

THE UNIVERSITY OF SHEFFIELD



Novel Biomarkers in the Management of HPV-Positive & -Negative Oropharyngeal Carcinoma

Thesis submitted to the University of Sheffield
for the degree of Doctor of Philosophy

Robert Bolt

Department of Oral & Maxillofacial Pathology

January 2016

Abstract

Human Papillomavirus (HPV)-related oropharyngeal carcinoma is considered to be in the early stages of an epidemic¹⁻¹². A marked rise in the incidence of this sexually-transmissible cancer has captured the public interest, and much debate exists over both the prophylactic and therapeutic strategies currently employed to manage this healthcare priority.

HPV-positive oropharyngeal carcinoma is associated with highly favourable oncological outcomes. Clinical attention over recent years has been paid to the potential de-escalation of therapy in order to account for the disease's favourable prognosis, in addition to reducing therapeutic burden in a well-prognosticating, younger patient cohort, for which consequences of radical chemo-radiotherapy strategies may disproportionately impact on longer-term quality of life. Whilst optimising the management of the ever-increasing proportion of HPV-positive oropharyngeal carcinomas is desirable and highly justifiable, it appears the poorer prognosticating HPV-negative oropharyngeal carcinoma has at least in part become overlooked.

Oropharyngeal carcinoma is unique in comparison to many other established HPV-related cancers inasmuch as a clear HPV-negative subset exists, to which established aetiological factors (tobacco smoking and alcohol consumption) strongly correlate. For most other HPV-related carcinomas, such as cervical, anal and penile, tumours classified as HPV-negative are either regarded as potentially-virus containing, or else cannot be correlated to a definitive aetiological agent. Comparison of HPV-positive and -negative oropharyngeal carcinoma therefore offers unprecedented insight into the biological significance of each aetiological agent, and how prognostication of each disease may relate to tumour behaviour at a molecular level. Whilst improved outcomes may be attributable in part to greater radio-sensitivity due to preservation of key wild-type genes in HPV-positive tumours, more comprehensive biological differences are likely to underpin the overall behaviour of disease – indeed, surgical outcomes are also favourable in HPV-positive disease.

This thesis explores the potential for the tumour microenvironment to differ between HPV-positive and -negative disease. We hypothesised that due to the strictly epitheliotropic nature of the Human Papillomavirus, activation of the tumour microenvironment would potentially be suppressed in order to avoid host clearance of pathogen during the natural history of viral infection, whereas penetrating carcinogens linked to tobacco smoking and alcohol consumption may either directly derange the stroma or, less contentiously, induce an increased mutational load which in turn in turn may offer greater opportunity for tumour evolution towards deranged microenvironmental signalling.

A 2D tissue culture model of the tumour microenvironment was created and used to test the hypothesis of a difference in microenvironmental interactions between HPV-positive versus HPV-negative disease, and normal stroma. Confirmation of an increase in migration-inducing signals from the modelled normal fibroblast stroma in HPV-negative disease led to further investigation at a molecular level using cytokine array technology. Further ELISA quantification and recombinant protein dose-response analysis ultimately identified Human Hepatocyte Growth Factor (HGF) as a primary candidate molecule for driving the additional migration observed in response to activated stroma. IL-6, co-secreted with HGF by stimulated fibroblasts, was also found to have a supporting role through the co-induction of STAT3. Final confirmation of HGF's principal role in inducing HPV-negative tumour migration was undertaken using the clinically relevant c-Met inhibitors, foretinib & INCB28060 (recently rebranded as capmatinib).

Further experimentation using 3D models of HPV-negative tumour spheroid invasion found fibroblast co-culture with tumour lines a necessary prerequisite for invasion. Moreover, disruption of HGF signalling within co-cultures led to near-total abrogation of invasion.

Acknowledgements

I would like to take this opportunity to give thanks for the huge amount of support I have received from colleagues within my direct research team and further afield. I would like to give particular thanks to the following people, who have been instrumental in the progress of my work;

I would like to thank my two supervisors, Dr. Keith Hunter and Dr. Bernadette Foran for their ongoing support and guidance throughout the project and its conception, in addition to their efforts in orchestrating collaborations with Leeds hospital for the clinical element of the study aimed to extend beyond the PhD. I would also like to thank Dr. Hunter for taking great personal effort to source, negotiate MTAs and travel to retrieve the cell lines used within this project, donated as kind gifts by Prof. Eric Blair (Leeds) and Dr. S. Thavaraj (London).

Particular thanks go to those who have helped with my training in tissue culture and directly related experimental techniques, including Dr. Vanessa Hearnden, Dr. Lav Darda, Dr. Fahad Hakami, Dr. Jill Callaghan, Dr. Sally Thomas and Dr. Taznuva Kabir. I would like to extend these thanks to acknowledge the particular efforts of Dr. Vanessa Hearnden, who has been invaluable in establishing a reproducible method of undertaking migration assay, in addition to patiently working through flow cytometry analysis of mitomycin treatments with me. I would like to point out the inclusion of a graph relating cell line UD SCC2 (Figure 1.6b), which represents Dr. Hearnden's own work undertaken with my support, used as a demonstration case for other cell lines. Special thanks also should be extended to Dr. Sally Thomas for the collaborative work on the western blot data depicted in Figures 5.6 a & b.

I would like to give additional thanks to Jill Callaghan for her guidance in PCR analysis, including her assistance in the sourcing and reconstitution of custom TaqMan probes. I would also like to give thanks to Dr. Fahad Hakami, Dr. Lav Darda, Dr. Genevieve Melling and Brenka McCabe for their advice in running PCR experiments.

Specific thanks also to Drs. Daniel Lambert, Craig Murdoch, Simon Whawell, Lynne Bingle, Eileen Crawford, Ali Khurram and Abigail Pinnock for offering direct guidance and sharing access to a number of resources and consumables, without which progress in particular elements of the project would have been unfeasible. I would also like to give thanks to Jason Heath, Brenka McCabe, Michelle Gaunt, David Thompson and Hailey Stanhope for their help in accessing and ordering a host of materials, in addition to guidance in the use of histopathology equipment and assistance with specimen processing.

Finally, I would like to extend my thanks to Yorkshire Cancer Research and Cancer Research UK for the joint-funded Clinical Research Fellowship which has allowed this research to be undertaken.

Contents

Literature Review	Page
1. Introduction	1
2. The Human Papillomavirus (HPV) as a causative agent in cancer	5
3. Epidemiology of HPV-positive Oropharyngeal Carcinoma (OPC)	14
4. Mechanism of HPV-related carcinogenesis	17
5. Accounting for prognosis	22
6. Methods of HPV detection in OPC	25
7. Management of HPV-positive disease	28
8. Management of HPV-negative disease	29
9. Stromal Derangement	31
10. Hypothesis, aims and objectives	34
Chapter 1: Confirmation of HPV Status, Validation of Cell Lines & Optimisation of Migration Assay	
1. Introduction	37
2. Methods	40
3. Results	51
4. Discussion	62
Chapter 2: 2D Modelling of the Microenvironment in HPV-positive & -negative Disease	
1. Introduction	65
2. Methods	67
3. Results	74
4. Discussion	82
Chapter 3: Cytokine Array Analysis of Tumour & Fibroblast Conditioned Media	
1. Introduction	85
2. Methods	88

	Page
3. Results	91
4. Discussion	113
 Chapter 4: Investigation of a CXCR-2/IL-6 Basis of Fibroblast Recruitment and Support	
1. Introduction	122
2. Methods	125
3. Results	133
4. Discussion	146
 Chapter 5: Progressive Analysis of Candidate Molecules Identified by Cytokine Array	
1. Introduction	152
2. Methods	158
3. Results	168
4. Discussion	180
 Chapter 6: The Role of HGF in 2D Modelled Migrations	
1. Introduction	187
2. Methods	195
3. Results	209
4. Discussion	237
 Chapter 7: Conditioned Media Induction of Fibroblast Senescence	
1. Introduction	246
2. Methods	248
3. Results	250
4. Discussion	254
 Chapter 8: Determining Validity of 2D Experimental Findings	
1. Introduction	256
2. Methods	258

3. Results	265
4. Discussion	280

Chapter 9: Further Work	Page
1. Introduction	283
2. Further Work I	288
3. Further Work II	295
4. Further Work III	306
5. Further Work IV	307
6. Further Work V	309
7. Further Work VI	311
References	313
Appendices	345

List of Abbreviations

2D	Two dimensional
3D	Three dimensional
ALI	Air-liquid interface
B2M	Beta-2-microglobulin
CAF	Cancer-Associated Fibroblast
CDK	Cyclin-Dependent Kinase
CK	Cytokeratin
c-Met	Human Hepatocyte Growth Factor Receptor
CXCL	Chemokine CXC-motif Ligand
DAB	Diaminobenzidine
DDR	DNA damage response
DED	De-Epidermised Dermis
DeESCALaTE	Determination of Epidermal growth factor receptor-inhibitor (cetuximab) vs Standard Chemotherapy early and Late Toxicity Events in Human Papilloma Virus Positive Oropharyngeal Carcinoma
dH ₂ O	Distilled water
DMEM	Dulbecco's Modified Eagle's Medium
DMSO	Dimethyl Sulphoxide
DNA	Deoxyribonucleic Acid
E1-E7	HPV "Early" Proteins 1-7
EDTA	Ethylenediaminetetraacetic acid
EGF	Epidermal Growth Factor
EGFr	Epidermal Growth Factor receptor
EMT	Epithelial to Mesenchymal Transition
ENA 78	Epithelial Neutrophil-Activating Protein 78 (also known as CXCL5)
FAM	Amine-reactive succinimidyl ester of carboxyfluorescein
FBS	Fetal Bovine Serum
FFPE	Formalin-Fixed, Paraffin Embedded
G	Grams
G	G-force - units equal to Earth's gravitational acceleration (9.80665 m/s ²)
Gal	Galectin
GCP 2	Granulocyte Chemotactic Protein 2 (also known as CXCL6)
GFP	Green fluorescent protein
GIST	Gastrointestinal Stromal Tumour
GRO	Growth-Regulated Oncogene
Gy	Grays
H&E	Haematoxylin and Eosin
h/ hrs	Hours
HGF	Human Hepatocyte Derived Growth Factor
HIRA	Histone Receptor Alpha
HPV	Human Papillomavirus
HPV 16	Human Papillomavirus type 16
HPV 18	Human Papillomavirus type 18
HRQoL	Health-Related Quality of Life
ICC	Immunocytochemistry

IF	Immunofluorescence
IL	Interleukin
INNO LiPA	Innogenetics genotyping assay
IRAS	Integrated Research Application System
ISH	In-Situ Hybridization
IU	International Units
L1-L2	HPV "Late" Proteins 1-2
M	Molar
MEM	Minimum Essential Media
µg	Micrograms
Mg	Milligrams
MHC	Major Histocompatibility Complex
Mins	Minutes
mL	Millilitres
µL	Microliters
MMP	Matrix Metalloproteinase
MTS	3-(4,5-dimethylthiazol-2-yl)-5-(3-carboxymethoxyphenyl)-2-(4-sulphophenyl)-2H-tetrazolium
NEAA	Non-Essential Amino Acid
NF-κB	Nuclear Factor Kappa-light-chain-enhancer of activated B cells
Ng	Nanograms
NHS	National Health Service
NIH	National Institute of Health, USA
°C	Degrees Celsius
OPC	Oropharyngeal Carcinoma
OSCC	Oral Squamous Cell Carcinoma
PBS	Phosphate Buffered Saline
PDGF	Platelet-Derived Growth Factor
PI	Principal Investigator
PIKK	Phosphatidylinositol 3-kinase-related kinase
pRb	Retinoblastoma protein
R&D	Research And Development
RB1	Retinoblastoma gene
REC	Research Ethics Committee
RFP	Red fluorescent protein
RNA	Ribonucleic Acid
ROS	Reactive Oxygen Species
Rpm	Revolutions per minute
RT	Room temperature
RTOG	Radiation Therapy Oncology Group
SA β-Gal	Senescence-associated β-galactosidase
SASP	Senescence-Associated Secretory Phenotype
SCC	Squamous Cell Carcinoma
SMA	Smooth Muscle Actin
SMG-1	Serine/threonine-protein kinase SMG1
Spp	Species pleuralis
SSI	Site Specific Information

STH	Sheffield Teaching Hospitals
TAE	Tris Acetic EDTA
TAMRA	Carboxytetramethylrhodamine, succinimidyl ester
TGF- β 1	Transforming Growth Factor - β 1
TBS	Tris-Buffered Saline
U	Units
VIC	Applied Biosystems proprietary reporter used in PCR, data unavailable for compound structure
WPH	Weston Park Hospital

List of Figures

Figure	Page	Description
0.1	2	The Human Papillomavirus Genome
0.2	4	Normal versus HPV-infected regulation of p53, pRB and p16
0.3	8	Genomic events seen in the multistep process of head and neck cancer formation
1.1	51	Nanodrop™ Analysis of extracted cell line RNA
1.2	52	HPV16 E1 qPCR amplification plot
1.3	53	HPV16 E6 qPCR amplification plot
1.4	54	Agarose Gel Electrophoresis of HPV16 E6 and E1 qPCR Reaction Products
1.5	56	Flow Cytometry Analysis of Cell Lines Exposed to a Range of Mitomycin C Concentrations
1.6	60	Trial Cell Seeding Densities for ORIS™ Assay Loading
2.1	68	Conceptual Model of Tumour-Stroma Microenvironmental Interactions, Plus 2D Tissue Culture Duplicate Model
2.2	74	Additional ORIS™ Assay Migration of Cell Lines Exposed to Respective Stimulated Fibroblast Media 1
2.3	76	Additional ORIS™ Assay Migration of Cell Lines Exposed to Respective Stimulated Fibroblast Media 2
2.4	77	Overlay Images of ORIS™ Assay Cell Migration Following Exposure to Media 1, Compared to Unstimulated Fibroblast Conditioned Media Control
2.5	79	Overlay Image of ORIS™ Assay Migration Following Exposure to Media 2, Compared to Unstimulated Fibroblast Conditioned Media Control
2.6	80	MTS Assay of HPV-positive Cell Line Proliferation in Response to Stimulated Fibroblast Media 2 Versus Unstimulated Fibroblast Control
2.7	81	MTS Assay of HPV-negative Cell Line Proliferation in Response to Stimulated Fibroblast Media 2 Versus Unstimulated Fibroblast Control
3.1	91	Raybiotech C6 Cytokine Array Analysis of Tumour Line Conditioned Media
3.2	93	Raybiotech C7 Cytokine Array Analysis of Tumour Line Conditioned Media
3.3	95	Raybiotech C8 Cytokine Array Analysis of Tumour Line Conditioned Media
3.4	97	Raybiotech C6 Cytokine Array Analysis of Simulated Fibroblast Conditioned Media
3.5	99	Raybiotech C7 Cytokine Array Analysis of Simulated Fibroblast Conditioned Media
3.6	101	Raybiotech C8 Cytokine Array Analysis of Simulated Fibroblast Conditioned Media
3.7	103	Densitometry Analysis of Tumour Line Conditioned Media Raybiotech C6 Cytokine Array
3.8	104	Densitometry Analysis of Tumour Line Conditioned Media Raybiotech C7 Cytokine Array
3.9	105	Densitometry Analysis of Tumour Line Conditioned Media Raybiotech C8 Cytokine Array
3.10	107	Densitometry Analysis of Simulated Fibroblast Media Raybiotech C6 Cytokine Array
3.11	109	Densitometry Analysis of Simulated Fibroblast Media Raybiotech C7 Cytokine Array
3.12	110	Densitometry Analysis of Simulated Fibroblast Media Raybiotech C8 Cytokine Array
4.0	124	Hypothesised Route through Which HPV-negative Cell Lines Derive Increased Migrational Activity from Fibroblasts

4.1	133	IL-6 ELISA Analysis of Cell Line Conditioned Media and Stimulated Fibroblast Media 1&2
4.2	134	IL-8 ELISA Analysis of Cell Line Conditioned Media and Stimulated Fibroblast Media 1&2
4.3	136	Solubilised IL-6R ELISA Analysis of Cell Line-Derived Conditioned Media
4.4	137	Flow Cytometry Analysis of CXCR1 Expression in DENOFO8 Normal Oral Fibroblasts Following Exposure to Cell Line Conditioned Media
4.5	139	Flow Cytometry Analysis of CXCR2 Expression in DENOFO8 Normal Oral Fibroblasts Following Exposure to Cell Line Conditioned Media
4.6	141	GRO-beta and GRO-gamma mRNA Expression in HPV-positive Versus HPV-negative Cell Lines
4.7	142	ELISA Analysis of Media 2 IL-6 Content Following Co-incubation of Fibroblasts with CXCR2 Inhibitor Versus DMSO Control.
4.8	143	ELISA Analysis of IL-6 Content Following Stimulation of Fibroblasts with Permutations of sIL-6R, IL-6, GRO-beta and GRO-gamma
4.9	144	ORIS™ Assay of UPCI SCC072 Migration in Response to recombinant GRO- β/γ - Stimulated Fibroblast Media 2
4.10	145	Recombinant IL-6 Dose-Response Curve for Additional ORIS™ Assay Migration, Compared to DMEM Control
5.1	168	Dose-Response Curves for Candidate Recombinant Proteins Identified by Cytokine Array
5.2	170	OSM ELISA Analysis of Cell Line Conditioned Media and Respective Media 1 & 2
5.3	171	HGF ELISA Analysis of Cell Line Conditioned Media and Respective Media 1 & 2
5.4	173	Dose-Response Analysis of Recombinant Human HGF for HPV-Negative Oropharyngeal Carcinoma Line UPCI SCC089
5.5	174	Flow Cytometric Analysis of c-Met Status in Oropharyngeal Carcinoma Cell Lines
5.6	177	Total and Phospho-STAT3 Western Blot Analysis of Cell Lines Following Exposure to Stimulated Fibroblast Media 2
5.7	179	ELISA analysis of Soluble c-Met release from Oropharyngeal Carcinoma Cell Lines
6.1	209	Effect of c-Met Inhibitors on UPCI SCC089 Migration Using 0.5 $\mu\text{g ml}^{-1}$ Recombinant Human HGF in Normal Media
6.2	211	Effect of c-Met Inhibitors on UPCI SCC072 Migration Using 0.5 $\mu\text{g ml}^{-1}$ Recombinant Human HGF in Normal Media
6.3	213	Cytotoxicity Assays of Foretinib and INCB28060 for Cell Line UPCI SCC072
6.4	215	Cytotoxicity Assays of Foretinib and INCB28060 for Cell Line UPCI SCC089
6.5	217	Effect of c-Met inhibitors on UPCI SCC89 ORIS™ Assay Migration Using DENOFO8 Stimulated Fibroblast Media 2
6.6	219	Effect of c-Met inhibitors on UPCI SCC072 ORIS™ Assay Migration Using DENOFO8 Stimulated Fibroblast Media 2
6.7	221	Dose-Response Analysis of HPV-negative Cell Lines Exposed to Logarithmically Increasing Concentrations of Recombinant Human EGF
6.8	223	Dose-Response Analysis of HPV-negative Cell Line UPCI SCC072 Exposed to Logarithmically Increasing Concentrations of Recombinant Human VEGF
6.9	225	EGF ELISA Analysis of Cell Line Conditioned Media and Stimulated DENOFO8 Fibroblast Media 1 & 2.
6.10	227	Effect of c-Met Inhibitors on UPCI SCC072 ORIS™ Assay Migration with 2 ng mL ⁻¹ EGF
6.11	229	Effect of c-Met Inhibitors on UPCI SCC089 ORIS™ Assay Migration with 2 ng mL ⁻¹ EGF

6.12	231	ORIS™ Assay Migration of Cell Line UPCI SCC072 Under Conditions of Co-incubation With Varying Concentrations of HGF and IL-6
6.13	233	ORIS™ Assay Migration of Cell Line UPCI SCC089 Under Conditions of Co-incubation With Varying Concentrations of HGF and IL-6
6.14	235	Flow Cytometry Analysis of IL-6 Receptor Expression on Oropharyngeal Carcinoma Cell Lines
6.15	240	Model of microenvironmental pathway of inducing HPV-negative tumour migration
7.1	250	Representative Micrographs of DENO F08 Fibroblast Cultures Following 13 Day Exposure to Cell Line Conditioned Media
7.2	252	Percentage SA-βGal Positive DENO F08 Fibroblasts in Cultures Following 13 Day Exposure to Cell Line Conditioned Media
8.0	264	Example Selection Tool Mark-Up of Cells in Escape Zone, Cultrex™ Assay
8.1	205	Representative Photomicrographs of DED Organotypic Models at 7 & 14 Days in Cell Lines HTE E6E7, UPCI SCC02, UPCI SCC072, UPCI SCC089 and UPCI SCC090
8.2	267	Representative Photomicrographs of Collagen-based Organotypic Models at 14 Days in Cell Lines UPCI SCC02 and UPCI SCC072
8.3	268	Cultrex™ Tumour Spheroid Invasion Assay, Cell Line UPCI SCC089
8.4	270	Cultrex™ Tumour Spheroid Invasion Assay, Cell Line UPCI SCC072
8.5	272	Bar Graphs: Cultrex™ Assay Invasion of Cell Lines UPCI SCC072 & UPCI SCC089
8.6	274	H&E Sections of Cultrex™ Tumour Spheroids, Cell Line UPCI SCC072
8.7	276	H&E Section of Cultrex™ Tumour Spheroid, Cell Line UPCI SCC089
8.8	277	Cytokeratin A1/A3 Staining of UPCI SCC072 Co-Culture Model
9.1	289	Western Blot Analysis of Fibroblast Total(t) and Phospho(p)STAT3 in Response to HPV-Positive Cell Line Conditioned Media
9.2	290	Western Blot Analysis of Fibroblast Total(t) and Phospho(p)STAT3 in Response to HPV-Negative Cell Line Conditioned Media
9.3	296	Effects of Ruxolitinib on HGF/IL-6 Signalling via STAT3
9.4	299	Effects of Ruxolitinib 1µM on ORIS™ Assay Migration of Cell Line UPCI SCC089 in the Presence of Stimulated Fibroblast Conditioned Media Versus Unstimulated Fibroblast Media Control
9.5	301	Effects of Ruxolitinib 1µM on ORIS™ Assay Migration of Cell Line UPCI SCC072 in the Presence of Stimulated Fibroblast Conditioned Media Versus Unstimulated Fibroblast Media Control
9.6	302	Ruxolitinib 1µM LDH Assay, UPCI SCC072 & UPCI SCC089
9.7	303	Ruxolitinib 1µM MTS Assay, UPCI SCC072 & UPCI SCC089

List of Tables

Table	Page	Description
0.1	6	Proportion of cancers attributable to Human Papillomavirus by anatomic site
0.2	8	A summary of clinical studies of HPV prognostication in Oropharyngeal cancer
1.1	41	Composition of Modified E-media, used for culture of HTE E6 E7
1.2	41	Composition of Media Used for expansion of Cell Lines UD SCC02, UPCI SCC072, UPCI SCC089 and UPCI SCC090
1.3	42	Summary of retrieved cell lines
1.4	44	Reagents used in Reverse Transcription reaction
1.5	44	Thermal Cycle Program for cDNA Formation
1.6	45	PCR Reagents
1.7	46	PCR Reagents
1.8	46	TAE Constituents (X50 solution)
1.9	59	Optimal Mitomycin concentration determined for each cell line
1.10	61	Optimal seeding densities determined following trial seeding in ORIS™ assay wells
3.1	111	Summary of Factors Present in Cell Line Conditioned Media
3.2	112	Summary of Factors Present in (Stimulated) Fibroblast Media
5.1	158	Details of recombinant proteins used in dose-response analysis
5.2	176	Additional Flow Cytometric Absorption of Cell Lines Co-incubated with c-Met Probe, Compared to Control
6.1	189	List of available small molecule/monoclonal antibody inhibitors of c-Met
8.1	261	Collagen Gel Constituents
8.2	261	Constituents of Green's Media
9.1	311	Summary of Data Collected for Retrospective Cohort Analysis

Foreword

A significant body of the work presented in this thesis relates to the experimental use of conditioned media. Where reference has been made to “normal media”, the plural term of “media” has been used exclusively in order to avoid any unnecessary confusion. Although “medium” may well be a more grammatically correct term for use in the singular, “normal media” is a commonly accepted phrase and was felt to avoid confusion with alternative definitions of “normal” and “medium”, which both relate to measures of central tendency.

Literature Review

Contents

	Page
1. Introduction	1
2. The Human Papillomavirus (HPV) as a causative agent in cancer	5
3. Epidemiology of Oropharyngeal Carcinoma (OPC)	14
4. Mechanism of HPV-related carcinogenesis	17
5. Accounting for prognosis	22
6. Methods of HPV detection in OPC	25
7. Management of HPV-positive disease	28
8. Management of HPV-negative disease	29
9. Stromal Derangement	31
10. Hypothesis, aims and objectives	34

1. Introduction

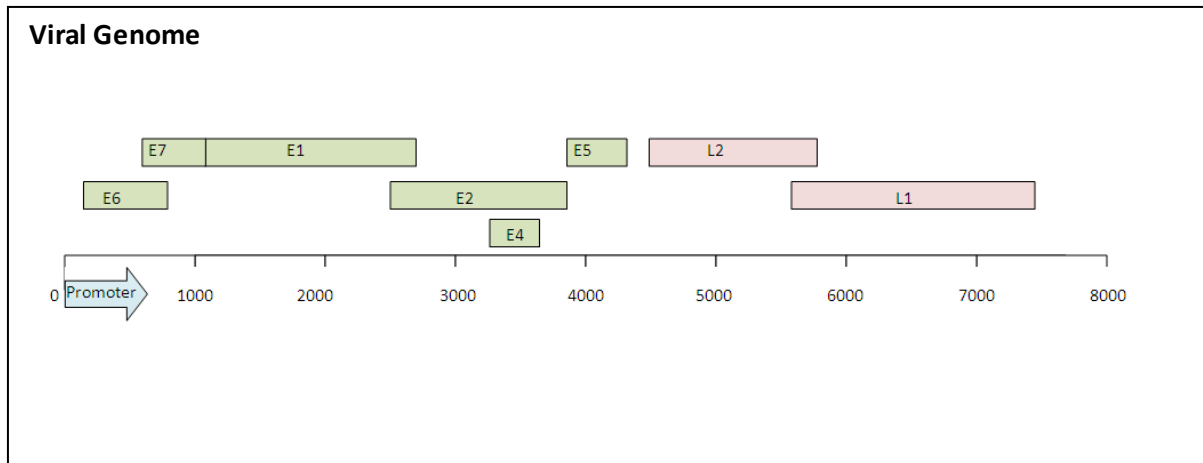
The Human Papillomavirus (HPV) is a non-enveloped, double stranded DNA virus capable of infecting skin and mucosa^{13, 14}. HPV infection has not been identified outside of the skin, oropharynx and anogenital mucosa, leading to the virus being considered as strictly epitheliotropic¹⁵. The reason for this is unknown although the virus has limited capacity for host invasion, requiring a breach in the continuity of epithelial lining in order to access and infect cells of the basal layer¹³. A prerequisite for successful host invasion also appears to be maintenance of an intact basement membrane in order for the virus to evade the immune response; sub-epithelial exposure to the virus appears to act as a stimulus to the adaptive immune system¹⁶, whilst has capacity to suppress underlying inflammation whilst residing in epithelia¹⁷.

The HPV particle consists of an icosahedral capsid that acts to enclose and also assist in packaging of the viral genome, as well as contributing to host entry by interacting with cell surface heparan sulfate to trigger endosomal absorption¹⁸. The major component of this shell is the L1 protein, so-called due to the “late” expression of the gene encoding this protein during the viral life cycle¹⁴. A further viral protein, L2, also has a minor contribution to the viral capsid structure.

To date, over 100 HPV “types” have been identified, with estimates of around 200 types being in existence^{19, 20}. A type is defined as having at least a 10% difference in the nucleotide sequence encoding the major viral capsid component (L1 gene) when compared to any other known HPV type¹⁹. Specific types have been heavily implicated with carcinogenesis, and have therefore been ascribed the term “high-risk”.

The HPV genome is very slowly evolving, and has remained relatively unchanged since the origin of the human species. It is estimated that between 1-5% of the HPV nucleotide sequence has evolved with the human species, leading to “variants” within each HPV type¹⁹. A variant of a specific HPV type is considered as having 2% variation in coding regions of the HPV genome, and 5% in non-coding regions^{19, 21}. Diversity between HPV types is thought to have evolved over several millions of years²².

Figure 0.1: The Human Papillomavirus Genome



The HPV genome comprises a circular DNA sequence of approximately 8 kilobase pairs, complexed by host cellular histones¹⁴. A total of 9 genes exist, encoding 7 early (“E”) and 2 late (“L”) proteins²³ (Figure 0.1). As aforementioned, the 2 “L” proteins form the viral capsid, and their late expression reflects the requirements of capsid production; virally infected keratinocytes must progress to the more superficial layers of epithelium before virion release can occur. In fact, L1 production is governed by the maturation process of basal to superficial epithelial cells, hence much stronger L1 expression is seen in the superficial epithelial layers²⁴⁻²⁶. The release of viral particles is assisted by the expression of the E4 protein (also expressed relatively late in the viral cycle despite its nomenclature), which acts to disrupt intermediate filaments of the cell cytoskeleton²⁷.

The other “E” proteins are largely involved in influencing viral replication. The E1 gene encodes a protein that binds to the viral origin of replication and acts as a helicase, separating the viral DNA strands so that replication can occur through the use of host cell factors¹⁴. The E2 protein acts as a major transcriptional regulator, in addition to tethering viral DNA to host chromosomes²⁸. The E2 protein further acts as a negative regulator of E6 and E7 expression – genes heavily implicated with carcinogenesis^{29, 30}. Inactivation of E2, which is thought to occur as a result of integration of viral DNA into the host chromosome, leads to the increased expression of E6 and E7³¹.

The E3 gene is not known to have any important function. E5, although oncogenic in some animal papillomavirus types, is generally regarded as having only an early destabilising function within human cells; a substantial portion of the E5 gene is deleted during viral

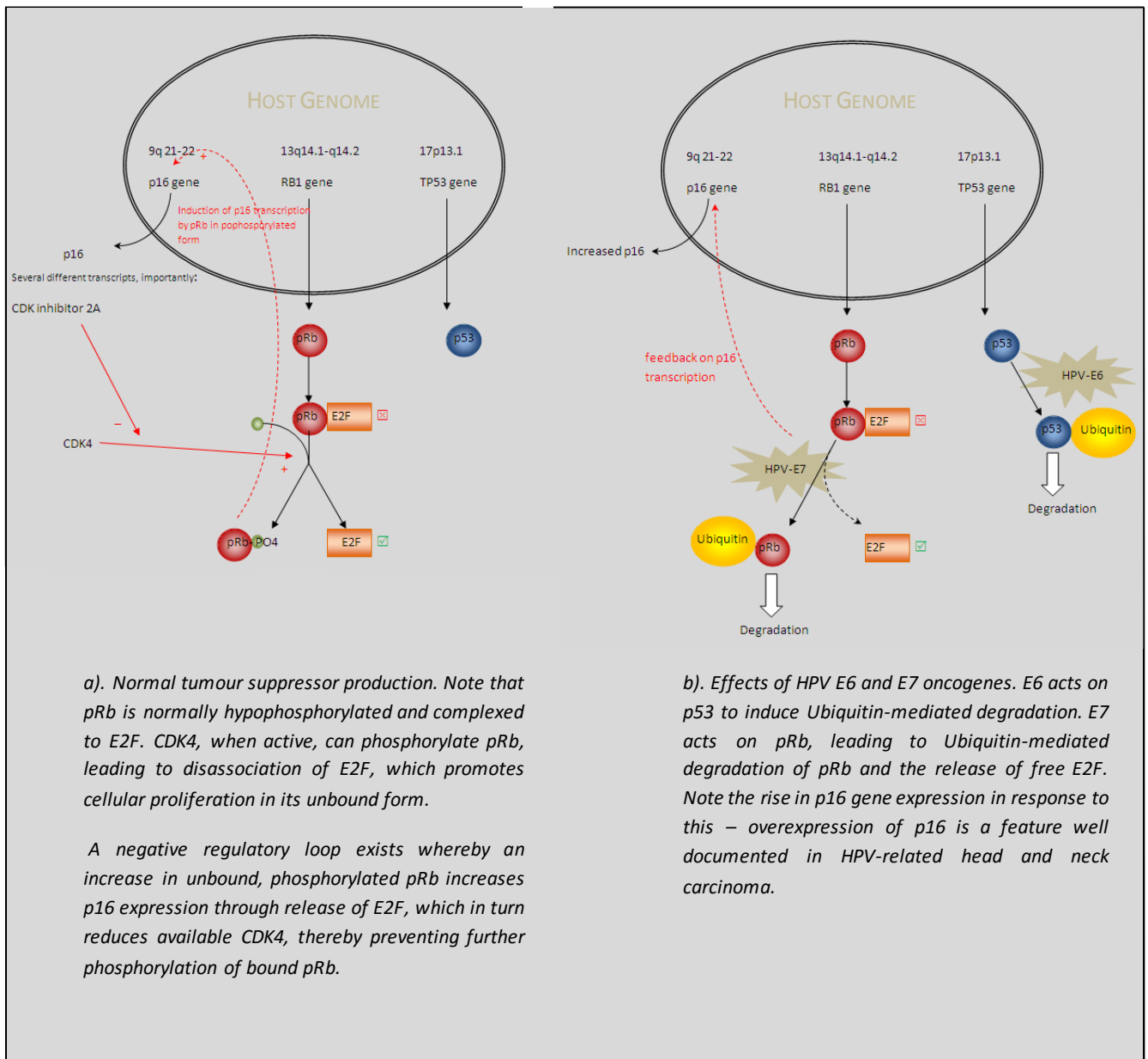
integration³². E5 does however act to upregulate EGFR in the early stages of infection, leading to the downregulation of p21³³; the potential for E5 to have a carcinogenic effect is therefore not entirely ruled out³⁴.

The E6 and E7 genes encode oncoproteins that deregulate cell cycle control^{31, 32}. Although both E6 and E7 proteins have effects on multiple intracellular signalling pathways, their major actions are on the tumour suppressor proteins p53 and pRb, respectively^{23, 35, 36}. E6 complexes with E6AP ("E6-associated protein" – a cellular protein ligase), which then binds P53 and induces Ubiquitin-mediated degradation^{15, 29}. E7 binds to hypophosphorylated pRb; this form of the pRb protein exists complexed with E2F³⁷. The interactions between E7 and pRb leads to the release of E2F, a factor that promotes DNA synthesis and cell cycle progression when in its free form¹⁴. Release of E2F by pRb usually only occurs as a result of phosphorylation, most notably by CDK4 (a cyclin-dependant kinase that is activated during cell proliferation)³⁸. This is summarised in Figure 0.2b.

The functional sequestration of p53 and pRb leads to the loss of important pathways in cell cycle control; p53 normally acts to hold the cell at the G1/S regulation point when DNA damage is detected, along with mediating DNA repair and when appropriate inducing apoptosis²⁹. Free E2F further compounds this through the activation of genes linked to cell cycle progression and turnover.

It is important to note that there is some degree of conflict between the actions of the E2 protein and E6&7. In addition to repressing E6&7, E2 also acts to arrest the cell cycle in S-phase²⁹. Arrest in S-phase allows replication of viral DNA, which would otherwise be limited if cell cycle were to progress.

Figure 0.2 Normal versus HPV-infected regulation of p53, pRb and p16



2. HPV as a Causal Agent in Cancer

In 1983 Harald Zur Hausen announced his discovery of HPV type 16 as the major causal agent in cervical carcinoma³⁹. Despite widespread recognition of Zur Hausen's groundbreaking work, the role of HPV-related lesions in carcinogenesis had for some time already been acknowledged. Malignant transformation of condyloma acuminata had been reported in the literature as far back as 1950⁴⁰, with Siegel's 1962 review concluding a role for such lesions in occasional malignancies of the anogenital region⁴¹. Dun *et al* described the presence of intranuclear viral particles in human genital wart tissue in 1968⁴², with Zur Hausen himself postulating the role of the as-yet undiscovered "condyloma agent" in carcinomas of the anogenital tract in a brief correspondence published in *Cancer Research* in 1976⁴³. Perhaps the greatest leap Zur Hausen took was to acknowledge the numerous reports of malignant transformation of condyloma acuminata, and divert his efforts away from attempting to confirm a then-popularised role of HSV-2 in carcinogenesis and instead search for the presence of the condyloma agent in cervical malignancies⁴⁴⁻⁴⁸.

Following the publication of Zur Hausen's paper, a snowballing of further research linking HPV to anogenital and other epithelial malignancies ensued. Whilst there was rapid acceptance of the role of the virus in other carcinomas, suggestions of its role in cancers of the orofacial region were met with some resistance. The International Agency for Research on Cancer (IARC) now recognises HPV as a risk factor for oropharyngeal carcinoma (OPC)⁴⁹⁻⁵¹. The acceptance of HPV as a causal agent in OPC has been delayed in comparison to its cervical cancer counterpart, largely due to the latter being almost exclusively linked to preceding HPV infection (Table 0.1). In contrast, the major risk factors for OPC are historically tobacco smoking and alcohol intake, with HPV (until recently) being linked to a small subset of carcinomas. Compounding this, HPV related OPC is linked to specific anatomical sub-sites, namely base of tongue and tonsils; inclusion of these tumours in the more generic group of "oropharyngeal carcinoma" leads to dilution of any correlative findings⁵.

Table 0.1: Proportion & Prognostic Significance of Tumours with a HPV-positive Status in Relation to Anatomical Location

Site	Proportion (%) of cancers HPV+	HPV Types occurring with significant frequency (descending order)	Proportion of virus-positive cancers HPV 16 (%)	HPV Prognostic Significance
Cervix ^{52, 53}	79-89	16, 18	60	HPV 16 favourable HPV 18 unfavourable
Vagina ⁵⁴	70	16, 18	77	Favourable in late stage disease
Vulva ^{52, 54}	40	16, 33	79	Favourable
Penis ⁵⁵	48	16, 6, 18	64	Inconclusive
Anus ⁵⁴	84	16, 18, 33	87	Favourable
Oropharynx ^{56, 57}	36	16	90	Favourable

There is now a good body of evidence for a causal relationship between HPV and OPC. Several studies have addressed many of the criteria set out by Bradford-Hill for the demonstration of causality⁵⁸. These are discussed below;

Strength of Association

Although there is clearly a much lower strength of association between HPV and OPC in comparison to cervical carcinoma, there is a marked increase in the relative risk of OPC in the base of tongue and tonsillar regions related to sexual practice. A higher number of lifetime sexual partners, younger age of sexual debut, higher number of oral sexual partners and history of oral-anal intercourse have all been implicated with an increase in relative risk of OPC⁵⁹⁻⁶⁵. Risk is particularly linked to males^{65, 66}; it is postulated that this is due to exposure to a higher HPV viral load in cervical secretions during oral sex in comparison to oral contact with penile tissue¹².

A further interesting relationship which reinforces direct evidence of association is the increased risk of OPC in husbands of females with a history of cervical carcinoma⁶⁷. Joint disease mapping of cervical carcinoma and male OPC also infers a shared risk⁶⁸.

Consistency

The presence of high risk HPV within a tonsillar/tongue base subset of OPC has been consistently demonstrated in a number of studies, a systematic review and a large multicentre trial^{49, 50, 56, 62, 69}. Serological markers of HPV infection have also been repeatedly linked to head and neck cancer risk⁷⁰. Furthermore, the improved prognosis of HPV-positive OPC is well documented, and has been subject to meta-analysis in addition to prospective clinical trial⁷¹⁻⁷⁷. A summary of studies assessing the prognostic significance of HPV status is given in Table 0.2.

Table 0.2: A Summary of Clinical Studies assessing HPV as a Prognostic Marker in OPC

Year	First Author	n	Method of analysis	Outcome measures	Treatment	HPV+ survival	HPV- survival	Conclusions
1996	Snijders ⁷⁸	63	C-PCR	OS, RR	S	-	-	No difference*
1997	Paz ⁷⁹	167	C-PCR	OS	Not stated	43.1 (3)	48.8 (3)	No difference*
1999	Pintos ⁸⁰	117	C-PCR	OS, DFS	Not stated	66.7 (5)	58.3 (5)	No difference*
2000	Gillison ⁸¹	253	C-PCR, TS-PCR, ISH	DSS	S/ RT/CRT	91 (3)	79 (3)	Favourable
2000	Mellin ⁸²	60	C-PCR	SR, CSMR	RT	53.5 (5)	31.5 (5)	Favourable
2001	Friesland ⁸³	40	C-PCR	OS	RT	30 (5)	19 (5)	Favourable
2002	Ringstrom ⁸⁴	89	C-PCR	DSS	Not stated	94.1 (5)	54 (5)	Favourable
2003	Klussmann ⁸⁵	34	C-PCR, p16	OS, DFS	S +/- CRT	62 (4)	33 (4)	Favourable
2003	Li ⁸⁶	86	C-PCR, TS-PCR, p16	DSS	S/ RT/SRT	89 (5)	65 (5)	Favourable
2003	Ritchie ⁸⁵	139	C-PCR	SR	S/ RT/CRT	71 (5)	49 (5)	Favourable
2004	Baez ⁸⁷	118	TS-PCR	OS, DFS	Not stated	50 (3)	31.8 (3)	No difference*
2005	Wittekindt ⁸⁸	34	C-PCR, p16	DFS, RR	Not stated	72 (4)	23 (4)	Favourable
2006	Licitra ⁸⁹	90	RT-PCR	OS	S +/- RT	79 [§] (5)	46 (5)	Favourable
2006	Weinberger ⁹⁰	79	RT-PCR, p16	OS, DFS	SRT/RT	79 (5)	20 (5)	Favourable
2007	Badaracco ⁹¹	115	TS-PCR	DFS, OS	S	66.1 (2)	53.2 (2)	No difference*
2007	Reimers ⁹²	106	C-PCR, p16	OS, DFS	S +/-RT / CRT	84 (5)	49 (5)	Favourable
2007	Na ⁹³	108	C-PCR	SR	S/ RT +/- C	100 (5)	44 (5)	Favourable
2008	Fakhry ⁹⁴	96	C-PCR, ISH	OS, RR	CRT	95 (2)	62 (2)	Favourable
2008	Klozar ⁹⁵	81	C-PCR	OS, DSS	S +/- RT	73 (3)	35 (3)	Favourable
2008	Smith ⁹⁶	294	C-PCR	DSS, RFS	S/ RT/SRT	58 (5)	15 (5)	Favourable
2009	Chung ⁹⁷	46	RT-PCR, ISH	OS, LRR, MFS	CRT	86 (5)	35 (5)	Favourable
2009	Kong ⁹⁸	82	C-PCR	OS	Not stated	79 (5)	50 (5)	Favourable
2009	Lassen ⁹⁹	195	ISH, p16	OS, DSS, LRR	RT	62 (5)	26 (5)	Favourable
2009	Shi ¹⁰⁰	111	RT-PCR, ISH, p16	OS, DFS	RT +/- C	88 (3)	67 (3)	Favourable
2009	Hafkamp ¹⁰¹	77	PCR, ISH, p16	DSS	Not stated	69 (5)	31 (5)	Favourable
2010	Rischin ¹⁰²	172	ISH, p16, PCR	OS, FFS	CRT	91 (2)	74 (2)	Favourable
2010	Hannisdal ¹⁰³	137	C-PCR	CS	S +/- RT	54 (5)	33 (5)	Favourable
2010	Fischer ¹⁰⁴	365	p16	OS	S/ CRT	76.7 (5)	41.5 (5)	Favourable
2010	Ang ¹⁰⁵	323	ISH, p16	OS	CRT	82.4 (3)	57.1 (3)	Favourable
2010	Fischer ¹⁰⁶	102	p16	OS	S/ RT +/- C	59.3 (5)	24.5 (5)	Favourable
2010	Smith ¹⁰⁷	237	C-PCR, p16	OS, DSS	Not stated	83 [§] (2)	54 (2)	Favourable
2010	Lewis ¹⁰⁸	239	ISH, C-PCR, p16	OS, DFS, DSS	S/ S +RT/ S + C	86.2 (2)	44.2 (2)	Favourable
2011	Chernock ¹⁰⁹	148	ISH, p16	DFS	RT	HR 0.41	-	Favourable
2012	Kim ¹¹⁰	33	PCR, p16	DFS	S(C)RT	HR 9.53	-	No difference
2012	Holzinger ¹¹¹	199	PCR	OS, PFS	S(C)RT	HR 0.55	-	Favourable
2012	Cheng ¹¹²	60	PCR	OS, DFS, PFS	(C)RT	HR 0.23	-	Favourable
2012	Huang ¹¹³ (Chinese: abstract only)	66	PCR	OS, DSS	Not stated	90 (3)	52 (3)	Favourable
2013	Lin ¹¹⁴	176	ISH, p16	OS, DFS	SRT/CRT	89 (5)	-	N/A

2013	Mizumachi ¹¹⁵	71	PCR	OS	SRT/CRT	79 (5)	51 (5)	Favourable
2013	Semrau ¹¹⁶	52	PCR, p16	OS, PFS	CRT	70 (3)	37 (3)	Improved PFS, no difference in OS; advanced disease
2013	Hong ¹¹⁷	489	PCR, p16	OS	RT +/- S/C	N/A	N/A	Favourable
2013	Oguejiofor ¹¹⁸	217	PCR, p16	CSS, RFS, LRR	RT +/- All	77 (5)	39 (5)	Favourable
2013	Kawakami ¹¹⁹	104	PCR, p16	OS	RT/CRT	HR 0.21		Favourable
2013	Evans ¹²⁰	138	PCR, ISH, p16	OS, PFS	SRT/CRT	75 (5)	25 (5)	Favourable
2013	Bledsoe ¹²¹	121	ISH +/- p16	OS, DFS, LRR	CRT	94 (2)	73 (2)	Favourable
2013	Cerezo ¹²²	102	p16	OS, DFS, LRC	CRT	67	50	Favourable
2013	Tural ¹²³	81	PCR	OS	RT +/- S/C		HR 2.4	Favourable
2013	Nichols ¹²⁴	95	PCR, p16	OS, DFS	Not stated	90 (3)	65 (3)	Favourable
2013	Psychogios ¹²⁵	83**	p16	DSS	S +/- C/RT	81	80	No difference
2014	Melkane ¹²⁶	133	RT-PCR	OS, PFS	SRT/CRT	68 (5)	40 (5)	Favourable
2014	Deng ¹²⁷	53	PCR, p16	RFS, DFS	Not stated	100 (3)	77 (3)	Favourable
2014	Meyer ¹²⁸	106	PCR, p16	OS	All	71 (5)	56 (5)	Favourable
2014	Elgoff ¹²⁹	69	ISH	OS	CRT + Cetuximab	90 (5)	33 (5)	Favourable
2014	Hasegawa ¹³⁰	39	PCR, p16	DFS, TTF	CRT +/- S	94 (3)	67 (3)	Favourable
2014	Nomura ¹³¹	77	PCR, p16	DSS	All	89.1/90.3 (3)	76.8/74.5 (3)	Favourable
2014	Cai ¹³²	54	RNA-ISH, p16	OS	S/R/CRT	86	30	Favourable
2014	Vermorken ¹³³	416	Cervista, p16	OS	CRT + Cetuximab	HR 0.59-0.83		Favourable
2015	Lorch ¹³⁴	500	PCR/p16/both	OS	CRT	91 (3)	85 (3)	Favourable
2015	Goodman ¹³⁵	529	PCR	OS	S +/- RT/CRT	65 (5) HPV16 46 (5) HPV other	28 (5)	Favourable
2015	Lam ¹³⁶	207	PCR	OS, DSS		63 (5)	30 (5)	Favourable
2015	Rosenthal	182	p16, ISH	OS, LRC, PFS	RT +/- Cetuximab	HR 0.40	-	Favourable
2007	Ragin ⁷¹	N/A	Systematic Review	OS, DFS	All	HR 0.72, 0.51	-	Favourable
2012	O'Rourke ⁷³	N/A	Systematic Review	OS, DSS, PFS	All	HR 0.46, 0.28, 0.40	-	Favourable
2013	Rainsbury ⁷⁵	N/A	Systematic Review	OS	All	HR 0.39	-	Favourable
2014	Petrelli ⁷⁴	N/A	Systematic Review	OS, DSS, DFS	RT +/- S/C	HR 0.33, 0.24, 0.31	-	Favourable
2015	Wang ⁷⁶	N/A	Systematic Review	OS	Surgery Vs CRT	HR 0.283 Tongue, 0.475 Tonsil	-	Favourable
2015	Yuanyuan ⁷⁷	N/A	Meta Analysis (article in Chinese; abstract reviewed)	DSS, DFS, PFS	Not reported in abstract	HR 0.31, 0.38, 0.46	-	Favourable

Table 0.2: OS – Overall Survival, PFS – Progression-Free Survival, DHR – Death Hazard Ratio, CS – Cumulative Survival, CSS – Cancer Specific Survival DSS – Disease-Specific Survival, DR – Disease Recurrence, FFS – Failure-Free Survival, SR – Survival Rate, CSMR – Cause Specific Mortality Risk, RFS – Recurrence Free Survival, PFS – Progression Free Survival, RR – Response Rate, LRR – Locoregional

Recurrence, MFS – Metastasis Free Survival, TTF – Time to Treatment Failure, HR – Hazard Ratio of respective outcome measure. (Legend continued overleaf)

** majority of samples not oropharyngeal*

***only 31% of overall study population assessed for p16 status without reason given*

Techniques: TS-PCR – Type-specific PCR, C-PCR – Consensus PCR, RT-PCR – Real-time PCR, ISH – In-situ hybridization, p16 – p16 Immunohistochemistry, SAb – Serum antibodies

Where multiple outcome measures have been utilised, the first quoted outcome measure has been used for HPV-positive/-negative disease survival

Specificity

There is a high degree of anatomical specificity seen in HPV-positive tumours. As previously stated, HPV-positive OPC is site-specific to the base of tongue and tonsils, although HPV is also detectable in a smaller proportion of oral carcinomas^{66, 137}. In-situ hybridization studies have further helped to demonstrate the specificity of HPV distribution to the nuclei of carcinoma cells, with absence of staining within the surrounding stroma/ invaded tissue.

p16 staining, a surrogate marker of HPV infection, is now an accepted method of determining a likely oropharyngeal primary in patients presenting with nodal disease from an occult source, due to its specificity to HPV-positive OPC.

A further marker of specificity is the viral type found in HPV-positive OPC. HPV 16 (a high risk HPV heavily implicated with cervical carcinoma) has consistently been found to be the predominant type detected (around 90% of HPV-positive tumours)^{56, 57, 81, 138}.

Temporality

The temporal sequence of events in proposed HPV-related carcinogenesis is supportive of a causal relationship (i.e. HPV infection as a result of sexual exposure will precede clinical carcinoma by several decades). Temporality is also supported through the findings that an earlier age of sexual debut and cumulative number of sexual/oral sexual partners increases HPV-positive OPC risk.

It should be noted, however, that some studies citing these relationships have detected positive markers of HPV infection within known tumours and then correlated HPV status to sexual history⁵⁹. This in isolation is not synonymous with evidence for HPV increasing risk of tumourigenesis; that is, it would be possible that previous HPV exposure could result in sub-clinical carriage in the oropharyngeal region, which, in the presence of phenotypically aberrant epithelium (i.e. tumour) leads to localised HPV invasion. However, further evidence through case-control study of OPC demonstrates that there is a statistically significant difference in sexual history for *all* cases of OPC when compared to a control group⁶²; this shows a specific increase in cancer risk associated with sexual behaviour rather than simple correlation of tumour-laden virus to sexual history.

Biological Gradient

There is little data available to support a clear dose-response relationship between HPV and OPC. Determining an appropriate objective measure of “dose” is more difficult than may be assumed in the first instance. For example, studies demonstrating the increased risk of OPC linked to number of oral/vaginal sexual partners present some evidence of a dose-dependent relationship (i.e. higher numbers of partners increases OPC risk), but utilise what is essentially a surrogate and non-specific marker of a sexually transmitted factor that may or may not be HPV. Furthermore, by utilising sexual history alone, there is no true quantitative measure of HPV “dose” – higher numbers of partners would increase the risk of exposure to HPV rather than influence the viral load within an individual.

Quantitative analysis of virus within tumour is difficult, as many methods of assessing for HPV involvement are dichotomous – for example PCR demonstrates presence or absence of viral DNA, in-situ hybridization assesses presence or absence of hybridization signals within tumour cell nuclei and p16 immunohistochemistry is ultimately interpreted as either positive or negative. Real time PCR is perhaps the only established method of quantitative analysis of viral load, although it has been found to have only 92% sensitivity in a small study assessing the reliability of HPV-positive OPC detection methods¹³⁸.

The sample to be assessed adds further complication, as viral load needs to be measured prior to tumour formation to demonstrate dose-response. Due to the relatively rare event of OPC formation, it may be concluded that assessing precursor lesions such as dysplasia may

be the most appropriate method, so as to isolate a population within which malignant transformation is more likely, and also allowing access to relevant tissue samples for viral quantification. However, even with a higher risk group such as dysplasia, one must bear in mind that not all dysplasia progresses to carcinoma, and in addition HPV-positive OPC accounts for only a proportion of OPCs – this, in combination with any therapeutic measures applied to dysplastic lesions, would lead to a high data set being required for dose-response to be demonstrable.

Plausibility

There is a highly plausible mechanism through which HPV infection can lead to carcinogenesis – this is discussed later. Molecular studies have corroborated a significant proportion of what is thought to be the early events in a multi-stage process¹³⁹. It is generally accepted that HPV infection is not capable of causing malignant transformation in isolation, but rather eliminates the need to acquire genetic mutations in two tumour suppressor genes important for the progression of head and neck carcinogenesis, namely p53 and pRb, and in addition sends the cell into unrestrained turnover whereby the acquisition of further mutations is more likely.

Coherence

There has been a recent increase in incidence of OPC in subsites linked to HPV positivity (i.e. tonsils and tongue base), whereas this trend has not been seen in other head and neck sites^{12, 140-142}. This rise in tonsillar and tongue base OPC has been coupled with an increase in the proportion of tumours identified as HPV-positive, demonstrating a level of coherence between the two variables¹⁴³. The rise is thought to be linked to changes in sexual behaviours subsequent to the 1960s, such as increased premarital sex and oral sex^{12, 140, 144, 145}.

Experiment

Due to the latent period between HPV inoculation and onset of OPC, any beneficial effect of preventive measures such as HPV vaccination on OPC incidence would take a significant

period of time to demonstrate. In addition to this, current estimates of cost-benefit preclude the introduction of a population-based male HPV vaccine, even with the assumption of high efficacy at preventing oral HPV infection and subsequent carcinogenesis^{146, 147}. However, cost-utility analyses have historically underestimated the contribution of HPV to carcinomas in males; more recent work also suggests that vaccination is cost-effective for men who have sex with men, and Australian vaccination programmes have now introduced male HPV vaccination¹⁴⁸⁻¹⁵⁰. It is therefore possible that future data may be available to demonstrate that HPV vaccination reduces OPC incidence in males.

Current proof of causality through preventive experiment is difficult due to the widespread limitation of vaccination programmes to females, although the effects of herd immunity as a consequence of female HPV immunisation may indeed be demonstrable. Assuming oral exposure to HPV in cervical secretions is the major source of inoculation in the male oropharynx, highly efficacious vaccination of females should theoretically reduce male exposure to HPV, with a demonstrable effect on OPC incidence in the future.

Therapeutic trials may go some way to provide experimental evidence for HPV as a causative agent. Improved outcome of OPC as a result of HPV-targeted therapy would infer causation, although one would have to consider the possibility of an idiosyncratic response.

Analogy

There are many similarities between HPV-positive OPC and cervical carcinoma. Comparable mucosal structure, the potential for sexual exposure, along with the HPV types associated with risk, makes both sites highly analogous. There is also recognition of distinct lesions that precede carcinoma formation by many years in both oropharyngeal and cervical tissues, within which HPV has been detected⁶⁶– lending to a common concept of a multistage process of carcinogenesis which may be initiated but not entirely achieved through the actions of HPV.

3. Epidemiology of OPC

OPC in the UK

CRUK's summary statistics for UK cancers, taken from data provided by the Office of National Statistics, ISD Scotland, Welsh Cancer Intelligence and Surveillance Unit and Northern Ireland Cancer Registry, currently groups OPC under the umbrella term of "oral cancer"¹⁵¹. The rationale for CRUK's grouping of oral/oropharyngeal/pharyngeal tumours relates to a large proportion of cases failing to have a specific site recorded in the cancer registry data. Although the summary utilises a definition of oral cancer disparate to that used in direct clinical context, CRUK's statistics offer a comprehensive review of UK-specific data, and also contextualises the proportion of oral/pharyngeal tumours attributable to OPC. OPC was found to account for 38% of male, and 24.9% of female tumours occurring in this region¹⁵¹. Conway *et al* reviewed 12 UK cancer registries from 1990-1999, finding an average annual rise in oral/oropharyngeal cancer incidence of approximately 3%¹⁵². Louie *et al* found a marginally higher annual rise of 3.7% in an English population from 1995-2011, and predicted a further 45% increase by 2025¹⁵³. UK oral and oropharyngeal incidence rates are currently estimated at around 11:100,000 people yr⁻¹ ¹⁵⁴, and account for 2% of all new cancers¹⁵¹.

Prevalence of HPV within Oropharyngeal Tumours

The reported prevalence of HPV in head and neck cancer varies considerably, with findings of 0-100% of all head and neck tumours testing positive⁵⁶. Several variables influence the proportion of tumour specimens testing positive for HPV, notably anatomical sub-site, method used to detect HPV, study date and geographic location.

As discussed above, HPV has carcinogenic site specificity, with a predilection for causing tonsillar and base of tongue tumours. Despite this, the reported prevalence of HPV-positive OPC still varies widely (11-100%)^{155, 156}. A systematic review conducted in 2005 found overall HPV prevalence to be 35.6%, with a 95% confidence interval of 32.6-38.7%⁵⁶. Data analysed suggested a higher prevalence in North America and Asia (47.0% and 46.3%,

respectively), and a lower prevalence in Europe (28.2%). More recent UK data suggest prevalence has now risen to around 45-57%¹⁵⁷.

HPV-positive OPC is felt by many authors to be on the increase, accounting for the 0.5%-4% per year rise in incidence rate of OPC seen over recent years^{5, 12, 100, 140, 141, 143, 154, 158}. Conversely, there has been a general decrease in incidence of head and neck cancers at sites other than oropharynx, largely attributed to changing trends in tobacco smoking⁵. These temporal changes will undoubtedly have an effect on the proportion of OPC specimens testing HPV-positive. Indeed, Nasman *et al* have found such a change in tonsillar specimens collected from 1970-2007, with a rise in HPV prevalence from 23% of tumour specimens taken between 1970-1979, to 79% of specimens taken between 2000-2007¹⁴³.

Incidence of HPV-Positive OPC

There is difficulty in directly assessing the incidence of HPV-positive OPC due to the absence of a reliable and rapidly applied test, compounded by the relatively rare event of OPC formation. However, it is possible to extrapolate data available from cancer registries with respect to overall oral/OPC incidence, taking into account the likely percentage of tumours attributable to HPV. US and UK age-adjusted rates of oral/OPC are 1.87:100,000 and 11:100,000 respectively¹⁵⁴. Using the European prevalence of HPV as determined by Kreimer *et al*'s systematic review, in addition to CRUK statistics on the proportion of oropharyngeal carcinomas contributing to tumours of the oral/pharyngeal region, the age-adjusted rate of HPV-positive OPC can be estimated at 1.2:100,000 people yr⁻¹ in the UK^{56, 151}.

Age, Sex, Risk Factors and Ethnicity

HPV-positive OPC has been generally found to occur in a younger cohort than HPV negative OPC^{65, 72, 84, 89, 107, 159, 160}, although this relationship has not been shown by some authors^{106, 161}. In those studies demonstrating an age difference, patients are around 3-5 years younger than HPV negative cases¹⁴⁰. As with HPV negative OPC, a significant male predominance is seen^{65, 72, 162}.

Risk factors appear to be significantly different for HPV-positive OPC. Many studies have shown that patients with HPV-positive tumours are less likely to smoke when compared to their HPV negative counterparts^{65, 72, 107}, although not all studies have found this relationship⁸⁴. Alcohol exposure is also thought to be less in this group^{72, 160}, although this finding is not as statistically significant or as consistently demonstrated as for smoking^{84 107, 159}.

Sexual exposure is the major risk factor for HPV-positive OPC. Risk from oral sexual exposure has a reported odds ratio of between 1.6-3.9 for developing HPV-positive OPC^{59, 62, 63, 65}. Higher numbers of vaginal sexual partners is also implicated, with a history of over 6 lifetime vaginal sex partners being of increased risk (odds ratio 2.7-6.4)^{62, 63, 65}. Less than 6 lifetime vaginal sex partners has only been implicated in some studies⁶⁵. History of oral-anal contact is associated with marked risk (adjusted odds ratio 19.5)⁵⁹.

A number of US studies have found a significant difference in the proportion of HPV-positive OPCs demonstrated in White and African-American patients^{160, 163, 164}. A greater percentage of HPV-negative tumours helps to account for the reduced prognosis of OPC seen in African-Americans when compared to Whites^{165, 166}. Overall survival of HPV-positive and negative OPC appears comparable for both ethnic groups, further supporting the notion that HPV is the responsible variable for the differences seen¹⁶³. It is thought that differences in oral sexual behaviour may account for this disparity⁶¹.

4. Mechanism of Carcinogenesis

As alluded to above, viral oncogenes E6 and E7 are known to have a critical role in HPV-related carcinogenesis. The major effect of E6/7 is a functional blockade of tumour suppressor genes encoding p53 and pRb; this is in stark contrast to HPV negative OPC, whereby genetic aberration must occur to result in loss of p53/pRb expression. Such losses of heterozygosity are acquired as a result of exposure to chemical carcinogens, principally as a result of tobacco smoking and alcohol intake¹⁶⁷.

Sporadic (HPV-negative) head and neck carcinogenesis is accepted as a multistage process, with clearly identified precursor lesions. Cumulative chromosomal loss and proto-oncogene mutations are thought to occur through the phenotypic stages from hyperplasia to dysplasia, carcinoma *in situ* and then invasive carcinoma¹⁶⁸ (Figure 0.3). TP53 (i.e. the gene encoding p53) aberration occurs early at chromosome 17p13, as does p16 (encoded on chromosome 9p21)^{168, 169}. Loss of heterozygosity at chromosome region 3p21 is also an early event that involves loss of tumour suppressor function mapped to that locus¹⁶⁹. Chromosome 3p has been shown to contain at least three distinct regions that represent tumour suppressor loci, all of which can be affected during carcinogenesis¹⁷⁰. Latter events include alterations of chromosome regions 11q13, encoding Cyclin D1 (a proto-oncogene), and 13q (housing Retinoblastoma)^{168, 171}. A characteristic feature of events seen in non-HPV related carcinogenesis is the loss of whole or large portions of chromosomal arms that result in gross deletions inclusive of the aforementioned regions.

Figure 0.3: Genomic events seen in the multistep process of head and neck cancer formation

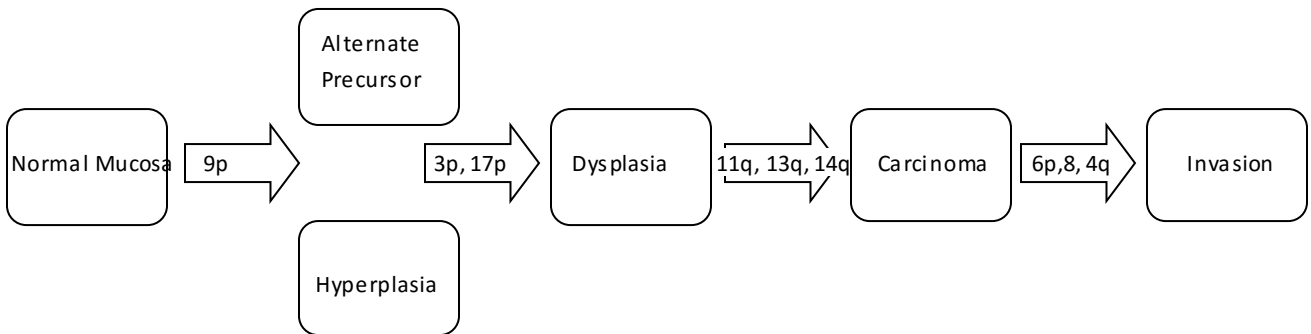


Figure 0.3: A summary of the genomic events associated with carcinogenesis in the head and neck region, adapted from Califano *et al*⁶⁸. Rectangles represent clinico-histopathologically classifiable lesions, arrows denote genomic aberrations (principally losses of heterozygosity) that are linked to progression into the next clinically discernible stage. It should be noted that Califano’s original model made careful reference to the fact that it is the accumulation of genetic aberrations and not the order of acquisition that is important to cancer progression; arrows illustrate the point at which the frequency of each aberration plateaus in a cohort of lesions. Although no recognised precursor lesion exists in the case of HPV-related oropharyngeal carcinoma, the model proposes either hyperplasia or an alternative precursor lesion precedes clinical dysplasia.

Califano’s analysis of areas of apparently benign mucosa adjacent to premalignant lesions suggested that early genetic events are shared by cells in the anatomical region, inferring a common clonal ancestor. This feature supports the concept of field cancerisation. Chromosome 9p encodes the tumour suppressor protein p16; loss of heterozygosity may therefore be linked to reduced binding of E2F (please refer to Figure 0.2 for a summary of p16’s regulatory function of E2F), allowing promotion of cell turnover leading to hyperplasia. Loss of p53 (located on chromosome 17p) may permit the transition from hyperplasia into dysplasia, with subsequent genomic aberrations progressing unchecked. The subsequent aberrations may be illustrated by the progressive haphazard cellular arrangements and visible cellular atypia observed in dysplasia as lesions progress from “mild” through to “severe”. Additional allelic losses may mark the transition from dysplasia to carcinoma, with further aberrations linked to regulators of E2F – Retinoblastoma protein (an E2F-binder) and cyclin D1 (a controller of CDKs 4&6, which in turn regulate Retinoblastoma binding to E2F) are encoded within chromosomes 11q and 13q; loss may therefore exaggerate the derangements in cell turnover, in addition to further accrual of derangements that select for an invasive phenotype.

Conversely, HPV-related carcinogenesis involves much fewer genetic events, as demonstrated in microsatellite analysis of HPV-positive OPC in comparison to HPV negative OPC¹⁶⁹. Genetic aberrations are also more conservative in comparison to the gross deletions seen in HPV negative OPC. Deletions of 17p, 9p and 13q are unnecessary due to the actions of viral oncogenes E6 and E7, which is reflected by infrequent allelic loss in these regions¹⁶⁹. Chromosome 3p aberrations are also rare in HPV-positive OPC (whereas common in HPV negative OPC) – this is not easily explained through the classical functions of E6 and E7, although it has been hypothesised that there may be further inhibitory effects of HPV proteins on the tumour suppressor proteins encoded in this region, which would account for the lack of aberrations seen¹⁶⁹.

If there is indeed a viral mechanism of inhibiting the tumour suppressor proteins encoded by chromosome 3p, all important mutational events seen in the carcinogenesis model proposed by Califano *et al* are bypassed to the stage of dysplasia (Figure LR3). In cervical carcinoma models, expression of E6 and E7 is considered as necessary but not independently sufficient to achieve cell immortalisation without further genetic events^{15, 172}. The features of HPV related carcinogenesis described above would suggest that this is also true in the case of OPC, with virally infected cells requiring subsequent genetic events to progress beyond dysplasia.

The loss of p53 and pRb activity promotes the acquisition of such aberrations, as cellular proliferation is allowed to proceed unchecked. High risk HPV E7 causes further instability by inducing centromere over-duplication during cell division, an effect independent of its actions on pRb²⁰. Accumulation of relatively small chromosomal changes (in both size and number when compared to the large deletions seen in non-HPV OPC) may ultimately lead to phenotype change from dysplasia through carcinoma in situ, to invasive carcinoma.

Viral integration into host chromosomes has been implicated with carcinogenesis, particularly in cervical cancer¹⁴. It is considered that the major effect of integration is through the loss of E2, which subsequently leads to E6 and E7 expression as discussed earlier. Viral integration does not normally occur in benign HPV lesions; HPV is usually episomal and in low copy number^{20, 173}. As keratinocytes terminally differentiate during their progress through the more superficial epithelial layers, E2 expression is switched off; this allows for florid viral replication and release²⁰. By restricting replication within the basal layer, viral immunogenicity is kept to a minimum, avoiding a host response¹⁷³. This also has the host

advantage of avoiding potentially mutagenic cellular turnover through the actions of E6 and E7; integration of virus bypasses this protective effect.

Although the change in viral proteins triggered by chromosomal integration is adequate to account for HPV's carcinogenic potential, it is unclear as to whether this is the sole mechanism by which the virus has its effect. The role of insertional mutagenesis at viral integration sites may also be of importance, although this is of contention. A systematic review of genomic integration sites of HPV in cervical dysplasia and invasive cancer showed a random distribution of viral integration over the whole genome, albeit with a strong predilection for common fragile sites¹⁷⁴. A study included in the systematic review corroborated this specifically for HPV16, the viral type most heavily implicated with OPC¹⁷⁵. However, subsequent studies have concluded that although there is indeed a spread seen throughout the genome, integration occurred commonly around cytogenetic bands 4q13.3, 8q24.21, 13q22.1 and 17q21 (23% of integrations detected)^{176, 177}. Of particular note is 8q24.21, as integrations in this region were found to be 1-860kb upstream of the MYC gene – a gene commonly dysregulated in cancer¹⁷⁶. Furthermore, in vitro study of genital tumour-derived cell lines have shown MYC overexpression to only occur in cell lines that contain integrated viral DNA at the 8q24 region¹⁷⁸. Whether these findings are reliable, and if so, whether they translate to OPC is yet to be determined. Relatively little data is available from the direct study of HPV related head and neck cancer, although it appears that integration at common fragile sites is also likely in these tumours^{179, 180}.

In addition to bypassing need for losses of heterozygosity through the activity of viral oncoproteins, virus-related epigenetic aberrations also occur. A key function of HPV E6 oncoprotein appears to be activation of the hTERT promoter¹⁸¹, leading to activation of the telomerase complex¹⁸². Capacity of E6 to activate telomerase via increased expression of hTERT appears to be one of the defining features of virally-induced immortalisation; this telomerase activity is regarded as independent of E6's effect on p53, and moreover has been documented as a crucial process in combination with p16 abrogation for immortalisation¹⁸³. This view is not shared by all authors, however – McMurray *et al* found that keratinocyte transfection with a combination of wild-type E7 plus a mutant form of E6 capable of inducing telomerase but incapable of inducing p53 degradation, did not induce immortalisation, whereas mutant E6 capable of inducing p53 degradation without telomerase function retained capacity to induce immortalisation. The authors concluded that p53 degradation was therefore the necessary process via which E6 induces immortalisation

when in combination with E7. There are however some limitations of McMurray's work; telomerase-inducing-but-p53-retaining E6 clones demonstrated an extended lifespan compared to control (53 population doublings versus 28 for control), and measurements to confirm cell crisis leading to mortality was difficult; p16 elevation, a usual marker of cell crisis was appropriately deemed irrelevant due to the effects of E7, and the authors therefore assessed accumulation of p21^{CIP1} – a product of p53 activity. Whilst this may be a reasonable marker of cell crisis, a caveat is that results may by definition be confounded by those lines expressing E6 capable of degrading p53; cell crisis may not necessarily be ascertained using this marker in the presence of wild-type or p53-degrading E6. A final comment regarding McMurray's findings also lies in the fact that *in vivo*, wild-type E6 oncoprotein will exert an effect on both telomerase and p53 simultaneously; concomitant lack of p53 activity may support E6's telomerase-inducing effects.

Irrespective of the absolute nature of virally-induced immortalisation, increased telomerase activity has been identified as being linked to an increased risk of progression of cervical premalignant lesions¹⁸⁴. Moreover, telomerase activity has been found to be stringently repressed in mortal tissue and reactivated in approximately 90% of cancers¹⁸⁵. The telomerase-inducing activity of the E6 protein is therefore a clinically significant parameter which may contribute to the process of carcinogenesis.

5. Accounting for Prognosis

The favourable prognosis of HPV-positive OPC is well documented (Table 0.2). It was initially thought that the improvement seen in outcome was a function of increased tumour radiosensitivity. Although HPV-positive OPCs are indeed more responsive to radiotherapy, the improved outcome of these tumours appears to also be translated to surgery^{89, 104}. A more comprehensive effect of viral carcinogenesis must therefore be responsible for tumour behaviour. The contemporary view is that the improved prognosis of HPV-positive cancers is largely accounted for by the lack of genetic aberration seen in tumour tissue¹⁶⁹; persistence of wild-type TP53 and RB1 genes is thought to underpin the altered behaviour in response to therapy. It has been proposed that the cellular insult sustained as a result of radiotherapy may send the cell beyond a critical threshold necessary to overcome the effects of viral oncogenes, allowing p53 expression to become re-established¹⁸⁶. Indeed, use of siRNA to TP53 in E6/E7 expressing lines led to increased radioresistance¹⁸⁷.

Despite the generic effects of viral infection on treatment success, modality-specific effects have also been noted. Gubanova *et al* recently demonstrated the downregulation of SMG-1, a potential tumour suppressor protein, in a small cohort of patients with HPV-positive OPC. This downregulation also occurred in both normal keratinocytes and HPV-negative cell lines in response to E6/E7 transfection as a consequence of SMG-1 promoter hypermethylation. Gubanova went on to demonstrate that experimentally downregulating SMG-1 in HPV-negative cell lines led to increased radiosensitivity, whereas upregulating SMG-1 in HPV-positive cells decreased sensitivity¹⁸⁸. SMG-1 is a Phosphatidylinositol 3-kinase-related kinase (PIKK), and one of many regulators of the DNA damage response (DDR). It is itself activated in response to ionising radiation¹⁸⁹. In the absence of SMG-1, the accumulation of irreparable DNA double strand breaks triggers apoptosis; HPV-positive tumour depletion of SMG-1 may therefore account for a significant proportion of its radiosensitivity.

Tumour repopulation after radiotherapy also appears compromised in HPV-positive disease¹⁸⁶. Signalling cascades which drive surviving tumour cells to proliferate may be an important aspect of radioresistance. Conflicting reports exist as to the degree of EGFR signalling in HPV-positive versus HPV-negative head and neck cancer, although experimental data suggest that Akt (downstream of EGFR signalling) is less active in HPV-positive disease^{186, 190}.

Immunomodulation may also play an important role in the HPV-positive tumour response to therapy; it has been proposed that radiotherapy may cause an increased immune response through many potential pathways. These pathways include increased antigen presentation as a result of uptake of necrotic, viral-loaded cells; improved penetrance of immune cells into tumour as a result of reduced cellular adhesion post-radiotherapy; upregulation of MHC class I; and induction of pro-inflammatory cytokines such as TNF, which may act to reverse viral tolerance¹⁹¹. Alterations in viral antigenicity as a response to therapy may also explain improvements in outcome seen in the surgical management of HPV-positive OPC. Local inflammatory response to the trauma of tissue excision, in addition to the release of cellular contents at incomplete surgical margins may very well influence immunity in a similar way.

One must also consider the potential for a phenotypically less aggressive tumour, which by virtue is more responsive to treatment, irrespective of the therapeutic modality chosen. Lack of field cancerization is well recognised in HPV-positive tumours, and may contribute in part to the improved outcome seen¹⁹². The true cause of survival benefit will have implications on providing targeted treatment for HPV-positive OPC, as HPV infection may ultimately be a non-manipulable prognostic factor.

Ang *et al* identified a reduction in the prognostic benefit of a HPV-positive status when associated with OPCs occurring in smokers; Ang *et al* proposed an “intermediate” group, where prognosis lay in between that of non-smoker HPV-positive disease and that of HPV-negative disease in heavy smokers¹⁰⁵. The underlying mechanism through which outcome is reduced in this intermediate group is unclear – again, this may represent a change in cellular process triggered in response to smoking which is subject to targeted therapy, or alternatively may represent more general accrual of genetic aberrations which cannot be targeted with a standardised approach but may offer opportunity for the development of stratified medicine in the management of HPV-negative disease.

6. Methods of HPV Detection

There is currently no accepted standard test for the detection of HPV in OPC specimens¹⁹³. No single method is available that can be applied to both frozen and formalin-fixed paraffin-embedded (FFPE) specimens, that is also 100% sensitive and specific. Proxy measures of HPV infection, such as serum analysis of antibodies to E6, E7 and L1, are poorly specific due to the potential for HPV infection at other sites¹³. No other systemic markers of HPV infection exist, as there is no blood-borne phase of HPV infection⁵¹.

Reverse transcriptase polymerase chain reaction (PCR) amplification of viral E6/E7 mRNA is now considered as “gold standard” for the detection of clinically significant HPV infection within tumour specimens^{100, 194}. However, the method is only reliable when applied to fresh frozen specimens, with an estimated 50% reduction in sensitivity when applied to FFPE samples¹⁹⁵. This reduction in sensitivity is related to RNA instability in specimens which have not been fresh frozen¹⁹⁶.

PCR amplification of viral DNA is a highly sensitive method of HPV detection, and can be applied to either a single HPV type by amplification of a sequence specific to that type, or can be used less specifically to assess presence of multiple HPV types by use of a consensus primer¹⁹⁵. Despite this, there are significant limitations of the method due to its inability to distinguish clinically relevant HPV infection. Presence of latent virus leads to false positive results due to the ability of PCR to detect just a few copies of HPV DNA per cell¹³⁸. Attempts have been made to resolve this issue through use of real-time PCR, which provides a quantitative analysis of viral load. However, a criticism of this method is that it still provides no direct evidence of viral integration or oncogene expression. Furthermore, sensitivity is estimated at 92% and specificity 97% when using a cut-off viral load of >0.5 copies per cell; false positives and false negatives therefore still exist¹³⁸. Increasing the cut-off for viral load improves the specificity of this method, but at the expense of further reductions in sensitivity.

DNA in-situ hybridization (DNA-ISH) is felt to overcome some of the limitations of PCR in detecting only clinically relevant infection. Nuclear hybridization signals can be visually inspected for punctuate or diffuse staining, representing integrated and episomal viral DNA respectively^{197, 198}. Presence of a punctate hybridization signal, either alone or in

combination with diffuse nuclear signals, therefore reflects clinically relevant HPV infection. Although specificity of this method is high (100%), sensitivity is not ideal (83%)¹³⁸. It has been estimated that around 10 copies of virus per cell must be present in order for DNA-ISH to detect HPV, although newer ISH kits are thought to be more sensitive¹⁹⁵.

p16 immunohistochemistry (IHC) has become an established surrogate marker of HPV infection and has been used in studies to determine HPV-positive OPC. The method identifies clinically relevant infection, as p16 overexpression is in response to the loss of bound pRb (Figure 0.2b), which in turn implies active transcription of viral oncogene E7. However, there appears to be a number of HPV negative tumours that also overexpress p16, leading to false positives¹⁹⁵. Although sensitivity is quoted as high (100%)^{138, 195}, Weinberger *et al.* have reported a subset of HPV-positive tumours which do not overexpress p16; this would infer a sensitivity of less than 100%¹⁹⁹. However, Weinberger used real time PCR as conclusive evidence of HPV infection, with a lower cut-off of 1 viral copy per 10 cell genomes' worth of DNA⁹⁰. Given the specificity of 97% for a lower cut-off of 0.5 copies per cell, Weinberger's work would almost certainly include a number of false positives. The existence of true HPV-positive tumours that do not overexpress p16 is therefore contentious, as it may be such false positives that are p16 negative. However, Wiest *et al* also noted HPV E6/E7 positive, p16 negative tumours, albeit with a lower prevalence than that seen by Weinberger *et al* (14% versus 37%)²⁰⁰. Those tumours of multifactorial aetiology (that is, HPV-positive tumours arising in smoker/drinkers) would indeed appear to offer a route through which the p16 axis can be abrogated through mutagenesis whilst otherwise maintaining DNA/mRNA features of viral infection. Irrespective of the existence of a non-p16 overexpressing subset of HPV-positive tumours, p16 IHC is not an ideal test in isolation due to its low specificity (79%)^{138, 195}, in addition to variability in defining what constitutes a positive test²⁰¹. A number of authors have suggested criteria for a p16 IHC H-scoring system, although proposals have not been in full agreement. Jordan *et al* proposed a system of multiplying semi-quantitative IHC intensity staining score by percentage of tumour positivity in order to achieve a final H-score, with ROC analysis against HPV16E6/E7 gold standard – leading to a proposed cut-off of 60 on a scale of 0-300, yielding a sensitivity of 91.6% and specificity of 90.4%²⁰². El Naggari & Westra on the contrary have advised a more generic definition until a consensus view is agreed, limiting their definition to “strong and uniform” p16 staining and recommending additional HPV testing for weak/negative p16 staining tumours²⁰³. A number of recent articles have utilised a definition of 70% or more tumour staining strongly positive²⁰⁴⁻²⁰⁶; indeed, a systematic review correlating human

papillomavirus and p16 status also advocated a 70% cut-off²⁰¹. Although this cut-off may infer greatest correlation between p16 IHC and other HPV-specific tests, this is not necessarily synonymous with the clinically most valuable point at which to ascribe positivity.

In the absence of a single, ideal method of HPV detection, some authors have applied a combination of tests to improve reliability. Smeets *et al* recommended p16 immunostaining, followed by GP5+/6+ PCR (general primer consensus PCR) in those samples p16 positive¹³⁸. Their rationale for using this method was based on data suggesting 100% sensitivity and specificity when compared to an E6 mRNA gold standard. However, it should be noted that there were independently several false positives for both p16 IHC and GP5+/6+ PCR, and the size of the study (48 samples) makes interpretation difficult, as the absence of simultaneous false positive results for p16/general primer analysis may have occurred by chance. Smeets *et al* acknowledged this, and calculated a likely 2% chance of concurrent false positives when using the technique.

The combination of two tests considered 100% sensitive should improve specificity with no detriment to sensitivity and is therefore commendable. As discussed above, p16 IHC is not necessarily 100% sensitive and one must therefore consider the potential for false negatives in using this technique. Despite this, p16 IHC is perhaps the most appropriate marker to use in combination with another test, as it assesses a very different parameter to other available techniques. HPV16 PCR, GP5+/6+ PCR and in-situ hybridization all assess for presence of viral DNA; combining such tests is therefore of questionable value.

Determining the most appropriate DNA-based method to compliment p16 immunostaining should take into account the relative merits of each available test. For PCR, the use of consensus primers such as GP5+/6+ has an advantage over HPV16-specific primers in that any tumours attributable to HPV types other than HPV16 will also be detected as positive. The disadvantage of GP5+/6+ is the reduction in specificity in comparison to HPV 16 PCR, due to false positive results that would occur from the other viral types. DNA-ISH is a highly (100%) specific test, and combining p16 IHC with this test therefore has no benefit.

It therefore follows that many authors have adopted a PCR-based technique in combination with p16 IHC to identify HPV-positive tumours. Whilst E6/E7 mRNA detection remains the gold standard, its limitations with FFPE specimens have thus far precluded the technique from becoming universally adopted. DNA-ISH also has its advantages due to a high

specificity, and is therefore an appropriate test for research in which sensitivity is not of paramount concern.

RNA-ISH is a recent advancement which allows detection of transcriptionally active HPV infection and offers (in combination with p16-IHC) the most accurate prognostication of patient outcome to date²⁰⁷. E6/E7 mRNA hybridization is achieved using a number of “Z” stranded DNA probes complimentary to the target mRNA sequence. Once aligned, two adjacent “Z” strands can be subjected to a sequential chromogenic amplification reaction. This process circumvents the inherent difficulties with RNA instability in FFPE specimens. Schache *et al* found RNAScope RNA-ISH to have a sensitivity and specificity of 97% and 93%, respectively¹⁹⁶. Schache also found that all RNAScope RNA-ISH false negatives and false positives were similarly misclassified using p16 IHC, when compared to the E6/E7 mRNA qPCR standard¹⁹⁶. These findings may suggest there is no additional benefit of undertaking p16 IHC in conjunction with RNA-ISH, although the relatively small data set in Schache’s study (n=79) precludes any definitive judgement in this respect.

HPV Typing

The HPV detection techniques described above are generally incapable of discerning HPV type. Type specificity is often sacrificed in order to achieve a single test capable of determining tumour HPV status through the use of consensus probes capable of flagging a number of high-risk HPV types. It is possible to achieve specific HPV typing by use of multiple type-specific, rather than pooled probes. Alternative methods of typing include the use of western blot or through use of newer techniques such as INNO LiPA HPV genotyping or next generation sequencing²⁰⁸.

Studies into cervical carcinoma suggest HPV 18 infection imparts a poorer prognosis than even sporadic cancers, whereas HPV 16 infection is associated with a highly favourable prognosis²⁰⁹⁻²¹¹. HPV typing therefore has direct clinical implications in the management of cervical carcinoma. However, due to the almost exclusive role of HPV16 in OPC, the prognostic influence of HPV 18 remains less clear in head and neck disease, although recent work suggests HPV types other than 16 carry less survival benefit²¹².

7. Management of HPV-Positive Disease

Current oropharyngeal cancer chemo-radiotherapy regimens have been established through the addition of concurrent chemotherapy to radical radiotherapy prior to any appreciation of the existence of a HPV-related subset²¹³. Whilst this has improved the overall survival of non-surgically managed oropharyngeal carcinoma per se²¹⁴, it remains unclear whether current standard therapy is necessary to treat HPV-positive disease successfully; there is at present no high-quality evidence to either support or refute the de-escalation of therapy in HPV-positive disease²¹⁵. As previously discussed, HPV-positive oropharyngeal carcinomas are extremely radiosensitive²¹⁶, calling the role of concomitant systemic treatment into question. Proposals for de-escalation of therapy have been met with reservation within the head and neck oncology community, due to the potential for a worsened outcome should withdrawn therapy in fact prove beneficial. Despite this, it is accepted that there is an urgent need for evaluation of de-escalated therapy through clinical research²¹⁷. It is essential to research potential withdrawal of treatment through either successive prospective randomised trials, or to retrospectively assess clinical outcome of HPV-positive disease prior to and after the introduction of therapeutic escalation.

Two large clinical trials are currently underway to address the feasibility of therapeutic de-escalation in HPV-positive disease; RTOG 1016 and DeESCALaTE-HPV^{218, 219}. Both studies aim to compare standard cisplatin-based chemotherapeutic regimens against cetuximab, an EGFR inhibitor. Although not specified, the approach of each trial appears consistent with non-inferiority assessment of cetuximab when analysing overall survival rates. A criticism of this approach relates to the assumption of definite benefit from current chemotherapeutic strategies in HPV-positive disease; cisplatin-based treatment is therefore defined as a “positive” control against which to demonstrate cetuximab’s non-inferiority. Should chemotherapy in fact provide no additional benefit over radiotherapy alone in HPV-positive disease, both trials actually compare two unnecessary treatments, and vindication of cetuximab’s use in HPV-positive disease will ensue on the grounds of lower toxicity in comparison to cisplatin – irrespective of any true effect of this expensive drug²²⁰⁻²²². Indeed, there is some evidence that in the case of T1-3 HPV-positive tumours with N0-2c nodal status, chemotherapy may be of little benefit²²³. Fortunately, both RTOG 1016 and DeESCALaTE have exclusion criteria of all T0-2 N0 carcinomas; this may reduce the potential confounding population of tumours to those of T3 N0 status.

8. Management of HPV-Negative Disease

Blanchard *et al* recently published an updated meta-analysis of the efficacy of chemotherapy as additional treatment in head and neck cancer²²⁴. Preceding meta-analyses by Pignon *et al*, as part of the same “meta-analysis of chemotherapy in head and neck cancer” (MACH-NC) collaborative group found “only a small significant survival benefit in favour of chemotherapy” when compared to radiotherapy alone, corresponding to an absolute survival benefit of 4% over 2-5 years²²⁵. Pignon *et al* failed to recommend chemotherapy for routine use on this basis. Interestingly, a further updated MACH-NC meta-analysis published in 2009 found a more appreciable 6.5% absolute survival advantage of additional chemotherapy²²⁶. Blanchard’s most recent update included analysis of benefit to specific anatomical sub-sites, confirming a 5 year absolute survival benefit of 8.1% in oropharyngeal carcinoma. The period reviewed by the 2011 study was from 1965-2000, inferring that the majority of carcinomas within the oropharyngeal sub-group were HPV-negative. Brotherston *et al* recently published data to show that 69% of oropharyngeal carcinoma patients considered a survival benefit of 5% or less as reason to switch from radiotherapy alone to chemoradiotherapy; the data from MACH-NC’s reviews therefore provide evidence for both a clinically and statistically significant increase in survival rates with chemoradiotherapeutic regimens²²⁷.

On the basis of MACH-NC’s analyses, platinum-based chemoradiotherapy remains treatment as standard for the management of oropharyngeal carcinoma in the UK. A number of alternative therapeutic approaches are available including transoral laser microsurgery (TLM) & transoral robotic surgery (TORS), although no studies directly comparing surgery to chemoradiotherapy in a randomised fashion have been undertaken²²⁸. The ORATOR trial may offer preliminary evidence of TORS efficacy, although primary outcome measures are quality of life, with overall survival and progression-free survival being limited to secondary outcome measures²²⁹. Surgery is generally limited to stage I and II disease²³⁰, and is reliant on access to both specialist surgical equipment and highly skilled operators. Some operators reserve this approach to HPV-positive disease, driven by calls to de-escalate management in order to reduce post-therapeutic sequelae²³¹, although others have presented data to suggest that oncological outcomes are not sacrificed regardless of HPV status²³².

It remains beyond the scope of this thesis to discuss the intricacies of current therapy beyond that outlined above, other than to make passing reference to the vast combinations of modified chemotherapeutic and radiotherapeutic strategies which are available. A number of these techniques have been subject of further recent meta-analyses, including altered fractionation in locoregionally advanced disease (improved outcome)²³³, induction chemotherapy in locoregionally advanced disease (no difference in outcome)²³⁴, cetuximab versus platinum-based chemotherapy in locally advanced disease (platinum more effective)²³⁵ and use of intensity-modulated radiotherapy (IMRT; reduced incidence of grade 2-4 xerostomias)²³⁶. What is clear even in this brief summary is that although chemoradiotherapeutic strategies for HPV-negative oropharyngeal carcinoma have developed as part of the management of head and neck cancer as a single entity, contemporary data suggest that current management strategies offer greater absolute survival benefit than most other cancers of the head and neck region²²⁴, and furthermore survival benefit is of paramount importance²²⁷. Therapeutic advances in HPV-negative disease are therefore likely to be aimed at therapeutic escalation; indeed, the current CompARE trial (Institute of Head and Neck Studies and Education, University of Birmingham, UK) aims to validate the benefit of therapeutic escalation by comparing 3 treatment arms against a concomitant cisplatin plus IMRT standard in intermediate and high risk disease, as classified by Ang¹⁰⁵. Treatment arms will investigate the benefits of induction chemotherapy, dose-escalated radiotherapy and primary resection as addition to current standard therapy, offering great scope in refining outcomes in oropharyngeal-specific cohort.

9. Stromal Derangement

Differences in the molecular characterisation of HPV-positive tumours may not be limited to the epithelium; the importance of epithelial-connective tissue interplay in the progression of cancer is becoming increasingly recognised. Thurlow *et al*²³⁷ used a combination of spectral clustering and gene ontology analysis to determine the most significant pathways influencing prognostication in head and neck cancer. Expression of genes associated with the composition of the extracellular environment, along with genes linked to cytokine-cytokine receptor interaction, highly correlated with clinical outcome. Notably, the over-expression of genes encoding a number of matrix metalloproteinases (discussed below in the context of fibroblast senescence) was found to be linked with poor clinical outcome. Similarly, Lim *et al* noted a fibroblast gene expression profile that correlated with tumour progression; fibroblast expression of α -SMA and ITGA6 correlated with survival, and furthermore IGFBP7 (a marker of the fibroblast senescence-associated secretory profile) was upregulated in those tumours demonstrating greatest genetic aberration. Roepman *et al* also demonstrated a metastasis-associated pattern of stromal-specific genes in head and neck cancers through laser capture microdissection. Upregulated stromal genes included CTGF, MMP-2, Thrombospondin 2 (a TGF- β inducer) and ADAM12²³⁸, inferring a strong role of the microenvironment in supporting tumour metastasis.

HPV is a strictly epitheliotropic virus and tumour stroma may therefore remain relatively undisturbed, in stark contrast to tumours of tobacco/ alcohol origin in which the associated connective tissue has been chronically exposed to penetrating carcinogens. Recent progress in assessing the role of epithelial-connective tissue interaction in cancer formation suggests that penetrating carcinogens may lead to oxidative damage of the principal cell residing in connective tissue, the fibroblast²³⁹. Furthermore, the instructive capacity of HPV-related carcinomas may be less than that of their sporadic counterparts; Hassona *et al* found that conditioned medium from genetically unstable oral squamous cell carcinoma lines (defined as those lines carrying greater chromosomal damage) more readily instructed fibroblasts to acquire a secretory phenotype supportive of tumour invasion compared to genetically stable comparators, with TGF- β central to this process²⁴⁰. The lack of chromosomal damage linked to HPV-positive OPC may lead to a weaker instructive capacity

of tumour epithelia, which may in turn lead to a disparity between stromal behaviour in virus-positive and -negative disease.

There is some conflict against the concept of decreased stromal support in HPV-positive disease; Erez *et al* found that in cervical carcinoma, epithelial-stromal interaction was active through the NF- κ B pathway²⁴¹. Moreover, HPV-positive OPCs present at a more advanced stage than sporadic tumours, with nodal metastases being more frequent². In isolation, this observation could be attributed to the invasive capacity of the epithelia alone, or may alternatively reflect patient demographics. However, recognised difficulties with culturing non-smoker, non-drinker HPV-positive cell lines *in-vitro* would suggest that virus-positive tumours are highly reliant on the support of their microenvironment.

Those connective tissue markers linked to cancer progression and prognostication, such as smooth muscle actin (SMA)²⁴² and markers of fibroblast senescence (HIRA and SA- β Gal)²⁴³ are yet to be characterised for HPV positive disease. Similarly, epithelial-stromal interaction *in-vitro* remains undocumented.

Fibroblast Senescence

Penetrating carcinogens from cigarette smoke and smokeless tobacco have been shown to raise levels of reactive oxygen species (ROS) within fibroblasts²⁴⁴. Oxidative damage occurs within the cell, driving entry into a viable, but replicatively quiescent state, known as senescence²⁴⁵. In addition to cell cycle arrest, an altered secretory phenotype has been demonstrated in a number of senescent cells²⁴⁶, including fibroblasts associated with various oral cavity lesions²⁴⁴. Pitiyage *et al* observed that in oral submucous fibrosis (OSMF), senescent fibroblasts accumulate as lesions progress; 1.9% of fibroblasts from early OSMF were noted to be senescent (compared to 0.4% of control fibroblasts), increasing to 3.7% of fibroblasts in cases of advanced OSMF with dysplasia²⁴³. Pitiyage demonstrated cell culture evidence that oxidative stress resulting from mitochondrial damage was the major process through which senescence had been induced, and furthermore demonstrated that the senescent population expressed high levels of MMP-1 and MMP-2. Increased secretion of osteopontin and matrix metalloproteinases (particularly MMP-3), in addition to a reduction in tissue regulators have been identified as a characteristic feature of tumour-associated

senescent fibroblasts, leading to a connective tissue microenvironment that is supportive of tumour invasion^{244, 245, 247}. The findings of Thurlow *et al* suggest that poor prognosis head and neck tumours have increased genetic expression of these aforementioned factors, further corroborating the influence of the microenvironment on tumour behaviour²³⁷. There is also evidence that gene expression varies greatly between HPV-positive and -negative tumours, with marked differences seen in expression of genes involved in cell cycle control²⁴⁸. Although these analyses of gene expression have fundamentally addressed the cellular processes undertaken within neoplastic epithelium, the influence this has on the surrounding connective tissue and associated microenvironment is anticipated to be appreciable.

Senescent fibroblasts, due to their lack of mitotic activity, become highly resistant to radiotherapy and chemotherapeutic strategies. Thus, following (chemo)radiotherapy, an environment highly supportive of any surviving tumour cells will persist. Experimentally-induced senescent fibroblasts have been shown to confer radio-resistance to co-cultured breast carcinoma cells in such a manner²⁴⁹.

Myofibroblast Activation and Smooth Muscle Actin (SMA)

Carcinogen exposure may potentiate fibroblast differentiation into myofibroblasts within tissue stroma. Myofibroblast secretory function differs from that of the native fibroblast, demonstrating a change in epithelial-connective tissue interplay through $\alpha v\beta 6$ integrin-dependent activation TGF- $\beta 1$, of which SMA acts as a marker²⁴². This altered secretory function appears to support tumours in an analogous way to the altered secretory function induced through fibroblast senescence.

Stromal smooth muscle actin (SMA) expression has recently been demonstrated as the single most reliable predictor of mortality in oral squamous cell carcinoma, superseding even established measures such as tumour staging and grading²⁴². SMA therefore represents a highly robust measure of stromal derangement, and characterisation of SMA expression in HPV-positive disease is of importance in establishing the role of epithelial-connective tissue interplay. HPV-positive and negative disease may also show a difference in epithelial-connective tissue interplay relating to $\alpha v\beta 6$ integrin dependent activation TGF- $\beta 1$.

10. Hypothesis, Aims & Objectives

Hypothesis

HPV-positive oropharyngeal carcinoma is microenvironmentally less active than HPV-negative disease. This feature may account for prognosis and may be reflected in how conditioned medium from representative oropharyngeal carcinoma cell lines interact with fibroblasts. A characteristic, tumour-supportive fibroblast secretory response may be accomplished *de novo* in normal oral fibroblasts exposed to cell line conditioned medium, rather than requiring the presence of “pre-conditioned” cancer-associated fibroblasts. Those factors secreted by fibroblasts in response to oropharyngeal cancer cell lines may be a definitive feature in distinguishing HPV-positive and -negative disease, and may furthermore be subject to clinical blockade.

(A) Aims & (O) Objectives

A1. To acquire and authenticate two HPV-positive and two HPV-negative oropharyngeal carcinoma cell lines in order to model microenvironmental interactions in HPV-positive and HPV-negative disease

O1. Acquisition and successfully culture a number of oropharyngeal carcinoma lines of mixed HPV status, validate the HPV status of each cell line using PCR in addition to external validation of cell lines to confirm authenticity – inclusive of STR profiling. Determine the most representative HPV-positive and -negative cell lines to take forward in experiments by reviewing the available literature

A2. To optimise a 2D tissue culture model of microenvironmental interactions between cell lines and fibroblasts, using conditioned medium incubations

O2. Collect optimised and normalised conditioned medium from cell lines in order to stimulate normal oral fibroblast cultures. Stimulate fibroblasts and collect a second normalised conditioned medium containing the secretory response. Determine the most

suitable periods over which conditioned medium should be collected, along with the most suitable concentrations of conditioned medium in order to observe biological effect

A3. To determine any changes in biological activity of oropharyngeal carcinoma lines in response to conditioned medium taken from fibroblasts stimulated by cell line conditioned medium

O3. Optimise and undertake suitable 2D migration and proliferation experiments of cell lines exposed to stimulated fibroblast conditioned medium versus unstimulated fibroblast control

A4. To determine any difference between HPV-positive and HPV-negative cell lines in terms of their interactions with fibroblasts in conditioned medium experiments

O4. Statistically compare HPV-positive and HPV-negative cell line behaviour in 2D migration and proliferation assays following exposure to stimulated fibroblast conditioned medium. Use a triplicate of fibroblast cultures in order to robustly validate *in-vitro* findings

A5. To determine the underlying molecular profile of any changes observed

O5. Undertake cytokine array analysis of cell line and fibroblast conditioned medium, identify key factors expressed differently in HPV-positive versus HPV-negative cell lines and/or stimulated fibroblasts

A6. To identify potential therapeutic targets for the management of disease stratified by virus status and microenvironmental biomarkers

O6. Validate those candidate factors identified by cytokine array in order to identify molecules responsible for driving any changes observed. Use clinically-relevant inhibitor drugs in order to confirm therapeutic potential of targeting the respective molecules and also to further validate the respective candidates

A7. To apply 2D findings to a 3D model of disease

O7. Successfully culture cell lines in an appropriate 3D model of invasion using either DED, matrigel or alternative 3D matrix. Repeat inhibitor experiments in 3D as appropriate

A8. To validate tissue culture findings in a pilot cohort of oropharyngeal carcinomas

O8. Collate biopsy specimens taken from a pilot cohort of oropharyngeal carcinomas, confirm HPV status using a combination of p16 immunohistochemistry and RNA in-situ hybridization, undertake biomarker analysis relevant to tissue culture findings using standard immunohistochemistry and/or RNA in-situ hybridization

Chapter 1: Confirmation of HPV Status, Validation of Cell Lines & Optimisation of Migration Assay

Introduction

Analysis of HPV Status in Cell Lines

Analysis of HPV status remains a contentious issue within the realms of the clinical assessment of oropharyngeal tumour specimens. Contention largely lies around the analysis of formalin fixed tissue – whilst a gold standard exists for fresh specimens (E6/E7 mRNA analysis)^{138, 196}, this method of analysing formalin-fixed tissue specimens is recognised as highly unreliable. For means of cohort analysis (see Chapter 8), a combination of p16 IHC and RNAScope RNA ISH have been determined as providing the most clinically valuable index of HPV status, as these two tests carry the greatest prognostic significance of all HPV analyses²⁰⁷.

HPV analysis of oropharyngeal cell lines using PCR remains less disputed, presumably due to PCR analysis being a common standard in the validation of any gene *in vitro*, along with access to an unlimited source of “fresh tissue” equivalent and use of multiple probes²⁵⁰. Unlike pathological specimens, cell cultures should contain a pure sample of the carcinoma line and therefore a positive finding of HPV DNA infers infection within that specific line; there is no potential for incidental infection of surrounding tissue as may be seen in the former.

PCR analysis of clinical specimens has commonly involved the use of general primers in order to improve sensitivity²⁵¹, although type-specific probes are available¹³⁸. Irrespective of which probe is used in the clinical environment, as extensive an approach to PCR analysis as *in-vitro* is likely prohibited by the fixation process and the cost of clinically-validated kits.

An HPV16 E1 PCR Taqman probe, based on DNA sequencing work by Seedorf *et al* and Kennedy *et al* has been validated and is commercially available (Applied Biosystems, UK) for use in cell culture^{252, 253}, whereas PCR involving other HPV genes/ types has been undertaken using custom probes^{180, 250, 254}.

Analysis of Migration In-Vitro

Invasion is considered a hallmark of malignancy²⁵⁵; clinical “invasion” of tumour relies on a group of aberrant characteristics including motility, directionality and enzymatic digestion of extracellular matrix. Whilst not reflecting the comprehensive properties of invasion, analysis of cellular migration remains an accessible method of tissue culture tumour modelling. It is therefore an important component in the analysis of carcinoma behaviour *in-vitro*, although methods used to undertake such migration analyses vary. A common approach is to review cellular movement in two dimensions; that is, migration of a confluent cell culture across a predetermined gap. Perhaps the most intuitive method of introducing such a gap in an otherwise confluent cell culture is to mechanically debride a portion of the confluent culture using an instrument tip – the so-called “scratch” assay. Whilst this method is an established, cheap and readily accessible technique²⁵⁶, there are some limitations in its validity.

One major factor in the validity of any migration assay lies in deciphering true cellular migration from the net effects of cellular proliferation within an already-confluent culture leading to passive gap infill. Whilst a recent Nature Protocols publication bears no reference to addressing cellular proliferation whilst undertaking the scratch assay technique²⁵⁶, and indeed many publications do not take proliferation into account²⁵⁷⁻²⁵⁹, the literature also commonly sites serum starvation or the use of an inhibitor of cellular turnover such as mitomycin C or DMSO²⁶⁰⁻²⁶³. The variability in choice of technique may reside in whether a particular piece of research needs to distinguish cell turnover from true migration. Some authors have undertaken migration assays both with and without mitomycin C in order to more accurately reflect migratory and proliferative contributions to wound closure^{260, 261, 264}.

Mitomycin C is an aziridine-containing isolate from *Streptomyces* spp, and is a potent DNA crosslinker. DNA crosslinking leads to replication arrest, thereby inhibiting cellular proliferation. Whilst mitomycin C's anti-proliferative effect offers a reproducible method of isolating true migration, a truly representative migration profile is not guaranteed – there may be subtherapeutic mitomycin dosing, or conversely toxic effects leading to cell death. Moreover, the intracellular consequences of DNA crosslinking may adversely affect cellular motility. These features may have dissuaded some authors from its use.

The method of “scratch” introduction may also present a challenge in terms of disturbing the immediate cellular milieu. Cell rupture during the mechanical scratch may lead to release of a number of factors, thereby creating variability in subsequent migrational behaviour. The

force at which the scratch is introduced may not only influence the behaviour of cells, but also determine the width of scratch that is produced. Methods to circumvent these issues include the use of silicone stoppers attached to the base of a culture well prior to cell seeding and subsequent confluence; the removal of the stopper at the start of the assay aims to avoid cell rupture and may potentially offer a process of creating a uniform gap. Manufacturer's data suggest that in fact the reproducibility of gap size is comparable between mechanical scratches introduced using a pipette tip and voids left by silicone stoppers. The reproducibility of the subsequent cellular migration does however appear to be superior using the silicone stopper technique²⁶⁵.

This chapter addresses the initial confirmation of HPV status & validation of cell lines, and optimisation of a contemporary silicone stopper migration assay technique, taking into account the limitations discussed above in order to achieve a method which is both reproducible and representative of cellular migration in isolation from proliferation.

Methods

Retrieval of Cell Lines

Seven head and neck cancer cell lines (UD SCC 02, UPCI SCC 072, UPCI SCC 089, UPCI SCC090, UPCI SCC 152, UPCI SCC154 and VU 147T) were received as a kind gift from Dr. S. Thavaraj, London following completion of appropriate Material Transfer Agreement with Prof. S. Gollin, University of Pittsburgh School of Public Health, Pittsburgh for lines with the prefix "UPCI". VU 147T (also known as 93-VU-147T) was originally cultured at the Free University Hospital, Amsterdam¹⁷⁹, and UD SCC 02 (UD SCC-2) was originally cultured at the University of Dusseldorf, Germany²⁶⁶. A further Human Tonsillar Epithelium (HTE) line, experimentally-immortalised through insertion of HPV 16 E6 and E7 oncogenes (HTE E6 E7) was received as a kind gift from Prof. E. Blair, Leeds, serving as a positive control for the HPV16 E6/E7 oncogenes, and negative control for all other viral genes.

All lines were expanded in the recommended media (Tables 1.1 & 1.2) and then frozen in liquid nitrogen for stock. Lines were then carefully observed and weaned onto normal media (DMEM plus 10 % FCS, with 2 mM L-glutamine & 50 IU/50 µg mL⁻¹ penicillin-streptomycin) in order for conditioned medium experiments outlined in Chapter 2 to be undertaken using identical media in all cell lines and primary cultures. The literature was then reviewed to confirm reported HPV status and to determine the most representative HPV-positive and HPV-negative oropharyngeal carcinoma lines to be used in experimentation. Table 1.3 summarises the HPV status and demographics linked to each cell line, as reported in the literature^{179, 180, 250, 254, 267-269}. UPCI SCC072 and UPCI SCC 089 were chosen as representative HPV-negative lines, whereas UD SCC2, and UPCI SCC090 were chosen as representative HPV-positive lines. A further cell line, FaDu was initially trialled in the migration experiments described later in the chapter, but was discarded from use in further work due to failure of trial ORIS™ migration assays, whereby cells retracted to form thin anastomosing strands of non-viable cells.

All cell lines were tested for mycoplasma on a monthly basis using the Ez-PCR mycoplasma test kit (Biological Industries, Kibbutz Beit Haemek, Israel).

Table 1.1: Composition of Modified E-media, used for culture of HTE E6 E7

Additive	Volume & Concentration	Final Concentration	Storage	Supplier
DMEM	330 mL	67%	4 °C	Sigma, Poole UK
Ham's F12	108 mL	22%	4 °C	Sigma, Poole UK
FBS	50 mL	10%	4 °C	Sigma, Poole UK
L-glutamine	5 mL: 200 mM	2 mM	-20 °C	Sigma, Poole UK
3, 3, 5- Tri-iodothyronine	500 µL; 1.36 µg mL ⁻¹	1.36 ng mL ⁻¹	-20 °C	Sigma, Poole UK
Apo-Transferrin	500 µL; 5 mg mL ⁻¹	5 µg mL ⁻¹	-20 °C	Sigma, Poole UK
Hydrocortisone	80 µL; 2.5 mg mL ⁻¹	4 µg mL ⁻¹	4 °C	Sigma, Poole UK
EGF	25 µL; 100 µg mL ⁻¹	5 ng mL ⁻¹	-20 °C	Sigma, Poole UK
Cholera Toxin	500 µL; 8.47 ng mL ⁻¹	8.47 ng mL ⁻¹	4 °C	Sigma, Poole UK

Table 1.2: Composition of Media Used for expansion of Cell Lines UD SCC02, UPCI SCC072, UPCI SCC089 and UPCI SCC090

Additive	Volume & Concentration	Final Concentration	Storage	Supplier
MEM with Earle's salts	450 mL	87 %	4°C	Sigma, Poole UK
FBS	50 mL	10 %	4°C	Sigma, Poole UK
L-glutamine	5 mL; 200 mM	2 mM	-20°C	Sigma, Poole UK
Penicillin/streptomycin	5 mL; 5,000 U penicillin and 5 mg streptomycin mL ⁻¹	50 U mL ⁻¹ 50 µg mL ⁻¹	-20°C	Sigma, Poole UK
NEAA	5 mL; 100X solution	1X	4°C	Sigma, Poole UK

Table 1.3: Summary of Retrieved Cell Lines

Cell line	Site	Nature	HPV status	p53 status	11q13	Smoker	Drinker
UPCI SCC090 ^{180, 250, 267, 269}	Base of tongue	Recurrence	Positive	Wild Type	Not	Y	Y
UPCI SCC072 ²⁶⁷⁻²⁶⁹	Tonsil	New primary	Negative	Mut (179)	Amplified	Y	Y
UPCI SCC089 ²⁶⁷⁻²⁶⁹	Tonsil	New primary	Negative	- (**)	Amplified	Y	Y
UPCI SCC154 ^{267, 269}	Tongue	New primary	Positive	Wild Type	Not	Y	Y
UPCI SCC152 ^{180, 267}	Hypopharynx	New primary*	Positive	Wild Type	Not	Y	Y
93-VU-147T ^{179, 254}	Floor of Mouth	New primary	Positive	Wild Type		Y	Y
UD SCC2 ^{254, 266, 269}	Hypopharynx		Positive	Wild Type			
HTE E6 E7	N/A	Experimental	Positive				

Cell line	Family History	Outcome	Age	Gender	Histology	Grade	Stage
UPCI SCC 090	Y	No evidence of disease (*)	46	M	Poorly differentiated, basaloid	3	T2N0
UPCI SCC 072	Y	No evidence of disease	61	F	Moderately differentiated	2	T3N2b
UPCI SCC 089	N	Died of disease	58	M	Moderately differentiated	2	T4N2b
UPCI SCC 154	N		54	M		3	T4N2
UPCI SCC 152	Y		47	M		2	- (**)
93-VU-147T			58	M	Moderately differentiated		T4N2
UD SCC 2				M			T1N2M0
HTE E6 E7							

* despite reports of no recurrence of disease in papers linked to UPCI SCC090, UPCI SCC152 is widely documented as a cell line derived from a recurrence in the same patient²⁶⁷. Conflicting reports of the origins and viability of UPCI SCC152 can be found, whereby the line was considered as a new primary and even failed to grow in cell culture¹⁸⁰. UPCI SCC152 was a hypopharyngeal tumour occurring 1 year following UPCI SCC090; the timescale and proximity to the anatomical origin of UPCI SCC090 may have led to the conflicting reports of recurrence/new primary. ** reported with a strikethrough in the literature, without explanation²⁶⁷

M1.1: Validation of Cell Line HPV Status

Cell Pellet

For each cell line, a confluent 75 cm² flask was trypsinised and the cell suspension centrifuged at 1,000 rpm for 5 minutes. The supernatant was then discarded, and remaining cell pellet resuspended in PBS and centrifuged for a further 2 mins at 3,000 rpm. The final cell pellet was immediately stored at -80 °C until use. Triplicate biological repeats were undertaken for each cell line (HTE E6 E7, UD SCC02, UPCI SCC072, UPCI SCC089, UPCI SCC090).

RNA Extraction

RNA extraction was undertaken for each cell line (ISOLATE RNA kit, Bioline Reagents Ltd. London, UK). Cell pellets were suspended using 450 µL lysis buffer and incubated for 3 mins at room temperature. The cell suspension was then centrifuged for 2 mins at 10,000 x *g* in a spin column, allowing separation of filtrate from cellular debris. 450 µL 70% Ethanol was then added as an antisolvent. The ethanolised filtrate was then transferred to a second spin column, and again centrifuged for 2 mins at 10,000 x *g*. The filtrate was discarded, and the spin column placed over a fresh collection tube, 700 µL wash buffer added and then centrifuged at 10,000 x *g* for 1 min to remove co-precipitated salts. The collection tube was then discarded and a further centrifugation process undertaken at 10,000 x *g* for 3 mins. 50 µL RNAase-free water was then added to the spin column membrane to dissolve precipitated RNA, incubated at room temperature for 1 min and then centrifuged at 6,000 x *g* for 1 minute to elute the retained RNA. Successful RNA extraction was then confirmed using a Nanodrop 1000 Spectrophotometer (Thermo Fischer Scientific), quantifying RNA concentration and comparing absorbencies at 230, 260 and 280 nm to assess RNA purity. A 260 nm:280 nm absorbance ratio of approximately 2.0, in addition to a monophasic absorption peak, were used as criteria to confirm RNA purity.

cDNA Formation

Each RNA sample was diluted to 500 ng μL^{-1} prior to cDNA formation. An initial PCR run using cDNA from 100 ng μL^{-1} RNA led to late amplification, and therefore prompted the use of 500 ng μL^{-1} RNA samples. cDNA reverse transcription reactions were undertaken using 10 μL RNA samples from each cell line in combination with 10 μL reverse transcription reagent mixture, prepared according to manufacturer's instructions (Applied Biosystems UK). Components of the final reagent mixture are summarised in Table 1.4, below. cDNA formation was undertaken using a DYAD™ "DNA Engine" PCR machine, using a thermal cycling program summarised in Table 1.5.

Table 1.4: Reagents used in Reverse Transcription reaction

Component	Volume (μL) per reaction
10 X RT buffer	2.0
25X dNTP mix (100mM)	0.8
10 X RT random primers	2.0
Multiscribe™ reverse transcriptase	1.0
Nuclease-free H ₂ O	4.2
500 ng μL^{-1} RNA sample	10.0
Total	20.0

Table 1.5: Thermal Cycle Program for cDNA Formation

Temperature	Time
25 °C	10 mins
37 °C	2 hrs
85 °C	5 mins
4 °C	Indefinite

HPV16 E1 qPCR

A commercially available Taqman probe for HPV16 E1 (FAM reporter) was purchased from Applied Biosystems, UK. A probe for the B2M housekeeping gene was used in parallel to the E1 probe (VIC reporter). Concomitant 10 μL experiments on cDNA extracted from each cell line were run in a 96-well PCR plate; each experiment was undertaken in triplicate repeat. Table 1.6, below, summarises the components of the 10 μL PCR mixture. Reagents were

centrifuged for 1 min at 1,000 rpm and then exposed to PCR reaction conditions of 50 °C for 2 mins, 95 °C for 10 mins, followed by 40 cycles of 15 s at 95 °C/ 1 min at 60 °C using a 7900 Fast real-time PCR Machine.

Table 1.6: PCR Reagents

	Volume (μL)
Mastermix (<i>Applied Biosystems, UK</i>)	5
Nuclease free H ₂ O	3.5
B2M reporter (<i>Applied Biosystems, UK</i>)	0.5
E1 probe (<i>Applied Biosystems, UK</i>)	0.5
cDNA sample	0.5

HPV16 E6 qPCR

A custom Taqman probe for HPV16 E6 (FAM reporter) was purchased from Applied Biosystems, UK, using a previously published sequence of 5'-(FAM)-CCCAGAAAGTTACCACAGTTATGCACAGAGCT-(TAMRA)-3'²⁷⁰. The following primers were used for HPV 16-specific E6 amplification: HPV 16 E6 forward primer, 5'-TCAGGACCCACAGGAGCG-3' HPV 16 E6 reverse primer, 5'-CCTCACGTTCGCAGTAACTGTTG-3'.

rtPCR was undertaken using a 7900 Fast real-time PCR Machine. A probe for the B2M housekeeping gene was initially used in parallel to the E6 probe using a VIC reporter. Concomitant 10 μL experiments on cDNA extracted from each cell line were run in a 96-well PCR plate; each experiment was undertaken in triplicate repeat. Reagents were prepared as summarised in Table 1.7, centrifuged for 1 min at 1,000 rpm and then exposed to PCR reaction conditions of 50 °C for 2 mins, 95 °C for 10 mins, followed by 40 cycles of 15 s at 95 °C/ 1 min at 60 °C. Due to parabolic amplification plots encountered during initial experimentation (see results section), PCR was initially re-run with increasing dilutions of HPV16 E6 probe/primer to rule out a “hook” effect from using an over-concentrated probe/primer solution and then further repeated without B2M reporter; identical amplification plot patterns occurred in all experiments. Amplification products were therefore finally run

under agarose gel electrophoresis to confirm presence/absence of PCR products of the correct molecular weight, as described below.

Table 1.7: PCR Reagents

	Volume (μL) with B2M	Volume (μL) without B2M for agarose electrophoresis
Mastermix (<i>Applied Biosystems, UK</i>)	5	5
Nuclease free H ₂ O	3.5	4
B2M reporter (<i>Applied Biosystems, UK</i>)	0.5	-
E1 probe (<i>Applied Biosystems, UK</i>)	0.5	0.5
cDNA sample	0.5	0.5

2.5 % Agarose Gel Electrophoresis

Parabolic graphs obtained from HPV16 E6 Taqman PCR in cell lines HTE E6 E7, UD SCC2 and UPCI SCC090 prompted further investigation to determine whether correct amplification products had been created. Final confirmation of reaction products was achieved by means of agarose gel electrophoresis appropriate to <100 kbp²⁷¹. A 2.5% agarose gel was created by dissolving 2.5 g anhydrous agarose in 100 mL X1 TAE (TAE constituents are summarised in Table 1.8). 1 μL Ethidium Bromide was added to the solution before allowing the gel to set in an electrophoresis tray. 2 μL loading dye was added to each 10 μL PCR well, before loading separate lanes of the gel. A 100 bp DNA ladder was used as reference. PCR reaction products from E1/B2M and E6 amplification were run for all cell lines. Electrophoresis was undertaken at 120 V for 45 minutes.

Table 1.8: TAE Constituents (X50 solution)

Constituent	Amount
Tris base	242 g
Glacial acetic acid	57.1 mL
EDTA 0.5M (pH8)	100 mL

DNA Extraction for STR Profiling

Cell pellet formation was undertaken as described in PCR analysis, above, for each cell line. DNA extraction was then performed on a cell pellet for each line using a Wizard[®] Genomic DNA Purification Kit (Promega, Madison, USA). Cells were washed and resuspended in PBS, then exposed to 600 μ L Nuclei Lysis Solution and pipetted until all visible cell clumps were dissolved. 3 μ L RNase Solution was then added to the nuclear lysate and mixed by inverting 5 times, followed by incubation at 37 °C for 20 mins. After 5 mins cooling to RT, 200 μ L Protein Precipitation Solution was added to the sample and vortexed for 20 s. The sample was then chilled on ice for 5 mins, followed by centrifugation at 13,000 X *g* for 4 mins. The DNA-containing supernatant was then removed and pipetted into a microcentrifuge tube containing 600 μ L isopropanol. The solution was mixed through gentle inversion until strands of precipitated DNA became visible, and then centrifuged for 1 min at 13,000 X *g*. The supernatant was then discarded and 600 μ L 70% Ethanol added in order to wash the precipitated DNA. The tube was then centrifuged at 13,000 X *g* for 1 min, and the Ethanol supernatant carefully removed before allowing the DNA pellet to dry for 15 mins at 50 °C. The DNA pellet was then resuspended in 50 mL dH₂O and stored at -20 °C until use. DNA samples were then transported on ice for external STR profiling by the CRUK Cancer Centre Genomics Facility, Leeds Institute of Cancer and Pathology. STR profiling summaries are given in Appendix 1.

M1.2: Optimisation of ORIS™ Migration Assays

Trial Seeding Densities

The appropriate seeding densities for each cell line to be used in experimentation were determined using serial dilutions of each cell line cultured to approximately 80 % confluence, trypsinised and then resuspended in media. All cells lines were initially suspended to a concentration of 1 million cells mL⁻¹, other than UD SCC02 and UPCI SCC 090 (suspended at 2.5 million cells mL⁻¹). The increased concentration used for UD SCC02 and UPCI SCC 090 was in response to initial practice seeding, for which 1 million cells mL⁻¹ was inadequate for achieving overnight confluent seeding into assay wells.

For each cell line, 100 µL of suspension was pipetted into a well of a manufacturer-supplied 96-well ORIS™ assay-compatible plate at target concentration, with 100 µL of subsequent dilutions from 90 % to 10 % of initial concentration pipetted into adjacent wells. Each well was reviewed after overnight incubation to determine which dilution corresponded to the optimal cellular confluence at the given time.

Optimisation of Mitomycin C Concentration for Migration Assay

Due to potential cellular toxicity at higher doses, optimal lowest dose of mitomycin C concentration for the inhibition of proliferation in each cell line (UD SCC02, UPCI SCC072, UPCI SCC089, UPCI SCC090) was confirmed through flow cytometry, using plots of cell replication (CellTrace™, Far Red Invitrogen, Life Technologies, Paisley, UK). mitomycin C was purchased from Sigma (Poole, UK, Cat number M4287-2MG), reconstituted in distilled water to a concentration of 0.5 mg mL⁻¹, filter sterilised, snap-frozen in liquid nitrogen and stored in a light-protected container at -80 °C. The available literature was then used as a guide for appropriate mitomycin exposure period and concentrations in order to inhibit cell proliferation^{272, 273}.

CellTrace™ was added to separate 70 % confluent 75 cm² flasks containing each cell line at a concentration of 0.5 µM in PBS, and incubated at 37 °C for 15 mins. The flasks were then washed in PBS before adding standard media for 30 mins in order for cells to recover. Each cell line was then trypsinised and seeded into 15 wells, using multiple 12-well plates, at a concentration of 100,000 cells per well and left overnight to adhere. A 3.5 hr incubation with

mitomycin C at concentrations of 10, 2, 0.5, 0.25 and 0 $\mu\text{g mL}^{-1}$ in triplicate repeat was then undertaken 24 hrs post-seeding. A PBS wash was then undertaken before adding fresh standard media into each well and then incubating at 37 °C for 3 days.

After 3 days' incubation at 37 °C, each experimental well was trypsinised, centrifuged at 6,000 rpm for 2 mins, supernatant carefully aspirated, washed X 2 by resuspension of pellet in 1 mL PBS, repeat centrifugation for 2 mins at 6,000 rpm and supernatant aspiration. The final pellet was resuspended in 300 μL 37 % formaldehyde, stored overnight at 4 °C protected from light and then analysed using a Calibur flow cytometer, recording absorbance at 660 nm.

Trial ORIS™ Migration Assay

Following optimisation of mitomycin C exposure and seeding densities for each cell line, a trial ORIS™ migration assay was run in normal media (DMEM plus 10 % FCS, with 2 mM L-glutamine & 50 IU/50 $\mu\text{g mL}^{-1}$ penicillin-streptomycin) in order to determine the optimal period over which to run each migration assay.

Cell lines UD SCC02, UPCI SCC072, UPCI SCC089 and UPCI SCC090 were grown to 70 % confluence in separate 75 cm^2 flasks. Cells were washed twice in PBS, trypsinised, centrifuged at 1,000 rpm and then resuspended in normal media. Each cell suspension was then counted using a haemocytometer, appropriately diluted using normal media, and re-counted in order to achieve the preoptimised seeding concentrations summarised in Table 1.10. ORIS™ assay plates were prepared under sterile conditions, mounting silicone stoppers into each well using the manufacturer-supplied location device. 100 μL of each cell suspension was then pipetted into respective ORIS™ assay wells and left overnight to adhere.

Following cell adherence and confirmation of well confluency using an inverted lens microscope, preoptimised mitomycin C suspension in normal media (please refer to Table 1.9) was prepared for each cell line from snap-frozen 0.5 mg mL^{-1} aliquots of mitomycin C stored at -80 °C. All handling of mitomycin C was undertaken in a darkened tissue culture hood in order to avoid excessive light exposure.

Silicone stoppers were then removed from assay wells using the manufacturer supplied retrieval tool, exposing the respective cell exclusion zone, and normal media carefully aspirated off each well ensuring contact was avoided with the well base. 2 X 100 μL PBS

washes were then undertaken, and then 100 μ L mitomycin C in normal media carefully pipetted into respective wells and incubated for 3.5 hours at 37 °C in the dark. Following 3.5 hours incubation in mitomycin C, baseline void photomicrographs were taken using a X4 objective lens.

Following mitomycin C incubation, assay wells were washed X2 in PBS and then 100 μ L HGF/inhibitor suspension carefully pipetted into respective wells. ORIS™ assay plates were then incubated and visually inspected at 10 h, 15 h, 20 h, 24 h, 48 h and 72 h.

Results

Figure 1.1: Nanodrop™ Analysis of extracted RNA

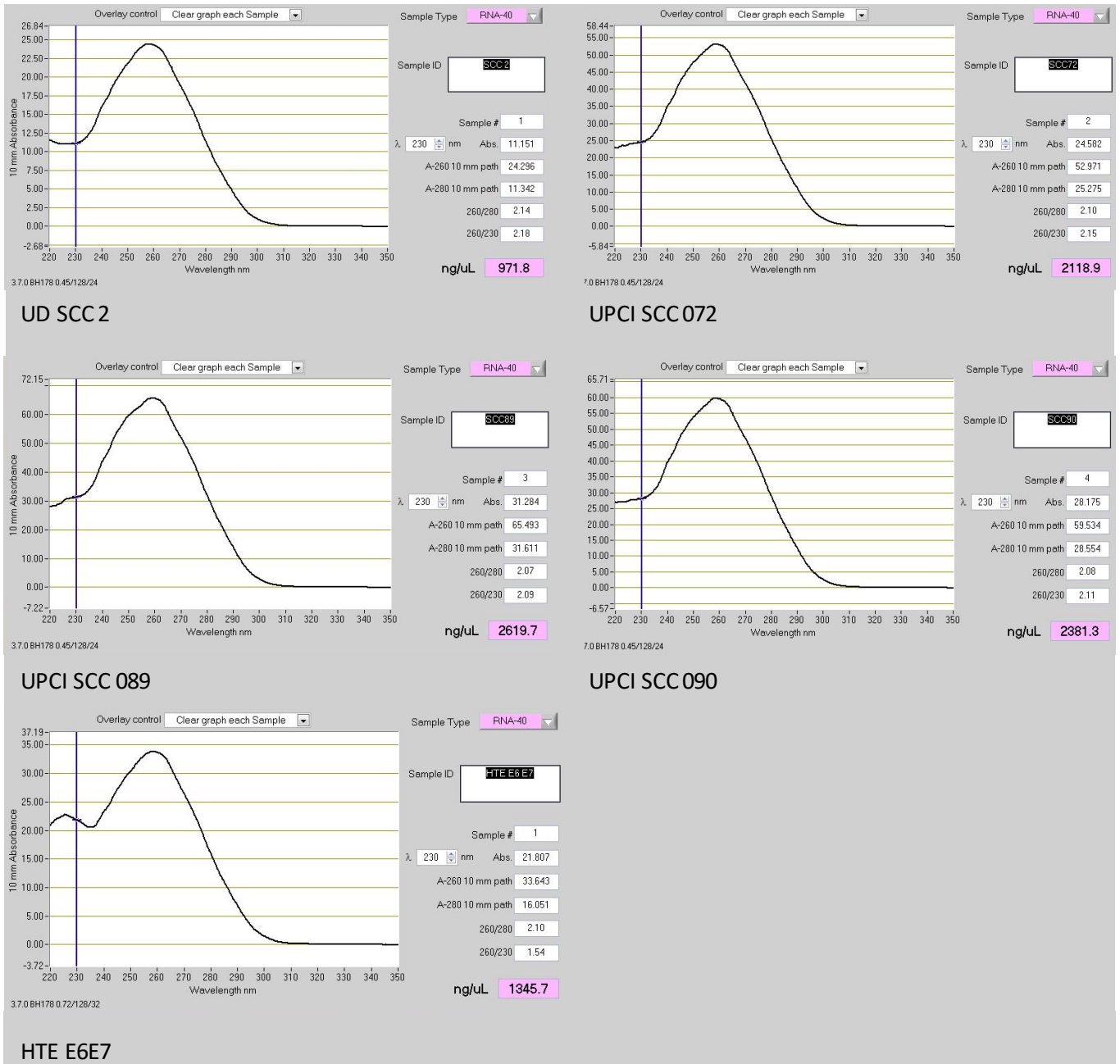


Figure 1.1: Nanodrop™ analysis of extracted RNA, demonstrating a monophasic peak plus 260/230 nm light absorption ratios of approximately 2.0 in all specimens, confirming high quality RNA extraction throughout.

Figure 1.2: HPV16 E1 qPCR amplification plot

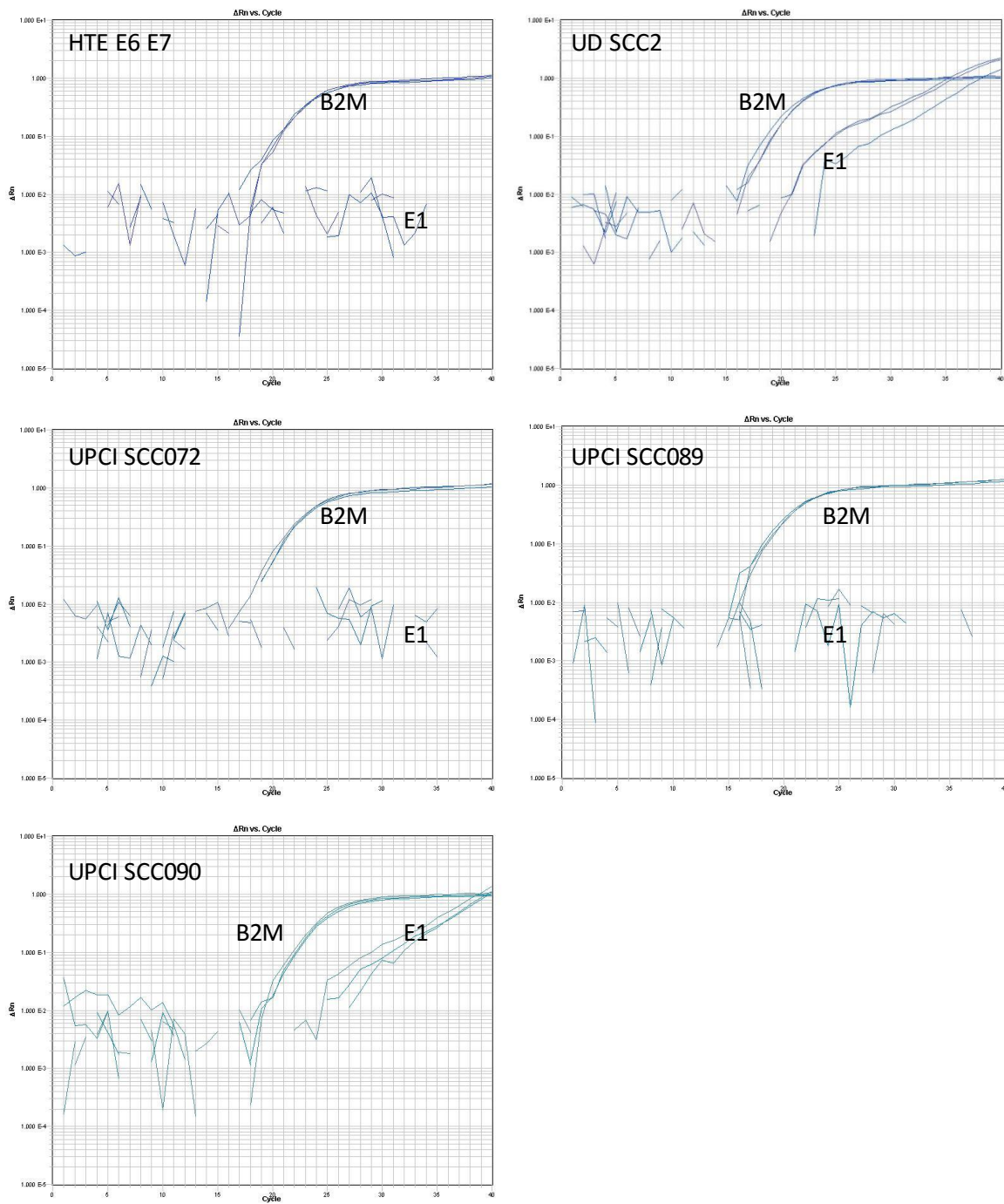


Figure 1.2: HPV16 E1 qPCR amplification plots for cell lines HTE E6 E7, UD SCC02, UPCI SCC072, UPCI SCC089 and UPCI SCC090. X-axis denotes time, Y-axis denotes absorbance. Note HPV16 E1 expression in lines UD SCC2 and UPCI SCC090, consistent with their reported HPV16-positive status. Note the absence of amplification of HPV16 E1 in the HPV negative cell lines UPCI SCC072 and UPCI SCC089, in addition to HTE E6 E7 negative control. B2M control gene expression can be seen as tight amplification plots for triplicate repeats in all cell lines.

Figure 1.3: HPV16 E6 qPCR amplification plot

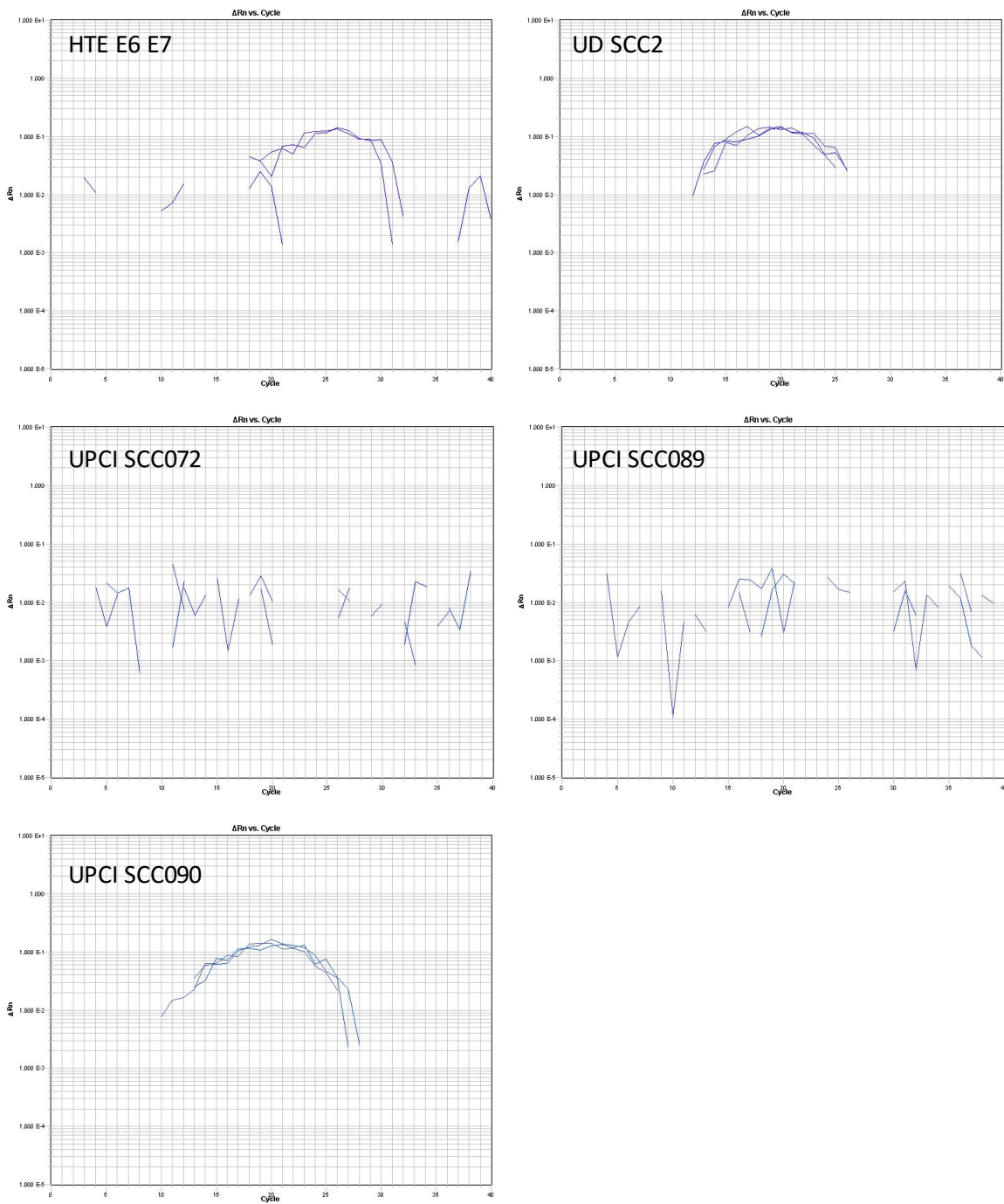


Figure 1.3: HPV16 E6 qPCR amplification plots for cell lines HTE E6 E7, UD SCC02, UPCI SCC072, UPCI SCC089 and UPCI SCC090. X-axis denotes time, Y-axis denotes absorbance. Note the parabolic shape of amplification curves for HTE E6 E7, UD SCC02 and UPCI SCC090, prompting further validation through agarose gel electrophoresis. As discussed further in the methods section, PCR was repeated using a range of primer/probe concentrations to rule out “hook effect”, without change to amplification plot pattern. Note the complete absence of amplification of HPV16 E6 in the HPV negative cell lines UPCI SCC072 and UPCI SCC089.

Figure 1.4: Agarose Gel Electrophoresis of HPV16 E6 and E1 qPCR Reaction Products. *Inverted image.*

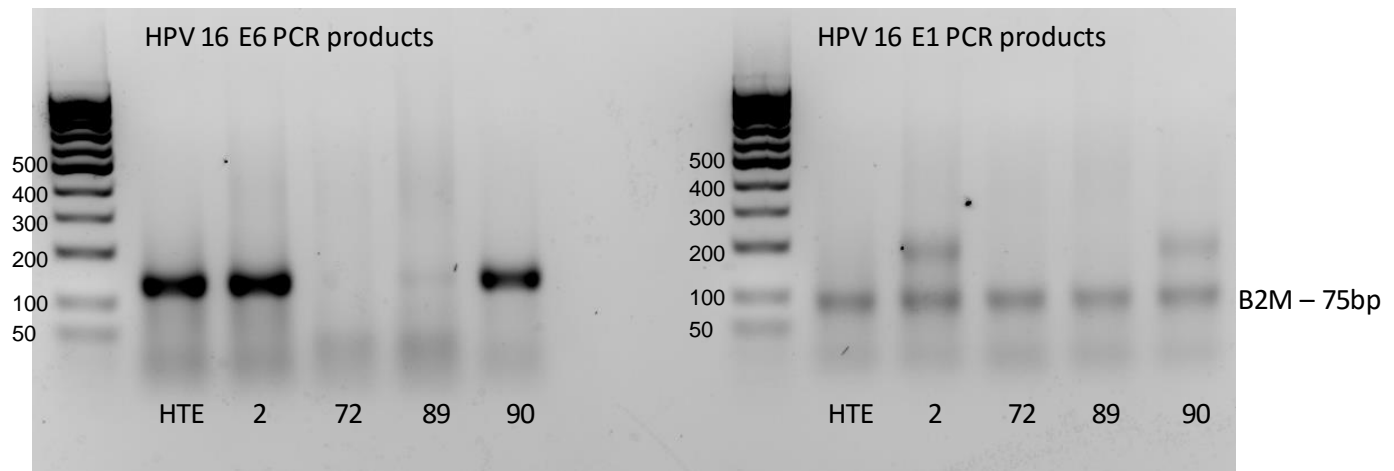


Figure 1.4: Agarose Gel Electrophoresis of qPCR reaction products for cell lines HTE E6 E7, UD SCC02, UPCI SCC72, UPCI SCC089 and UPCI SCC090.

HTE – HTE E6 E7 2 – UD SCC02
 72 – UPCI SCC072 89 – UPCI SCC089
 90 – UPCI SCC090

DNA ladder reference depicted to the left of each experiment; numerical figures denote size of ladder bands, in base pairs (bp).

HPV16 E6 PCR products:

Note that a dense 150 bp band can be observed for HPV16 E6 reaction products of cell lines HTE E6 E7, UD SCC02 and UPCI SCC090. A faint band can also be observed for cell line UPCI SCC089; although this band represents a very low amount of PCR product, as PCR amplification was undertaken from a high initial RNA sample concentration of 500 ng mL⁻¹, even a small amount of amplification product relating to a viral gene is an aberrant finding in a reputedly HPV-negative cell line.

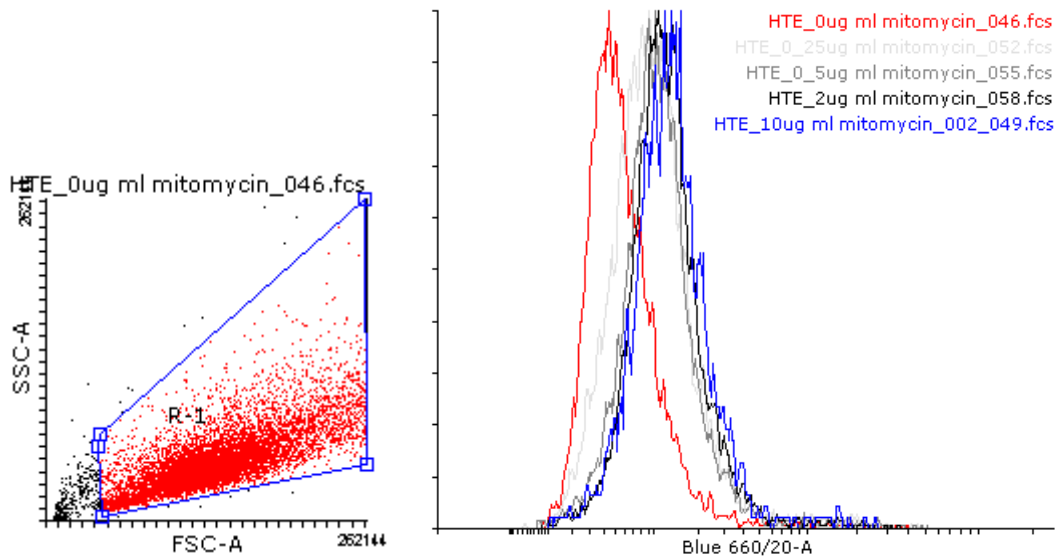
HPV16 E1 PCR products:

Note the presence of a 75 bp band in all cell lines, consistent with B2M reaction products. Note also presence of a 200 bp band in HPV-positive cell lines UD SCC02 and UPCI SCC090, consistent with HPV16 E1 amplification products. Note also the absence of any bands additional to B2M in cell lines HTE E6 E7, UPCI SCC072 and UPCI SCC089, consistent with a HPV-negative status of the latter two lines and E6/E7 oncogene-specific status of HTE E6 E7.

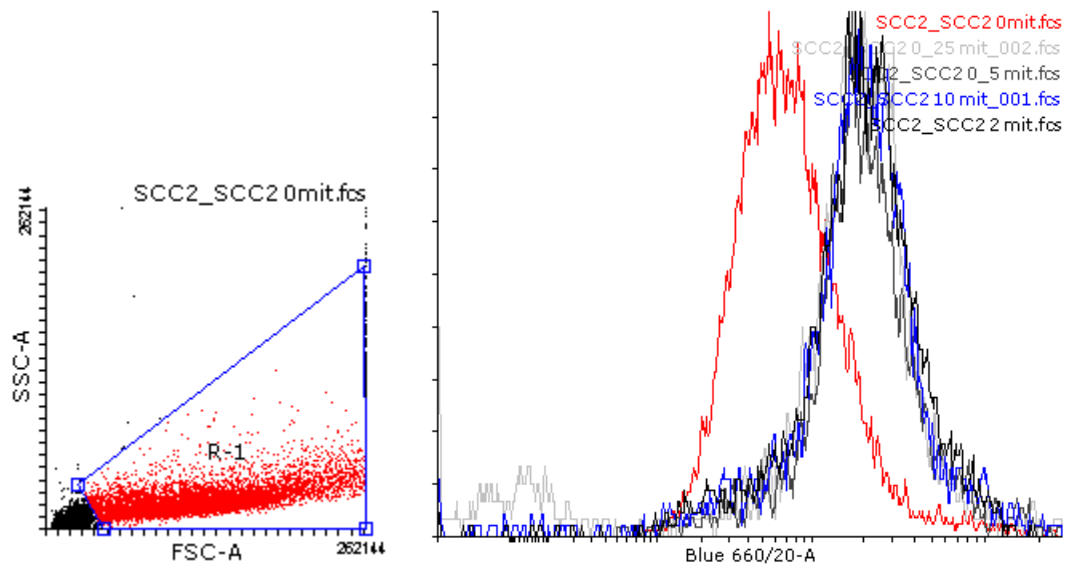
Due to the weak band noted for UPCI SCC089 on HPV16 E6 electrophoresis, samples of each cell line were finally sent for external PCR validation of HPV status, confirming a HPV-positive status of UPCI SCC02 and UPCI SCC090, and HPV negative status of UPCI SCC072 and UPCI SCC089. External validation was undertaken by the Royal Hallamshire Hospital department of cytology, using the Cobas® HPV Test multiplex assay (Roche, New Jersey, USA).

Figure 1.5: Flow Cytometry Analysis of Cell Lines Exposed to a Range of Mitomycin C Concentrations.

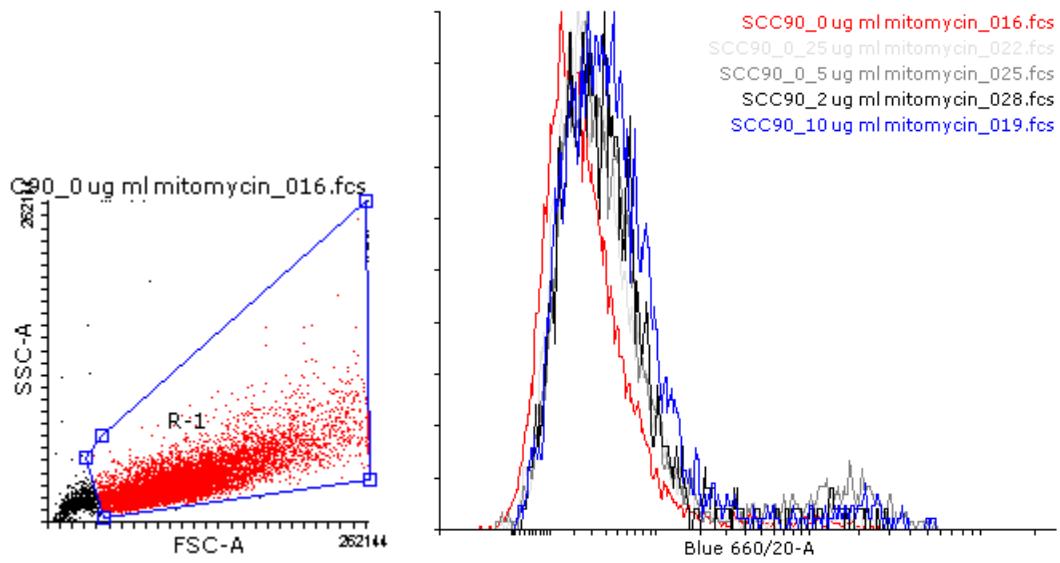
a). HTE E6 E7



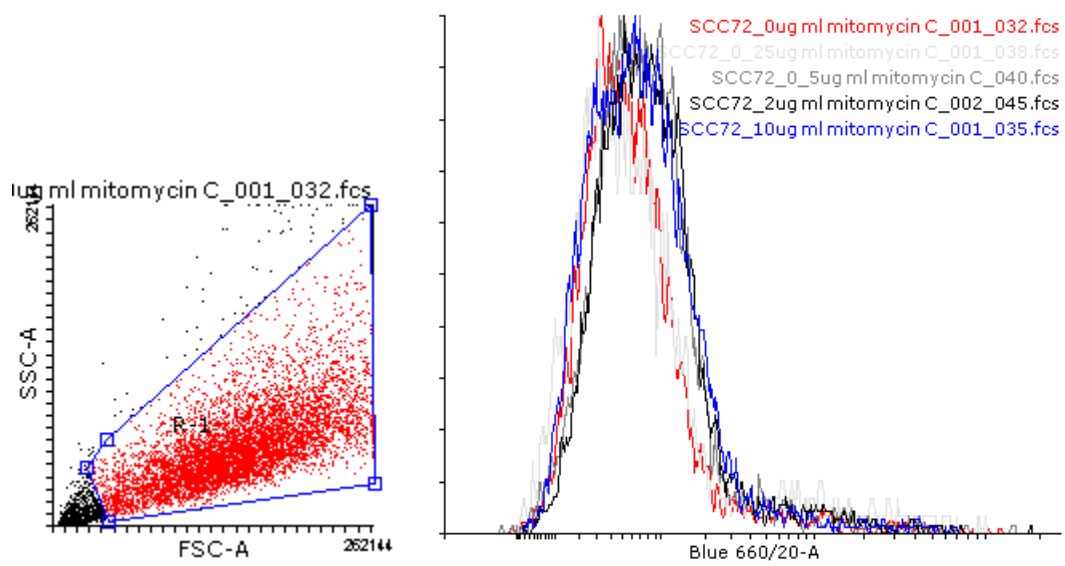
b). UD SCC02



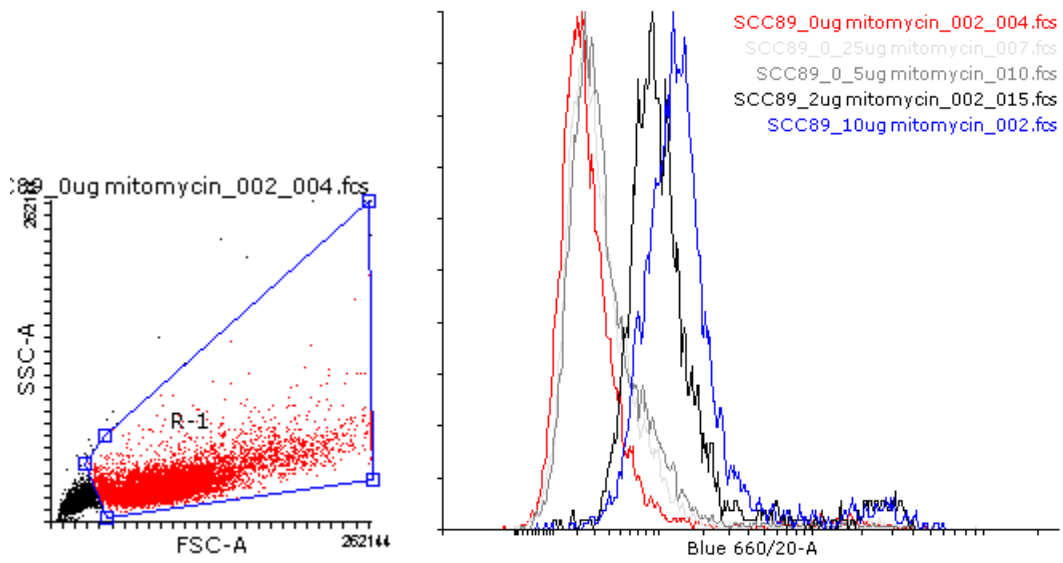
c). UPCI SCC090



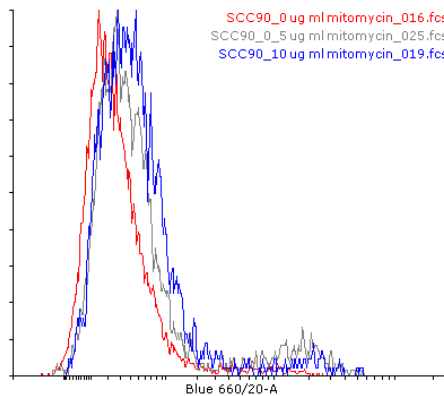
d). UPCI SCC072



e). UPCI SCC089



f). UPCI SCC090



g). UPCI SCC072

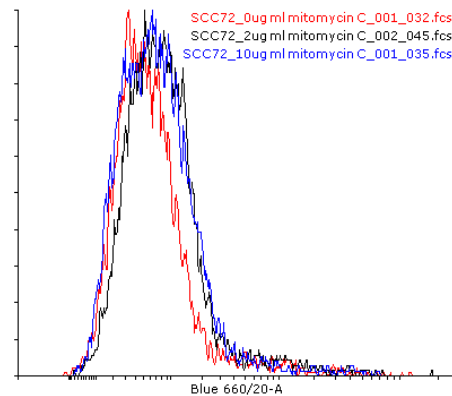


Figure 1.5: Flow cytometry analysis of cell turnover using CellTrace™ following pre-incubation with mitomycin C at respective concentrations for 3.5 h.

- a). HTE E6 E7 (E6/E7 immortalised tonsillar keratinocyte control)
- b). UD SCC02 (HPV-positive line)
- c). UPCI SCC090 (HPV-positive line)

d). UPCI SCC072 (HPV-negative line)

e). UPCI SCC089 (HPV-negative line)

f). & g). Optimal mitomycin C histogram compared to 0 $\mu\text{g mL}^{-1}$ negative control and 10 $\mu\text{g mL}^{-1}$ positive control

Left images depict raw data of forward/side scatter and positioning of gating to exclude regions of debris. Right images depict flow cytometric fluorescence histogram at 660 nm, corresponding to CellTrace™ emission spectra. Figure legends adjacent to histogram denote corresponding mitomycin C concentrations; “0” represents negative control sample incubated without mitomycin C prior to analysis, and is depicted in red. “10” represents 10 $\mu\text{g mL}^{-1}$ positive control, and is depicted in blue. All other numerical postscripts denote mitomycin C concentration in $\mu\text{g mL}^{-1}$, and are illustrated by progressively dark greyscale histograms corresponding to increasing concentrations. HTE E6 E7 was used as an immortalised tonsillar keratinocyte control.

Note the clear separation of histogram distributions between 0 and 10 $\mu\text{g mL}^{-1}$ mitomycin C incubations in cell lines HTE E6 E7, UPCI SCC089 and UD SCC02. A left histogram shift denotes continued proliferation following mitomycin C exposure, with CellTrace™ content halving with each cell division. The lowest mitomycin C concentration inducing a histogram distribution comparable to that observed with 10 $\mu\text{g mL}^{-1}$ mitomycin C was therefore determined as the optimal dose for each cell line: this is summarised in Table 1.9, below.

A less discernible split between peaks is noted in the slower growing cell lines UPCI SCC072 and UPCI SCC090, reflecting a lower rate of cell division, and therefore reduced histogram shift between 0 and 10 $\mu\text{g mL}^{-1}$ mitomycin C. Data relating to intermediate mitomycin C doses for these lines has been censored in figures f & g for ease of viewing, with lowest adequate dose of mitomycin C illustrated; note the general mirroring of 10 $\mu\text{g mL}^{-1}$ mitomycin C histograms with 2 $\mu\text{g mL}^{-1}$ mitomycin C for cell line UPCI SCC072 and 0.5 $\mu\text{g mL}^{-1}$ mitomycin C for cell line UPCI SCC090.

N.B. Optimisation of mitomycin C exposure in cell line UD SCC02 was undertaken with the kind guidance of Dr. V. Hearnden

Table 1.9: Optimal Mitomycin concentration determined for each cell line

	Mitomycin C Concentration, $\mu\text{g mL}^{-1}$
HTE E6 E7	2
UD SCC 02	0.25
UPCI SCC 072	2
UPCI SCC 089	2
UPCI SCC 090	0.5

Figure 1.6: Trial Cell Seeding Densities for ORIS™ Assay Loading

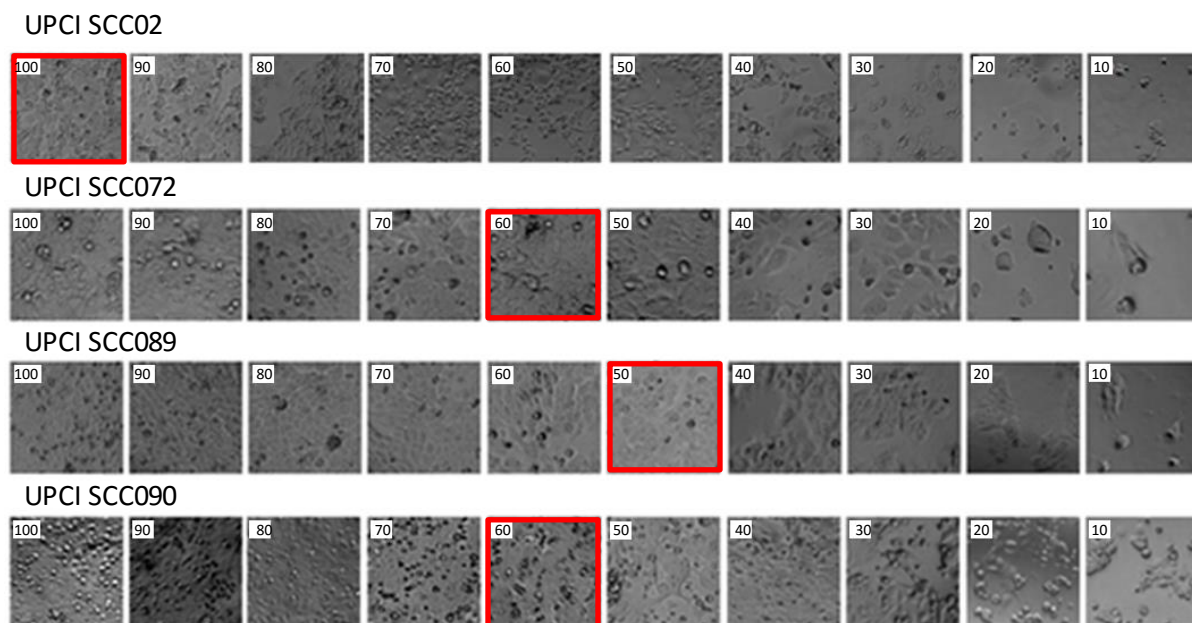


Figure 1.6: ORIS™ assay confluence following overnight seeding of cell lines UD SCC02, UPCI SCC072, UPCI SCC089 and UPCI SCC090 at progressive dilutions. Numbers denote percentage concentration of original cell suspension – e.g. “100” denotes 100%, “90” denotes 90%. The following cell concentrations were used for each cell line:

UD SCC02- 2.2 million cells mL⁻¹

UPCI SCC072 – 3.2 million cells mL⁻¹

UPCI SCC089 – 1.76 million cells mL⁻¹

UPCI SCC090 – 1.93 million cells mL⁻¹

Red squares denote the percentage dilution for each cell line that provided optimal confluent seeding. Note that concentrations exceeding the optimal seeding density led to non-adherent cells being visible overlying the confluent monolayer (visualised as blackened areas in the above images), whereas cell-free regions can be noted at concentrations lower than highlighted in red. Images taken at X10 magnification, width of each square denotes 400 µm.

Table 1.10: Optimal seeding densities determined following trial seeding in ORIS™ assay wells.

	Concentration, cells mL⁻¹	Number of Cells in 100µL Aliquot
UD SCC 02	2,200,000	220,000
UPCI SCC 072	1,600,000	160,000
UPCI SCC 089	880,000	88,000
UPCI SCC 090	1,160,000	116,000

Discussion

HPV Status of Cell Lines

The HPV status of all cell lines has been comprehensively assessed using recognised PCR and electrophoresis techniques to confirm presence/absence of HPV16 E1 & E6 mRNA. All oropharyngeal carcinoma cell lines were validated as retaining a HPV status as described in the literature^{179, 180, 250, 254, 267-269}. Although the experimentally-induced HTE E6 E7 control remains poorly described in the literature, validation of viral E6 oncogene expression in the absence of E1 infers experimental induction of E6 rather than acquisition through viral infection, and is therefore consistent with the mRNA expression pattern expected of this cell line. One limitation of using this line as a control is that whilst the line adequately acts as a positive control for E6 mRNA expression, it is limited to being a negative control for E1 mRNA expression. Unfortunately, HeLa, the commonly available HPV-positive cervical carcinoma line is HPV18 infected and therefore could not be used as a positive control due to primer specificity to the HPV16 sequence. HTE E6 E7 therefore offered a pragmatic and accessible control for PCR analysis.

In order to fully validate UPCI SCC089 given the faint band noted with electrophoresis of E6 PCR products (Figure 1.4), a cell sample of each line was sent for external PCR validation against a panel of HPV types including HPV16 and 18, confirming UPCI SCC089's HPV-negative status. The faint band seen on agarose E6 electrophoresis is therefore not of biological significance. This is also in keeping with the complete absence of E1 banding noted in agarose gel electrophoresis of PCR products derived from this line (Figure 1.4), In addition to external validation of HPV status using the Cobas[®] HPV Test.

Final confirmation of cell line authenticity was achieved through STR profiling, allowing the confident use of the cell lines in further experimentation.

Difficulties in Obtaining Representative HPV-Positive Cell Lines for Use in Cell Culture

As detailed in Table 1.3, all HPV-positive cell lines have been established from tumours of mixed aetiology; that is, HPV-positive disease arising in known smoker/drinkers. As discussed in more detail in the preceding literature review, data from Ang *et al's* seminal

paper suggests tumours of mixed aetiology carry a prognosis intermediate to that seen in HPV-positive and -negative disease¹⁰⁵. Caution must be therefore employed not to over-interpret cell culture findings relating to these cell lines, as they may not be fully representative of HPV-positive disease. There are however, no reports in the literature of an established HPV-positive oropharyngeal line derived from a non-smoker, due to sensitivities leading to cell culture failure. This likely represents the less aggressive clinical nature of HPV-positive disease. The obtained lines therefore offer the only pragmatic approach to *in-vitro* comparisons between HPV-positive and -negative disease, although they do offer the prospect that any observable difference between the available HPV-positive lines and HPV-negative lines may in fact be more pronounced had a non-smoker/drinker HPV-positive line been available.

ORIS™ Assay Optimisation

Each cell line has been optimised for application in ORIS™ migration assay. Mitomycin C exposure has been optimised for each line, albeit with limited effect noted in flow cytometric analysis of cell lines UPCI SCC072 and UPCI SCC090 due to their inherently low basal proliferative rate. It is important however, to bear in mind that cell line incubation with conditioned medium containing tumour-supportive factors could potentially alter proliferation rate during the assay: the use of mitomycin C for these two lines is therefore critical to ensure void closure relates to migration alone, and not passive infill as a result of cell division. Cell lines UD SCC02 and UPCI SCC089 demonstrated marked shift of flow cytometry histograms in response to appropriate doses of mitomycin C, demonstrating unambiguous requirements of mitomycin C in order to assess migration alone.

Use of 10 µg mL⁻¹ mitomycin C throughout the duration of migration assay in order to inhibit proliferation has been cited in the literature²⁶⁰, however this concentration led to marked cell death during initial optimisation. Two possible explanations may account for the cell death seen – perhaps the most forthcoming relates to the drug being incorrectly stored by other authors, leading to loss of activity. Storage instability of mitomycin C has indeed been noted by co-researchers in our group. The oropharyngeal carcinoma cell lines used may alternatively exhibit greater sensitivity to mitomycin C in comparison to other lines quoted in the literature, an effect which may become particularly notable due to the relatively protracted time taken for cell migration to be observed in these lines²⁵⁶.

Optimal ORIS™ assay cell seeding densities have been established for each cell line under investigation. Lines demonstrated appreciable differences in seeding density requirements, with UD SCC02 requiring seeding at an approximate 2-fold cell density in comparison to other lines. This variation in seeding density in part appears to correlate to cell size, although attempts to optimise seeding on cheaper, non-fibronectin coated 96-well assay plates derived lower seeding densities than were necessary in ORIS™ assay wells. Well coating/wettability may therefore also determine the final optimal seeding density for a given cell line.

ORIS™ assay void closure was noted to be near complete at 24 h using cell line UPCI SCC089. An optimal migration end-point for this line was therefore determined as 20 h. All other cell lines (UD SCC02, UPCI SCC072, UPCI SCC090) demonstrated progressive migration to 48 h, with apparent migration arrest at 72 h: an optimal migration end-point for these 3 lines was therefore determined as 48 h.

The ORIS™ assay offers a reproducible method of creating a standardised cell exclusion zone for migration analysis through the removal of a silicone barrier rather than inducing cellular trauma through the use of pipette scratches, as has historically been applied to the “scratch” assay. Cell number and media requirements are also greatly reduced using this method in comparison to individual scratches being introduced into a confluent 12-well plate. The assay appears to have additional advantages over other commercially available assays in that high throughput analysis may be undertaken due to the incorporation of the assay into a 96-well plate set-up. Introduction of a circular void rather than linear scratch also offers greater reproducibility with respect to measuring closure: void margins can be measured in their entirety, and the assay therefore avoids risk of measuring different regions between baseline and end-point.

Limitations of the assay include the more labour-intensive analysis necessary in order to accurately measure the volume of an often irregular-shaped void, as compared to measurement of distance across a simple scratch assay margin. The assay is also limited to providing 2D migration data, and cannot readily distinguish between migration with directionality versus the more random process of cell scatter; it does, however offer a reproducible method of assessing cellular motility which may thereafter be analysed further using more complex models.

Chapter 2: 2D Modelling of the Microenvironment in HPV-positive & -negative Disease

Introduction

The tumour microenvironment comprises a complex molecular network derived from the dynamic interactions between tumour cells, surrounding stroma and immigrating vascular and immune cell populations. Little has been reported on the role of the microenvironment in HPV-positive versus HPV-negative oropharyngeal carcinoma, although a wealth of data is available regarding the heterogenous group of diseases that fall under the umbrella term of “head and neck cancer”. More generically, activation of the microenvironment has been linked to aggressive behaviour in a wide range of cancers, and has major prognostic implications.

Much data is available on the capacity of tumours to hijack acute inflammatory pathways linked to wound healing. Such inflammatory factors have the capacity to promote epithelial proliferation, migration and Epithelial to Mesenchymal Transition (EMT), angiogenesis and immune cell infiltration - properties that under the correct conditions, can all lead to the progression of cancer through acquisition of an evolutionary advantage. Common derangements in biomarkers linked to wound healing have been noted in a range of tumour types; for example, elevated EGF is a feature of a number of head and neck, hepatocellular²⁵⁶, breast²⁷⁴ and lung²⁷⁵ carcinomas, and has a characteristic activity of promoting proliferation, migration and invasion of all these tumour types. It appears however, that certain microenvironmental factors have more varied effect on different cancer types; this often reflects the varied physiological influence the given factor has on normal tissue, in addition to the biology of the specific neoplastic disease.

In oropharyngeal carcinoma, HPV-positive tumour status is established as offering favourable prognosis, and has been discussed in greater detail in the literature review. Although the role of the microenvironment has yet to be confirmed, it is intuitive that given the favourable prognosis of HPV-positive disease; in addition to the strictly epitheliotropic nature of the virus, which actively evades immune recognition; that differences in HPV-positive and -negative tumour microenvironments could offer insight into not only the reason for the favourable prognosis in HPV-positive disease, but also offer therapeutic targets in the management of HPV-negative disease.

Hassona *et al* investigated the role of oral squamous cell carcinoma genetic instability in the tumour microenvironment²⁴⁰. Hassona defined those oral cancers expressing significant genetic mutation, with specific reference to loss of p53, as “genetically unstable” (GU-OSCC). Conversely, those cancers retaining wild type p53 and having fewer mutations were considered “genetically stable” (GS-OSCC). Hassona found that conditioned medium from GU-OSCC cell lines more readily induced fibroblast expression of SA β -Gal, a marker of senescence, than did conditioned medium taken from GS-OSCC or dysplastic cell lines. Conditioned medium taken from senescent versus normal oral fibroblasts was also demonstrated as having a more profound effect on GU-OSCC cell line invasion into collagen gels, whereas normal oral keratinocytes failed to demonstrate a change. It should be noted however, that only a single normal oral keratinocyte cell line was assessed in this latter experiment, and moreover no GS-OSCC lines were assessed. Hassona also went on to demonstrate that normal oral fibroblasts could be induced into a senescent state through 4 hourly pulsatile exposure to TGF- β 1; conditioned medium taken from the induced senescent state increased invasion in a similar manner to senescent fibroblasts retrieved from genetically unstable tumours.

Several inferences can be made from Hassona’s article in terms of HPV-positive oropharyngeal carcinoma; the low number of genetic mutations seen in HPV-positive tumours, in addition to a characteristic preservation of wild-type p53 and p16, render these tumours analogous to GS-OSCC. HPV-negative tumours contain the genetic aberrations surmised by Hassona as GU-OSCC. It is therefore feasible that conditioned medium taken from HPV-positive oropharyngeal cell lines have less ability to induce a fibroblast response in comparison to HPV-negative counterparts, and thereafter HPV-positive tumours may not be as responsive to instruction from fibroblast-derived conditioned medium.

This chapter explores the potential for HPV-positive versus HPV-negative tumours to induce a secretory phenotype in normal oral fibroblasts and the potential for this phenotype to instruct the tumours to migrate and proliferate.

Methods

Overview

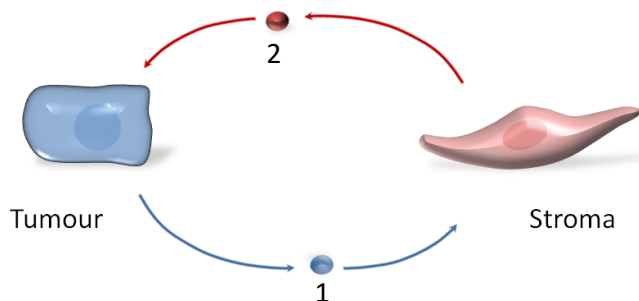
In order to model tumour-stroma microenvironmental interactions, a conceptual model was translated into a 2D tissue culture duplicate model (Figure 2.1). We hypothesised those tumours with greatest microenvironmental interactions *in vivo* would be, at a molecular level, more instructive to the normal stroma; exposure of stromal fibroblasts to tumour conditioned medium should therefore precipitate a fibroblast response to such instructions.

In order to precipitate the fibroblast response *in vitro*, tumour cell line conditioned medium was first collected and then incubated with fibroblast cultures for 24 h (a more detailed methodology is given below). Tumour conditioned medium was then aspirated from fibroblast cultures, cultures washed, and then fresh normal media incubated with the activated fibroblast cultures for a further 24 h to collect a “stimulated fibroblast” conditioned medium. It became apparent that in fact an initial fibroblast secretory response could occur concurrently with the initial 24 h incubation in tumour conditioned medium. Two sets of conditioned media were therefore collected from each experiment: firstly, the original tumour conditioned medium subsequently incubated with fibroblasts and therefore containing the initial fibroblast response, hereon referred to as “Medium 1”; and a second conditioned medium collected after washing activated fibroblasts and then incubating with fresh normal media for the 24-48 h post-stimulation period – exclusively contributed to by stimulated fibroblasts, hereon referred to as “Medium 2”. Media 1 & 2 were then use to determine whether stimulating fibroblasts in such manner could lead to altered behaviour in the original tumour cell line by assessing migration and proliferation compared to unstimulated fibroblast conditioned medium control.

Conditioned medium was therefore collected from each cell line (UD SCC02, UPCI SCC072, UPCI SCC089, UPCI SCC090), and used to induce cell line-specific stimulated fibroblast Medium 1 & 2; each cell line was then exposed to its own respective stimulated fibroblast medium in the ensuing experiments.

Figure 2.1: Conceptual Model of Tumour-Stroma Microenvironmental Interactions, Plus 2D Tissue Culture Duplicate Model

a). Conceptual Model



b). 2D Tissue Culture Duplicate Model

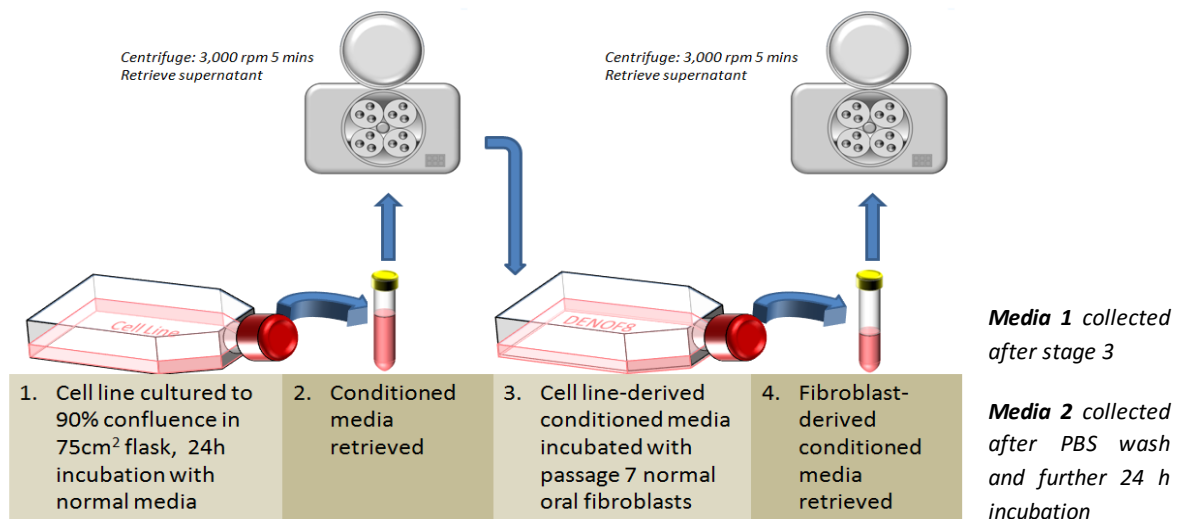


Figure 2.1a: Conceptual model of microenvironmental interactions. The above model proposes that microenvironmentally-active tumours (represented by blue cell) secrete activating factors (1), which may lead to stromal activation (stromal fibroblast represented by red cell). This in turn leads to stromal release of further factors (2), which may reinforce the hallmarks of malignancy, such as tumour proliferation, migration and invasion.

Figure 2.1b: Tissue culture duplicate model. Tumour cell lines are cultured to near confluence (step 1) and conditioned medium retrieved (step 2); this initial conditioned medium hypothetically contains the activating factors depicted in Figure 2.1a (labelled “1” on diagram). Subsequent incubation with fibroblast cultures (step 3) may lead to similar activation as occurs *in vivo*, leading to a fibroblast secretory response that can be collected in further conditioned medium (step 4) that also reflects the response *in vivo*, as labelled “2” in Figure 2.1a.

M2.1: ORIS™ Assay Migration Analysis of Modelled Microenvironmental Interactions

Collection of Cell Line Conditioned Medium

Cell lines UD SCC02, UPCI SCC072, UPCI SCC089 and UPCI SCC090 were cultured in 75 cm² flasks using normal media (DMEM with 10 % FCS, plus 2 mM L-glutamine & 50 IU/50 µg mL⁻¹ penicillin-streptomycin) until near-confluent. Flasks were then washed X3 in PBS and then incubated for 24 h with 7 mL normal media. After 24 h, conditioned medium was aspirated from each flask and centrifuged for 5 minutes at 3,000 rpm in order to remove cellular debris. 6 mL supernatant was then carefully aspirated in order to avoid resuspension of precipitated debris, and then immediately stored in a universal container at -21 °C until use in experiments.

Flasks were washed X2 in PBS, trypsinised and then cells counted in order to calculate the number of cells contributing to each mL of conditioned medium. Only conditioned media of a cell count of 3 (+/- 1) million cells mL⁻¹ conditioned medium 24 h⁻¹ were kept for use in experiments. A record of the exact cell count was maintained to allow conditioned medium to be normalised to exactly 3 million cells mL⁻¹ immediately prior to experiments. Where necessary, normalisation was undertaken by thawing two separate vials of conditioned media from the same cell line (one vial over-concentrated and one vial under-concentrated) and mixing media at a ratio that equalled a final conditioned medium concentration of 3 million cells mL⁻¹. All remaining thawed media was then discarded.

Fibroblast Stimulation with Cell Line Conditioned Medium and Collection of Media 1 & 2

Passage 6 DENOF08 normal oral fibroblasts were cultured in a 75 cm² flask to approximately 80 % confluence. Cells were then washed X2 in PBS, trypsinised, centrifuged and resuspended in approximately 6 mL normal media. In order to establish equal seeding densities in multiple 75 cm² flasks for the subsequent passage, a sterile 1,000 µL pipette was used to aspirate 1 mL of cell suspension and thereafter transfer the suspension into 5 separate 75 cm² flasks containing normal media.

The 5 separate 75 cm² flasks of passage 7 DENOFO8 fibroblasts were then cultured to early confluence. Flasks were visually inspected on a daily basis using a X10 objective lens until intracellular spaces had been obliterated due to fibroblast culture confluence. Flasks were also visually compared to confirm cell density was equal in each separate culture.

Confluent fibroblast cultures were then washed X3 in PBS and then incubated with 6 mL cell line conditioned medium for 24 h to create "Medium 1". Medium 1 was aspirated, centrifuged at 3,000 rpm and 5 mL of supernatant carefully aspirated and immediately stored at -21 °C until use in experiments. The fibroblast cultures were then washed X3 in PBS and then 6 mL normal media added and incubated for a further 24 h to create "Medium 2". Medium 2 was then aspirated, centrifuged at 3,000 rpm and 5mL of supernatant carefully aspirated and immediately stored at -21 °C until use in experiments. Fibroblast cultures were then washed X2 in PBS, trypsinised and counted using a haemocytometer to confirm a final cell density of 4 X 10⁵ cells per mL conditioned medium collected.

Preparation of Migration Assays & Inhibition of Cell Division

Two HPV-negative oropharyngeal carcinoma cell lines UPCI SCC072 and UPCI SCC089, and two HPV-positive oropharyngeal carcinoma cell lines UD SCC02 and UPCI SCC089 were grown to 70 % confluence in separate 75 cm² flasks. Cells were washed twice in PBS, trypsinised, centrifuged at 1,000 rpm for 5 minutes and then resuspended in normal media. Each cell suspension was then counted using a haemocytometer, appropriately diluted using normal media, and re-counted in order to achieve the pre-optimised seeding concentrations of 1.6 X 10⁶ cells mL⁻¹ for UPCI SCC072, 8.8 X 10⁵ cells mL⁻¹ for UPCI SCC089, 2.2 X 10⁶ cells mL⁻¹ for UD SCC02 & 1.2 X 10⁶ cells mL⁻¹ for UPCI SCC090, allowing confluent ORIS™ assay well loading as described in Chapter 1. ORIS™ assay plates were prepared under sterile conditions, mounting silicone stoppers into each well using the manufacturer-supplied location device. 100 µL of each cell suspension was then pipetted into respective ORIS™ assay wells and left overnight to adhere.

Following cell adherence and confirmation of well confluency using an inverted lens microscope, preoptimised (please refer to Chapter 1, Table 1.9) concentrations of 2, 0.5 & 0.25 µg mL⁻¹ mitomycin C suspension in normal media were prepared from snap-frozen 0.5 mg mL⁻¹ aliquots of mitomycin C stored at -80 °C. All handling of mitomycin C was undertaken in a darkened tissue culture hood in order to avoid excessive light exposure.

Silicone stoppers were then removed from assay wells using the manufacturer supplied retrieval tool, exposing the respective cell exclusion zone, and normal media carefully aspirated off each well ensuring contact was avoided with the well base. 2 X 100 μ L PBS washes were then undertaken, and then 100 μ L mitomycin C carefully pipetted into respective wells at preoptimised concentrations for each respective cell line (please refer to Chapter 1, Table 1.9) and incubated for 3.5 hours at 37 °C in the dark. Following 3.5 hours incubation in mitomycin C, baseline void photomicrographs were taken using a X4 objective lens.

Following mitomycin C incubation, assay wells were washed X2 in PBS and then 100 μ L of either Medium 1, Medium 2 or unstimulated fibroblast conditioned medium control carefully pipetted into respective wells. ORIS™ assay plates were then incubated for either 20 h (UPCI SCC089) or 48 h (UD SCC02, UPCI SCC072, UPCI SCC090) in order for migration to occur, and then endpoint photomicrographs taken using a X4 objective lens.

Analysis of Cell Migration

Analysis of cell migration was undertaken by comparison of baseline versus endpoint micrograph images taken at X4 objective. The area of each stopper-induced cell exclusion zone at baseline and endpoint was measured with ImageJ software (freeware, NIH, USA), using the polygon selection tool. Percentage void closure was then calculated by dividing area of closure at experimental endpoint by total baseline area of cell exclusion zone.

M2.2: MTS Assay Analysis of Cell Proliferation

Following the observed results in ORIS™ assay migrations, Medium 2 was selected as the most appropriate conditioned medium to assess the effects of stimulated fibroblast conditioned medium on cell line proliferation. Further stimulated fibroblast Medium 2 was collected as described above for migration assays, and immediately stored at -21 °C until use in experiments.

Cell proliferation of UD SCC2, UPCI SCC72, UPCI SCC89 and UPCI SCC90 in the presence of either respective stimulated fibroblast Medium 2 or unstimulated fibroblast conditioned medium control was assessed by means of MTS proliferation assay. Cells were grown to 70-80 % confluence in 75 cm² flasks, trypsinised, counted using a haemocytometer, divided, centrifuged at 1,000 rpm for 5 minutes, resuspended in the respective Medium 2 or control medium, re-counted and then 100 µL of cell suspension seeded at a density of 10,000 cells per well into a 96-well plate, using triplicate repeats for each condition. Wells were incubated at 37 °C in a 5 % CO₂ environment, and time points taken at baseline, 24, 48, 72 and 96 h in order to assess proliferation over the observed period. At each time point of interest, respective triplicate wells were rinsed with 100 µL PBS, then 100 µL normal media added. 20 µL MTS (CellTiter, Promega, Madison, USA) was then added in each well to be analysed, and incubated for 1.5 hours. Light absorbance at 492 nm was then assessed using a Tecan Infinite M200 plate reader.

M2.3 Repetition of Migration Assay Work to Include Tonsillar Fibroblast Cultures

In order to ensure reproducibility of cell line/fibroblast interactions, migration experiments were repeated to include two further fibroblast cultures derived from normal human tonsils. Colleagues from the Murdoch research group recently isolated two tonsillar fibroblast cultures from a total of 13 tonsillar excisions, named NTF01 and NTF06. These cultures offered anatomically representative stromal fibroblasts, and allowed experimentation to be undertaken in triplicate biological and experimental repeat, on triplicate cell cultures.

All experimental methods were repeated as described above, substituting DENOF08 cultures with NTF1/NTF6. Again, where specified, fibroblast cultures were taken to early confluence prior to incubation with cell line conditioned medium. A cell count was again

undertaken following the collection of Medium 2; returning final conditioned medium concentrations of 1×10^6 cells mL^{-1} conditioned medium for NTF1, and 5×10^5 cells mL^{-1} conditioned medium for NTF6. Although NTF1-derived conditioned medium had been contributed to by a greater cell population compared to DENO08 & NTF6, normalisation was not undertaken due to the potential influence of media nutrient depletion on migratory behaviour.

Results

Figure 2.2: Additional ORIS™ Assay Migration of Cell Lines Exposed to Respective Stimulated Fibroblast Medium 1

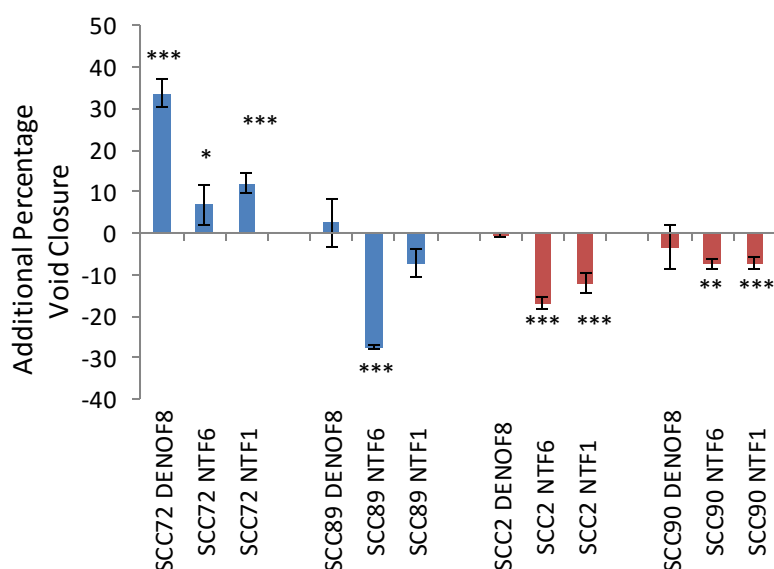


Figure 2.2: Additional ORIS™ Assay Migration of cell lines UD SCC02, UPCI SCC072, UPCI SCC089 and UPCI 090 exposed to respective stimulated fibroblast Medium 1, compared to unstimulated fibroblast control conditioned medium, expressed as additional percentage void area closure. Blue bars represent HPV-negative cell lines; red bars represent HPV-positive cell lines. Postscripts denote the respective fibroblast culture contributing to Medium 1 (derived from either DENOF08, NTF1 or NTF6). Error bars denote SEM. Asterisks denote statistical significance: * $p < 0.05$, ** $p < 0.01$, *** $p < 0.001$, Mann-Whitney U-test (Levene's test demonstrates unequal variance between treatment and control). Note that the HPV-negative cell line UPCI SCC072 consistently demonstrates increased migration throughout the range of fibroblast cultures tested. All other cell lines demonstrate either insignificant change in migration compared to control, or a reduced migration consistent with nutrient exhaustion within the conditioned medium.

Migration analyses were assessed against appropriate unstimulated fibroblast control medium which had not been pre-incubated with an equivalent epithelial control, due to difficulty incubating mortal epithelia or appropriate comparator in media other than KGM; early optimisation experiments had also demonstrated that cell line migration in 24 h cell line conditioned medium not exposed to fibroblasts led to inferior migration compared to DMEM control; this general reduction in migration was regarded as due to depletion of nutrients within conditioned medium.

Note that for cell line UPCI SCC072, migration in DENO08-derived stimulated fibroblast Medium 1 vastly out-competed all migrations observed with other fibroblast cultures, and also for the data presented in Figure 2.3 relating to Medium 2.

Figure 2.3: Additional ORIS™ Assay Migration of Cell Lines Exposed to Respective Stimulated Fibroblast Medium 2

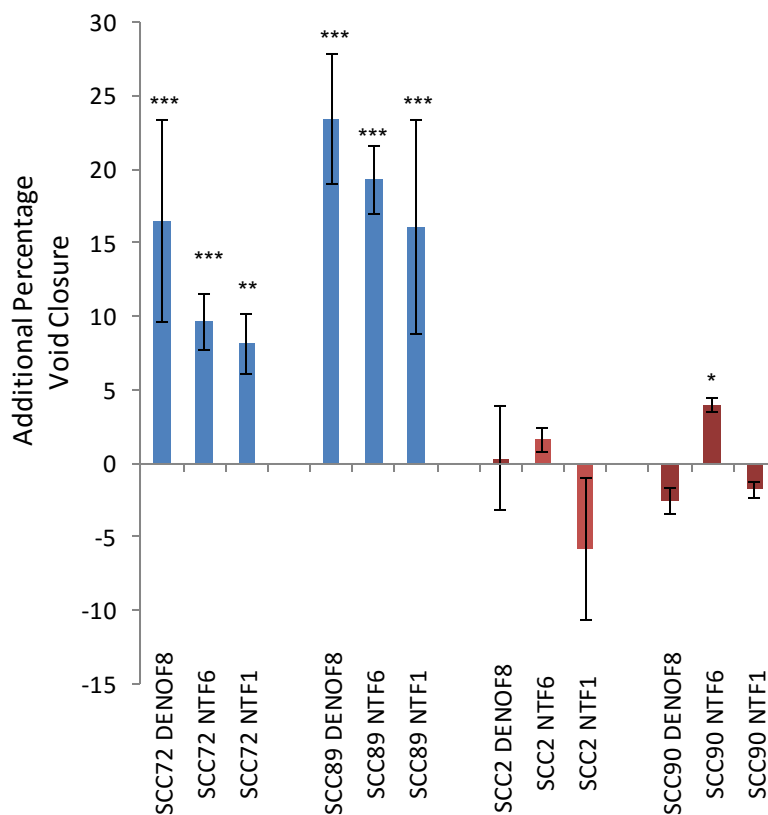
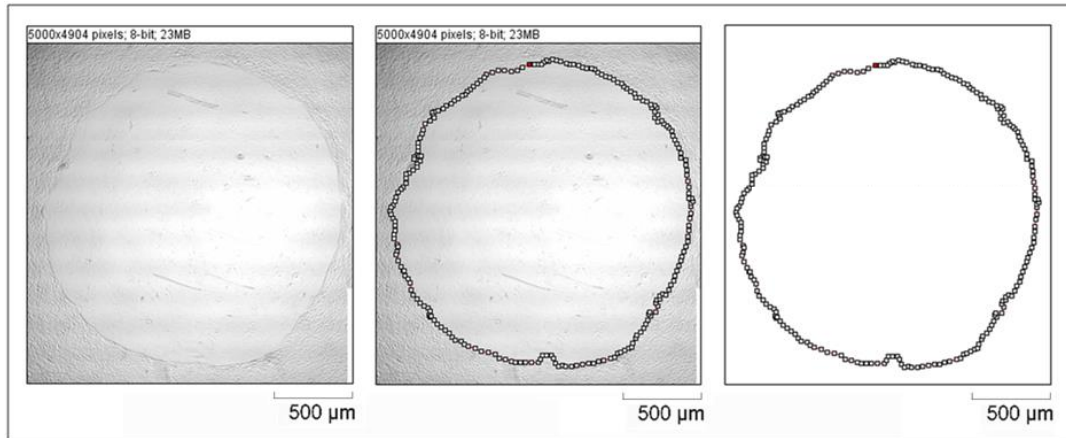


Figure 2.3: Additional ORIS™ Assay Migration of cell lines UD SCC02, UPCI SCC072, UPCI SCC089 and UPCI 090 exposed to respective stimulated fibroblast Medium 2, compared to unstimulated fibroblast control conditioned medium. Blue bars represent HPV-negative cell lines; red bars represent HPV-positive cell lines. Postscripts denote the respective fibroblast culture contributing to Medium 2 (derived from either DENOF08, NTF1 or NTF6). Error bars denote SEM, n=9. Asterisks denote statistical significance: * p<0.05, ** p<0.01, ***p<0.001, Mann-Whitney U-test (Levene’s test demonstrates unequal variance between treatment and control). Note the absence of any consistent pattern of additional migration in HPV-negative cell lines throughout the range of fibroblast media tested, whereas all HPV-negative cell line-stimulated Medium 2 led to consistent additional migration in both HPV-negative lines. Note also the reproducible trends in the degree of migration observed with each Medium 2 in both HPV negative lines (i.e. greatest degree of migration with DENOF08 Medium 2, least migration with NTF1).

Figure 2.4: Overlay Images of ORIS™ Assay Cell Migration Following Exposure to Medium 1, Compared to Unstimulated Fibroblast Conditioned Medium Control & Cell Line Conditioned Medium Control

a).



b).

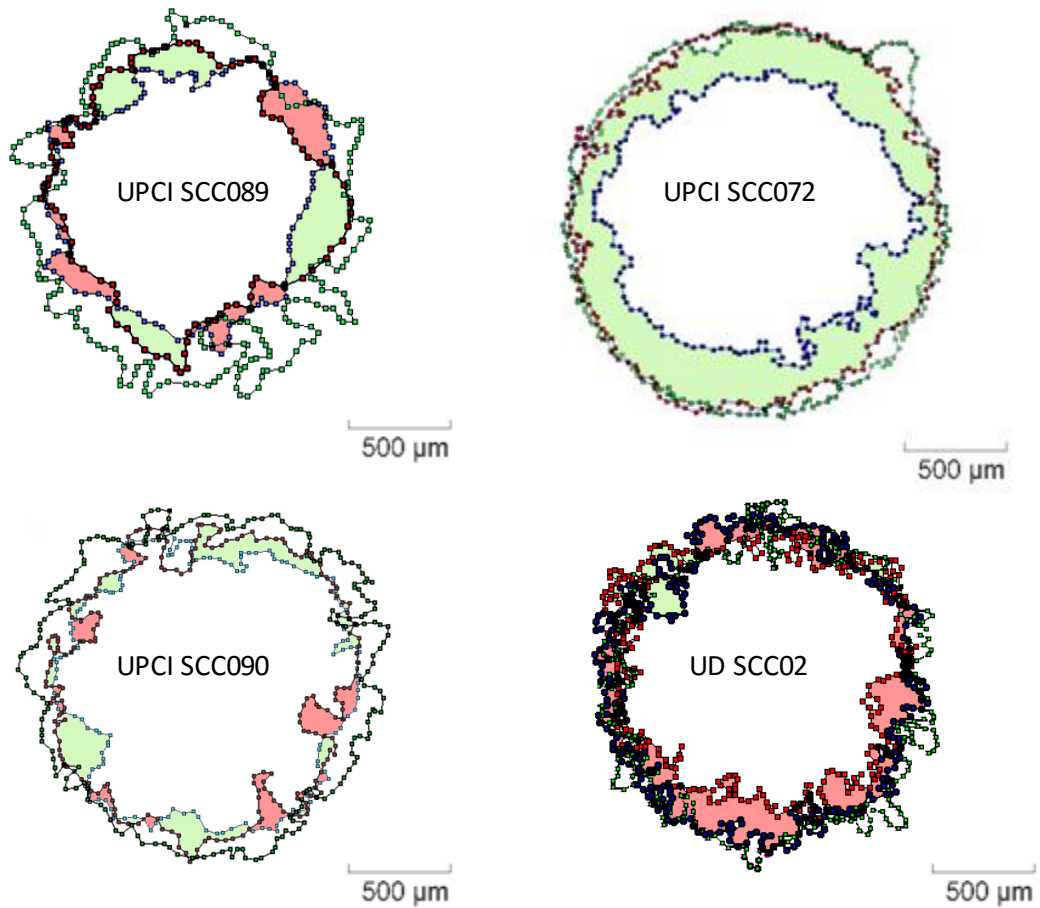


Figure 2.4:

a). Example of Image J analysis undertaken to obtain overlay plot of void margin. Left image denotes original micrograph, centre image denotes Image J polygon selection tool mark-up with approximately 200 mark-up squares identifying the void margin, right image denotes retrieved overlay plot following subtraction of original micrograph.

b). Overlay images of first experimental repeat of ORIS™ assay migrations for DENOF8 Medium 1-induced migration versus unstimulated fibroblast control. Note the marked additional migration observed with Medium 1 compared to control (green area) in cell line UPCI SCC072 only. Baseline void positions have been excluded from this overlay image for ease of visual interpretation, but were comparable for all three experimental conditions for each cell line. All migration endpoints taken at 48 h, other than UPCI SCC089 (taken at 20 h).

Green squares – end position of void margin, cell line conditioned medium control

Red squares – end position of void margin, unstimulated fibroblast conditioned medium control

Blue squares – end position of void margin, Medium 1 not exposed to fibroblasts

Green area – additional closure with Medium 1

Pink area – additional closure with Control

Figure 2.5: Overlay Images of ORIS™ Assay Cell Migration Following Exposure to Medium 2, Compared to Unstimulated Fibroblast Conditioned Medium Control

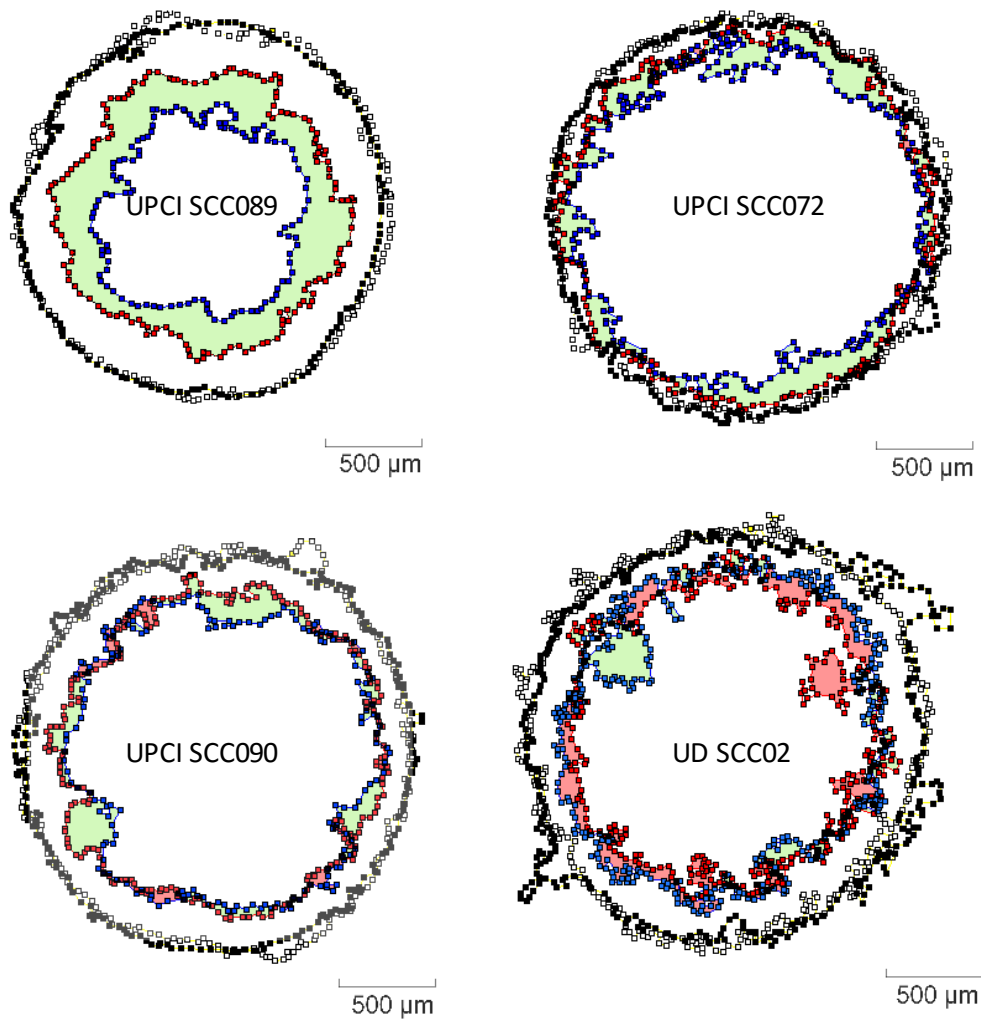


Figure 2.5: Overlay images of first experimental repeat of ORIS™ assay migrations for DENO8 Medium 2-induced migrations versus unstimulated fibroblast control. Note that both HPV-positive cell lines (UPCI SCC072, UPCI SCC089) demonstrate a clear net increase in migration compared to control, whereas both HPV-positive lines (UD SCC02, UPCI SCC090) show no evidence of additional migration, despite control migration being intermediate to that observed in the two HPV-negative cell lines. All migration endpoints taken at 48 h, other than UPCI SCC089 (taken at 20 h).

Black squares - position of void margin at baseline for incubation with Medium 2
White squares – position of void margin at baseline for control medium
Blue squares – end position of void margin, Medium 2
Red squares – end position of void margin, control medium
Green area – additional closure with Medium 2
Pink area – additional closure with control

Figure 2.6: MTS Assay of HPV-positive Cell Line Proliferation in Response to Stimulated Fibroblast Medium 2 Versus Unstimulated Fibroblast Control

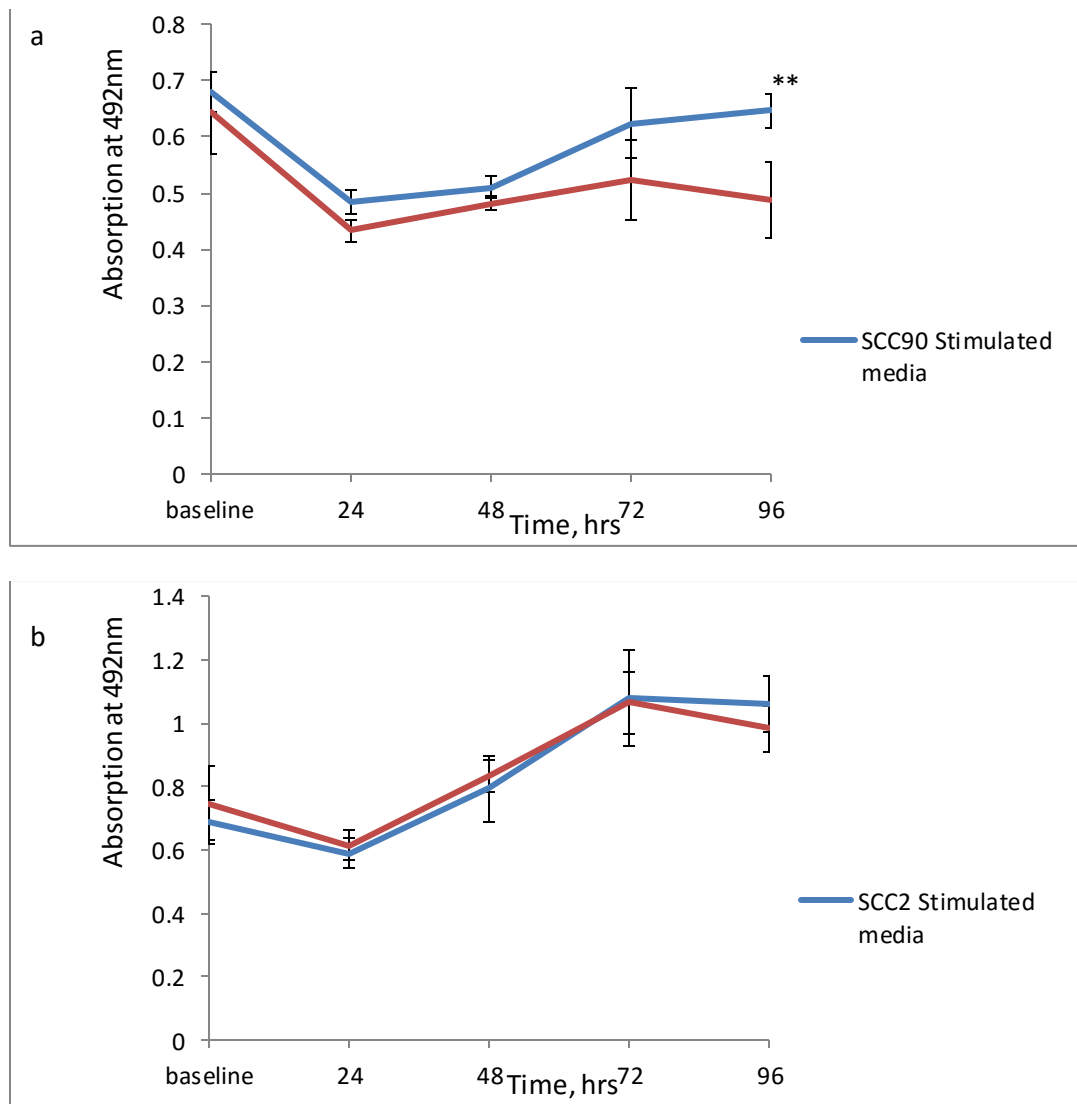


Figure 2.6: Graphs depicting MTS assay absorbance of HPV-positive cell lines UD SCC02 (a) and UPCI SCC090 (b), following incubation with DENO08 stimulated fibroblast Medium 2 versus control (light absorption at 492 nm). Blue lines denote absorbance following incubation in stimulated fibroblast Medium 2, red lines denote absorbance using control medium. Error bars denote S.E.M. * = significance at 0.05, **= significance at 0.01 (Independent samples T-test, following Levene’s test to confirm equal variance). n=9

Note that baseline absorbance was measured using respective conditioned medium due to cells remaining in suspension, whereas all other timepoints were measured following PBS wash and replacement with normal media: variation at baseline may therefore be attributed to differences in conditioned medium background absorbance. Note the significant increase in absorbance ($P < 0.01$) with cell line UPCI SCC090 at 96 hours. No significant change was noted for cell line UD SCC02.

Figure 2.7: MTS Assay of HPV-negative Cell Line Proliferation in Response to Stimulated Fibroblast Medium 2 Versus Unstimulated Fibroblast Control

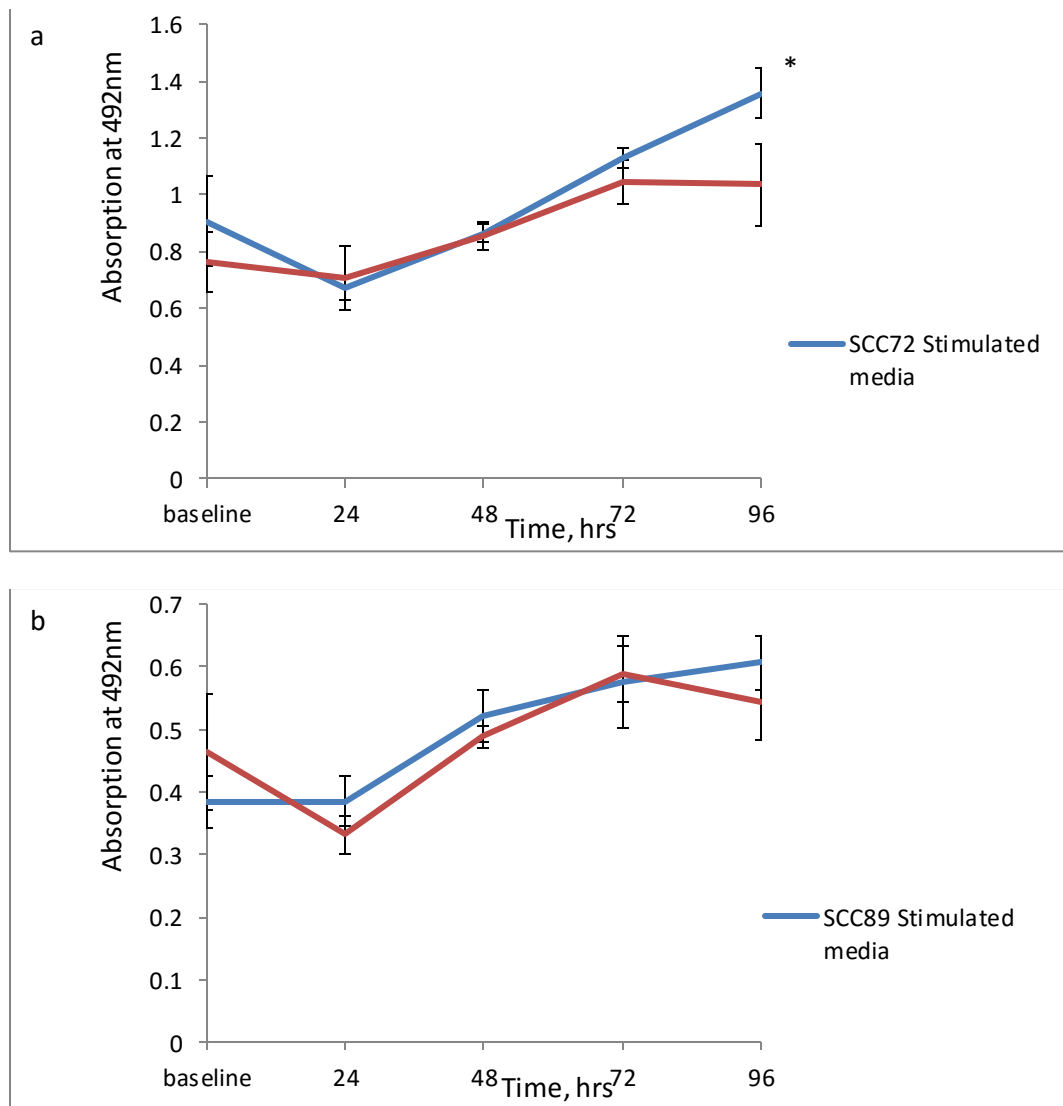


Figure 2.7: Graphs depicting MTS assay absorbance of HPV-negative cell lines UPCI SCC072 (a) and UPCI SCC089 (b), following incubation with DENOFO8 stimulated fibroblast Medium 2 versus control (light absorption at 492 nm). Blue lines denote absorbance following incubation in stimulated fibroblast Medium 2, red lines denote absorbance using control medium. Error bars denote S.E.M. * = significance at 0.05, **= significance at 0.01 (Independent samples T-test, following Levene’s test to confirm equal variance). n=9

Note that baseline absorbance was measured using respective conditioned medium due to cells remaining in suspension, whereas all other timepoints were measured following PBS wash and replacement with normal media: variation at baseline may therefore be attributed to differences in conditioned medium background absorbance. Note the significant increase in absorbance ($P < 0.05$) with cell line UPCI SCC072 at 96 hours. No significant change was noted for cell line UPCI SCC089.

Discussion

HPV-negative cell lines were observed to induce a fibroblast response capable of promoting additional void closure in contemporary 2D migration assays. Although Medium 2 consistently induced migration in both HPV-negative cell lines throughout the range of fibroblasts tested, Medium 1 was observed to also induce migration in the cell line UPCI SCC072. The significance of the additional migration in UPCI SCC072 Medium 1 is uncertain based on the data presented in this chapter; although this phenomenon may be linked to an inductive pathway unique to UPCI SCC072/fibroblast interactions, it is also plausible that the underlying molecular basis of increased migration with UPCI SCC072 Medium 1 is the same as that observed for Medium 2. The temporality of factor secretion in response to UPCI SCC072 versus UPCI SCC089 conditioned medium may either differ, or alternatively UPCI SCC089 Medium 1 may constitutively repress additional migration through factor inhibition or alternatively nutrient depletion.

All cell lines other than UPCI SCC072 demonstrated a general trend of reduced migration in the presence of Medium 1 compared to control medium, suggesting that media exhaustion may have occurred as a result of the preceding 48 h incubation with near confluent cell lines/fibroblast cultures. Due to limitations relating to keratinocyte incompatibility with normal media, control media was not exposed to a suitable epithelial equivalent prior to incubation with fibroblasts: control conditioned medium nutrient and metabolite content may therefore be more favourable than experimental media, leading to the suboptimal migrations observed in cell lines other than UPCI SCC072.

HPV-positive cell lines demonstrated no additional migration in response to either Medium 1 or 2. Lack of response may reflect either inability to induce fibroblast secretion of factors supportive of migration, inability of the cell lines to respond in the same manner as HPV-negative cell lines, or alternatively a combination of both reduced fibroblast induction and also reduced cell line responsiveness.

An apparent anomaly exists between the behaviour of the HPV-positive cell lines observed *in-vitro* in response to stimulated fibroblast medium and the clinical observation that HPV-positive disease presents at a more advanced stage than HPV-negative disease. Whilst this conflict may arguably undermine the validity of our model of HPV-positive disease, which as previously stated undoubtedly carries the flaws associated with the acquired cell lines being

derived from smokers, a number of points exist to corroborate the model. Foremost, our model references *additional*, rather than *absolute* migration; therefore, whilst HPV-positive cell lines demonstrated no *additional* migration compared to their own respective internal control exposed to unstimulated fibroblast medium (Figure 2.3), the cell lines can clearly be seen to outstrip the *absolute* migration of HPV-negative cell line UPCI SCC072 in the overlay images presented in Figure 2.5. Our data therefore offer the proposition that HPV-negative disease utilises factors from the microenvironment to assist migration whereas HPV positive disease does not; it should be made clear that the *absolute* invasiveness of HPV-positive versus HPV-negative disease bears no direct relation to these observations.

Furthermore, the overall migratory rates of each cell line in the presence of stimulated fibroblast medium may not be robustly comparable in 2D, and may also translate poorly to a three dimensional, anatomical setting; the presented data therefore more appropriately demonstrate the ability of HPV-negative lines to induce stromal support, and respond to that support through increased motility. This interaction may have major implications in the distant spread of disease, whereby HPV-negative tumour cells may retain potential to more rapidly prime and respond to the stromal milieu, leading to greater potential for cancer progression through extracapsular spread and production of viable metastasis, and may also provide local resilience to conventional therapeutics²⁷⁷.

The biological significance of the finding that HPV-positive disease presents at a more advanced stage than its HPV-negative counterpart remains uncertain. Indeed, this finding does not translate to the most pertinent of clinical measures, that is, patient survival. A number of socio-economic and cultural confounders, in addition to greater anatomical plasticity linked to the more youthful HPV-positive patient base, may lead to a more delayed period from carcinogenesis to the threshold at which symptoms prompt clinical assessment. The static measure of tumour stage at the time of clinical presentation may therefore not correlate with migration/invasion at a cellular level, which may markedly influence outcome in the manner described above.

MTS assay data (Figure 2.7) demonstrated no characteristic difference in proliferation between HPV-positive and -negative cell lines in response to respective stimulated fibroblast medium. Cell lines UPCI SCC072 and UPCI SCC90 showed evidence of increased cell proliferation at 96 h in the presence of conditioned media, although all other timepoints showed no significant difference to control. Cell lines UD SCC02 and UPCI SCC089 demonstrated no significant difference to control throughout all timepoints. It was however

noted that all cell lines demonstrated a general trend of increased proliferation at 96 h, albeit not statistically significant for cell lines UD SCC02 and UPCI SCC090.

The magnitude of effect linked to the DENOF08 fibroblast culture warrants its use in further experiments to ascertain the nature of the observed migratory phenomenon. The marked influence of UPCI SCC072-activated DENOF08 Medium 1, in addition to UPCI SCC089-activated DENOF08 Medium 2 outcompeting NTF1 and NTF6, allows DENOF08 to be considered the most useful fibroblast culture of the three cultures used in this chapter.

Chapter 3: Cytokine Array Analysis of Tumour & Fibroblast Conditioned Media

Introduction

Data presented in Chapter 2 demonstrated that conditioned media from the HPV-negative cell lines UPCI SCC072 and UPCI SCC089 induced a fibroblast secretory response supportive of cell migration. In terms of the microenvironment in head and neck disease, much interest resides in TGF- β as a major factor underlying microenvironmental activity and tumour motility through the induction of EMT²⁷⁸⁻²⁸¹. Moreover, studies have highlighted a link between TGF β R1 gene expression and susceptibility to HPV-positive oropharyngeal carcinoma²⁸², in addition to TGF β 1 T869C polymorphisms being linked to a HPV-positive oropharyngeal carcinoma status²⁸³, and viral oncoproteins E6 & E7 inducing TGF β 1 promoter activation²⁸⁴. TGF β is therefore an enticing factor to study in relation to our data, although this HPV-specific relationship infers that greater EMT (and therefore motility) would be expected in HPV-positive tumours. Conversely, recent data suggest that HPV-negative tumours more commonly express markers of EMT²⁸⁵; this is more in keeping with the findings of Chapter 2. Levovitz *et al* found TGF β 1 to be expressed greater in oropharyngeal carcinoma than in HPV-positive head and neck cancer; the virally heterogenous status of the “oropharyngeal carcinoma”, as opposed to “HPV-positive head and neck cancer” could suggest that in fact HPV-negative oropharyngeal tumours therefore express greater TGF β 1 than HPV-positive tumours²⁸².

As briefly reviewed in Chapter 2, a recent article by Hassona *et al* found that conditioned medium from genetically unstable oral cancer cell lines (“GU-OSCC”; defined as those lines carrying greater mutations, with particular reference to p53 and p16) readily induced fibroblast expression of markers of cellular senescence²⁴⁰. Conditioned medium taken from senescent fibroblasts also had a more profound effect on GU-OSCC cell line invasion into collagen gels when compared to media taken from normal oral fibroblasts. A key feature of genetically unstable head and neck cancers as a group of heterogenous, yet comparably aggressive diseases may therefore be the ability to instruct underlying stroma to create an environment supportive of tumour cell invasion; this is in-keeping with our observations for HPV-negative cell lines. As has been discussed in the literature review, HPV-positive oropharyngeal carcinomas carry fewer mutations than their HPV-negative counterparts due

to viral E6 and E7 proteins acting to bypass a number of critical mutational steps necessary for carcinogenesis. In addition to the avoidance of highly specific gene mutations, namely that of p53 and RB1, HPV-positive disease has also been shown to carry lower overall genetic aberrations, both in terms of number and degree of mutations¹⁶⁹. The relative genetic stability of HPV-positive oropharyngeal carcinoma suggests that behaviour may be comparable to other genetically stable tumours, and microenvironmental interactions may therefore be reduced. Hassona's principal conclusions were that the induction of TGF- β expression by fibroblasts occurred in response to Reactive Oxygen Species (ROS), and was linked to the support of tumour invasion.

Whilst the definition of genetically stable and unstable cancers closely parallel the features that characteristically distinguish HPV-positive versus -negative oropharyngeal carcinoma as a result of viral oncogene activity (that is, wild-type p53 and elevated p16), and therefore make TGF- β an enticing factor for consideration of the migratory phenomena discussed in Chapter 2, a proportion of Hassona *et al*'s work on the mechanisms of migratory support is circumstantial. For example, the authors found 8-oxo-dG (a marker of oxidative stress) to be elevated in fibroblasts expressing SA β -Gal and p16 – from this, Hassona concluded that senescence was a direct result of the oxidative stress. Whilst oxidative stress is indeed a recognised aetiological agent in the precipitation of fibroblast senescence²⁸⁶, Hassona merely supplied evidence of correlation rather than causality in terms of fibroblast senescence, although did demonstrate that malignant keratinocyte collagen gel invasion in response to senescent fibroblast conditioned medium became partially inhibited with the addition of the antioxidant, PBN (phenyl-alpha-tert-butyl nitron). A further factor could however plausibly contribute to a significant proportion of the senescence observed by the authors. Similarly, anti-TGF- β antibody led to an approximate 50% reduction of fibroblast senescence in the presence of conditioned medium (the remainder of senescence induction left unaccounted for), as measured in the presence of conditioned medium from only a single cell line; H357. Furthermore, although data presented with respect to 3D collagen gel invasion correlated to the fibroblast senescence profile, the data were neither demonstrated to be reliant on senescence, nor was it demonstrated to be linked to any specific factor.

Given the uncertainty underlying the final effectors driving cell line migration in Hassona's work, in addition to confirmation of a number of correlations rather than causal links, potential for a factor other than TGF- β was considered in relation to our data. Whilst TGF- β remained of interest as a potential driver of the observed migrations, a broader screen of

conditioned media appeared a measured approach compared to more specific analyses such as TGF- β ELISA.

A number of techniques offered a broader screen for candidate molecules, including mass spectrometry, cytokine array and cytometric bead array. Of the available tests, cytokine array analysis was considered the most suitable, due to the ability to screen for several hundred factors in a single experiment, in addition to being comparatively cheap and requiring only standard laboratory equipment. Each technique listed above, including cytokine array, has a number of limitations. Mass spectrometry requires highly specialist equipment and technician time, along with generating data that relate to the probability of each spectrometry peak being due to a specific factor, rather than displaying absolute factor specificity. Cytometric bead array analysis, whilst still requiring relatively specialist equipment, is a more accessible option and maintains the advantage over standard cytokine array techniques in that data are quantitative, with a high degree of intra- and inter-assay precision²⁸⁷; the number of factors included in a single screen is however limited to around 30²⁸⁸. Whilst cytokine array advantages have been discussed above, a limitation is the generation of semi-quantitative data – further quantitative analysis of factors of interest, for example, via ELISA, is therefore necessary. As an initial screen, the advantages of cytokine array analysis were considered to outweigh the disadvantages relating to semi-quantitative analysis and was therefore undertaken on cell line conditioned medium, in addition to stimulated fibroblast Medium 2 for lines UD SCC02, UPCI SCC072, UPCI SCC089 and UPCI SCC090. A further cytokine array analysis of UPCI SCC072-stimulated fibroblast Medium 1 was also considered of value, due to the unique capacity of this conditioned medium to induce additional cell line migration in ORIS™ assay (please refer to Chapter 2, Figures 2.2 & 2.4).

Methods

Collection of Serum-Free Cell Line Conditioned Medium

Cell lines UD SCC02, UPCI SCC072, UPCI SCC089 and UPCI SCC090 were grown to near confluence in normal media (DMEM plus 10 % FCS, with 2mM L-glutamine & 50 IU/50 $\mu\text{g mL}^{-1}$ penicillin-streptomycin), washed X3 in PBS and then incubated with 7 mL serum-free normal media for 24 h. After 24 h, conditioned medium was aspirated from each flask and centrifuged for 5 minutes at 3,000 rpm in order to remove cellular debris. 6 mL supernatant was then carefully aspirated in order to avoid resuspension of precipitated debris, and then immediately stored at $-21\text{ }^{\circ}\text{C}$ in a universal container until use in experiments.

Flasks were washed X2 in PBS, trypsinised and then cells counted in order to calculate the number of cells contributing to each mL of conditioned media. Conditioned medium was then normalised in the same manner as described in Chapter 2, methods section M2.1, with a final normalised count of 2.7 million cells mL^{-1} conditioned medium. A slightly reduced count compared to serum-containing conditioned medium was accounted for as a result of serum starvation over the incubation period.

Collection of Serum-Free Stimulated DENO08 Conditioned Medium

Serum-free cell line conditioned medium was collected as described above. 75 cm^2 flasks of passage 7 DENO08 fibroblasts were cultured to early confluence washed X3 in PBS and then incubated for 24 h with 6 mL respective serum-free cell line conditioned medium, or a serum-free normal media control. After 24 h, serum-free Medium 1 was aspirated from each flask and centrifuged for 5 minutes at 3,000 rpm in order to remove cellular debris. 5 mL supernatant was then carefully aspirated in order to avoid resuspension of precipitated debris, and then immediately stored at $-21\text{ }^{\circ}\text{C}$ in a universal container until use in experiments. Fibroblast cultures were then washed X3 in PBS and incubated with 6mL fresh serum-free normal media for a further 24 h in order to retrieve a serum-free Medium 2. Again, Medium 2 was aspirated, centrifuged and stored as outlined for Medium 1. Fibroblast cultures were then washed X2 in PBS, trypsinised and a final cell count undertaken to confirm equal cell population sizes in each flask, contributing to conditioned medium of 4×10^5 cells mL^{-1} .

Serum-free normal media from the same stock was used for all conditioned media collected from both cell lines and fibroblast cultures.

Cytokine Array Analysis of Conditioned Media

Cell line conditioned media and Medium 2 for all cell lines were thawed immediately prior to experiments, along with Medium 1 derived from cell line UPCI SCC072, due to its exclusive capacity to induce cell migration compared to Medium 1 derived from all other cell lines. A more comprehensive approach of cytokine array analysis of Medium 1 for all lines was deemed cost-prohibitive. Respective controls were also thawed, namely, serum-free normal media (cell line conditioned medium control) and unstimulated fibroblast conditioned medium control (control for Media 1/2).

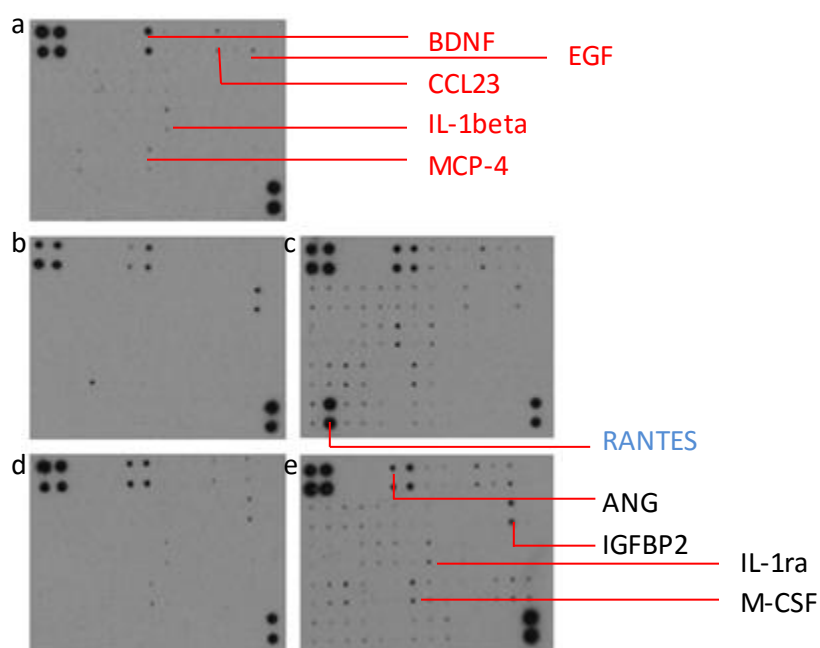
Raybiotech C2000 Human Cytokine Arrays (Raybiotechnology, Norcross, USA, cat number: AAH-CYT-2000) were purchased from a UK distributor (Insight Biotechnology, Middlesex, UK). Each C2000 kit comprised a 174-probe assay derived from 3 separate assay membranes (C6, C7 and C8) also available for separate purchase from Raybiotech. Manufacturer's instructions were adhered to throughout experimentation.

Each Raybiotech cytokine array kit was thawed to room temperature, and cytokine array membranes placed in separate wells of the manufacturer-supplied Incubation Tray. 2 mL Blocking Buffer was then pipetted over each membrane and incubated for 20 minutes at room temperature using a rocking machine. Blocking buffer was then aspirated, and 1 mL undiluted conditioned medium pipetted into each respective well and incubated overnight for 18 h at 4 °C on a rocking machine. Samples were then aspirated from each well, and membranes washed with 2 mL 1 X Wash Buffer 1, and incubated at room temperature for 5 minutes on a rocking machine. A further two repeat washes using Wash Buffer 1 were undertaken, followed by two further 5 minute washes using Wash Buffer 2. Complete buffer aspiration was carefully undertaken between washes. 1 mL freshly-prepared biotinylated antibody cocktail was then pipetted into each well and incubated for 1.5 hours at room temperature. The antibody cocktail was then carefully aspirated, and a further 3 X Wash Buffer 1 & 2 X Wash Buffer 2 washes undertaken as outlined above. 2 mL 1 X HRP-streptavidin solution was then incubated with each membrane for 2 h at room temperature and then carefully aspirated from each well. A third wash using Wash Buffers 1 & 2 as outlined above was then undertaken, and then membranes transferred printed side up onto tissue paper. Excess wash buffer

was then carefully blotted along the edges of each membrane to retrieve excess wash buffer, and membranes transferred onto cling film. Detection Buffer items C & D were then mixed in equal volumes and 500 μ L solution carefully pipetted onto each membrane for 2 minutes before covering and then processed using standard radiographic film following 1, 2 and 5 minute exposures. Developed films were then scanned at high resolution and analysed using Quantity One software (Version 4.5.0; Bio-Rad, Hertfordshire, UK). Densitometry data were then normalised to positive/negative control spot densitometry undertaken on appropriate control arrays (serum-free normal media for cell line conditioned medium arrays, serum-free unstimulated fibroblast conditioned medium for Media 1&2 arrays).

Results

Figure 3.1: Raybiotech C6 Cytokine Array Analysis of Tumour Line Conditioned Media



	A	B	C	D	E	F	G	H	I	J	K	L	M	N
1	POS	POS	NEG	NEG	BLANK	ANG	BDNF	BLC	BMP 4	BMP 6	CCL23	CNTF	EGF	Eotaxin 1
2	POS	POS	NEG	NEG	BLANK	ANG	BDNF	BLC	BMP 4	BMP 6	CCL23	CNTF	EGF	Eotaxin 1
3	Eotaxin 2	Eotaxin 3	FGF-6	FGF-7	Flt-3 Ligand	Fractalkine	GCP-2	GDNF	GM CSF	I-309	IFN gamma	IGFBP 1	IGFBP 2	IGFBP 4
4	Eotaxin 2	Eotaxin 3	FGF-6	FGF-7	Flt-3 Ligand	Fractalkine	GCP-2	GDNF	GM CSF	I-309	IFN gamma	IGFBP 1	IGFBP 2	IGFBP 4
5	IGF-1	IL-10	IL-13	IL-15	IL-16	IL-1 alpha	IL-1 beta	IL-1ra	IL-2	IL-3	IL-4	IL-5	IL-6	IL-7
6	IGF-1	IL-10	IL-13	IL-15	IL-16	IL-1 alpha	IL-1 beta	IL-1ra	IL-2	IL-3	IL-4	IL-5	IL-6	IL-7
7	Leptin	LIGHT	MCP-1	MCP-2	MCP-3	MCP-4	M-CSF	MDC	MIG	MIP-1 delta	MIP-3 alpha	NAP-2	NT-3	PARC
8	Leptin	LIGHT	MCP-1	MCP-2	MCP-3	MCP-4	M-CSF	MDC	MIG	MIP-1 delta	MIP-3 alpha	NAP-2	NT-3	PARC
9	PDGF BB	RANTES	SCF	SDF-1 alpha	TARC	TGF beta 1	TGF beta 3	TNF alpha	TNF beta	BLANK	BLANK	BLANK	BLANK	POS
10	PDGF BB	RANTES	SCF	SDF-1 alpha	TARC	TGF beta 1	TGF beta 3	TNF alpha	TNF beta	BLANK	BLANK	BLANK	BLANK	POS

Figure 3.1: RayBiotech cytokine array C6 analysis of serum-free conditioned medium taken from cell lines UD SCC02, UPCI SCC072, UPCI SCC089 and UPCI SCC090.

- a. Serum-free DMEM control
- b. UPCI SCC072 conditioned medium (HPV-negative)
- c. UPCI SCC089 conditioned medium (HPV-negative)
- d. UD SCC02 conditioned medium (HPV-positive)
- e. UPCI SCC090 conditioned medium (HPV-positive)

Inferior table: array map, reproduced with kind permission of Raybiotechnology (Norcross, USA).

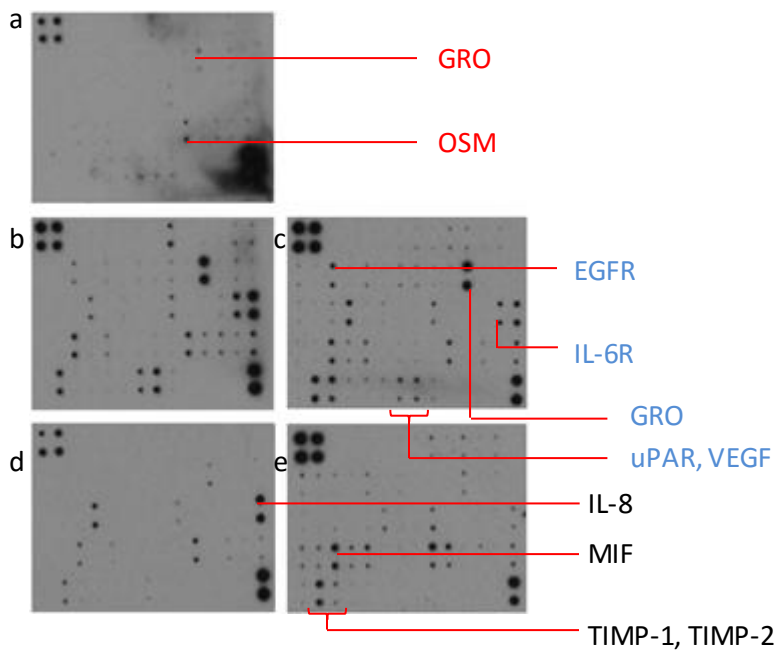
Red text denotes positive spots on normal media control array, signifying high background absorbance, blue text denotes RANTES upregulated more significantly in a single HPV-negative cell line medium, black text denotes factors present in all cell line-derived media but absent from normal media control.

Note the absence of any consistent trend in cytokine release by HPV-positive, versus HPV-negative cell lines (images d & e versus b & c, respectively). An isolated, yet marked, uptake for RANTES was noted in line UPCI SCC089 (image c). Note also absence of TGF- β 1/3 absorption throughout the samples.

C6 arrays for cell lines UPCI SCC072 (HPV-negative, image b) and UD SCC02 (HPV-positive, image d) demonstrate no significant uptake other than for ANG, BDNF, EGF, CLL23, IL-1ra and IGFBP2 (densitometries summarised along with RANTES in Figure 3.7), all of which do not demonstrate any pattern of uptake between HPV-positive and -negative cell lines. Although high intensity uptake is noted for BDNF in all cell line conditioned media, a comparable densitometry measurement of BDNF can also be observed in serum-free DMEM control (image a, above, also illustrated in figure 3.7). The absorbance for BDNF was therefore regarded as background uptake. Similar background absorbencies can also be seen for EGF, CCL23, IL-1beta and MCP-4. Indeed, further investigation by ELISA (please refer to Chapter 6, Figure 6.9) proved all cell line conditioned media to contain undetectable levels of EGF.

Cell lines UPCI SCC072 (image c, HPV-negative) and UPCI SCC090 (image e, HPV-positive) can be observed to have a small degree of uptake in most array spots. This was regarded as background uptake, and did not follow a consistent pattern with the other cell line conditioned media (images b and d).

Figure 3.2: Raybiotech C7 Cytokine Array Analysis of Tumour Line Conditioned Media



	A	B	C	D	E	F	G	H	I	J	K	L	M	N
1	POS	POS	NEG	NEG	BLANK	Acrp30	AgRP	ANGPT2	AREG	Axl	bFGF	b-NGF	BTC	CCL28
2	POS	POS	NEG	NEG	BLANK	Acrp30	AgRP	ANGPT2	AREG	Axl	bFGF	b-NGF	BTC	CCL28
3	CTACK	Dtk	EGFR	ENA-78	Fas	FGF-4	FGF-9	G-CSF	GITR Ligand	GITR	GRO	GRO alpha	HCC-4	HGF
4	CTACK	Dtk	EGFR	ENA-78	Fas	FGF-4	FGF-9	G-CSF	GITR Ligand	GITR	GRO	GRO alpha	HCC-4	HGF
5	ICAM-1	ICAM-3	IGFBP 3	IGFBP 6	IGF-1 sR	IL-1 R4	IL-1 R1	IL-11	IL-12 p40	IL-12 p70	IL-17	IL-2 R alpha	IL-6 R	IL-8
6	ICAM-1	ICAM-3	IGFBP 3	IGFBP 6	IGF-1 sR	IL-1 R4	IL-1 R1	IL-11	IL-12 p40	IL-12 p70	IL-17	IL-2 R alpha	IL-6 R	IL-8
7	I-TAC	XCL1	MIF	MIP-1 alpha	MIP-1 beta	MIP-3 beta	MSP alpha	NT-4	OPG	OSM	PLGF	sgp130	sTNFRII	sTNFRI
8	I-TAC	XCL1	MIF	MIP-1 alpha	MIP-1 beta	MIP-3 beta	MSP alpha	NT-4	OPG	OSM	PLGF	sgp130	sTNFRII	sTNFRI
9	TECK	TIMP-1	TIMP-2	THPO	TRAIL R3	TRAIL R4	uPAR	VEGF	VEGF-D	BLANK	BLANK	BLANK	BLANK	POS
10	TECK	TIMP-1	TIMP-2	THPO	TRAIL R3	TRAIL R4	uPAR	VEGF	VEGF-D	BLANK	BLANK	BLANK	BLANK	POS

Figure 3.2: RayBiotech cytokine array C7 analysis of serum-free conditioned medium taken from cell lines UD SCC02, UPCI SCC072, UPCI SCC089 and UPCI SCC090.

- a. Serum-free DMEM control
- b. UPCI SCC072 conditioned medium (HPV-negative)
- c. UPCI SCC089 conditioned medium (HPV-negative)
- d. UD SCC02 conditioned medium (HPV-positive)
- e. UPCI SCC090 conditioned medium (HPV-positive)

Inferior table: array map, reproduced with kind permission of Raybiotechnology (Norcross, USA).

Red text denotes positive spots on normal media control array, signifying high background absorbance, blue text denotes factors upregulated more significantly in HPV-negative cell line media,

black text denotes factors present in all cell line-derived media but absent from normal media control.

Note presence of developer solution contamination and “bleed-through” from positive control spots in the lower right quadrant of the serum-free DMEM control array (image a). More nebulous regions of developer contamination can also be observed in the superior and inferior central aspects of the control array. This led to a high control densitometry reading of array spots in each of the 3 aforementioned regions (C7 densitometry is summarised in Figure 3.8). The marked contamination of the lower right quadrant prompted censorship of the respective positive control spots, with the 4 positive control spots sited in the upper left quadrant being used in isolation for means of densitometry normalisation. All other spots directly contaminated by the main point of developer uptake represented blank arrays, as depicted in the lower right quadrant of the C7 array map (inferior image, courtesy of Raybiotechnology, Norcross, USA). The contamination therefore led to minor over-representation of control medium cytokine content for the associated spots. Minimal evidence of developer contamination is noted for cell line conditioned media other than the superior right region of cell line UPCI SCC072 and the inferior central region of cell line UPCI SCC089.

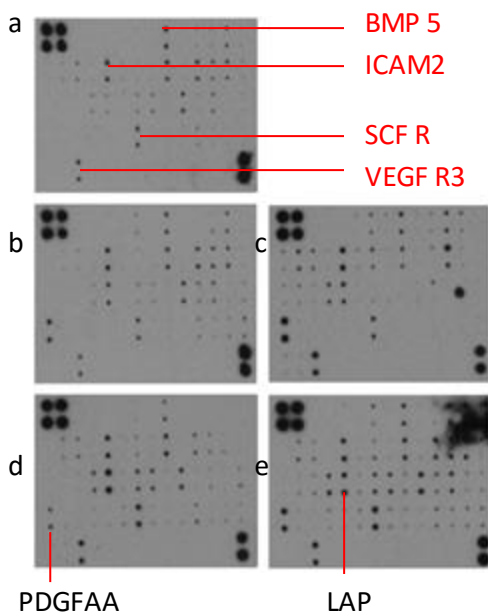
Despite the limitations linked to contamination of the control array, background uptake can be observed in control array spots for GRO and (more notably) OSM. The comparable uptake of OSM in control medium in proportion to cell line conditioned media, undermines the significance of this cytokine array spot, as can be further observed in the unstimulated fibroblast control C7 array (Figure 3.5); the high background cytokine array absorbance for OSM shall be discussed further in Chapter 5, in the context of OSM ELISA findings (Figure 5.2).

Note marked uptake in both HPV-negative cell line conditioned media (images b & c) for GRO, IL-6R and IL-8. IL-8 uptake is also noted in the conditioned medium of the HPV-positive cell line UPCI SCC02, although GRO and IL-6R uptake is minimal in both HPV-positive cell line conditioned medium arrays (images d & e). As the GRO- α specific array spot remains unstained, it can be inferred that the non-specific GRO array spot uptake in HPV-negative cell line conditioned media is a result of GRO- β /GRO- γ . EGFR, uPAR and VEGF are also elevated in HPV-negative cell line conditioned media.

In summary, a number of factors characteristic of all cell line conditioned media were noted, including MIF, TIMP-1 and TIMP-2. HPV-negative lines UPCI SCC072 and UPCI SCC089 secreted a number of additional factors, including GRO, IL-6R, EGFR, uPAR and VEGF. These additional factors are consistent with a more aggressive tumour profile (please refer to the discussion section for further consideration of these factors).

A number of the aforementioned factors, namely GRO, uPAR and VEGF, were also noted to be induced in fibroblast populations as a result of stimulation with cell line-derived conditioned media (please refer to Figure 3.5), suggesting that both autocrine and paracrine stimulation by a common inducing factor may be responsible for the release of these cytokines in both cell lines and fibroblasts.

Figure 3.3: Raybiotech C8 Cytokine Array Analysis of Tumour Line Conditioned Media



	A	B	C	D	E	F	G	H	I	J	K	L	M	N
1	POS	POS	NEG	NEG	BLANK	Activin A	ALCAM	CD80	BMP 5	BMP 7	CT-1	CD14	CXCL16	DR6
2	POS	POS	NEG	NEG	BLANK	Activin A	ALCAM	CD80	BMP 5	BMP 7	CT-1	CD14	CXCL16	DR6
3	Endoglin	ErbB3	E Selectin	Fas Ligand	ICAM 2	IGF-2	IL-1 R 2	IL-10 R beta	IL-13 R alpha 2	IL-18 BP alpha	IL-18 R beta	MMP 3	IL-2 R beta	IL-2 R gamma
4	Endoglin	ErbB3	E Selectin	Fas Ligand	ICAM 2	IGF-2	IL-1 R 2	IL-10 R beta	IL-13 R alpha 2	IL-18 BP alpha	IL-18 R beta	MMP 3	IL-2 R beta	IL-2 R gamma
5	IL-21 R	IL-5 R alpha	IL-9	IP-10	LAP	Leptin R	LIF	L Selectin	M-CSF R	MMP 1	MMP 13	MMP 9	MPIF-1	NGFR
6	IL-21 R	IL-5 R alpha	IL-9	IP-10	LAP	Leptin R	LIF	L Selectin	M-CSF R	MMP 1	MMP 13	MMP 9	MPIF-1	NGFR
7	PDGF AA	PDGF AB	PDGFR alpha	PDGFR beta	PECAM 1	PRL	SCFR	SDF-1 beta	Siglec 5	TGF alpha	TGF beta 2	TIE-1	TIE-2	TIMP-4
8	PDGF AA	PDGF AB	PDGFR alpha	PDGFR beta	PECAM 1	PRL	SCFR	SDF-1 beta	Siglec 5	TGF alpha	TGF beta 2	TIE-1	TIE-2	TIMP-4
9	VE Cadherin	VEGF R2	VEGF R3	BLANK	BLANK	BLANK	BLANK	BLANK	BLANK	BLANK	BLANK	BLANK	BLANK	POS
10	VE Cadherin	VEGF R2	VEGF R3	BLANK	BLANK	BLANK	BLANK	BLANK	BLANK	BLANK	BLANK	BLANK	BLANK	POS

Figure 3.3: RayBiotech cytokine array C8 analysis of serum-free conditioned medium taken from cell lines UD SCC02, UPCI SCC072, UPCI SCC089 and UPCI SCC090.

- a. Serum-free DMEM control
- b. UPCI SCC072 conditioned medium (HPV-negative)
- c. UPCI SCC089 conditioned medium (HPV-negative)
- d. UD SCC02 conditioned medium (HPV-positive)
- e. UPCI SCC090 conditioned medium (HPV-positive)

Inferior table: array map, reproduced with kind permission of Raybiotechnology (Norcross, USA).

Red text denotes positive spots on normal media control array, signifying high background absorbance, blue text denotes factors upregulated more significantly in HPV-negative cell line media, black text denotes factors present in all cell line-derived media but absent from normal media control.

Note again, presence of developer solution contamination in the superior right field of image e (UPCI SCC089). Contamination did not preclude overall interpretation of the C8 array, due to absence of any pattern of array uptake being noted between images a-d in this region of the assay membrane other than for MMP 3, as discussed below.

A number of array spots appear to have background absorbencies, as observed in serum-free media (image a), including BMP-5, ICAM-2, IL-13 R alpha 2, IL-18R beta, MMP1, SCF R and VEGF R3.

Findings of the C8 array are by and large unremarkable under direct visual scrutiny, with much uptake in cell line conditioned medium being comparable to normal media control (image a). Uptake of PDGFAA and LAP did however appear to be consistently upregulated in cell line conditioned media, with some evidence of HPV-status specific effect (as shall be discussed further with respect to densitometry, Figure 3.9).

MMP 3, LIF and SCFR also returned HPV-status specific differences, although visual inspection of UPCI SCC90 cytokine array (image e) confirms that developer contamination is in the vicinity of the respective MMP 3 array spot, leading to censorship of data for this cell line. HPV-negative cell line MMP 3 densitometry was therefore only directly compared to UD SCC02, and status-specific differences cannot be considered as a reliable on this basis. LIF and SCFR both returned densitometry measures that were elevated for HPV-negative lines, although LIF densitometry was of a low magnitude, and SCFR background densitometry was relatively high, leaving potential for these observations to be artefactual.

Figure 3.4: Raybiotech C6 Cytokine Array Analysis of Simulated Fibroblast Conditioned Media

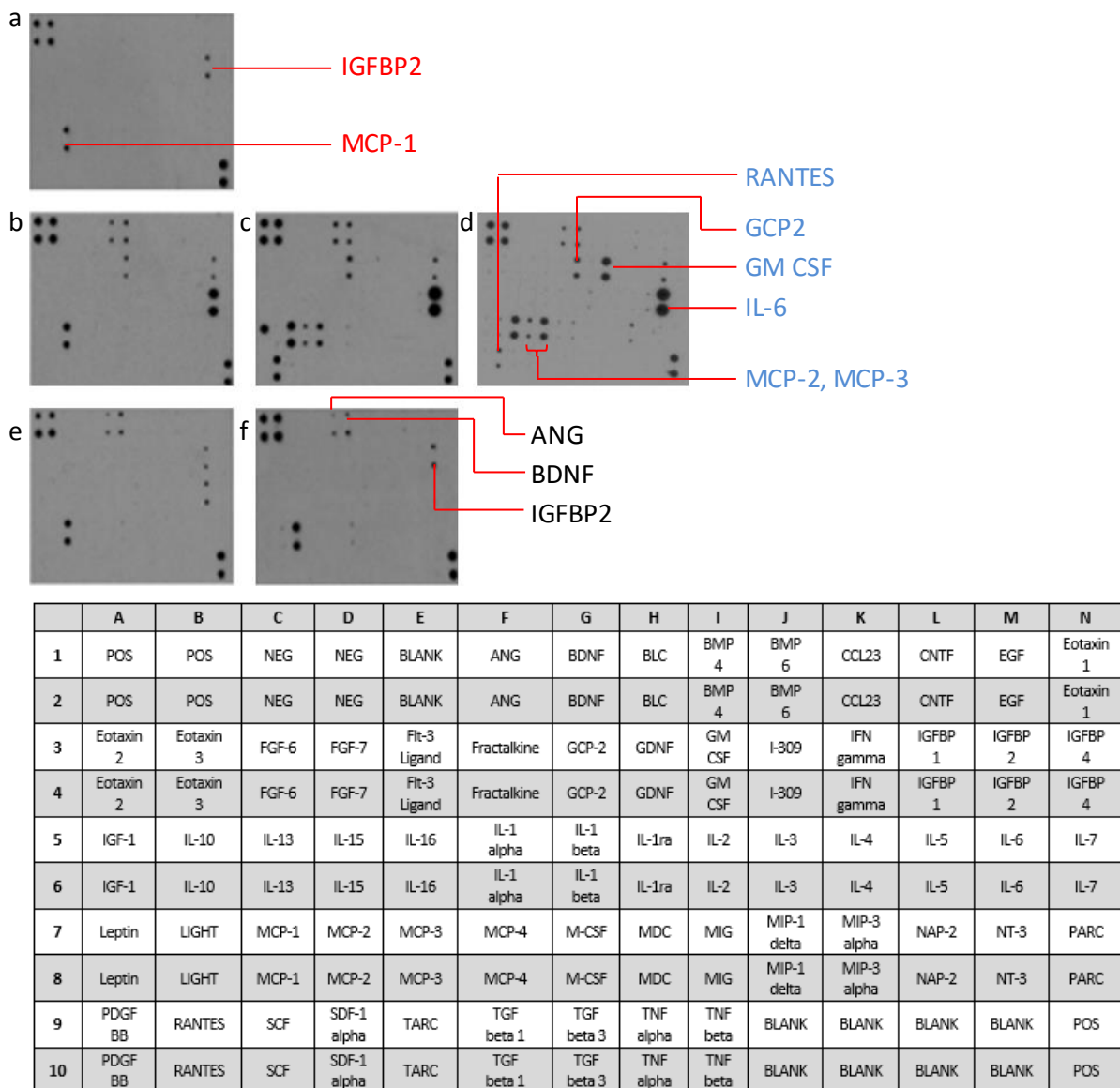


Figure 3.4: RayBiotech cytokine array C6 analysis of serum-free stimulated fibroblast medium taken after stimulation with cell lines UD SCC02, UPCI SCC072, UPCI SCC089 and UPCI SCC090.

- a. Serum-free unstimulated DENOFO8 fibroblast conditioned medium control
- b. UPCI SCC072-stimulated DENOFO8 Medium 2 (HPV-negative stimulated)
- c. UPCI SCC089-stimulated DENOFO8 Medium 2 (HPV-negative stimulated)
- d. UPCI SCC072-stimulated DENOFO8 Medium 1 (HPV-negative stimulated)
- e. UD SCC02-stimulated DENOFO8 Medium 2 (HPV-positive stimulated)
- f. UPCI SCC090-stimulated DENOFO8 Medium 2 (HPV-positive stimulated)

Inferior table: array map, reproduced with kind permission of Raybiotechnology (Norcross, USA).

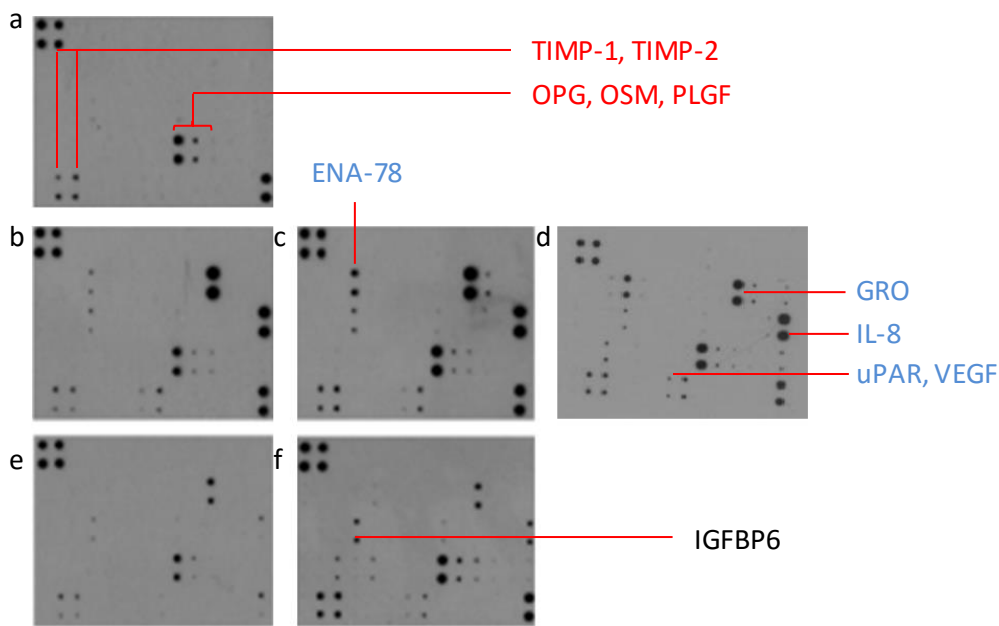
Red text denotes positive spots on unstimulated fibroblast medium control array, signifying basal secretion (please compare to Figure 3.1, which illustrates background absorbance due to normal media and excludes factors highlighted in red), blue text denotes factors upregulated more significantly in HPV-negative cell line media, black text denotes factors present in all cell line derived media but absent from normal media control.

Note the absence of BDNF, IL-1beta and MCP-4 background signals observed with serum free media (depicted in Figure 3.1) in the unstimulated fibroblast control (image a); this finding is inconsistent and not readily explained other than by experimental variability. IGFBP2 and MCP-1 (aka CCL2) are however observed to be present in unstimulated fibroblast control and absent in normal media control, suggesting that unstimulated fibroblasts secreted these two factors basally. BDNF is noted in all other media, which, on the basis of background uptake with the normal media control depicted in Figure 3.1, may be considered as further background uptake, although due consideration to the fact that this array spot is not observed in the unstimulated fibroblast control must be taken. Lack of developer solution on the unstimulated fibroblast control membrane could account for the absence of signal for BDNF, IL-1beta and MCP-4, although this appears unlikely given the consistent uptake in positive control spots, in addition to positive signals noted in all four quadrants of the array.

IL-6 and GCP2 can be observed to be elevated in all fibroblast conditioned media stimulated by HPV-negative lines, whereas these two factors are minimal in conditioned media stimulated by HPV-positive lines. RANTES and MCPs 2 & 3 (aka CCL8 and CCL7, respectively) can also be observed to be elevated in UPCI SCC089 Medium 2 (image c) and UPCI SCC072 Medium 1 (image d). The absence of RANTES and MCPs 2&3 from UPCI SCC072 Medium 2 suggests that the factors are secreted early in response to fibroblast stimulation. This finding, albeit with the lack of array data for Medium 1 derived from HPV-positive cell lines, infers that MCP 2&3 may still potentially be released from fibroblasts in response to HPV-negative cell line conditioned medium only.

UPCI SCC072 Medium 1 also demonstrated marked uptake of GM-CSF; again, the significance of this finding is uncertain without interrogating Medium 1 induced by the other cell lines.

Figure 3.5: Raybiotech C7 Cytokine Array Analysis of Simulated Fibroblast Conditioned Media



	A	B	C	D	E	F	G	H	I	J	K	L	M	N
1	POS	POS	NEG	NEG	BLANK	Acpr30	AgRP	ANGPT2	AREG	Axl	bFGF	b-NGF	BTC	CCL28
2	POS	POS	NEG	NEG	BLANK	Acpr30	AgRP	ANGPT2	AREG	Axl	bFGF	b-NGF	BTC	CCL28
3	CTACK	Dtk	EGFR	ENA-78	Fas	FGF-4	FGF-9	G-CSF	GITR Ligand	GITR	GRO	GRO alpha	HCC-4	HGF
4	CTACK	Dtk	EGFR	ENA-78	Fas	FGF-4	FGF-9	G-CSF	GITR Ligand	GITR	GRO	GRO alpha	HCC-4	HGF
5	ICAM-1	ICAM-3	IGFBP 3	IGFBP 6	IGF-1 sR	IL-1 R4	IL-1 R1	IL-11	IL-12 p40	IL-12 p70	IL-17	IL-2 R alpha	IL-6 R	IL-8
6	ICAM-1	ICAM-3	IGFBP 3	IGFBP 6	IGF-1 sR	IL-1 R4	IL-1 R1	IL-11	IL-12 p40	IL-12 p70	IL-17	IL-2 R alpha	IL-6 R	IL-8
7	I-TAC	XCL1	MIF	MIP-1 alpha	MIP-1 beta	MIP-3 beta	MSP alpha	NT-4	OPG	OSM	PLGF	sgp130	sTNFRII	sTNFRI
8	I-TAC	XCL1	MIF	MIP-1 alpha	MIP-1 beta	MIP-3 beta	MSP alpha	NT-4	OPG	OSM	PLGF	sgp130	sTNFRII	sTNFRI
9	TECK	TIMP-1	TIMP-2	THPO	TRAIL R3	TRAIL R4	uPAR	VEGF	VEGF-D	BLANK	BLANK	BLANK	BLANK	POS
10	TECK	TIMP-1	TIMP-2	THPO	TRAIL R3	TRAIL R4	uPAR	VEGF	VEGF-D	BLANK	BLANK	BLANK	BLANK	POS

Figure 3.5: RayBiotech cytokine array C7 analysis of serum-free stimulated fibroblast medium taken after stimulation with cell lines UD SCC02, UPCI SCC072, UPCI SCC089 and UPCI SCC090.

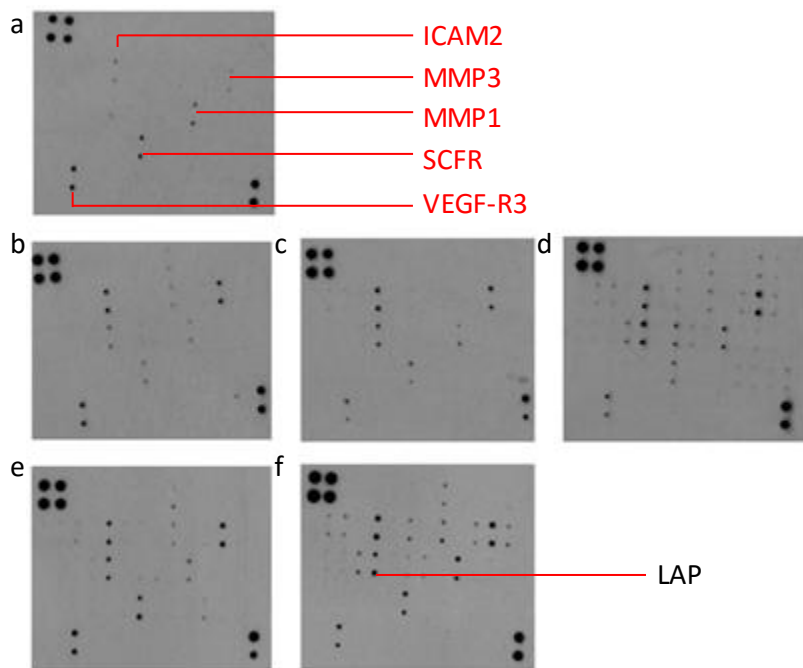
- a. Serum-free unstimulated DENOFO8 fibroblast conditioned media control
- b. UPCI SCC072-stimulated DENOFO8 Medium 2 (HPV-negative stimulated)
- c. UPCI SCC089-stimulated DENOFO8 Medium 2 (HPV-negative stimulated)
- d. UPCI SCC072-stimulated DENOFO8 Medium 1 (HPV-negative stimulated)
- e. UD SCC02-stimulated DENOFO8 Medium 2 (HPV-positive stimulated)
- f. UPCI SCC090-stimulated DENOFO8 Medium 2 (HPV-positive stimulated)

Inferior table: array map, reproduced with kind permission of Raybiotechnology (Norcross, USA).

Red text denotes positive spots on unstimulated fibroblast medium control array, signifying basal secretion (please compare to Figure 3.2, image a, which illustrates background absorbance due to normal media and excludes factors highlighted in red other than OSM), blue text denotes factors upregulated more significantly in HPV-negative cell line media, black text denotes factors present in all cell line derived media but absent from normal media control.

Note that a number of ligands which interact with CXCR-1/2 are released in HPV-negative stimulated fibroblast conditioned media, namely ENA78, GRO and IL-8. GCP2, noted to be elevated in HPV-negative stimulated media in Figure 3.4, is a further ligand of CXCRs 1 & 2. The overall secretory profile of HPV-negative cell line-stimulated fibroblasts, inclusive CXCR-1/2 ligands shall be considered further in the discussion with specific reference to senescence. uPAR and VEGF, although noted in HPV-positive cell line-stimulated fibroblast media, are also more upregulated in HPV-negative cell line-stimulated fibroblast media. In addition to ligands upregulated HPV-negative cell line-stimulated fibroblast media, IGFBP6 was noted to be upregulated in all stimulated fibroblast media, although more so for HPV-positive lines (please refer to Figure 3.11 for densitometry analysis).

Figure 3.6: Raybiotech C8 Cytokine Array Analysis of Simulated Fibroblast Conditioned Media



	A	B	C	D	E	F	G	H	I	J	K	L	M	N
1	POS	POS	NEG	NEG	BLANK	Activin A	ALCAM	CD80	BMP 5	BMP 7	CT-1	CD14	CXCL16	DR6
2	POS	POS	NEG	NEG	BLANK	Activin A	ALCAM	CD80	BMP 5	BMP 7	CT-1	CD14	CXCL16	DR6
3	Endoglin	ErbB3	E Selectin	Fas Ligand	ICAM 2	IGF-2	IL-1 R 2	IL-10 R beta	IL-13 R alpha 2	IL-18 BP alpha	IL-18 R beta	MMP 3	IL-2 R beta	IL-2 R gamma
4	Endoglin	ErbB3	E Selectin	Fas Ligand	ICAM 2	IGF-2	IL-1 R 2	IL-10 R beta	IL-13 R alpha 2	IL-18 BP alpha	IL-18 R beta	MMP 3	IL-2 R beta	IL-2 R gamma
5	IL-21 R	IL-5 R alpha	IL-9	IP-10	LAP	Leptin R	LIF	L Selectin	M-CSF R	MMP 1	MMP 13	MMP 9	MPIF-1	NGF R
6	IL-21 R	IL-5 R alpha	IL-9	IP-10	LAP	Leptin R	LIF	L Selectin	M-CSF R	MMP 1	MMP 13	MMP 9	MPIF-1	NGF R
7	PDGF AA	PDGF AB	PDGF R alpha	PDGF R beta	PECAM 1	PRL	SCF R	SDF-1 beta	Siglec 5	TGF alpha	TGF beta 2	TIE-1	TIE-2	TIMP-4
8	PDGF AA	PDGF AB	PDGF R alpha	PDGF R beta	PECAM 1	PRL	SCF R	SDF-1 beta	Siglec 5	TGF alpha	TGF beta 2	TIE-1	TIE-2	TIMP-4
9	VE Cadherin	VEGF R2	VEGF R3	BLANK	BLANK	BLANK	BLANK	BLANK	BLANK	BLANK	BLANK	BLANK	BLANK	POS
10	VE Cadherin	VEGF R2	VEGF R3	BLANK	BLANK	BLANK	BLANK	BLANK	BLANK	BLANK	BLANK	BLANK	BLANK	POS

Figure 3.6: RayBiotech cytokine array C8 analysis of serum-free stimulated fibroblast medium taken after stimulation with cell lines UD SCC02, UPCI SCC072, UPCI SCC089 and UPCI SCC090.

- a. Serum-free unstimulated DENOFO8 fibroblast conditioned media control
- b. UPCI SCC072-stimulated DENOFO8 Medium 2 (HPV-negative stimulated)
- c. UPCI SCC089-stimulated DENOFO8 Medium 2 (HPV-negative stimulated)
- d. UPCI SCC072-stimulated DENOFO8 Medium 1 (HPV-negative stimulated)
- e. UD SCC02-stimulated DENOFO8 Medium 2 (HPV-positive stimulated)
- f. UPCI SCC090-stimulated DENOFO8 Medium 2 (HPV-positive stimulated)

Inferior table: array map, reproduced with kind permission of Raybiotechnology (Norcross, USA).

Red text denotes positive spots on unstimulated fibroblast medium control array. Black text denotes factors present in all cell line derived media but absent from normal media control. Note that a number of positive spots in the unstimulated fibroblast medium control array were also observed to be positive in normal media (please refer to Figure 3.3), namely ICAM2, SCF R and VEGF R3. These “positive” spots were therefore concluded as a result of background absorbance. Array spots for MMPs 1 & 3 do however appear to be positive in the unstimulated fibroblast medium control (a), but negative for the normal media control illustrated in Figure 3.3, suggesting that MMPs 1&3 are secreted basally by unstimulated fibroblasts.

No factor was noted to be elevated in only HPV-negative stimulated fibroblast media (please refer to densitometry, Figure 3.12), although LAP (latency associated peptide) can be observed to be elevated in all stimulated fibroblast media.

Figure 3.7: Densitometry Analysis of Tumour Line Conditioned Media Raybiotech C6 Cytokine Array

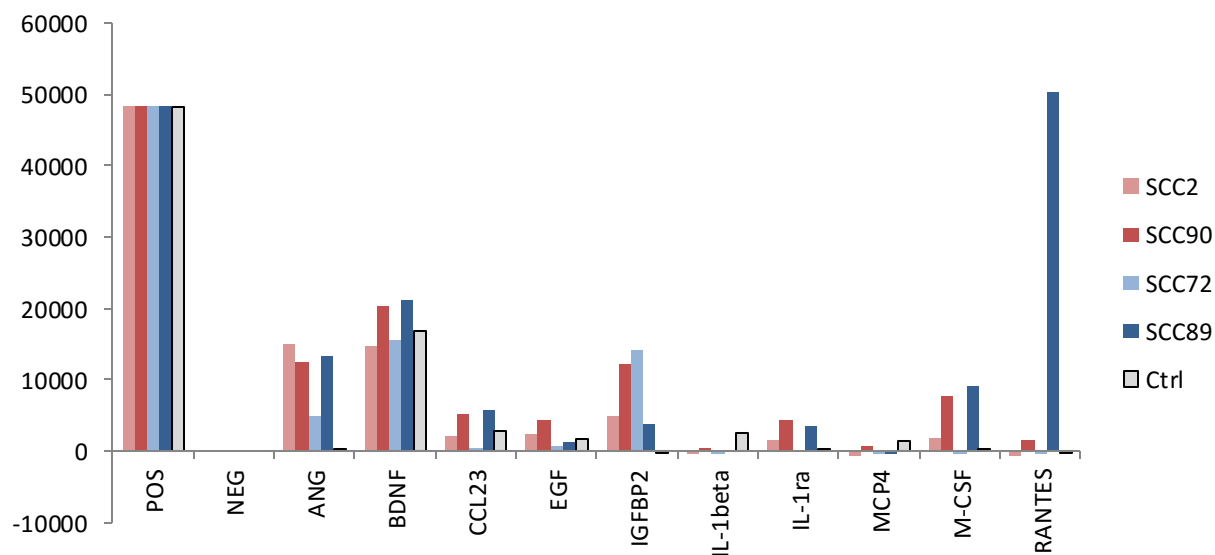


Figure 3.7: Densitometry analysis of cell line conditioned media Raybiotech C6 cytokine array. Blue bars denote HPV-negative cell lines (light blue: UPCI SCC072, dark blue: UPCI SCC089), whereas red bars denote HPV-positive cell lines (pink/light red: UD SCC02, dark red: UPCI SCC090). Grey bars denote serum-free medium control. Y-axis in arbitrary units, all bars derived from the average densitometry of each array’s duplicate repeat spot. All densitometry is normalised to control medium positive control spots. Array spots with complete absence of uptake in at least one HPV-positive and one HPV-negative cell line have been excluded for ease of viewing (please refer to Figure 3.1, images b & d). POS/NEG – normalised positive and negative control spots, respectively.

Note that BDNF, CCL23, IL-1beta and MCP4 array uptake is generally comparable to control in all cell lines, confirming visual features of array films presented in Figure 3.1. As noted from visual inspection of cell line medium C6 arrays, ANG, IGFBP2, IL-1ra, M-CSF and RANTES all demonstrate uptake that exceeds control spot uptake, although no consistent pattern of difference is noted between HPV-positive (UD SCC02, UPCI SCC090) and HPV-negative (UPII SCC072, UPCI SCC089) cell lines.

Figure 3.8: Densitometry Analysis of Tumour Line Conditioned Media Raybiotech C7 Cytokine Array

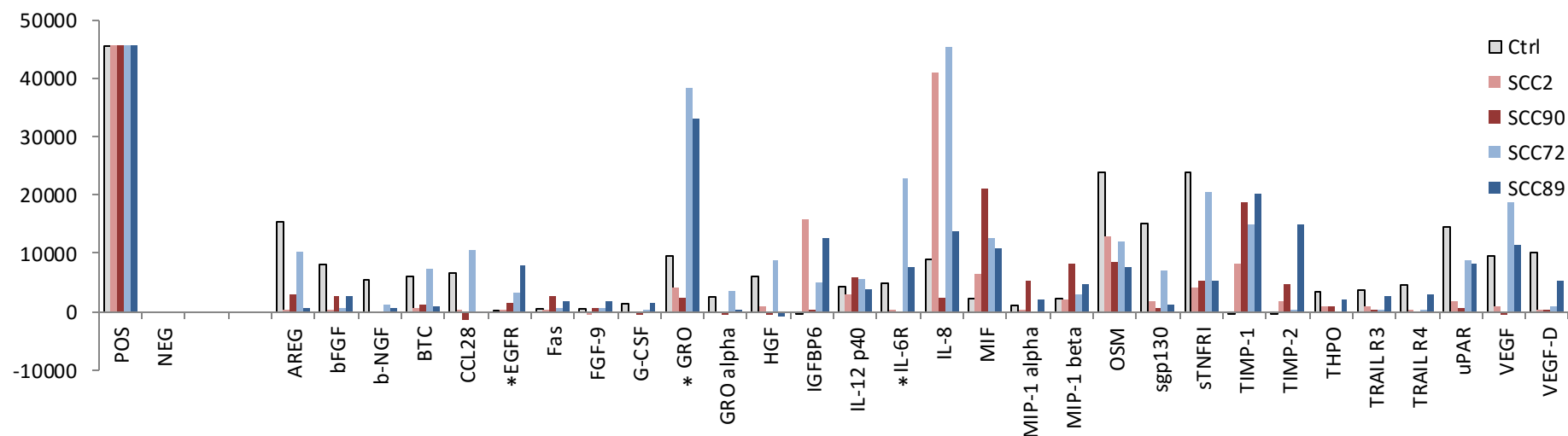


Figure 3.8: Densitometry analysis of cell line conditioned media Raybiotech C7 cytokine array. Blue bars denote HPV-negative cell lines (light blue: UPCI SCC072, dark blue: UPCI SCC089), whereas red bars denote HPV-positive cell lines (pink/light red: UD SCC02, dark red: UPCI SCC090). Grey bars denote serum-free medium control. Y-axis in arbitrary units, all bars derived from the average densitometry of each array’s duplicate repeat spot. All densitometry is normalised to control medium positive control spots. All densitometry is normalised to control medium positive control spots. Array spots with complete absence of uptake in at least one HPV-positive and one HPV-negative cell line have been excluded for ease of viewing (please refer to Figure 3.2, images b & d). POS/NEG – normalised positive and negative control spots, respectively.

As noted in Figure 3.2, a clear increase in HPV-negative cell line conditioned media densitometry is noted in the following array spots: EGFR, GRO, IL-6R (asterisked). Control absorbance can be observed to be high in uPAR and VEGF spots, although correlating the densitometry of control spots to images presented in Figure 3.2 identifies bleed-through of developer as the source of high control absorbance: it is therefore likely that HPV-negative cell lines truly release higher concentrations of these two factors. As also noted in Figure 3.2, all cell lines can be observed to release MIF. Densitometry of IL-8 suggests that, although significantly raised, does not follow a consistent pattern between HPV-positive and HPV-negative lines.

Figure 3.9: Densitometry Analysis of Tumour Line Conditioned Media Raybiotech C8 Cytokine Array

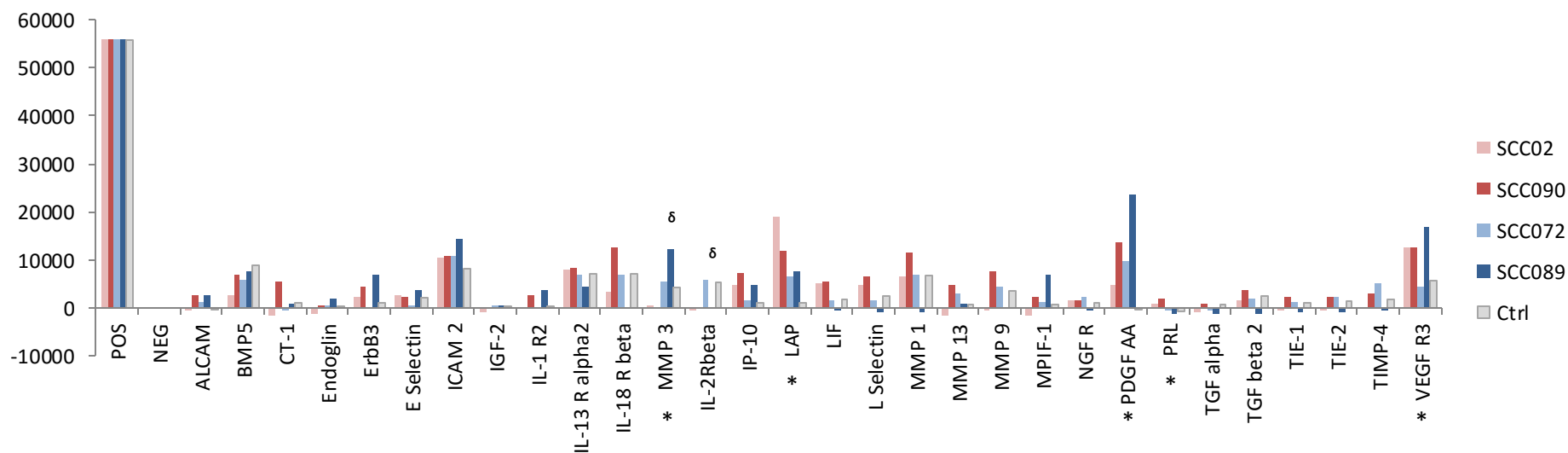


Figure 3.9: Densitometry analysis of cell line conditioned media Raybiotech C8 cytokine array. Blue bars denote HPV-negative cell lines (light blue: UPCI SCC072, dark blue: UPCI SCC089), whereas red bars denote HPV-positive cell lines (pink/light red: UD SCC02, dark red: UPCI SCC090). Grey bars denote serum-free medium control. Y-axis in arbitrary units, all bars derived from the average densitometry of each array’s duplicate repeat spot. All densitometry is normalised to control medium positive control spots. POS/NEG – normalised positive and negative control spots, respectively. Noteworthy array features asterisked. Array spots with complete absence of uptake in at least one HPV-positive and one HPV-negative cell line have been excluded for ease of viewing.

^δDenotes array spots for which UPCI SCC090 densitometry was not possible due to developer bleed-through.

Note that for most array spots, densitometry is comparable to normal media control. MMP-3, PDGFAA and VEGFR3 demonstrated absorbencies that exceeded control, although a definitive relationship to HPV status is not apparent. Although PDGFAA does not perfectly demonstrate a clear difference between HPV-positive and -negative cell line stimulation, the magnitude of absorbance approximates the pattern seen for IL-6 and IL-8 ELISA undertaken on

stimulated fibroblast medium in Chapter 4 (please refer to Figures 4.1 & 4.2), retaining potential for the factor to be linked to the mechanism of fibroblast stimulation. The limitations in valid MMP-3 interpretation due to UPCI SCC090 array developer bleed have been discussed in Figure 3.3. LAP appears to be more upregulated in HPV-positive cell line conditioned media, as did PRL (albeit with low readings throughout).

Figure 3.10: Densitometry Analysis of Simulated Fibroblast Media Raybiotech C6 Cytokine Array

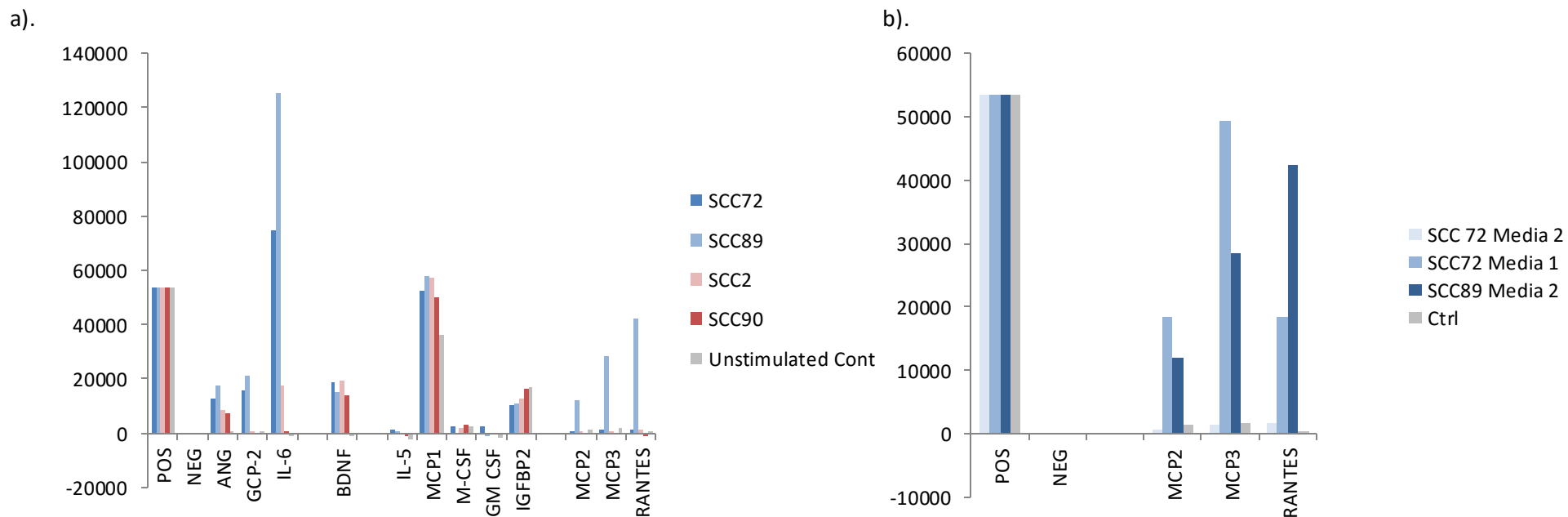


Figure 3.10: Densitometry analysis of stimulated fibroblast conditioned media Raybiotech C6 cytokine array.

Figure a: Stimulated fibroblast medium 2, all cell lines. Blue bars denote HPV-negative cell lines (light blue: UPCI SCC072, dark blue: UPCI SCC089), whereas red bars denote HPV-positive cell lines (pink/light red: UD SCC02, dark red: UPCI SCC090). Grey bars denote unstimulated fibroblast conditioned medium control. Y-axis in arbitrary units, all bars derived from the average densitometry of each array's duplicate repeat spot. All densitometry is normalised to control medium positive control spots. Consistently negative array spots have been excluded for ease of viewing. POS/NEG – normalised positive and negative control spots, respectively.

Note that for ANG, GCP2 and IL-6, marked upregulation is seen in HPV-negative stimulated fibroblast media. For BDNF, all stimulated fibroblast media uptake exceeded control, although background absorbance noted in serum-free normal media (Figure 3.1) suggests this finding may be artefactual. Although positive absorbencies were recorded for IL-5, MCP1, M-CSF, GM-CSF and IGFBP2, densitometry did not differ significantly from control. MCP2, MCP3 and RANTES were noted to be only elevated in Medium 2 derived from cell line UPCI SCC089, although please refer to findings in Figure b relating to UPCI SCC072 stimulated fibroblast Medium 1.

Figure b: Stimulated fibroblast Media 1&2, HPV-negative cell lines. Light blue bar denotes UPCI SCC072 Medium 2, medium blue bar denotes UPCI SCC072 Medium 1, dark blue bar denotes UPCI SCC089 Medium 2. Grey bars denote unstimulated fibroblast conditioned medium control. Y-axis in arbitrary units, all bars derived from the average densitometry of each array's duplicate repeat spot. All densitometry is normalised to control medium positive control spots.

Note that for UPCI SCC072 stimulated fibroblast Medium 1, MCP-2, MCP-3 and RANTES all approximate closer to UPCI SCC089 Medium 2 absorbencies. This can also be observed in Figure 3.4.

Figure 3.11: Densitometry Analysis of Simulated Fibroblast Media Raybiotech C7 Cytokine Array

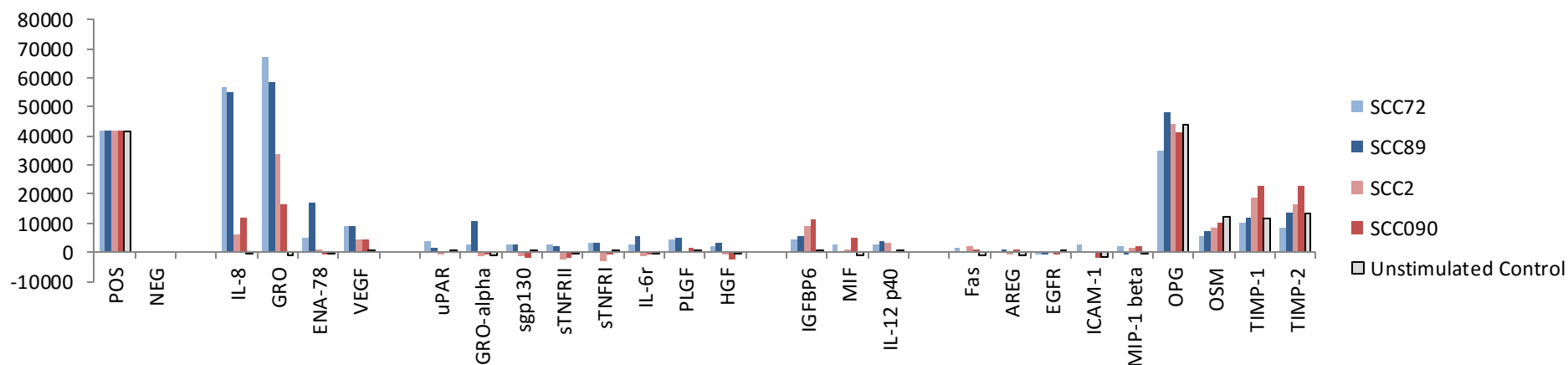


Figure 3.11: Densitometry analysis of stimulated fibroblast conditioned media Raybiotech C6 cytokine array, stimulated fibroblast medium 2, all cell lines. Blue bars denote HPV-negative cell lines (light blue: UPCI SCC072, dark blue: UPCI SCC089), whereas red bars denote HPV-positive cell lines (pink/light red: UD SCC02, dark red: UPCI SCC090). Grey bars denote unstimulated fibroblast conditioned medium control. Y-axis in arbitrary units, all bars derived from the average densitometry of each array's duplicate repeat spot. All densitometry is normalised to control medium positive control spots. Consistently negative array spots have been excluded for ease of viewing. POS/NEG – normalised positive and negative control spots, respectively.

Note the considerable upregulation of IL-8, GRO, ENA-78 and VEGF, all of which demonstrate a pattern of increased densitometry with fibroblasts activated by HPV-negative cell line conditioned media. Consistent patterns of increased fibroblast secretion following HPV-negative cell line stimulation can also be observed for uPAR, GRO α , sgp130, sTNFR1, IL-6R, PLGF and HGF, albeit with lower densitometry. MIF and IL-12p40 appear upregulated, although no consistent difference is noted between HPV-positive and -negative stimulated media. IGFBP2 may be moderately upregulated in HPV-positive cell lines. Fas, AREG, EGFR, ICAM-1, OPG and OSM demonstrated no significant difference from control absorbance despite positive array uptake. TIMP-1 and TIMP-2 demonstrated a small increase in absorbance in HPV-positive stimulated media, whereas HPV-negative stimulated media approximate to control absorbance.

Figure 3.12: Densitometry Analysis of Simulated Fibroblast Media Raybiotech C8 Cytokine Array

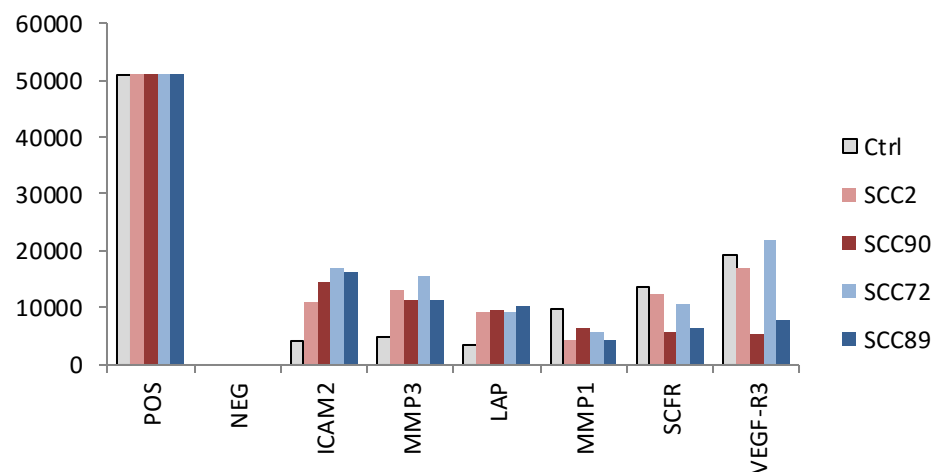


Figure 3.12: Densitometry analysis of stimulated fibroblast conditioned media Raybiotech C6 cytokine array, stimulated fibroblast medium 2, all cell lines. Blue bars denote HPV-negative cell lines (dark blue: UPCI SCC072, light blue: UPCI SCC089), whereas red bars denote HPV-positive cell lines (dark red: UD SCC02, pink/light red: UPCI SCC090). Grey bars denote unstimulated fibroblast conditioned medium control. Y-axis in arbitrary units, all bars derived from the average densitometry of each array's duplicate repeat spot. All densitometry is normalised to control medium positive control spots. Consistently negative array spots have been excluded for ease of viewing. POS/NEG – normalised positive and negative control spots, respectively.

Note that no convincing distinction between HPV-positive and -negative stimulated fibroblasts can be seen. Although ICAM 2 does show increased densitometry for HPV-negative stimulated fibroblasts, this difference is small in comparison to absorbencies from HPV-positive stimulated fibroblasts and is likely artefactual.

Table 3.1: Summary of Factors Present in Cell Line Conditioned Media

Present in All Cell Line Conditioned Media Without Evidence of HPV Status Specificity	More Elevated in HPV-positive Cell Line Conditioned Media	More Elevated in HPV-negative Cell Line Conditioned Media
ANG IGFBP2 IL-1ra M-CSF IL-8 MIF TIMP-1 TIMP-2 PDGFAA	LAP PRL	EGFR IL-6R GRO uPAR VEGF

Table 3.1: Summary of factors present in cell line conditioned media, data taken from cytokine array densitometry presented in Figures 3.7-3.9. Data have been divided into those factors secreted by all cell lines investigated, those factors secreted in greater concentrations by HPV-positive lines, and those factors secreted in greater concentrations by HPV-negative lines.

Table 3.2: Summary of Factors Present in (Stimulated) Fibroblast Media

Basal Fibroblast Secretion	Elevated in All Stimulated Fibroblast Media	More Elevated in HPV-positive Stimulated Fibroblast Media	More Elevated in HPV-negative Stimulated Fibroblast Media
IGFBP2	ANG	TIMP-1	RANTES*
MCP-1	BDNF	TIMP-2	MCP-2*
TIMP-1	MCP-1	IGFBP6	MCP-3*
TIMP-2	LAP		GCP2
OPG	MMP3		ENA78
PLGF			GRO
MMP3			IL-8
MMP1			uPAR
			VEGF
			ICAM2
			sgp-130
			STNFR1
			STNFR2
			IL-6R
			HGF
			PLGF
			IL-6

Table 3.2: Summary of factors present in stimulated/unstimulated fibroblast conditioned media; data taken from cytokine array densitometry presented in Figures 3.10-3.12. Data have been divided into those factors secreted basally by unstimulated fibroblasts (positive uptake on unstimulated fibroblast control array without comparable uptake on normal media control array), those factors secreted by fibroblasts in response to all cell line conditioned media, and those factors released in greater concentrations following HPV-positive/-negative cell line stimulation.

*Signifies those factors which demonstrate upregulation in UPCI SCC089-stimulated Medium 2 and UPCI SCC072 Medium 1, but not UPCI SCC072 Medium 2.

Discussion

Cytokine array analysis demonstrated a consistent cell line secretory profile based on HPV status. Conditioned media from all oropharyngeal carcinoma lines demonstrated positive array uptake for ANG, IGFBP2, IL-1ra, IL-8, MIF, TIMP 1&2, PDGFAA and M-CSF. In addition to those factors apparently ubiquitous to the oropharyngeal carcinoma lines, a further group of factors, namely EGFR, IL-6R, GRO, uPAR and VEGF – were noted to be released in greater concentrations by HPV-negative cell lines. These latter factors clearly have potential to be implicated in the mechanism of additional cell line migrations discussed in Chapter 2, due to a correlation between cytokine array densitometry and cell migration in response to conditioned media. The preceding factors common to all cell lines may however, also be implicated if the lack of HPV-positive cell line migration is linked to tumour line responsiveness to a given factor that becomes generically released upon fibroblast stimulation. Viral inhibition of tumour response remains a plausible mechanism through which only virus-negative cell lines migrate in the presence of a factor found in all stimulated fibroblast media.

Only two factors, prolactin (PRL) and latency-associated peptide (LAP) were found to be more upregulated in HPV-positive cell line conditioned media. Although LAP densitometry for the HPV-positive cell line UD SCC02 does appear appreciably elevated compared to the HPV-negative cell lines (please refer to Figure 3.9), the relatively high sensitivity of the LAP array spot (1 pg mL^{-1}) along with the low magnitude of difference in densitometry between the HPV-positive cell line UPCI SCC090 and the HPV-negative cell lines suggests that this relationship may be a result of experimental error rather than a bona fide upregulation in HPV-positive lines. Conversely, the PRL array spot has low sensitivity ($1,000 \text{ pg mL}^{-1}$), inferring that a small difference in densitometry between HPV-positive and -negative line conditioned media translates to a significant biological difference. It is however, important to note that all cell line conditioned media PRL densitometries were particularly low, and densitometry cannot therefore be guaranteed to be an accurate reflection of absolute concentrations. A key limitation of cytokine array densitometry is its semi-quantitative nature, and the difficulties in interpreting weak densitometry uptake, as illustrated for PRL along with a number of other factors discussed below, warrants quantitative follow-up of data of interest through supplemental methods, such as ELISA analysis.

Fibroblast conditioned media again contained a number of common factors secreted in response to stimulation by all cell lines, namely ANG, BDNF, MCP-1, LAP and MMP-3. As

with cell line conditioned media, HPV-negative cell line-stimulated fibroblasts secreted a number of additional factors leading to observable differences in array absorbencies, namely GCP2, GM-CSF, IL-6, ENA78, GRO, VEGF, IL-6 and IL-8. Densitometry demonstrated a further sub-set of factors that again produced low intensity absorbencies, yet a consistent upregulation in HPV-negative stimulated fibroblast media, including uPAR, sgp-130, STNFR1, STNFR2, IL-6r, PLGF and HGF. Whilst the relationship of these latter factors retain higher potential to have occurred as a result of relatively high experimental variance in relation to their low overall absorbance, as was discussed for PRL above, their potential to underlie the migratory phenomenon in Chapter 2 is not ruled out; particularly given the low array sensitivity to a number of these latter factors. A small number of factors were noted to be more elevated in HPV-positive cell line-stimulated fibroblast media, namely TIMP-1, TIMP-2 and IGFBP6. Again, experimental variability may account for the higher densitometry of these latter 3 factors, particularly given the high control absorbance noted for TIMP-1 and TIMP-2.

To summarise cytokine array findings, there are 3 remarkable features of the additional secretory profile of HPV-negative cell lines and their respective fibroblast response: firstly, a number of the factors released by fibroblasts in response to HPV-negative lines signal via CXCRs 1&2 (GCP2, ENA78, GRO and IL-8) – the implication of this observation is that CXCR-expressing cellular populations are likely to become more activated in HPV-negative disease. Secondly, an inflammatory profile, reflected by marked array uptake of IL-6 and IL-8, is induced in response to HPV-negative cell line conditioned media. Thirdly, a number of receptor ectodomains are observed in HPV-negative cell line conditioned media, including EGFR and IL-6R (further examples shall also be discussed in Chapter 5). A common source of membrane cleavage, as shall be discussed in Chapter 4, may underlie this feature of HPV-negative cell line conditioned media.

As shall be discussed further in Chapter 4, Acosta *et al* noted a near-identical secretory profile to our HPV-negative-induced fibroblast findings, whereby fibroblasts undergoing oncogene-induced senescence (via MEK-1) developed expression of CXCR-2, in addition to release of IL-6, IL-8, GRO- α , IL-1 β and increased mRNA transcription of all known CXCR2 ligands²⁸⁹. The induction of fibroblast senescence as a process through which HPV-negative cell lines induce fibroblast support of migration therefore appears plausible. Rudisch *et al* also noted a similar “cytokine fingerprint” of GM-CSF, GRO- α , GCP2, VEGF, RANTES and IL-8 following co-culture of NSCLC lines with fibroblasts²⁹⁰, attributing canonical NF κ B

signalling to fibroblast secretion of the aforementioned factors – albeit that the authors only formally demonstrated canonical NF κ B signalling with respect to GM-CSF. Coppe *et al* also induced an IL-6, IL-8, GRO, GM-CSF and HGF-expressing fibroblast phenotype following the induction of senescence through both oxidative stress and ionising radiation²⁴⁶.

A further limitation of cytokine array technology is that due to relatively high expense, triplicate repeat analysis is unfeasible for the large amount of data presented in this chapter. Duplicate repeat spots are however included for each factor within a single array membrane, and high concordance was noted between spots throughout the arrays, other than for sites of developer excess, as can be observed for uPAR, VEGF & VEGFD in the Raybiotech C7 control array (Figure 3.2) and densitometry plot (Figure 3.8), Figure C8 cytokine arrays were noted as producing considerable background absorbance in most array spots; the use of appropriate controls allowed standardisation of results to this background absorbance, although concern remained as to the risk of background absorbance varying between membranes, thereby inducing experimental error. Indeed, BDNF, IL-1 β and MCP-4 were all noted to be represented by positive array uptake on serum-free normal media control (Figure 3.1), whereas factors were observed to be absent in unstimulated fibroblast control medium (Figure 3.4). There is no simple explanation for this difference; DMEM with serum-free supplements should not have capacity to contain the aforementioned proteins, and a conclusion of background absorbance is consistent with the similar pattern of BDNF/IL-1 β /MCP-4 uptake in cell line conditioned media. Background uptake should however be expected in the unstimulated fibroblast control medium array, which is seen to be devoid of any positive uptake in the aforementioned spots. Enzymatic breakdown of BDNF/IL-1 β /MCP-4 by fibroblasts remains a feasible, yet unlikely alternative explanation.

Interestingly, neither cell line conditioned media nor stimulated fibroblast media demonstrated any evidence of TGF β expression, despite comprehensive array spots for TGF β 1, TGF β 2 and TGF β 3. It was however, observed that latency-associated peptide (LAP) densitometry was increased in both cell line conditioned media and stimulated fibroblast media compared to respective controls. Latency-associated peptide is a protein derived from the N-terminal region of the TGF β gene, forming part of the latent TGF β complex prior to extracellular secretion²⁹¹. Personal correspondence with Raybiotech confirmed the C8 “LAP” array spot consists of two antibody pairs, responsive to both human LAP and the latent TGF- β 1 complex. A residual possibility of TGF β existing in a latent form is therefore feasible,

although a functional role of TGF β in conditioned medium-induced migration appears unlikely given the absence of uptake in array spots responsive to its active forms.

A broad range of the factors (IL-6R, GRO α , GRO β , GRO γ , ENA78, GCP2, IL-6, IL-8, OSM, OPG, HGF, identified through cytokine array analysis shall be considered in Chapters 4-6; review of these respective factors can be found in the introduction of Chapter 5. Consideration here shall therefore be limited to those factors not directly followed up in this thesis, and the impact they may have on disease progression.

EGF Receptor (EGFR)

EGFR was noted to be elevated in HPV-negative cell line conditioned media. Although this may well be an inadvertent consequence of more generic membranous receptor and factor shedding via upregulated ADAM activity²⁹², as shall be discussed later in the thesis, there may be significant implications of EGFR release on the therapeutic management of oropharyngeal carcinoma. Interestingly, among other factors, ADAM17 is capable of inducing the release of EGFR ligands²⁹³, inferring a balance may be necessary between tumour EGFR shedding and EGF upregulation via ADAM17 activity. Cetuximab, a monoclonal antibody to the EGF receptor ectodomain²⁹⁴, has been FDA approved for management of patients with head and neck disease that have had prior platinum-based chemotherapy. Cetuximab has proven efficacy in locoregionally advanced²⁹⁵, recurrent and metastatic disease²⁹⁶. EU approval has been given for use of cetuximab in combination with radiation therapy for the management of locally advanced head and neck disease, and also in combination with platinum-based chemotherapy for the treatment of recurrent and/or metastatic disease²⁹⁷. Unfortunately, although cetuximab has benefit in the management of advanced head and neck cancer, its cost efficacy has been brought into question²²². A more accurate method of determining patient response to therapy may therefore be warranted.

Several trials of cetuximab in the management of HPV-positive oropharyngeal carcinoma are ongoing, including DeESCALaTE, RTOG 1016, UMCC 2009.078, ECOG-E1308 and TROG 12.01²⁹⁸. Indeed, experimental evidence suggests that the HPV E5 protein has capacity to amplify ligand-dependent EGFR signalling^{299, 300}, providing a scientific rationale for the application of cetuximab in the management of HPV-positive oropharyngeal cancer. Moreover, our data suggest that receptor decoy, in the form of cleaved EGFR ectodomain is less likely to be of concern in HPV-positive disease. Despite this, care has to be taken when

interpreting the results of the ongoing trials; O'Sullivan *et al* have reported comparable efficacy of radiotherapy alone compared to chemoradiotherapy in HPV-positive N0-N2a oropharyngeal disease and in N2b disease related to <10 pack years cigarette exposure²²³; those studies such as DeESCALaTE (clinicaltrials.gov identifier: NCT01874171), which include N0 – N2b disease, are designed to report survival data as a secondary outcome measure in terms of non-inferiority to a potentially flawed chemoradiotherapy “standard”, on the assumption that standard chemotherapy in the control group has adjunctive benefit over radiotherapy alone. Measuring cetuximab efficacy in a study skewed to local disease or early nodal spread may therefore deliver a result of comparable effect to chemotherapy, irrespective of any true benefit from either therapeutic.

Irrespective of the findings of ongoing trials, our data identify soluble EGFR as a potential supplemental biomarker for response to cetuximab. Historically, attempts at biomarker-driven cetuximab therapy through analysis of membranous EGFR status have been unsuccessful³⁰¹; membranous receptor status does not appear to accurately predict response to cetuximab therapy. Indeed, it has also been noted that high concentrations of EGF and TGF α may compete with cetuximab for EGFR binding³⁰¹; a more complex relationship between membranous and solubilised receptor status, in combination with ligand concentration may underlie the limitations in predicting efficacy of cetuximab, and response may be discerned more accurately by use of an index of tumour EGFR status based on serum soluble EGFR status as a ratio to tumour membranous EGFR status and ligand concentration.

The use of concurrent erlotinib, a kinase domain EGF inhibitor which is therefore not competitively inhibited by the shed EGFR ectodomain, nor EGFR ligand concentration, may also help circumvent some of the limitations of cetuximab alone. Cetuximab plus erlotinib therapy has delivered promising results in the management of colon cancer³⁰², and may be an appropriate therapeutic strategy in HPV-negative disease. Further research using xenograft models has also identified the benefit of combining cetuximab with gefitinib, a small molecule tyrosine kinase domain inhibitor of EGF³⁰³; researchers found that combined therapy led to tumour regression and maintenance of a disease-free state 4 months after drug withdrawal, whereas monotherapy, even at higher concentrations, led to tumour progression upon drug withdrawal.

uPAR

Urokinase plasminogen activator (uPA), a component of the plasminogen system, acts through the uPAR receptor in order to catalyse plasminogen to plasmin. Activation of the membranous receptor therefore directs proteolysis at the margin of carcinomas, leading to invasion and metastasis³⁰⁴. A study of breast cancers using laser capture microdissection found both tumour and stroma act as sources of uPA and uPAR, although there appears to be slightly greater production by stroma³⁰⁵. Membranous cleavage of uPAR may occur after receptor binding, leading to release of the solubilised form of the receptor, which also has capacity to induce chemotaxis³⁰⁶. Serum uPAR has been found to be a determinant of survival in both malignancy^{305, 307} and also infective diseases such as TB and HIV^{308, 309}, although some conflicting reports exist as to its role in specific cancers³¹⁰.

Available data on the role of uPAR in head and neck disease is limited. Ying-na *et al* found uPAR to promote nasopharyngeal carcinoma cell growth and migration in vitro, and also found uPAR to be elevated in metastatic disease compared to normal tissue controls in a small cohort of 36 patients³¹¹. Recent work by Magnussen *et al* has also demonstrated that uPAR and uPA are both predictors of mortality in T1 oral tumours³¹².

Our findings are consistent with the above publications, whereby the characteristically poor-prognosticating HPV-negative carcinoma lines both expressed uPAR, and also induced more significant fibroblast release of uPAR compared to HPV-positive lines. The overall densitometry of cell line conditioned media (Figure 3.8) did however exceed the densitometry of fibroblast conditioned media (Figure 3.11) suggesting fibroblast secretion of uPAR may be less significant than tumour secretion, although it is important to bear in mind that densitometry is a semi-quantitative measure, and also that cell line conditioned media was contributed to by a cellular population 7.5 times greater than the fibroblast population contributing to Media 1&2.

RANTES

RANTES (CCL5, Regulated on Activation, Normal T Cell Expressed and Secreted) was noted to be elevated in both UPCI SC089 cell line medium and also UPCI SCC089 stimulated fibroblast Medium 2. Although UPCI SCC072 did not release RANTES into cell line conditioned medium or Medium 2, RANTES was observed in UPCI SCC072 Medium 1.

As has been discussed for previous factors noted in UPCI SCC072 Medium 1, the absolute significance of RANTES in UPCI SCC072 Medium 1 is indeterminate without further analysis of Medium 1 for other cell lines. Despite this limitation, it can be concluded that both HPV-negative line conditioned media showed evidence of RANTES induction in fibroblasts, albeit over different timepoints.

RANTES is a chemotactic factor, with a principal physiological function of attracting immune cells to sites of inflammation. It has been implicated in the attraction of tumour-associated macrophages and progression of breast carcinoma³¹³, and has been reported as concomitantly expressed with MCP-1³¹⁴, a factor noted to be only modestly upregulated in cytokine array densitometry of stimulated fibroblast media (Figure 3.10). HPV-negative oropharyngeal carcinomas may contain a macrophage subpopulation more supportive of tumour progression should RANTES be a distinguishing feature between HPV-positive and -negative disease. Considerable further follow-up of our data would be necessary to confirm this role in both an experimental and clinical setting.

VEGF

VEGF has a well-documented role in the progression of cancer. Head and neck-specific data generally support an association between VEGF status and poor prognosis/ nodal metastasis³¹⁵, although some reviews have not found such a relationship with nodal metastasis³¹⁶, and a role of VEGF in laryngeal & pharyngeal carcinoma is disputed^{316, 317}. VEGF has been reported to adversely affect prognosis in both HPV-positive and HPV-negative oropharyngeal carcinoma³¹⁸, although no relationship was noted between tumour VEGF and HPV status³¹⁸; conflicting data has been reported, whereby HPV-negative tumours are associated with higher circulating levels of VEGF³¹⁹. Our data appear to concur with this latter study, and suggests that although VEGF is induced in fibroblast populations by both HPV-positive and -negative cell lines, HPV-negative cell lines induced greater amounts of VEGF release by fibroblasts (Figure 3.11), and moreover, HPV-negative cell lines also secreted modest amounts of VEGF into conditioned media (Figure 3.8). Whilst the inconsistency between our observed data and some clinically reported data may be a result of the lack of external validity of the employed *in-vitro* methodology, and also may reflect the limited number of cell lines analysed, the inconsistency may also be a consequence of qualitative assessment of VEGF immunohistochemistry status as opposed to quantitative

analysis of circulating VEGF, which closely mirrored our findings. Indeed, experimental overexpression of HPV16 oncoproteins E6 & E7 via transfection of non-small cell lung cancer lines has been demonstrated to upregulate VEGF secretion³²⁰, suggesting VEGF is not exclusive to HPV-negative cancers.

MCP-2 & MCP-3

Monocyte chemotactic proteins (MCP) 2 & 3 (CCL8 and CCL7, respectively) act as monocytic chemoattractants³²¹. Cytokine array data infer rapid release of these factors from fibroblasts in response to exposure to conditioned medium from the cell line UPCI SCC072 (please refer to Medium 1 C6 array densitometry data, Figure 3.10), although release rapidly declined after washing and media change – leading to minimal levels of both factors in UPCI SCC072 stimulated fibroblast Medium 2. The second experimental HPV-negative cell line, UPCI-SCC089, demonstrated induction of MCP 2&3 release in the respective stimulated fibroblast Medium 2.

As cytokine array assessment of HPV-positive cell line-stimulated fibroblast Media 1 was not undertaken, it is not possible to confirm whether MCP-2/3 release was specific to HPV-negative cell lines. It is feasible that in assessing only HPV-positive stimulated Media 2, transient MCP 2/3 release, as was observed with the cell line UPCI SCC072, has been overlooked. Speculation is therefore made in this discussion on the assumption, rather than confirmation, of MCP-2/3 release as a HPV-negative tumour phenomenon.

Whilst there are clear connotations linked to the release of monocytic chemoattractants, which may act to develop a favourable leukocytic population within the mature tumour microenvironment, there is little clinical data available on the role of MCP-2/3 in cancer progression. A study of both factors in gastric carcinoma progression found MCP-3 (CCL7) to be linked to lymph node metastasis and poor outcome, whilst MCP-2 (CCL8) was not³²². Jung *et al* used a range of oral carcinoma lines in co-culture with cancer-associated fibroblasts (CAF) to show that IL-1 α secreted by carcinoma lines promoted MCP-3 release by fibroblasts in a similar manner to our data³²³. Perhaps what is most novel about our finding is that MCP-3 can be induced within a normal fibroblast population, and therefore fibroblast priming to a CAF phenotype is unnecessary. Jung *et al* further discussed their findings of upregulated GRO α , β & γ , along with IL-8 in their co-culture experiments, further corroborating the findings of our cytokine array data.

STNFR I & II

Soluble TNF receptors 1&2 were upregulated in HPV-negative cell line-stimulated fibroblast media. These soluble receptors are known to be cleaved from membranes by proteolytic enzymes³²⁴ and may be elevated in both malignant³²⁵⁻³²⁷ and inflammatory processes³²⁸⁻³³⁰. Dong *et al* (article in Chinese, abstract accessed via PubMed) also reported elevation for sTNFRI in head and neck cancer³³¹, although little further data are available for the head and neck region.

Conclusion

Cytokine array assessment of HPV-negative cell line and HPV-negative stimulated fibroblast media confirmed upregulation of a number of factors consistent with a senescence-associated secretory phenotype. Little evidence was found to support a TGF- β linked induction of cell migration, although differences in the data presented by Hassona *et al*²⁴⁰ may be explained by a separate biology of oropharyngeal and oral carcinoma.

Whilst cytokine array data have offered considerable insight into the potential nature of microenvironmental interactions within HPV-positive versus HPV-negative oropharyngeal disease, one must bear in mind a number of limitations relating to the technology. Foremost, although a comprehensive list of chemokines has been studied, this list is not exhaustive, and the migrations observed in Chapter 2 may be attributable to a factor absent from the Raybiotechnology C2000 array. Moreover, the previously discussed limitations relating to variations in cytokine array spot sensitivity and semi-quantitative analysis necessitate further follow-up and validation. Despite these limitations, the array data presented in this chapter offer directionality for subsequent research and also affirms a “signature” secretory profile in HPV-negative cell lines and stimulated fibroblasts, which is consistent with the more aggressive nature of HPV-negative disease.

Chapter 4: Investigation of a CXCR-2/IL-6 Basis of Fibroblast Recruitment and Support

Introduction

Cytokine array densitometry data presented in Chapter 3 demonstrated a signature secretory profile of DENOFO8 fibroblasts in response to HPV-negative cell line conditioned media. A number of the principal findings of densitometry related to an inflammatory secretome, with IL-6 and IL-8 dominating the overall picture of stimulated fibroblast array data in terms of array spot intensity. The findings of IL-6 and IL-8 upregulation prompted a review of the available literature; both factors are quoted as having capacity to induce EMT^{280, 332, 333}, and furthermore IL-6 has recently been found to induce migration in oral cancer cell lines³³⁴ and invasion in colorectal carcinoma lines³³⁵. Conversely, no current data are available on the role of IL-8 in inducing tumour migration. Activation of the receptor CXCR-2 by ligands such as GRO (found in HPV-negative cell line conditioned media – please refer to Chapter 3, Figures 3.2 & 3.8) has been found to induce senescence via a p53-dependent pathway in human fibroblasts²⁸⁹. The exact mechanism by which CXCR-2 activation leads to senescence is unresolved, although there is evidence that Rac activation through CXCR-2 leads to NADPH oxidases producing reactive oxygen species, which in turn trigger DNA damage and thereafter a p53 response that drives senescence³³⁶. Irrespective of the intricacies of the CXCR-2 induced pathway to senescence, the result is an established senescence-associated secretory profile (SASP), which includes products such as IL-6, IL-8 and GRO α ³³⁶; factors noted in HPV-negative stimulated fibroblast Media 2 cytokine arrays. A senescence-induced pathway may therefore underlie the secretory response noted in HPV-negative stimulated fibroblast media cytokine arrays (Chapter 3, Figures 3.4-3.6 and 3.10-3.12), and may also act as a basis for the additional migrations noted in ORISTM assay experiments (Chapter 2, Figures 2.2 & 2.3). Reinforcing signals for further paracrine CXCR-2 activation of senescence have also been described in response to initial CXCR-2 induction; Acosta *et al* reported that mRNA for most known CXCR-2 ligands becomes upregulated, including ENA78, GCP2, IL-8 and GRO α ²⁸⁹; factors again noted to be upregulated in HPV-negative stimulated fibroblast media cytokine arrays. CXCR-2 itself also becomes upregulated in this process. Non-canonical cytokines such as IL-6 have also been implicated in establishing the senescent response³³⁶. A hypothetical model of GRO-activated CXCR-2

leading to fibroblast release of reinforcing factors, in addition to production of IL-6, which thereafter has the capacity to induce cell line migration is summarised in Figure 4.0. Underlying this hypothesis is the potential for IL-6 to act as a principal driver of the additional migrations observed in HPV-negative cell lines in response to stimulated fibroblast media.

Conditioned media collected from HPV-negative cell lines demonstrated increased cytokine array uptake of the solubilised form of the IL-6 receptor (sIL-6R). Whilst it is not uncommon for solubilised receptor release to be upregulated in tumours as a result of ADAM snippase activity leading to generic shedding of Type I membranous receptor ectodomains³³⁷, sIL-6R is relatively unique in that it retains capacity to have biological effect following cleavage, through a route referred to as “trans-signalling”. Most other receptors cleaved by ADAM snippases become deactivated, as signalling is reliant on the integrity of the receptor’s intracellular tyrosine kinase domain for signal transduction; cleaved receptor ectodomains therefore commonly act as competitive inhibitors of their membranous precursors, as they retain capacity for ligand binding without capacity for signalling. IL-6 is an exception due to its ability to signal via gp130, a transmembrane protein which can complex with either membranous or solubilised IL-6R in order for signal transduction to occur. It appears that there are subtle differences in biological effect between sIL-6R trans-signalling and canonical signalling via the membranous receptor. Limited data are available on the significance of sIL-6R trans-signalling in either carcinomas or normal epithelia, although the observation that HPV-negative cell lines actively released sIL-6R as well as inducing stromal production of IL-6 offers an enticing receptor-ligand relationship that could bear significance to the migratory phenomena in the presence of HPV-negative stimulated fibroblast media.

This chapter seeks to test the hypothesis that fibroblast release of IL-6 is responsible for the additional migrations observed in HPV-negative cell lines in the ORIS™ assay experiments discussed in Chapter 2, and that fibroblast CXCR-2 activation in response to cell line-released GRO leads to fibroblast release of IL-6.

Figure 4.0: Hypothesised Route through Which HPV-negative Cell Lines Derive Increased Migrational Activity from Fibroblasts

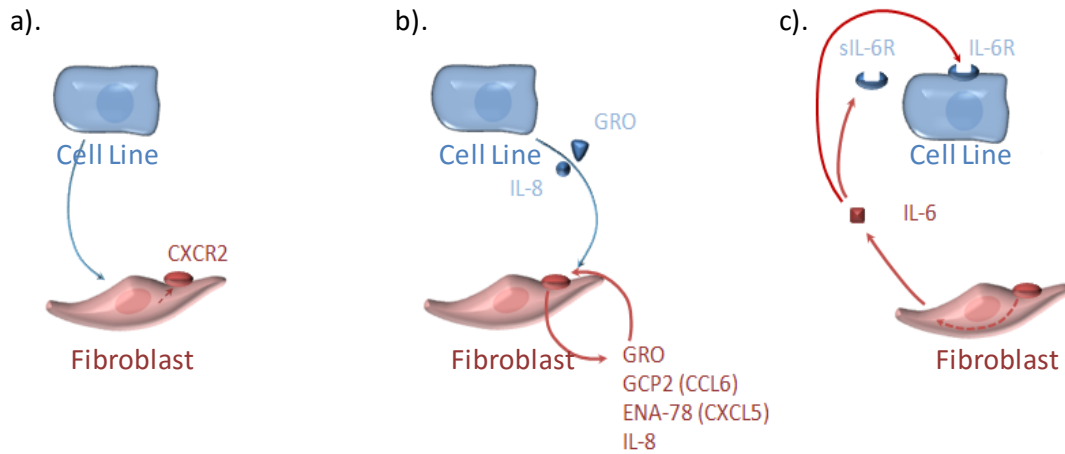


Figure 4.0: Schematic to illustrate hypothetical pathway through which HPV-negative cell lines may derive increased migrational activity from Stimulated Fibroblast Media 1 & 2 in ORIS™ assay experiments (Chapter 2, Figures 2.2 & 2.3).

- a). HPV-negative cell lines release a factor capable of inducing CXCR2 expression in stromal fibroblasts
- b). HPV-negative lines also release Growth Regulated Oncogene, either independently or in combination with IL-8. Fibroblast-induced secretion of other CXCR2-stimulating factors may supplement IL-8 and Growth Regulated Oncogene
- c). The net effect of CXCR stimulation is the release of IL-6, which binds to solubilised IL-6 receptor released by HPV-negative lines, stimulating cell motility through the IL-6 trans-signalling pathway

Methods

M4.1: ELISA Analysis of IL-6 in Cell Line and Stimulated Fibroblast Conditioned Media

Conditioned media was collected, normalised and stored at -21 °C in an identical manner as described in Chapter 2, methods section M2.1.

A Human IL-6 OptEIA™ ELISA Set was purchased from BD Bioscience (California, USA, Cat number 555220). Immediately prior to ELISA experiments, all conditioned media was thawed and homogenised on an agitator. Standards were prepared according to manufacturer's instructions (serial 50 % dilutions of 300 pg mL⁻¹ standard). ELISA-compatible 96-well plates were coated with 100 µL diluted stock capture antibody (1:250 in PBS). Plates were then sealed with adherent film and incubated overnight at 4 °C. Following overnight incubation, capture antibody was discarded and wells carefully washed X3 using a minimum of 300 µL wash buffer per well (freshly prepared PBS with 0.05 % Tween-20), with blotting of upturned wells undertaken between each wash. Plates were then blocked with 200 µL Assay Diluent (PBS with 10 % FBS) and incubated at room temperature for 1 hr. Assay diluent was then discarded and a further 3X washes undertaken with blotting between washes. 100 µL appropriately diluted assay standard or sample was then pipetted into each respective well, the 96-well plate sealed with adherent film and then incubated for 2 h at room temperature. All conditioned media samples were prepared to 1:20 and 1:50 dilution. Following incubation, media was aspirated and a further 5X washes undertaken with blotting between each wash. 100 µL detection antibody plus streptavidin reagent was then prepared according to manufacturer's instructions, pipetted into each well, sealed and then incubated for a further 1 h at room temperature. Antibody/streptavidin reagent was then aspirated and a further 7X washes undertaken with blotting between washes. 100 µL TMB substrate (BD Biosciences, Franklin Lakes, New Jersey, USA, Cat number 555214) was then added to each well, and incubated in the dark for 30 minutes with periodic observation to ensure excessive chromogenic reaction did not occur. 50 µL 2N sulphuric acid "stop" solution was then added to terminate the chromogenic reaction, and absorbance immediately measured at 450 nm using a Tecan Infinite M200 plate reader, with correction at 570 nm. Plate reader absorbencies were tabulated in Microsoft Excel, then imported into DeltaSoft ELISA analysis software (BioMetallics, Princeton, New Jersey, USA), and interpreted using manufacturer-advised log-log plot.

M4.2: ELISA Analysis of IL-8 in Cell Line and Stimulated Fibroblast Conditioned Media

Conditioned media was collected, normalised and stored at -21 °C in an identical manner as described in Chapter 2, methods section M2.1.

A Human IL-8 OptEIA™ ELISA Set was purchased from BD Bioscience (California, USA, Cat number 555244). Immediately prior to ELISA experiments, all conditioned media was thawed and homogenised on an agitator. Standards were prepared according to manufacturer's instructions (serial 50 % dilutions of 200 pg mL⁻¹ standard). ELISA-compatible 96-well plates were coated with 100 µL capture antibody diluted 1:250 in PBS. Plates were then sealed with adherent film and incubated overnight at 4 °C. Following overnight incubation, capture antibody was discarded and wells carefully washed X3 using a minimum of 300 µL wash buffer per well (freshly prepared PBS with 0.05 % Tween-20), with blotting of upturned wells undertaken between each wash. Plates were then blocked with 200 µL Assay Diluent (PBS with 10 % FBS) and incubated at room temperature for 1 hr. Assay diluent was then discarded and a further 3X washes undertaken with blotting between washes. 100 µL appropriately diluted assay standard or sample was then pipetted into each respective well, the 96-well plate sealed with adherent film and then incubated for 2 h at room temperature. All conditioned media samples were prepared to 1:20 and 1:50 dilution, with UPCI SCC089 stimulated fibroblast medium analysed at a further dilution of 1:100 (due to exceeding standard curve absorbance during initial optimisation). Following incubation, media was aspirated and a further 5X washes undertaken with blotting between each wash. 100 µL detection antibody plus streptavidin reagent was then prepared according to manufacturer's instructions, pipetted into each well, sealed and then incubated for a further 1 h at room temperature. Antibody/streptavidin reagent was then aspirated and a further 7X washes undertaken with blotting between washes. 100 µL TMB substrate (BD Biosciences) was then added to each well, and incubated in the dark for 30 minutes with periodic observation to ensure excessive chromogenic reaction did not occur. 50 µL 2N sulphuric acid "stop" solution was then added to terminate the chromogenic reaction, and absorbance immediately measured at 450 nm using a Tecan Infinite M200 plate reader, with correction at 570 nm. Plate reader absorbencies were tabulated in Microsoft Excel, then imported into DeltaSoft ELISA analysis software, and interpreted using manufacturer-advised log-log plot.

M4.3: ELISA Analysis of IL-6R in Cell Line Conditioned Media

Conditioned media was collected, normalised and stored at -21 °C in an identical manner as described in Chapter 2, methods section M2.1.

A Human IL-6R Raybiotech pre-coated IL-6R ELISA kit was purchased from Raybiotech (Raybiotechnology, Norcross, USA, cat number: ELH-IL6sR). Immediately prior to ELISA experiments, all conditioned media was thawed and then homogenised on an agitator. Standards were prepared according to manufacturer's instructions (serial 60 % dilutions of 1,000 pg mL⁻¹ standard), using manufacturer-supplied Assay Diluent B. 100 µL assay standard, or cell line conditioned media sample diluted 1:20 using Assay Diluent B, was then pipetted into each respective well. The plate was then covered and incubated overnight at 4 °C on a rocking machine. Following overnight incubation, wells were aspirated and washed X4 using 300 µL manufacturer-supplied wash buffer, with careful blotting between washes. 100 µL prepared biotinylated antibody was then added to each well, sealed and incubated for 1 h at room temperature on a rocking machine. Plates were again aspirated and subjected to 4X washes as described above. 100 µL prepared streptavidin solution was then added to each well and incubated at room temperature for 45 mins. A further 4X washes were then undertaken as described above, and then 100 µL manufacturer-supplied TMB One-Step Substrate Reagent added to each well and incubated for 30 mins in the dark. 50 µL manufacturer-supplied Stop Solution was then used to terminate the chromogenic reaction, and absorbance immediately measured at 450 nm using a Tecan Infinite M200 plate reader. Plate reader absorbencies were tabulated in Microsoft Excel, then imported into DeltaSoft ELISA analysis software, and interpreted using 4-parametric analysis.

M4.4 – 4.5: Flow Cytometric Analysis of CXCR-1 and CXCR-2 Status in Stimulated and Unstimulated DENOFO8 Fibroblast Cultures

Cell line conditioned media was collected, normalised and stored at -21 °C in an identical manner as described in Chapter 2, methods section 2.1.

DENOFO8 normal oral fibroblasts were grown to approximately 70 % confluence in T75 flasks. Human peripheral blood monocytes were used as a positive control. Flasks were then washed X3 in PBS and then incubated at 37 °C for 24 h with either cell line conditioned media or normal media control. Cells were then washed, non-enzymatically retrieved using cell dissociation solution (Sigma-Aldrich, Dorset, England, Cat C5914-100ML), diluted in cold FACS buffer (PBS with 0.1 % Sodium Azide and 1 % BSA) and then centrifuged at 1,000 rpm for 5 minutes to form a pellet. Cells were then resuspended in cold FACS buffer, and then centrifuged again at 1,000 rpm for 5 minutes. Cell pellets were then resuspended in FACS buffer and 50 µL suspension transferred to a microtube and incubated on ice for 45 minutes with either 50 µL monoclonal mouse anti CXCR-1 antibody (R&D Systems, Minneapolis, USA, Cat. number MAB330), monoclonal mouse CXCR-2 antibody (R&D Systems, Minneapolis, USA, Cat. Number MAB331) or FACS buffer control. Final antibody concentrations over the incubation period were 10 µg mL⁻¹ for both anti-CXCR-1 and anti-CXCR-2. Suspensions were then washed with 1 mL cold FACS buffer, centrifuged at 6,000 rpm for 2 minutes, supernatant discarded and then resuspended in 50 µL fluorescent conjugated secondary antibody (Life Technologies, AlexaFluor 488 labelled goat anti-mouse antibody, Cat A11001) at a 1:50 dilution in cold FACS buffer. Cells were then washed X2 in cold FACS buffer, with centrifugation at 6,000 rpm for 2 minutes between washes. The final pellet was resuspended in 300 µL FACS buffer and immediately analysed using a Calibur flow cytometer set to analyse 10,000 events. Flow cytometry data were then plotted and converted into overlay histogram images using Flowing 2.5.1 software (freeware, Turku, Finland).

M4.6: PCR analysis of Cell Line GRO- β and GRO- γ mRNA Expression

Cytokine array data presented in Chapter 3, Figure 3.2 demonstrated elevated non-specific GRO (reactive to GRO - α , - β & - γ) array densitometry in cell line conditioned media without comparable elevation of GRO- α specific array densitometry. Cytokine arrays did not include GRO- β or GRO- γ specific spots; upregulation of GRO- β and/or GRO- γ expression was therefore inferred. Due to prohibitively high ELISA costs, preliminary analysis of GRO- β and GRO- γ was instead undertaken at the mRNA level in order to determine which candidate molecules demonstrated promise in accounting for the non-specific GRO signal uptake on cytokine array.

cDNA for cell lines UD SCC02, UPCI SCC072, UPCI SCC089 and UPCI SCC090 was prepared as described in Chapter 1, methods section 1.1.

Commercially available Taqman probes for GRO- β and GRO- γ (FAM reporter) were purchased from Applied Biosystems, UK (Cat numbers Hs00601975_m1 and Hs00171061_m1). A probe for the B2M housekeeping gene was used in parallel to each GRO probe (VIC reporter). Concomitant 10 μ L experiments on cDNA extracted from each cell line were run in a 96-well PCR plate; each experiment was undertaken in triplicate repeat. Table 1.5, Chapter 1, summarises the components of the 10 μ L PCR mixture. Reagents were centrifuged for 1 minute at 1,000 rpm and then exposed to PCR reaction conditions of 50 $^{\circ}$ C for 2 mins, 95 $^{\circ}$ C for 10 minutes, followed by 40 cycles of 15 s at 95 $^{\circ}$ C/ 1 min at 60 $^{\circ}$ C using a 7900 Fast real-time PCR Machine.

Results were tabulated using Microsoft Excel, and relative expression calculated, normalised to the cell line UPCI SCC090.

M4.7: ELISA Analysis of Media 2 IL-6 Content Following

Experimental Blockade of Fibroblast CXCR-2

Cell line conditioned media was collected, normalised and stored at -21 °C in an identical manner as described in Chapter 2, methods section 2.1.

DENOF08 normal oral fibroblasts were grown to early confluence in T75 flasks and then washed X3 in PBS. 6 mL conditioned media from HPV-negative cell lines UPCI SCC072 and UPCI SCC089 was then added to separate flasks and incubated for 24 h in the presence of either the CXCR-2 antagonist SB265610, or DMSO control. SB265610 had been pre-optimised by co-workers to a concentration of 500 ng mL⁻¹ when used to block CXCR2 activity in keratinocyte cultures; in order to safeguard adequate CXCR inhibition, a ten-fold increase in inhibitor concentration was used, with intention to repeat experiments using dose-response analysis and cytotoxicity assays should inhibition of IL-6 secretion occur.

Cells were then washed X3 in PBS, and incubated with normal media for a further 24 h to obtain a stimulated fibroblast Medium 2 in a similar manner as described in Chapter 2. Medium 2 was therefore collected from fibroblasts exposed to each HPV-negative cell line conditioned medium in the presence or absence of SB265610. Conditioned media were then subjected to ELISA analysis of IL-6 concentration, as described in methods section 4.1, above.

M4.8: ELISA Analysis of Fibroblast Conditioned Media IL-6 Content

Following Co-Incubation with Recombinant Human GRO β / GRO γ

Following the inability of CXCR inhibition to restrain IL-6 release in stimulated DENOF08 normal fibroblasts, the role of GRO- β and GRO- γ were directly assessed using recombinant human proteins. Due to the potential for IL-6 to induce positive feedback of its own secretion when in combination with other IL-6-inducing factors such as IL-17A³³⁸, 2 ng mL⁻¹ IL-6 plus 2 ng mL⁻¹ sIL-6R (the solubilised receptor observed in HPV-negative cell line cytokine array analysis) were also added to experimental media.

Recombinant human IL-6, sIL-6R, GRO- β and GRO- γ were purchased from Insight Biotechnology (Cat numbers 10-1018-C, 10-1252-C, 10-1118-B and 10-1157-B, respectively).

DENOF08 normal fibroblasts were grown to early confluence, washed X3 in PBS and then co-incubated with either normal media control or normal media containing 2 ng mL⁻¹ IL-6 plus/minus IL-6R, plus/minus GRO- β or GRO- γ .

Experimental medium recombinant GRO- β /GRO- γ concentration was 2 ng mL⁻¹, comparable in magnitude to the limited experimental data available on GRO- α release by head and neck cell lines³³³. Recombinant sIL-6R was added at a concentration of 2 ng mL⁻¹, which is comparable to UPCI SCC072 sIL-6R release into cell line conditioned medium when taking into account 3 million cells contributing to 1 mL cell line conditioned media (please refer to Figure 4.3).

Following 24 h incubation, media were retrieved and stored as a recombinant Medium 1 equivalent. Fibroblasts were then washed X3 in PBS and then 6 mL normal media added. Stimulated fibroblasts were incubated with the normal media for 24 h and then recombinant protein-stimulated Medium 2 retrieved. All media was stored immediately at -21 °C. Media were subsequently thawed and assessed via IL-6 ELISA analysis as described in M4.1, above.

M4.9: Use of GRO-Stimulated Fibroblast Conditioned Media in ORIS™ Assay Experiments

After failure to demonstrate an IL-6 secretory response in DENOF08 fibroblasts following exposure to recombinant GRO- β/γ , the collected recombinant protein-stimulated Medium 2 was used in ORIS™ migration experiments to rule out the induction of an alternative factor via GRO-stimulation that could account for the migratory phenomenon observed in Chapter 2.

ORIS™ assays were undertaken in an illustrative cell line and recombinant protein-stimulated Medium 2 in order to reduce overall experimental costs and workload, due to the low anticipation of significant effect. Recombinant GRO- γ -stimulated Medium 2 was therefore used against unstimulated fibroblast conditioned medium control in cell line UPCI

SCC072 ORIS™ assay migrations. In brief, ORIS™ assay methods were identical to that described in Chapter 2, experimental methods 2.1, albeit with recombinant GRO- γ -stimulated fibroblasts replacing cell line-stimulated fibroblast media.

M4.10: ORIS™ Assay Analysis of Cell Line UPCI SCC072 Migration in Response to IL-6

In order to fully assess a role of IL-6 in HPV-negative cell line migrations, irrespective of the underlying precipitant of the HPV-negative stimulated fibroblast IL-6 response, ORIS™ assays were repeated for cell line UPCI SCC072 in the presence of either normal media control or logarithmically-increasing doses of recombinant human IL-6 in normal media. Experimental methods were again identical to that described in Chapter 2, experimental methods 2.1, other than for the use of recombinant IL-6-containing media in place of stimulated fibroblast conditioned medium.

Results

Figure 4.1: IL-6 ELISA Analysis of Cell Line Conditioned Media and Stimulated Fibroblast Media 1&2

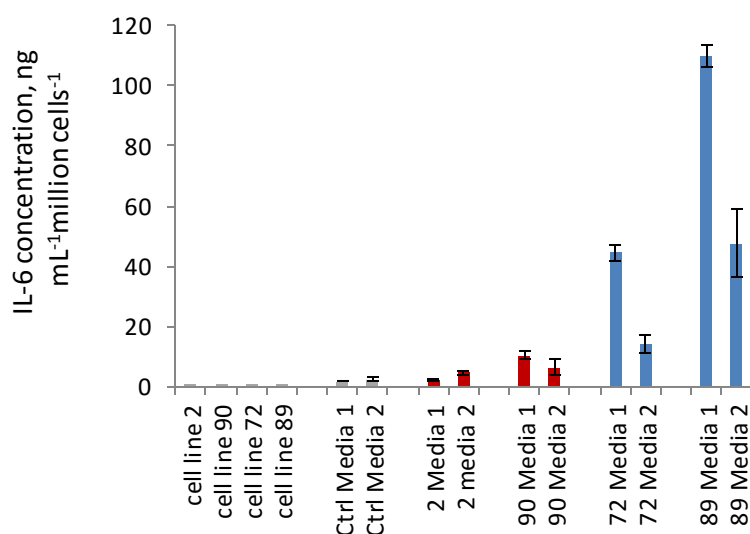


Figure 4.1: IL-6 ELISA analysis of cell line 24 h conditioned media and stimulated DENOFO8 fibroblast Media 1 & 2. $n=9$, Y-axis denotes standardised IL-6 concentration, in ng per mL, per million cells. Grey bars denote cell line conditioned media/ unstimulated fibroblast control Media 1 & 2. Red bars denote HPV-positive cell line-stimulated fibroblast Media 1 & 2, blue bars denote HPV-negative cell line-stimulated fibroblast Media 1 & 2. All conditioned media contained significantly greater IL-6 compared to respective fibroblast control medium (Mann-Whitney U-test, $P<0.05$), other than UPCI SCC02 stimulated fibroblast Medium 1.

Cell line – denotes cell line-derived 24 h conditioned media, numerical suffix denotes specific cell line (2 – UD SCC02, 72 – UPCI SCC072, 89 – UPCI SCC089, 90 – UPCI SCC090)

Ctrl – unstimulated fibroblast conditioned medium control

Media 1 – stimulated fibroblast Media 1 (please refer to Chapter 2 for definitions of Media 1 & 2). Numerical prefix denotes specific cell line (2 – UD SCC02, 72 – UPCI SCC072, 89 – UPCI SCC089, 90 – UPCI SCC090)

Media 2 – stimulated fibroblast Media 2

Consistent with cytokine array findings (please refer to Chapter 3, Figures 3.4 & 3.10), HPV-negative cell lines induced marked IL-6 secretion by DENOFO8 fibroblasts. An initial secretory response can be observed in Media 1, with a subsequent tail-off of response in Media 2. HPV-positive cell lines can be observed to also induce an IL-6 response, although the magnitude of the response is low compared to HPV-negative cell lines.

All cell line and unstimulated fibroblast control media demonstrated minimal IL-6 release, confirming fibroblast stimulation by conditioned media had led to the secretory response observed in Media 1 & 2.

Figure 4.2: IL-8 ELISA Analysis of Cell Line Conditioned Media and Stimulated Fibroblast Media 1&2

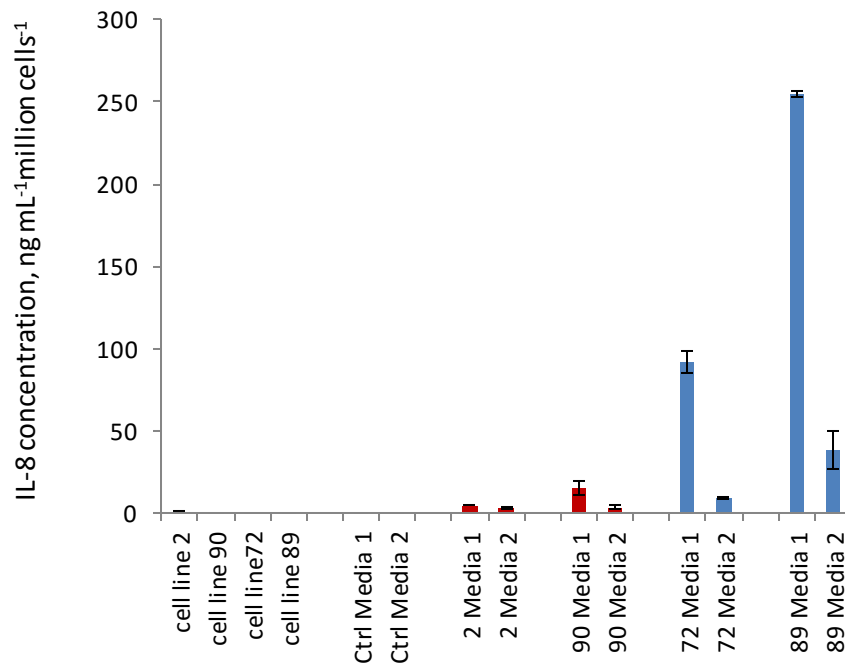


Figure 4.2: IL-8 ELISA analysis of cell line 24 h conditioned media and stimulated DENOF08 fibroblast Media 1 & 2. n=9, Y-axis denotes standardised IL-8 concentration, in ng per mL, per million cells. Grey bars denote cell line conditioned media/unstimulated fibroblast control Media 1 & 2. Red bars denote HPV-positive cell line-stimulated fibroblast Media 1 & 2, blue bars denote HPV-negative cell line-stimulated fibroblast Media 1 & 2. All conditioned media contained significantly greater IL-8 compared to respective fibroblast control medium (Mann-Whitney U-test, P<0.05).

Cell line – denotes cell line-derived 24h conditioned media, numerical suffix denotes specific cell line (2 – UD SCC02, 72 – UPCI SCC072, 89 – UPCI SCC089, 90 – UPCI SCC090)

Ctrl – unstimulated fibroblast conditioned medium control

Media 1 – stimulated fibroblast Media 1. Numerical prefix denotes specific cell line (2 – UD SCC02, 72 – UPCI SCC072, 89 – UPCI SCC089, 90 – UPCI SCC090)

Media 2 – stimulated fibroblast Media 2

As seen for IL-6 ELISA, HPV-negative cell lines induced marked IL-8 secretion by DENOF08 fibroblasts. An initial secretory response can be observed in Media 1, with a subsequent tail-off of response in Media 2. HPV-positive cell lines can be observed to also induce an IL-8 response, although the magnitude of the response is low compared to HPV-negative cell lines. The mirrored pattern of fibroblast secretion of IL-8 compared to IL-6 infers that a common stimulatory mechanism may underlie the release of both factors.

All cell line and unstimulated fibroblast control media demonstrated minimal IL-8 release compared to the observed concentrations of IL-8 produced in Media 1 & 2, confirming that fibroblast stimulation by cell line conditioned media had led to the secretory response observed in Media 1 & 2. Note that although dwarfed by the degree of fibroblast secretory response, UD SCC02 basally secreted $2,000 \text{ pg mL}^{-1} \text{ million cells}^{-1}$ IL-8, which vastly exceeded other cell line basal IL-8 secretion of approximately $50 \text{ pg mL}^{-1} \text{ million cells}^{-1}$.

Figure 4.3: Solubilised IL-6R ELISA Analysis of Cell Line-Derived Conditioned Media

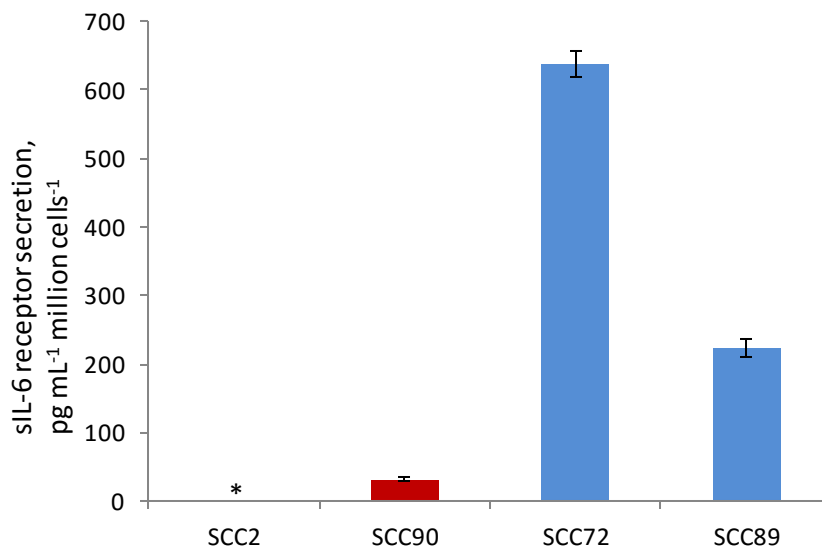
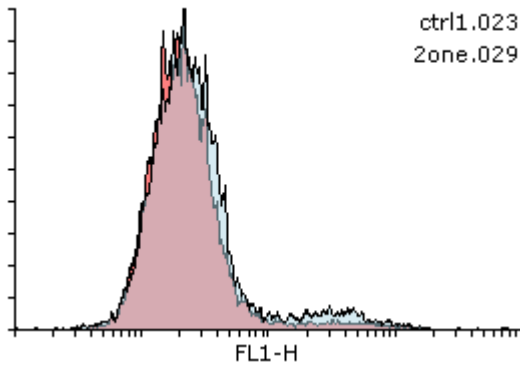


Figure 4.3: ELISA analysis of 24 hours Soluble IL-6 Receptor release into conditioned media, standardised to pg per mL, per million cells. n=9, error bars denote +/- 1 S.E. *UD SCC02 levels undetectable in all triplicate samples and all triplicate repeats using 4-para analysis (Raybiotech Human IL-6sR ELISA sensitivity reported at <3 pg mL⁻¹). Red bars denote HPV-positive cell lines (UD SCC2; SCC2, UPCI SCC090; SCC90), blue bars denote HPV-negative cell lines (UPCI SCC072; SCC72, UPCI SCC089; SCC89).

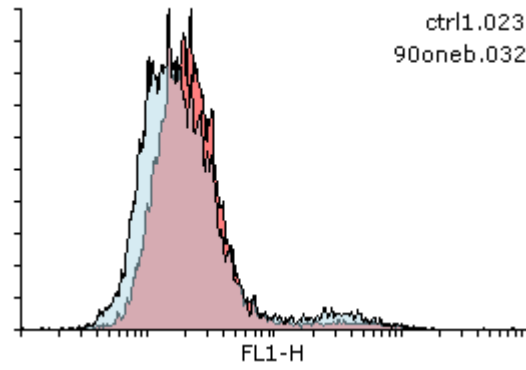
Marked release of the solubilised IL-6 receptor is observed in both HPV-negative cell lines, whereas HPV-positive cell lines produce little or no solubilised receptor. A statistically significant increase in IL-6R secretion was observed in both HPV-negative cell line conditioned media compared to UPCI SCC090 (Mann-Whitney U-test, P<0.05). Note the particularly elevated release of sIL-6R by cell line UPCI SCC072, which may be postulated as having a role in the increased migrations observed in UPCI SCC072 Medium 1 compared to UPCI SCC072 Medium 2 – Media 1 contained 24 h cell line-derived secretions which includes sIL-6R; Media 1 therefore retains greater potential for IL-6 trans-signalling via sIL-6R compared to Media 2, which may only contain sIL-6R following commencement of the migration assay, whereby assay-containing cells may secrete sIL-6R into the medium.

Figure 4.4: Flow Cytometry Analysis of CXCR-1 Expression in DENOF08 Normal Oral Fibroblasts Following Exposure to Cell Line Conditioned Media

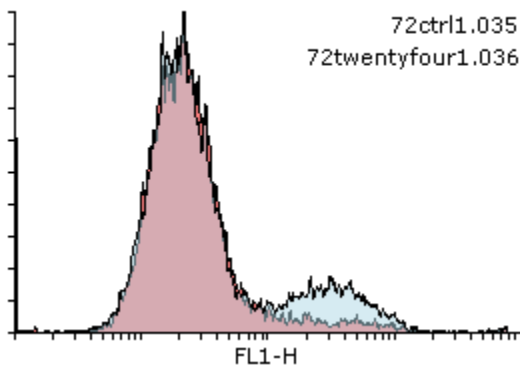
a).UD SSC02



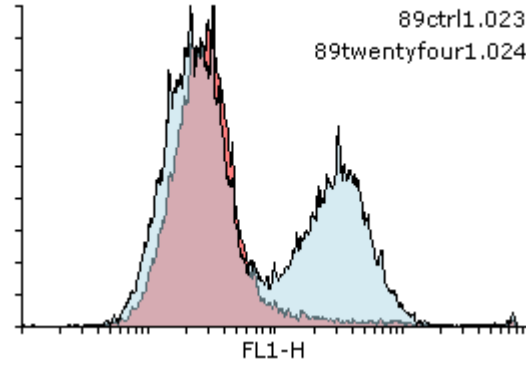
b).UPCI SCC090



c). UPCI SCCC072



d). UPCI SCC089



e). Monocyte Control

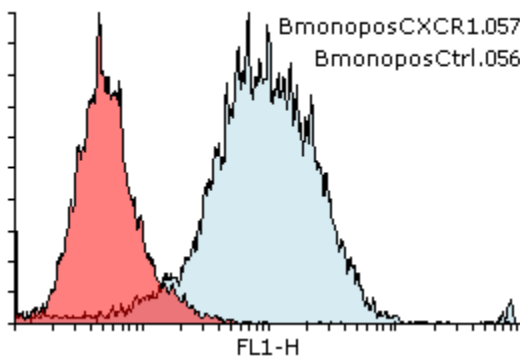
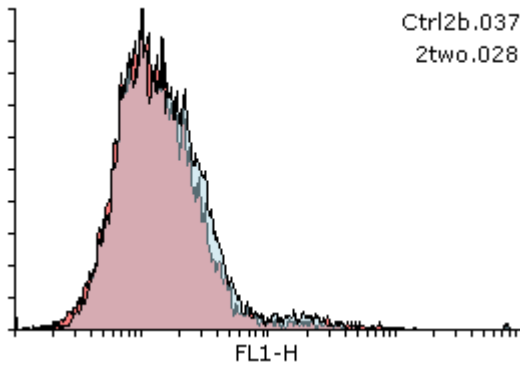


Figure 4.4: Flow cytometry analysis of CXCR-1 expression in DENO08 normal oral fibroblast cultures following 24 h exposure to conditioned media taken from cell lines UD SCC02, UPCI SCC072, UPCI SCC089 and UPCI SCC090 (n=3 biological repeats). Figures a, b, c and d: flow cytometry FL1-H (488 nm) overlay histograms for DENO08 fibroblast CXCR-1 expression after 24 h incubation with tumour line conditioned media (blue) versus CXCR-1 expression in unstimulated fibroblast control (red) for respective cell lines. Figure e: flow cytometry FL1-H overlay histogram for monocyte positive control; red denotes incubation with IgG control, blue denotes incubation with CXCR-1 specific antibody.

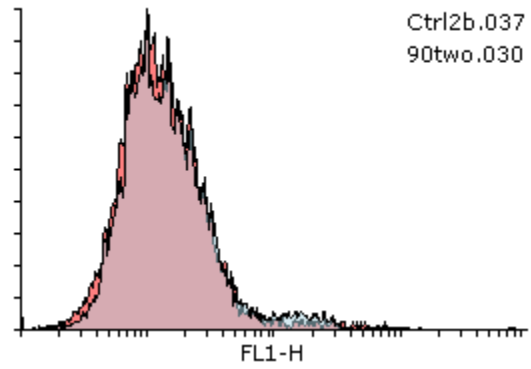
CXCR-1 is seen to be constitutively absent in the unstimulated fibroblast population. Following 24 h incubation with both HPV-negative cell line conditioned media (Figures c and d), a CXCR-1 positive subpopulation is established - observed as a second peak. Conversely, HPV-positive cell line conditioned media did not induce a clear subpopulation of CXCR-1 positive fibroblasts (Figures a and b).

Figure 4.5: Flow Cytometry Analysis of CXCR-2 Expression in DENO08 Normal Oral Fibroblasts Following Exposure to Cell Line Conditioned Media

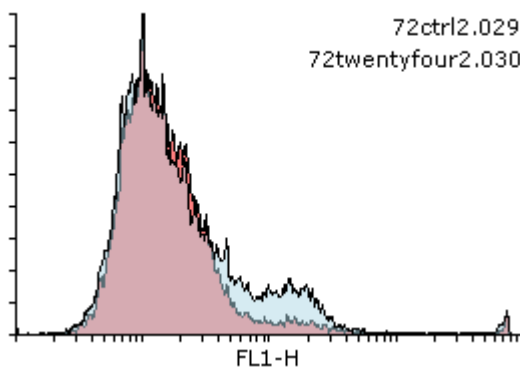
a).UD SSC02



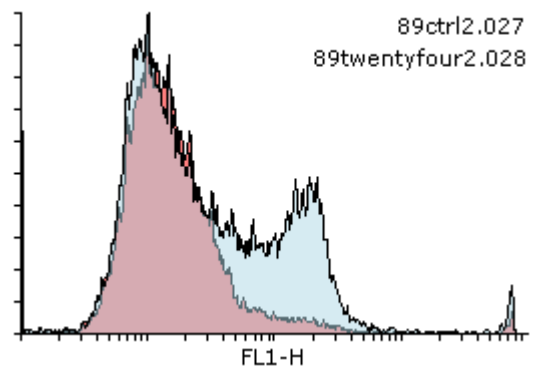
b).UPCI SCC090



c). UPCI SCCC072



d). UPCI SCC089



e). Monocyte Control

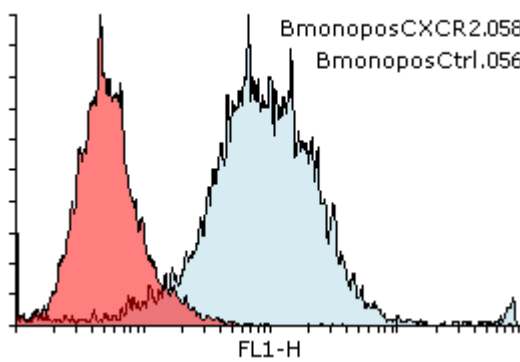


Figure 4.5: Flow cytometry analysis of CXCR-2 expression in DENO08 normal oral fibroblast cultures following 24 h exposure to conditioned media taken from cell lines UD SCC02, UPCI SCC072, UPCI SCC089 and UPCI SCC090 (n=3 biological repeats). Figures a, b, c and d: flow cytometry FL1-H (488 nm) overlay histograms for DENO08 fibroblast CXCR-2 expression after 24 h incubation with tumour line conditioned media (blue) versus CXCR-2 expression in unstimulated fibroblast control (red) for respective cell lines. Figure e: flow cytometry FL1-H overlay histogram for monocyte positive control; red denotes incubation with IgG control, blue denotes incubation with CXCR-2 specific antibody.

In a similar manner to CXCR-1, CXCR-2 is seen to be constitutively absent in the unstimulated fibroblast population. Following 24 h incubation with both HPV-negative cell line conditioned media (Figures c and d), a CXCR-2 positive subpopulation is established - observed as a second peak. Conversely, HPV-positive cell line conditioned media again did not induce a clear subpopulation of CXCR2 positive fibroblasts (Figures a and b).

Figure 4.6 GRO- β and GRO- γ mRNA Expression in HPV-positive Versus HPV-negative Cell Lines

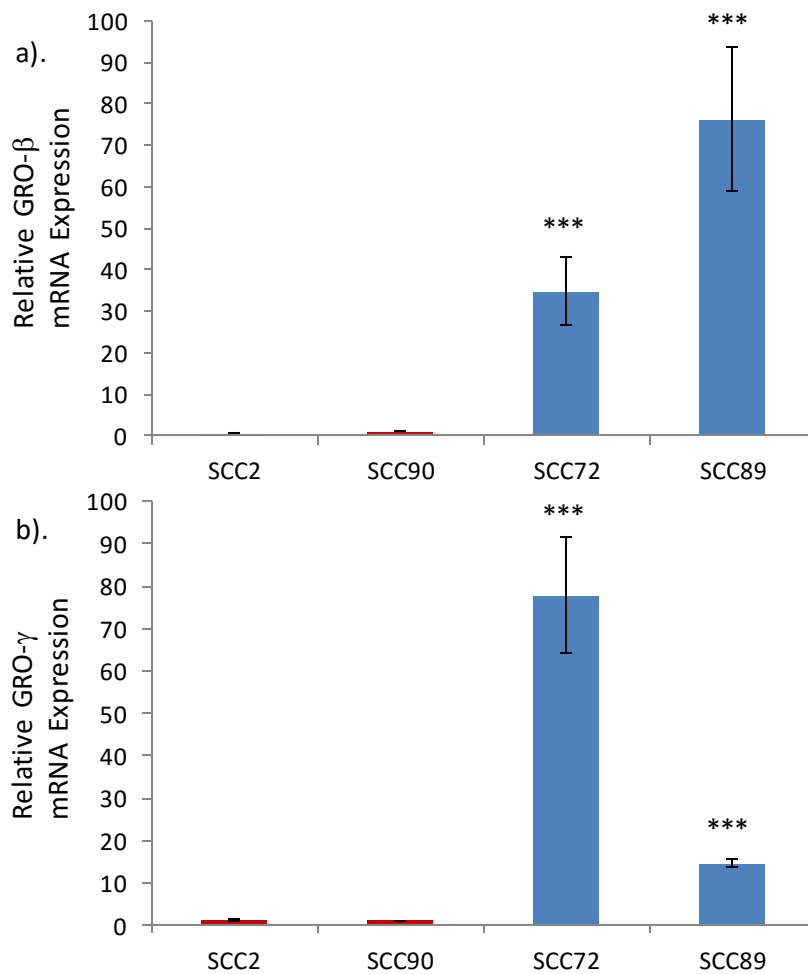


Figure 4.6 a). PCR analysis of GRO- β expression in respective cell lines. Error Bars denote ± 1 SEM, n=9. Red bars denote HPV-positive cell lines, Blue bars denote HPV-negative cell lines. Y-axis represents GRO- β mRNA expression relative to UPCI SCC090. Note the marked increase in GRO- β expression seen in both HPV-negative lines (blue bars) compared to HPV-positive lines (red bars).

Figure 4.6 b). PCR analysis of GRO- γ expression in respective cell lines. Error Bars denote ± 1 SEM, n=9. Red bars denote HPV-positive cell lines, Blue bars denote HPV-negative cell lines. Y-axis represents GRO- γ mRNA expression relative to UPCI SCC090. There is again an increased expression of GRO- γ compared to HPV-positive lines, although the proportional relationship between expression in UPCI SCC072 and UPCI SCC089 is the inverse of that seen for GRO- β . It was postulated that the increased GRO- γ expression in cell line UPCI SCC072 compared to UPCI SCC089 may account for the increased migration observed in the respective fibroblast Medium 1, as GRO- γ is known to have a greater avidity and stimulatory capacity for CXCR-2³³⁹.

A highly significant difference in both GRO- β and GRO- γ expression was observed for both HPV-negative cell lines compared to UPCI SCC090, whereas UD SCC02 demonstrated no significant difference (Mann-Whitney U-test, ***P<0.001).

Figure 4.7: ELISA Analysis of Media 2 IL-6 Content Following Co-incubation of Fibroblasts with 5 $\mu\text{g mL}^{-1}$ SB265610 Versus DMSO Control.

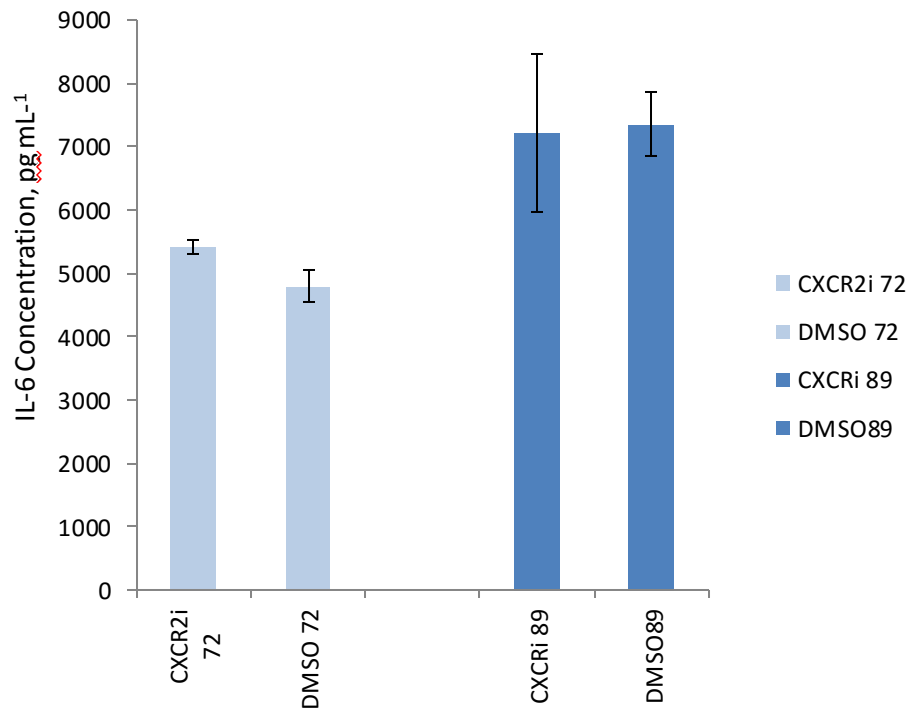


Figure 4.7: IL-6 ELISA analysis of HPV-negative cell line-stimulated DENOFO8 Media 2 following co-incubation with the CXCR-2 inhibitor SB265610, versus DMSO control. Error bars denote SEM, n=9.

CXCRi – co-incubation with 5 $\mu\text{g mL}^{-1}$ SB265610

DMSO – co-incubation with DMSO control

72 – UPCI SCC072-stimulated DENOFO8 Medium 2

89 – UPCI SCC089-stimulated DENOFO8 Medium 2

Note that for both cell lines tested, no significant difference (Mann-Whitney U-test, $P > 0.05$) in IL-6 secretion was found following co-incubation with SB265610, versus DMSO control. Note also that IL-6 concentration is plotted in pg mL^{-1} , and therefore does not directly correlate to data presented in Figure 4.1, which is displayed in pg mL^{-1} million cells⁻¹ in order to normalise data between cell line and fibroblast conditioned media. DENOFO8 concentration was 4×10^5 cells mL^{-1} , accounting for the approximate 2.5 fold change in magnitude between the two figures.

Lack of change in IL-6 secretion following co-incubation with the CXCR-2 inhibitor SB265610 suggests that CXCR-2 receptor stimulation is not important in the induction of the IL-6 response by HPV-negative cell lines.

Figure 4.8: ELISA Analysis of IL-6 Content Following Stimulation of Fibroblasts with Permutations of sIL-6R, IL-6, GRO β and GRO γ

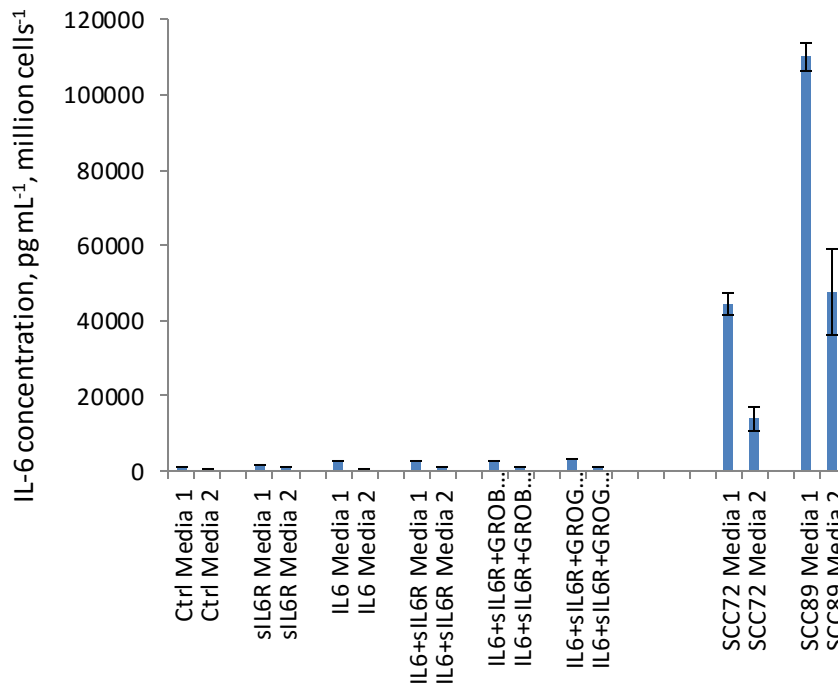


Figure 4.8: Fibroblast IL-6 secretory response, measured by ELISA, following incubation with 2 ng mL⁻¹ GRO- β or GRO- γ in combination with 2 ng mL⁻¹ IL-6 plus recombinant 2 ng mL⁻¹ solubilised IL-6 receptor in order to allow for any potential positive feedback interaction with IL-6 via the trans-signalling route. Error bars denote SD, n=3 (single biological repeat) for all recombinant protein conditions.

Ctrl – unstimulated fibroblast control medium

sIL6R – 50 ng mL⁻¹ sIL-6R added to medium

IL6 – 2 ng mL⁻¹ IL-6 added to medium

GRO β - 2 ng mL⁻¹ GRO β added to medium

GRO γ – 2 ng mL⁻¹ GRO γ added to medium

SCC72 – UPCI SCC072 stimulated positive control

SCC89 – UPCI SCC089 stimulated positive control

Note that no combination of GRO β /GRO γ /IL-6/sIL-6R precipitated a fibroblast secretory response comparable to that observed in positive control media. Statistical testing was not undertaken due to n=3, in addition to the magnitude of change observed in HPV-negative cell line Media 1&2 versus that observed in all recombinant protein groups. Minor rises of IL-6 concentration in Media 1 of all experimental groups other than sIL-6R alone, are attributable to the presence of 2 ng mL⁻¹ recombinant human IL-6 in respective conditions and therefore do not infer a fibroblast secretory response. In conclusion, the above data suggest that GRO- β / GRO- γ are not responsible for inducing the IL-6 secretory response in stimulated fibroblast media.

Figure 4.9: ORIS™ Assay of UPCI SCC072 Migration in Response to recombinant GRO- β/γ - Stimulated Fibroblast Media 2

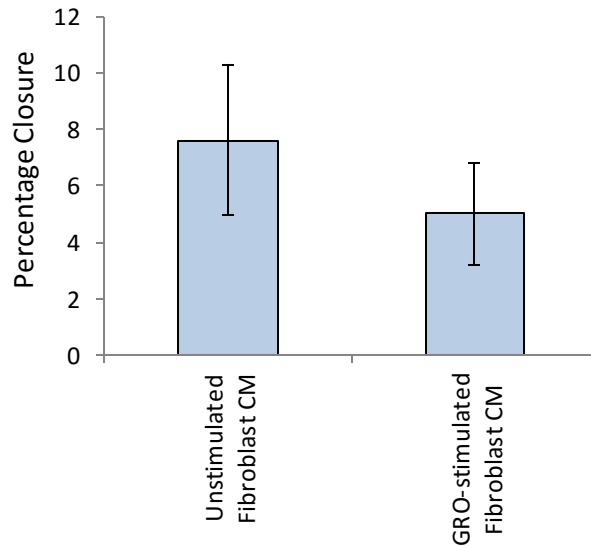


Figure 4.9: ORIS™ migration assay of cell line UPCI SCC072 cultured in the presence of recombinant GRO- β/γ - stimulated fibroblast Medium 2 versus unstimulated fibroblast control. $n=9$, error bars denote SEM. GRO-stimulated fibroblast medium induced no additional migration compared to unstimulated fibroblast medium control, and no significant difference in migration was noted between experimental and control groups (Mann-Whitney U-test, $P>0.05$), suggesting that GRO- β/γ are not responsible for inducing the migratory response observed in HPV-negative cell line-stimulated fibroblast conditioned media. Note that both treatment and control media led to the same degree of void closure observed in control migrations for cell line UPCI SCC072 in preceding experiments, and were much less than that observed for UPCI SCC072-stimulated fibroblast medium (please refer to Chapter 2, Figure 2.3).

Figure 4.10: Recombinant IL-6 Dose-Response Curve for Additional ORIS™ Assay Migration, Compared to DMEM Control

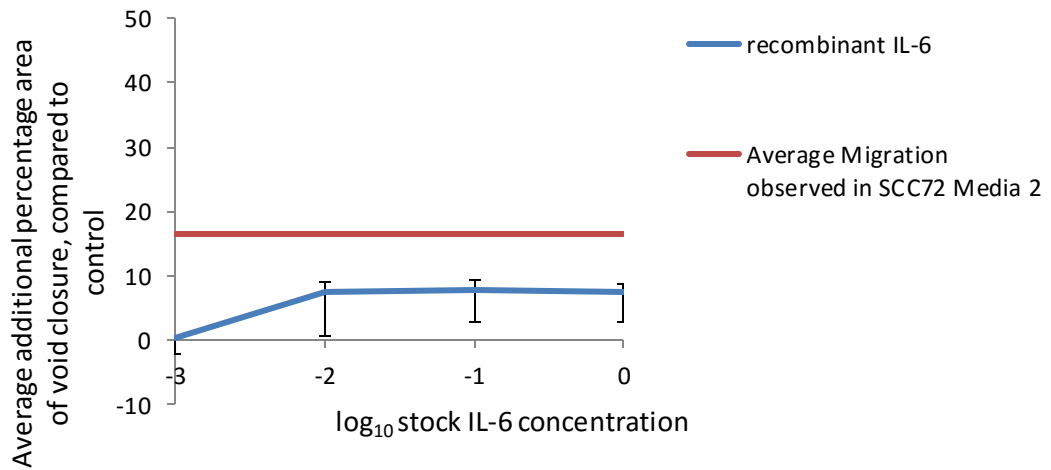


Figure 4.10: Dose-response curve for additional ORIS™ assay migration in cell line UPCI SCC072 in the presence of recombinant IL-6. Y-axis denotes additional percentage void closure, compared to respective control. Blue line denotes median additional closure following incubation with logarithmically-increasing concentrations of recombinant human IL-6 in normal media, error bars denote range. Stock concentration of IL-6 was 2 µg mL⁻¹. Control medium was normal media (compare to Medium 2, below). Repeats were limited to n=3 (3 biological repeats of n=1).

As a comparison, red line denotes average additional percentage migration observed in UPCI SCC072-stimulated DENOFO8 Medium 2 compared to unstimulated fibroblast control (please refer to Chapter 2, Figure 2.3).

IL-6 can be observed to have a weak overall influence on additional migration, illustrated by lower range of error bars nearing zero. Note that irrespective of any meaningful additional migration in the presence of recombinant IL-6 in at concentrations between 1 X 10⁻³ – 1 X 10⁻² stock (reflecting a biologically-relevant range of recombinant IL-6 concentrations; please refer to Figure 4.1), migration did not approach the degree of additional migration that was achieved with Medium 2.

Note that although the respective controls differ between Medium 2 and recombinant IL-6 experiments, the unstimulated fibroblast control for Medium 2 was ultimately found to outperform normal media in inducing cell migration (please refer to Chapter 6, Figures 6.5-6.6), and therefore the difference in controls weakens the illustrated difference in effect size between recombinant IL-6/Medium 2 induced additional migrations, whereas the true difference in effect is greater.

It was therefore concluded that IL-6 did not have the capacity to act as a sole driver of the HPV-negative cell line migrations observed in Media 1 & 2.

Discussion

Discussion of Results

This chapter has tested and disproved the hypothesis that IL-6 acts as a principal inducer of the additional migrations observed in HPV-negative cell lines. Intense cytokine array uptake of both IL-6 & IL-8 in HPV-negative stimulated fibroblast media (Chapter 3, Figures 3.4 & 3.5) had initially prompted both molecules to be regarded as alluring candidates on which to form a hypothetical basis for the observed migrations. This saliently illustrates a major shortcoming of cytokine array technology, which is to lead the unassuming researcher to ascribe greatest significance to the most intense spot densities noted within an array. There is considerable variation in array spot sensitivities; RayBiotech cytokine array minimum sensitivities for both IL-6 & IL-8 are 1 pg mL^{-1} , whereas sensitivity to HGF is 200 pg mL^{-1} , and thrombospondin-1 is 100 ng mL^{-1} ; a 100,000-fold difference in sensitivity (Raybiotech cytokine array manufacturer-supplied data). Moreover, variance in spot sensitivity may be further complicated by variations in the bioactivity of each candidate molecule; spot sensitivity is not directly calibrated to bioactivity and these two variables may therefore compound each other.

Presence of intense array uptake for the solubilised IL-6 receptor in HPV-negative cell line conditioned media prompted further assumptions relating to the significance of IL-6 release by HPV-negative stimulated fibroblasts in the context of migration, as a potential receptor-ligand relationship that correlated to the conditioned medium-induced migrations was evident. ELISA quantification of IL-6 and sIL-6R in the respective media (Figures 4.1 & 4.3), added emotional weighting to the notion that IL-6 may have potential to drive cell migration. Whilst IL-6 & sIL-6R ELISAs allowed more accurate quantification of cytokine array findings, and are indeed valuable in combination with IL-8 ELISA data to confirm the inflammasome of the HPV-negative microenvironment suggested by our experimental model, ELISA quantification offered no additional evidence over cytokine array data to support IL-6 driven migration. Caution has to be taken to remain impartial to such supplementary data, which can only offer a pseudoscientific “theory-confirmation approach” to an established hypothesis, as was originally outlined by Popper³⁴⁰. Application of a more appropriate “theory falsification approach” to hypothesis testing, as addressed by subsequent experiments, has provided evidence to robustly disprove a principal IL-6 basis for microenvironmentally-supported tumour migration, with repeated acceptance of the null hypothesis of no significant effect throughout latter experimentation.

Initial work regarding GRO- β and/or GRO- γ as a hypothetical basis for stromal induction offered promising results. PCR analysis of both GRO- β and GRO- γ mRNA demonstrated upregulation of both sequences in HPV-negative cell lines in comparison to HPV-positive cell lines (Figures 4.6 a & b). Due to the lack of reliable, commercially-available ELISA kits for GRO- β and GRO- γ , ELISA was not undertaken to confirm GRO- β and GRO- γ concentrations at the protein level in the first instance; the role of both molecules in inducing migration was disproved prior to the purchasing and optimisation of custom GRO-ELISA plates. Cytokine array data confirming upregulated “non- α ” GRO secretion by cell lines (Figure 3.2), in combination with PCR data, suggested that increased levels of both GRO- β and GRO- γ secretion at a protein level by HPV-negative lines was highly probable. This prompted further analysis of a potential GRO-based interaction with fibroblasts via confirmation of fibroblast CXCR receptor status.

Whilst basal fibroblast CXCR-1 & CXCR-2 receptor status was found to be negative, stimulation with HPV-negative cell line conditioned media led to a fibroblast subpopulation expressing both CXCRs (Figures 4.4 & 4.5). It is unclear whether the same cellular subpopulation expressed both CXCR-1 and CXCR-2, although further investigation using multiple-colour flow cytometry would allow confirmation had this been desirable. The induction of CXCR-1/2 expression, along with release of GRO from HPV-negative cell lines, offered initial evidence to confirm the hypothesis of IL-6 induction via GRO stimulation of CXCR2.

Despite the initial findings, fibroblast stimulation with recombinant GRO- β or GRO- γ in combination with recombinant solubilised IL-6 receptor led to no release of IL-6 (Figure 4.8). A limitation of this experiment was that it had been assumed that fibroblast expression of CXCR-1/2 would be induced during either GRO stimulation or IL-6/sIL-6R stimulation, although this had not been confirmed as the process via which HPV-negative cell line conditioned media induced CXCR expression. It therefore remained feasible that CXCR expression may be triggered by an alternative route, thereby not completely ruling out the potential for GRO to be responsible for stimulating IL-6 release by fibroblasts. Furthermore, experimental GRO- β and GRO- γ recombinant protein concentrations had been estimated using cytokine array sensitivities and densitometry comparison to positive array spots, along with the limited data available in the literature³³³, and therefore may not have been within biologically relevant concentrations. Supplemental experimentation was therefore undertaken using a CXCR inhibitor at concentrations previously optimised by colleagues

within the research group, in order to determine whether blockade of CXCR-2 would inhibit IL-6 release from fibroblasts when stimulated by HPV-negative cell line conditioned media (Figure 4.7). Again, incubation of fibroblasts in the presence of 5 $\mu\text{g mL}^{-1}$ of the CXCR-2 inhibitor SB265610 in both SCC72 and SCC89 cell line conditioned media led to no decrease in IL-6 release when compared to conditioned media containing DMSO control (Mann-Whitney U-test, $P=0.270$ 2-tailed, $P=0.297$ 1-tailed). In combination with the preceding recombinant protein stimulation data, this provided satisfactory evidence to reject the hypothesis that GRO- β/γ was responsible for inducing significant fibroblast release of IL-6.

Indeed, a relatively recent paper, Guo *et al* provided evidence to refute an interdependent relationship between CXCR-2 expression and release of both IL-6 & IL-8³⁴¹. The authors noted that following exposure to 10 Gy ionising radiation, peaks in CXCR-2 mRNA expression and IL-6/IL-8 mRNA expression followed differing temporal relationships. This work did however involve non-oncogenic induction of senescence in U2OS osteosarcoma cells, and one must also take care to avoid interpreting Guo's data in a dogmatic fashion not only due to the experimental conditions, but also due to the fact that Guo assessed the relationship of induction of CXCR-2 *expression* and IL-6/IL-8 release rather than the relationship between CXCR-2 *stimulation* and IL-6/IL-8 release.

Final experimentation in order to disprove a role of GRO in inducing fibroblast support for cell migration was to use Medium 2 taken from fibroblasts stimulated by GRO- γ and assess whether this medium promoted cell migration via a factor other than IL-6 that had been induced by the respective GRO molecule. Again, migration data failed to demonstrate an effect in response to recombinant proteins; repeats were therefore limited to $n=3$ due to assay expense.

Following the abandonment of GRO- β/γ as potential inducers of fibroblast activation, attention was placed on determining the role of IL-6 as a candidate molecule for inducing cell migration. The presence of the solubilised form of the receptor in HPV-negative cell line conditioned media (Figure 4.3) as quantified via ELISA, offered support for a potential IL-6-based role in cell line migration. This solubilised form of the IL-6 receptor has been extensively studied for its unusual capacity to signal in a similar manner to its membranous counterpart once bound to its ligand, via trans-signalling – as discussed in the chapter introduction. Furthermore, the absence of solubilised IL-6 receptor release by HPV-positive

cell lines offered an explanation for the specificity of fibroblast stimulated media to induce HPV-negative cell line migration alone.

In order to confirm a role for IL-6 in inducing cell migration, dose-response curves were constructed using ORIS migration assays of the HPV-negative cell line UPCI SCC072, exposed to logarithmic dilutions of recombinant human IL-6 in normal media. Those concentrations of recombinant IL-6 that approximated to the levels quantified in SCC72 stimulated fibroblast Media 1&2 (40-100 ng mL⁻¹; Figure 4.1) induced punitive additional migration compared to that observed when exposing cell lines to UPCI SCC072-stimulated fibroblast medium (red line, Figure 4.1). Furthermore, even at IL-6 doses excessive to that observed in conditioned media, cell line migration was inferior to that observed with stimulated fibroblast medium. It was therefore concluded that as recombinant IL-6 did not retain potential to induce comparable levels of migration to that seen using SCC72-stimulated fibroblast Medium 1&2, even when using concentrations of recombinant IL-6 higher than was determined in SCC72-stimulated fibroblast Media 1&2, IL-6 was not the primary factor responsible for inducing the additional cell migration.

Conclusions

Following the rejection of all aspects of the hypothetical model illustrated in Figure 4.0, the following conclusions could be drawn:

Whilst there is evidence of both GRO- β and GRO- γ upregulation in HPV-negative cell lines in comparison to HPV-positive cell lines, GRO does not appear to be responsible for stimulating fibroblasts to provide secretory support for HPV-negative cell line migration. Fibroblasts do not basally express canonical receptors to GRO, although expression of CXCRs 1&2 appears to be induced by HPV-negative cell line conditioned media. The importance of GRO in microenvironmental fibroblast stimulation cannot therefore be ruled out, although it remains unimportant to the migratory phenomenon under investigation. IL-6 appears to have a low capacity for inducing cell line migration; irrespective of whether this capacity is biologically significant, IL-6 is incapable of independently inducing the degree of cell migration observed with stimulated fibroblast conditioned media.

HPV-negative cell line conditioned media has the capacity to rapidly induce fibroblast secretion of significant levels of both IL-6 and IL-8 *in-vitro*; these molecules are potent

inflammatory mediators and have been implicated in a number of processes important to the tumour microenvironment, including leukocyte recruitment and neovascularisation³⁴²⁻³⁴⁷. The release of solubilised IL-6 receptor by HPV-negative cell lines allows potential for non-canonical IL-6 signalling to take place in those cells lacking the membranous form of the IL-6 receptor, and may therefore have the consequence of a broader number of cells in the microenvironment becoming stimulated, and contentiously could even offer potential for endocrine-like effects on distant organs via sIL-6R/IL-6 complexes absorbed into the systemic circulation. Indeed, systemic effects derived from a cancer-associated fibroblast population has been proposed³⁴⁸. Membranous cleavage of sIL-6R may however be a biologically unimportant consequence of ADAM snippase activation, of which may have greater significance in the cleavage of unrelated factors, as discussed in Chapters 5 & 9.

Whether solubilised IL-6 receptor trans-signalling offers a competitive advantage over canonical IL-6 signalling via a direct effect on tumour cells is uncertain; a number of downstream effects unique to IL-6 trans-signalling have indeed been reported – particularly with respect to pro-inflammatory as opposed to reparative activity³⁴⁹, although it is difficult to confirm the significance of this in terms of tumour benefit without measurable biological effects equated to the hallmarks of cancer^{255, 350}.

Plan for Further Experimentation

Aside from the exclusion of IL-6 as the principal molecule for inducing cell line migration, the experimental conclusions of this chapter unfortunately provide minimal progress in determining the molecular basis for the additional migrations observed in HPV-negative cell lines when exposed to stimulated fibroblast media. Whilst disappointing, a compilation of candidate molecules identified by cytokine array remained untested and offered further promise. A key limitation to the experimental approach within this chapter was to concentrate on extensively testing a single hypothesis regarding a small number of factors taken from a wider selection of potential candidates. Although comprehensive analysis of any identified molecule/ pathway driving migration remains an ultimate necessity, undertaking extensive experimentation on further candidate pathways in a similar manner to that described in this chapter would remain unfeasibly time-consuming and inefficient. A decision was therefore

made to concentrate on validating the constituent(s) of the stimulated fibroblast secretome responsible for inducing cell line migration rather than determine a more extensive pathway inclusive of the factor(s) responsible for initiating that fibroblast secretory response.

Review of stimulated fibroblast cytokine array data allowed segregation of candidate molecules into four groups, namely: *i.* those factors displaying markedly upregulated densitometry exclusively following the stimulation with HPV-negative cell line conditioned media, *ii.* those factors with a clear trend of increased array uptake following stimulation with HPV-negative cell line conditioned media in comparison to HPV-positive cell line conditioned media, *iii.* those factors upregulated by all cell lines in comparison to control, and *iv.* those factors inducing positive densitometry readouts yet showing no frank pattern of their secretion from HPV-positive versus -negative cell lines, or densitometry not exceeding that of control. Factors from all four groups were considered as potential drivers of cell migration, despite groups *iii.* and *iv.* not directly correlating with the observed migrations; although less likely, molecules within these two groups were still considered as retaining potential to induce migration in HPV-negative lines only, should HPV-positive cell lines demonstrate a comparative downregulation of the respective receptor. Further consideration was given to factors not included in the cytokine arrays, but also reported in the literature to induce cell migration. A final list of the following factors was compiled: IL-6, IL-8, GRO- α , GRO- β , GRO- γ , ENA78, GCP2, uPAR, solubilised GP130, solubilised IL6-R, STNFR1 STNFR2, PLGF, HGF, IGFBP6, OPG, OSM, TMP1, TMP2 and CTGF; the latter having been absent from cytokine arrays, but reported in the literature as promoting cell migration and having been linked to factors present in cell line conditioned media; it has also been noted to be upregulated in the stroma of metastatic head and neck cancer^{238, 351, 352}. From this list, solubilised receptors and carrier proteins were initially excluded, in addition to those factors for which purchase of the recombinant protein was deemed cost-prohibitive (PLGF and uPAR). This allowed a working list of 11 candidate molecules inclusive of IL-6 to be carried forward for initial assessment via recombinant protein dose-response analysis of migration.

Chapter 5: Progressive Analysis of Candidate Molecules Identified by Cytokine Array

Introduction

A total of 11 candidate molecules identified by cytokine array as potential drivers of HPV-negative oropharyngeal cell line migrations were selected for further analysis. Initial experimental plans included assessment of each of the 11 candidate molecules through dose-dependent effect on cell line migration using recombinant proteins. Those recombinant proteins showing a convincing dose-response relationship with cell migration in HPV-negative cell lines would then be analysed further to determine biological plausibility of driving migration, by flow cytometric analysis of membranous receptors to that specific factor in HPV-negative cell lines in addition to analysis of stimulated fibroblast media 1 & 2 for presence of that factor. In doing so, many of the criteria for providing adequate evidence of causality, as originally described by Bradford-Hill, are satisfied – namely:

Strength – a marked increase in ORIS™ assay cell migration when exposed to the respective recombinant protein, comparable to that observed in conditioned medium experiments, would be required for any candidate molecule to retain its position as a plausible driver of migration in the stimulated fibroblast media. Previous experimentation with recombinant IL-6 led to a minor degree of cell migration that was not consistent with the overall effect of conditioned media. One would have to consider the prospect of multiple secreted factors contributing to cell migration in conditioned medium experiments, although in the first instance a convincing prime candidate would be sought.

Consistency – the candidate molecule would have to demonstrate capacity to drive migration in both cell lines SCC72 and SCC89 throughout triplicate biological repeat of dose response experimentation. Additional reference to the candidate molecule in the literature for driving tumour migration would offer further support of consistency.

Temporality – an increase in cell migration should be demonstrated following exposure of each cell line to the candidate molecule.

Biological Gradient – the candidate molecule should show evidence of a clear dose-response relationship with cell migration.

Plausibility – confirmation of canonical membranous receptor expression in HPV-negative oropharyngeal cell lines, in addition to quantitative confirmation of presence of the respective candidate molecule in a biologically active concentration in HPV-negative stimulated fibroblast media would provide evidence of plausibility.

Further experimentation to confirm a final criterion set by Bradford-Hill, *Specificity*, shall be addressed in Chapter 6. Individual consideration of the literature for each of the 10 remaining candidate molecules (following exclusion of IL-6 in Chapter 4) with respect to inducing cellular migration shall now be given.

CTGF

Connective tissue growth factor (CTGF, CCN2), although not included in the Raybiotech cytokine array panel, has been found to be upregulated in tumour-fibroblast co-culture, and correlates with EMT changes³⁵³. CTGF has been observed to induce lung fibroblast migration and myofibroblast differentiation³⁵⁴. Interestingly, stromal release of CTGF in models of pancreatic tumour-stromal interactions has been attributed to CXCR-2 activation, and tumour progression can be abrogated in a xenograft model via CXCR-2 inhibition³⁵². These findings offer a potential explanation for driving both HPV-negative oropharyngeal carcinoma migration (Chapter 2, Figure 2.3), in addition to upregulation of CXCR-2 in stimulated fibroblasts (Chapter 4, Figure 4.5). CTGF was therefore considered a noteworthy addition to those candidate molecules identified via cytokine array for further analysis.

IL-8

IL-8 (interleukin 8) is a chemokine secreted by a broad range of cells, including keratinocytes, head and neck carcinoma lines and fibroblasts. IL-8 had been observed to be markedly elevated in HPV-negative stimulated fibroblast cytokine array data (Figure 3.5), and had been further quantified by ELISA (Figure 4.2). Intriguingly, IL-8 signals via the CXCR receptors 1 & 2, which had been noted to be induced in a sub-population of fibroblasts following exposure to HPV-negative cell line conditioned media (Figures 4.4 &

4.5). CXCR-1 & 2 expression was not formally assessed in cell lines, although it remained plausible that CXCR induction as an exclusive property of the HPV-negative cell lines could be linked to the additional migrations observed in conditioned medium experiments. Moreover, IL-8 stimulation has been found to transiently induce EGFR tyrosine kinase activity via promoting the release of heparin-binding EGF-like growth factor, leading to colon carcinoma cell line migration³⁵⁵. EGFR transactivation via IL-8 has been further reported in small cell lung carcinoma lines, albeit with respect to induction of proliferation rather than migration³⁵⁶, in addition to acting as a mechanism of inducing motility in endothelia³⁵⁷. Furthermore, conditioned media taken from iNKT cells, a T-cell subset was found to induce both EGFR transactivation in endothelia this manner, in addition to inducing CXCR-2 expression³⁵⁷.

GRO- α

Growth-regulated oncogene- α (GRO- α , CXCL1), is a chemokine that signals via the CXCR2 receptor. Its role in cancer has largely been reported with respect to the induction of mitogenesis in melanoma, although has also been found to induce neutrophil chemotaxis in a similar manner to IL-8³⁵⁸. GRO- α has been linked to thrombin-induced angiogenesis and chemotaxis of endothelia³⁵⁹, although a direct role in cancer cell migration has not been shown. Despite the lack of direct evidence relating to migration, GRO- α has been found to be more elevated in metastatic colonic carcinoma lines compared to non-metastatic lines³⁶⁰. Despite this observation, its role in tumour progression is largely attributed to angiogenesis³⁶¹, and moreover clinical data suggest GRO- α may in fact correlate with favourable outcome in colonic carcinoma³⁶². Bieche *et al* found through PCR analysis of tumour specimens that upregulation of GRO- α , GRO- γ and IL-8 in breast carcinoma correlated with metastasis and poor disease control with Tamoxifen. Whilst IL-8 was identified in a number of tissue types in Bieche's study, GRO- α and - γ were noted to be produced by cells of vascular origin, a finding consistent with the consensus view of GROs' role in cancer progression³⁶³. Limited data exist on the role of GRO- α in oropharyngeal carcinoma, although a rise in concentration of this cytokine, along with VEGF, HGF, IL-6 and IL-8, has been noted to precede mortality in advanced disease³⁶⁴. Its exclusive receptor, CXCR-2, is clinically implicated with oral cancer and also cell line invasion and metastasis³⁶⁵.³⁶⁶. Although CXCR-2 exists as an exclusive receptor to the GRO- α ligand, the converse is

not true; in fact, a number of candidate chemokines addressed in this chapter, including IL-8, GCP2, GRO- β , GRO- γ and ENA78 signal via this receptor. Implication of this receptor in disease therefore, is not necessarily specific to any single ligand. Irrespective of the available literature, GRO- α was found to be elevated in HPV-negative stimulated fibroblast media (Figure 3.5), retaining it as a potential candidate molecule in the induction of the observed migrations with stimulated fibroblast media.

GRO- β

Growth-regulated oncogene- β (GRO- β , CXCL2), as with GRO- α , signals via the CXCR2 receptor and has been similarly implicated with early neutrophil recruitment in inflammation³⁶⁷. Although tumour migration has not been reported in response to GRO- β , the molecule has been linked with poor prognosis in GISTs³⁶⁸, and the degree of GRO- β expression in colonic carcinoma correlates with staging, although has no bearing on metastasis or survival³⁶⁹. GRO- β has no reported influence on carcinoma migration, and its effects appear to be limited to inducing proliferation *in-vitro*^{370, 371}.

GRO- γ

Growth-regulated oncogene- γ (GRO- γ , CXCL3, MIP2b) is a known regulator of migration of neutrophils³⁷², monocytes³⁷³, airway smooth muscle cells³⁷⁴ and cerebellar neurones³⁷⁵. Although GRO- γ has a much greater affinity for CXCR-2³³⁹, it has been reported that activity of both CXCR-1 and CXCR-2 are necessary for its effects on migration; neutralising antibody to either receptor reduced the migratory effect of GRO- γ on airway smooth muscle *in-vitro*³⁷⁴. There are no data to support its direct role in carcinoma migration.

ENA78

Epithelial-derived neutrophil-activating peptide 78 (ENA78, CXCL5) is a further CXC cytokine that signals via the CXCR-2 receptor. ENA78 has been reported as chemoattractant to neutrophils³⁷² and endothelia³⁷⁶, although has no reported effects on carcinoma migration.

GCP2

Granulocyte chemotactic protein 2 (GCP2, CXCL6) has the capacity to signal via both CXCR-1 & 2³⁷⁷. Although regarded as a neutrophil chemoattractant^{372, 378}, GCP2 has recently been found to induce hepatocellular carcinoma line migration³⁷⁹, although there are no reports of a role in head and neck carcinoma migration.

HGF

HGF (Hepatocyte growth factor, scatter factor, SF) is a highly motogenic cytokine released principally by fibroblasts in wound repair³⁷⁹. Its effect on keratinocyte motility is achieved via STAT3 upregulation and can be inhibited by the SOCS3 protein^{380, 381}. Head and neck carcinoma line migration in response to HGF has been well documented^{382, 383}, and downregulation of c-Met (HGF's classical receptor) by miR-143 has been shown to inhibit migration in-vitro³⁸⁴. Similar experimentation using RNA interference of c-Met also led to reduced tumour size and improved survival in an animal model of head and neck cancer³⁸⁵.

Cytokine array densitometry data showed upregulation of HGF in HPV-negative cell line-stimulated fibroblast media compared to HPV-positive stimulated fibroblast media (Chapter 3, Figure 3.11). Although all HGF densitometry measures were low compared to positive control, low densitometry uptake may be attributed to reduced array HGF sensitivity as discussed in Chapter 4, and a proportionate relationship between HPV-positive and -negative stimulated fibroblast media is therefore more valid than overall array spot density. Low array uptake does however introduce greater potential for background variability to account for variance between HPV-positive and -negative stimulated media, although one can conclude that the correct relationship exists for HGF to be considered a candidate molecule. HGF's profile of acting as a highly motogenic cytokine, in addition to being characteristically released by fibroblasts, further supports the potential for this cytokine to underlie the additional migrations observed in the conditioned medium experiments (Chapter 2).

OPG

Osteoprotegerin (OPG) is a secreted glycoprotein that has capacity to block osteoclast differentiation³⁸⁶. Its principal role is to act as a receptor decoy to the RANK ligand. OPG has no reported role in head and neck cancer, and moreover OPG has been proposed as a potential cancer therapeutic in the management of bone tumours³⁸⁷. OPG therefore retains minimal potential as a driver of the observed cell migrations, although one cannot rule out the potential for OPG to downregulate a basally-secreted inhibitor of migration through its receptor decoy activity. Despite this, RANK ligand, the only ligand known to bind to OPG, has a pro-tumourigenic effect and blockade of stromal release of OPG appears important for bone tumour progression³⁸⁸.

OSM

Oncostatin M (OSM) is a pleiotropic cytokine, sharing a similar amino acid sequence to cytokines CTNF, G-CSF, IL-6, IL-11 and LIF³⁸⁹. It is thought that a common evolutionary ancestor gave rise to OSM and these homologous cytokines, which led to a shared receptor signal transduction system between OSM, IL-6, IL-11 and LIF involving the gp130 transmembrane protein. OSM characteristically activates two intracellular signalling pathways, namely JAK/STAT and MAPK³⁹⁰. Despite characteristic signalling cascades, OSM can bind to two receptors capable of complexing with gp130; the exclusive OSM receptor (OSMR)³⁹¹, and a “shared” LIF-receptor, which is capable of being activated by both OSM and LIF³⁹². OSM also directly binds gp130 with low affinity³⁹³.

OSM's pleiotropic nature leaves uncertainty with respect to its potential activity on oropharyngeal carcinoma lines. OSM has been noted to act as a potent mitogen in myeloma and Kaposi's sarcoma, yet has been found to inhibit gastric, ovarian, lung and breast carcinoma line proliferation³⁹⁴. There are some data to support a role for OSM in cell migration; OSM has been found to induce migration of extravillous trophoblasts³⁹⁵, as well as inducing matrigel invasion of osteosarcoma lines³⁹⁶, and has been recently found to induce endometrial carcinoma cell migration³⁹⁷.

Methods

M5.1: Recombinant Protein Dose-Response Analysis

Recombinant human CTGF, ENA78, GCP2, GRO- α , GRO- β , GRO- γ , HGF, IL-6, IL-8, OPG and OSM were purchased from Insight Biotechnology (Wembley, UK). Each vial of lyophilised protein was reconstituted with 1,000 μ L normal media (DMEM plus 10 % FCS, plus 50 U mL⁻¹/50 μ g mL⁻¹ penicillin-streptomycin, plus 2mM l-glutamine) to produce a stock solution, aliquoted and stored at -21 °C prior to use in experiments. All stock solutions were prepared to a micro-gram per millilitre concentration, although absolute concentrations varied as depicted in Table 5.1, below; use of a standardised solvent volume to ensure accurate dilution of each recombinant protein, in addition to achieving an adequate volume to run triplicate experimental repeats was considered more critical than achieving identical concentrations of each biologically distinct recombinant protein. Serial 1:10 dilutions were then undertaken using normal media to obtain logarithmically decreasing doses of each recombinant protein. Normal media containing identical DMEM, penicillin-streptomycin, L-glutamine and FCS batches were used for all serial dilutions, in order to maintain experimental consistency.

Table 5.1: Details of recombinant proteins used in dose-response analysis

Recombinant Protein	Supplier	Catalogue Number	Manufacturer supplied amount, μ g	Concentration of Stock Solution, μ g mL ⁻¹
CTGF	Insight Biotechnology	10-1811-B	5	5
ENA78	Insight Biotechnology	10-1050-B	5	5
GCP2	Insight Biotechnology	10-1115-B	5	5
GRO- α	Insight Biotechnology	10-1052-B	5	5
GRO- β	Insight Biotechnology	10-1118-B	2	2
GRO- γ	Insight Biotechnology	10-1157-B	2	2
HGF	Insight Biotechnology	10-1194-B	2	2
IL-6	Insight Biotechnology	10-1018-C	20	20
IL-8	Insight Biotechnology	10-1054-C	25	25
OPG	Insight Biotechnology	10-1191-B	10	10
OSM	Insight Biotechnology	10-1740-B	2	2

UPCI SCC072 was selected as a representative HPV-negative cell line for initial investigation, and was grown to 70 % confluence in a T75 flask. Cells were washed twice in

PBS, trypsinised, centrifuged at 1,000 rpm and then resuspended in normal media. The cell suspension was then counted using a haemocytometer, with appropriate dilutions using normal media in order to achieve the preoptimised seeding concentration of 1.6×10^6 cells mL^{-1} for confluent ORIS™ assay well loading, as described in Chapter 1. ORIS™ assay plates were prepared under sterile conditions, mounting silicone stoppers into each well using the manufacturer-supplied location device. 100 μL of each cell suspension was then pipetted into respective ORIS™ assay wells and left overnight to adhere.

Following cell adherence and confirmation of well confluency using an inverted lens microscope, a preoptimised (please refer to Chapter 1, Figure 1.5) $2 \mu\text{g mL}^{-1}$ mitomycin C suspension in normal media was created from snap-frozen 0.5 mg mL^{-1} aliquots of mitomycin C stored at $-80 \text{ }^\circ\text{C}$. All handling of mitomycin C was undertaken in a darkened tissue culture hood in order to avoid excessive light exposure. Silicone stoppers were then removed from assay wells using the manufacturer supplied retrieval tool, exposing the respective cell exclusion zone, and normal media carefully aspirated off each well ensuring contact was avoided with the well base. $2 \times 100 \mu\text{L}$ PBS washes were then undertaken. 100 μL mitomycin C at preoptimised concentrations to inhibit cell proliferation was then pipetted into each well and incubated for 3.5 hours at $37 \text{ }^\circ\text{C}$ in the dark. Following 3.5 hours incubation in mitomycin C, baseline void photomicrographs were taken under X4 magnification. Wells were then immediately washed X 2 with 100 μL PBS and then incubated with 100 μL normal media control/serially-diluted recombinant protein-containing media for 48 h. End-point migration photomicrographs were taken of each cell exclusion zone at 48 h.

Analysis of cell migration was undertaken by comparison of baseline versus 48 h micrograph images taken at X4 objective. The area of each stopper-induced cell exclusion zone at baseline and 48 h was measured using ImageJ using the polygon selection tool (freeware, NIH, USA). Percentage void closure was then calculated by dividing area of closure over 48 h by total baseline area of cell exclusion zone.

Each recombinant protein was tested at serial dilutions of 10^0 , 10^{-1} , 10^{-2} and 10^{-3} stock solution concentrations, in addition to normal media control. Triplicate biological repeats of each experimental condition ($n=1$) were undertaken, with median additional percentage void closure (compared to closure in control medium) calculated and plotted graphically (Figure 5.1).

Collection of Conditioned Media for ELISA Analysis of Candidate Cytokines

Collection of Conditioned Media for ELISA Analysis: Cell Line Conditioned Media

Cell lines UD SCC02, UPCI SCC072, UPCI SCC089 and UPCI 090 were grown to near confluence in T75 flasks, washed X3 in PBS and incubated with 7 mL normal media for 24 h. Following 24 h incubation, conditioned media were retrieved, centrifuged at 3,000 rpm for 5 minutes and then supernatant retrieved taking care to avoid resuspension of precipitated cellular debris, and then stored at -21 °C. The respective T75 flask was trypsinised and a cell count undertaken to confirm collection of a conditioned medium that had been contributed to by 3 million cells per mL of media.

Collection of Conditioned Media for ELISA Analysis: Stimulated Fibroblast Media

Passage 7 DENO08 normal oral fibroblasts were cultured in T75 flasks to confluence, washed X3 in PBS and then incubated with 6ml cell line conditioned medium, derived in the same manner as described above for ELISA analysis, again normalised to 3 million cells mL⁻¹. Following incubation with either cell line conditioned media taken from UD SCC02, UPCI SCC072, UPCI SCC089, UPCI 090 or normal media control, the medium was retrieved, centrifuged and the supernatant (hereon referred to as stimulated fibroblast Medium 1) comprising the initial cell line conditioned medium plus immediate fibroblast response, stored at -21 °C. Fibroblast cultures were then washed X3 in PBS, and then 6 mL normal media co-incubated for a further 24 hours in order to collect the tail-off of any fibroblast response to stimulation (hereon referred to as stimulated fibroblast Medium 2). Following incubation, stimulated fibroblast Medium 2 was retrieved, centrifuged at 3,000 rpm and then supernatant collected and stored at -21 °C.

Following collection of fibroblast media 2, fibroblast cultures were washed X3 in PBS, trypsinised and counted. All flasks were counted to confirm stimulated fibroblast media had been collected at a standard count of 400,000 fibroblasts per mL of conditioned medium.

M5.2: OSM ELISA Analysis

Oncostatin M quantification of cell line conditioned media and stimulated fibroblast Media 1 & 2 was undertaken using Raybiotech OSM ELISA kits (Raybiotech, Norcross, USA, Cat ELH-OSM). Manufacturer instructions were adhered to throughout ELISA analysis. In brief, manufacturer-supplied recombinant human OSM standard was prepared to a $1,000 \text{ pg mL}^{-1}$ concentration in assay buffer. Serial 1:3 dilutions were then undertaken using assay buffer in order to achieve a control reference range. Assay buffer was used as a zero standard. All conditioned media were diluted in assay buffer using a manufacturer-suggested 1:20 dilution. A further biologically-active 2 ng mL^{-1} recombinant OSM protein control (Insight Biotechnology, cat 10-1740-B) was assayed in 1:20 dilution order to validate ELISA plates.

100 μL standard/sample was added to each well of the Raybiotech OSM capture antibody preconditioned ELISA plates and incubated overnight with gentle rocking. The conditioned media/standard were then discarded and each well washed X4 with 300 μL manufacturer-supplied wash buffer using a multi-channel pipette, ensuring complete removal of solution after each wash through blotting of the inverted plate against tissue paper. Each well was then incubated at room temperature with 100 μL 1X biotinylated detection antibody for 1 hour on an automated rocker machine. Following incubation, the biotinylated antibody solution was discarded and again wells washed X4 with 300 μL manufacturer-supplied wash buffer using a multi-channel pipette, ensuring complete removal of solution after each wash through blotting of the inverted plate against tissue paper.

100 μL freshly-prepared 1X streptavidin solution (concentrate diluted 300-fold in assay diluent) was then pipetted into each well using a multi-channel pipette and incubated for 45 minutes at room temperature on an automated rocker machine. Following incubation, the streptavidin solution was discarded and a further X4 washes undertaken as described above.

100 μL of manufacturer-supplied TMB One-Step Substrate Reagent was then added to each well and incubated for 30 minutes at room temperature, protected from light, on an automated rocker machine. 50 μL of manufacturer-supplied Stop Solution was then added to each well and the plate read at 450 nm using a Tecan Infinite M200 plate reader. Results were tabulated using Microsoft Excel and imported into DeltaSoft ELISA analysis software (BioMetallics, Princeton, New Jersey, USA), and interpreted using 4-parameter best-fit plot.

M5.3: HGF ELISA Analysis

HGF quantification of cell line conditioned media and stimulated fibroblast Media 1 & 2 was undertaken using Raybiotech HGF ELISA kits (Raybiotech, Norcross, USA, Cat ELH-HGF). Manufacturer instructions were adhered to throughout ELISA analysis. In brief, manufacturer-supplied recombinant human HGF standard was prepared to a 2,000 pg mL⁻¹ concentration in assay buffer. Serial 1:3 dilutions were then undertaken using assay buffer in order to achieve a control reference range. Assay buffer was used as a zero standard. All conditioned media were diluted in assay buffer using a manufacturer-suggested 1:20 dilution.

100 µL standard/sample was added to each well of the Raybiotech HGF capture antibody preconditioned ELISA plates and incubated overnight with gentle rocking. The conditioned media/standard were then discarded and each well washed X4 with 300 µL manufacturer-supplied wash buffer using a multi-channel pipette, ensuring complete removal of solution after each wash through blotting of the inverted plate against tissue paper. Each well was then incubated at room temperature with 100 µL 1X biotinylated detection antibody for 1 hour on an automated rocker machine. Following incubation, the biotinylated antibody solution was discarded and again wells washed X4 with 300 µL manufacturer-supplied wash buffer using a multi-channel pipette, ensuring complete removal of solution after each wash through blotting of the inverted plate against tissue paper.

100 µL freshly-prepared 1X streptavidin solution (concentrate diluted 300-fold in assay diluent) was then pipetted into each well using a multi-channel pipette and incubated for 45 minutes at room temperature on an automated rocker machine. Following incubation, the streptavidin solution was discarded and a further X4 washes undertaken as described above.

100 µL manufacturer-supplied TMB One-Step Substrate Reagent was then added to each well and incubated for 30 minutes at room temperature, protected from light, on an automated rocker machine. 50 µL of manufacturer-supplied Stop Solution was then added to each well and the plate read at 450 nm using a Tecan Infinite M200 plate reader. Results were tabulated using Microsoft Excel and imported into DeltaSoft ELISA analysis software, and interpreted using 4-parameter best-fit plot.

M5.4: Dose-Response Analysis of HGF in HPV-Negative Cell Line UPCI SCC089

Following identification of HGF as a principal candidate for driving migration in cell line UPCI SCC072, dose-response analysis was repeated for a second HPV-negative cell line, UPCI SCC089. Cell line UPCI SCC089 was grown to 70-80 % confluence in a T75 flask. Cells were washed twice in PBS, trypsinised, centrifuged at 1,000 rpm and then resuspended in normal media. The cell suspension was then counted using a haemocytometer, with appropriate dilutions using normal media in order to achieve the preoptimised seeding concentration of 8.8×10^5 cells mL^{-1} for confluent ORIS™ assay well loading, as described in Chapter 1. ORIS™ assay plates were prepared under sterile conditions, mounting silicone stoppers into each well using the manufacturer-supplied location device. 100 μL of each cell suspension was then pipetted into respective ORIS™ assay wells and left overnight to adhere.

Following cell adherence and confirmation of well confluency using an inverted lens microscope, a preoptimised (please refer to Chapter 1, Figure 1.5) $2 \mu\text{g mL}^{-1}$ mitomycin C suspension in normal media was created from snap-frozen 0.5 mg mL^{-1} aliquots of mitomycin C stored at $-80 \text{ }^\circ\text{C}$. All handling of mitomycin C was undertaken in a darkened tissue culture hood in order to avoid excessive light exposure. Silicone stoppers were then removed from assay wells using the manufacturer supplied retrieval tool, exposing the respective cell exclusion zone, and normal media carefully aspirated off each well ensuring contact was avoided with the well base. $2 \times 100 \mu\text{L}$ PBS washes were then undertaken. 100 μL mitomycin C at preoptimised concentrations to inhibit cell proliferation was then pipetted into each well and incubated for 3.5 hours at $37 \text{ }^\circ\text{C}$ in the dark. Following 3.5 hours incubation in mitomycin C, baseline void photomicrographs were taken under X4 magnification. Wells were then immediately washed $\times 2$ with 100 μL PBS and then incubated with 100 μL normal media control/serially-diluted recombinant protein-containing medium for 20 hours. End-point migration photomicrographs were taken of each cell exclusion zone at 20 h.

Analysis of cell migration was undertaken by comparison of baseline versus 20h micrograph images taken at X4 objective. The area of each stopper-induced cell exclusion zone at baseline and 20 h was measured with ImageJ software, using the polygon selection tool (freeware, NIH, USA). Percentage void closure was then calculated by dividing area of closure over 20 h by total baseline area of cell exclusion zone.

Recombinant HGF was tested at serial dilutions of 10^0 , 10^{-1} , 10^{-2} , 10^{-3} , 10^{-4} and 10^{-5} stock solution concentration ($2 \mu\text{g mL}^{-1}$), in addition to normal media control. Triplicate biological repeats of each experimental condition were undertaken, with median additional percentage void closure (compared to migration with control media) calculated and plotted graphically (Figure 5.4).

M5.5: Flow Cytometric Analysis of c-Met Status Oropharyngeal Carcinoma

Cell Lines

FITC-conjugated anti-human c-Met antibody for use in flow cytometry was purchased from Affymetrix e-Bioscience (Hatfield, UK, Cat number 11-8858-41), along with rat IgG1 κ isotype control probe (Cat number 11-4301-81).

Cell lines UD SCC2, UPCI SCC072, UPCI SCC089 and UPCI SCC090 were grown to 70-80 % confluence in T75 flasks, along with HeLa (cervical carcinoma) and HepG2 (hepatocellular carcinoma) lines to act as c-Met positive controls. Cells were dissociated from respective flasks using EDTA cell dissociation solution (Sigma-Aldrich, Dorset, England, Cat C5914-100ML), suspended in FACS buffer (PBS with 0.1 % Sodium Azide plus 1 % BSA) cooled on ice, and centrifuged at 1,000 rpm for 5 minutes. The supernatant was then decanted and cells resuspended in 900 μL cooled FACS buffer. Each cell suspension was then divided equally into three Eppendorph containers and again centrifuged at 2,000 rpm for 2 minutes. Following careful aspiration of supernatant, cells were resuspended in 100 μL cooled FACS buffer containing either no additive, 5 μL ($1.0 \mu\text{g}$) FITC-conjugated c-Met probe, or 5 μL ($1.0 \mu\text{g}$) rat IgG1 κ isotype control. Each suspension was then incubated on ice and in the dark for 40 minutes. Following incubation, cells were centrifuged at 2,000 rpm for 2 minutes, supernatants carefully aspirated and cell pellets resuspended in 1,000 μL cold FACS buffer. A repeat centrifugation and cold FACS buffer wash was undertaken, followed by final centrifugation at 2,000 rpm for 2 minutes, aspiration of supernatant and then resuspension in 300 μL cold FACS buffer. Cells were then immediately stored on ice and analysed using a Calibur flow cytometer. Flow cytometry data were then plotted and converted into overlay histogram images using Flowing 2.5.1 software (freeware, Turku, Finland).

M5.6: Western Blot Analysis of Total & Phosphorylated STAT3

Following ELISA confirmation of presence of HGF in elevated concentrations in HPV-negative cell line-stimulated fibroblast media, in addition to recombinant HGF retaining capacity to drive migration, activation of the secondary messenger STAT3 was interrogated by western blot analysis.

Collection of Conditioned Media

Stimulated Fibroblast Media 2 were collected from DENOF08 normal fibroblasts as described in Chapter 2, methods section 2.1 for cell lines UD SCC02, UPCI SCC072, UPCI SCC089 and UPCI SCC090.

Exposure of Cell Lines to Stimulated Fibroblast Media and Collection of Protein for Western Blot Analysis

Cell lines UD SCC02, UPCI SCC072, UPCI SCC089 and UPCI 090 were grown in T75 flasks to approximately 70 % confluence. Cultures were washed X3 in PBS and then exposed to either unstimulated fibroblast conditioned medium control or stimulated fibroblast Media 2 for 0 mins, 20 mins or 12 hrs. On completion of each respective incubation period, flasks were washed X3 in cold TBS and then incubated with 1 mL cell dissociation solution at 4 °C on a rocking machine for 10 mins. Cells were then removed with the assistance of a cell scraper, the suspension transferred to an Eppendorph container, centrifuged at 1,000 rpm 5 mins, supernatant removed and then immediately stored at -80 °C.

Protein extraction

Cell pellets were lysed on ice in a buffer containing 50 mM Tris HCL pH 7.4, 250 mM NaCl, 5 mM EDTA, 0.3% Triton X-100 and protease inhibitor (Complete mini EDTA free protease inhibitor cocktail, Roche, Cat 05892791001).

Western Blotting

Samples were boiled for 5 minutes in an equal volume of Laemmli sample buffer (125 mM Tris HCl pH 6.8, 20 % glycerol, 4 % SDS, 0.005 % Bromophenol blue and 5 % Beta Mercaptoethanol). Samples were separated using 4-15 % pre-cast gels (Mini-Protean TGX, Bio-Rad, California, USA, Cat 4561081) run at 75 mV for 10 mins and 90 mV for 80 mins. Separated samples were transferred to a nitrocellulose membrane (Amersham Hybond ECL, GE Healthcare, Cat RPN2020D) at 85 mV for 1 hour 20 minutes. Membranes were blocked for thirty minutes in 5 % skimmed milk in Tris buffered saline (pH 7.4) with 0.1 % Tween-20, then incubated with either Tyr 705-phosphorylated/non-phospho specific STAT3 antibodies (Cell Signalling Technology, Danvers, USA, Cat 9145 & 9139 respectively; both antibodies used at 1: 1,000 dilution) or anti-Beta Actin control (1:2,000 dilution) in 5 % BSA/TBST overnight at 4 °C. Membranes were then incubated in horseradish peroxidase conjugated secondary antibodies at a dilution of 1:10,000 for 45 minutes and imaged using ECL reagent (GE Healthcare, Cat RPN2106).

M5.7: Soluble c-Met ELISA Analysis of Oropharyngeal Carcinoma Cell Lines

Collection of Conditioned Media

Cell lines UD SCC02, UPCI SCC072, UPCI SCC089 and UPCI 090 were grown to near confluence in T75 flasks, washed X3 in PBS and incubated with 7 mL normal media for 24 h. Following 24 h incubation, conditioned media were retrieved, centrifuged at 3,000 rpm for 5 minutes and then supernatant retrieved taking care to avoid resuspension of precipitated cellular debris, and then stored at -21 °C. The respective T75 flask was trypsinised and a cell count undertaken to confirm collection of a conditioned medium that had been contributed to by 3 million cells per mL.

ELISA Analysis

Soluble c-Met quantification of cell line conditioned media and stimulated fibroblast Media 1 & 2 was undertaken using Life Technologies soluble c-Met ELISA kit (Life Technologies, Paisley, UK, cat number KHO2031). Manufacturer instructions were adhered to throughout

ELISA analysis. In brief, manufacturer-supplied recombinant human soluble c-Met standard was prepared to a 50 ng mL⁻¹ concentration in standard diluent buffer. Serial 1:2 dilutions were then undertaken using standard diluent buffer in order to achieve a control reference range. Standard diluent buffer was used as a zero standard. All conditioned media were diluted in standard diluent buffer using a 1:20 dilution.

100 µL standard/sample was added to each well of the Life Technologies soluble c-Met capture antibody preconditioned ELISA plates and incubated at room temperature for 2 hours. The conditioned media/standard were then discarded and each well washed X4 with 300 µL manufacturer-supplied wash buffer using a multi-channel pipette, ensuring complete removal of solution after each wash through blotting of the inverted microtitre plate against tissue paper. Each well was then incubated at room temperature for 1 hour with 100 µL biotinylated detection antibody, after an initial 30 seconds agitation through gentle tapping of the side of the microtitre plate. Following incubation, the biotinylated antibody solution was discarded and again wells washed X4 with 300 µL manufacturer-supplied wash buffer using a multi-channel pipette, ensuring complete removal of solution after each wash through blotting of the inverted plate against tissue paper.

100 µL freshly-prepared streptavidin-HRP working solution was then pipetted into each well using a multi-channel pipette and incubated for 30 minutes at room temperature. Following incubation, the streptavidin solution was discarded and a further X4 washes undertaken as described above.

100 µL manufacturer-supplied Stabilised Chromogen was then added to each well and incubated for 30 minutes at room temperature, protected from light using a non-metallic cover. 100 µL of manufacturer-supplied Stop Solution was then added to each well and the plate read at 450 nm using a Tecan Infinite M200 plate reader. Results were tabulated using Microsoft Excel and imported into DeltaSoft ELISA analysis software (BioMetallics, Princeton, New Jersey, USA), and interpreted using 4-parameter best-fit plot.

Results

Figure 5.1: Dose-Response Curves for Candidate Recombinant Proteins Identified by Cytokine Array

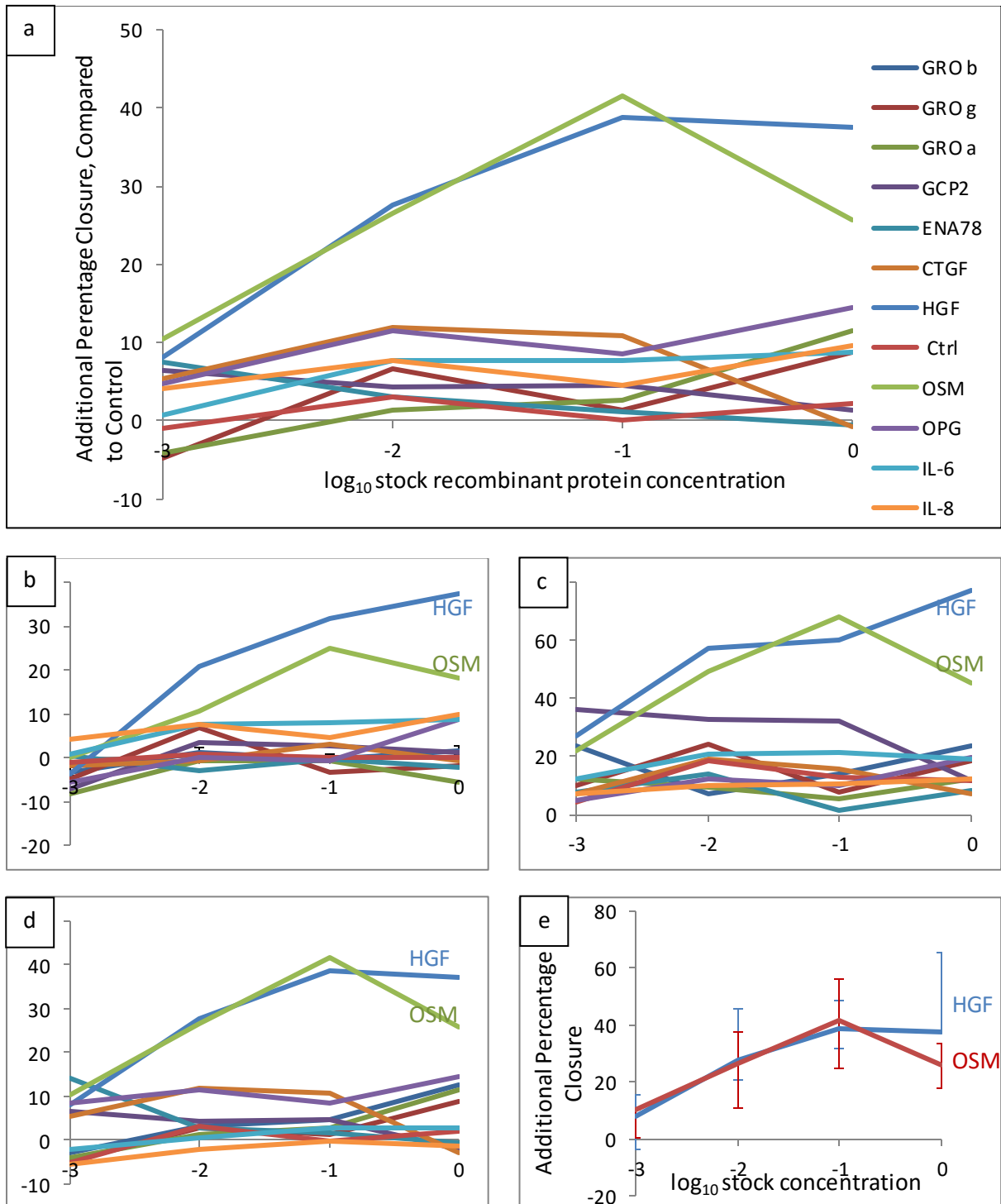


Figure 5.1: Dose-response curves for candidate recombinant proteins identified by cytokine array:

a). Median dose-response curve for ORIS™ assay migration over 48h in cell line SCC72 using candidate recombinant proteins identified by cytokine array of stimulated fibroblast medium. Error bars omitted for clarity, but reproduced in figure e). for proteins HGF and OSM. X-axis represents \log_{10} stock recombinant protein concentration. Stock recombinant protein concentrations used in experiments (created through dissolution of commercially-supplied lyophilised protein in 1ml standard medium) were as follows:

25 $\mu\text{g mL}^{-1}$: IL-8

10 $\mu\text{g mL}^{-1}$: OPG

5 $\mu\text{g mL}^{-1}$: GRO α , GRO β , ENA78, CTGF

2 $\mu\text{g mL}^{-1}$: HGF, GRO γ , OSM, GCP2, IL-6

Figure a). demonstrates a clear dose-response relationship between recombinant proteins HGF and OSM with increased cell migration. All other recombinant proteins demonstrated no reproducible dose-response relationship.

Please note that as median data has been presented, the same data appear in the subsequent graphs

b), c) & d). Data for biological repeats 1,2 & 3 (n=1), illustrating the reproducible dose-response relationship between migration and HGF/OSM concentration (axes same as Figure a).

e). Triplicate biological repeats for recombinant OSM and HGF dose-response data. Error bars denote range – note the skewed distribution of HGF data. Variance for OSM and HGF has been illustrated in a separate graph for ease of interpretation.

Figure 5.2: OSM ELISA Analysis of Cell Line Conditioned Media and Respective Media 1 & 2

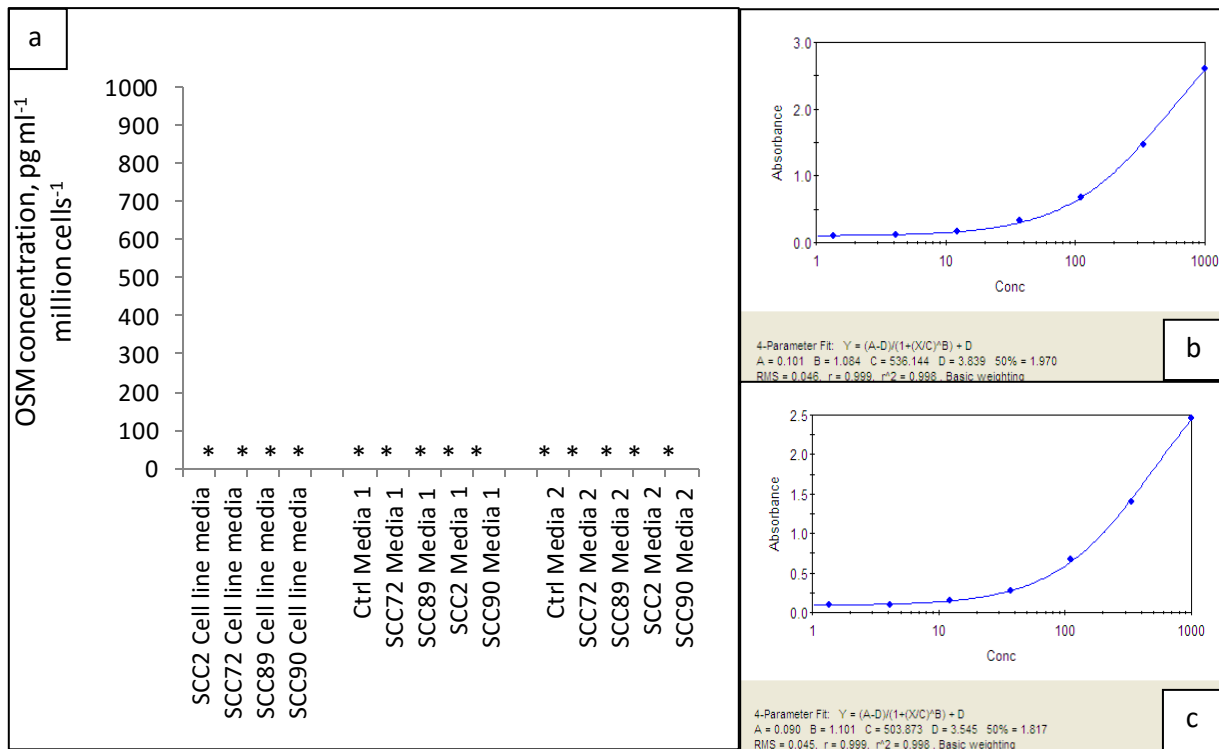


Figure 5.2: OSM ELISA analysis of cell line conditioned media and respective stimulated fibroblast media 1 & 2

a). ELISA analysis of OSM concentration in cell line conditioned media and fibroblast Media 1 & 2 for cell lines UD SCC02, UPCI SCC072, UPCI SCC089 and UPCI SCC090, plus respective unstimulated fibroblast controls (n=9). *represents a reading below detectable levels in all triplicate experimental and biological repeats, as interpreted by 4-parameter best-fit plot. Note that all conditioned media returned negative findings. In addition to ELISA standards, a second positive control of recombinant, biologically active 2 ng mL⁻¹ OSM in normal media used for migration dose-response curves in Figure 4.1 (Insight Biotechnology, Wembley, UK.) was incubated with fibroblasts, collected and washed at 24 h and then replaced with normal media in the same manner as cell line media in order to get a comparable recombinant OSM co-incubated fibroblast Media 1&2. OSM co-incubated fibroblast Medium 1 (containing the recombinant protein) returned a positive ELISA reading (exceeded detectable levels and therefore censored from the above graph), and fibroblast Medium 2 returned a negative ELISA reading (below detectable levels), helping confirm the reliability of the ELISA kit. Standard curves using 4-parameter plotting are illustrated (insets b and c) in order to further illustrate the validity and accuracy of the ELISA analysis despite ubiquitous sample negatives.

b). & c). 4-parametric-fit curve of ELISA standards for OSM ELISA plates 1 & 2, respectively. Y-axis denotes absorbance, X-axis denotes recombinant OSM concentration in pg mL⁻¹. Note a high correlation coefficient (r=0.999, both plates), confirming a highly reproducible ELISA system despite the absence of OSM detection in all media.

Figure 5.3: HGF ELISA Analysis of Cell Line Conditioned Media and Respective Media 1 & 2

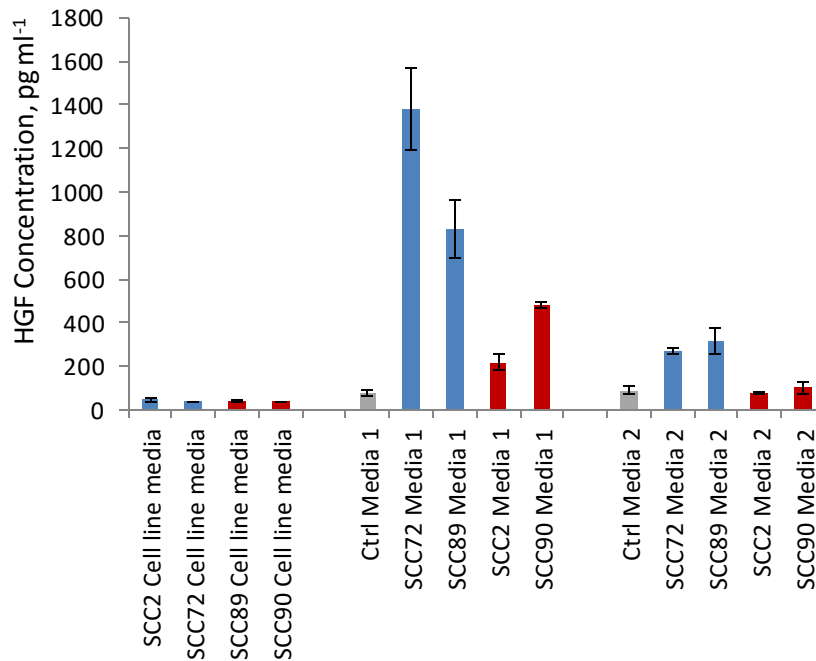


Figure 5.3: ELISA analysis of HGF concentration in cell line conditioned media and fibroblast Media 1 & 2 for cell lines UD SCC02, UPCI SCC072, UPCI SCC089 and UPCI SCC090, plus respective unstimulated fibroblast controls (n=9). Y-axis is not normalised to number of cells contributing to the media due to differences between cell line media concentrations (3.5×10^6 cells contributing to 1 mL of conditioned media) and fibroblast concentrations (3.5×10^5 cells contributing to 1 mL of conditioned media); presenting the concentration of HGF in non-normalised format allows direct comparison of the HGF content of each conditioned medium. Error bars denote SEM, Blue columns denote data for HPV-negative cell line/ stimulated fibroblast media, red bars denote HPV-positive cell line/ stimulated fibroblast media. Grey columns denote unstimulated fibroblast controls.

Note that irrespective of a 10-fold increase in cell numbers contributing to the cell line conditioned media, HGF release from cell lines was low/absent. Log-log interpretation of ELISA data have been undertaken as per manufacturers' instructions: very low ELISA readings, such as for all cell line conditioned media, may therefore represent variance in background absorbance.

Although all cell lines induced a significant increase in HGF secretion in Media 1 (Mann-Whitney U-test, $P < 0.05$), a higher amount of HGF release was observed in fibroblasts stimulated by HPV-negative cell lines (UPCI SCC072 and UPCI SCC089 versus UPCI SCC090; Mann-Whitney U-test $P < 0.05$), with the majority of the HGF release occurring within the first 24 h (Media 1 data). A tail-off of the HGF response can be seen in Medium 2 for each line (representing the 24-48 h period post-initial stimulation). Only HPV-negative lines induced a significantly increased concentration of HGF in Media 2 (Mann-Whitney U-test, $p < 0.05$).

Note the lower, yet still significant increase in HGF release from fibroblasts stimulated by cell lines UD SCC02 and UPCI SCC090, as observed in respective fibroblast Medium 1. Also note a small basal release of HGF by fibroblasts in both unstimulated control Media 1 & 2.

It can be observed that the concentration of HGF measured in stimulated fibroblast Media 1&2 for cell line UPCI SCC072 is below the concentration of recombinant HGF necessary to induce the degree of migration comparable to that seen using conditioned media. Mean HGF concentration in UPCI SCC072 Media 1&2 is 1.38 ng mL^{-1} and 0.27 ng mL^{-1} respectively, whereas migration comparable to that observed in Medium 1 (approximately 35 % overall void closure) was observed at an approximate 10-fold increase in recombinant HGF concentration (Figure 4.1).

Despite the mean HGF concentration of UPCI SCC089-stimulated fibroblast Medium 1 (0.83 ng mL^{-1}) being within the range of recombinant HGF concentrations observed to induce significant additional ORIS™ assay migration (Figure 5.4, below), no additional migration compared to control was noted using this conditioned medium. Lack of effect was postulated to be due to either conditioned medium exhaustion of nutrients, or may alternatively represent inhibition of HGF by another factor present within the conditioned medium.

The above inconsistency suggests that whilst HGF is present in a biologically active concentration in HPV-negative stimulated fibroblast media, the measured concentrations of HGF do not fully account for the degree of migrations observed with stimulated fibroblast media, and moreover raises the potential for an HGF-inhibiting factor to be present, further complicating the relationship between HGF and cell migration.

Figure 5.4: Dose-Response Analysis of Recombinant Human HGF for HPV-Negative Oropharyngeal Carcinoma Line UPCI SCC089

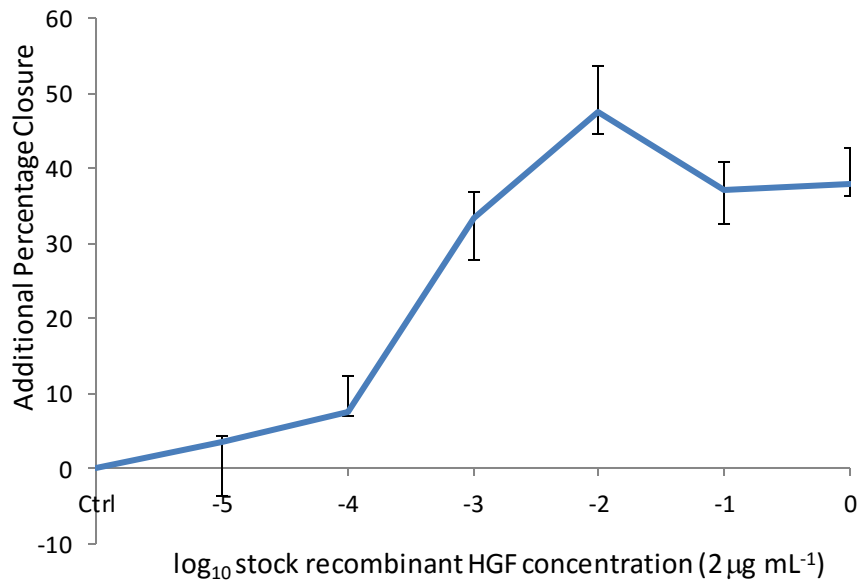
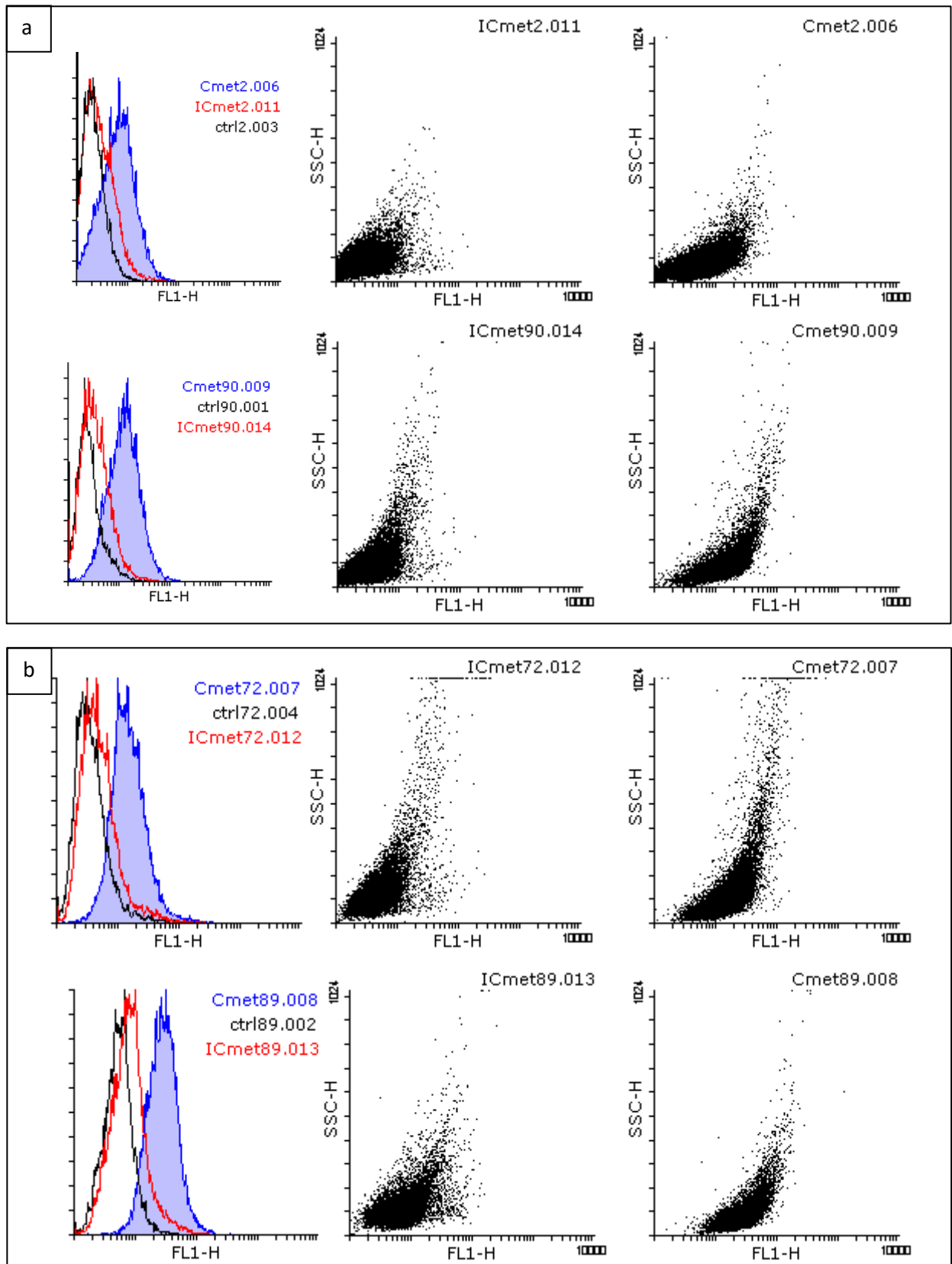


Figure 5.4: Dose-response curve of additional ORIS™ assay migration observed in cell line UPCI SCC089 in response to logarithmic dilutions of 2 µg mL⁻¹ stock recombinant HGF in normal media. Error bars denote range (n=3: triplicate biological repeats of n=1), with median used as measure of central tendency (blue line). Migration expressed as additional percentage closure of baseline void, compared to control.

Note that a parabolic increase in migration occurs between 0.2-2 ng mL⁻¹ HGF (stock HGF concentration X 10⁻⁴ - 10⁻³), and peak stimulation of cell line SCC89 occurs at 20 ng mL⁻¹ HGF (stock HGF concentration X 10⁻²); an approximate 10-fold increase in responsiveness compared to cell line UPCI SCC072 (Figure 5.1).

Figure 5.5: Flow Cytometric Analysis of c-Met Status in Oropharyngeal Carcinoma Cell Lines



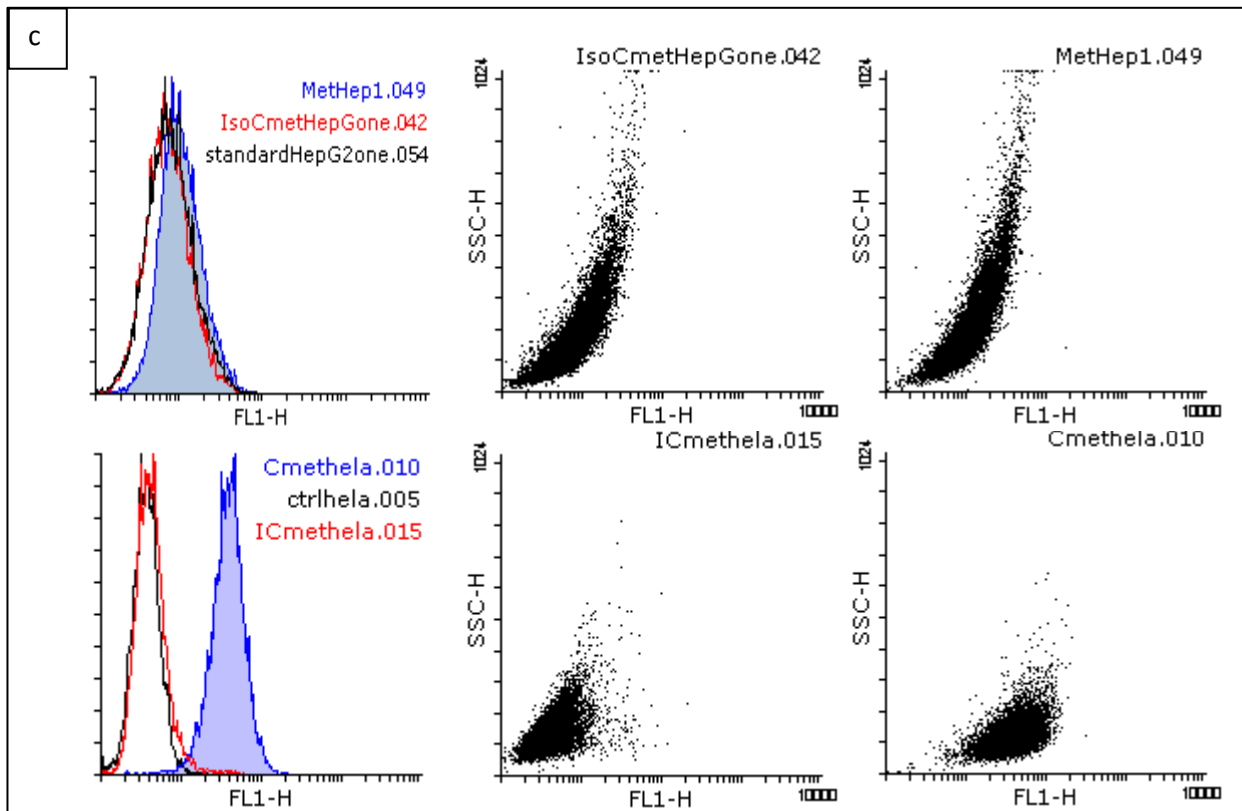


Figure 5.5: Flow cytometric analysis of membranous c-Met versus untreated standard & isotype control (n=3 biological repeats). Left images: overlay histograms summarising c-Met status of each cell line. X-axis: FL1-H, absorption using Alexafluor488 conjugated c-Met and isotype control probes. Y-axis: cell count. Black line represents untreated standard, red line represents isotype control, blue line/shaded area represents absorption following incubation with c-Met probe. Right images: dot plot of raw data: isotype control and c-Met probe.

a). HPV-positive oropharyngeal carcinoma cell lines UD SCC02 (superior images) and UPCI SCC090 (inferior images). Note the separation of absorption peaks for c-Met probe versus isotype control, consistent with c-Met expression in both lines.

b). HPV-negative oropharyngeal carcinoma cell lines UPCI SCC072 (superior images) and UPCI SCC089 (inferior images). Note the separation of absorption peaks in each line is comparable to HPV-positive cell lines illustrated in a).

c). Positive control cell lines HepG2 (superior images) and HeLa (inferior images). Note the marked separation of absorption peaks for HeLa c-Met versus isotype control. HepG2, a low c-Met-expressing hepatocellular carcinoma line^{398, 399} can be seen to have minimal separation of absorption peaks between c-Met probe and isotype control. All oropharyngeal carcinoma cell lines demonstrated c-Met probe absorption that exceeds HepG2 and is less than HeLa, confirming c-Met expression in all lines.

Median absorption shift was calculated using Flowing software by subtracting median absorption of control from median absorption with c-Met probe, with an average of three values taken from triplicate repeats. No significant pattern was noted between HPV-positive and HPV-negative lines, although all oropharyngeal lines other than UD SCC02 demonstrated greater absorption shift than the low c-Met-expressing cell line HepG2. Hela demonstrated a marked shift in absorption compared with all other lines. Additional absorption values are summarised in Table 5.2.

Table 5.2: Additional Flow Cytometric Absorption of Cell Lines Co-incubated with c-Met Probe, Compared to Control

Cell Line	UD SCC02	UPCI SCC72	UPCI SCC89	UPCI SCC90	HepG2	Hela
Median additional absorption	2.62	7.88	16.4	8.65	3.12	35.02

Figure 5.6: Total and Phospho-STAT3 Western Blot Analysis of Cell Lines Following Exposure to Stimulated Fibroblast Media 2

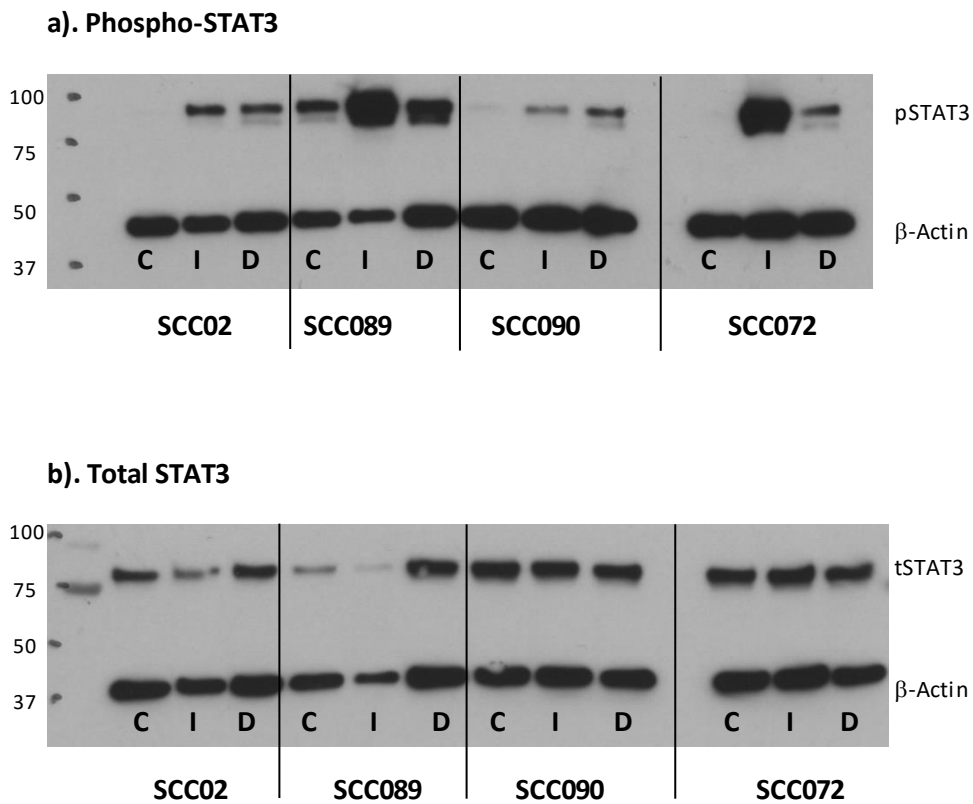


Figure 5.6: Western blot analysis of phosphorylated versus total STAT3 in cell lines UD SCC02, UPCI SCC072, UPCI SCC089 and UPCI SCC090 (n=3 biological repeats).

SCC02 – UPCI SCC02 (HPV-positive cell line)

SCC072 – UPCI SCC072 (HPV-negative cell line)

SCC089 – UPCI SCC089 (HPV-negative cell line)

SCC090 – UPCI SCC090 (HPV-positive cell line)

C – “Control”; 20 minute exposure to normal media control

I – “Immediate effect”: 20 minute exposure to respective stimulated fibroblast Medium 2

D – “Delayed effect”: 12 hour exposure to respective stimulated fibroblast Medium 2

a). Phospho-STAT3 western blot analysis of cell lines following exposure to their respective stimulated fibroblast Medium 2. Note that for HPV-negative cell lines, a marked increase in blot density can be observed following 20 minutes' exposure to stimulated fibroblast Media 2, whereas HPV-positive cell lines demonstrate an observable, yet much lower amount of pSTAT3 at 20 minutes. This finding is consistent with HPV-negative stimulated fibroblast Media 2 containing higher concentrations of one or more factors which signal via STAT3, such as HGF. Note that UPCI SCC089 demonstrated basal expression of pSTAT3, which may represent constitutive activation of a STAT3-signalling receptor. A smaller amount of sustained phospho-STAT3 elevation can be observed for cell lines at 12 h, although this is reduced compared to the marked elevation observed in HPV-negative lines at 20 mins. β -actin control bands can be observed to be consistent throughout, other than for UPCI SCC089, for which a minor decrease in concentration is apparent in the "immediate stimulation" lane – despite the reduction, the proportion of phospho-STAT3 is markedly elevated in this sample.

b). Total STAT3 western blot analysis of cell lines following exposure to their respective stimulated fibroblast Medium 2, identical experimental repeat to Figure a. No frank pattern of change in total STAT3 expression over each time-point can be observed in HPV-positive or -negative cell lines. Despite an apparent reduction in total STAT3 in cell line UPCI SCC089 at baseline and 20 mins, overall total STAT3 expression remained comparable in all cell lines, and at all time-points, when taking experimental repeats into account. Reductions of total STAT3 observed in the illustrated experimental repeat appear consistent in part with a reduction in respective β -actin band intensity.

Western blotting undertaken in collaboration with Dr. S. Thomas, who kindly undertook initial western blot analysis of first experimental repeat, and provided supervision and guidance for subsequent experimental repeats.

Figure 5.7: ELISA analysis of Soluble c-Met release from Oropharyngeal Carcinoma Cell Lines

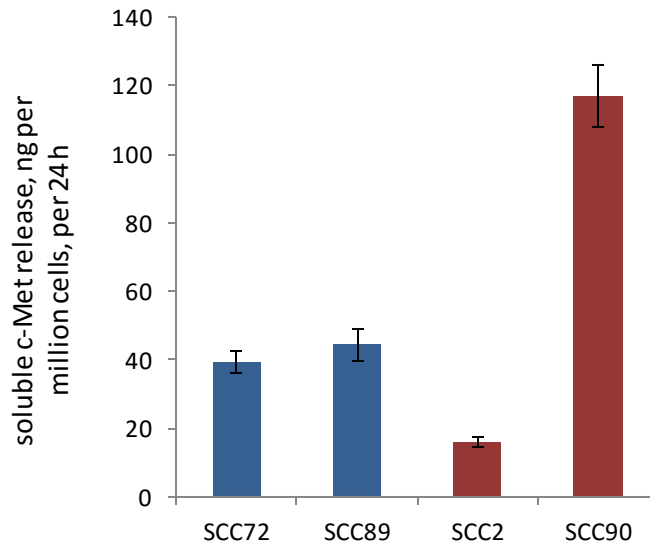


Figure 5.7: ELISA analysis of the concentration of the soluble form of the HGF receptor, c-Met in cell line conditioned media. Y-axis is normalised to ng million cells⁻¹ (original media concentration 3.5 X 10⁶ cells mL⁻¹). Error bars denote SEM, n=9. Red bars denote HPV-positive cell lines, blue bars denote HPV-negative cell lines.

Note that all cell lines release soluble c-Met. The two HPV-negative lines (UPCI SCC072 and UPCI SCC089) release an appreciable level of c-Met compared to UD SCC02. UPCI SCC090 demonstrates the greatest level of soluble c-Met release of all cell lines. Data for cell lines UPCI SCC072 and UPCI SCC089 are consistent with upregulated receptor cleavage, as noted for other ADAM-cleaved receptors (see Figures 3.2 and 4.3), although this statement is only proportional to the amount of c-Met released from cell line UD SCC02. The considerable c-Met release by UPCI SCC90 is noteworthy due to the absence of other ADAM-cleaved receptors noted in the cell line conditioned medium (Figures 3.2 and 4.3), suggesting soluble c-Met release may be due to an alternative mechanism to that seen in the HPV-negative lines, such as alternate splicing. The marked c-Met released by UPCI SCC090 may act as a competitive inhibitor to HGF stimulation of this cell line.

Statistical significance testing deemed inappropriate due to HPV-positive cell line c-Met release (UDSCC02 and UPCI SCC090) lying either side of HPV-negative cell line c-Met secretion (UPCI SCC072 and UPCI SCC089), inferring no overall trend.

Discussion

Initial experimentation using recombinant forms of candidate proteins identified by cytokine array analysis in Chapter 3 demonstrated two factors exhibiting a clear dose-response relationship with migration in cell line UPCI SCC072, namely HGF and OSM (Figure 5.1). All other recombinant proteins, excluding IL-6, showed no convincing dose-response effect on migration. As discussed in Chapter 4, although IL-6 did appear to induce a modest amount of additional migration at concentrations exceeding 2 ng mL^{-1} , this effect was not consistent with the degree of migration noted with cell line UPCI SCC072 when exposed to stimulated fibroblast medium. Moreover, the entire dose-response curve for recombinant IL-6 illustrated in Figure 5.1 can be observed to lie within the range of apparent background variability in migration linked to all other recombinant proteins tested. Statistical significance testing was not undertaken on the dose-response results, as the limited number of overall repeats ($n=3$) precluded significance testing from being an appropriate method of data analysis. Figures 5.1 b, c & d therefore includes all three biological repeats of $n=1$, to further illustrate a consistent trend of dose-response by HGF and OSM throughout all biological repeats, and unconvincing effects relating to all other factors tested. Undertaking triplicate biological and experimental repeats ($n=9$) was not feasible for the broad range of recombinant proteins tested due to high costs. HGF and OSM were therefore considered principal candidates for further investigation, with intent to subsequently validate migration using the recombinant version of each protein if presence was confirmed in conditioned media via ELISA. Recombinant HGF-induced migration was therefore ultimately repeated in dose-response experiments for both cell lines UPCI SCC072 and UPCI SCC089 in triplicate experimental and biological repeats, as shall be discussed in Chapter 6.

ELISA analysis of HGF & OSM allowed exclusion of OSM as a candidate molecule for inducing migrations: all conditioned media taken from both cell lines and stimulated fibroblasts contained undetectable levels of OSM (Figure 5.2). OSM had initially been regarded as a candidate molecule based on cytokine array densitometry data (Chapter 3, Figure 3.5); the inconsistency between cytokine array and ELISA analysis was due to high background absorption for OSM in the unstimulated fibroblast control medium. The background absorbance registered for normal media control (Figure 3.2) could not be confirmed as valid due to bleed-through of developer solution in that respective portion of the cytokine array and therefore was regarded as a potential false positive. In retrospect, the

OSM densitometry measurement for normal media control appears consistent with ELISA results; this reflects a clear limitation of the cytokine array experiments, whereby lack of biological repeats due to high array costs led to ambiguous results. Raybiotech OSM ELISA minimum sensitivity is quoted as 1 pg mL⁻¹; as a 1:20 dilution of conditioned media was used to perform ELISA analysis, this represents a minimum overall sensitivity of 20 pg mL⁻¹. Recombinant OSM dose-response analysis of ORIS™ assay migration (Figure 5.1) demonstrated that an OSM concentration of approximately 10 ng mL⁻¹ was necessary to induce the degree of migration seen in stimulated fibroblast media, and a concentration of approximately 2 ng mL⁻¹ in order to achieve any appreciable difference from control migration. It can therefore be concluded that ELISA sensitivity is of an appropriate degree to exclude OSM as a candidate molecule.

Although OSM appears to have no role in driving the additional migrations in HPV-negative stimulated fibroblast Media 1 & 2, the observation of a dose-dependent increase in migration with exposure of cell line UPCI SCC072 to recombinant OSM is in itself a novel finding. The capacity of OSM to drive EMT has been reported in breast carcinoma lines⁴⁰⁰, although the role of OSM in cancer progression is contentious – with reports of OSM having capacity to both reinforce and obstruct cancer progression⁴⁰¹⁻⁴⁰⁴. There is some level of consistency between findings relating to cancer type, and OSM may therefore have variable effects depending on cancer site of origin. Authors have suggested the use of OSM in therapeutic management of cancer⁴⁰⁵ – our data suggest management of oropharyngeal carcinoma in this manner may lead to catastrophic consequences through induction of tumour migration. Indeed, OSM is recognised as mediating cell migration through STAT3 induction and E-Cadherin downregulation³⁹⁵.

Conversely, HGF ELISA analysis confirmed all stimulated fibroblast media contained elevated amounts of HGF compared to unstimulated fibroblast control, with HPV-negative stimulated fibroblast media containing markedly higher amounts of HGF compared to HPV-positive stimulated fibroblast media (Figure 5.3). An intriguing observation was that for all stimulated fibroblast media, Medium 1 contained a greater concentration of HGF. This feature was inconsistent with the biological effects of Media 1 & 2 on migration in cell line UPCI SCC089, whereby Medium 2, albeit with a lower concentration of HGF, induced marked additional cell migration whereas Medium 1 did not. Moreover, the HPV-positive cell line UPCI SCC090 induced greater HGF release by fibroblasts in the respective Medium 1 compared to UPCI SCC089-stimulated fibroblast Medium 2. A general relationship

consistent with the observed migratory phenomenon was therefore established for HGF, although the absolute amount of HGF in each specific medium did not directly correlate with effect. This relationship mirrored earlier findings relating to IL-6 and IL-8 (Chapter 4, Figures 4.1 and 4.2), and therefore HGF's role in driving cell migration could not be assumed, despite its capacity to induce migration in the preceding recombinant protein experiments.

A number of explanations were considered for the inconsistencies between HGF concentration and cell migration, including potential nutrient exhaustion in Media 1 as a result of pre-incubation for 24 h with near-confluent cell lines followed by a further 24 h incubation with confluent fibroblasts. Indeed, the reduction in migration of cell lines UD SCC02, UPCI SCC089 and UPCI SCC090 when exposed to stimulated fibroblast Media 1 derived from the tonsillar fibroblast lines NTF06 and NTF01 (Chapter 2, Figure 2.2) suggested media exhaustion may have taken place.

An alternative explanation included release of a HGF-inhibiting agent by either cell lines (therefore present in Media 1) or by stimulated fibroblasts. Indeed, C7 cytokine array densitometry data for both HPV-negative cell line-stimulated fibroblast media indicates the presence of sgp130. The soluble gp130 receptor subunit is recognised as having an inhibitory effect on IL-6 trans-signalling⁴⁰⁶, and may have been released as a control mechanism following fibroblast stimulation through the trans-signalling route. Although this observation is not confirmatory of any factor being released with the capacity of directly blocking HGF signalling, it does illustrate the potential for inhibitory molecules to be released in response to stimulation.

The prospect of soluble c-Met release interfering with HPV-negative cell line response to stimulated fibroblast media was therefore considered given the confirmed release of sIL-6R in HPV-negative cell line conditioned media (cytokine array data: Figure 3.2, ELISA data: Figure 4.3), and also release of sEGFR (cytokine array data: Figure 3.2); both EGFR and IL-6R are type I tyrosine kinase receptors, and may be potentially cleaved by the snippase enzymes ADAMs 10 & 17^{407, 408}. Variable release of soluble TNFR1 & TNFR2 was also noted in HPV-negative line conditioned medium cytokine arrays; again, these soluble receptors are cleaved by ADAM17⁴⁰⁹. The scope for ADAM upregulation in HPV-negative cell lines therefore offered promise for cleavage of other type I receptors, including c-Met. Due to Medium 1 containing secretions from pre-incubation with each respective cell line, release of solubilised c-Met by HPV-negative lines, in combination with media exhaustion offered a feasible explanation for Media 2 more readily promoting migration despite

containing a lower concentration of HGF. Soluble c-Met ELISA (Figure 5.7) did indeed confirm the presence of this factor in HPV-negative cell line media, in addition to a surprisingly elevated amount of solubilised c-Met released by cell line UPCI SCC090. It may be postulated that as UPCI SCC090 did not release solubilised IL-6R and EGFR in the same manner as HPV-negative cell lines, the cellular mechanism for soluble c-Met release may differ. In addition to snippase cleavage, it is recognised that soluble c-Met may be formed from differentially-spliced mRNA⁴¹⁰; this would account for soluble c-Met release in UPCI SCC090 without release of EGFR/sIL-6R. Alternatively, UPCI SCC090 may simply express a lower membranous receptor density of sIL-6R and EGFR; although flow cytometry analysis of membranous IL-6R expression was found to bear no relationship to cell line HPV-status (data are presented in the subsequent chapter to maintain an appropriate narrative, Figure 6.14), this finding is in the context of receptor release by HPV-negative cell lines; basal membrane expression may therefore not reflect the true membranous receptor load preceding enzyme activity. ADAMs 10 & 17 are known to cleave type 1 receptors at threshold receptor densities; this may have only been exceeded by HPV-negative cell lines.

The biological relevance of soluble c-Met release in Media 1 was not formally tested, although any soluble c-Met may be assumed to have bound and competitively inhibited a proportion of available HGF on the basis of the findings of Coxon *et al*⁴¹¹, who noted avid HGF binding by the human c-Met ectodomain leading to HGF inhibition in human prostate and glioblastoma cell lines at a concentration of 2 nM and greater, when exposed to 50 ng mL⁻¹ HGF. Although Coxon did not analyse soluble c-Met at concentrations below 2 nM, a tail-off of efficacy of soluble c-Met as an HGF inhibitor was noted at this concentration in comparison to logarithmically increasing doses of 20 nM and 200 nM soluble c-Met. ELISA analysis of HPV-negative line derived conditioned media confirmed soluble c-Met concentrations of approximately 40 ng mL⁻¹, which equates to approximately 0.5 picoM of this 75-85 kDa cleaved protein^{412, 413}; a significantly lower concentration than used by Coxon. Despite this, HGF concentration in stimulated fibroblast media was approximately 25-50 times more dilute than utilised by Coxon, and therefore the absolute ratio of c-Met:HGF is approximately 40 times higher in Coxon's work; it therefore remains plausible that soluble c-Met release could have a partial, yet biologically significant effect on the *in-vitro* migration experiments.

Although HPV-negative cell line release of c-Met was regarded as insufficient to create any meaningful blockade of HGF, and therefore did not account for the lower migrations

observed with HPV-negative Media 1, the release of soluble c-Met in HPV-negative cell lines was a finding counterintuitive to a generalised view of HGF-driven migration exclusive to HPV-negative tumours. Retention of membranous c-Met would be more advantageous in HGF-induced migration; it may therefore be that partial membranous c-Met cleavage is a result of generalised ADAM snippase activity, the net effect of which is beneficial to tumour progression. It may be postulated that partial c-Met cleavage is a necessary consequence of ADAM-induced release of soluble mediators of tumour progression, such as sIL-6R, TNF- α , TGF- α and IL-1 β ^{409, 414}.

Following confirmation of HGF in stimulated fibroblast media, dose-response analysis of cell line UPCI SCC089 was undertaken in a similar manner to line UPCI SCC072 (Figure 5.4). Again, a clear dose-response relationship was observed in this cell line, although the line was noted to be approximately 10-fold more responsive to HGF compared to UPCI SCC072, with a parabolic increase in migration occurring between 0.2-2 ng mL⁻¹ HGF for UPCI SCC089, whereas UPCI SCC072 displayed a similar trend in migration between 2-20 ng mL⁻¹ HGF. Furthermore, it was noted that whilst the amount of HGF quantified via ELISA for SCC089-stimulated fibroblast Medium 2 was consistent with the dose of recombinant HGF necessary to induce ORIS™ assay migrations observed with UPCI SCC089-stimulated Medium 2, the amount of HGF measured in UPCI SCC072 Medium 2 was approximately 10-fold less than the dose of recombinant HGF required to induce the degree of migration observed with UPCI SCC072 Medium 2. It was therefore unclear whether HGF was a key inducer of the additional migrations observed in the conditioned media experiments, and if so, whether HGF acted alone or in combination with other factors.

To confirm that c-Met stimulation was a plausible mechanism of inducing HPV-negative cell line migration, flow cytometry was used to assess the amount of membranous c-Met expressed by each cell line. Surprisingly, all HPV-positive and -negative cell lines expressed comparable levels of membrane-bound c-Met (Figure 5.5), which exceeded that of HepG2 positive³⁹⁸ control (Figure 5.5c). Although hepatocellular carcinoma represents a classic disease of parenchymal HGF overexpression, HepG2 is known to produce relatively low levels of c-Met in comparison to other hepatocellular carcinoma lines³⁹⁹; the HeLa cell line was therefore run as a second positive control, due to its confirmed membranous expression of c-Met via immunocytochemistry⁴¹⁵. HeLa c-Met expression exceeded that of all oropharyngeal lines (Figure 5.5c). This comparable expression of c-Met in all oropharyngeal cell lines was consistent with clinical findings of Kwon *et al*²⁷⁶, who noted that although HGF

expression in HPV-negative oropharyngeal carcinomas is linked to poor prognosis, the degree of cell bound c-Met expression has no correlation with outcome. A study conducted by Choe *et al*⁴¹⁶ further demonstrated no correlation between tumour p16 status and c-Met expression, although only 17 of the 82 tumours sampled were oropharyngeal in origin.

A number of in-vitro studies have found HGF to be an important component of tumour-stromal interactions in HNSCC⁴¹⁷⁻⁴¹⁹, and have linked stromal HGF release to the induction of tumour migration and invasion in a similar manner to our findings with respect to HPV-negative oropharyngeal carcinoma lines^{418, 419}. A key difference however, is that our data suggest that pre-conditioned tumour-associated fibroblasts are unnecessary for tumour-stromal interactions to occur, and that normal stromal fibroblasts may be recruited to adopt a supportive secretory profile within 24 h.

HGF and its classical receptor, c-Met, have been implicated with poor survival in a wide range of malignancies, including non-small cell lung cancer⁴²⁰, ovarian carcinoma⁴²¹, gastric carcinoma^{422, 423} and colon carcinoma^{424, 425}. Although HGF/c-Met status has been contentious in predicting head and neck cancer outcomes^{75, 129, 426, 427}, recent data suggest that c-Met status may be important in predicting outcome in locally-advanced, HPV-negative (p16-negative) disease⁴²⁸. Recent oropharyngeal-specific data suggest that HGF status predicts outcome in HPV-negative disease, although c-Met status was found to have no prognostic value²⁷⁶. c-Met expression has also been linked to poor outcome in nasopharyngeal tumours⁴²⁹.

Conclusion

Following recombinant protein dose-response experimentation, along with interrogation of both cell lines and conditioned media, HGF remained as a single most plausible candidate for driving cell line migrations. A number of inconsistencies were observed with regards to potential HGF-induced migration, including the high concentrations of HGF in UPCI SCC089 Medium 1 which did not appear to induce migration as readily as UPCI SCC089 Medium 2, and lower concentrations of HGF in all UPCI SCC072 stimulated fibroblast media compared to the concentration of recombinant HGF required to drive migration comparable to that observed in conditioned media experiments. Analysis of migration blockade by use of c-Met inhibitors was determined as a method of both confirming HGF as a responsible molecule, in

addition to potentially validating clinically available drugs in the management of HPV-negative disease.

Chapter 6: The Role of HGF in 2D Modelled Migrations

Introduction

Many of the Bradford-Hill criteria⁵⁸ for affirmation of a causal relationship between fibroblast HGF release and cell line migration have been addressed in Chapter 5, with the exclusion of *Specificity*. Bradford-Hill stated that the more specific the association between a factor and the effect of concern, the more likely a causal relationship exists. Repetition of stimulated fibroblast media migrations with experimental inhibition of HGF signalling offers both validation of specificity, as well as offering a theory-falsification approach to assessing whether HGF is a major driver of the stimulated fibroblast media-induced migrations. Much of the data relating to HGF presented in Chapter 5, albeit valuable, may be regarded as circumstantial; although HGF has been measured by ELISA in conditioned media and is indeed present in higher concentrations in HPV-negative cell line stimulated media, and although HGF has been demonstrated to induce HPV-negative cell line migration, no conclusive evidence has been put forward to confirm a direct relationship between presence of HGF in stimulated fibroblast media and the induction of cell migration. This chapter therefore seeks to theory test the role of HGF in driving stimulated fibroblast media-induced migrations.

An established approach to the obstruction of cellular signalling pathways is the use of small molecule inhibitor drugs/blocking antibodies. In addition to demonstrating the biological relevance of pathway inhibition, clinically valid inhibitors have the additional benefit of offering insight into how currently available therapeutic agents may be used to take advantage of *in-vitro* phenomena in a clinical setting. Blockade of the HGF receptor, c-Met, provides an accessible method of analysing the role of HGF in driving cell migrations in the stimulated fibroblast conditioned media experiments through a theory falsification approach; if HGF stimulation of c-Met is responsible for cell migration in response to stimulated fibroblast media, then obstructing c-Met signalling should lead to abrogation of media-induced migrations – any failure of c-Met inhibitors to restrain cell migration in stimulated fibroblast media therefore acts as a method of theory falsification.

A considerable number of small molecule and monoclonal antibody inhibitors to c-Met are available (please refer to Table 6.1), each of which demonstrate marked variation in c-Met affinity and specificity. Of all available c-Met-specific inhibitors, INCB28060 offers greatest potency, with an IC_{50} of 0.13 nM⁴³⁰. INCB28060 is also a highly specific inhibitor of c-Met, and shows no reported cross-reactivity with other receptors. Although a single dose-escalation study has been completed for INCB28060 (further discussed below), no Phase II trials have yet been undertaken. Foretinib, a c-Met inhibitor capable of blocking a range of cytokine receptors with tyrosine kinase activity, has been trialled in a number of Phase II studies⁴³¹⁻⁴³³, and shows promise in the management of cancer. Foretinib moreover demonstrates the greatest potency of all inhibitors that have currently completed Phase II trial. The highly active and specific inhibitor INCB28060, and the clinically-relevant, yet less specific inhibitor foretinib, shall be considered in further detail; experimental inhibition of c-Met activity using these two drugs offers both comprehensive analysis of HGF's role in conditioned media-induced migrations, in addition to assessing the ability of a clinically-applicable drug (i.e. foretinib) to inhibit microenvironmental interactions.

Table 6.1: List of available small molecule/monoclonal antibody inhibitors of c-Met (arranged in descending order of potency, expressed as IC_{50}).^{430, 434-455}

Inhibitor	c-Met IC_{50} , nM	Other Targets	Reference
INCB28060	0.13		2011 Lui
TAK-701	0.3		2012 Cecchi
Foretinib	0.4	KDR, Tie-2, VEGFR1 & 3, EGFR, RON	2009 Qian
Exelixis	0.4	VEGFR2	2009 Eder
MGCD-265	1	RON, VEGFR2, VEGFR1	2012 Bonfils
AMG-458	1.2	VEGFR2	2008 Liu
Cabozantinib	1.3	VEGFR2/KDR, Kit, VEGFR3/FLT4	2011 You
RP1040	1.3		2012 Cecchi
MK8033	1.3	Ron	2012 Cecchi
BMS-794833	1.7	VEGFR2	referenced by Selleckchem without valid article
Rilotumumab	2.1		2012 Cecchi
MK-2461	0.4-2.6	c-Met mutants, Flt1, RON	2010 Pan, 2012 Cecchi
Tepotinib	3	IRAK4, TrkA, Axl	2013 Bladt
BMS-777607	3.9	Axl, RON, Tyro3, VEGFR2	2009 Schroeder
JNJ-38877605	4		referenced by Selleckchem without valid article
SGX-523	4		2009 Buchanan
PF-04217903	4.8		2009 Timofeevski
EMD1214063	1.0-6.0		2012 Cecchi
Onartuzumab (MetMab)	2.6-8.7		2012 Cecchi
BMS-754807	6	Insulin Receptor, IGF-1R, TrkB	2009 Carboni
AMG-208	9		2008 Albrecht
PHA-665752	9	RON, Flk1, c-Abl	2006 Smolen
PHA-665752	9	RON, VEGFR2	2003 Christensen
Crizotinib	11	ALK	2007 Zou
CEP-A	13		2012 Cecchi
Golvatinib	14	VEGFR2	2010 Nakagawa
NVP-BVU972	14		PMID: 21697284
SU11274	20	Flk1, RON, FGFR1	2012 Cecchi
SU11271	40	RON, FGFR1, FLK-1	PMID: 14617781
ARQ197	100		PMID: 21632449 (?Tivantinib)
S49076	1-200	FGFR1, 2 & 3, AXL	2012 Cecchi
SU11606	170	RON, FGFR1, FLK-1	2003 Wang
Tivantinib	100-550		2010 Munshi, 2011 Eathiraj
Amuvatinib	4,790	c-Kit, PDGFR alpha	2010 Taverna
MP470	5,000	c-KIT, MET, PDGFR, Flt3, and AXL	2009 Welsh
K252a	10,000	c-Met mutant M1268T, partial PDGFR	2002 Morotti

Foretinib

Foretinib is a Class II ATP-competitive small molecule inhibitor of c-Met. Inhibitor classification has been derived from the historical development of small molecule c-Met-inhibiting drugs: two of the forerunners of the vast number of currently available compounds were SU-11274 and AM7. SU-11274's activity relies on an acyl thiourea group, which allows penetration into a hydrophobic pocket expressed by the c-Met receptor's ATP binding site in order to cause blockade; those modern drugs demonstrating a similar activity to SU-11274 are referred to as "Class I" c-Met inhibitors. AM7 attaches to the kinase linker domain of c-Met, leading to a conformation change of a C-helix⁴⁵⁶ within the tyrosine kinase domain, which in turn exposes an alternative hydrophobic region that AM7 is capable binding⁴⁵⁷. The conformation change occurring in c-Met's ATP processing site in response to AM7 binding renders it inactive. Drugs acting in a similar fashion to AM7 are termed "Class II" inhibitors. Both Class I and II drugs act through initially binding to c-Met and then lodging a further domain within the kinase subunit's ATP processing region; they are therefore termed "ATP-competitive" inhibitors. A further class has been discovered, which acts as a non-ATP competitive inhibitor – this group of drugs prevent kinase activity by inducing a conformation change that either prevents ATP & substrate binding (for example, ARQ197⁴⁵²), or prevents catalytic residues interacting (for example, tivantinib).

As for other Class II ATP-competitive small molecule inhibitors, foretinib's activity is not limited to inhibition of c-Met; similar inhibitory properties have been noted for VEGFR and EGFR, among other receptors. It appears the nature of Class II inhibitor interactions with the tyrosine kinase domain is less specific than Class I inhibitors, leading to cross reactivity with other tyrosine kinase receptors. Indeed, Class II c-Met inhibitors were initially derived from modified PDGFR and VEGFR2 inhibitors⁴⁵⁸.

Foretinib has been subject to a number of Phase II trials, including a trial in advanced head and neck cancer⁴³³. Seiwert *et al* trialled oral foretinib 240 mg, administered for 5 consecutive days of a 14-day cycle in patients with recurrent/metastatic head and neck cancer. The trial was of a two-stage design; stage 1 of the trial involved enrolment and treatment of 14 patients. Stage 2 of the trial was halted due to progression criteria requiring at least one patient demonstrating either complete or partial regression of disease. Despite the lack of progression to stage 2, the study demonstrated that 50 % of patients had stabilisation of their disease, with mean stabilisation of 4.1 months. Two patients demonstrated prolonged stabilisation of disease of 13 and 13.9 months.

Foretinib dosing has been reviewed in a Phase II study of 74 patients with metastatic gastric carcinoma⁴³¹; Manish *et al* compared daily 80 mg dosing to the 240 mg cyclic regimen used by Siewert *et al*, and found that daily dosing led to lower incidence of adverse reactions, whilst maintaining comparable effect. Again, best response was found to be stable disease, with no evidence of complete/partial response to therapy⁴³¹.

Further Phase II trials of foretinib include the management of papillary renal carcinoma⁴⁵⁹ and advanced hepatocellular carcinoma⁴⁶⁰. Both trials demonstrated evidence of tumour regression in select patients; whilst this was limited to 2 of 13 patients in the case of advanced hepatocellular carcinoma, a more profound effect was noted in papillary renal carcinoma, with 50 of 68 patients demonstrating some decrease in tumour size, and 21 % of tumours decreasing in size by 30 % or more. This profound influence on tumour size in renal carcinoma may reflect HGF's known effects on renal cell proliferation *in vivo* and *in vitro*, which include induction of DNA synthesis and promotion of resilience to ischaemia⁴⁶¹.

INCB28060 (Capmatinib)

INCB28060, recently rebranded as capmatinib, is a Class I ATP-competitive small molecule inhibitor of c-Met. As with other Class I competitors INCB28060 demonstrates marked c-Met specificity compared to foretinib and other Class II inhibitors. Despite INCB28060's highly specific activity against the c-Met receptor, it has been shown to have inhibitory effects on downstream cross-talk with EGFR and HER-3 via receptor activation and ligand release⁴³⁰. As with foretinib, INCB 28060 has been found to reduce tumour size in specific xenograft models of cancer in combination with gemcitabine⁴⁶². Again, the authors reported prolonged survival rather than tumour regression, and noted that although tumour cell proliferation was reduced, apoptosis was absent; the authors further stated that INCB28060 had no effect on advanced tumour growth, findings that appear consistent with clinical studies of c-Met inhibition with foretinib. To date, no clinical trial data have been published for INCB28060, although a Phase Ia trial has been completed (ClinicalTrials.gov identifier: NCT01072266), and a Phase Ib trial in combination with bevacizumab is planned (ClinicalTrials.gov identifier: NCT02386826).

HGF/c-Met Signalling

The role of HGF in cancer progression has been discussed in Chapter 5. Consideration shall therefore be limited here to the HGF receptor, c-Met (also known as MET, AUTS9, HGFR, RCCP2 and DFN97) and the related intracellular migratory signalling pathways which may be influenced by c-Met inhibition. Conflicting reports exist as to the source of c-Met's nomenclature, with some citing that the receptor was initially identified as an oncogenic fusion protein in cells treated with N-methyl-N'-nitrosoguanidine, from which the receptor derives its name⁴⁵⁸. Alternative reports include "MET" acting as shorthand for mesenchymal epithelial transition factor receptor⁴³³, although this appears a misnomer given that "mesenchymal-epithelial transition" refers to a process reverse to that of "epithelial-mesenchymal transition", which is more characteristically ascribed to epithelial stimulation with HGF^{278, 463}.

c-Met is a transmembrane protein consisting of an extracellular receptor domain and an intracellular tyrosine kinase domain. The tyrosine kinase domain has capacity to activate a complicated network of secondary messenger signalling pathways including Beta-catenin, Notch, PI3K, Raf-MEK-ERK, RAS, STAT1 and STAT3⁴⁶⁴⁻⁴⁷⁰. RAS, PI3K and STAT3 appear responsible for inducing HGF-mediated cellular motility⁴⁷⁰⁻⁴⁷². STAT3, specifically, has been identified as a key pathway for induction of tumour migration/invasion in response to HGF⁴⁷²⁻⁴⁷⁵. In addition to the somewhat prolific effects on intracellular signalling cascades, c-Met has numerous synergistic interactions with other cellular receptors: this shall be reviewed in further detail in the discussion.

Multi-Cytokine Control of Cell Migration

As discussed in Chapter 5 (please refer to discussion section and Figures 5.1 & 5.3), the cell line UPCI SCC072 demonstrated a convincing dose-response relationship of additional ORIS™ assay migration in the presence of logarithmically increasing doses of recombinant human HGF. Despite this relationship, ELISA-assayed HGF concentration in UPCI SCC072-stimulated Medium 2 was below that required to induce an equivalent degree of migration when using recombinant HGF protein. A number of explanations may underlie the disparity between the two observations; HGF may either be entirely unimportant to the migratory phenomenon; or alternatively may be central to the migratory phenomenon, yet biologically more active when produced in-situ in comparison to recombinant protein. It is moreover

feasible that reconstituted recombinant HGF may lack the same degree of effect as the equivalent concentration of in-situ protein for a number of technical reasons, including protein sequence, degradation during transportation and storage, or as a result of reconstitution/ dilution errors. A third possibility, as shall be addressed in this chapter, is that HGF may influence cell migration in combination with (a) further factor(s) secreted by fibroblasts in response to stimulation by HPV-negative cell lines.

The most plausible factor which may supplement HGF's effect, based on data presented in Chapter 4, is IL-6; Figure 4.10 illustrates a potential dose-response relationship, albeit punitive in comparison to conditioned media experiments, between IL-6 concentration and cell migration. All other factors tested (excluding OSM) failed to demonstrate a convincing dose-response relationship throughout triplicate biological repeat experimentation. IL-6 has also been measured as elevated in HPV-negative cell line-stimulated fibroblast media (please refer to Figure 4.1), and characteristically stimulates EMT, a process that would be favourable for migration to occur, as discussed in more detail in Chapter 4. Whilst the conclusion of Chapter 4 was that IL-6 did not appear to have a principal effect on driving the migratory phenomenon observed in conditioned media experiments, the factor does retain potential to interact with HGF-driven cell migration. Recombinant IL-6 has also been reported as inducing HGF release in cancer patients⁴⁷⁶, and furthermore signals via STAT3, offering scope for HGF-reinforcing signals to occur in response to IL-6 stimulation.

Secondary Targets of Foretinib

As discussed above, both EGFR and VEGFR have been identified as secondary targets of foretinib. The IC₅₀ for each respective receptor is reported by commercial suppliers, Selleckchem, as 2.99 μ M and 2.8 nM; some tenfold higher than for c-Met⁴⁷⁷. Although Selleckchem appropriately quote work by Fawn *et al* as establishing data for the IC₅₀ of VEGFR, no reference is made to EGFR in their article⁴³⁵. Other researchers referenced by suppliers have indeed found EGFR to be inhibited by foretinib, although interpretation has been via semi-quantitative Phospho-RTK array in the presence a standardised dose of 1 μ M foretinib⁴⁷⁸. Furthermore, IC₅₀ for receptor phosphorylation versus biological effect have been found by the same authors to vary by approximately 100-fold⁴³⁵. The quoted inhibitory concentration of foretinib for each tyrosine kinase receptor therefore acts as a noteworthy reference point rather than an absolute; biologically relevant effect certainly appears to

exceed receptor phosphorylation data⁴³⁵ and therefore a phosphorylation-based IC₅₀ cannot be relied upon for functional assays.

The comparable IC₅₀ quoted for both c-Met and VEGFR does however illustrate the potential for receptor inhibition to occur simultaneously in c-Met-inhibition experiments using the drug. This is further complicated by uncertainties surrounding the supplier-quoted IC₅₀ of EGFR, which cannot be identified in the respective literature and therefore may approximate closer than expected to the inhibitory concentrations required for c-Met and VEGF.

Although VEGF/VEGFR signalling has been historically regarded as an angiogenic phenomenon, more recent work have identified that tumour-expressed VEGFR is important for progression of many cancers, including those of the head and neck^{316, 479}. Whilst the current body of research does not necessarily support the role of VEGF signalling in tumour motility, cross-reactivity of foretinib with this receptor must be borne in mind as an alternative mechanism to c-Met inhibition when analysing restraint of conditioned media-induced cell migration. Much data are available to support EGFR-induced cellular motility in both keratinocytes and head and neck cancer⁴⁸⁰⁻⁴⁸³; foretinib's cross-reactivity with EGFR signalling must therefore also be considered alongside VEGFR.

This chapter shall therefore theory-test the role of HGF in HPV-negative cell line-stimulated fibroblast conditioned media induced migration through c-Met blockade, using the inhibitors INCB28060 and foretinib. Further consideration shall be paid to potential bystander effects of each of these drugs on EGF and VEGF signalling, and further experimental methods undertaken to rule out EGF/ VEGF signalling as a contributor to the observed migrations. The role of IL-6 shall be revisited in the context of HGF-induced migration, with specific consideration of the cell line UPCI SCC072, for which HGF in isolation may not account fully for the effects of stimulated fibroblast conditioned media on cell migration.

Methods

M6.1-6.2: Analysis of Effect of c-Met Inhibitors on Migration of HPV-Negative Oropharyngeal Carcinoma Cell Lines Exposed to Recombinant Human HGF

Purchasing, Preparation and Storage of HGF and c-Met Inhibitors

Foretinib and INCB28060 were purchased from Selleckchem (Stratech Scientific Ltd, Newmarket, Suffolk: UK distributors to Selleckchem). Each vial of anhydrous drug was dissolved in DMSO to a stock concentration of 4 mM and 1 mM for foretinib and INCB28060, respectively. Each stock solution was aliquoted and stored immediately at -80 °C until use in experiments.

Recombinant human HGF was purchased from Insight Biotechnology (Wembley, UK. Catalogue number 10-1194-C). The lyophilised protein was briefly centrifuged and then reconstituted with 1,000 µL normal media (DMEM plus 10 % FCS, plus 50 U mL⁻¹/50 µg mL⁻¹ penicillin-streptomycin, plus 2 mM L-glutamine) to produce a stock solution of 10 µg mL⁻¹, aliquoted and stored at -21 °C prior to use in experiments.

Preparation of Migration Assays, Inhibition of Cell Division and Pre-experimental Conditioning with c-Met Inhibitors/DMSO Control

HPV-negative cell lines UPCI SCC072 and UPCI SCC089 were grown to 70 % confluence in separate T75 flasks. Cells were washed twice in PBS, trypsinised, centrifuged at 1,000 rpm and then resuspended in normal media. Each cell suspension was then counted using a haemocytometer, appropriately diluted using normal media, and re-counted in order to achieve the preoptimised seeding concentration of 1.6 X 10⁶ cells mL⁻¹ for UPCI SCC072, and 8.8 X 10⁵ cells mL⁻¹ for UPCI SCC089, allowing confluent ORIS™ assay well loading as described in Chapter 1. ORIS™ assay plates were prepared under sterile conditions, mounting silicone stoppers into each well using the manufacturer-supplied location device. 100 µL of each cell suspension was then pipetted into respective ORIS™ assay wells and left overnight to adhere.

Following cell adherence and confirmation of well confluency using an inverted lens microscope, a preoptimised (please refer to Chapter 1, Figure 1.9) $2 \mu\text{g mL}^{-1}$ mitomycin C suspension in normal media was prepared from snap-frozen 0.5 mg mL^{-1} aliquots of mitomycin C stored at $-80 \text{ }^{\circ}\text{C}$. All handling of mitomycin C was undertaken in a darkened tissue culture hood in order to avoid excessive light exposure. The mitomycin C suspension was then divided into multiple universal containers, and either foretinib/INCB28060/DMSO control added from stock solutions in order to achieve the desired concentrations of 0.4, 4 & 40nM foretinib, 0.1, 1 & 10nM INCB28060, or DMSO control. Foretinib and INCB28060 stock solutions were diluted 10-fold and 100-fold in DMSO in order to achieve three initial solutions that each required a 1:100,000 dilution to achieve desired working concentrations in mitomycin C, thereby retaining equal levels of DMSO solvent in each final dilution. Foretinib and INCB28060 concentrations were determined using the available literature on receptor IC₅₀ and also data on biologically relevant effect^{430, 435}.

Silicone stoppers were then removed from assay wells using the manufacturer supplied retrieval tool, exposing the respective cell exclusion zone, and normal media carefully aspirated off each well ensuring contact was avoided with the well base. 2 X 100 μL PBS washes were then undertaken, and then 100 μL mitomycin C with foretinib/INCB28060/DMSO control was then carefully pipetted into respective wells and incubated for 3.5 hours at $37 \text{ }^{\circ}\text{C}$ in the dark. Following 3.5 hours incubation in mitomycin C, baseline void photomicrographs were taken using a X4 objective lens.

Preparation of $0.5 \mu\text{g mL}^{-1}$ HGF Plus c-Met Inhibitor/ DMSO Control Solutions, Completion of ORIS™ Assay

$0.5 \mu\text{g mL}^{-1}$ HGF was determined as an optimal concentration for analysing blockade of HPV-negative cell migration based on data presented in Figure 5.1, whereby higher concentrations of HGF led to a decline in migration in cell line UPCI SCC072. Although cell line UPCI SCC089 demonstrated a slight reduction in additional migration at concentrations above $0.2 \mu\text{g mL}^{-1}$ HGF, $0.5 \mu\text{g mL}^{-1}$ was still considered a favourable concentration as more rapid migration of UPCI SCC089 had potential to result in complete ORIS™ assay void closure, thereby obscuring minor changes in migration that may occur in the presence of foretinib/ INCB28060.

Thawed stock $10 \mu\text{g mL}^{-1}$ HGF was diluted in normal media to a concentration of $0.5 \mu\text{g mL}^{-1}$ immediately prior to experimentation. The $0.5 \mu\text{g mL}^{-1}$ HGF suspension was then divided into multiple universal containers, and either foretinib/INCB28060/DMSO control added from stock solutions in order to achieve the desired concentrations of 0.4, 4 & 40 nM foretinib, 0.1, 1 & 10 nM INCB28060, or DMSO control. Foretinib and INCB28060 stock solutions were again diluted 10-fold and 100-fold in DMSO in order to achieve three initial solutions that each required a 1:100,000 dilution to achieve desired working concentrations in mitomycin C, thereby retaining equal levels of DMSO solvent in each final dilution.

Following mitomycin C incubation, assay wells were washed X2 in PBS and then $100 \mu\text{L}$ HGF/inhibitor suspension carefully pipetted into respective wells. ORIS™ assay plates were then incubated for either 20 h (UPCI SCC089) or 48 h (UPCI SCC072) in order for migration to occur, and then endpoint photomicrographs taken using a X4 objective lens.

Analysis of Cell Migration

Analysis of cell migration was undertaken by comparison of baseline versus endpoint micrograph images taken at X4 objective. The area of each stopper-induced cell exclusion zone at baseline and endpoint was measured with ImageJ software (freeware, NIH, USA), using the polygon selection tool. Percentage void closure was then calculated by dividing area of closure at experimental endpoint by total baseline area of cell exclusion zone.

M6.3-6.4: Foretinib/INCB28060 Cytotoxicity Assays using Cell Lines UPCI SCC072 and UPCI SCC089

LDH Assay

Cytotox 96[®] Non-Radioactive Cytotoxicity Assays were purchased from Promega Corporation (Madison, USA, Cat number G1780). Manufacturer's instructions were adhered to throughout experimentation, although are summarised below.

HPV-negative Cell Lines UPCI SCC072 and UPCI SCC089 were grown to approximately 70-80 % confluence in T75 flasks, trypsinised, resuspended in normal media, counted using a haemocytometer, diluted to 1×10^5 cells mL⁻¹ and then re-counted. 10,000 cells in 100 μ L normal media were then pipetted into wells of a 96-well plate and left overnight to adhere.

Foretinib/INCB28060/DMSO control was then added to normal media to achieve the desired concentrations of 0.4, 4, 40, 400 and 4,000 nM foretinib, 0.1, 1, 10, 100, 1,000 & 10,000 nM INCB28060, or DMSO control. Following overnight adherence, each 96-well plate was washed X2 in PBS and then 100 μ L normal media containing foretinib/INCB28060/DMSO control added and incubated at 37 °C for 24 hours. Normal media containing foretinib/INCB28060/DMSO control was also incubated in cell-free wells in order to act as background absorbance controls.

Following 24 h incubation, target maximum LDH release control was prepared using wells incubated with DMSO-containing normal media control. 10 μ L manufacturer-supplied lysis buffer was added cellular "target maximum" and acellular "volume control" wells and incubated for 45 minutes at 37 °C. 50 μ L media from each assay well was then transferred to a fresh 96-well plate and co-incubated with 50 μ L reconstituted substrate solution (prepared through dissolution of manufacturer-supplied substrate mix in 12 mL assay buffer) at room temperature for 30 minutes, protected from light. 50 μ L manufacturer-supplied stop solution was then added to each well, and absorbance at 492 nm measured using a Tecan Infinite M200 plate reader.

Percentage cytotoxicity for each dose of foretinib/INCB28060 was then calculated using the following manufacturer-advised formula:

$$\% \text{ Cytotoxicity} = \frac{(\text{Experimental absorption} - \text{Spontaneous absorption}) \times 100}{\text{Target Maximum} - \text{Spontaneous absorption}}$$

MTS Assay

CellTiter 96[®] AQueous One Solution Cell Proliferation Assay was purchased from Promega Corporation (Madison, USA, Cat number G3580). Manufacturer's instructions were adhered to throughout experimentation, although are summarised below.

HPV₋negative Cell Lines UPCI SCC072 and UPCI SCC089 were grown to approximately 70-80 % confluence in T75 flasks, trypsinised, resuspended in normal media, counted using a haemocytometer, diluted to 1×10^5 cells mL⁻¹ and then re-counted. 10,000 cells in 100 μ L normal media were then pipetted into wells of a 96-well plate and left overnight to adhere.

Foretinib/INCB28060/DMSO control was then added to normal media to achieve the desired concentrations of 0.4, 4, 40, 400 and 4,000 nM foretinib, 0.1, 1, 10, 100, 1,000 & 10,000 nM INCB28060, or DMSO control. Following overnight adherence, each 96-well plate was washed X2 in PBS and then 100 μ L normal media containing foretinib/INCB28060/DMSO control added and incubated at 37 °C for 24 hours. Normal media containing foretinib/INCB28060/DMSO control was also incubated in cell-free wells in order to act as background absorbance controls.

Following 24 h incubation, media were aspirated and wells washed X2 in PBS. 100 μ L normal media was then added to each well and co-incubated with 20 μ L MTS solution for 1.5 hours. Absorption was then immediately read at 490 nm using a Tecan Infinite M200 plate reader.

M6.5 - 6.6: Analysis of Effect of c-Met Inhibitors on Migration of HPV-Negative Oropharyngeal Carcinoma Cell Lines Exposed to Stimulated Fibroblast Media

Preparation of Migration Assays, Inhibition of Cell Division and Pre-experimental Conditioning with c-Met Inhibitors/DMSO Control

HPV-negative cell lines UPCI SCC072 and UPCI SCC089 were grown to 70 % confluence in separate T75 flasks. Cells were washed twice in PBS, trypsinised, centrifuged at 1,000 rpm and then resuspended in normal media. Each cell suspension was then counted using a haemocytometer, appropriately diluted using normal media, and re-counted in order to achieve the preoptimised seeding concentration of 1.6×10^6 cells mL^{-1} for UPCI SCC072, and 8.8×10^5 cells mL^{-1} for UPCI SCC089, allowing confluent ORIS™ assay well loading as described in Chapter 1. ORIS™ assay plates were prepared under sterile conditions, mounting silicone stoppers into each well using the manufacturer-supplied location device. 100 μL of each cell suspension was then pipetted into respective ORIS™ assay wells and left overnight to adhere.

Following cell adherence and confirmation of well confluency using an inverted lens microscope, a pre-optimised (please refer to Chapter 1, Figure 1.5) 2 $\mu\text{g mL}^{-1}$ mitomycin C suspension in normal media was prepared from snap-frozen 0.5 mg mL^{-1} aliquots of mitomycin C stored at $-80\text{ }^\circ\text{C}$. All handling of mitomycin was undertaken in a darkened tissue culture hood in order to avoid excessive light exposure. The mitomycin C suspension was then divided into multiple universal containers, and either foretinib/INCB28060/DMSO control added from stock solutions in order to achieve the desired concentrations of 0.4, 4 & 40 nM foretinib, 0.1, 1 & 10 nM INCB28060, or DMSO control. Foretinib and INCB28060 stock solutions were diluted 10-fold and 100-fold in DMSO in order to achieve three initial solutions that each required a 1:100,000 dilution to achieve desired working concentrations in mitomycin C, thereby retaining equal levels of DMSO solvent in each final dilution.

Silicone stoppers were then removed from assay wells using the manufacturer supplied retrieval tool, exposing the respective cell exclusion zone, and normal media carefully aspirated off each well ensuring contact was avoided with the well base. 2 X 100 μL PBS washes were then undertaken, and then 100 μL mitomycin C with foretinib/INCB28060/DMSO control was then carefully pipetted into respective wells and

incubated for 3.5 hours at 37 °C in the dark. Following 3.5 hours incubation in mitomycin C, baseline void photomicrographs were taken using a X4 objective lens.

Preparation of Stimulated Fibroblast Media Plus c-Met Inhibitor/ DMSO Control Solutions, Completion of ORIS™ Assay

The most experimentally-inductive stimulated fibroblast media for cell lines UPCI SCC072 (DENOF08 stimulated fibroblast Medium 1) and UPCI SCC089 (DENOF08 stimulated fibroblast Medium 2) were collected and immediately stored at -21 °C ahead of experiments, as outlined in Chapter 2. Stimulated fibroblast media were then thawed, aliquoted and either foretinib/INCB28060/DMSO control added from stock solutions in order to achieve the desired concentrations of 0.4, 4 & 40 nM foretinib, 0.1, 1 & 10 nM INCB28060, or DMSO control. Foretinib and INCB28060 stock solutions were diluted 10-fold and 100-fold in DMSO in order to achieve three initial solutions that each required a 1:100,000 dilution to achieve desired working concentrations in the fibroblast conditioned media, thereby retaining equal levels of DMSO solvent in each final dilution.

Following mitomycin C incubation, assay wells were washed X2 in PBS and then 100 µL Stimulated fibroblast medium with foretinib/INCB28060/DMSO control carefully pipetted into respective wells. ORIS™ assay plates were then incubated for either 20 h (UPCI SCC089) or 48 h (UPCI SCC072) in order for migration to occur, and then endpoint photomicrographs taken using a X4 objective lens.

Analysis of Cell Migration

Analysis of cell migration was undertaken by comparison of baseline versus endpoint micrograph images taken using a X4 objective lens. The area of each stopper-induced cell exclusion zone at baseline and endpoint was measured with ImageJ software (freeware, NIH, USA), using the polygon selection tool. Percentage void closure was then calculated by dividing area of closure at experimental endpoint by total baseline area of cell exclusion zone.

M6.7-6.8: Dose-response Analysis of HPV-Negative Cell Lines to Ligands of Non-c-Met Receptors Known to be Inhibited by Foretinib

Following the inhibition of cell line migration in response to non-toxic doses of foretinib & INCB28060, we analysed the potential for other receptors known to be inhibited by foretinib (but not INCB28060) to have a role in the migrations induced by stimulated fibroblast media. EGF and VEGF were identified as two further candidate molecules due to their known role in head and neck cancer progression^{319, 484-490}, in addition to an increased densitometry of VEGF in HPV-negative stimulated fibroblast medium cytokine arrays (Figures 3.5 & 3.11) and were therefore subjected to the dose-response analyses undertaken for candidate molecules discussed in Chapter 5 (please refer to Figure 5.1).

Recombinant human EGF and VEGF were purchased from Insight Biotechnology (Wembley, UK. Catalogue number 10-1001 and 10-1037-C, respectively). Each vial of lyophilised protein was reconstituted with 1,000 μL normal media (DMEM plus 10 % FCS, plus 50 U mL^{-1} /50 $\mu\text{g mL}^{-1}$ penicillin-streptomycin, plus 2 mM L-glutamine) to produce a 2 $\mu\text{g mL}^{-1}$ stock solution, aliquoted and stored at $-21\text{ }^{\circ}\text{C}$ prior to use in experiments. Serial 1:10 dilutions were then undertaken using normal media to obtain logarithmically decreasing doses of each recombinant protein. Normal media containing identical DMEM, penicillin-streptomycin, L-glutamine and FCS batches were used for all serial dilutions in order to maintain experimental consistency.

UPCI SCC072 was selected as a representative HPV-negative cell line for initial investigation, and was grown to 70 % confluence in a T75 flask. Cells were washed twice in PBS, trypsinised, centrifuged at 1,000 rpm and then resuspended in normal media. The cell suspension was then counted using a haemocytometer, with appropriate dilutions using normal media in order to achieve the preoptimised seeding concentration of 1.6×10^6 cells mL^{-1} for confluent ORIS™ assay well loading, as described in Chapter 1. ORIS™ assay plates were prepared under sterile conditions, mounting silicone stoppers into each well using the manufacturer-supplied location device. 100 μL of each cell suspension was then pipetted into respective ORIS™ assay wells and left overnight to adhere.

Following cell adherence and confirmation of well confluency using an inverted lens microscope, a preoptimised (please refer to Chapter 1, Figure 1.5) 2 $\mu\text{g mL}^{-1}$ mitomycin C suspension in normal media was created from snap-frozen 0.5 mg mL^{-1} aliquots of

mitomycin C stored at -80 °C. All handling of mitomycin C was undertaken in a darkened tissue culture hood in order to avoid excessive light exposure. Silicone stoppers were then removed from assay wells using the manufacturer supplied retrieval tool, exposing the respective cell exclusion zone, and normal media carefully aspirated off each well ensuring contact was avoided with the well base. 2 X 100 µL PBS washes were then undertaken. 100 µL mitomycin C 2 µg mL⁻¹ was then pipetted into each well and incubated for 3.5 hours at 37 °C in the dark. Following 3.5 hours incubation in mitomycin C, baseline void photomicrographs were taken under X4 magnification. Wells were then immediately washed X 2 with 100 µL PBS and then incubated with 100 µL normal media control/serially-diluted recombinant EGF/VEGF-containing media for 48 h. End-point migration photomicrographs were taken of each cell exclusion zone at 48 h.

Analysis of cell migration was undertaken by comparison of baseline versus 48 h micrograph images taken at X4 objective. The area of each stopper-induced cell exclusion zone at baseline and 48 h was measured with ImageJ (freeware, NIH, USA) using the polygon selection tool. Percentage void closure was then calculated by dividing area of closure at 48 h by total baseline area of cell exclusion zone.

Both recombinant proteins were tested at serial dilutions of 10⁰, 10⁻¹, 10⁻², 10⁻³ and 10⁻⁴ stock solution concentrations, in addition to normal media control. Triplicate biological repeats of each experimental condition (n=1) were undertaken, with median additional percentage void closure (compared to closure in control media) calculated and plotted graphically.

Due to EGF response in cell line UPCI SCC072, experimental methods were then repeated for cell line UPCI SCC089, using a 20 h endpoint in place of 48 h.

M6.9: EGF ELISA Analysis

Cell line and stimulated fibroblast Media 1 & 2 were collected for cell lines UD SCC02, UPCI SCC072, UPCI SCC089 and UPCI SCC090, as described for ELISA analysis in Chapter 5.

EGF quantification of cell line conditioned media and stimulated fibroblast Media 1 & 2 was undertaken using Raybiotech HGF ELISA kits (Raybiotech, Norcross, USA, Cat ELH-EGF). Manufacturer instructions were adhered to throughout ELISA analysis. In brief, manufacturer-supplied recombinant human EGF standard was prepared to a 200 pg mL⁻¹ concentration in assay buffer. Serial 1:2.5 dilutions were then undertaken using assay buffer in order to achieve a control reference range. Assay buffer was used as a zero standard. All conditioned media were diluted in assay buffer using a manufacturer-suggested 1:20 dilution.

100 µL standard/sample was added to each well of the Raybiotech EGF capture antibody preconditioned ELISA plates and incubated overnight with gentle rocking. The conditioned media/standard were then discarded and each well washed X4 with 300 µL manufacturer-supplied wash buffer using a multi-channel pipette, ensuring complete removal of solution after each wash through blotting of the inverted plate against tissue paper. Each well was then incubated at room temperature with 100 µL 1X biotinylated detection antibody for 1 hour on an automated rocker machine. Following incubation, the biotinylated antibody solution was discarded and again wells washed X4 with 300 µL manufacturer-supplied wash buffer using a multi-channel pipette, ensuring complete removal of solution after each wash through blotting of the inverted plate against tissue paper.

100 µL freshly-prepared 1X streptavidin solution (concentrate diluted 300-fold in assay diluent) was then pipetted into each well using a multi-channel pipette and incubated for 45 minutes at room temperature on an automated rocker machine. Following incubation, the streptavidin solution was discarded and a further X4 washes undertaken as described above. 100 µL manufacturer-supplied TMB One-Step Substrate Reagent was then added to each well and incubated for 30 minutes at room temperature, protected from light, on an automated rocker machine. 50 µL of manufacturer-supplied Stop Solution was then added to each well and the plate read at 450 nm using a Tecan Infinite M200 plate reader. Results were tabulated using Microsoft Excel and imported into DeltaSoft ELISA analysis software (BioMetallics, Princeton, New Jersey, USA), and interpreted using 4-parameter best-fit plot.

M6.10-6.11: Analysis of Effect of c-Met Inhibitors on Migration of HPV-Negative Oropharyngeal Carcinoma Cell Lines Exposed to 2 ng mL⁻¹ Recombinant Human EGF

To further exclude the role of EGF in the observed stimulated fibroblast media/c-Met inhibitor experiments, in addition to providing a functional cytotoxicity assay of c-Met inhibitors, experimental method 6.1 was repeated using 2 ng mL⁻¹ EGF in place of 0.5 µg mL⁻¹ recombinant human HGF.

M6.12 – 6.13: Co-Stimulation of Cell Lines UPCI SCC072 and UPCI SCC089 with Recombinant Human IL-6 and HGF

Recombinant human IL-6 and HGF were purchased from Insight Biotechnology as detailed above. Logarithmic dilutions of HGF in normal media, ranging from 0.2-200 ng mL⁻¹ were prepared, aliquoted and then recombinant IL-6 added at concentrations of 0, 5, 50 or 500 ng mL⁻¹.

HPV-negative cell lines UPCI SCC072 and UPCI SCC089 were grown to 70 % confluence in separate T75 flasks. Cells were washed twice in PBS, trypsinised, centrifuged at 1,000 rpm and then resuspended in normal media. Each cell suspension was then counted using a haemocytometer, appropriately diluted using normal media, and re-counted in order to achieve the preoptimised seeding concentration of 1.6 X 10⁶ cells mL⁻¹ for UPCI SCC072, and 8.8 X 10⁵ cells mL⁻¹ for UPCI SCC089, allowing confluent ORIS™ assay well loading as described in Chapter 1. ORIS™ assay plates were prepared under sterile conditions, mounting silicone stoppers into each well using the manufacturer-supplied location device. 100 µL of each cell suspension was then pipetted into respective ORIS™ assay wells and left overnight to adhere.

Following cell adherence and confirmation of well confluency using an inverted lens microscope, a pre-optimised (please refer to Chapter 1, Figure 1.5) 2 µg mL⁻¹ mitomycin C suspension in normal media was prepared from snap-frozen 0.5 mg mL⁻¹ aliquots of mitomycin C stored at -80 °C. All handling of mitomycin C was undertaken in a darkened tissue culture hood in order to avoid excessive light exposure. Silicone stoppers were then removed from assay wells using the manufacturer supplied retrieval tool, exposing the respective cell exclusion zone, and normal media carefully aspirated off each well ensuring contact was avoided with the well base. 2 X 100 µL PBS washes were then undertaken, and then 100 µL mitomycin C 2 µg mL⁻¹ in normal media was then carefully pipetted into respective wells and incubated for 3.5 hours at 37 °C in the dark. Following 3.5 hours incubation in mitomycin C, baseline void photomicrographs were taken using a X4 objective lens.

Following mitomycin C incubation, assay wells were washed X2 in PBS and then 100 µL HGF 0.2-200 ng mL⁻¹ with IL-6 0-500 ng mL⁻¹ in normal media carefully pipetted into respective wells. ORIS™ assay plates were then incubated for either 20 h (UPCI SCC089)

or 48 h (UPCI SCC072) in order for migration to occur, and then endpoint photomicrographs taken using a X4 objective lens.

Analysis of cell migration was undertaken by comparison of baseline versus endpoint micrograph images taken at X4 objective. The area of each stopper-induced cell exclusion zone at baseline and endpoint was measured with ImageJ software (freeware, NIH, USA), using the polygon selection tool. Percentage void closure was then calculated by dividing area of closure at experimental endpoint by total baseline area of cell exclusion zone.

M6.14: Flow Cytometry Analysis of Membranous IL-6 Receptor Status

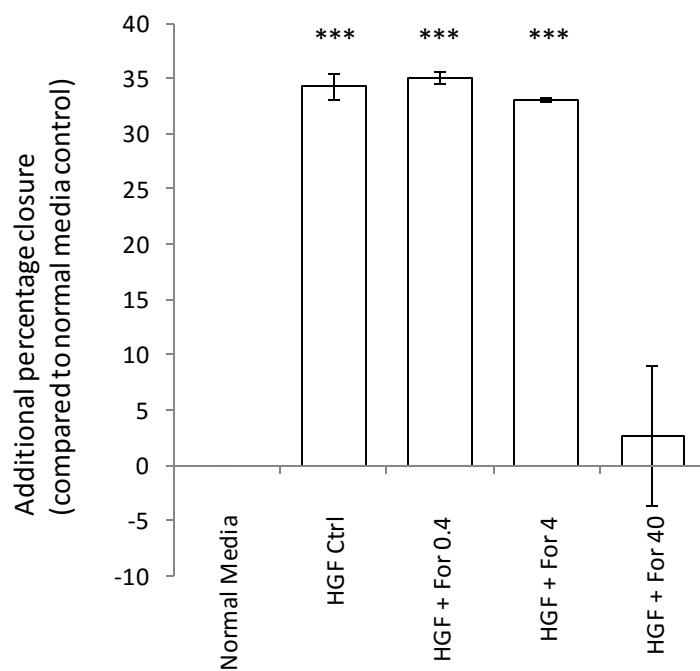
Anti-human IL-6 receptor antibody for use in flow cytometry was purchased Abcam (Cambridge, UK, Catalogue number ab47215), along with mouse monoclonal IgG isotype control probe and anti-mouse Alexa-Fluor 488 secondary probe (Life Technologies/ Thermo Fisher Scientific, Massachusetts, USA, Cat A11001)

Cell lines UD SCC2, UPCI SCC072, UPCI SCC089 and UPCI SCC090 were grown to 70-80 % confluence in T75 flasks. Further flasks of DENO08 normal oral fibroblasts were cultured to comparable confluence, and also the THP-1 monocytic line to act as an IL-6R positive control line^{491, 492}. Excluding the non-adherent THP-1 line, cells were dissociated from respective flasks using EDTA cell dissociation solution (Sigma-Aldrich, Dorset, England, Cat C5914-100ML), suspended in FACS buffer (PBS with 0.1 % Sodium Azide plus 1 % BSA) cooled on ice, and centrifuged at 1,000 rpm for 5 minutes. The supernatant was then decanted and cells resuspended in 900 μ L cooled FACS buffer. Each cell suspension was then divided equally into three Eppendorph containers and again centrifuged at 2,000 rpm for 2 minutes. Following careful aspiration of supernatant, cells were resuspended in 100 μ L cold FACS buffer containing either no additive, monoclonal mouse anti-IL-6R antibody (1:250 dilution), or mouse IgG isotype control. Each suspension was then incubated on ice and in the dark for 40 minutes. Following incubation, cells were centrifuged at 2,000 rpm for 2 minutes, supernatants carefully aspirated and cell pellets resuspended in 1,000 μ L cold FACS buffer. A repeat centrifugation and cold FACS buffer wash was undertaken, and then pellets resuspended in 50 μ L cold FACS buffer and 50 μ L Alexafluor488-labelled anti-mouse secondary antibody added (final dilution of 1:50), before incubating on ice for a further 30 minutes. After secondary antibody incubation, a further 2X FACS buffer wash/ centrifugation steps were undertaken, followed by a final centrifugation at 2,000 rpm for 2 minutes, aspiration of supernatant and then resuspension in 300 μ L cold FACS buffer. Eppendorph containers were then immediately placed on ice and cells analysed using a Calibur flow cytometer set to analyse 10,000 events. Flow cytometry data were then plotted and converted into overlay histogram images using Flowing 2.5.1 software (freeware, Turku, Finland).

Results

Figure 6.1: Effect of c-Met Inhibitors on UPCI SCC089 Migration Using $0.5 \mu\text{g mL}^{-1}$ Recombinant Human HGF in Normal Media

a).



b).

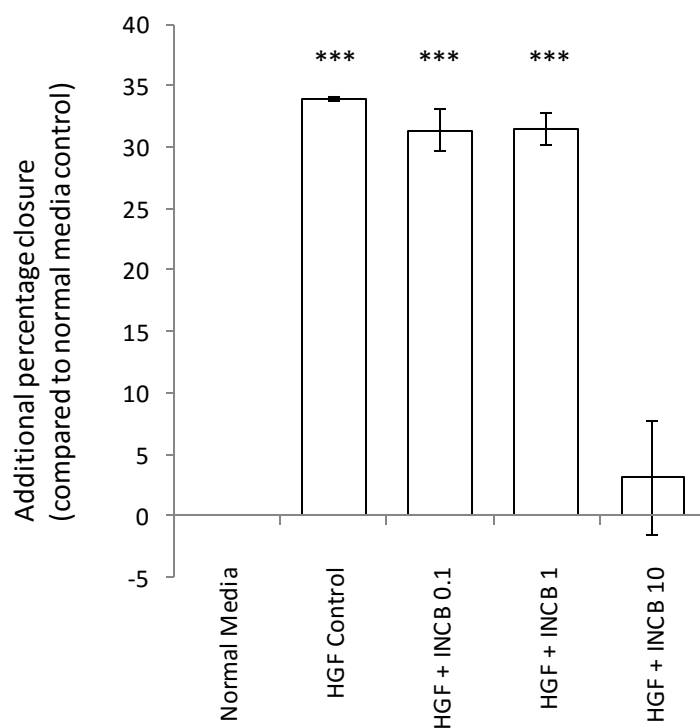


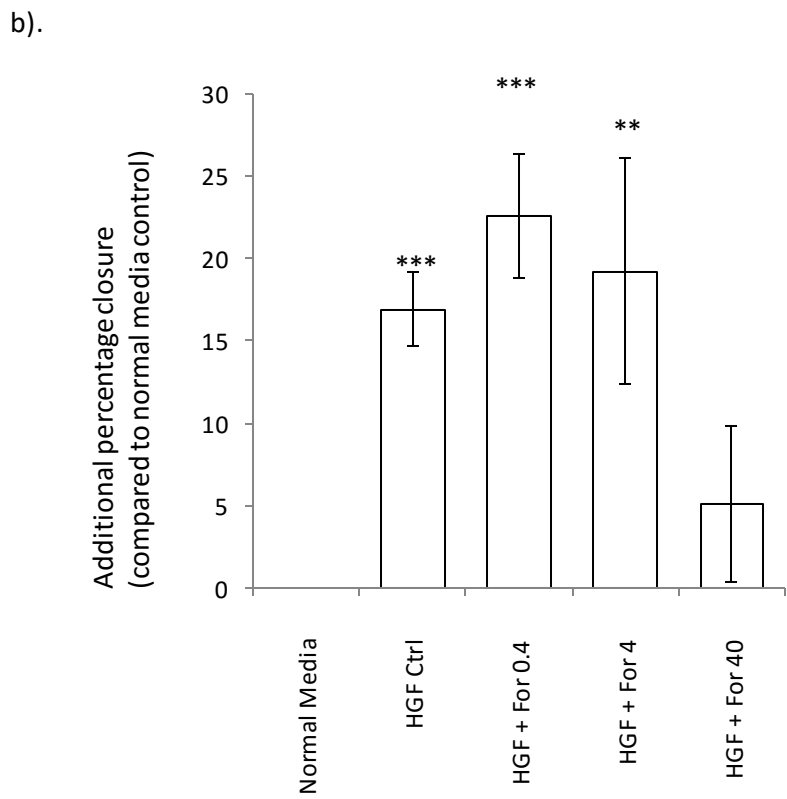
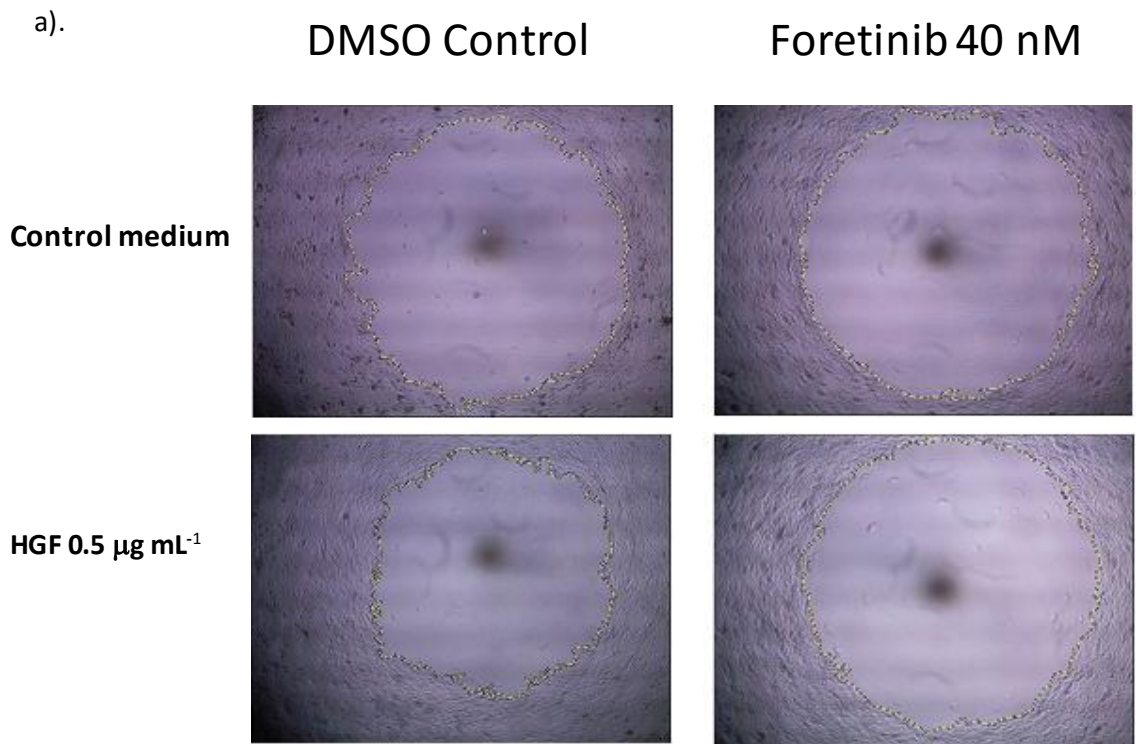
Figure 6.1: Bar graphs depicting the effect of adding c-Met inhibitors to normal media containing $0.5 \mu\text{g mL}^{-1}$ recombinant HGF on SCC89 migration in ORIS™ assays over a 20 h period. Error bars represent SEM, Y-axis represents additional migration compared to HGF-free normal media DMSO control, expressed as additional percentage closure of baseline void. *** = Mann-Whitney U-test, compared to normal media control, $P < 0.001$. $n = 9$

Note that both foretinib (Figure a) and INCB28060 (Figure b) inhibit HGF-induced migration to levels not significantly different to control (Mann-Whitney U-test, $P = 0.453$ foretinib, $P = 0.142$ INCB28060) with drug concentrations of 40 nM and 10 nM, respectively. These results are consistent with the literature, with Fawn *et al* reporting an IC_{50} of 0.4 nM and a biologically-relevant IC_{50} for HGF-mediated growth in cell lines B16F10, A549, and HT29 at 40nM with foretinib⁴³⁵, and an IC_{50} of 0.13 nM and complete inhibition of c-Met phosphorylation at 3.9 nM using western blot with INCB28060⁴³⁰.

Note the important observation that migration is brought to baseline in both experiments; this differs from the control presented in Figure 6.5 (unstimulated fibroblast conditioned medium), which demonstrates a reduction in migration to below that of the unstimulated fibroblast control, but again comparable to normal media, suggesting that HGF is secreted at low levels by the unstimulated fibroblast population and therefore basal fibroblast secretions reinforcing of cell line movement are also inhibited by foretinib and INCB28060. Basal secretion of HGF is consistent with ELISA data presented in Figure 5.3.

(*HGF Ctrl*; normal media containing DMSO and $0.5 \mu\text{g mL}^{-1}$ recombinant HGF as positive control, *For*; foretinib, *INCB*; INCB28060, all numerical postscripts refer to drug concentration in nM)

Figure 6.2 Effect of c-Met Inhibitors on UPCI SCC072 Migration Using 0.5 $\mu\text{g mL}^{-1}$ Recombinant Human HGF in Normal Media



c).

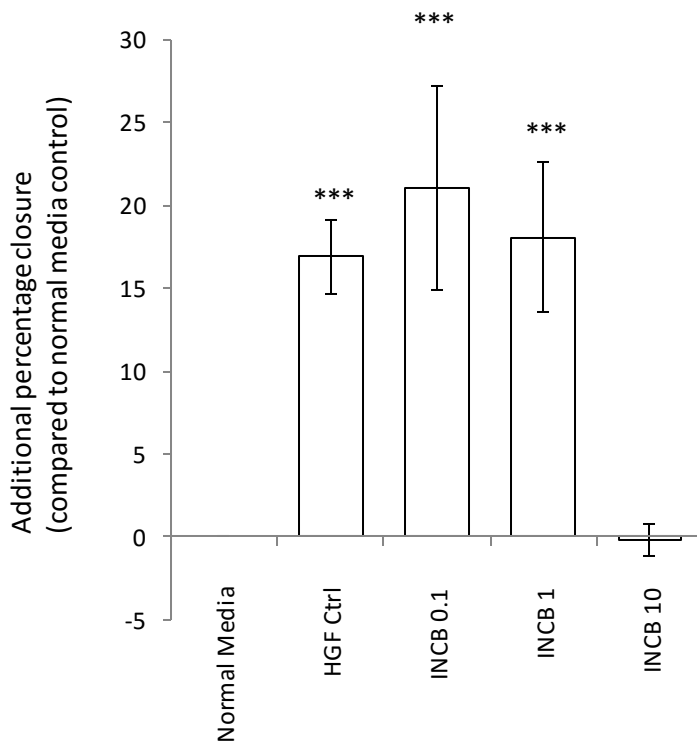


Figure 6.2:

a). Micrographs illustrating effect of 40 nM foretinib on cell migration. Note that a basal rate of migration is observed in control medium with little optically discernible change in the presence of 40 nM foretinib. Addition of normal media containing $0.5 \mu\text{g mL}^{-1}$ recombinant HGF leads to visually notable additional migration (lower left image), which is restrained upon co-incubation with 40 nM foretinib (lower right image)

b). & c). Bar graphs depicting the effect of adding c-Met inhibitors to normal media containing $0.5 \mu\text{g mL}^{-1}$ recombinant HGF on SCC72 migration in ORIS™ assays over a 48 h period. Error bars represent SEM, Y-axis represents additional migration compared to HGF-free normal media DMSO control, expressed as additional percentage closure of baseline void. Mann-Whitney U-test, compared to normal media control, ** $P < 0.05$, *** $P < 0.001$, $n = 9$

Note that both foretinib (Figure b) and INCB28060 (Figure c) inhibit HGF-induced migration to levels not significantly different to control (Mann Whitney U-test, $P = 0.171$ foretinib, $P = 0.895$ INCB28060) with drug concentrations of 40 nM and 10 nM, respectively. These results are consistent with data presented for UPCI SCC089 and also the literature, as discussed in Figure Legend 6.1.

(HGF Ctrl; normal media containing DMSO and $0.5 \mu\text{g mL}^{-1}$ recombinant HGF as positive control, For; foretinib, INCB; INCB28060, all numerical postscripts refer to drug concentration in nM)

Figure 6.3: Cytotoxicity Assays of Foretinib and INCB28060 for Cell Line UPCI SCC072

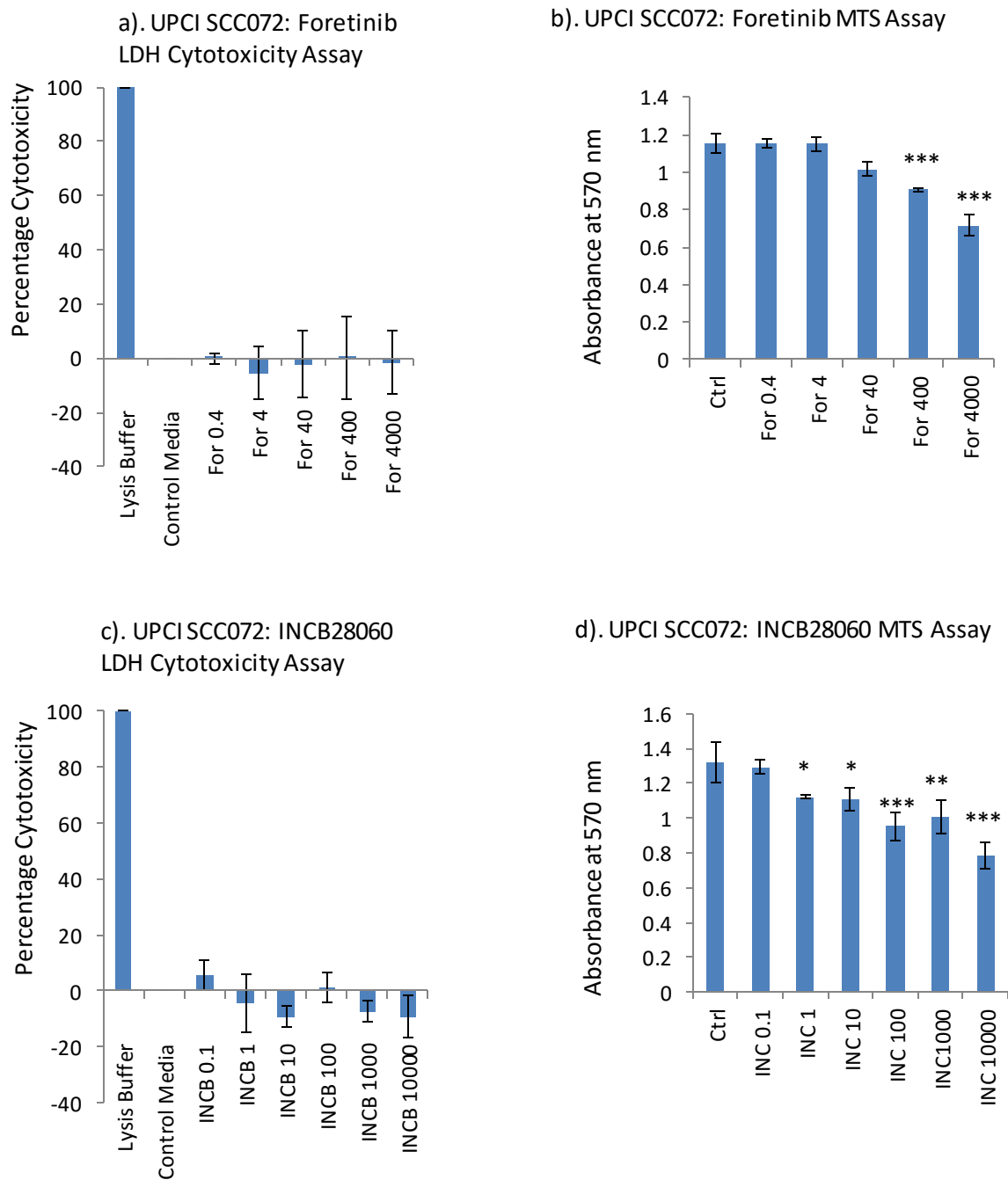


Figure 6.3: Cytotoxicity assays of foretinib and INCB28060 for cell line UPCI SCC072. All numerical post-scripts along X-axis denote foretinib/INCB28060 concentration, in nM. “Lysis buffer” denotes LDH positive control with use of manufacturer-supplied lysis buffer (100 % cytotoxicity reference),

Ctrl/Control Media denote cells incubated in normal media with DMSO. Error bars denote SEM. *For* – foretinib, *INC(B)* – INCB28060. n=9

* Mann Whitney U-test, $P < 0.05$

** Mann Whitney U-test, $P < 0.01$

*** Mann Whitney U-test, $P < 0.001$

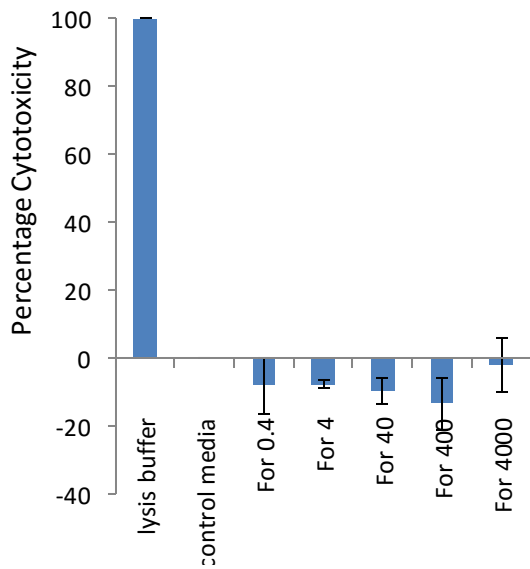
Figures a & b: LDH and MTS assays, respectively, of cell line UPCI SCC072 exposed to logarithmically increasing doses of foretinib. Note that there is no evidence of change in LDH assay from baseline with all doses of foretinib tested (Figure a). There is a gradual decrease in MTS assay absorbance at doses greater than 4 nM, however this pattern is not consistent with the precipitous drop in migration noted at 40 nM foretinib for cell line UPCI SCC072 (Figure 6.2a). Although a statistically significant drop in MTS absorbance is seen only of 400 nM foretinib and above (Mann Whitney U-test, compared to control), there is a weakly significant reduction in absorbance at 40 nM ($P = 0.07$). No statistically significant change was noted in LDH assay over the range of foretinib tested (Mann Whitney U-test, $P > 0.05$, compared to control).

Figures c & d: LDH and MTS assays, respectively, of cell line UPCI SCC072 exposed to logarithmically increasing doses of INCB28060. Note that there is no evidence of change in LDH assay from baseline with all doses of INCB2860 tested (Figure c). There is a gradual decrease in MTS assay absorbance, with statistical significance achieved at doses greater than 0.1 nM INCB28060 (Mann Whitney U-test), however this pattern is not consistent with the precipitous drop in migration noted at 10 nM INCB28060 for cell line UPCI SCC072 (Figure 6.2b). This drop is consistent with the gradual growth-inhibiting effects of INCB28060 noted in pancreatic carcinoma lines, producing a similar pattern using MTT assay⁴⁶². No statistically significant change was noted in LDH assay over the range of INCB28060 tested (Mann Whitney U-test, $P > 0.05$, compared to control).

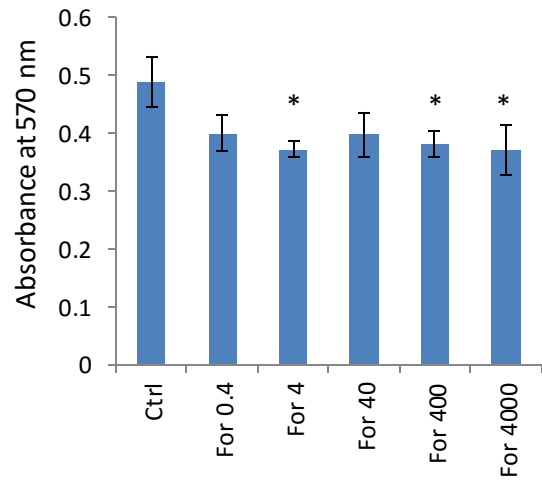
In combination, Figures a-d suggest that the inhibition of cell migration noted with 40 nM foretinib and 10 nM INCB2806 in Figure 6.2 is due to receptor-specific effects rather than direct cytotoxicity.

Figure 6.4: Cytotoxicity Assays of Foretinib and INCB28060 for Cell Line UPCI SCC089

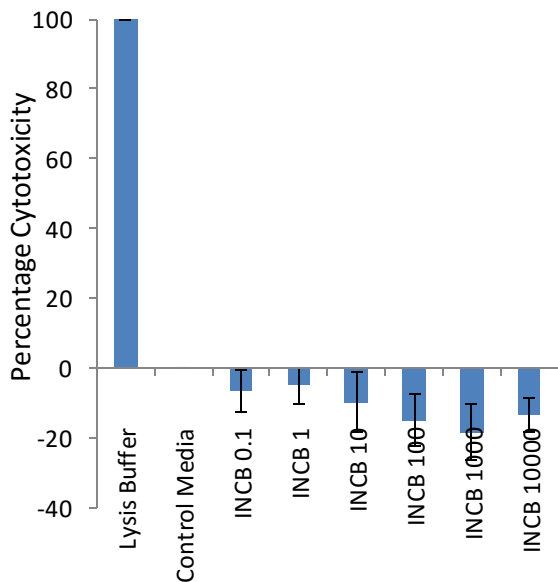
a). UPCI SCC089: Foretinib LDH Cytotoxicity Assay



b). UPCI SCC089: Foretinib MTS Assay



c). UPCI SCC089: INCB28060 LDH Cytotoxicity Assay



d). UPCI SCC089: INCB28060 MTS Assay

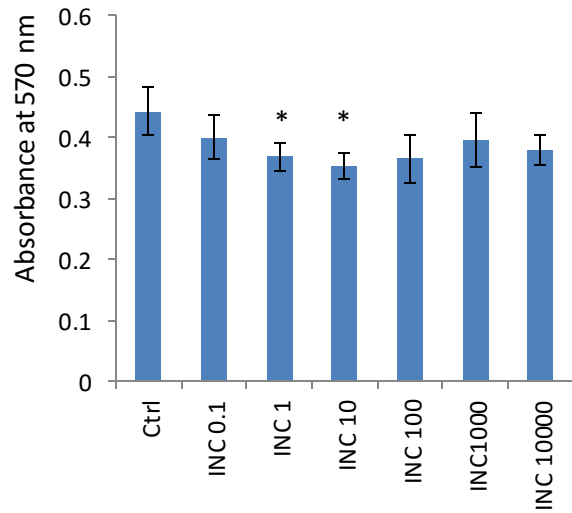


Figure 6.4: Cytotoxicity assays of foretinib and INCB28060 for cell line UPCI SCC089. All numerical post-scripts along X-axis denote foretinib/INCB28060 concentration, in nM. “Lysis buffer” denotes LDH positive control with use of manufacturer-supplied lysis buffer (100 % cytotoxicity reference), *Ctrl/Control Media* denote cells incubated in normal media with DMSO. Error bars denote SEM. *For* – foretinib, *INC(B)* – INCB28060. n=9

* P<0.05, Mann Whitney U-test

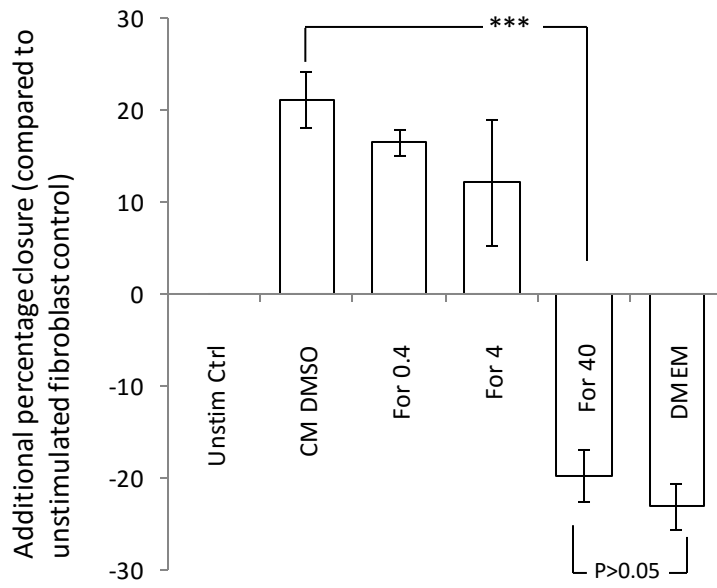
Figures a & b: LDH and MTS assays, respectively, of cell line UPCI SCC089 exposed to logarithmically increasing doses of foretinib. Note that there is no evidence of increase in LDH assay from baseline with all doses of foretinib tested (Figure a). There is a decrease in MTS assay absorbance with all doses of foretinib; this decrease is statistically significant (Mann Whitney U-test, P<0.05) for all foretinib doses other than 0.4 nM and 40 nM (P=0.077 and 0.050, respectively). It should be noted however, that there is no MTS assay absorbance drop coinciding with the inhibition of migration noted at 40 nM foretinib for cell line UPCI SCC089 (Figure 6.1a); all tested doses of foretinib demonstrated no significant difference in assay absorption when compared to foretinib 0.4 nM (Mann Whitney U-test, P>0.05). This suggests that whilst a difference in absorbance may be noted between foretinib and control, any change in cellular metabolism linked to that difference does not correlate with the inhibition of migration observed at 40 nM in ORIS™ assay experiments, and may again be linked to growth-inhibiting effects as discussed in Figure 6.3.

Figures c & d: LDH and MTS assays, respectively, of cell line UPCI SCC089 exposed to logarithmically increasing doses of INCB28060. Note that again, there is no evidence of increased LDH release from baseline with exposure of cell lines to all doses of INCB28060 tested (Figure c). There is again a small decrease in MTS assay absorbance for all concentrations of INCB28060 compared to that of control, achieving significance at 1 nM and 10 nM INCB28060, however this pattern is again not consistent with the precipitous drop in migration noted at 10 nM INCB28060 for cell line UPCI SCC089 (Figure 6.1b), and MTS assay at higher INCB28060 concentrations demonstrated no significant difference to control.

In combination, Figures a-d suggest that, as for UPCI SCC072, the inhibition of cell migration noted with 40 nM foretinib and 10 nM INCB2806 in Figure 6.1 is due to receptor-specific effects rather than direct cytotoxicity.

Figure 6.5: Effect of c-Met inhibitors on UPCI SCC089 ORIS™ Assay Migration Using DENOFO8 Stimulated Fibroblast Medium 2

a).



b).

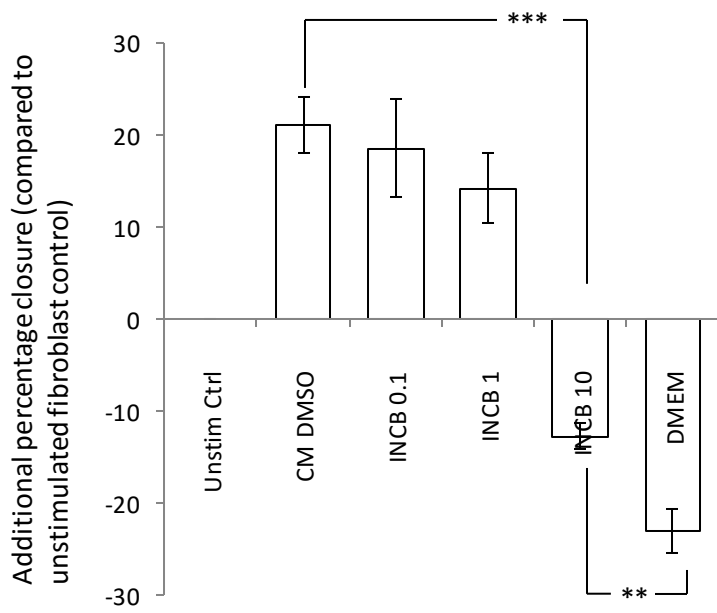


Figure 6.5: Bar graphs depicting the effect of adding c-Met inhibitors to UPCI SCC089 exposed to UPCI SCC089 stimulated DENO08-derived Medium 2, on migration in ORIS™ assays over a 20 h period. Error bars represent SEM, Y-axis represents additional migration compared to unstimulated fibroblast DMSO control, expressed as additional percentage closure of baseline void. n=9

** - $P < 0.01$, Mann Whitney U-test

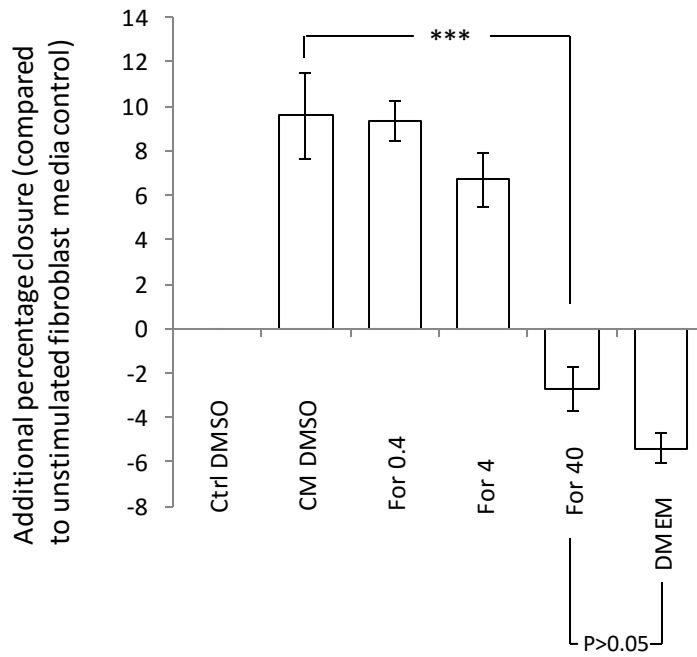
*** - $P < 0.001$, Mann Whitney U-test

Note that both foretinib (Figure a) and INCB28060 (Figure b) inhibit migration to levels lower than unstimulated control, with foretinib achieving restriction of migration to that seen using normal media (“DMEM” on graphs, Mann Whitney U-test $P > 0.05$). This characteristic suggests presence of a foretinib/INCB28060-sensitive factor which is basally secreted by the fibroblast population, hence reduction of migration to below that of unstimulated fibroblast medium control. This finding is consistent with the basal release of HGF noted in ELISA analysis of unstimulated fibroblast media (Figure 5.3). INCB28060 did not abrogate migration to the same level as normal media control; this may be due to either suboptimal dosing, or alternatively the presence of a second, foretinib-sensitive factor in the conditioned medium such as EGF.

(*Unistim Ctrl*; unstimulated fibroblast conditioned medium control containing DMSO, *CM DMSO*; SCC89-stimulated fibroblast conditioned medium positive control containing DMSO, *DMEM* – normal media plus DMSO negative control, *For*; foretinib, *INCB*; INCB28060, all numerical postscripts refer to drug concentration in nM).

Figure 6.6: Effect of c-Met inhibitors on UPCI SCC072 ORIS™ Assay Migration Using DENOFO8 Stimulated Fibroblast Medium 2

a).



b).

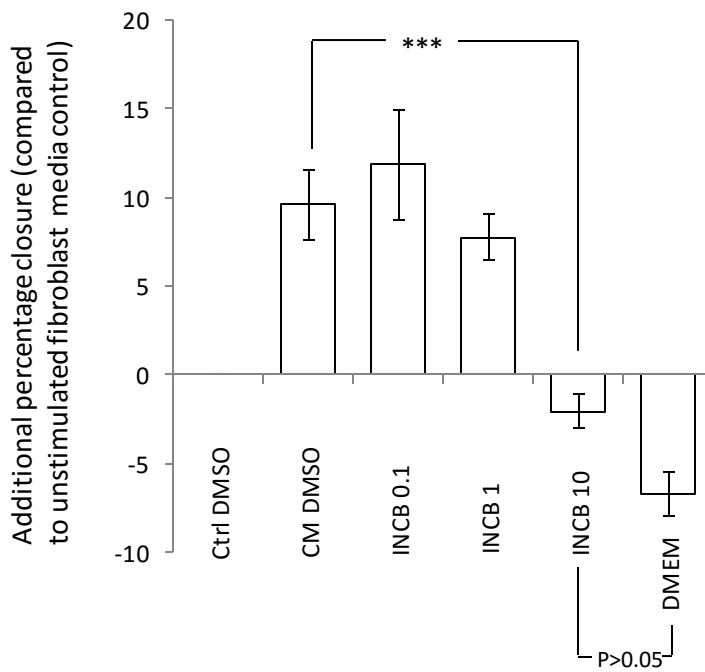


Figure 6.6: Bar graphs depicting the effect of adding c-Met inhibitors to UPCI SCC72 exposed to UPCI SCC072 Medium 1, on migration in ORIS™ assays over a 48 h period. Error bars represent SEM, Y-axis represents additional migration compared to unstimulated fibroblast DMSO control, expressed as additional percentage closure of baseline void. n=9

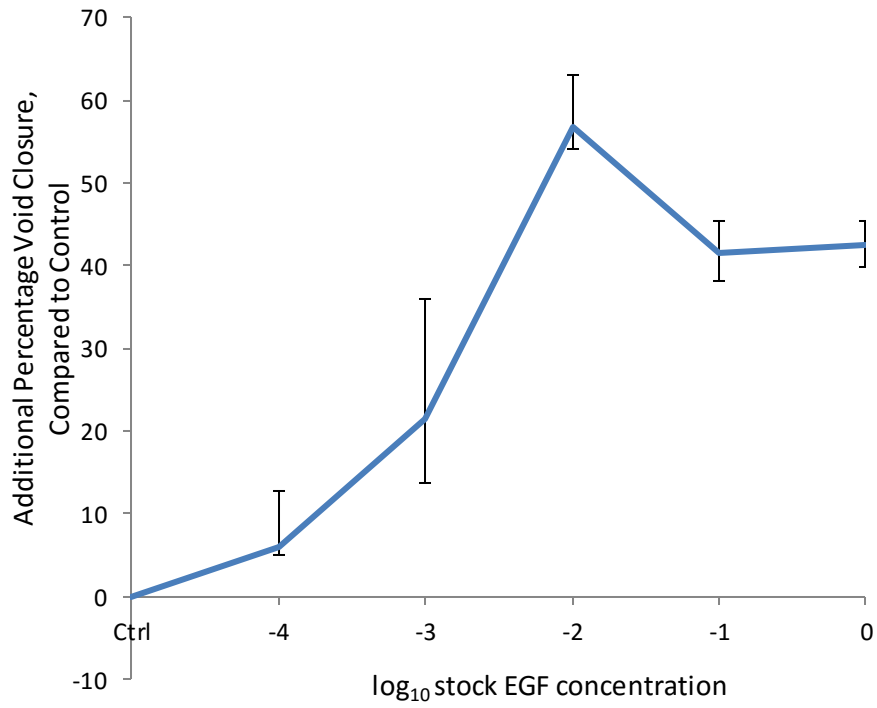
*** - $P < 0.01$, Mann Whitney U-test

Note that both foretinib (Figure a) and INCB28060 (Figure b) inhibit migration to levels lower than unstimulated control, as observed for cell line UPCI SCC089. Again, this finding is consistent with basal secretion of HGF by the unstimulated fibroblast population. No significant difference was found between either foretinib 40 nM/ INCB28060 10 nM versus DMEM control, although a near-significant difference was observed for INCB28060 (Mann Whitney U-test $P = 0.054$).

(*Unistim Ctrl*; unstimulated fibroblast conditioned medium control containing DMSO, *CM DMSO*; UPCI SCC072-stimulated fibroblast conditioned medium positive control containing DMSO, *DMEM* – normal media plus DMSO negative control, *For*; foretinib, *INCB*; INCB28060, all numerical postscripts refer to drug concentration in nM).

Figure 6.7: Dose-Response Analysis of HPV-negative Cell Lines Exposed to Logarithmically Increasing Concentrations of Recombinant Human EGF

a) Cell line UPCI SCC072



b) Cell line UPCI SCC089

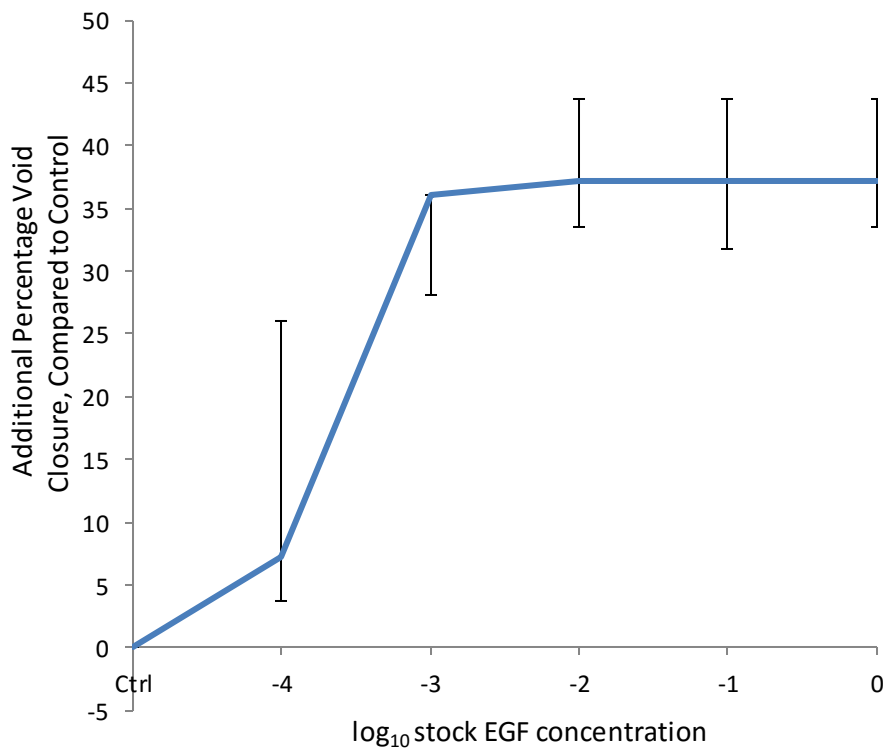


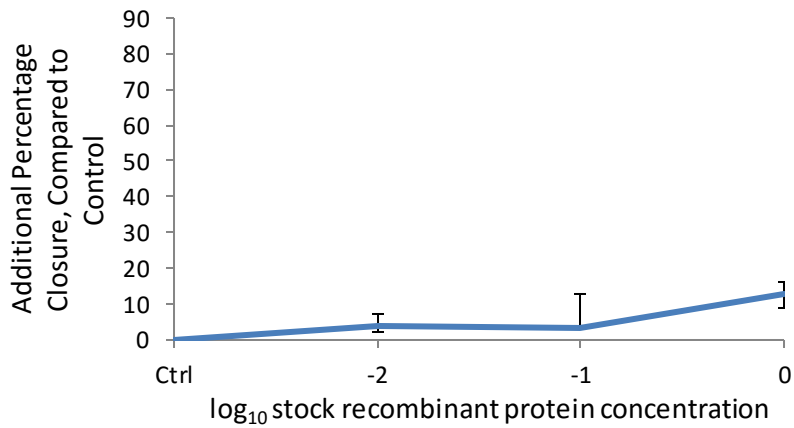
Figure 6.7: Dose response curves of additional ORIS™ assay migration over 48 h and 20 h in cell lines UPCI SCC072 (Figure a) and UPCI SCC089 (Figure b), respectively in response to logarithmic dilutions of 2 µg mL⁻¹ stock recombinant EGF in normal media (n=3 biological repeats). Error bars denote range, with median used as measure of central tendency (blue line). Migration expressed as additional percentage closure of baseline void, compared to control void closure.

Both of the HPV-negative cell lines are observed to migrate in response to stimulation with recombinant human EGF, rendering EGF as a candidate driver of cell migration in the conditioned media experiments, albeit with less consistency than HGF due to reported EGFR inhibition only occurring in response to foretinib, and not INCB28060.

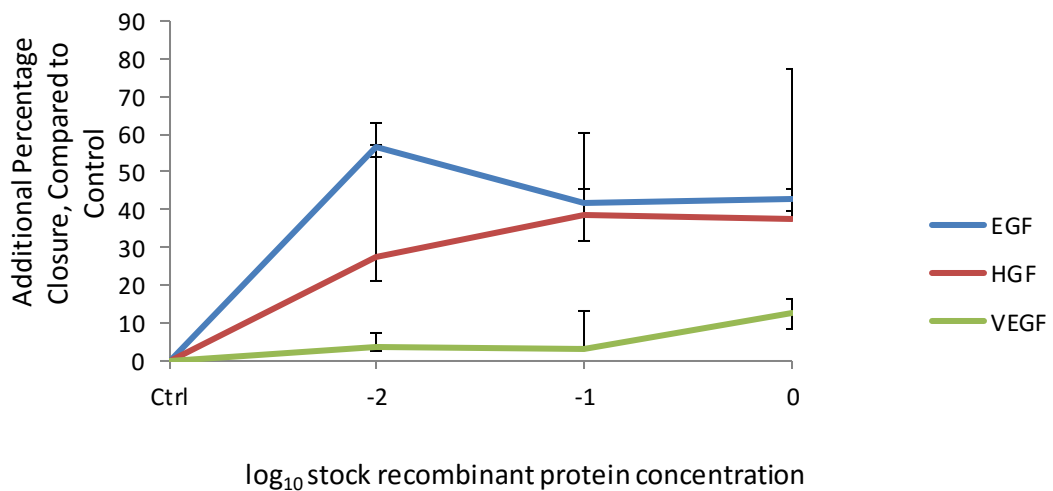
Note the peak stimulation of cell line UPCI SCC072 occurring at 20 ng mL⁻¹ EGF (stock EGF concentration X 10⁻²), inferring receptor saturation has occurred at higher doses, whereas no peak is observed in UPCI SCC089 due to complete void closure at all doses above 2 ng mL⁻¹ EGF (stock EGF concentration X 10⁻³), masking any potential decrease in effect at higher concentrations. 2 ng mL⁻¹ EGF (stock concentration X 10⁻³) was determined as the optimal concentration for subsequent inhibitor experiments to assess the effect of foretinib and INCB28060 on the EGF pathway, due to subtotal migration at this concentration in both HPV-negative cell lines, as illustrated in Figures a & b, above. Full void closure in cell line UPCI SCC089 could potentially mask partial inhibition of an EGF-stimulated positive control due to potential concomitant closure of both control and inhibitor voids at 20 h.

Figure 6.8: Dose-Response Analysis of HPV-negative Cell Line UPCI SCC072 Exposed to Logarithmically Increasing Concentrations of Recombinant Human VEGF

a).



b).



c).

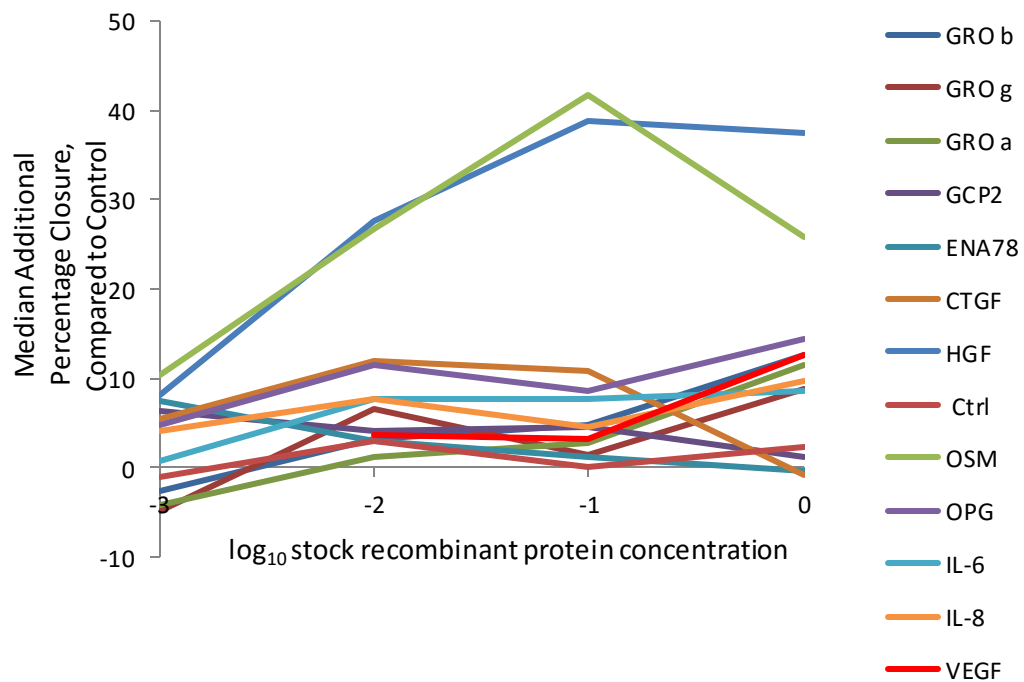


Figure 6.8a: Dose response curves of additional ORIS™ assay migration observed in cell line UPCI SCC072 in response to logarithmic dilutions of 2 µg mL⁻¹ stock recombinant human VEGF in normal media (n=3 biological repeats). Error bars denote range, with median used as measure of central tendency (blue line). Migration expressed as additional percentage closure of baseline void, compared to control.

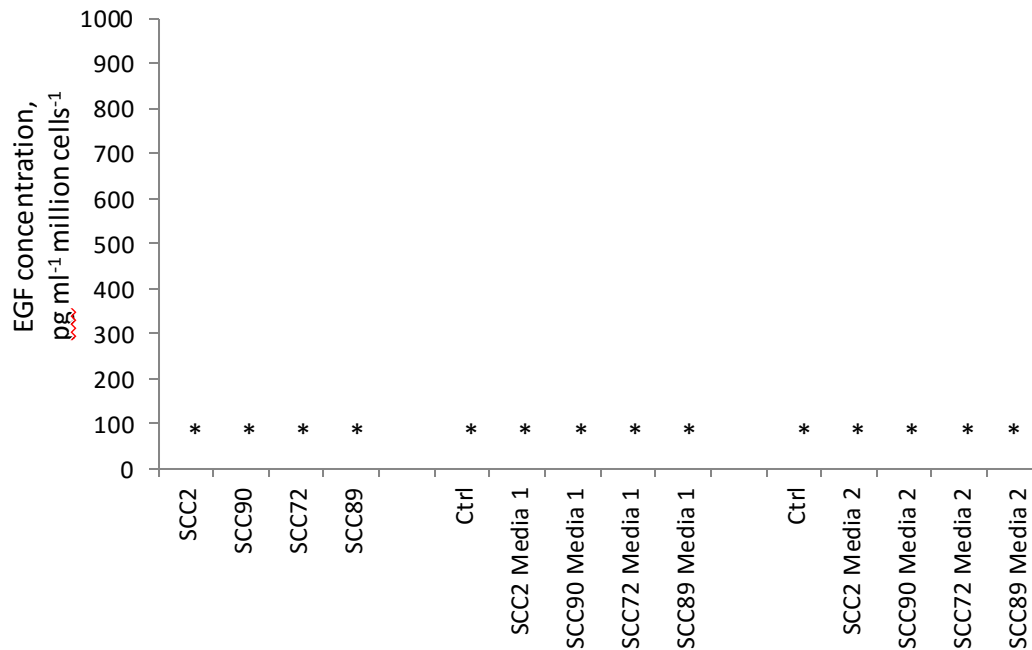
Figure b: comparison of VEGF-induced migration (same data as presented in a) against HGF & EGF in normal media. Error bars denote range, with median used as measure of central tendency (coloured lines). Migration expressed as additional percentage closure of baseline void, compared to control.

Figure c: comparison of VEGF-induced migration against all candidate molecules tested in Chapter 5. Coloured lines represent median. Migration expressed as additional percentage closure of baseline void, compared to control.

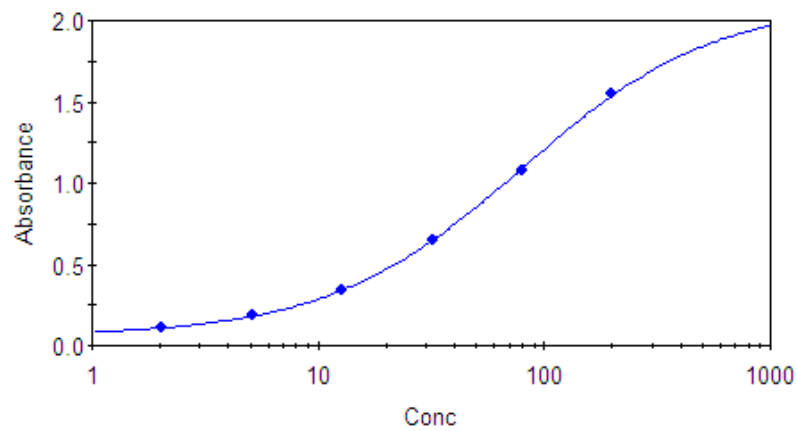
VEGF can be observed to have negligible effect on migration at concentrations of 200 ng mL⁻¹ and less. 2 µg mL⁻¹ VEGF (1 X 10⁰) led to a median additional closure of 12.6 %. This modest additional closure at high concentrations may be regarded as biologically irrelevant, particularly in the context of the degree of additional migration observed with recombinant EGF & HGF (Figure b), and also with the background variability noted for all candidate cytokines tested in Chapter 5 (Figure c). VEGF was therefore excluded as a potential foretinib-sensitive cytokine with capacity to drive migration in the conditioned media experiments, and not followed up with ELISA analysis in the manner that is described for EGF.

Figure 6.9: EGF ELISA Analysis of Cell Line Conditioned Media and Stimulated DENOFO8 Fibroblast Media 1 & 2.

a).



b).



4-Parameter Fit: $Y = (A-D)/(1+(X/C)^B) + D$
 A = 0.061 B = 1.016 C = 79.031 D = 2.112 50% = 1.086
 RMS = 0.030, r = 1.000, r² = 0.999, Basic weighting

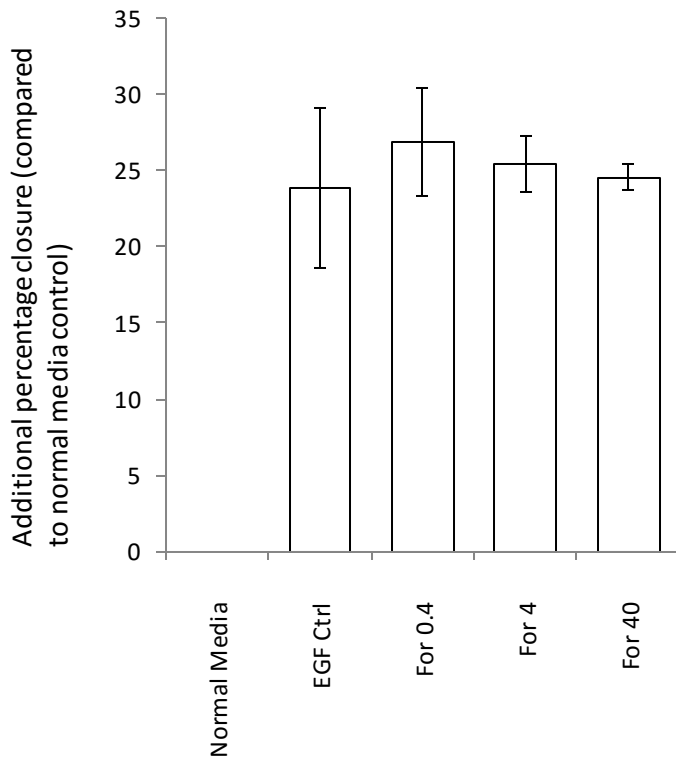
Figure 6.9a: EGF ELISA analysis of cell line conditioned media and stimulated fibroblast Media 1&2 (n=9). Y-axis: EGF concentration in pg mL⁻¹ million cells⁻¹. X-axis denotes medium type; SCC2, SCC72, SCC89 and SCC90 represent cell line conditioned media derived from the respective UD/UPCI line, suffix of Media1/Media2 denote stimulated DENOFO8 fibroblast media derived from respective UD/UPCI line. Note that all media contained undetectable levels of EGF using 4-parametric analysis.

Figure b illustrates a highly consistent standard curve for the respective Raybiotech EGF ELISA kit ($r^2=0.999$).

One limitation of the ELISA data presented is the absence of a positive control other than manufacturer-supplied standard. In the unlikely event that the highly reproducible EGF standard had been an inappropriate control, and in order to fully exclude EGF as a driver of cell migration which had been inhibited by foretinib/ INCB28060 in Figures 6.5 & 6.6, inhibitor experiments were repeated using 2 ng mL^{-1} EGF (please refer to Figure 6.10).

Figure 6.10: Effect of c-Met Inhibitors on UPCI SCC072 ORIS™ Assay Migration with 2 ng mL⁻¹ EGF

a).



b).

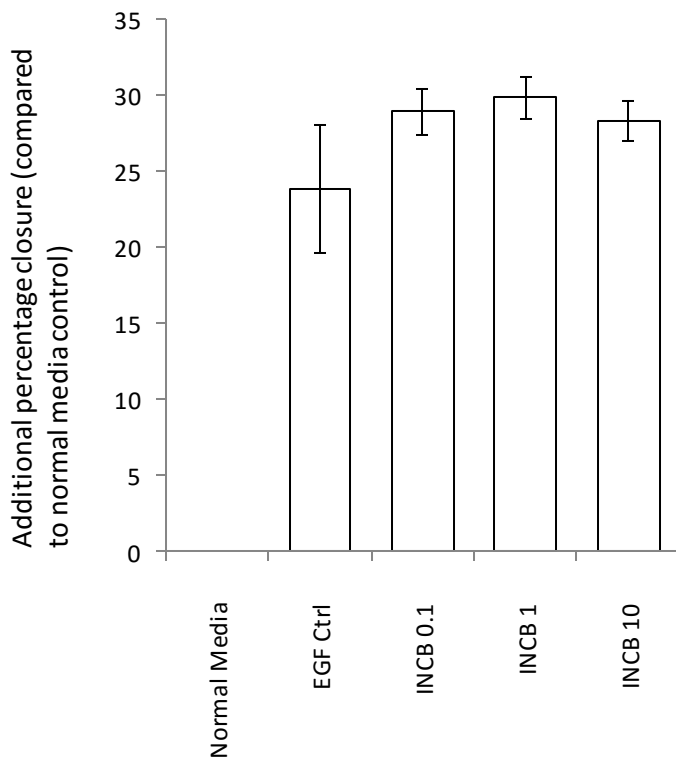


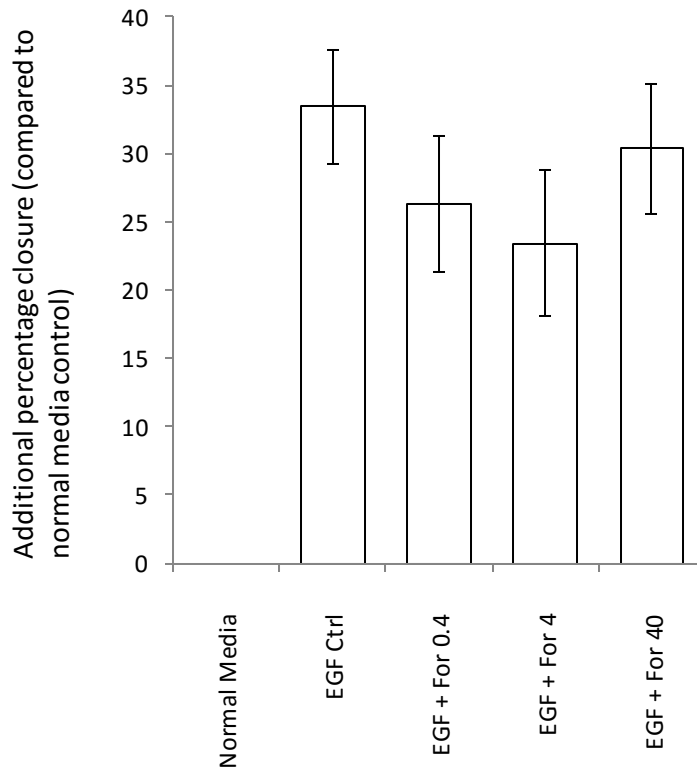
Figure 6.10: Effect of c-Met inhibitors on UPCI SCC072 ORIS™ assay migration over a 48 hour period using 2 ng mL⁻¹ EGF (n=9). Figure a – logarithmically increasing concentrations of foretinib, Figure b: logarithmically increasing concentrations of INCB28060. Y-axis: additional percentage closure of assay void, compared to normal media control. X-axis: *Normal Media* – normal media with DMSO control, *EGF Ctrl* – 2 ng mL⁻¹ EGF in normal media with DMSO, *For* – foretinib, *INCB* – INCB28060, all numerical postscripts refer to drug concentration in nM.

Note that for both foretinib and INCB, there is no decrease in cell line migration within the range of concentrations tested. Furthermore, no significant difference was found between 2 ng mL⁻¹ EGF positive control and EGF with inhibitor over the range of concentrations tested (Mann Whitney U-test, P>0.05). This finding is in contrast to the inhibition of all stimulated fibroblast media with 40 nM foretinib and 10 nM INCB28060. The inability of foretinib/ INCB28060 to inhibit cell migration in Figure 6.10 not only further discounts EGF as a candidate driver of cell migration in the conditioned media experiments, but also offers functional evidence that the effects of foretinib/INCB28060 on inhibiting cell line migration in Figures 6.5 & 6.6 are due to receptor-specific inhibition rather than direct cellular cytotoxicity.

As previously discussed, foretinib is reported to inhibit EGF, with a reported IC₅₀ of 2.99 μM⁴³⁵. The lack of significant inhibition in Figure 6.10 is consistent with the use of foretinib at a maximum concentration of approximately 75-fold lower than this reported IC₅₀. Moreover, a biologically relevant degree of EGFR inhibition may require a significantly higher foretinib concentration than the reported IC₅₀ for receptor phosphorylation, as noted for recombinant HGF experiments in Figures 6.1 & 6.2.

Figure 6.11: Effect of c-Met Inhibitors on UPCI SCC089 ORIS™ Assay Migration with 2 ng mL⁻¹ EGF

a).



b).

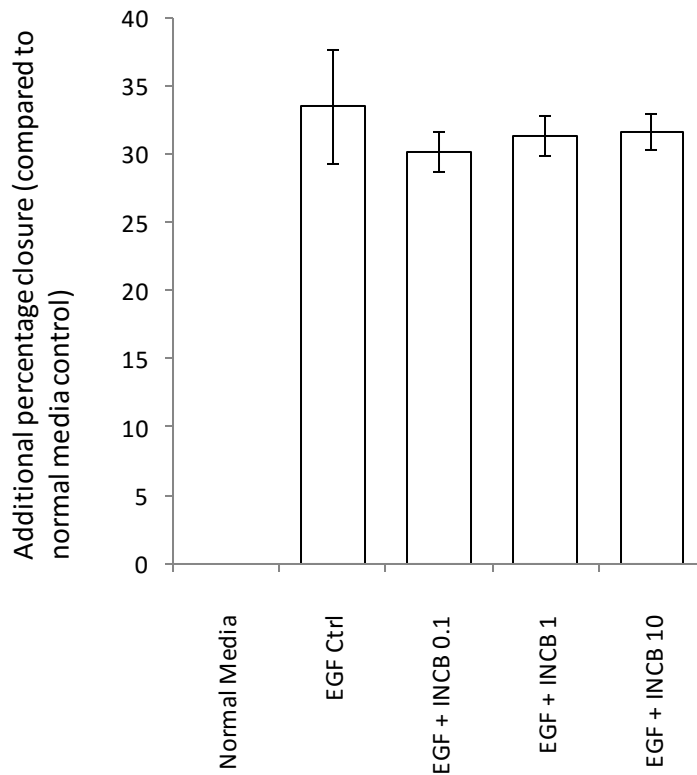
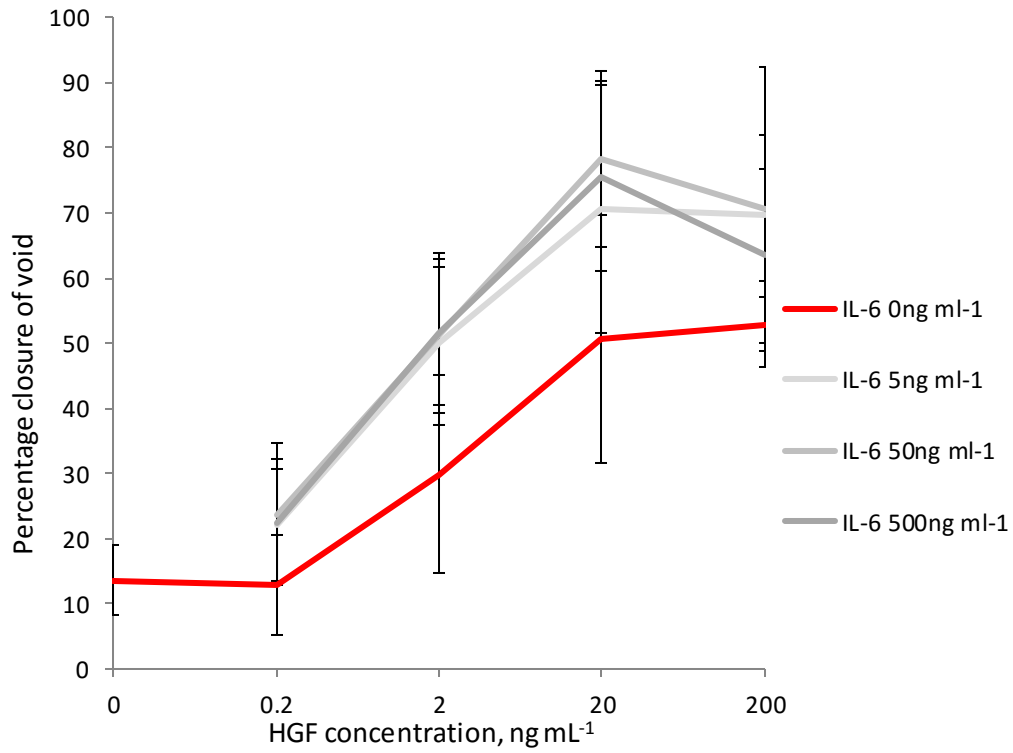


Figure 6.11: Effect of c-Met inhibitors on UPCI SCC089 ORIS™ assay migration over a 20 hour period using 2 ng mL⁻¹ EGF (n=9). Figure a – logarithmically increasing concentrations of foretinib, Figure b: logarithmically increasing concentrations of INCB28060. Y-axis: additional percentage closure of assay void, compared to normal media control. X-axis: *Normal Media* – normal media with DMSO control, *EGF Ctrl* – 2 ng mL⁻¹ EGF in normal media with DMSO, *For* – foretinib, *INCB* – INCB28060, all numerical postscripts refer to drug concentration in nM.

Note that, as for cell line UPCI SCC072 (Figure 6.10), there is no significant decrease in cell line migration within the range of foretinib/ INCB28060 concentrations tested (Mann Whitney U-test, P>0.05).

Figure 6.12: ORIS™ Assay Migration of Cell Line UPCI SCC072 under Conditions of Co-incubation with Varying Concentrations of HGF and IL-6

a).



b).

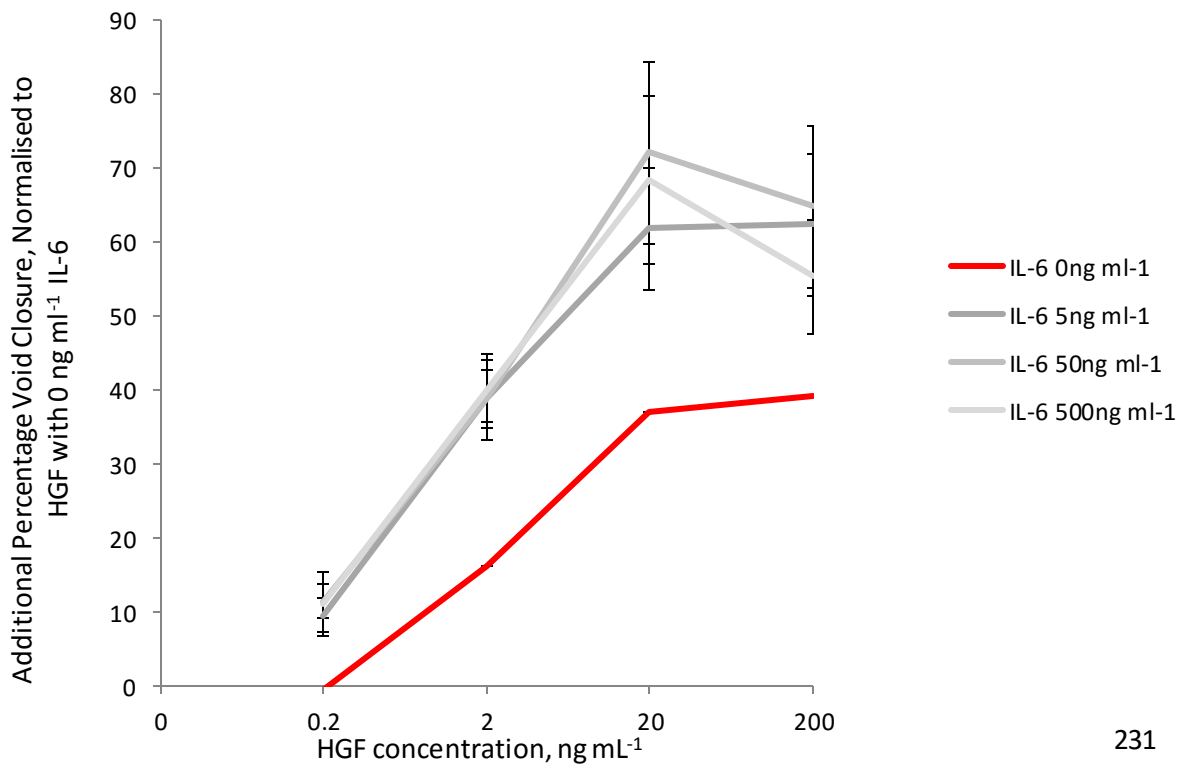


Figure 6.12a: Graph to show percentage ORIS™ assay void closure attributable to co-stimulation of cell line UPCI SCC072 with HGF plus IL-6 at respective doses. X-axis denotes HGF concentration in ng mL⁻¹; Y-axis denotes percentage closure of ORIS assay void by cell line UPCI SCC072 over 48 h. Error bars denote SEM, n=9. Note the marked variability in void closure linked to stimulation with HGF alone (red line), contributing to overlapping error bars when comparing to plots for HGF with IL-6 at 5, 50 & 500 ng mL⁻¹. Despite the variability linked to HGF, the addition of IL-6 was consistently observed to increase cell line migration compared to HGF alone: wide error bars were attributed to variability between biological repeats.

Figure 6.12b: Graph to show additional percentage void closure in cell line UPCI SCC072 (percentage closure minus control), normalised to account for HGF variability. Average migration for each HGF concentration plus 0 ng mL⁻¹ IL-6 for each triplicate biological repeat was normalised to the overall experimental average for each respective HGF concentration, hence error bars equal zero for IL-6=0 ng mL⁻¹. IL-6 containing media were then normalised to the respective HGF concentration using the same ratio. Note the tighter error bars (denoting SEM) attributable to IL-6 alone, inferring 95 % confidence intervals (1.96X SEM) which do not overlap HGF + 0 ng mL⁻¹ IL-6; a significant increase in migration with all concentrations of IL-6 was therefore observed. Note the separation of each IL-6 plot (grey lines) from the HGF control (red line): a difference of approximately 10 % additional closure can be seen at HGF=0.2 ng mL⁻¹, whereas a difference of approximately 25-35 % additional closure can be seen at HGF=20 ng mL⁻¹. This separation of curves suggests that HGF and IL-6 are acting in a synergistic manner.

Figure 6.13: ORIS™ Assay Migration of Cell Line UPCI SCC089 under Conditions of Co-incubation with Varying Concentrations of HGF and IL-6

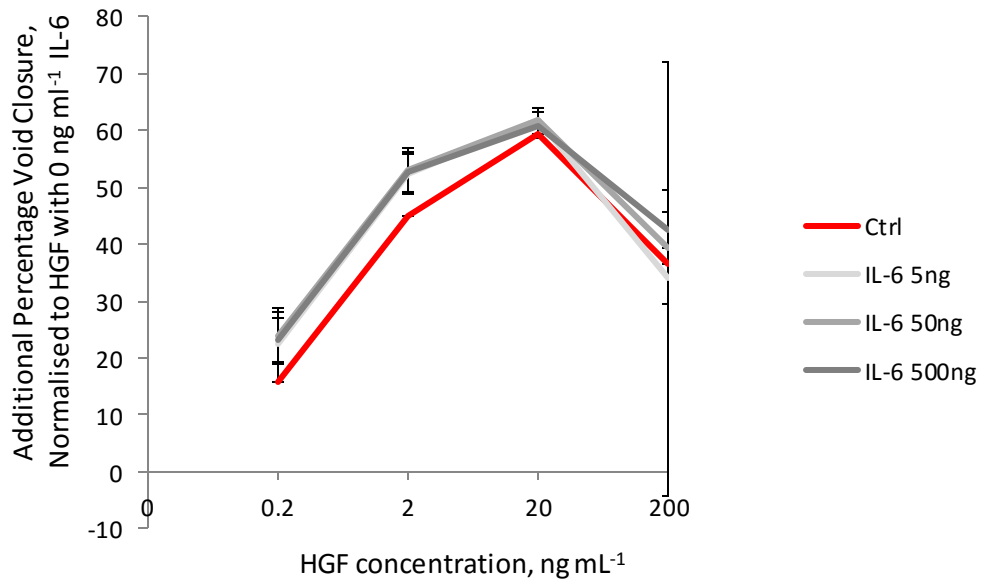
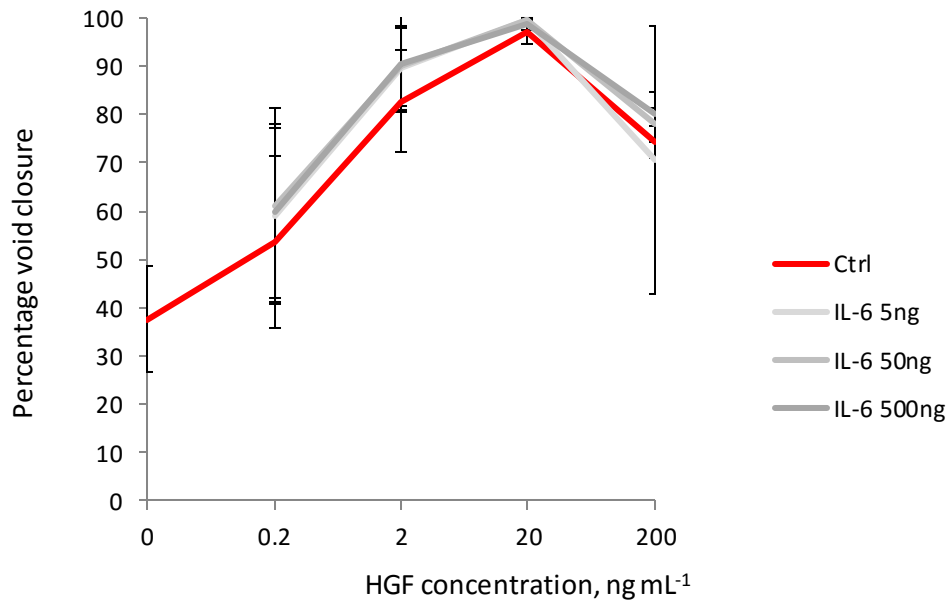


Figure 6.13a: Graph to show percentage ORIS™ assay void closure attributable to co-stimulation of cell line UPCI SCC089 with HGF plus IL-6 at respective doses. X-axis denotes HGF concentration in ng mL⁻¹; Y-axis denotes percentage closure of ORIS assay void by cell line UPCI SCC089 over 20 h. Error bars denote SEM, n=9. Note the marked variability in void closure linked to stimulation with HGF alone (red line), contributing to overlapping error bars when comparing to plots for HGF with IL-6 at 5, 50 & 500 ng mL⁻¹. Note that in contrast to cell line UPCI SCC072, cell line UPCI SCC089 demonstrated minimal increase in migration in response to addition of IL-6, with negligible effect at higher concentrations.

Figure 6.13b: Graph to show additional percentage void closure in cell line UPCI SCC089 (percentage closure minus control), normalised to account for HGF variability. Average migration for each HGF concentration plus 0 ng mL⁻¹ IL-6 for each triplicate biological repeat was normalised to the overall experimental average for each respective HGF concentration, hence error bars equal zero for IL-6=0 ng mL⁻¹. IL-6 containing media were then normalised to the respective HGF concentration using the same ratio.

Error bars denote SEM, demonstrating 95% confidence intervals (1.96XSEM) which overlap control, therefore inferring no significant difference between treatment and control groups.

Figure 6.14: Flow Cytometry Analysis of IL-6 Receptor Expression on Oropharyngeal Carcinoma Cell Lines

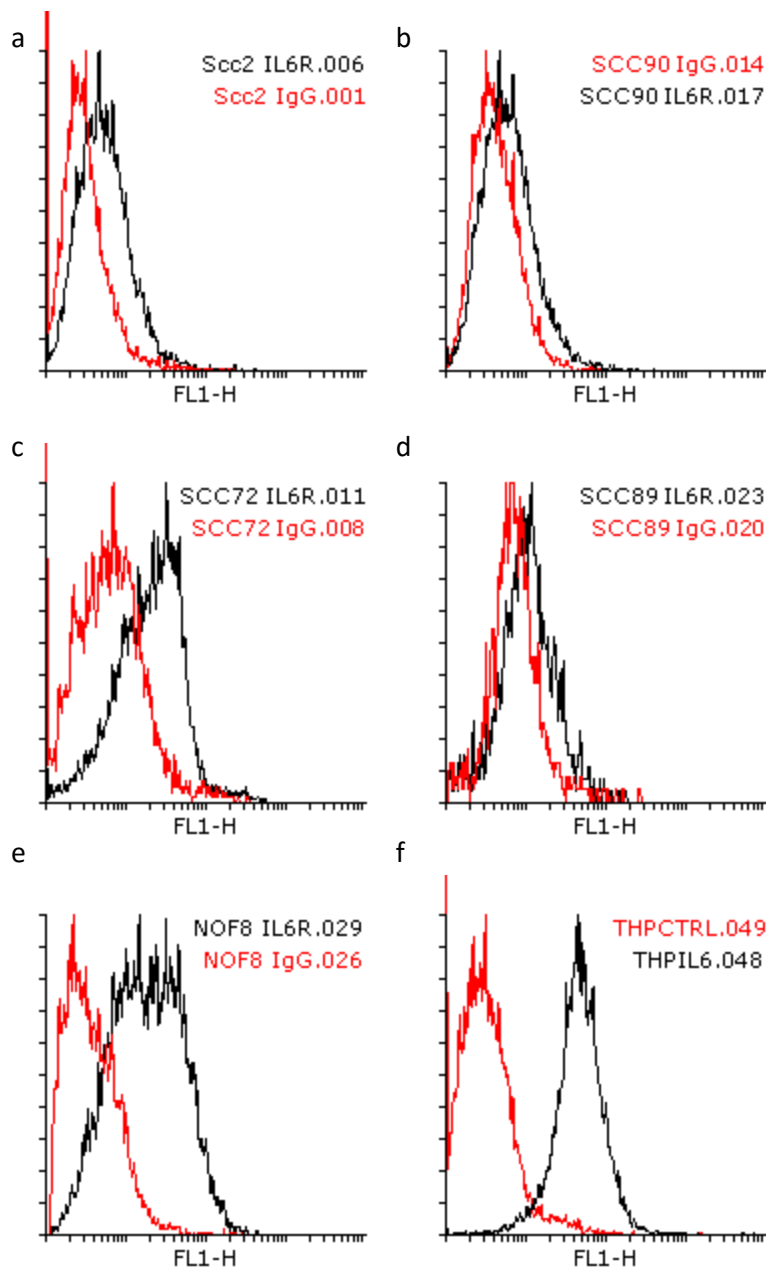


Figure 6.14: Flow cytometry analysis of DENO08 fibroblast culture/ oropharyngeal carcinoma cell line membranous IL-6 receptor status. FL1-H (X-axis) plotted against cell count (Y-axis); red lines denote IgG isotype control, black lines denote co-incubation with IL-6R primary antibody. Note low expression of IL-6 receptor in cell lines UD SCC02, UPCI SCC089 and UPCI SCC090. UPCI SCC072 demonstrated a more appreciable expression of IL-6 receptor, as did DENO08 fibroblasts.

- a. UD SCC02 (HPV-positive oropharyngeal carcinoma cell line)
- b. UPCI SCC090 (HPV-positive oropharyngeal carcinoma cell line)
- c. UPCI SCC 072 (HPV-negative oropharyngeal carcinoma cell line)
- d. UPCI SCC089 (HPV-negative oropharyngeal carcinoma cell line)
- e. DENO08 (normal oral fibroblast culture)
- f. THP-1 (acute monocytic leukaemia IL-6R positive control)

Discussion

In order to determine whether HGF had a principal role in inducing the additional migrations observed with stimulated fibroblast media, migration experiments were repeated using the clinically relevant c-Met inhibitors foretinib and INCB28060. Manufacturer data report a c-Met IC₅₀ of 0.4 nM and 0.13 nM for foretinib⁴³⁵ and INCB28060⁴³⁰, respectively; the literature, however, reports that biologically relevant inhibition is achieved at levels approximately 100-fold higher than the IC₅₀ of each drug^{430, 435, 478}. Dose-response curves were therefore created to assess ORIS™ assay migration of HPV-negative cell lines UPCI SCC072 and UPCI SCC089 in response to 0.5 µg mL⁻¹ recombinant HGF in the presence of varying amounts of each inhibitor (Figures 6.1 & 6.2). Experiments were then repeated using the most potent stimulated fibroblast medium for each HPV-negative cell line (SCC72-stimulated DENOFO8 Medium 1, and SCC089-stimulated DENOFO8 Medium 2) to determine the overall role of HGF in driving the additional migrations. As reported in the literature, a marked decrease in migration was noted in both recombinant HGF-induced migration and stimulated fibroblast medium-induced migration at concentrations of 40 ng mL⁻¹ foretinib and 10 ng mL⁻¹ INCB28060 (Figures 6.1, 6.2, 6.5 & 6.6).

Although INCB28060 is regarded as a highly specific c-Met inhibitor, foretinib has the capacity to inhibit further cytokine receptors in high concentrations, namely EGFR (at approximately 3 µM) and VEGFR (at approximately 3 nM)^{435, 478}. Whilst inhibition experiments were undertaken using concentrations of foretinib capable of blocking only VEGFR, both EGF and VEGF have been implicated in head and neck cancer progression and were therefore assessed further.

Initial recombinant protein dose-response analysis of cell migration was undertaken in a similar manner to recombinant HGF. Whilst recombinant EGF induced comparable dose-response curves to HGF in both cell lines UPCI SCC072 and UPCI SCC089 (Figure 6.7), recombinant VEGF demonstrated minimal evidence of inducing cell migration and was therefore discounted as a candidate molecule. Again, cell line UPCI SCC089 responded to EGF at concentrations approximately 10-fold lower than required for UPCI SCC072; this phenomenon shall be discussed in further detail later in the chapter. To provide final analysis of EGF's role in Media 1&2 -induced migrations, EGF ELISA was undertaken on DENOFO8 Media 1&2 for all cell lines, along with cell line-derived conditioned media (Figure 6.9). EGF

was undetectable in all conditioned media despite a highly robust recombinant human EGF standard curve. Although ELISA analysis had effectively ruled out EGF as a candidate for contributing to the stimulated fibroblast media-induced migrations, EGF served as a functional comparator in the confirmation of inhibitor specificity rather than toxicity. Foretinib and INCB28060 were therefore co-incubated with EGF at doses used to inhibit cell line migration in the preceding experiments (Figures 6.5 & 6.6), with no observable change in migration in the presence of foretinib or INCB28060 throughout the dose range tested. It was therefore concluded that foretinib and INCB28060 were acting in a receptor-specific manner rather than inhibiting migration as a consequence of exposing cell lines to a toxic dose of inhibitor.

The inconsistency between HGF ELISA-quantified HGF concentrations in UPCI SCC072-stimulated fibroblast media and the concentration of recombinant HGF necessary to induce an identical response prompted further toxicity assays, in order to confirm foretinib and INCB28060 had inhibited cell migration in a receptor-specific manner. LDH and MTA assays were therefore undertaken to supplement the functional evidence provided by co-incubation of inhibitors with recombinant EGF. LDH assay following co-incubation of both inhibitors with cell lines UPCI SCC072 and UPCI SCC089 demonstrated no evidence of toxicity throughout the dose range utilised in the preceding experiments. Similarly, MTS assay demonstrated no frank evidence of change in mitochondrial activity over this dose range for cell line UPCI SCC089 (Figure 6.4), although a gradual decline in activity was noted in cell line UPCI SCC072 (Figure 6.3). The decline in MTS assay absorbance noted in cell line UPCI SCC072 did not correlate with the precipitous drop in migration observed with 40 nM foretinib/ 10 nM INCB28060, and was therefore considered as unimportant to the inhibition of cell migration.

It was therefore concluded that foretinib and INCB28060 had acted in a receptor-specific manner, and that HGF blockade through c-Met inhibition had led to the restraint of stimulated fibroblast media-induced migrations. Two final considerations were however left unresolved. Foremost, HGF appeared an unlikely sole inducer of migration in cell line UPCI SCC072 due to a significant mismatch between conditioned medium HGF concentration and the concentration of recombinant HGF required to drive comparable migration; a second factor was therefore likely to be interacting alongside HGF. Secondly, it was noted that c-Met inhibition did not completely reduce cell migration to that of DMEM control in either cell line (Figures 6.5 & 6.6) – although subtotal c-Met inhibition could explain this phenomenon, a

further factor could in part have contributed to the residual migration induced by stimulated fibroblast conditioned media following c-Met inhibition.

Of all recombinant proteins initially assessed for dose-response effect on migration, IL-6 retained the greatest potential as a second factor to supplement HGF. Preceding ELISA quantification (Chapter 4, Figure 4.1) had confirmed a significant amount of this factor to be present in stimulated fibroblast conditioned media, and moreover IL-6 has been reported to synergise both HGF and EGF signalling, albeit in a non-migratory context^{493, 494}. Dose-response curves were therefore constructed using logarithmically increasing doses of IL-6 co-incubated with recombinant HGF (Figures 6.12 & 6.13). Due to the significant background variability of migration induced by HGF, graphs were normalised to each respective HGF dose in order to demonstrate the independent influence of IL-6 on migration. IL-6 was noted to synergise HGF's effect of cell line UPCI SCC072 in a similar manner to that reported for EGF, as can be observed by the divergent gradients of IL-6 containing media with increasing HGF concentrations, compared to HGF in the absence of IL-6 (Figure 6.12). UPCI SCC089 demonstrated minimal response to supplementation of HGF with IL-6 (Figure 6.13), although migrations using IL-6 containing media consistently outcompeted HGF alone, as again is illustrated following normalisation for HGF variability. The capacity of IL-6 to induce migration in cell line UPCI SCC072 and not cell line UPCI SCC089 correlates well with membrane-bound IL-6 receptor status (Figure 6.14), although UPCI SCC089's lack of response may also be attributable to constitutional STAT activation, negating the requirement for IL-6 supplementation via a paracrine route.

A model of HGF induction, with supplementation of the HGF signal via STAT activation through either IL-6 signalling, constitutional STAT activation, or both, was devised as an underlying mechanism through which HPV-negative cell line stimulated fibroblast media may induce additional migration (please see Figure 6.15, below for a diagrammatic representation of this interaction). Constitutional STAT activation in this theoretical model affirms the observed increased sensitivity of line SCC089 to HGF, and also explains the minimal response of UPCI SCC089 to IL-6 in combination with HGF despite a similar sIL-6R secretome compared to cell line UPCI SCC072.

Co-incubation of recombinant IL-6 plus HGF at concentrations comparable to that measured in UPCI SCC072-stimulated fibroblast media led to a comparable degree of migration to that of the conditioned media, further validating the potential for HGF/IL-6 interactions to account for migration of cell line UPCI SCC072 in response to stimulated fibroblast media. Moreover,

synergism between IL-6/ constitutional STAT activation and HGF (which also signals via STAT) supports the observation that the majority of stimulated fibroblast medium-induced migration could be restrained using c-Met inhibitors alone.

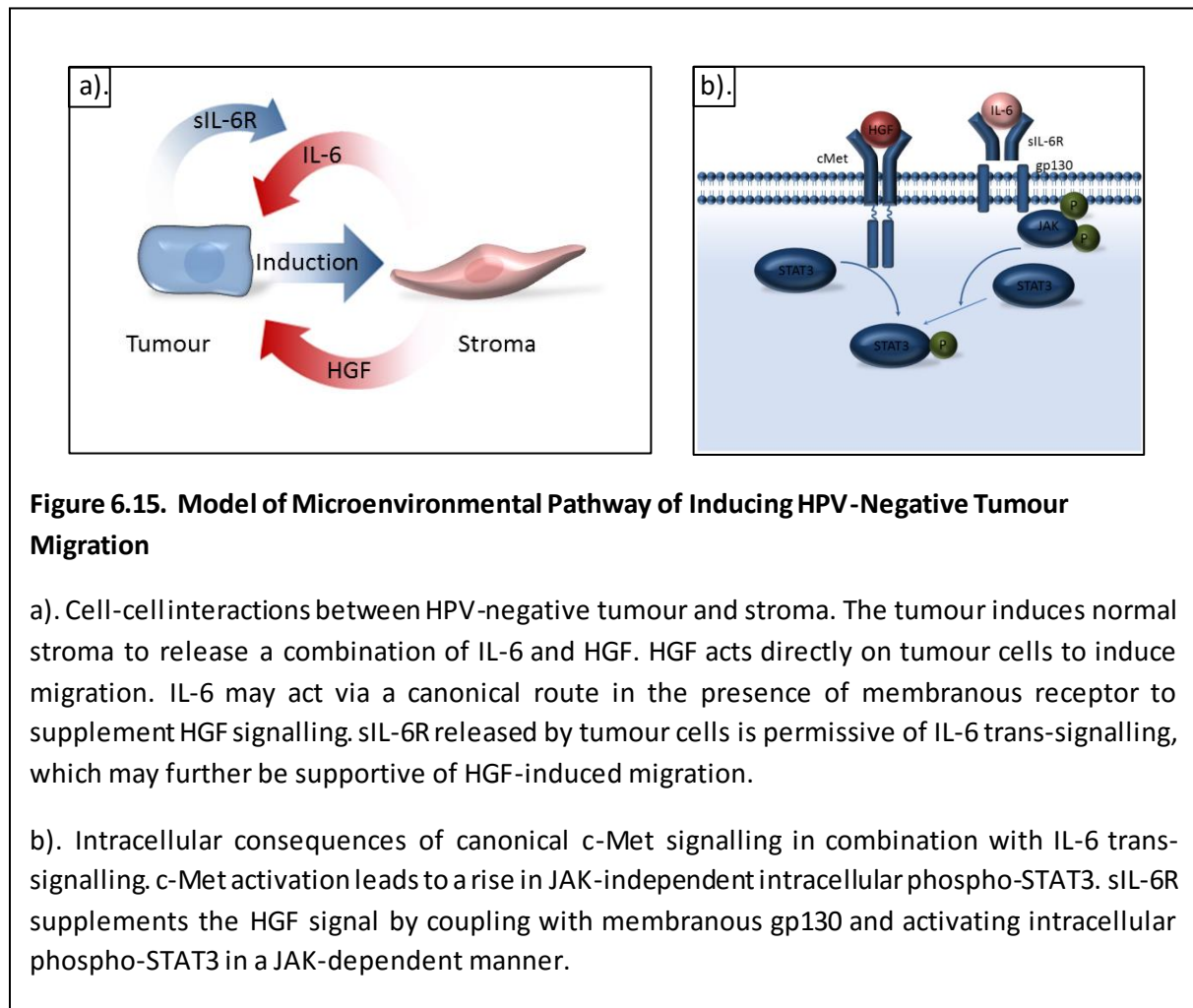


Figure 6.15. Model of Microenvironmental Pathway of Inducing HPV-Negative Tumour Migration

a). Cell-cell interactions between HPV-negative tumour and stroma. The tumour induces normal stroma to release a combination of IL-6 and HGF. HGF acts directly on tumour cells to induce migration. IL-6 may act via a canonical route in the presence of membranous receptor to supplement HGF signalling. sIL-6R released by tumour cells is permissive of IL-6 trans-signalling, which may further be supportive of HGF-induced migration.

b). Intracellular consequences of canonical c-Met signalling in combination with IL-6 trans-signalling. c-Met activation leads to a rise in JAK-independent intracellular phospho-STAT3. sIL-6R supplements the HGF signal by coupling with membranous gp130 and activating intracellular phospho-STAT3 in a JAK-dependent manner.

Cooperation between HGF and IL-6 trans-signalling has been reported in models of acute liver injury⁴⁹⁵, although findings were linked to hepatocyte mitosis rather than cellular migration. The authors found however, that PI3K/AKT was necessary for the cooperative effects on mitosis rather than STAT3 or MAPK, the main alternative intracellular pathways linked to IL-6 signalling⁴⁹⁶. Although the authors conclusively demonstrated that blockade of PI3K/AKT with the inhibitor wortmannin led to obstruction of this cooperative effect, co-transfection of HGF with either IL-6 or HIL-6 (an IL-6-bound soluble IL-6 receptor analogue) was associated with less PI3K/AKT upregulation compared to IL-6 or HIL-6 alone. The authors appropriately concluded that PI3K/AKT activation was necessary for the cooperative

effect of IL-6 on proliferation, but conceded that AKT activation was not linked to HGF-induced proliferation. AKT activation therefore appears to be a single component of a more complex interactive pathway between IL-6 trans-signalling and HGF. There are several limitations in contextualising the authors' work to the interactions between IL-6 and HGF in HPV-negative cell line migration, not least that a proportion of experimental methods involved transfection of HGF rather than protein exposure, in addition to the fact that mitosis was under scrutiny rather than migration. The article does however illustrate the potential for HGF and IL-6 to interact synergistically, and moreover provides an insight into the fact that the secondary messenger system through which interactions occur may be a complex relationship involving multiple pathways. In a *Nature* correspondence, Boccaccio *et al* also noted the complex relationship between HGF-induced STAT activation and other secondary messenger pathways, remarking that although the STAT pathway is necessary in HGF-induced tubulogenesis, STAT signalling alone is insufficient, and likely relies on crosstalk from other pathways in order to have its morphogenetic effects³⁸¹. Boccaccio went on to cite that MAP kinase activity positively reinforces STAT DNA-binding through serine phosphorylation, and concluded that the HGF receptor families' unique ability to induce branching morphogenesis may be explained by its ability to activate both STAT and other intracellular signalling pathways. It is therefore feasible that IL-6 derived support observed in HPV-negative cell line migrations relies on a similar activation of STAT-supportive messenger pathways rather than relying on the incidental additional rise in STAT that occurs with IL-6 stimulation.

A 2012 *Nature* review of c-Met in cancer also noted that crosstalk between c-Met and other signalling systems had "emerged as a major mechanism in human cancer". Established interactions include cooperation between c-Met and EGFR⁴⁹³, and WNT- β -catenin signalling⁴⁹⁷. Further experimental data suggest cooperation of HGF with TGF- β , IGF-1 and EGF in keratinocyte migration in-vitro⁴⁹⁸. More specifically, Hov *et al* noted c-Met signalling potentiated the effect of IL-6 on proliferation in myeloma cell lines⁴⁹⁴. Hov *et al* also assessed cell line migration in response to HGF in combination with IL-6, and although a trend of increased migration was noted, findings failed significance testing ($P=0.14$). Unlike Nechemia-Arbely *et al*'s work on acute liver injury, Hov *et al* concluded that synergy in the context of proliferation may be due to further HGF being produced in response to IL-6 (an established consequence of IL-6 signalling^{499, 500} or may be due to MAPK activation. The authors did not, however, derive any suitable evidence that their observed changes in levels

of MAPK following HGF/IL-6 co-stimulation were directly responsible for changes in proliferation.

HGF-induced keratinocyte migration has been comprehensively analysed and attributed to STAT3 activation^{380, 381}. Although HGF does not directly induce SOCS proteins, both SOCS 1&3 are capable of negatively regulating phosphorylated STAT3 produced by HGF stimulation³⁸⁰. IL-6, an inducer of SOCS3⁵⁰¹, has therefore been postulated to act as a restraining mechanism for HGF-induced migration³⁸⁰. Our data refute this proposition and suggests that, at least in the concentrations relevant to 2D tissue culture, IL-6 supports HGF-induced migration. IL-6 induced carcinoma migration has been recently confirmed in oral squamous cell carcinoma lines³³⁴, although longitudinal serum IL-6 has been implicated with survival for many years^{129, 364, 502}. Chuang *et al* found that IL-6 mediated migration was linked to membranous IL-6 receptor stimulation, with subsequent activation of Syk and JNK intracellular signalling pathways, leading to ICAM-1 expression. Interfering with ICAM-1 using siRNA led to abrogation of IL-6 mediated migration³³⁴.

It is uncertain as to the role of sIL-6R in driving migration in the stimulated fibroblast media experiments. Whilst it is enticing that the release of significant levels of sIL-6R is limited to HPV-negative cell lines (Chapter 4, Figure 4.3), this process may be a less significant consequence of global ADAM snippase activity leading to the release of a number of membrane-harboured cytokines which thereafter drive cancer progression, as previously discussed. Analysis of the relative contributions of sIL-6R and mIL-6R activity is testable via universal receptor inhibition using tocilizumab, versus solubilised receptor inhibition using sgp130. Due to difficulties in accessing both tocilizumab and validated sgp130, this consideration shall be discussed in “future work”.

Trans-signalling via the solubilised IL-6 receptor may offer advantages over canonical signalling via the membranous form of the receptor, such as IL-6 activation of non-IL-6R expressing cells⁵⁰³, differences in effector function of canonical and non-canonical pathways⁵⁰⁴ and more contentiously endocrine-like effects on target organs capable of releasing further HGF in response to trans-signalling, such as the liver⁴⁷⁶. Furthermore, there is evidence that early STAT3 phosphorylation is more pronounced via the IL-6 trans-signalling route^{505, 506} and has been found to be prolonged compared to canonical signalling in a model of murine liver regeneration⁵⁰⁷, although experimental data relate to use of a covalently bonded IL-6/sIL-6R designer cytokine complex to replicate IL-6 trans-signalling rather than use of IL-6 in combination with sIL-6R; the experimental use of a permanently-

bound receptor-ligand complex may have implications for bioactivity and sustained signal transduction. Greater induction of STAT would offer a clear benefit of solubilised IL-6 receptor signalling in the potential support of HGF activity.

Dominitzki *et al*⁵⁰⁸ concluded that IL-6 trans-signalling via the soluble IL-6R diminishes induction of adaptive regulatory T-cells (Treg) in a murine model, blocking immune tolerance. Dominitzki *et al* also found that whilst stimulating naïve CD4⁺CD25⁻ T-cells with high levels of IL-6 in primary cell culture led to only partial inhibition of FoxP3 induction (a key regulator of CD4⁺CD25⁺ Treg cell development⁵⁰⁹, IL-6 trans-signalling almost completely abolished FoxP3. The consequence of FoxP3 abrogation is to induce T-helper₁₇ (TH₁₇) subset development^{349, 510}. From a pathogenic perspective, switching from Treg immune tolerance to a pro-inflammatory TH₁₇ phenotype may be unfavourable for persistence of HPV infection, and may offer further insight into the HPV-negative status-specific nature of soluble IL-6R release observed in our data. Indeed, Treg frequency in isolated peripheral blood mononuclear cells has been found to correlate with HPV persistence in cervical premalignant lesions⁵¹¹.

It remains unclear whether alternative receptors that also signal via STAT3 could have a similar supplemental effect on HGF-induced migration, or whether this is a property exclusive to IL-6. Although STAT signalling is one of the best understood intracellular signalling pathways, much is still elusive as to how numerous cytokine receptors can utilise the same small number of phosphoproteins to elicit characteristic cellular responses. The SOCS 3 protein may account in part for the specific nature of IL-6 signalling^{505, 512, 513}, although again it is unclear as to whether this could drive IL-6-specific tumour evolution or whether more generic STAT activation is as effective in supporting HGF. Constitutional STAT activation may be a final process of achieving cell-autonomous responsiveness to HGF; this may account for marked sIL-6R secretion by cell line SCC089 despite a low migratory response to co-incubation with HGF and IL-6 – UPCI SCC089's solubilised receptor secretion may represent an evolutionary artefact that was accrued prior to gaining subsequent mutations that led to constitutionally activated STAT signalling.

STAT supplementation of HGF signalling offers a valuable biological explanation for recent clinical observations relating to the role of HGF in HPV-positive versus -negative disease. Kwon *et al*²⁷⁶ concluded that tumour HGF status correlated with overall survival rates in only HPV-negative oropharyngeal carcinomas; HGF status was not a prognosticator for HPV-positive tumours. Our data suggest that the degree of HGF release, along with further

derangements in tumour biology, namely IL-6 activation, are necessary in order for tumour cells to gain full migratory benefit from the microenvironment. sIL-6/mIL-6 receptor status, microenvironmental IL-6 release, STAT activity and soluble c-Met release may all have impact on a more comprehensive HGF/IL-6 synergistic pathway, and multiple cellular derangements may be necessary in order for these variables to become evolutionarily optimised. HPV-positive tumours are well recognised for carrying low overall mutational loads, and may under the majority of circumstances never accrue the degree of mutations necessary to fully take advantage of microenvironmental HGF. One may also postulate that the prognostic implications of smoking in HPV-positive disease could in part be linked to either introducing mutations that may support HGF signalling, or more alluringly, may directly induce STAT. Indeed, cigarette smoke extract has been found to increase JAK2 and STAT3 activation in a vascular smooth muscle model⁵¹⁴; similar effects on HGF-expressing, HPV-positive carcinomas could be profound. Tumour reliance on maintained cigarette smoking in order to derive STAT activation could have major therapeutic implications; smoking cessation upon diagnosis of HPV-positive, HGF-positive disease would be a paramount clinical consideration.

The ability of foretinib and INCB28060 to inhibit the migration induced by stimulated fibroblast media in both cell lines UPCI SCC072 and UPCI SCC089 demonstrates their potential value in the clinical setting. As previously discussed, foretinib has the additional advantage of blocking EGFR in higher concentrations, and therefore may be a suitable alternative to cetuximab; an EGFR blocking drug currently under randomised trial against platinum-based chemotherapy in the management of HPV-positive oropharyngeal carcinoma, in addition to having received NICE approval for locally-advanced head and neck cancer where platinum-based chemotherapy is considered inappropriate⁵¹⁵. c-Met mutations have become an established escape mechanism through which progression can occur in EGF-blocked tumours⁵¹⁶⁻⁵²², as has IL-6/STAT3 signalling⁵²³. Primary therapy with a Class II ATP-competitive small molecule inhibitor such as foretinib, offers not only dual restraint of any microenvironmental derangements in EGF & HGF release, but also obstructs potential c-Met mutation as an escape mechanism of EGF blockade due to foretinib's activity on the intracellular tyrosine kinase component of the c-Met receptor. Moreover, cytokine array data (Figure 3.8) suggest that HPV-negative cell lines released soluble EGFR; this may act as a decoy to EGF inhibitors such as cetuximab that act through binding the extracellular domain.

A number of recent studies on the efficacy of foretinib have investigated co-delivery of the drug with a further inhibitor⁵²⁴⁻⁵²⁶. Potential co-delivery of tocilizumab with foretinib may provide a valuable combination of receptor inhibiting effects that blockade EGF signalling, along with IL-6 and HGF signalling pathways; restraining migration in addition to obstructing known EGF-inhibitor tumour escape-routes for cancer progression.

As discussed in the introduction, Seiwert *et al's* trial of oral foretinib in recurrent/metastatic head and neck cancer failed to progress to stage 2 of the study, although reassuring findings were noted on the stabilisation of disease. Our data support the application of c-Met inhibitors in order to refrain tumour migration rather than proliferation, and the finding of foretinib-induced stabilisation rather than tumour regression is therefore intuitive. A more viable application of foretinib, or indeed any c-Met inhibitor in the management of head and neck cancer, is likely to be in the management of early disease rather than late, whereby inhibition of invasion and micrometastasis through the blockade of c-Met-driven tumour motility could offer significant improvements to outcome.

Chapter 7: Conditioned Media Induction of Fibroblast Senescence

Introduction

There has been increasing recognition of the role of fibroblasts in cancer over the past two decades⁵²⁷, both in terms of tumour initiation and progression⁵²⁷⁻⁵²⁹. Cancer-associated fibroblasts (CAFs) comprise a variety of tumour-supportive altered fibroblast phenotypes, including myfibroblasts and senescent fibroblasts; the former cell type referring to fibroblasts that have undergone partial smooth muscle differentiation⁵³⁰ and thereafter support tumour progression through the release of numerous growth factors including VEGF, IGF-1, EGF, HGF and TGF β -1⁵³¹, in addition to mechanically deranging stroma to create force- and protease- mediated tracks through which tumour cells may invade^{532, 533}. Fibroblasts entering a senescence pathway may also acquire a more active secretome. The so-called senescence-associated secretory phenotype (SASP) offers an alternative route to support tumour progression, and also includes the production of a number of factors supportive of tumour progression, as outlined in the preceding chapters. Senescent fibroblasts undergo a process termed “autophagy”, whereby oxidative stress drives lysosomal degradation and mitochondrial dysfunction, leading to induction of a catabolic state, and thereafter transfer of high energy products such as L-lactate, ketone bodies, glutamine, and free fatty acids to tumour cells^{534, 535}, providing further support for tumour progression.

The overall taxonomy of CAF subsets remains somewhat ill-defined³⁴⁸, with additional complexities with *in-vivo* classification linked to CAF heterogeneity occurring both within a single tumour and also between tumour types. Such heterogeneity is thought to account for difficulties in conclusively demonstrating a prognostic link between individual CAF markers and cancer prognosis⁵²⁷, with a general assumption that multiple yet-to-be-identified CAF subtypes may express similar markers, of which only some may bear prognostic significance.

CAFs are reported to originate from a number of sources, including resident fibroblasts, marrow-derived progenitors and also epithelia/endothelia via trans-differentiation³⁴⁸. Our model of tumour-stromal interactions has demonstrated that HPV-negative oropharyngeal

carcinoma lines have capacity to induce the resident fibroblast population to support tumour progression. Cytokine array data presented in Chapter 3 suggest that in addition to inducing a fibroblast secretory profile supportive of tumour migration, HPV-negative cell lines also induced a secretory profile typical of a SASP. Many factors linked by Elkhattouti *et al* to an age-related senescent profile, such as IL-6, IL-8 and stimulators of CXCR-2 (GRO, GCP-2, ENA-78)⁵³⁶ have been observed to be elevated in fibroblast cultures in response to HPV-negative cell line conditioned media. Furthermore, GRO- α expression, in addition to CXCR-2 expression, have been found to be linked to entry into a senescent pathway^{289, 537}, and have also been noted to contribute to a positive feedback loop⁵³⁶. Further factors linked to a SASP include MCP-1, MCP-2, HGF and VEGF⁵³⁸, all of which were upregulated in cytokine array analysis of HPV-negative stimulated fibroblast media. Data presented in Chapter 3 therefore suggest a senescent route of fibroblast induction.

From the perspective of tumour evolution, induction of an immediate fibroblast secretory profile offers clear selection pressure for expansion of those cellular populations with greatest capacity to drive senescence; there is less tangible evolutionary advantage of inducing the features of senescence which become observed only after protracted stimulation, although these latter features may allow establishment of a permanently supportive secretory profile. Many of the characteristic features of senescence (although beneficial to tumour progression) may therefore be a consequence of the immediate process of deriving evolutionary benefit from the initial secretory profile we have observed, rather than representing the characteristic evolutionary end-point of selection pressure. Nonetheless, an established senescent fibroblast phenotype is reflective of those tumours which are microenvironmentally active, and may offer clinically accessible measures of tumour-stromal interaction, which in turn may help define the prognostic disparity between HPV-positive and -negative disease.

This brief chapter examines whether protracted exposure to HPV-negative cell line conditioned media leads to fibroblast senescence, as an assumed biological end-point of the process linked to the initial secretory profile discussed in Chapter 3.

Methods

M7.1: Analysis of Senescence Following Culture of DENOFO8 Fibroblasts in Cell Line Conditioned Media

Culture of DENOFO8 Fibroblasts in Cell Line Conditioned Media

24 h conditioned media from cell lines UD SCC02, UPCI SCC072, UPCI SCC089 and UPCI SCC090 were collected at a concentration of 3 million cells mL⁻¹ conditioned medium and stored in an identical manner to that described in Chapter 2. Following initial trials of protracted incubation of DENOFO8 fibroblasts in cell line conditioned media, it was determined that conditioned media required supplementation with normal media in order to avoid nutrient exhaustion over the period of a 13-day incubation. Cell line conditioned media were therefore diluted with 30 % normal media (DMEM plus 10 % FCS, plus 50 U mL⁻¹/50 µg mL⁻¹ penicillin-streptomycin, plus 2mM L-glutamine) immediately prior to use in the experiment, achieving a working concentration of 2.13 million cells mL⁻¹.

Passage 7 DENOFO8 fibroblasts were grown in 25 cm tissue culture flasks to a confluence of approximately 15 %, washed X3 and then incubated with cell line conditioned media diluted with 30 % normal media. Concurrent flasks were incubated for each respective cell line (UD SCC02, UPCI SCC072, UPCI SCC089 and UPCI SCC090) conditioned media, along with separate normal media negative control and 10 µM cisplatin in normal media positive control. Medium change was undertaken every 48 h, with an additional medium change undertaken for cisplatin positive control after 24 h exposure. Cell cultures were reviewed for confluence daily, with sub-culture of flasks undertaken at day 8, except for cisplatin control due to low confluence throughout the experiment.

SA-βGal Analysis of Senescence

At day 13, media were removed, each flask washed in PBS, and then 1 mL fixative added from a commercial SA-βGal staining kit (Abcam, Cambridge, UK) for 15 mins. Each flask was then washed X2 with PBS and then proprietary SA-β Gal staining solution added using manufacturer's guidelines for preparation. Wells were then incubated at 37 °C for 20 hrs, protected from light exposure. Flasks were subsequently reviewed using a light microscope,

and 3 random areas photographed using a USB camera under X10 objective. The total number of cells in each field were then counted, along with total number of cells staining SA- β Gal positive – defined as all cells demonstrating distinct uptake of chromogen in the perinuclear region of the respective fibroblast cell body. Results were then expressed as percentage of total cells in each field staining SA- β Gal positive, and triplicate experimental and biological repeats summarised graphically.

Results

Figure 7.1: Representative Micrographs of DENOFO8 Fibroblast Cultures Following 13-Day Exposure to Cell Line Conditioned Media

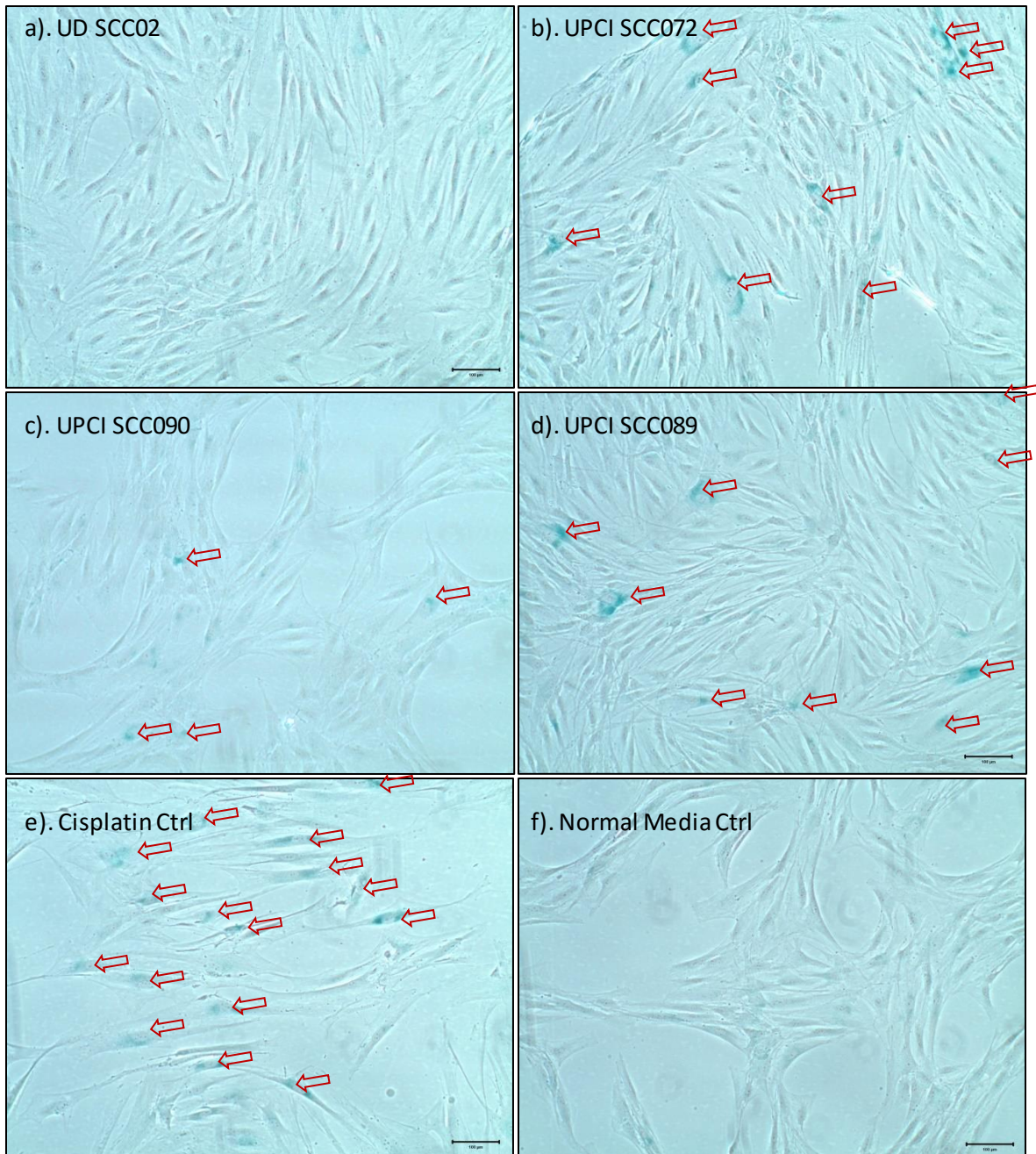


Figure 7.1: Representative micrographs of DENO F08 fibroblast cultures following 13-day exposure to conditioned media taken from cell lines UD SCC02, UPCI SCC072, UPCI SCC089 and UPCI SCC090 (Figures a-d). Red arrows denote cells displaying SA- β Gal positive staining. Cisplatin positive and normal media negative controls illustrated in figures e & f, respectively. Note the marked SA- β Gal positivity (blue perinuclear uptake of stain) observed in a significant number of fibroblasts in the cisplatin group. Note also clear SA- β Gal positivity can be seen in a proportion of fibroblasts exposed to HPV-negative cell line conditioned media (UPCI SCC072 and UPCI SCC089; Figures b & d). Note that weak staining can be observed in a number of fibroblasts exposed to UPCI SCC090 conditioned medium (Figure c), although the proportion of cells expressing weak positivity were less than the proportion of cells expressing strong positivity (please refer to Figure 7.2).

Figure 7.2: Percentage SA-βGal Positive DENO08 Fibroblasts in Cultures Following 13-Day Exposure to Cell Line Conditioned Media

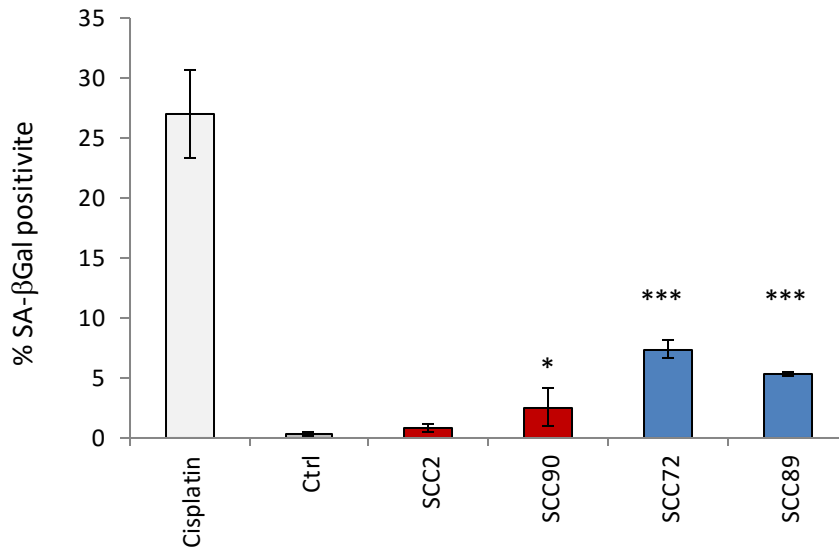


Figure 7.2: Bar graph to show percentage of total fibroblast population SA-βGal positive following 13-day exposure to cell line conditioned media. n=9, error bars denote SEM.

* - Mann Whitney U-test, P<0.05 (compared to control)

** - Mann Whitney U-test, P<0.01 (compared to control)

*** - Mann Whitney U-test, P<0.001 (compared to control)

Cisplatin – cisplatin positive control; 24 h exposure to cisplatin

Ctrl – Normal media negative control

SCC2 – Following 13-day exposure to UD SCC02 (HPV-positive) conditioned media

SCC90 – Following 13-day exposure to UPCI SCC090 (HPV-positive) conditioned media

SCC72 – Following 13-day exposure to UPCI SCC072 (HPV-negative) conditioned media

SCC89 – Following 13-day exposure to UPCI SCC089 (HPV-negative) conditioned media

Note the greater proportion of fibroblasts exposed to HPV-negative cell line conditioned media that express SA- β Gal, reflecting a greater proportion of cells entering senescence. As discussed in Figure 7.1, fibroblasts exposed to UPCI SCC090 conditioned media also demonstrated a proportion of cells entering senescence, although this proportion remained less than that induced by HPV-negative conditioned media, moreover the intensity of stain in response to UPCI SCC090 conditioned media (please refer back to legend of Figure 7.1) was less than observed in fibroblasts exposed to HPV-negative line conditioned media.

Note also that graphs for fibroblast senescence in response to cell lines UD SCC02, UPCI SCC072, UPCI SCC089 and UPCI SCC090 follow a similar trend to that seen for ELISA analysis of HGF, IL-6 and IL-8 (please refer to Figures 5.3, 4.1 & 4.2, respectively), whereby HPV-negative lines UPCI SCC072 and UPCI SCC089 secrete high levels of the aforementioned cytokines, with UPCI SCC090 producing modest amounts, and UD SCC02 inducing minimal response.

Discussion

As anticipated, HPV-negative cell line conditioned media demonstrated greater capacity to induce fibroblast senescence over the 13-day period of experimentation. Although a direct link between SA β -Gal expression and the initial secretory profile observed in stimulated fibroblast Media 1&2 (Chapters 2-5) is not confirmed, the observed pattern of SA β -Gal staining does appear consistent with a common process linking the initial secretory response and latter expression of markers of senescence. Further markers of senescence, such as HIRA foci, could be used to further validate our findings relating to SA- β Gal, although a more pertinent challenge is to identify the factor(s) released by cell lines which are responsible for driving the HGF response observed in stimulated fibroblasts. The findings of this chapter, in addition to the fibroblast secretory profile summarised in Chapters 3-5, offer clues as to the likely nature of the characteristic HPV-negative tumour secretome driving the fibroblast response. Identification of an established senescence-inducing factor may ultimately preclude the necessity for more comprehensive analyses of fibroblast senescence, although analysis of the transformed fibroblast phenotype is discussed further in Chapter 9.

Despite fibroblast senescence being generally regarded as a consequence of either cellular ageing or protracted exposure to oncogenes or alternative stressors, HPV-negative tumour conditioned media induced a comparable secretory profile in a normal fibroblast population within a 24-hour period (Chapters 2-5). Moreover, senescence is considered linked to an established cellular subpopulation distinct from the normal stroma, often referred to collectively as cancer-associated fibroblasts (CAFs); our data suggest the secretory profile classically ascribed to such populations is inducible within a comparatively short period of time, with markers of senescence occurring after protracted exposure.

Interestingly, CXCR-1 and CXCR-2 expression occurred in a subpopulation of normal fibroblasts stimulated by HPV-negative tumour conditioned media for 24h (Please refer to Chapter 4, Figures 4.4 & 4.5); this may reflect the initial stages of cellular entry into senescence, and may signify those fibroblasts which proceed to positive SA β -Gal staining at 13 days. This process would be consistent with the GRO/CXCR-2 feedback loop discussed in the chapter introduction. CXCR-2 linked flow cytometric cell sorting may allow for such populations to be isolated and studied in greater detail, allowing direct correlation of early CXCR expression to entry into senescence, although such further experimentation is beyond the scope of this thesis.

The function of only partial fibroblast entry into senescence (Figure 7.2) may relate to the physiological role of this process outside the context of the tumour microenvironment; it is intuitive that senescence of an entire fibroblast population would lead to loss of tissue dynamics and capacity to remodel/recover from a highly inflammatory milieu, and therefore only partial fibroblast population entry into senescence is desirable at a tissue level. Alternatively, entry may relate to either stage of cell cycle, or an alternative phenotypic difference occurring between fibroblasts within a given population. A higher proportion of cells entering senescence may therefore be observed over more protracted conditioned media incubations, as more fibroblast subpopulations enter a phenotypic state responsive to senescence induction.

A senescent profile may offer some light on the lack of TGF β -related findings linked to our model of the microenvironment. Although TGF β has been linked to the acquisition of both myofibroblastic and senescent fibroblastic profiles, the molecule may act as both a tumour suppressor and tumour promoter⁵³⁹⁻⁵⁴¹. Notably, loss of TGF β responsiveness has been linked to HGF expression⁵⁴², with inhibition of TGF β also potentiating HGF-induced invasion⁵⁴³. Our model may therefore illustrate entry into senescence via a route alternative to TGF β , such as IL-17A or IL-1 β ^{544, 545}, thereby retaining greater capacity to induce microenvironmental benefit from HGF.

Cytokine array and PCR data presented in Figures 3.2, 3.5 and 4.6 demonstrate that GRO- α , β & γ all appear elevated in the HPV-negative microenvironment as a result of both tumour and stromal release. GRO therefore offers both autocrine and paracrine CXCR-2 reinforcing signals for maintaining a persistent senescence profile. Indeed, the role of GRO- α in the induction of a SASP is clearly documented^{537, 546}.

In summary, the confirmation of a greater degree of senescence in HPV-negative conditioned media-stimulated fibroblasts provides further insight into the likely process through which HGF release has been induced. A number of reinforcing signals released by HPV-negative tumours, such as GRO, may supplement the induction of fibroblast senescence, although data presented in Chapter 4 suggest that GRO- β/γ alone did not retain capacity to drive HGF secretion. Candidate pathways other than GRO capable of driving the fibroblast response shall be discussed in "Further Work", Chapter 9.

Chapter 8: Determining Validity of 2D Experimental Findings

Introduction

Invasion Assay

The experimental data presented in Chapters 2-6 confirm a principal role of HGF in inducing cell migration within a 2D culture model. There are clear limitations with respect to the external validity of 2D modelling, and therefore a 3D model was sought for analysis of HGF's role in an anatomically representative setting. Our initial trials of De-Epithelialised Dermis (DED) and collagen matrix-based organotypic models appeared unrepresentative of tumour invasion; although cell lines UD SCC02, UPCI SCC090, UPCI SCC72 and UPCI SCC089 all created viable 3D cultures at 14 days, this was restricted to a stratified squamous-type lining being established in each model at the air-liquid interface. No reliable evidence of cell invasiveness was noted within any experimental repeat of each model, suggesting that the model was not representative of the known biology of the original disease from which each cell line was established (please refer to Chapter 1 Table 1.3, itemising published clinical data for cell lines UD SCC02, UPCI SCC090, UPCI SCC072 and UPCI SCC089). One major limitation of the use of anatomically-derived tissue as a platform for *in-vitro* modelling is that *in-vivo* carcinomas do not necessarily demonstrate significant progression over a period of 2 weeks, and it is therefore unsurprising that 3D culture often fails to reproduce the pattern of invasion characteristic of the original disease over the feasible period for which such experiments can be run. Moreover, difficulties have been encountered with respect to quantitatively analysing results of many organotypic models⁵⁴⁷, particularly in the presence of anatomical artefacts within DED such as sweat pores, which can lead to ingress of carcinoma lines and create an appearance similar to that of invasion.

Co-workers have been unsuccessful in culturing cell lines UPCI SCC072 and UPCI SCC089 into cell spheroids for means of 3D modelling by use of agar-based techniques routine to the department. Although colleagues found cell lines to be partially viable, the results of experimentation precluded any meaningful research being undertaken due to breakdown of the incubated cell mass. Alternative methods are available in order to form spheroids within 3D culture, including the use of low-adherence plates and hanging-drop models^{548, 549}, although the lack of cohesion noted in agar-based experiments may transfer to alternative,

de-novo methods of spheroid formation. AMSBIO (Abingdon, Oxford, UK) have recently produced a 3D “Cultrex™” spheroid invasion assay kit (Cat number 3500-096-K), which incorporates an extracellular matrix (ECM) constituent; this constituent is initially co-incubated with cell lines in a low adherence plate in order to help promote spheroid formation. The opportunity to supplement spheroid formation in cell lines UPCI SCC072 and UPCI SCC089 using commercially pre-optimised ECM supplements, given colleagues’ observations using agar techniques, therefore offered a viable alternative to the limitations of DED/collagen models we had also encountered, and offered the ability to simultaneously apply an invasion assay to each spheroid after formation, which could be adopted to investigate the role of HGF inhibition in restricting tumour invasion.

This chapter applies 2D *in-vitro* findings relating to HGF to a 3D Cultrex™ model of invasion, as further assessment of HGF as a potential biomarker of aggressive HPV-negative disease and also the potential clinical value of HGF inhibitors using an anatomically representative model.

Methods

M8.1: Trial DED Organotypic Models

Organotypic models were created using standardised protocols previously established by co-workers⁵⁵⁰.

Preparation of DED

Sterilised cadaveric dermis stored in glycerol was washed repeatedly in PBS and then hydrated at 37 °C for 48 h in fresh PBS, with further washing and PBS changes at 24 h. A final overnight incubation was then performed using 1 M NaCl to promote epidermal separation from the underlying dermis. Final epidermal removal was undertaken using sterile forceps. The DED was then stored in PBS at 4 °C until use in organotypic culture. Immediately prior to use in organotypic culture, DED was divided into 1.5 cm² segments and placed in a 6-well plate with papillary surface orientated superiorly, and a sterilised 1 cm diameter stainless steel ring firmly abutted to the surface. A total of 10 sections were prepared in order to provide 7-day and 14-day timepoints for each cell line of interest.

Seeding of Fibroblast Population

Passage 4 DENO8 Normal Oral Fibroblasts were grown to 60-80 % confluence, trypsinised and resuspended in normal media at a concentration of 2.5 million cells mL⁻¹. 200 µL of cell suspension was then pipetted into the inner aspect of each 1 cm diameter stainless steel ring, in order to seed 5 X 10⁵ fibroblasts onto each isolated DED surface. The DED/cell suspension was then incubated for 24 h at 37 °C in order to allow fibroblast redistribution within the model and conditioning of media.

Seeding of Cell Lines

Cell lines UD SCC2, UPCI SCC 072, UPCI SCC089, UPCI SCC090 and HTE E6E7 were grown to 60-80 % confluence, trypsinised and resuspended in normal media. For each cell line, 2.5×10^5 cells suspended in a small volume of normal media were then pipetted into the inner aspect of the 1 cm stainless steel ring for each duplicate repeat. Models were incubated at 37 °C for 24 h and then the superficial 400 μ L of medium removed from each well and replaced with fresh medium.

Establishing an Air-Liquid Interface (ALI)

Models were raised to ALI 72h after seeding cell lines. In brief, each DED model was carefully transferred onto a stainless steel grid sited in a 6-well plate, and normal media pipetted into each well to the level at which the inferior aspect of the DED was submerged, whilst leaving the superficial aspect of the DED exposed. Media were changed every 3 days until the models were harvested.

Harvesting of Organotypic Models

At the relevant timepoint (7 or 14 days), a single model for each cell line was submersed in 10 % formalin and stored overnight to ensure adequate fixation. The model was then bisected, paraffin-embedded and mounted in 5 μ m sections on histological slides in the usual manner. Sections were then stained with H&E, examined under light microscopy, and photomicrographs taken from representative portions of each model.

M8.2: Trial Collagen-based Models

Collagen-based 3D models were created using standardised protocols previously established by co-workers and based on recommendations by Dongari-Bagtzoglou & Kashleva's Nature protocol^{551, 552}. UD SCC02 and UPCI SCC072 were selected as representative HPV-positive and HPV-negative lines, respectively, in order to undertake preliminary analysis of collagen models prior to extending experimentation to include UPCI SCC089 and UPCI SCC090 should models appear superior to that observed using DED.

Passage 7 DENO08 normal oral fibroblasts were grown to 80% confluence, trypsinised, centrifuged at 1,000 rpm for 5 mins and then resuspended in CDMEM (DMEM supplemented with 10 % foetal calf serum, 50 U mL⁻¹ penicillin, 50 U mL⁻¹ streptomycin and 625 ng mL⁻¹ amphotericin B). A final fibroblast concentration of 1.25 X 10⁶ mL⁻¹ was achieved and confirmed using a haemocytometer.

The fibroblast/DMEM suspension was then mixed with reagents itemised in Table 8.1, using pipette tips pre-cooled at -21 °C overnight and ensuring thorough mixing of reagents by gentle swirling prior to addition of the fibroblast suspension, taking care to avoid introduction of air bubbles into the gel. All reagents were stored on ice during preparation. 1 M NaOH was then carefully titrated into the suspension in order to neutralise collagen acidity, confirmed using phenol red indicator (colour change from orange to pink). 800 µL suspension was then pipetted into 24 well plate tissue culture inserts using pipette tips pre-cooled at -21 °C overnight. Gels were then incubated at 37 °C for 2 hrs in order to set. Gels were then submerged in CDMEM and incubated at 37 °C overnight. Media change was undertaken the following day, followed by a further 24 hrs incubation at 37 °C.

UD SCC02 and UPCI SCC072 were grown to approximately 60-80 % confluence, trypsinised, centrifuged and resuspended in Green's media (constituents summarised in Table 8.2) in order to achieve a count of 5 X 10⁶ cells ml⁻¹. 200 µL suspension was then carefully pipetted onto the surface of respective collagen gels. Further Green's media was carefully pipetted to surround the collagen insert to the level of the keratinocyte suspension and incubated overnight at 37 °C. Media change was then undertaken, fully submerging models with medium and incubating for a further 24 hrs at 37 °C. Models were then raised to the air-liquid interface using stainless steel mesh supports and incubated at 37 °C for 2

weeks, undertaking media change every 2-3 days in order to maintain air-liquid interface at the level of the collagen/keratinocyte junction.

Models were retrieved at a 2-week endpoint, formalin fixed and paraffin embedded, 5 μm sections mounted on standard histological slides, stained with haemotoxylin & eosin and then imaged at X20 objective.

Table 8.1: Collagen Gel Constituents

Volume (μL)	Constituent
940	DMEM (10x)
940	Reconstitution buffer (10x) (22 mg mL ⁻¹ sodium bicarbonate and 20 mM HEPES in 0.062 N NaOH)
780	FCS
96	L-glutamine
6060	Rat tail collagen (5 mg mL ⁻¹)
360	Fibroblasts 1.25x10 ⁶ mL ⁻¹ in DMEM supplemented with 10 % FCS, 50 U mL ⁻¹ penicillin/streptomycin, 625 ng mL ⁻¹ amphotericin B

Table 8.2: Constituents of Green's Media

Volume	Constituent, Stock Concentration	Final Concentration
330 mL	DMEM	66 %
108 mL	Ham's F12 nutrient mixture	21.6 %
50 mL	Fetal calf serum	10 %
5 mL	Penicillin/streptomycin 10,000 IU/10,000 $\mu\text{g mL}^{-1}$	100 IU/100 mg μL^{-1}
1.25 mL	Amphotericin B 250 $\mu\text{g mL}^{-1}$	0.625 $\mu\text{g mL}^{-1}$
2 mL	Adenine 6.25 $\mu\text{g mL}^{-1}$	0.025 $\mu\text{g mL}^{-1}$
2.5 mL	Insulin 1 mg mL ⁻¹	5 $\mu\text{g mL}^{-1}$
0.5 mL	3,3,5 Tri-iodo thyronine/apo-transferrin 1.36 mg mL ⁻¹ / 5 mg mL ⁻¹	1.36 ng mL ⁻¹ / 5 $\mu\text{g mL}^{-1}$
80 μL	Hydrocortisone 2.5 mg mL ⁻¹	4 $\mu\text{g mL}^{-1}$
25 μL	Epidermal growth factor 100 $\mu\text{g mL}^{-1}$	5 ng mL ⁻¹
500 μL	Cholera toxin 8.47 $\mu\text{g mL}^{-1}$	8.47 ng mL ⁻¹

M8.3: Cultrex™ 3D Spheroid Invasion Assay

Following successful trials, in addition to completion of experimental findings discussed in the preceding chapters, the Cultrex™ 3D spheroid invasion assay (AMSBio, Oxford, UK) was determined as the most suitable method of 3D modelling HPV negative tumour invasion in the presence/absence of fibroblasts.

Passage 7 DENOFO8 normal oral fibroblasts and HPV-negative cell lines UPCI SCC072 & UPCI SCC089 were grown to approximately 70 % confluence in separate 75 cm² flasks. Each cell culture was trypsinised, centrifuged at 1,000 rpm for 5 mins, resuspended in normal media and counted using a haemocytometer, achieving an accurately counted stock cell suspension to the order of 1 million cells mL⁻¹. An appropriate volume of each cell suspension was then pipetted into universal containers along with 4 mL normal media minus the volume of cell suspension pipetted, in order to achieve a final exact 4 mL suspension with accurate cell concentration of 60,000 cells mL⁻¹. Two further cell suspensions containing both DENOFO8 normal oral fibroblasts mixed with each cell line were created in an identical manner; each DENOFO8/ cell line stock suspension was pipetted into a universal container and then made to exactly 4 mL by adding 4 mL normal media minus the sum volume of the two pipetted volumes. DENOFO8 fibroblasts were admixed to each cell line in a ratio of 1:6 – that is, a final suspension of 60,000 cells mL⁻¹ was created containing 10,000 fibroblasts mL⁻¹ and 50,000 carcinoma cells mL⁻¹.

60 µL Cultrex™ ECM solution, thawed on ice, was then added to a 1,140µL aliquot of each suspension in order to achieve a 5 % ECM supplement. 100 µL of each solution was then pipetted into respective wells of a Cultrex™ low-adherence 96-well plate and then incubated for 3 days, with review every 24 h to confirm spheroid formation and growth. At day 3, Cultrex™ invasion matrix was thawed on ice and the 96 well plate transiently cooled on ice before adding 50 µL invasion matrix to each respective well. The 96-well plate was then centrifuged at 1,000 rpm for 3 minutes and then incubated at 37 °C for 1 hour in order to allow the invasion matrix to set. 100 µL normal media containing 120 nM foretinib or DMSO control was then pipetted into each respective well. This provided a final well concentration of 60 nM foretinib, when allowing for dilution in the preceding 100 µL volume of medium/invasion matrix added to each well. Final foretinib concentration was elevated slightly from that optimised for ORIS™ migration assays (40 nM; see Chapter 6, Figures 6.1-

6.6) in order to compensate for any pipetting error or concentration gradient introduced by the invasion matrix; the 60 nM concentration remained well within appropriate limits of the toxicity assays discussed in Chapter 6, and also reflected 3D findings by other groups, who had found restraint of HGF-induced invasion at concentrations exceeding 40 nM, with borderline inhibition at 40 nM ⁴³⁵.

Wells were then cultured at 37 °C and monitored with daily micrographs at X4 objective for 6 days to assess invasion. At the end of the experiment, the medium supernatant was carefully aspirated and 200 µL 30 % formaldehyde pipetted over the residual invasion matrix in order to fix and liberate the intact spheroid-containing matrix from the base of each well. Each fixed matrix was then carefully aspirated into a 1,000 µL pipette using a cut pipette tip to allow atraumatic retrieval, and then stored in formalin to complete the fixation process.

Day 6 Inverted lens micrographs were analysed using ImageJ software, utilising single cell invasion counting, as recently described by Rudisch *et al* ²⁹⁰. An example selection tool mark-up of cells escaping tumour spheroid can be observed in Figure 8.0.

Formalin-fixed spheroid-containing matrices were paraffin embedded, cut in 5 µm sections and mounted on standard histological slides. H&E staining was undertaken for all conditions where spheroids survived the embedding process. Invasive co-culture models were also subjected to Cytokeratin AE1/3 immunohistochemistry to confirm the nature of cells escaping the body of the main tumour spheroid. Immunohistochemical staining was undertaken by the STH Histopathology Service, using validated positive and negative tissue controls.

Figure 8.0: Example Selection Tool Mark-Up of Cells in Escape Zone

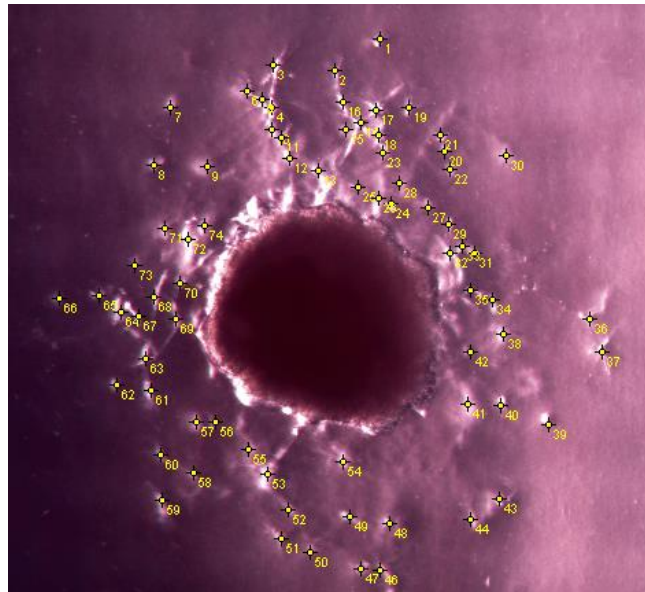


Figure 8.0: Photomicrograph demonstrating Image J count of in-focus cells in peri-spheroid escape zone (defined as the region without direct cellular contact against the established tumour spheroid surface). UPCI SCC072 co-cultured with fibroblasts in the absence of inhibitor has been used for illustrative purposes. Numbered cross-hashes indicate each counted cell; note that single cell bodies versus tight cell clusters are likely to be indistinguishable.

Results

Figure 8.1: Representative Photomicrographs of DED Organotypic Models at 7 & 14 Days in Cell Lines HTE E6E7, UPCI SCC02, UPCI SCC072, UPCI SCC089 and UPCI SCC090

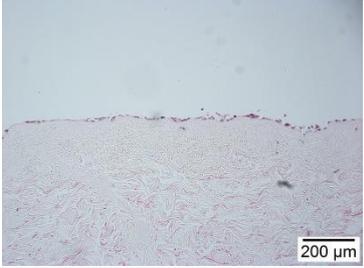
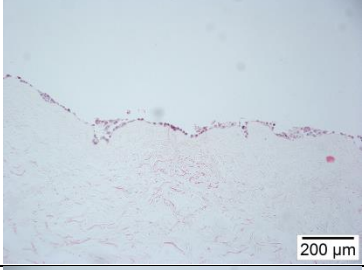
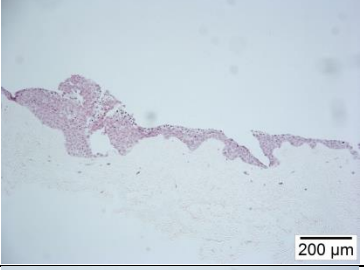
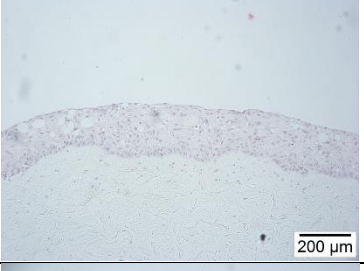
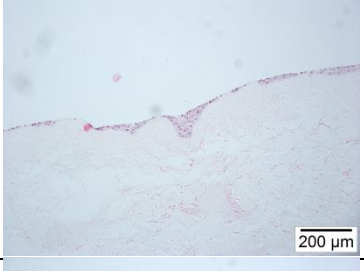
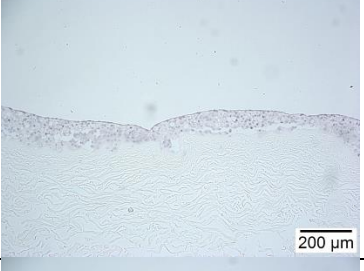
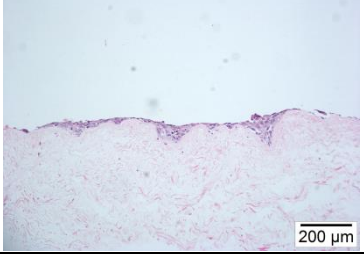
Cell Line	7 days	14 days
HTE E6 E7		
UPCI SCC 02		
UPCI SCC072		
UPCI SCC089		
UPCI SCC090		

Figure 8.1: Representative photomicrographs of DED organotypic models (n=3) of cell lines UD SCC02, UPCI SCC072, UPCI SCC089, UPCI SCC090, plus HTE E6 E7 immortalised tonsillar keratinocytes at days 7 & 14, taken under X10 objective lens. Note that all cell lines developed a stratified squamous-type epithelial layer. Minimal evidence of frank invasion can be observed; pseudo-invasion was observed in cell line UPCI SCC02 at 14 days, whereby a hair follicle became populated by tumour, although the remainder of the specimen comprised a stratified surface lining. No islands of bona fide invasion can be observed in any of the lines. A number of isolated cells can be observed beneath the basal layer in the 14-day models for lines UD SCC02 and UPCI SCC072, although the significance of this is uncertain; concern was raised that the small cell size of UD SCC02 may have allowed apparent invasion as a result of progression through artefactual porosities in the DED as a result of processing prior to use. Irrespective of the true nature of the sub-basal cells, a quantitative measure of invasion was deemed unfeasible.

The appearance of 14-day models for cell lines UPCI SCC072 and UPCI SCC089 was consistent with H&E sections of Cultrex™ spheroid models presented in Figures 8.6 & 8.7. Cell line UPCI SCC072 can be observed as densely packed cells with poor, yet discernible basal organisation, along with microcystic regions appearing in the equivalent of the spinous layer – attempts at basal layer formation along with microcystic regions are also visible in H&E sections of Cultrex™ models (Figure 8.6). Similarly, UPCI SCC089 adopted a comparable profile to that observed in Cultrex™ models, with numerous intercellular spaces and haphazard cell arrangement throughout (Figure 8.7).

Figure 8.2: Representative Photomicrographs of Collagen-based Organotypic Models at 14 Days in Cell Lines UPCI SCC02 and UPCI SCC072

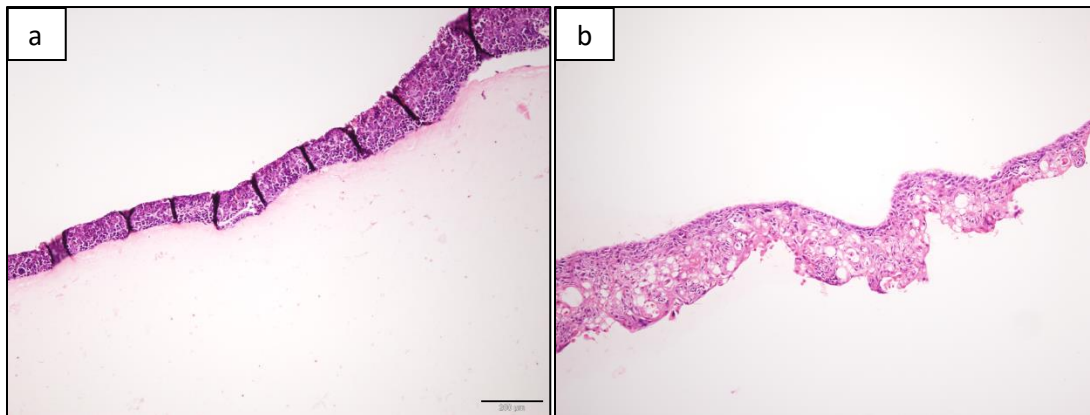


Figure 8.2: Representative photomicrographs of collagen-based organotypic models of cell lines UD a). SCC02 and b). UPCI SCC072 at 14 days, taken under X10 objective lens (n=3). Note that both lines developed a stratified squamous-type epithelial layer comparable to DED models, albeit with a general trend towards thinner overall stratification. Cell line UPCI SCC072 separated from underlying collagen matrix on processing in all repeats, although the matrix was reviewed separately to confirm absence of invading cells/epithelial islands. As with DED-based models, minimal evidence of bona fide islands of cellular invasion can be observed with both lines. Again, a quantitative measure of invasion was deemed unfeasible.

Figure 8.3: Cultrex™ Tumour Spheroid Invasion Assay, Cell Line UPCI SCC089

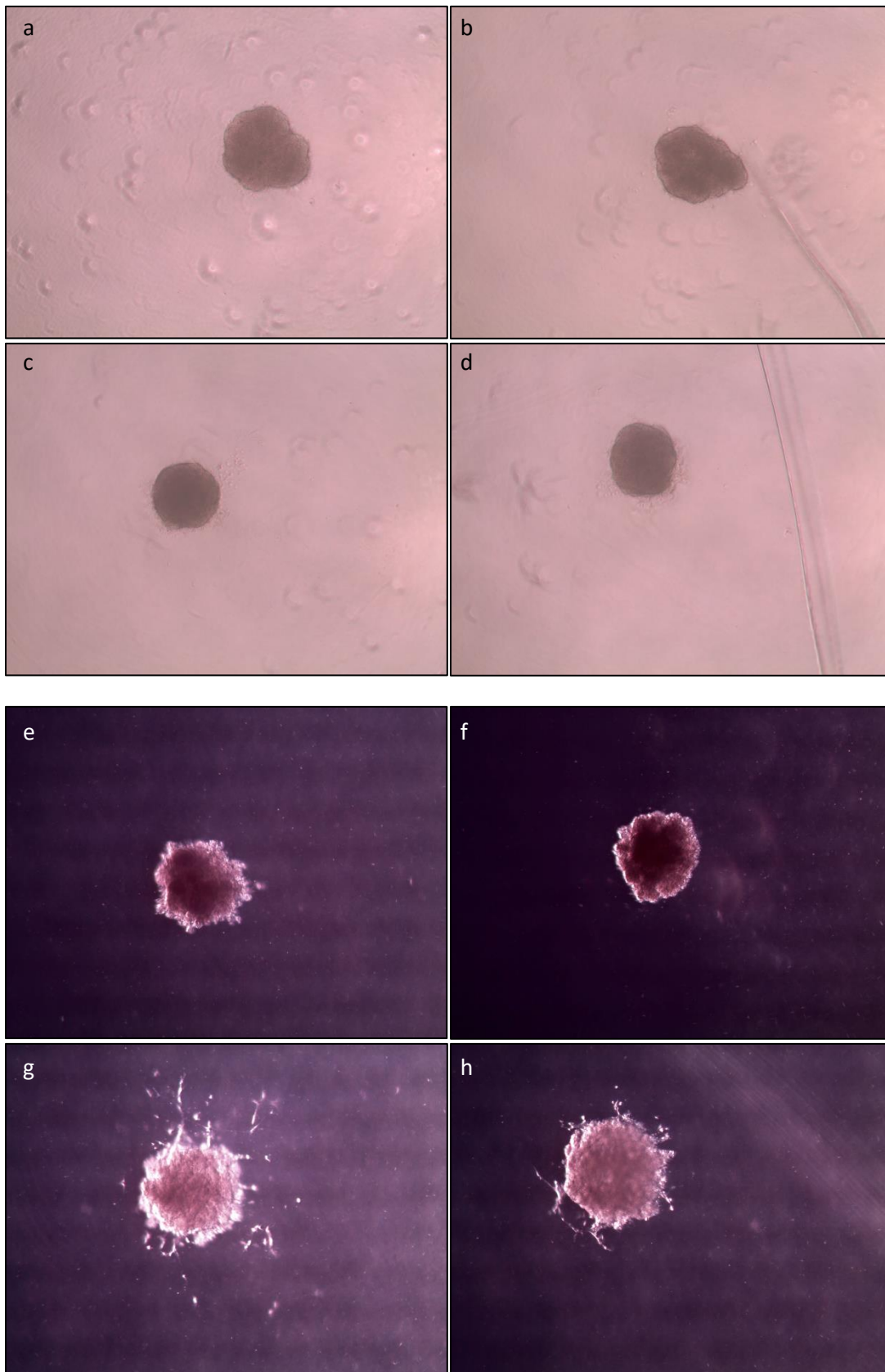


Figure 8.3: Cultrex™ spheroid invasion assay, cell line UPCI SCC089. Baseline (a-d) and invasion day 6 endpoint (e-h) micrographs taken at X4 objective. Note that for endpoint micrographs, a different filter was used with identical microscope and objective lens in order for more accurate imaging as a result of increased spheroid density over the experimental period. Representative images selected, based on quantitative data presented in Figure 8.5, images of baseline and endpoint invasions are paired.

a). & e). Spheroid comprising cell line UPCI SCC089 alone, exposed to DMSO control over the invasion period

b). & f). Spheroid comprising cell line UPCI SCC089 alone, exposed to 60 nM foretinib over the invasion period

c). & g). Spheroid comprising cell line UPCI SCC089 with 1:6 admixed DENOF08 fibroblasts, exposed to DMSO control over the invasion period

d). & h). Spheroid comprising cell line UPCI SCC089 with 1:6 admixed DENOF08 fibroblasts, exposed to 60 nM foretinib over the invasion period

Note that spheroids comprising cell lines alone demonstrated minimal evidence of migration, both in foretinib and control experiments (Figures e & f). Spheroids comprising both cell lines and admixed fibroblasts can be seen to clearly invade the surrounding matrix in the presence of DMSO control (Figure g). This invasion is abrogated in the presence of 60 nM foretinib (Figure h), although a smaller proportion of invading cells is still observed.

Figure 8.4: Cultrex™ Tumour Spheroid Invasion Assay, Cell Line UPCI SCC072

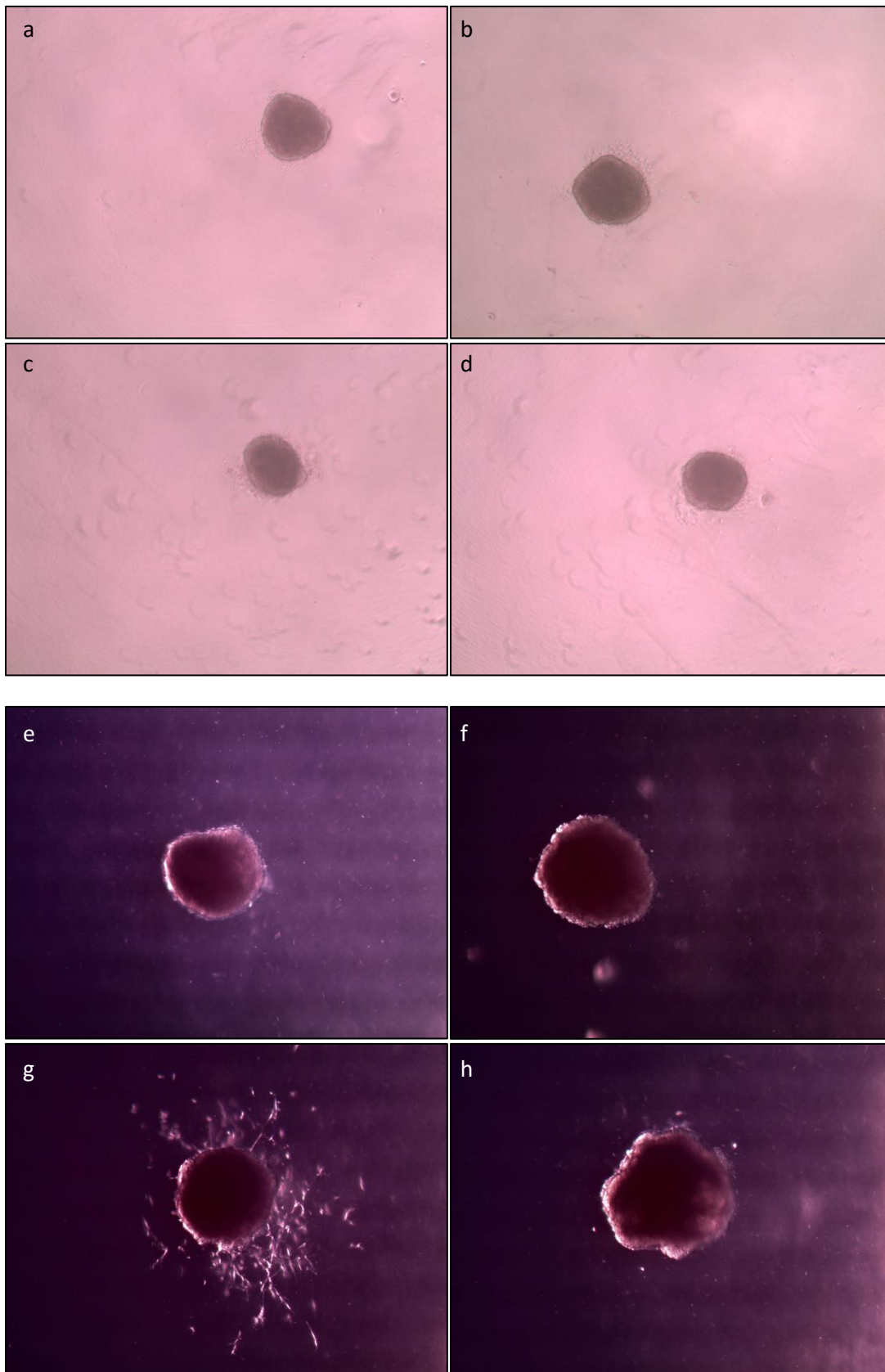


Figure 8.4: Cultrex™ spheroid invasion assay, cell line UPCI SCC072. Baseline (a-d) and invasion day 6 endpoint (e-h) micrographs taken at X4 objective. Note that for endpoint micrographs, a different filter was used with identical microscope and objective lens in order for more accurate imaging as a result of increased spheroid density over the experimental period. Representative images selected, based on quantitative data presented in Figure 8.5, images of baseline and endpoint invasions are paired.

a). & e). Spheroid comprising cell line UPCI SCC072 alone, exposed to DMSO control over the invasion period

b). & f). Spheroid comprising cell line UPCI SCC072 alone, exposed to 60 nM foretinib over the invasion period

c). & g). Spheroid comprising cell line UPCI SCC072 with 1:6 admixed DENO08 fibroblasts, exposed to DMSO control over the invasion period

d). & h). Spheroid comprising cell line UPCI SCC072 with 1:6 admixed DENO08 fibroblasts, exposed to 60 nM foretinib over the invasion period

Note that spheroids comprising cell lines alone demonstrated minimal evidence of migration, both in foretinib and control experiments (figures e & f). Spheroids comprising both cell lines and admixed fibroblasts can be seen to clearly invade the surrounding matrix in the presence of DMSO control (figure g). This invasion is abrogated in the presence of 60 nM foretinib (figure h), although a small number of invading cells are still observed.

Figure 8.5a: Cultrex™ Assay Invasion of Cell Line UPCI SCC089

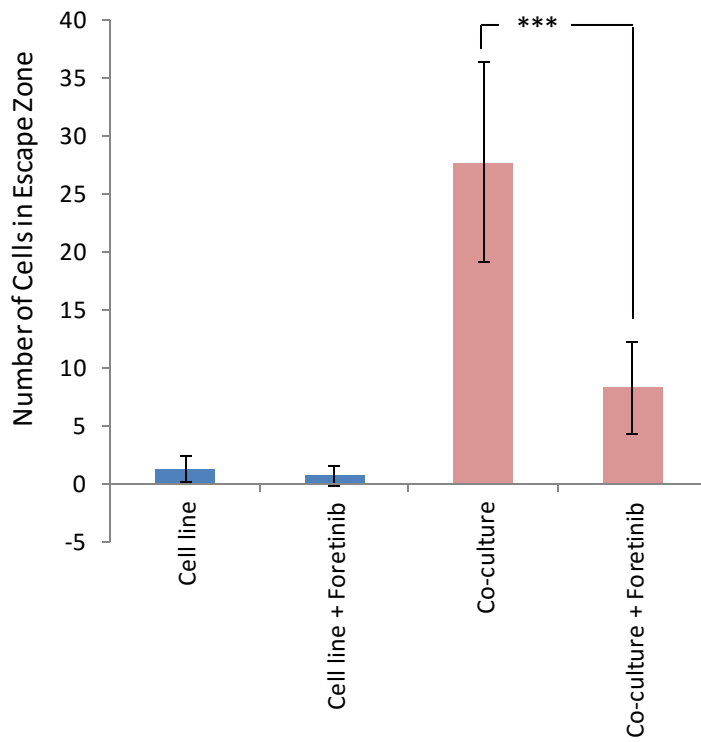


Figure 8.5b: Cultrex™ Assay Invasion of Cell Line UPCI SCC072

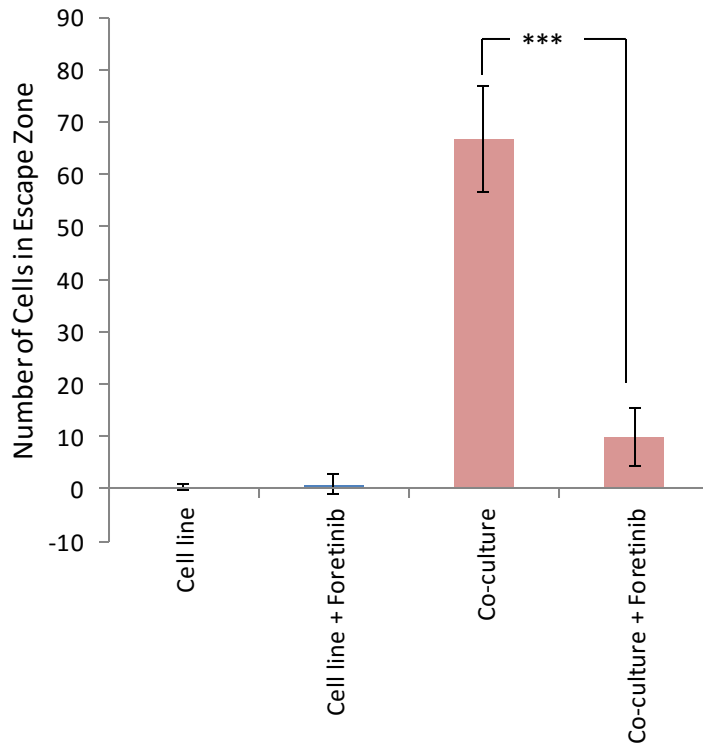


Figure 8.5a & b: Bar charts summarising Cultrex™ invasion assay of cell lines UPCI SCC089 (a) and UPCI SCC072 (b). Y-axis denotes number of in-focus cells counted in the peri-spheroid escape zone. n=9, Error bars denote Standard Deviation. Pink bars denote Co-culture spheroids (cell line plus fibroblasts), blue bars denote cell line monoculture.

*** - $P < 0.001$, Mann Whitney U-test, comparison between indicated groups

Note that in the case of both cell lines, minimal evidence of invasion was observed in the absence of co-cultured fibroblasts (blue bars). Co-culture of cell lines with admixed fibroblasts led to significant invasion (pink bars), although exposure to inhibitor over the experimental period led to marked abrogation of the number of cells counted in the peri-spheroid escape zone.

Figure 8.6: H&E Sections of Cultrex™ Tumour Spheroids, Cell Line UPCI SCC072

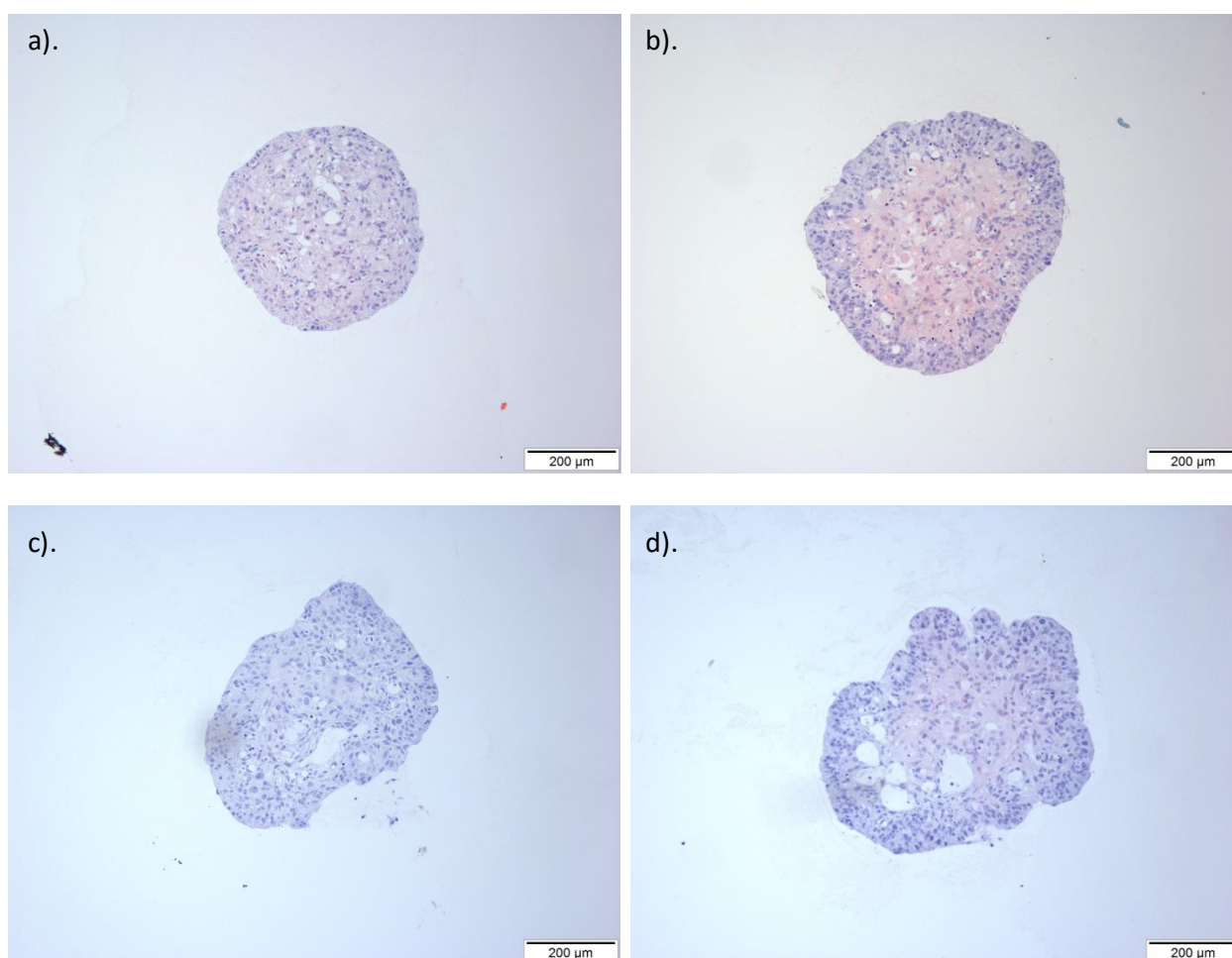


Figure 8.6: H&E sections of day 6 Cultrex™ spheroid invasion assay, cell line UPCI SCC072. Micrographs taken at X10 objective. Representative images selected, based on those inspection of spheroids surviving the paraffin embedding process.

a). Spheroid comprising cell line UPCI SCC072 alone, exposed to DMSO control over the invasion period. Note that a single eosinophilic cell can be observed free of the tumour spheroid in the lower right region of the micrograph. No other evidence of invasion into the surrounding matrix can be observed.

b). Spheroid comprising cell line UPCI SCC072 alone, exposed to 60 nM foretinib over the invasion period. Note that a single cell can be observed free of the tumour spheroid in the upper right region of the micrograph. No other evidence of invasion into the surrounding matrix can be observed.

c). Spheroid comprising cell line UPCI SCC072 with 1:6 admixed DENOF08 fibroblasts, exposed to DMSO control over the invasion period. Note that a number of cells free of the tumour spheroid can be observed to the lower right of the image, in addition to occasional cells to the lower left of the image. This is consistent with inverted lens microscope findings presented in Figure 8.4.

d). Spheroid comprising cell line UPCI SCC072 with 1:6 admixed DENO08 fibroblasts, exposed to 60 nM foretinib over the invasion period. Note that again, there is minimal evidence of invasion into the surrounding matrix. Two isolated cells can be observed to the left of the image.

Note also that the gross histological features of the spheroids are consistent with organotypic models presented in Figures 8.1 & 8.2, whereby microcystic lesions in combination with attempts of cellular organisation at the spheroid periphery can be observed.

Figure 8.7: H&E Section of Cultrex™ Tumour Spheroid, Cell Line UPCI SCC089

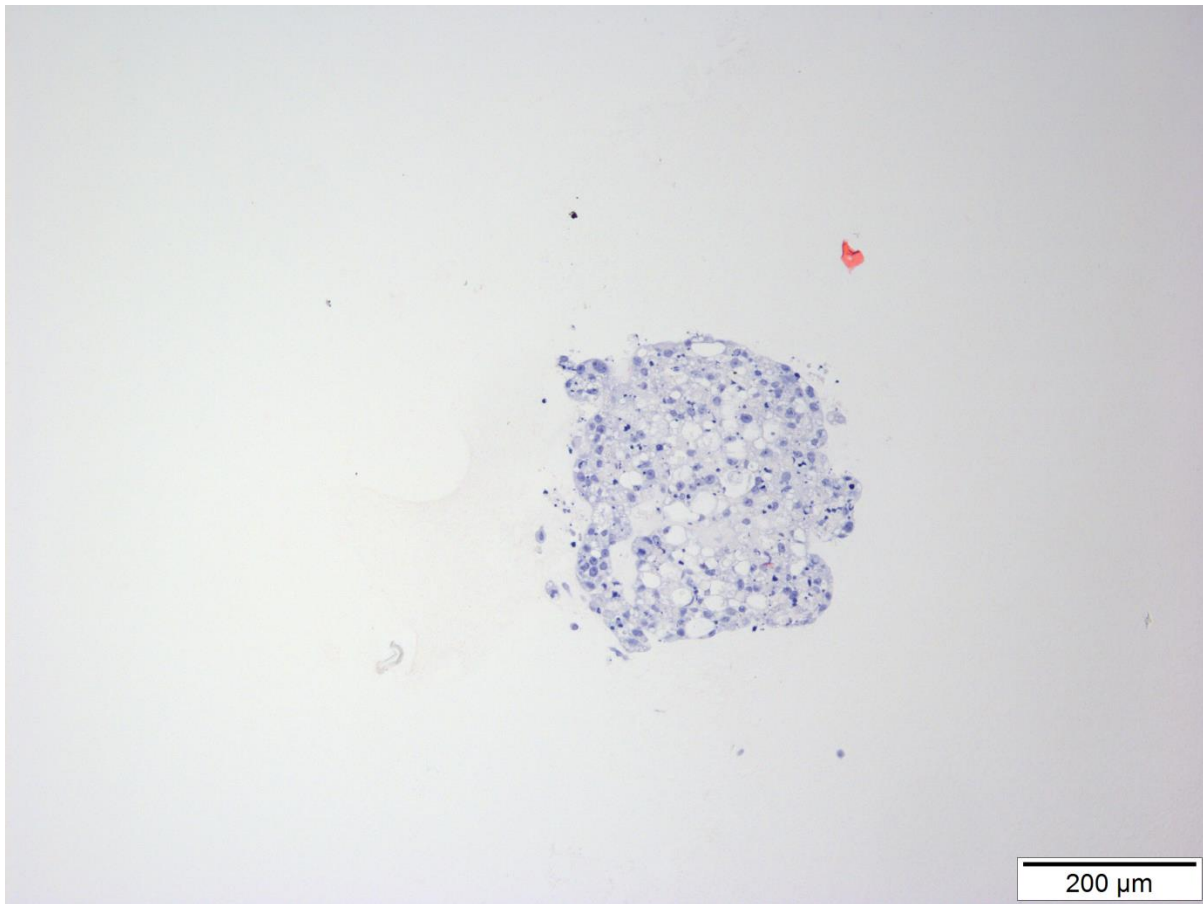
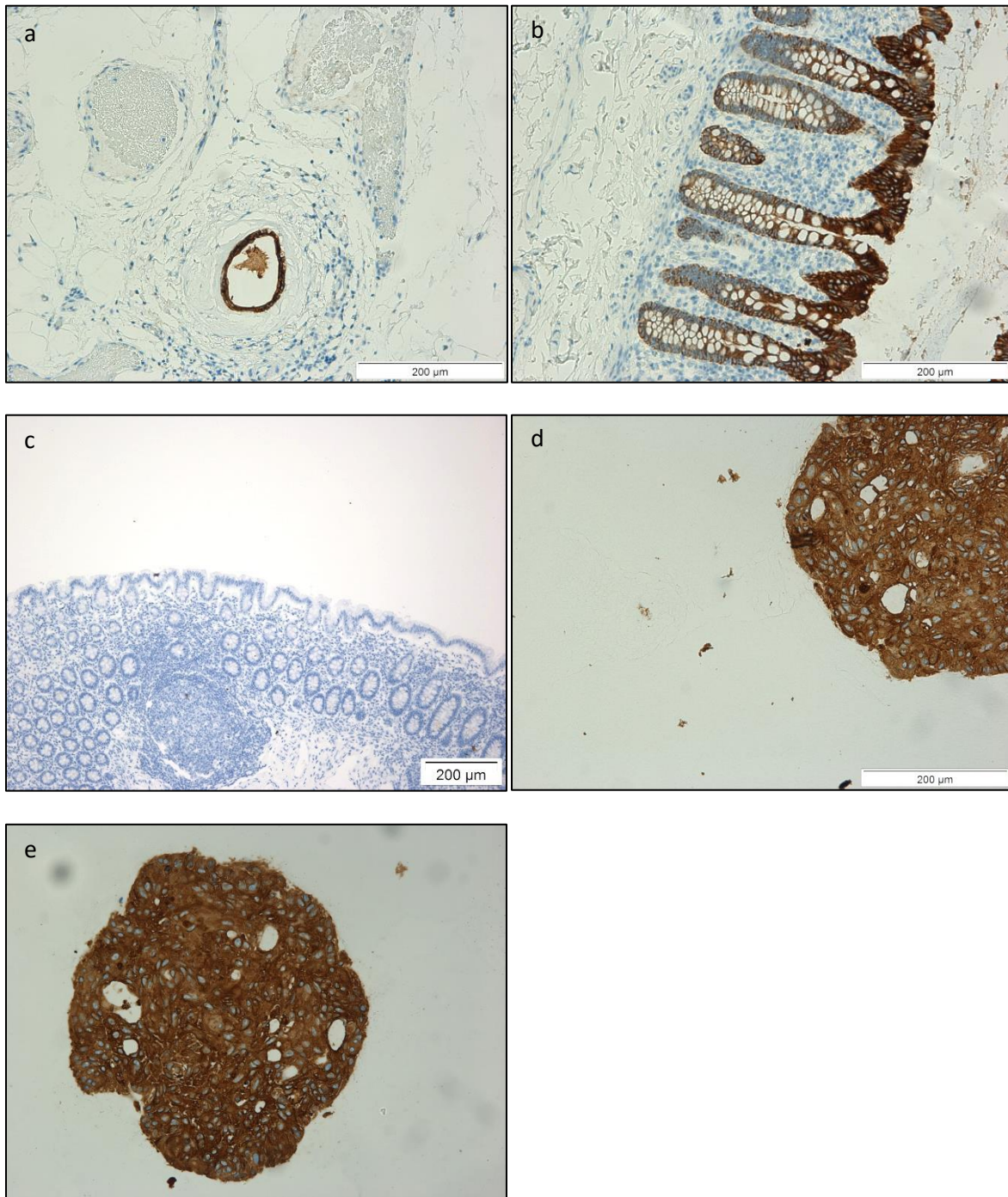


Figure 8.7: H&E section of day 6 Cultrex™ spheroid invasion assay, cell line UPCI SCC089. Micrographs taken at X10 objective. Representative image selected of single experimental condition; all other conditions did not survive the paraffin embedding process.

Spheroid comprising cell line UPCI SCC089 with 1:6 admixed DENO08 fibroblasts, exposed to DMSO control over the invasion period. Note that a number of cells free of the tumour spheroid can be observed to the left of the image, in addition to occasional cells to the lower right of the image. A further eosinophilic cell can be observed in the upper region of the image. As for cell line UPCI SCC072, H&E sectioning are again consistent with inverted lens microscope findings presented in Figures 8.1 and 8.2.

Note that all other conditions relating to Figure 8.3 failed to survive the paraffin embedding process.

Figure 8.8: Cytokeratin AE1/3 Staining of UPCI SCC072 Co-Culture Model



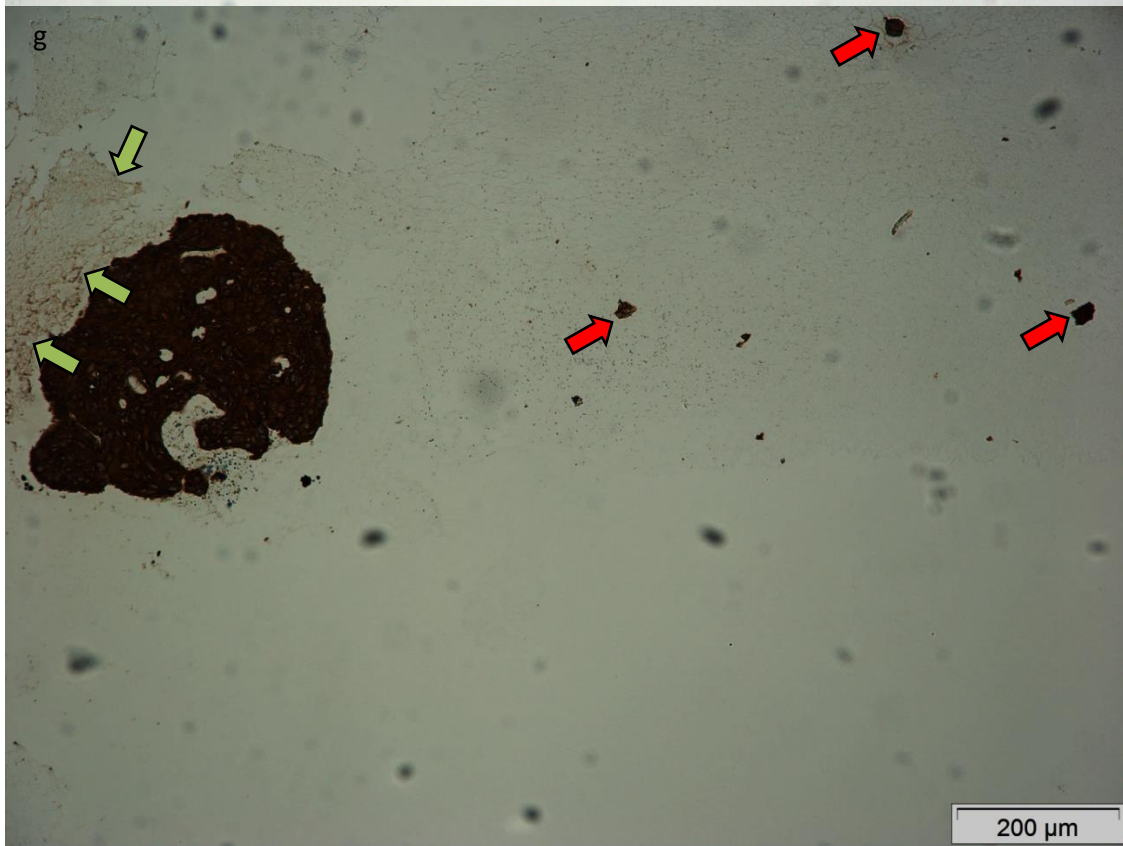
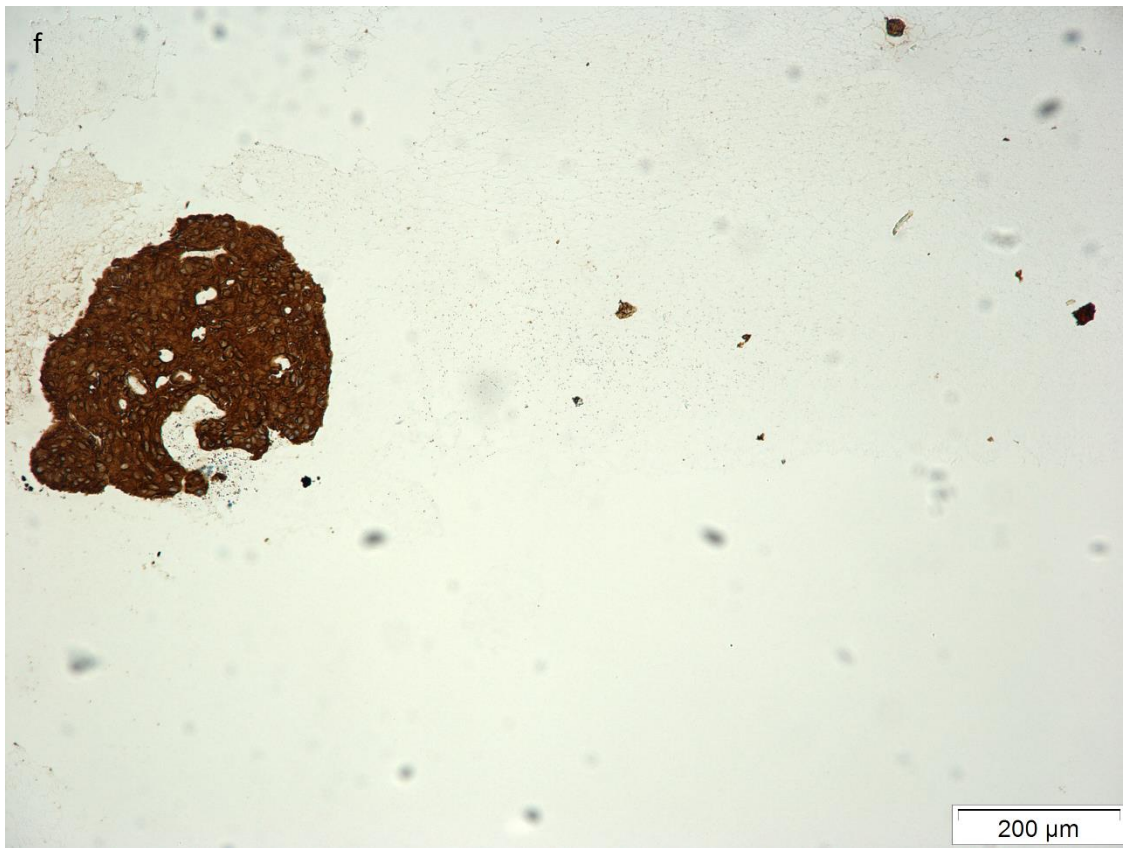


Figure 8.8: Cytokeratin AE1/3 immunohistochemistry staining of UPCI SCC072/DENOF08 spheroid co-culture in the presence of DMSO control.

a). & b). Lung & colorectal control tissue – note the highly specific positive staining of lining epithelium

c). Negative control (direct incubation with secondary antibody without exposure to primary), X10 objective view – note the absence of staining throughout the specimen

d). & e). X20 objective views of UPCI SCC072/DENOF08 spheroid co-culture models. A number of cytokeratin-positive cells can be observed free of the main spheroids

f). X10 objective view of UPCI SCC072/DENOF08 spheroid co-culture model. Again, a number of cytokeratin-positive cells can be observed free of the main spheroid

g). X10 object view of co-culture model illustrated in f, manipulated to -30 % brightness & +30 % contrast in order to visualise invasion matrix surrounding the main tumour spheroid. Note that although a small portion of invasion matrix tearing and retraction can be observed from the main tumour spheroid (green arrows), a number of cytokeratin-positive cells are embedded within the invasion matrix, confirming cellular escape from the tumour spheroid rather than a processing artefact. Positive cytokeratin staining of cells escaping the main tumour spheroid confirms that the imaged cells are tumour lines rather than fibroblasts

Discussion

The limitations of 3D organotypic modelling of tumour invasion have been broached in the introduction section of this chapter. A major drawback of using anatomically representative tissue such as DED is that inherent variations in tissue structure may influence the interpretation of apparent differences between treatment and control groups. Even the use of more homogenous dermal substitutes, such as collagen and/or matrigel are often limited to qualitative interpretation⁵⁵³. Jenei *et al* developed a computer-assisted method of analysing organotypic model invasion in order to ascribe quantitative analysis to such models⁵⁵³, although the distinct lack of invasion observed with the oropharyngeal carcinoma lines studied, as illustrated in Figures 8.1 & 8.2 rendered attempts of quantifying invasion as futile. Far greater success in quantifying 3D interactions was achieved using Cultrex™ 3D spheroid models, where quantitative, measurable differences were observed between experimental conditions.

3D spheroids comprising the HPV-negative carcinoma lines UPCI SCC072 or UPCI SCC089 with admixed DENO08 fibroblasts undertook marked invasion in Cultrex™ assays, which became significantly restricted in the presence of 60 nM foretinib. Those spheroids containing carcinoma lines alone demonstrated almost no evidence of invasion, irrespective of the presence of c-Met inhibitor. These findings suggest that as observed in 2D migration experiments, invasion is reliant on microenvironmental support, and HGF appears to be a fundamental mechanism by which cellular escape from the body of a HPV-negative tumour may occur.

Ideally, dose-response analysis of foretinib in 3D spheroid invasion assays for both cell lines, including greater concentrations of foretinib than were utilised in the presented data, would allow more comprehensive assessment of foretinib's capacity to fully refrain invasion *in-vitro*. Unfortunately, due to assay expense, extending work to include 3D dose-response analysis was not feasible. Irrespective of this limitation, foretinib demonstrated a profound capacity to inhibit invasion at concentrations relevant to both our 2D tissue culture experiments and also work by Qian *et al*, who found inhibition of matrigel invasion of the melanoma line B16F10 at concentrations above 40 nM⁴³⁵.

Cytokeratin AE1/3 analysis of UPCI SCC072/DENO08 spheroid co-cultures presented in Figures 8.8d-g confirm the invading population imaged in Figure 8.6c comprises cells of

epithelial origin, and therefore represent bona-fide tumour cell invasion rather than simple migration of stroma. Rudisch *et al*²⁹⁰ undertook invasion assay analyses of NSCLC spheroids in a comparable manner to our work; the group found similar promotion of invasiveness upon co-culture of two NSCLC cell lines with a range of stromal fibroblasts. Rudisch *et al* also employed a method of counting single cells to quantify invasion into the surrounding matrix; as with our data, the size of the spheroid mass presented in Rudisch's paper varied little between treatment and control groups, whereas profound cellular invasion and scatter can be observed in response to co-culture. The group undertook tagRFP (red) stable transfection of fibroblasts, along with TurboGFP (green) stable transfection of cell lines; whilst this method offered immediate visual distinction between tumour lines and fibroblasts, the additional steps of undertaking stable transfection were necessary in place of a relatively simple process of cytokeratin analysis. This method does however represent an expensive, yet robust alternative to the cytokeratin analysis undertaken in this chapter. Rudisch also referred to a "cytokine fingerprint" of GM-CSF, GRO- α , GCP-2, VEGF, IL6, RANTES and IL8 occurring in co-cultures, which is again consistent with the findings of our cytokine array data, and furthermore went on to demonstrate that a c-Met inhibitor, crizotinib, led to a reduction of cell line invasion.

Many authors have noted significant differences in drug performance when transferring work from a 2D to 3D *in-vitro* setting, due to the introduction of concentration gradients and hypoxic barriers to therapeutic effect that are not of concern in 2D culture. Foretinib appears to have been exceptional to this phenomenon, with significant biological effects occurring at comparable concentrations in both 2D and 3D cultures. This finding is not entirely idiosyncratic, as the functional effect of foretinib has been measured through analysis of cellular escape from tumour spheroid surface, whereby a number of the features of 3D tumour drug resistance which protect cells at the central core of the spheroid are no longer relevant. This finding may infer a clinical benefit from foretinib irrespective of tumour size, as it appears that unimpeded drug access to the tumour surface alone may be adequate for efficacy. It is however, likely that the greatest therapeutic benefit of foretinib may be in the management of early disease, whereby the arrest of cellular escape from the leading front of a tumour may translate into avoidance of micrometastasis and therefore a greater chance of tumour clearance with standard therapy. Induction therapy may therefore offer additional value in the clinical application of this drug; a strategy which has not been employed to

date^{554, 555}. Indeed, the prognostic significance of a discohesive-type invasive front in oral carcinoma has for some time been acknowledged⁵⁵⁶, and steps to therapeutically downgrade this invasive pattern through restraint of HGF in early tumours prior to standard therapy appear sensible, in addition to a post-therapeutic maintenance schedule. This concept may also have significant implications for the broader context of surgical management of head and neck disease, whereby marginal integrity of excisions are hard to confirm in terms of single /small cell populations.

Use of foretinib in the management of early disease in the manner described above may limit disease relapse to local recurrences rather than regional or metastatic spread, due to restriction of cellular motility. Care must therefore be taken to ensure appropriate primary outcome measures are selected for any prospective clinical study of early disease management; for example, analysis of locoregional control may potentially infer an insignificant or even deleterious effect of foretinib, whereas metastatic spread may be reduced, or overall survival improved.

In conclusion, 3D modelling of the microenvironment has confirmed findings relating to earlier 2D experiments. HGF inhibition in 3D models has the alluring prospect of retaining as great an efficacy in 3D as was observed in 2D experiments. HGF inhibitors offer great scope in the management of HPV-negative oropharyngeal carcinoma, although our findings suggest an application in the prevention of early cancer spread, rather than delivery of c-Met inhibition with curative intent. It is therefore not surprising that HGF inhibitor trials conducted on late stage, chemo- and/or radiotherapy-resistant disease have often demonstrated modest results. Combination of HGF inhibitors with standard chemo-radiotherapy protocols in early disease is an intuitive method of integrating the benefits of motility inhibition into treatment that can still be delivered with curative intent.

Chapter 9: Further Work

Introduction

A number of findings discussed within this thesis warrant further investigation. *In-vitro* modelled tumour-stromal interactions have been investigated in terms of the fibroblast secretory response to tumour stimulation and the effect thereafter on tumour behaviour, yet we have not assessed the factor(s) responsible for initial fibroblast stimulation. Whilst the mechanism of the fibroblast response to HPV-negative cell line conditioned media appears linked to induction of a senescence-associated secretory profile, offering insight into likely factors released by HPV-negative carcinoma lines, much work is necessary to confirm the basis of initial fibroblast recruitment. Discerning key fibroblast-inducing factors may offer exciting therapeutic opportunity, which may in turn be progressed to clinical trial in a similar manner is outlined for HGF inhibitors (discussed below).

In addition to analysing upstream regulators of the fibroblast response, further investigation of the nature of IL-6 synergism with HGF may also offer greater insight into the most favourable tailored therapeutics to manage HPV-negative disease. Chapter 6 has presented the hypothesis of STAT3 induction by both HGF and IL-6 leading to a synergistic effect on cell migration. STAT3 is one of many possible secondary messenger systems that could be responsible for the synergism, due to the pleiotropic nature of the cytokine IL-6. A number of alternative pathways remain plausible, as have been described by Nechemia-Arbely *et al* in the context of acute liver injury⁴⁹⁵ (reviewed in further detail in Chapter 6). Deciphering the secondary messenger pathway responsible for the IL-6 bolstering of HGF-induced migration may again offer scope for therapeutics – a common migratory pathway of synergistic STAT3 signalling by both IL-6 and HGF would offer a single target for therapeutic blockade, whereas interactions between HGF and IL-6 via alternative pathways as reported by Nechemia-Arbely *et al* would infer that upstream blockade of the chief fibroblast inducing factor may be more appropriate in order to control IL-6/HGF signalling using a single drug.

We have alluded to the potential role of ADAMs 17 & 10 in driving the membranous release of activating factors from HPV-negative lines. A number of soluble receptors were found to be released into HPV-negative cell line conditioned media, including sIL-6R, sEGFR and uPAR. As well as offering scope for further investigation, membrane snippase activity may

contribute to a disparity between transcriptome and secretome – care must therefore be taken when employing strategies to determine fibroblast activating factors released by HPV-negative lines; simple PCR quantification, although insightful, may not directly correlate to the secretome and therefore insignificant findings at the RNA level may represent false negatives.

We have also discussed the cytokine array finding of sEGFR within HPV-negative tumour conditioned media, and have discussed the potentially complex relationship between membranous EGFR, EGFR activating mutations and solubilised receptor “decoy” release; each of these variables may influence the overall value of cetuximab in the management of resistant oropharyngeal carcinoma. Erlotinib, a tyrosine kinase inhibitor active against EGFR signalling, offers a therapeutic strategy to circumnavigate limitations of cetuximab with respect to receptor decoy release and also potentially with respect to activating mutations. ELISA analysis of oropharyngeal carcinoma line release of sEGFR in combination with analysis of cetuximab/erlotinib toxicities may help determine whether targeting the tyrosine kinase domain of EGFR (erlotinib) has advantages over receptor domain blockade (cetuximab).

Indeed, there is recent evidence published by Hartmann *et al* that oral and laryngeal HNSCC cell lines may be more responsive to the EGFR tyrosine kinase domain-inhibitors, erlotinib and gefitinib, than to the ectodomain-inhibitor cetuximab⁵⁵⁷, although much of the improved response may be attributable to the investigated cell lines expressing EGF-independent receptor activations rather than a consequence of tyrosine kinase domain inhibitors circumnavigating the influence of receptor decoy release. Clinical data have for some time iterated the role of tyrosine kinase domain activating mutations in predicting therapeutic response to gefitinib in NSCLC⁵⁵⁸; an evidence-based analysis commissioned by Medical Advisory Secretariat, Ontario, found moderate-quality evidence to support EGFR activating mutations in predicting gefitinib response and similar, low-quality evidence to support erlotinib’s use in a comparable manner⁵⁵⁹. It is therefore feasible that the aforementioned observations linked to HNSCC cell lines relate in part to a self-selecting group responsive to erlotinib/gefitinib, as 4/5 cell lines in Hartmann’s study displayed EGF-independent growth behaviour due to receptor activation. Nonetheless, EGFR mutations are common in HNSCC, and therefore the findings of Hartmann *et al* may have direct applicability to this common mutated subset of tumours.

We propose that as an ectodomain-targeting therapeutic, cetuximab's activity may be obstructed by sEGFR decoy; suggesting that in the case of high sEGFR load, tyrosine kinase domain-inhibitors may be more effective at restraining EGFR signalling. Conversely, cetuximab's efficacy would be anticipated to be greater against non-sEGFR secreting tumours. This proposition has a subtle, yet important difference to the experimental questions posed by Hartmann *et al*, as sEGFR status may be a prognosticator independent of EGFR mutation status, and may be used as a predictor of cetuximab efficacy, and potentially as decision aid in determining whether to deliver cetuximab versus erlotinib/gefitinib. Importantly, kinase-domain inhibitors appear to have limited benefit in the management of wild-type EGFR-expressing tumours⁵⁵⁸, and cetuximab may therefore have a greater role in managing low sEGFR secreting, wild-type mEGFR disease. These features may also be characteristic of HPV-positive oropharyngeal carcinoma due to low mutational load in addition to our findings of low sEGFR secretion in HPV-positive cell lines.

Lococo *et al* found sEGFR to be elevated in the serum of patients with NSCLC in comparison to a normal cohort, and further found sEGFR concentration to correlate with tumour grade⁵⁶⁰. No prognostic impact of sEGFR was noted by the group despite careful analysis of plasma sEGFR concentration as both a continuous variable and using a minimum cut-off value. It should however be noted that the therapeutic regime used for the patient cohort was unreported – it is therefore feasible that treatment either excluded EGFR inhibitor therapy, or alternatively involved the use of erlotinib/gefitinib, whereby soluble receptor decoy may be irrelevant to therapeutic effect. The function of sEGFR in predicting tumour response to cetuximab may be somewhat disparate from that of gefitinib and erlotinib for the reasons outlined above. Moreover, experimental data presented in Lococo's paper further demonstrated an inhibitory effect of sEGFR on cell line proliferation and migration – it is therefore feasible that in addition to acting as a receptor decoy, cetuximab binding of sEGFR may negate the intrinsic inhibitory properties of the solubilised receptor.

HGF as a principal molecule for microenvironmental support of cell migration offers great scope in therapeutic management of HPV-negative disease. The potential for HGF inhibition in the management of early, rather than late disease, has been discussed in Chapter 8. In order to progress to a Phase II clinical trial, xenograft modelling of HGF inhibitors in HPV-negative tumours for both early and late disease is an important step. Previous Phase II trials of HGF inhibition in late stage solid tumours inclusive of the head and neck region have shown limited benefit⁴³³, and therefore may undermine support for clinical trial of the

respective inhibitors in early disease without further evidence from an animal model, in order to distinguish the role of treatment in early rather than late stage disease. Xenograft data are available with respect to the use of HGF inhibitors in the management of murine model of HNSCC, although the primary outcome measure assessed was tumour xenograft volume at 12 days⁴¹⁸. The authors found a 60-70 % reduction in tumour volume in the presence of crizotinib; whilst this finding suggests further benefit of HGF inhibitors in the management of HPV-negative oropharyngeal disease through the inhibition of tumour growth, no direct analysis of tumour invasion and metastasis was undertaken.

IL-6 support of HGF-induced migration has not been conclusively demonstrated in response to stimulated fibroblast media; its role has been assumed on the basis of ELISA quantification and co-incubation of biologically relevant concentrations of recombinant IL-6 with HGF in migration experiments – the use of an IL-6 inhibitor such as tocilizumab may offer confirmation of this initial evidence in a similar manner to foretinib/INCB28060 for HGF (please refer to Chapter 6). Tocilizumab is a monoclonal IL-6 receptor antibody, and is the first drug in its class to have progressed to late clinical trial⁵⁶¹. Negotiation of supply of tocilizumab for use in research is ongoing, although provisional scientific approval has been granted by Roche (St. Albans UK); supply of the drug for use in research has been hampered by international supply agreements between US and European branches.

As discussed in Chapters 3 & 7, induction of fibroblast senescence appears central to the secretory profile observed in conditioned media experiments. Although fibroblast senescence has been investigated in detail, broader analysis of the fibroblast phenotypic change in response to conditioned media may be beneficial. Markers of myofibroblast formation, such as α -SMA, may help determine whether the fibroblast response is purely senescent, or whether further aberrations occur in non-senescent sub-populations, leading to a more complex fibroblast profile. Provisional work suggests that TGF- β , a classic inducer of myofibroblast formation, is absent from conditioned media (please refer to Chapter 3); a negative finding in terms of a HPV-negative cell line induced myofibroblastic profile may therefore be as insightful as a positive result, as this would offer further evidence of a microenvironmental pathway exclusive of TGF- β .

Histopathological analysis of markers of both senescence and myofibroblastic differentiation in tumour specimens, in combination with IL-6/HGF/STAT status, may allow clinical validation of our *in-vitro* work. To date, we have progressed to retrieval of approximately 150 oropharyngeal carcinoma biopsies dating from 2004-2012, representing all oropharyngeal

carcinomas diagnosed at Sheffield Teaching Hospitals NHS Trust over an 8 year period, all of which have 3 year survival data available. Tissue microarray construction shall allow high-throughput analysis of the aforementioned biomarkers, and can be linked to outcome data which have already been collated.

The remainder of this section shall present initial data relating to a number of the above areas of further investigation and detail a plan of further experimentation.

I. STAT Signalling in Fibroblasts Following Exposure to Cell Line Conditioned Media

In addition to cell lines exposed to stimulated fibroblast media, provisional western blot analysis of STAT3 signalling in fibroblasts exposed to HPV-negative cell line conditioned media was undertaken (single experimental repeat).

Methods

Cell line conditioned media were collected as described in Chapter 2, methods section M2.1. DENO08 fibroblast cultures were raised in T75 flasks to near confluence, washed X3 in PBS and then incubated with either 6 ml normal media or cell line conditioned media for 0 mins, 20 mins or 12 hours. On completion of each respective incubation period, flasks were washed X3 in cold TBS and then incubated with 1 mL cell dissociation solution at 4° C on a rocking machine for 10 mins. Cells were then removed with the assistance of a cell scraper, the suspension transferred to an Eppendorph container, centrifuged at 1,000 rpm 5 mins and then supernatant removed and immediately stored at -80 °C. Protein extraction and western blotting were then undertaken as detailed in Chapter 5, section M5.6.

Experiments were undertaken separately for HPV-positive cell line conditioned media (UD SCC02 and UPCI SCC090) and HPV-negative cell line conditioned media (UPCI SCC072 and UPCI SCC089). Data presented relate to a single experimental repeat, and requires validation.

Results

Figure 9.1: Western Blot Analysis of Fibroblast Total(t) and Phospho(p) STAT3 in Response to HPV-Positive Cell Line Conditioned Media

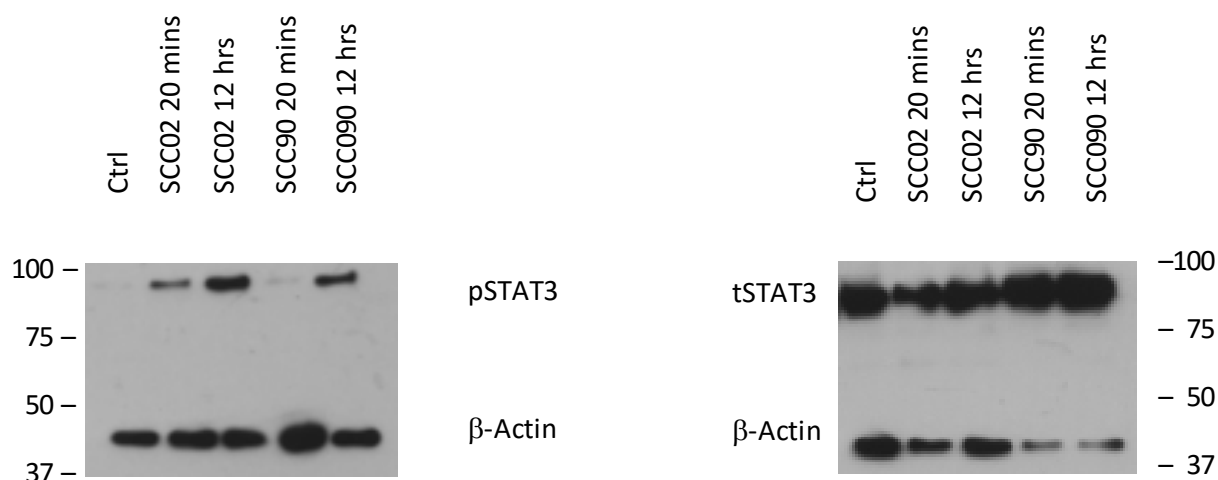


Figure 9.1: Provisional western blot analysis (n=1) of DENOF08 fibroblast cultures in response to HPV-positive cell line conditioned media

Ctrl – DENOF08 fibroblasts incubated for 20 mins in normal media control

SCC02 20 mins – DENOF08 fibroblasts exposed to UD SCC02 cell line conditioned medium for 20 mins

SCC02 12 hrs – DENOF08 fibroblasts exposed to UD SCC02 cell line conditioned medium for 12 hours

SCC90 20 mins – DENOF08 fibroblasts exposed to UPCI SCC090 cell line conditioned medium for 20 mins

SCC90 12 hrs – DENOF08 fibroblasts exposed to UPCI SCC090 cell line conditioned medium for 12 hours

Note that there is minimal evidence of STAT3 phosphorylation in response to UPCI SCC090 conditioned medium at 20 mins, and modest increase in response to UD SCC02 conditioned medium. STAT3 phosphorylation at 12 hours is more pronounced. Total STAT3 appears relatively constant throughout all conditions (Figure b), although uneven loading can be noted in the β-Actin bands, and tSTAT3 bands are overexposed.

Figure 9.2: Western Blot Analysis of Fibroblast Total(t) and Phospho(p) STAT3 in Response to HPV-Negative Cell Line Conditioned Media

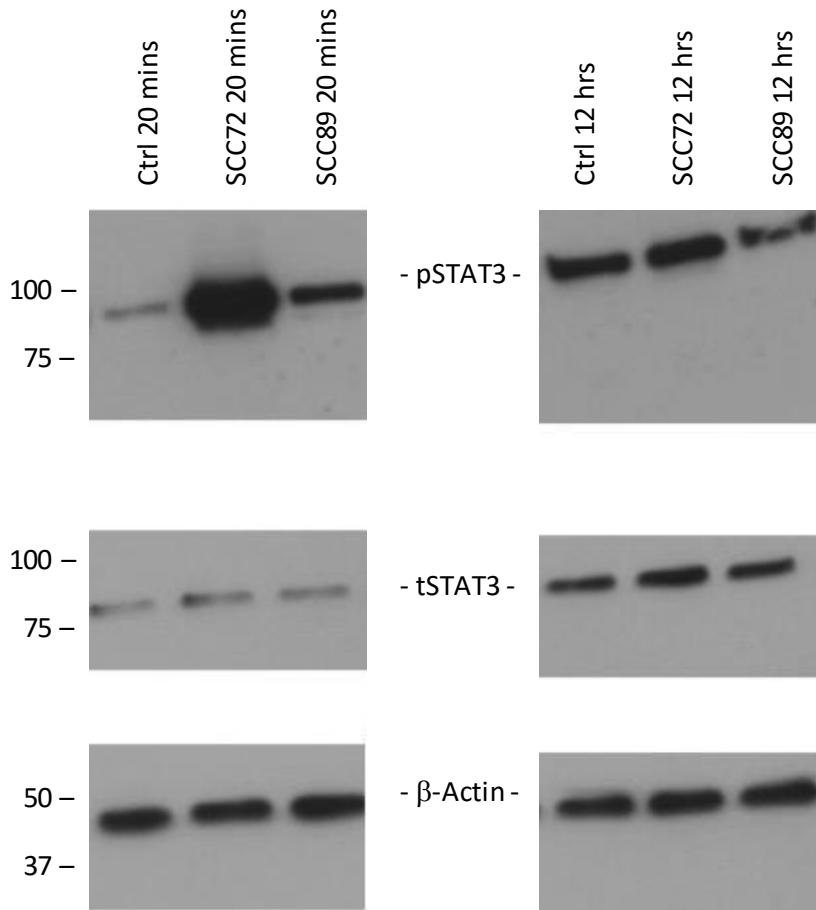


Figure 9.2: Provisional western blot analysis (n=1) of DENOF08 fibroblast cultures in response to HPV-negative cell line conditioned media

Ctrl 20 mins – DENOF08 fibroblasts incubated for 20 mins in normal media control

Ctrl 12 hrs – DENOF08 fibroblasts incubated for 12 hrs in normal media control

SCC72 20 mins – DENOF08 fibroblasts exposed to UPCI SCC072 cell line conditioned medium for 20 mins

SCC72 12 hrs – DENOF08 fibroblasts exposed to UPCI SCC072 cell line conditioned medium for 12 hours

SCC89 20 mins – DENOFO8 fibroblasts exposed to UPCI SCC089 cell line conditioned medium for 20 mins

SCC89 12 hrs – DENOFO8 fibroblasts exposed to UPCI SCC089 cell line conditioned medium for 12 hours

Note that there is minimal evidence of STAT3 phosphorylation in DENOFO8 fibroblasts in the 20-minute control band, whereas there is marked upregulation with exposure to UPCI SCC072 conditioned medium. A moderate degree of STAT3 phosphorylation is also noted with cell line UPCI SCC089 at 20 minutes. At 12 h, conditioned medium control expresses a similar degree of phosphorylated STAT3 as fibroblasts exposed to UPCI SCC072 and UPCI SCC089 cell line conditioned media; the significance of this in relation to 20-minute stimulations is uncertain. This preliminary data suggest that cell lines UPCI SCC072 and UPCI SCC089 may be activating fibroblasts via STAT3, although rises in STAT3 may not necessarily be related to the pathway through which HGF release is promoted. Although the preliminary blots for HPV-negative line-stimulated fibroblasts were undertaken separately from the HPV-positive blots depicted in Figure 9.1, there is a suggestion that STAT3 activation may be more pronounced at 20 mins in HPV-negative line-stimulated fibroblasts. STAT3 signalling may therefore represent a feature of the activating factor responsible for driving fibroblast HGF release, although this evidence is circumstantial. Further work directly comparing HPV-negative and HPV-positive stimulated fibroblasts is necessary to confirm the proportional relationship of STAT3 signalling in response to each respective conditioned medium.

Discussion

On the assumption that STAT3 activation is important to the observed fibroblast response to HPV-negative cell line conditioned media, interrogation of the STAT3 pathway may provide an indication of likely factors driving HGF and/or IL-6 secretion. As discussed in Figure 9.2, one has to bear in mind that even with validation of elevated STAT3 in response to HPV-negative cell line conditioned media, a direct relationship with induction of the HGF response cannot be assumed. However, a number of factors capable of inducing a secretory response similar to that presented in cytokine array data influence intracellular STAT3 levels, such as PDGFA^{562, 563} and IL-17A³³⁸; the finding of STAT3 elevation in response to cell line conditioned media may therefore direct further investigation towards such factors.

The role of STAT3 in driving the secretion of pro-inflammatory factors appears complex and potentially cell-specific; for example IL-8 (a factor noted to be markedly upregulated in the fibroblast response to HPV-negative cell line conditioned media) has been found to be elevated as a result of STAT3-induced Ox-PAPC transcription of IL-8 in aortic endothelia⁵⁶⁴, whereas direct repression of IL-8 by STAT3 has also been reported in Glioma⁵⁶⁵. The subtleties of STAT3 signalling in response to varying cytokines may further account for this discrepancy, with repressors such as SOCS potentially reducing direct STAT3 effects, whereas permitting earlier cellular events in response to STAT3 which may be responsible for IL-8 upregulation. A basis for STAT3 being correlated to upregulation of IL-6 and HGF appears less contentious, as both IL-6 itself and HGF may be upregulated in response to IL-6 signalling, which is known to lead to increased STAT3 (as discussed in Chapters 4 & 6).

Preliminary work has been undertaken through two experimental runs, in which fibroblasts exposed to HPV-positive and HPV-negative lines were separately assessed. HPV-positive versus -negative cell lines cannot therefore be reliably compared, although STAT3 expression does appear increased in fibroblasts stimulated by HPV-negative cell lines at 20 mins. Western blots for HPV-positive stimulated fibroblasts at 20 mins however, do not correlate with the proportionate secretion of HGF, IL-6 or IL-8 in response to cell lines UD SCC02 and UPCI SCC090 (please refer to Chapters 4 & 6 for ELISA data); UPCI SCC090 induced greater fibroblast secretion of HGF/IL-6/IL-8 than did UD SCC02, and therefore a greater amount of STAT3 phosphorylation of fibroblasts would be anticipated at 20 mins should STAT3 signalling underlie the induction of the fibroblast secretory response.

One cannot however fully assume that STAT3 phosphorylation within fibroblasts is occurring through a single mechanism in response to all cell lines. Whilst the fibroblasts response to HPV-negative cell lines is characteristic, and therefore may indeed be the result of a specific STAT3-inducing molecule, there remains potential for the HPV-positive cell line UD SCC02 to release an alternative STAT3 inducing factor which does not have the same effect as seen in HPV-negative stimulated fibroblasts. Indeed, UD SCC02 was noted to release significantly greater amounts of IL-8 compared to all other cell lines studied (dwarfed in ELISA data in Chapter 4 due to the marked rise seen in fibroblasts); whilst IL-8 does not induce STAT3 phosphorylation, the increased secretion of this factor by UD SCC02 does illustrate how another, unrelated factor could occur, leading to STAT3 activation in fibroblasts which is not significant to the process through which HGF and IL-6 are ultimately released.

Data relating to 12 h STAT3 expression are difficult to interpret; it is feasible that autocrine stimulation through fibroblast production of IL-6 by 12 hours may account for STAT3 elevation by 12 hours – this phenomenon has been reported by Gu *et al* in response to IL-17, and may be noted by as little as 3 hours post-stimulation⁵⁶⁶. As both HPV-positive and -negative lines induced some degree of IL-6 release by fibroblasts, autocrine stimulation by IL-6 is a feasible explanation for the elevation of pSTAT3 observed at 12 h with all cell line conditioned media, albeit that one would expect a greater degree of pSTAT3 elevation in response to HPV-negative cell line media due to a greater release of IL-6. It should be noted that the 12 h unstimulated fibroblast control in Figure 9.2 also demonstrated pSTAT3 by a similar degree to HPV-negative cell lines – it is therefore feasible that 12 h data represent a false positive.

Validation of western blots presented in Figures 9.1 & 9.2 is therefore required through appropriate triplicate experimental repeat of both HPV-positive and HPV-negative conditioned media stimulations, using a single gel for direct comparison. Should HPV-negative-stimulated fibroblasts consistently demonstrate upregulated STAT3 at 20 mins, STAT3 expression may be experimentally blocked with an appropriate inhibitor in order to determine its role in both the HGF and IL-6 response. As discussed above, “stattic” is a potent small molecule inhibitor of STAT3, demonstrating high selectivity over STAT1 & STAT5. Cell line conditioned media stimulation of fibroblasts in the presence/absence of stattic would therefore allow confirmation of the role of STAT3 in the fibroblast response, and could be measured through HGF and IL-6 ELISA. Further investigation of secondary

messenger pathways could be undertaken with ruxolitinib (as discussed below for inhibition of cell line migration), which would allow determination of whether STAT3 activation is reliant on Janus Kinase activity; further narrowing the list of plausible factors driving the fibroblast response. In addition to direct STAT3 blockade with stattic, more comprehensive STAT inhibition using nifuroxazide (Selleckchem, USA, Cat S41820) – an inhibitor of STAT1, 3 & 5 – would allow thorough determination of the role of STAT in driving the fibroblast secretory response. ELISA analysis of fibroblast secretion of HGF, IL-6 & IL-8 in the presence/absence of inhibitor would act as a rapid measure of inhibitor efficacy, with more protracted analyses of cell migration in response to respective fibroblast conditioned media being reserved for those conditions in which HGF, IL-6 & IL-8 secretion appear to have been influenced.

In addition to validation of the preliminary STAT3 data presented above, PCR analysis of a panel of HGF activating factors may also assist in identifying the chief inducer of the fibroblast HGF response. As already discussed with respect to ADAMs, post-transcriptional differences between HPV-positive and HPV-negative disease may account for HGF activation rather than a detectable difference in activating factors at the level of the transcriptome, although again, a marked difference in HPV-positive versus -negative expression of a recognised HGF activating factor may help identify a principal candidate. Viable candidate molecules for further investigation include HGFA (HGF activator), IL-17A, IL-17D, PDGF/PDGFA, bFGF and IL-1/IL-1 β , based on capacity to induce either direct release of HGF or alternatively a reported secretory profile consistent with our cytokine array data^{563, 566}.

II. Investigation of Secondary Messenger Pathways Linked to IL-6/ HGF Synergy

As discussed above, we are currently in the process of negotiating access to the IL-6 inhibitor, tocilizumab, for use in research. Whilst tocilizumab offers direct confirmation of the role of IL-6 in supporting HGF-mediated migration, difficulty in gaining access to this drug has prompted further investigation using more readily accessible inhibitors. Ruxolitinib is a selective JAK1/JAK2 inhibitor⁵⁶⁷ which offers a method of assessing IL-6 mediated support of HGF-induced migration in conditioned media, as well as interrogating the secondary messenger system responsible for the synergy between the two factors.

Although both HGF and IL-6 signal via STAT3, among other messenger systems, a distinguishing feature of HGF is that it promotes direct STAT3 phosphorylation via the c-Met receptor, whereas IL-6 activates STAT3 via JAK1 (Figure 9.3). Experimental blockade with ruxolitinib therefore offers the capacity to selectively inhibit IL-6-induced STAT3 signalling (blocked by ruxolitinib via JAK1 inhibition) whilst preserving HGF-induced STAT3 signalling. A number of other signalling pathways are also reliant on JAK1, including STAT5 and STAM2⁵⁶⁸⁻⁵⁷⁰; inhibition of IL-6-promoted support of HGF-mediated migration is therefore not direct proof of STAT3 supplementation driving the synergy between IL-6 and HGF-induced migration, although offers initial evidence to support or refute our hypothesis.

Figure 9.3: Effects of Ruxolitinib on HGF/IL-6 Signalling via STAT3

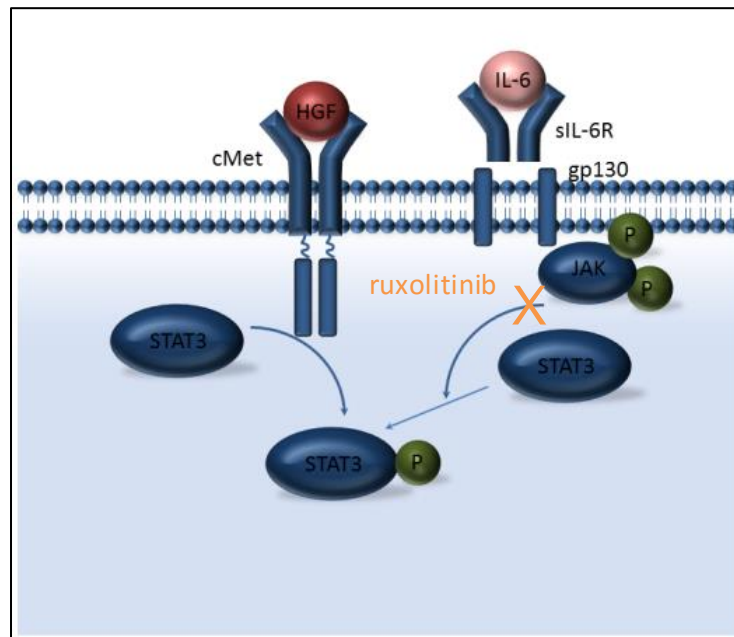


Figure 9.3: Effects of ruxolitinib on HGF/IL-6 signalling via the STAT3 secondary messenger system. Ruxolitinib is a JAK1/JAK2 selective inhibitor, and therefore inhibits JAK-dependent phosphorylation of STAT3. As HGF induces STAT3 phosphorylation in the absence of JAK, ruxolitinib has no effect on HGF-induced STAT3 activation, whereas IL-6 activation of STAT3 is JAK-dependent, and is therefore inhibited by ruxolitinib.

Methods

Inhibition of Cell Line Migration Using Ruxolitinib 1 μM

Preparation of Migration Assays, Inhibition of Cell Division and Pre-experimental Conditioning with Ruxolitinib/DMSO Control

HPV-negative cell lines UPCI SCC072 and UPCI SCC089 were grown to 70 % confluence in separate T75 flasks. Cells were washed twice in PBS, trypsinised, centrifuged at 1,000 rpm and then resuspended in normal media. Each cell suspension was then counted using a haemocytometer, appropriately diluted using normal media, and re-counted in order to achieve the preoptimised seeding concentration of 1.6×10^6 cells mL^{-1} for UPCI SCC072, and 8.8×10^5 cells mL^{-1} for UPCI SCC089, allowing confluent ORIS™ assay well loading as described in Chapter 1. ORIS™ assay plates were prepared under sterile conditions, mounting silicone stoppers into each well using the manufacturer-supplied location device. 100 μL of each cell suspension was then pipetted into respective ORIS™ assay wells and left overnight to adhere.

Following cell adherence and confirmation of well confluency using an inverted lens microscope, a pre-optimised (please refer to Chapter 1, Figure 1.5) 2 $\mu\text{g mL}^{-1}$ mitomycin C suspension in normal media was prepared from snap-frozen 0.5 mg mL^{-1} aliquots of mitomycin C stored at $-80\text{ }^\circ\text{C}$. All handling of mitomycin C was undertaken in a darkened tissue culture hood in order to avoid excessive light exposure. The mitomycin C suspension was then divided into multiple universal containers, and either ruxolitinib or equivalent DMSO control added from stock solutions in order to achieve the desired concentrations of ruxolitinib 1 μM , or DMSO control.

Silicone stoppers were then removed from assay wells using the manufacturer supplied retrieval tool, exposing the respective cell exclusion zone, and normal media carefully aspirated off each well ensuring contact was avoided with the well base. 2 X 100 μL PBS washes were then undertaken, and then 100 μL mitomycin C with ruxolitinib/DMSO control was then carefully pipetted into respective wells and incubated for 3.5 h at $37\text{ }^\circ\text{C}$ in the dark. Following 3.5 h incubation in mitomycin C, baseline void photomicrographs were taken using a X4 objective lens.

Preparation of Stimulated Fibroblast Media Plus Ruxolitinib/ DMSO Control Solution, Completion of ORIS™ Assay

The most experimentally-inductive stimulated fibroblast media for cell lines UPCI SCC072 (DENOF08 stimulated fibroblast Medium 1) and UPCI SCC089 (DENOF08 stimulated fibroblast Medium 2) were collected and immediately stored at -21 °C ahead of experiments, as outlined in Chapter 2. Stimulated fibroblast media were then thawed, aliquoted and either ruxolitinib or DMSO control added from stock solutions in order to achieve the desired concentration of 1 μ M ruxolitinib or equivalent DMSO control.

Following mitomycin C incubation, assay wells were washed X2 in PBS and then 100 μ L Stimulated fibroblast media with ruxolitinib/DMSO control carefully pipetted into respective wells. ORIS™ assay plates were then incubated for either 20 h (UPCI SCC089) or 48 h (UPCI SCC072) in order for migration to occur, and then endpoint photomicrographs taken using a X4 objective lens.

Analysis of Cell Migration

Analysis of cell migration was undertaken by comparison of baseline versus endpoint micrograph images taken using a X4 objective lens. The area of each stopper-induced cell exclusion zone at baseline and endpoint was measured with ImageJ software (freeware, NIH, USA), using the polygon selection tool. Percentage void closure was then calculated by dividing area of closure at experimental endpoint by total baseline area of cell exclusion zone.

MTS & LDH Cytotoxicity Assays

MTS and LDH assays of cell lines UPCI SCC072 and UPCI SCC089 in the presence of 1 μ M ruxolitinib were undertaken using identical methods as described for foretinib/INCB28060 in Chapter 6, Methods section M6.3-6.4.

Results

Figure 9.4: Effects of Ruxolitinib 1 μ M on ORIS™ Assay Migration of Cell Line UPCI SCC089 in the Presence of Stimulated Fibroblast Conditioned Media Versus Unstimulated Fibroblast Media Control

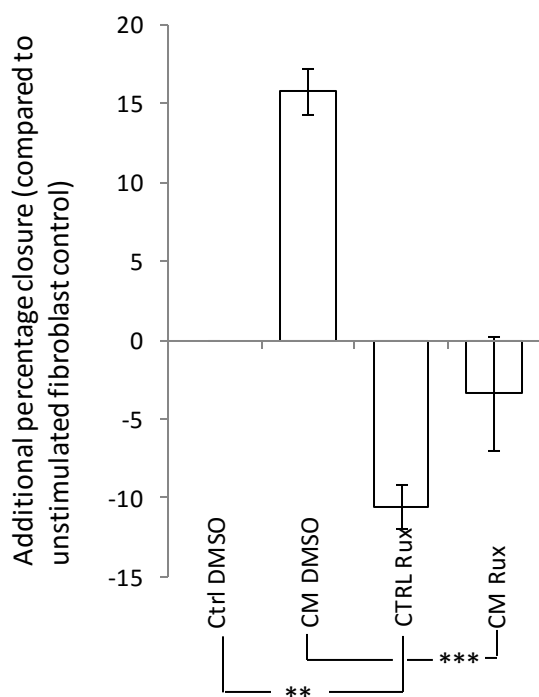


Figure 9.4: Effects of ruxolitinib on ORIS™ Assay migration of cell line UPCI SCC089 in the presence of stimulated fibroblast Medium 2 versus normal media control. Y-axis represents additional percentage closure, compared to migration in the presence of unstimulated fibroblast conditioned medium control. (n=9, Error Bars = SEM)

*- Mann Whitney U-test, $P < 0.05$

** - Mann Whitney U-test, $P < 0.01$

*** - Mann Whitney U-test $P < 0.001$

CM – UPCI SCC089 stimulated fibroblast Medium 2

Ctrl – Unstimulated fibroblast 24 h conditioned medium control

Rux – Incubation with ruxolitinib inhibitor for the duration of the experiment

DMSO – DMSO control (control for ruxolitinib)

Note that, as for previous experiments presented in Chapters 2 & 6, UPCI SCC089 stimulated fibroblast Medium 2 induced marked migration compared to unstimulated fibroblast conditioned medium control. Addition of ruxolitinib led to inhibition of basal migration in control media (Ctrl Rux; Mann Whitney U-test, $P < 0.01$). This inhibition suggests that JAK1/2 signalling is important for the constitutional migratory activity in cell line UPCI SCC089, although may also be due to basal fibroblast secretion of JAK-activating factors (however, basal fibroblast secretion of IL-6 is minimal – please refer to Chapter 4, Figure 4.1). Constitutional activation of JAK leading to basal activation of STAT3 is consistent with western blot data presented in Figure 5.6. UPCI SCC089 may therefore contain an activating mutation of IL-6R, gp130 or an alternative JAK-activating receptor.

Addition of ruxolitinib to stimulated fibroblast Medium 2 led to significant reduction of cell migration (Mann Whitney U-test, $P < 0.001$), although migration outcompeted that of ruxolitinib in combination with unstimulated fibroblast medium control (Mann Whitney U-test, $P = 0.019$). These features are consistent with HGF underlying a significant proportion of cell migration induced by stimulated fibroblast Medium 2; STAT3 signalling via the HGF route is not reliant on JAK.

Reduction of cell migration in stimulated Medium 2 with ruxolitinib was initially regarded as a surprising result, due to the apparent lack of effect of IL-6 in recombinant protein experiments presented in Figure 6.13. Constitutional JAK/STAT3 activation does however explain this phenomenon; recombinant IL-6 may not have effect on this cell line due to already constitutionally active IL-6R or alternatively gp130, which leads to saturation of the IL-6 signalling pathway, whereas JAK blockade will lead to a reduction of the synergistic effect on HGF-induced migration due to inhibition of constitutionally active IL-6 signalling, leading to an overall reduction in STAT3.

Figure 9.5: Effects of Ruxolitinib 1 μ M on ORIS™ Assay Migration of Cell Line UPCI SCC072 in the Presence of Stimulated Fibroblast Conditioned Media Versus Unstimulated Fibroblast Media Control

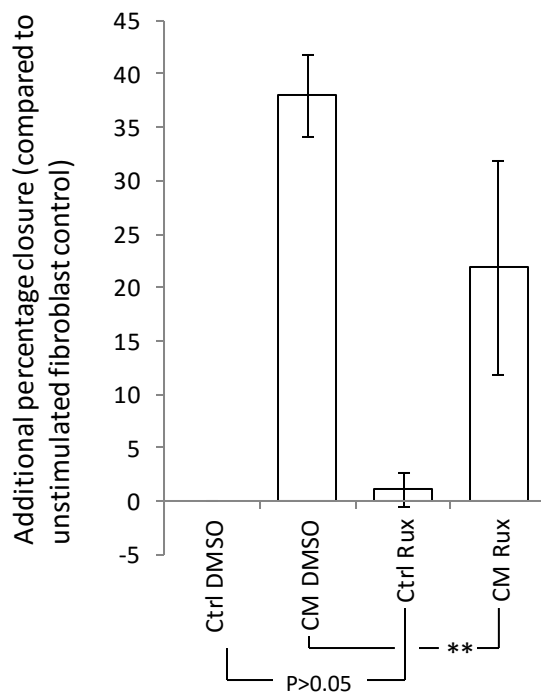


Figure 9.5: Effects of ruxolitinib on ORIS™ Assay migration of cell line UPCI SCC072 in the presence of stimulated fibroblast Medium 1 versus normal media control. Y-axis represents additional percentage closure, compared to migration in the presence of unstimulated fibroblast conditioned medium control. (n=9, Error Bars = SEM) **Mann Whitney U-test, P<0.01

CM – UPCI SCC072 stimulated fibroblast Medium 1

Ctrl – Unstimulated fibroblast 24 h conditioned medium control

Rux – Incubation with ruxolitinib inhibitor for the duration of the experiment

DMSO – DMSO control (control for ruxolitinib)

No significant difference in basal migration (unstimulated fibroblast medium) was noted with the addition of ruxolitinib (*Ctrl DMSO* Vs *Ctrl Rux*; Mann Whitney U-test P>0.05). Incubation with stimulated fibroblast media (*CM DMSO*) led to marked additional migration, as described in Chapter 2. Addition of ruxolitinib to stimulated fibroblast media led to subtotal inhibition of migration (*CM DMSO* Vs *CM Rux*; Mann Whitney U-test, P<0.01). These findings are consistent with inhibition of IL-6/JAK mediated STAT3 supplementation of the HGF signal.

Figure 9.6: Ruxolitinib 1 μ M LDH Assay, UPCI SCC072 & UPCI SCC089

a). UPCI SCC072 LDH Cytotoxicity Assay b). UPCI SCC089LDH Cytotoxicity Assay

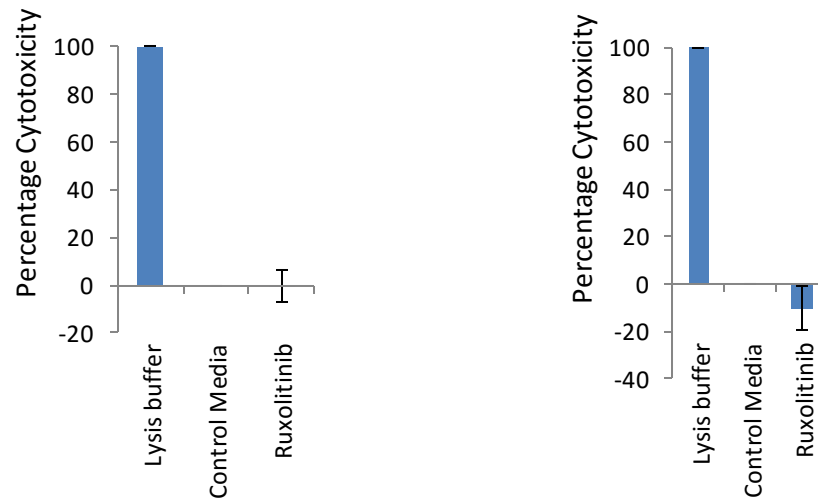
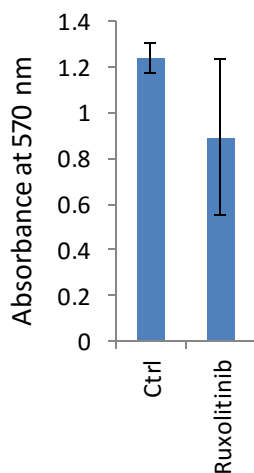


Figure 9.6: Bar graph summarising LDH assay of cell lines UPCI SCC072 (Figure a) & UPCI SCC089 (Figure b) exposed to ruxolitinib 1 μ M (*Ruxolitinib*), expressed as percentage cytotoxicity; calculated in the same manner as reported in Chapter 6, methods section 6.3-6.4. n=9, Error Bars = SEM. No evidence of increased LDH release was noted in either cell line (Mann Whitney U-test, P>0.05), suggesting that the effects of ruxolitinib on migrations reported in Figure 9.5 are due to receptor-specific effects rather than toxicity.

Figure 9.7: Ruxolitinib 1 μ M MTS Assay, UPCI SCC072 & UPCI SCC089

a). UPCI SCC072: MTS Assay of 1 μ M Ruxolitinib



b). UPCI SCC089: MTS Assay of 1 μ M Ruxolitinib

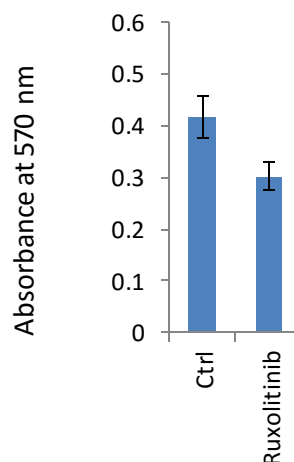


Figure 9.7: MTS assay of cell lines UPCI SCC072 (Figure a) and UPCI SCC089 (Figure b) in response to ruxolitinib 1 μ M. Y-axis represents absorbance at 570 nm, error bars denote SEM. An approximate 25 % average reduction in absorbance is observed following incubation of each cell line with ruxolitinib for 24 h, although statistical significance was not reached (Mann Whitney U-test, $P=0.508$ UPCI SCC072, $P=0.058$ UPCI SCC089). Note that contrary to LDH assay data presented in Figure 9.6, MTS assay as a measure of cytotoxicity suggests that ruxolitinib 1 μ M may have had borderline cytotoxic effect. Further experimental repeats may allow the effect of ruxolitinib 1 μ M on MTS assay to be more accurately quantified, as assay variance – particularly in the case of cell line UPCI SCC072, has led to statistical significance not being reached. Direct STAT3 inhibition has however been reported to reduce IL-6 mediated cellular proliferation, as measured by MTS assay⁵⁷¹, and reduced cellular proliferation rather than direct cytotoxicity may therefore account for the disparity between MTS and LDH assay data.

It should be noted, however, that despite the potential for STAT3 blockade to reduce cellular proliferation and therefore alter MTS absorbance, it can be observed that cell lines UPCI SCC072 and UPCI SCC089 both demonstrate a similar reduction in cell proliferation (approximately 28%). Although UPCI SCC089 demonstrates basal STAT3 activation, there is no greater reduction in assay absorbance for this cell line. Similarly, the basal inactivity of STAT3 in cell line UPCI SCC072 would suggest that STAT3 inhibition would not be a major determinant on proliferation. It is therefore feasible that ruxolitinib has influenced cellular proliferation through either alternative secondary messengers, or alternatively through cytotoxic effects. Dose-response analysis of ruxolitinib in a similar fashion to that undertaken for foretinib and INCB28060 would allow a more comprehensive analysis of cytotoxicity and could be correlated to dose-response analysis of ruxolitinib's capacity to inhibit cell migration in the presence of stimulated fibroblast media.

Discussion

Provisional data assessing JAK inhibition through the use of ruxolitinib support a role of for JAK-signalling in the supplementation of HGF-induced cellular migration. Although this finding provides further evidence to support the role of IL-6-induced STAT3 supplementation, direct IL-6 inhibition remains key to demonstrating this role. Similarly, JAK-reliant intracellular messenger systems other than STAT3 may be responsible for the supplemental effect observed, and a role of STAT3 appears likely, but cannot be assumed. Although elevation of phospho-STAT3 in response to cell line conditioned media, basal STAT3 activity in cell line UPCI SCC089, and preliminary JAK inhibitor data all correlate with the biological phenomenon of cell migration, the correlation may be due to a confounder. An immediately tangible example would include the scenario in which our hypothesis regarding IL-6 is indeed correct, yet an alternative intracellular messenger system remains responsible for HGF synergism. In such a scenario, STAT3 would still become elevated in response to conditioned media, yet would be redundant in terms of migrational effect. Similarly, constitutional activation of either IL-6R, gp130 or JAK-1 in cell line UPCI SCC089 would lead to a similar constitutional activation of STAT3, along with constitutional activation of an alternative messenger that drives UPCI SCC089's basal migratory activity. Direct analysis of STAT3 activity therefore remains central to confirmation of our hypothesis.

Stattic is a first in-class STAT3 inhibitor, demonstrating high specificity for STAT3 over closely related messengers such as STAT1 and STAT5. Migration analysis of cell line UPCI SCC089 using stattic would allow much insight into the role of STAT3 in driving migration. There is no structural or bioactive difference between HGF-induced versus IL-6-induced STAT3, making the proportionate response to stattic indecipherable between HGF and IL-6. However, data may be correlated to ruxolitinib data; if IL-6 derived STAT3 supplementation underlies IL-6's effects, one would anticipate an effect on migration that reflects that illustrated in Figure 9.4, albeit with greater inhibition of stimulated fibroblast media-induced migration due to stattic's additional effects on HGF-induced phospho-STAT3. In particular, one would expect basal migration in cell line UPCI SCC089 to become reduced in the presence of stattic, inferring the constitutional activation of STAT3.

Further investigation of activating mutations in cell line UPCI SCC089, for example by gene sequencing, may give further insight into the principal source of STAT3 activation. This may also contextualise the effects of tocilizumab on cell line UPCI SCC089; constitutive activation

of the IL-6 receptor through tyrosine kinase domain mutation may lead to tocilizumab resistance, due to the drug's activity against the extracellular receptor domain.

Madindoline A (Santa Cruz Biotechnology, USA, Cat sc-202702) may act as a suitable alternative to tocilizumab in confirming the role of IL-6 in supplementing HGF-mediated migration, should difficulty securing access to tocilizumab persist. Madindoline A is an indole alkaloid originally isolated from *Streptomyces nitrosporeus*, and competitively binds to the extracellular domain of gp130, leading to the inhibition of IL-6 and IL-11 signalling. Cytokine array data suggest that IL-11 secretion is not a significant feature of the fibroblast response to either HPV-positive or -negative cell line conditioned media, although absolute validation could be undertaken by means of IL-11 ELISA analysis.

III. Myofibroblast Formation in Response to Tumour Conditioned Media

Data presented in Chapter 7 have demonstrated that HPV-negative cell line conditioned media induced a greater degree of fibroblast senescence following protracted incubations, than did HPV-positive cell line conditioned media. Although data presented in Chapters 2-6 offer comprehensive insight into how this process may link in to earlier secretory phenomena, an intriguing comparator to senescence is myofibroblast formation. TGF β is a key inducer of myofibroblast formation, and therefore determining the capacity of HPV-positive versus -negative cell line conditioned media to induce myofibroblast formation would both provide a more detailed picture of the fibroblast phenotypes occurring in response to cell line conditioned media, in addition to potentially offering further evidence to confirm or refute a role of TGF β in the fibroblast response we have investigated. For a more direct analysis, TGF β ELISA could also be undertaken on cell line and stimulated fibroblast media.

Experimental analysis of myofibroblast formation has been optimised by co-workers. In brief, experimental conditions would involve 4-day serum free cell line conditioned media incubations, using a serum-free normal media negative control and serum-free recombinant TGF β containing normal media with positive control. Alpha Smooth Muscle Actin (α -SMA) ICC/IF could then be applied to determine staining intensity and cellular distribution of α -SMA, with comparison of the effects of HPV-negative cell line conditioned media against HPV-positive cell line conditioned media and positive/negative controls.

IV. ADAM 10 & 17 Analysis

Membrane snippase activity may underlie a number of observations made throughout this thesis. The introduction of this chapter has revisited the prospect of membrane-bound cytokines being released as a consequence of snippase activity, which may in turn lead to discrepancies between the transcriptome and secretome. Whilst PCR analysis of the transcriptome of each cell line investigated throughout the thesis may offer an immediate measure of a number of potential fibroblast activating factors, it is also possible that such investigation yields limited data. Investigation of ADAM activation may therefore offer an alternative route of investigation, which helps correlate the tumour secretome to the observed fibroblast response.

ADAM activity is not fully understood, although it has been identified that ras, src and v-src control ADAM activation post-translationally⁴¹⁴. A number of cytokines are released as a consequence of ADAM cleavage, including a pro-inflammatory form of TNF- α , TGF- α , AREG, EPGN, NRG1, HB-EGF, Pref1, Fractalkine, RANKL, CSF-1, SEMA4D, LAG-3, DLL1, KL-1, KL-2, MICA, MICB, Jagged, TMEFF2 and FLT-3L⁴¹⁴. Although these cytokines are not classically linked to induction of senescence, there is clearly a broad range of cytokine activity that may be induced as a consequence of ADAM activity.

An inherent starting point for analysing ADAM 10/17 activity in HPV-positive versus -negative cell lines is quantitative PCR analysis. Our preliminary work has included PCR analysis of both ADAMs 10 & 17, although demonstrated no frank relationship between viral status and mRNA expression. Due to post-translational activation, in addition to the enzymatic nature of ADAMs, it is difficult to conclude that PCR data have any direct relevance to functional activity. It may therefore be more appropriate to assess the effects of ADAM activation and inhibition on cell line conditioned media; inhibition of ADAM activity, for example with TAPI-2 (Santa Cruz, USA, Cat sc-205851)⁵⁷², in HPV-negative cell lines may lead to a conditioned medium that is less instructive to fibroblasts, thereby leading to a reduction in the HGF/IL-6/IL-8 response, as can be quantified by ELISA. Similarly, ADAM activation through use of PMA or anisomycin⁴¹⁴ may lead to a more florid fibroblast response on exposure to ADAM-activated cell line conditioned media. PCR analysis of known ADAM regulators, such as RNF41³³⁷ may also prove a valuable method of ascertaining the likely role of ADAMs in HPV-negative versus -positive disease.

Inhibitor experiments would also allow clarification of the role of ADAMs in HPV-negative cell line release of soluble receptors, such as sIL-6R and sEGFR. This may therefore link in to further work regarding sEGFR release and cetuximab resistance, as discussed in Section 5.

V. Cetuximab Resistance in sEGFR-releasing Oral & Oropharyngeal Carcinomas

Cytokine array data presented in Chapter 3 suggest that HPV-negative cell lines secreted soluble EGFR, whereas HPV-positive cell lines did not. As outlined, this feature may be related to a result of generic ADAM activity, rather than targeted membrane cleavage of EGFR. Alternatively, EGFR shedding could be linked to a higher membrane density of EGFR in HPV-negative cell lines; Perez-Torrez *et al* found a membrane density of 7×10^5 receptors per cell or greater led to ectodomain shedding of sEGFR⁵⁷³. Irrespective of the mechanism leading to EGFR release, the presence of soluble EGFR may have significant implications on the efficacy of cetuximab in the management of recurrent/late stage disease due to the release of receptor decoy.

ELISA analysis of sEGFR content in HPV-positive, versus -negative cell line conditioned media would allow quantitative analysis to confirm cytokine array findings. Cetuximab resistance could then be correlated to sEGFR release by calculating cetuximab's LD50 for each cell line. One would anticipate an increased LD50 for cell lines secreting sEGFR, particularly if cetuximab was added to established (i.e. 24 h+) cell line conditioned media. Further analysis could be undertaken by comparing results to erlotinib, an EGFR tyrosine kinase inhibitor that should theoretically not become inhibited by the solubilised EGFR ectodomain.

Finally, cetuximab efficacy versus tumour membranous: soluble EGFR ratio could be analysed in a clinical cohort of oropharyngeal carcinomas, although outcome data are likely to be difficult to interpret due to cetuximab being reserved in the UK for late stage/resistant disease. Current evidence supports this practice⁵⁷⁴. Studies such as DeESCALaTE, which have assessed the merits of cetuximab plus radiotherapy versus standard chemotherapy plus radiotherapy, may be used to undertake secondary data analysis of membranous/soluble EGFR status in the cetuximab cohort. Achieving of a valid method of sEGFR quantification may act as a barrier to any meaningful data, as tissue sEGFR may become either diffuse, diluted or may not be amenable to standard methods of assessment such as immunohistochemistry. Due to post-translational cleavage by ADAMs, techniques such as PCR or in-situ hybridization of RNA/DNA would not be valid; more expensive methods such as mass spectrometry may be necessary. A prospective cohort study may

therefore be necessary, whereby serum sEGFR may be used along with tumour membranous EGFR IHC status, and correlated to response to cetuximab.

VI. Retrospective Cohort Analysis and Translation to the Clinic

Approximately 150 cases of oropharyngeal carcinoma treated at Sheffield Teaching Hospitals NHS Trust from 2001-2011 have been identified through the Sheffield Teaching Hospitals pathology reporting database, and have been correlated to information stored on the Chemocare chemotherapy prescribing system. Clinical notes have been retrieved, and data collected with respect to variables listed in Table 9.1. Pathological blocks have been requested and STH are in the process of retrieving all original diagnostic biopsy blocks and respective slides. Diagnostic slides shall be used to identify target regions of FFPE specimen blocks for inclusion in tissue microarray, with 3 array samples being taken from all cases, except where exhaustion of the tissue specimen will occur.

Table 9.1: Summary of Data Collected for Retrospective Cohort Analysis

Sociodemographic	Timing	Tumour status	Therapy	Outcome	Other
sex	date of biopsy	anatomical location	radiotherapy regimen	response at 4 months	free text entry
date of birth	date of radiotherapy commencement	histological diagnosis	radiotherapy dose	local recurrence	
smoking status	date of radiotherapy completion	Grade	radiotherapy fractions	regional (nodal) recurrence	
pack years	date of surgery	T stage	chemotherapy regimen	metastasis during follow-up	
alcohol intake	date of recurrence	N stage	induction chemotherapy	method of 4 month assessment	
units/wk	date of last follow-up	M stage	date of chemotherapy commencement	cause of death	
performance status	date of death	stage grouping	number of chemotherapy cycles	last status of patient	
			surgical therapy		
			surgery type		
			treatment of recurrence		

Initial analyses shall include establishment of HPV status by p16 immunohistochemistry plus RNAScope HPV16/18 in-situ hybridization. Further investigation prompted by the findings of this thesis include IL-6 and HGF RNA in-situ hybridization plus IHC, along with IHC analysis of phospho-STAT3 and markers of fibroblast senescence such as SA-b Gal, γH2AX foci and Ki67⁵⁷⁵. Survival data and tumour HPV status can be correlated to IL-6 and HGF status, pSTAT3 intensity and fibroblast senescence to fully validate our *in-vitro* findings.

Tissue microarray construction will also allow high-throughput analysis of further biomarkers reflecting the characteristic HPV-negative cell line-induced fibroblast profile discussed in Chapter 4, along with yet to be confirmed biomarkers, such as the fibroblast-inducing factor(s) secreted by HPV-negative cell lines.

Our *in-vitro* data suggest much benefit may be gained from the use of HGF inhibitors in the management of early HPV-negative disease. As previously discussed, Phase II trial of foretinib in late stage solid tumours, including a small proportion of head and neck cancers, demonstrated limited benefit⁴³³. In order to translate our work to a trial of foretinib in HPV-negative oropharyngeal-specific disease, both clinical cohort analysis and xenograft *in-vivo* modelling are important. Kwon *et al*⁷⁶ have demonstrated the role of HGF IHC in prognosticating HPV-negative disease, and to some extent HGF-related findings of the cohort study outlined above are confirmatory, albeit with offering greater insight into the biological process through which HGF expression is brought about, along with tumour/stromal specific data achieved through RNA-ISH analysis.

Xenograft modelling of tumour invasion in the presence/absence of clinically relevant foretinib dosing regimens may offer final justification of a Phase II trial applied to early, rather than late disease. Indeed, ovarian carcinoma xenograft modelling has demonstrated utility of foretinib in the prevention of metastasis in the same manner as we predict for oropharyngeal carcinoma⁵⁷⁶.

References

1. Lewis A, Kang R, Levine A, Maghami E. The New Face of Head and Neck Cancer: The HPV Epidemic. *Oncology (Williston Park)*. 2015;29:616-626.
2. Massarelli E, Ferrarotto R, Glisson BS. New Strategies in Human Papillomavirus-Related Oropharynx Cancer: Effecting Advances in Treatment for a Growing Epidemic. *Clin Cancer Res*. 2015;21:3821-3828.
3. Moore KA, Mehta V. The Growing Epidemic of HPV-Positive Oropharyngeal Carcinoma: A Clinical Review for Primary Care Providers. *J Am Board Fam Med*. 2015;28:498-503.
4. Dalianis T. Human papillomavirus and oropharyngeal cancer, the epidemics, and significance of additional clinical biomarkers for prediction of response to therapy (Review). *Int J Oncol*. 2014;44:1799-1805.
5. Sturgis EM, Cinciripini PM. Trends in head and neck cancer incidence in relation to smoking prevalence: an emerging epidemic of human papillomavirus-associated cancers? *Cancer*. 2007;110:1429-1435.
6. Panwar A, Batra R, Lydiatt WM, Ganti AK. Human papilloma virus positive oropharyngeal squamous cell carcinoma: a growing epidemic. *Cancer Treat Rev*. 2014;40:215-219.
7. Hashibe M, Sturgis EM. Epidemiology of oral-cavity and oropharyngeal carcinomas: controlling a tobacco epidemic while a human papillomavirus epidemic emerges. *Otolaryngol Clin North Am*. 2013;46:507-520.
8. Nichols AC, Palma DA, Dhaliwal SS, et al. The epidemic of human papillomavirus and oropharyngeal cancer in a Canadian population. *Curr Oncol*. 2013;20:212-219.
9. Mroz EA, Forastiere AA, Rocco JW. Implications of the oropharyngeal cancer epidemic. *J Clin Oncol*. 2011;29:4222-4223.
10. Ramqvist T, Dalianis T. An epidemic of oropharyngeal squamous cell carcinoma (OSCC) due to human papillomavirus (HPV) infection and aspects of treatment and prevention. *Anticancer Res*. 2011;31:1515-1519.
11. Ramqvist T, Dalianis T. Oropharyngeal cancer epidemic and human papillomavirus. *Emerg Infect Dis*. 2010;16:1671-1677.
12. Marur S, D'Souza G, Westra WH, Forastiere AA. HPV-associated head and neck cancer: a virus-related cancer epidemic. *Lancet Oncol*. 2010;11:781-789.
13. Gillespie MB, Rubinchik S, Hoel B, Sutkowski N. Human papillomavirus and oropharyngeal cancer: what you need to know in 2009. *Curr Treat Options Oncol*. 2009;10:296-307.
14. McKaig RG, Baric RS, Olshan AF. Human papillomavirus and head and neck cancer: epidemiology and molecular biology. *Head Neck*. 1998;20:250-265.
15. zur Hausen H. Papillomaviruses causing cancer: evasion from host-cell control in early events in carcinogenesis. *J Natl Cancer Inst*. 2000;92:690-698.
16. Scott M, Nakagawa M, Moscicki AB. Cell-mediated immune response to human papillomavirus infection. *Clin Diagn Lab Immunol*. 2001;8:209-220.
17. Baumgarth N, Szubin R, Dolganov GM, et al. Highly tissue substructure-specific effects of human papilloma virus in mucosa of HIV-infected patients revealed by laser-dissection microscopy-assisted gene expression profiling. *Am J Pathol*. 2004;165:707-718.
18. Giroglou T, Florin L, Schäfer F, Streeck RE, Sapp M. Human papillomavirus infection requires cell surface heparan sulfate. *J Virol*. 2001;75:1565-1570.
19. Lizano M, Berumen J, García-Carrancá A. HPV-related carcinogenesis: basic concepts, viral types and variants. *Arch Med Res*. 2009;40:428-434.

20. Chow LT, Broker TR, Steinberg BM. The natural history of human papillomavirus infections of the mucosal epithelia. *APMIS*. 2010;118:422-449.
21. Bernard HU, Calleja-Macias IE, Dunn ST. Genome variation of human papillomavirus types: phylogenetic and medical implications. *Int J Cancer*. 2006;118:1071-1076.
22. Ong CK, Chan SY, Campo MS, et al. Evolution of human papillomavirus type 18: an ancient phylogenetic root in Africa and intratype diversity reflect coevolution with human ethnic groups. *J Virol*. 1993;67:6424-6431.
23. Ganguly N, Parihar SP. Human papillomavirus E6 and E7 oncoproteins as risk factors for tumorigenesis. *J Biosci*. 2009;34:113-123.
24. Yu L, Wang L, Zhong J, Chen S. Diagnostic value of p16INK4A, Ki-67, and human papillomavirus L1 capsid protein immunochemical staining on cell blocks from residual liquid-based gynecologic cytology specimens. *Cancer Cytopathol*. 2010;118:47-55.
25. Ozbun MA, Meyers C. Temporal usage of multiple promoters during the life cycle of human papillomavirus type 31b. *J Virol*. 1998;72:2715-2722.
26. Fang L, Budgeon LR, Doorbar J, Briggs ER, Howett MK. The human papillomavirus type 11 E1/E4 protein is not essential for viral genome amplification. *Virology*. 2006;351:271-279.
27. Doorbar J, Ely S, Sterling J, McLean C, Crawford L. Specific interaction between HPV-16 E1-E4 and cytokeratins results in collapse of the epithelial cell intermediate filament network. *Nature*. 1991;352:824-827.
28. Seo YS, Müller F, Lusk M, et al. Bovine papilloma virus (BPV)-encoded E2 protein enhances binding of E1 protein to the BPV replication origin. *Proc Natl Acad Sci U S A*. 1993;90:2865-2869.
29. Lazo PA. The molecular genetics of cervical carcinoma. *Br J Cancer*. 1999;80:2008-2018.
30. zur Hausen H. Immortalization of human cells and their malignant conversion by high risk human papillomavirus genotypes. *Semin Cancer Biol*. 1999;9:405-411.
31. Huang CF, Monie A, Weng WH, Wu T. DNA vaccines for cervical cancer. *Am J Transl Res*. 2010;2:75-87.
32. zur Hausen H. Papillomaviruses and cancer: from basic studies to clinical application. *Nat Rev Cancer*. 2002;2:342-350.
33. Tsai TC, Chen SL. The biochemical and biological functions of human papillomavirus type 16 E5 protein. *Arch Virol*. 2003;148:1445-1453.
34. Ragin CC, Modugno F, Gollin SM. The epidemiology and risk factors of head and neck cancer: a focus on human papillomavirus. *J Dent Res*. 2007;86:104-114.
35. Werness BA, Levine AJ, Howley PM. Association of human papillomavirus types 16 and 18 E6 proteins with p53. *Science*. 1990;248:76-79.
36. Vozenin MC, Lord HK, Hartl D, Deutsch E. Unravelling the biology of human papillomavirus (HPV) related tumours to enhance their radiosensitivity. *Cancer Treat Rev*. 2010;36:629-636.
37. Lizano M, Berumen J, Garcia-Carranca A. HPV-related carcinogenesis: basic concepts, viral types and variants. *Arch Med Res*. 2009;40:428-434.
38. Li Y, Nichols MA, Shay JW, Xiong Y. Transcriptional repression of the D-type cyclin-dependent kinase inhibitor p16 by the retinoblastoma susceptibility gene product pRb. *Cancer Res*. 1994;54:6078-6082.
39. Dürst M, Gissmann L, Ikenberg H, zur Hausen H. A papillomavirus DNA from a cervical carcinoma and its prevalence in cancer biopsy samples from different geographic regions. *Proc Natl Acad Sci U S A*. 1983;80:3812-3815.
40. MORIAME G. [Malignant transformation of venereal vegetations of the penis]. *Arch Belg Dermatol Syphiligr*. 1950;6:175-177.

41. SIEGEL A. Malignant transformation of condyloma acuminatum. Review of the literature and report of a case. *Am J Surg.* 1962;103:613-617.
42. Dun AE, Ogilvie MM. Intranuclear virus particles in human genital wart tissue: observations on the ultrastructure of the epidermal layer. *J Ultrastruct Res.* 1968;22:282-295.
43. zur Hausen H. Condylomata acuminata and human genital cancer. *Cancer Res.* 1976;36:794.
44. Plummer G, Masterson JG. Herpes simplex virus and cancer of the cervix. *Am J Obstet Gynecol.* 1971;111:81-84.
45. Centifanto YM, Hildebrandt RJ, Held B, Kaufman HE. Relationship of herpes simplex genital infection and carcinoma of the cervix: population studies. *Am J Obstet Gynecol.* 1971;110:690-692.
46. Cassai E, Rotola A, Meneguzzi G, et al. Herpes simplex virus and human cancer. I. Relationship between human cervical tumours and Herpes simplex type 2. *Eur J Cancer.* 1981;17:685-693.
47. Christenson B. Herpes virus-related antigens in herpes simplex virus type 2-transformed cells in the course of cervical carcinoma. *Eur J Cancer Clin Oncol.* 1982;18:1345-1352.
48. Smith JW. Herpes simplex virus. An expanding relationship to human cancer. *J Reprod Med.* 1983;28:116-122.
49. Attner P, Du J, Näsman A, et al. The role of human papillomavirus in the increased incidence of base of tongue cancer. *Int J Cancer.* 2010;126:2879-2884.
50. Herrero R, Castellsagué X, Pawlita M, et al. Human papillomavirus and oral cancer: the International Agency for Research on Cancer multicenter study. *J Natl Cancer Inst.* 2003;95:1772-1783.
51. Adelstein DJ, Ridge JA, Gillison ML, et al. Head and neck squamous cell cancer and the human papillomavirus: summary of a National Cancer Institute State of the Science Meeting, November 9-10, 2008, Washington, D.C. *Head Neck.* 2009;31:1393-1422.
52. Insinga RP, Liaw KL, Johnson LG, Madeleine MM. A systematic review of the prevalence and attribution of human papillomavirus types among cervical, vaginal, and vulvar precancers and cancers in the United States. *Cancer Epidemiol Biomarkers Prev.* 2008;17:1611-1622.
53. Ciapponi A, Bardach A, Glujovsky D, Gibbons L, Picconi MA. Type-specific HPV prevalence in cervical cancer and high-grade lesions in Latin America and the Caribbean: systematic review and meta-analysis. *PLoS One.* 2011;6:e25493.
54. De Vuyst H, Clifford GM, Nascimento MC, Madeleine MM, Franceschi S. Prevalence and type distribution of human papillomavirus in carcinoma and intraepithelial neoplasia of the vulva, vagina and anus: a meta-analysis. *Int J Cancer.* 2009;124:1626-1636.
55. Backes DM, Kurman RJ, Pimenta JM, Smith JS. Systematic review of human papillomavirus prevalence in invasive penile cancer. *Cancer Causes Control.* 2009;20:449-457.
56. Kreimer AR, Clifford GM, Boyle P, Franceschi S. Human papillomavirus types in head and neck squamous cell carcinomas worldwide: a systematic review. *Cancer Epidemiol Biomarkers Prev.* 2005;14:467-475.
57. Feller L, Wood NH, Khammissa RA, Lemmer J. Human papillomavirus-mediated carcinogenesis and HPV-associated oral and oropharyngeal squamous cell carcinoma. Part 2: Human papillomavirus associated oral and oropharyngeal squamous cell carcinoma. *Head Face Med.* 2010;6:15.
58. HILL AB. THE ENVIRONMENT AND DISEASE: ASSOCIATION OR CAUSATION? *Proc R Soc Med.* 1965;58:295-300.
59. Smith EM, Ritchie JM, Summersgill KF, et al. Age, sexual behavior and human papillomavirus infection in oral cavity and oropharyngeal cancers. *Int J Cancer.* 2004;108:766-772.

60. Maden C, Beckmann AM, Thomas DB, et al. Human papillomaviruses, herpes simplex viruses, and the risk of oral cancer in men. *Am J Epidemiol.* 1992;135:1093-1102.
61. Brawley OW. Oropharyngeal cancer, race, and the human papillomavirus. *Cancer Prev Res (Phila).* 2009;2:769-772.
62. D'Souza G, Kreimer AR, Viscidi R, et al. Case-control study of human papillomavirus and oropharyngeal cancer. *N Engl J Med.* 2007;356:1944-1956.
63. Gillison ML, D'Souza G, Westra W, et al. Distinct risk factor profiles for human papillomavirus type 16-positive and human papillomavirus type 16-negative head and neck cancers. *J Natl Cancer Inst.* 2008;100:407-420.
64. Nguyen NP, Chi A, Nguyen LM, Ly BH, Karlsson U, Vinh-Hung V. Human papillomavirus-associated oropharyngeal cancer: a new clinical entity. *QJM.* 2010;103:229-236.
65. Ritchie JM, Smith EM, Summersgill KF, et al. Human papillomavirus infection as a prognostic factor in carcinomas of the oral cavity and oropharynx. *Int J Cancer.* 2003;104:336-344.
66. Scully C. Oral cancer; the evidence for sexual transmission. *Br Dent J.* 2005;199:203-207.
67. Hemminki K, Dong C, Frisch M. Tonsillar and other upper aerodigestive tract cancers among cervical cancer patients and their husbands. *Eur J Cancer Prev.* 2000;9:433-437.
68. Onicescu G, Hill EG, Lawson AB, Korte JE, Gillespie MB. Joint disease mapping of cervical and male oropharyngeal cancer incidence in blacks and whites in South Carolina. *Spat Spatiotemporal Epidemiol.* 2010;1:133-141.
69. Hammarstedt L, Lindquist D, Dahlstrand H, et al. Human papillomavirus as a risk factor for the increase in incidence of tonsillar cancer. *Int J Cancer.* 2006;119:2620-2623.
70. Furniss CS, McClean MD, Smith JF, et al. Human papillomavirus 6 seropositivity is associated with risk of head and neck squamous cell carcinoma, independent of tobacco and alcohol use. *Ann Oncol.* 2009;20:534-541.
71. Ragin CC, Taioli E. Survival of squamous cell carcinoma of the head and neck in relation to human papillomavirus infection: review and meta-analysis. *Int J Cancer.* 2007;121:1813-1820.
72. Worden FP, Kumar B, Lee JS, et al. Chemoselection as a strategy for organ preservation in advanced oropharynx cancer: response and survival positively associated with HPV16 copy number. *J Clin Oncol.* 2008;26:3138-3146.
73. O'Rourke MA, Ellison MV, Murray LJ, Moran M, James J, Anderson LA. Human papillomavirus related head and neck cancer survival: a systematic review and meta-analysis. *Oral Oncol.* 2012;48:1191-1201.
74. Petrelli F, Sarti E, Barni S. Predictive value of human papillomavirus in oropharyngeal carcinoma treated with radiotherapy: An updated systematic review and meta-analysis of 30 trials. *Head Neck.* 2014;36:750-759.
75. Rainsbury JW, Ahmed W, Williams HK, Roberts S, Paleri V, Mehanna H. Prognostic biomarkers of survival in oropharyngeal squamous cell carcinoma: systematic review and meta-analysis. *Head Neck.* 2013;35:1048-1055.
76. Wang MB, Liu IY, Gornbein JA, Nguyen CT. HPV-Positive Oropharyngeal Carcinoma: A Systematic Review of Treatment and Prognosis. *Otolaryngol Head Neck Surg.* 2015;153:758-769.
77. Yuanyuan X, Suling H, Quan Z, et al. [The relationship between human papillomavirus and prognosis of oropharyngeal squamous cell carcinoma: a meta analysis]. *Zhonghua Er Bi Yan Hou Tou Jing Wai Ke Za Zhi.* 2015;50:236-243.
78. Snijders PJ, Scholes AG, Hart CA, et al. Prevalence of mucosotropic human papillomaviruses in squamous-cell carcinoma of the head and neck. *Int J Cancer.* 1996;66:464-469.

79. Paz IB, Cook N, Odom-Maryon T, Xie Y, Wilczynski SP. Human papillomavirus (HPV) in head and neck cancer. An association of HPV 16 with squamous cell carcinoma of Waldeyer's tonsillar ring. *Cancer*. 1997;79:595-604.
80. Pintos J, Franco EL, Black MJ, Bergeron J, Arella M. Human papillomavirus and prognoses of patients with cancers of the upper aerodigestive tract. *Cancer*. 1999;85:1903-1909.
81. Gillison ML, Koch WM, Capone RB, et al. Evidence for a causal association between human papillomavirus and a subset of head and neck cancers. *J Natl Cancer Inst*. 2000;92:709-720.
82. Mellin H, Friesland S, Lewensohn R, Dalianis T, Munck-Wikland E. Human papillomavirus (HPV) DNA in tonsillar cancer: clinical correlates, risk of relapse, and survival. *Int J Cancer*. 2000;89:300-304.
83. Friesland S, Mellin H, Munck-Wikland E, et al. Human papilloma virus (HPV) and p53 immunostaining in advanced tonsillar carcinoma--relation to radiotherapy response and survival. *Anticancer Res*. 2001;21:529-534.
84. Ringström E, Peters E, Hasegawa M, Posner M, Liu M, Kelsey KT. Human papillomavirus type 16 and squamous cell carcinoma of the head and neck. *Clin Cancer Res*. 2002;8:3187-3192.
85. Klussmann JP, Gültekin E, Weissenborn SJ, et al. Expression of p16 protein identifies a distinct entity of tonsillar carcinomas associated with human papillomavirus. *Am J Pathol*. 2003;162:747-753.
86. Li W, Thompson CH, O'Brien CJ, et al. Human papillomavirus positivity predicts favourable outcome for squamous carcinoma of the tonsil. *Int J Cancer*. 2003;106:553-558.
87. Báez A, Almodóvar JI, Cantor A, et al. High frequency of HPV16-associated head and neck squamous cell carcinoma in the Puerto Rican population. *Head Neck*. 2004;26:778-784.
88. Wittekindt C, Gültekin E, Weissenborn SJ, Dienes HP, Pfister HJ, Klussmann JP. Expression of p16 protein is associated with human papillomavirus status in tonsillar carcinomas and has implications on survival. *Adv Otorhinolaryngol*. 2005;62:72-80.
89. Licitra L, Perrone F, Bossi P, et al. High-risk human papillomavirus affects prognosis in patients with surgically treated oropharyngeal squamous cell carcinoma. *J Clin Oncol*. 2006;24:5630-5636.
90. Weinberger PM, Yu Z, Haffty BG, et al. Molecular classification identifies a subset of human papillomavirus--associated oropharyngeal cancers with favorable prognosis. *J Clin Oncol*. 2006;24:736-747.
91. Badaracco G, Rizzo C, Mafera B, et al. Molecular analyses and prognostic relevance of HPV in head and neck tumours. *Oncol Rep*. 2007;17:931-939.
92. Reimers N, Kasper HU, Weissenborn SJ, et al. Combined analysis of HPV-DNA, p16 and EGFR expression to predict prognosis in oropharyngeal cancer. *Int J Cancer*. 2007;120:1731-1738.
93. Na II, Kang HJ, Cho SY, et al. EGFR mutations and human papillomavirus in squamous cell carcinoma of tongue and tonsil. *Eur J Cancer*. 2007;43:520-526.
94. Fakhry C, Westra WH, Li S, et al. Improved survival of patients with human papillomavirus-positive head and neck squamous cell carcinoma in a prospective clinical trial. *J Natl Cancer Inst*. 2008;100:261-269.
95. Klozar J, Kratochvil V, Salakova M, et al. HPV status and regional metastasis in the prognosis of oral and oropharyngeal cancer. *Eur Arch Otorhinolaryngol*. 2008;265 Suppl 1:S75-82.
96. Smith EM, Wang D, Rubenstein LM, Morris WA, Turek LP, Haugen TH. Association between p53 and human papillomavirus in head and neck cancer survival. *Cancer Epidemiol Biomarkers Prev*. 2008;17:421-427.
97. Chung YL, Lee MY, Horng CF, et al. Use of combined molecular biomarkers for prediction of clinical outcomes in locally advanced tonsillar cancers treated with chemoradiotherapy alone. *Head Neck*. 2009;31:9-20.

98. Kong CS, Narasimhan B, Cao H, et al. The relationship between human papillomavirus status and other molecular prognostic markers in head and neck squamous cell carcinomas. *Int J Radiat Oncol Biol Phys.* 2009;74:553-561.
99. Lassen P, Eriksen JG, Hamilton-Dutoit S, Tramm T, Alsner J, Overgaard J. Effect of HPV-associated p16INK4A expression on response to radiotherapy and survival in squamous cell carcinoma of the head and neck. *J Clin Oncol.* 2009;27:1992-1998.
100. Shi W, Kato H, Perez-Ordóñez B, et al. Comparative prognostic value of HPV16 E6 mRNA compared with in situ hybridization for human oropharyngeal squamous carcinoma. *J Clin Oncol.* 2009;27:6213-6221.
101. Hafkamp HC, Mooren JJ, Claessen SM, et al. P21 Cip1/WAF1 expression is strongly associated with HPV-positive tonsillar carcinoma and a favorable prognosis. *Mod Pathol.* 2009;22:686-698.
102. Rischin D, Young RJ, Fisher R, et al. Prognostic significance of p16INK4A and human papillomavirus in patients with oropharyngeal cancer treated on TROG 02.02 phase III trial. *J Clin Oncol.* 2010;28:4142-4148.
103. Hannisdal K, Schjøberg A, De Angelis PM, Boysen M, Clausen OP. Human papillomavirus (HPV)-positive tonsillar carcinomas are frequent and have a favourable prognosis in males in Norway. *Acta Otolaryngol.* 2010;130:293-299.
104. Fischer CA, Zlobec I, Green E, et al. Is the improved prognosis of p16 positive oropharyngeal squamous cell carcinoma dependent of the treatment modality? *Int J Cancer.* 2010;126:1256-1262.
105. Ang KK, Harris J, Wheeler R, et al. Human papillomavirus and survival of patients with oropharyngeal cancer. *N Engl J Med.* 2010;363:24-35.
106. Fischer CA, Kampmann M, Zlobec I, et al. p16 expression in oropharyngeal cancer: its impact on staging and prognosis compared with the conventional clinical staging parameters. *Ann Oncol.* 2010;21:1961-1966.
107. Smith EM, Rubenstein LM, Hoffman H, Haugen TH, Turek LP. Human papillomavirus, p16 and p53 expression associated with survival of head and neck cancer. *Infect Agent Cancer.* 2010;5:4.
108. Lewis JS, Thorstad WL, Chernock RD, et al. p16 positive oropharyngeal squamous cell carcinoma: an entity with a favorable prognosis regardless of tumor HPV status. *Am J Surg Pathol.* 2010;34:1088-1096.
109. Chernock RD, Zhang Q, El-Mofty SK, Thorstad WL, Lewis JS. Human papillomavirus-related squamous cell carcinoma of the oropharynx: a comparative study in whites and African Americans. *Arch Otolaryngol Head Neck Surg.* 2011;137:163-169.
110. Kim TW, Choi SY, Ko YH, Baek CH, Son YI. The Prognostic Role of p16 Expression in Tonsil Cancer Treated by Either Surgery or Radiation. *Clin Exp Otorhinolaryngol.* 2012;5:207-212.
111. Holzinger D, Schmitt M, Dyckhoff G, Benner A, Pawlita M, Bosch FX. Viral RNA patterns and high viral load reliably define oropharynx carcinomas with active HPV16 involvement. *Cancer Res.* 2012;72:4993-5003.
112. Cheng NM, Chang JT, Huang CG, et al. Prognostic value of pretreatment ¹⁸F-FDG PET/CT and human papillomavirus type 16 testing in locally advanced oropharyngeal squamous cell carcinoma. *Eur J Nucl Med Mol Imaging.* 2012;39:1673-1684.
113. Huang H, Zhang B, Chen W, et al. [Human papillomavirus infection in oropharyngeal squamous cell carcinoma and prognosis: a preliminary analysis of 66 cases]. *Zhonghua Er Bi Yan Hou Tou Jing Wai Ke Za Zhi.* 2012;47:207-211.
114. Lin BM, Wang H, D'Souza G, et al. Long-term prognosis and risk factors among patients with HPV-associated oropharyngeal squamous cell carcinoma. *Cancer.* 2013.

115. Mizumachi T, Kano S, Sakashita T, et al. Improved survival of Japanese patients with human papillomavirus-positive oropharyngeal squamous cell carcinoma. *Int J Clin Oncol*. 2013;18:824-828.
116. Semrau R, Duerbaum H, Temming S, et al. Prognostic impact of human papillomavirus status, survivin, and epidermal growth factor receptor expression on survival in patients treated with radiochemotherapy for very advanced nonresectable oropharyngeal cancer. *Head Neck*. 2013;35:1339-1344.
117. Hong AM, Martin A, Armstrong BK, et al. Human papillomavirus modifies the prognostic significance of T stage and possibly N stage in tonsillar cancer. *Ann Oncol*. 2013;24:215-219.
118. Oguejiofor KK, Hall JS, Mani N, et al. The prognostic significance of the biomarker p16 in oropharyngeal squamous cell carcinoma. *Clin Oncol (R Coll Radiol)*. 2013;25:630-638.
119. Kawakami H, Okamoto I, Terao K, et al. Human papillomavirus DNA and p16 expression in Japanese patients with oropharyngeal squamous cell carcinoma. *Cancer Med*. 2013;2:933-941.
120. Evans M, Newcombe R, Fiander A, et al. Human Papillomavirus-associated oropharyngeal cancer: an observational study of diagnosis, prevalence and prognosis in a UK population. *BMC Cancer*. 2013;13:220.
121. Bledsoe TJ, Noble AR, Hunter GK, et al. Oropharyngeal squamous cell carcinoma with known human papillomavirus status treated with definitive chemoradiotherapy: patterns of failure and toxicity outcomes. *Radiat Oncol*. 2013;8:174.
122. Cerezo L, de la Torre A, Hervás A, et al. Oropharyngeal cancer related to Human Papilloma Virus: incidence and prognosis in Madrid, Spain. *Clin Transl Oncol*. 2014;16:301-306.
123. Tural D, Eliçin O, Batur S, et al. Human papillomavirus is independent prognostic factor on outcome of oropharyngeal squamous cell carcinoma. *Tumour Biol*. 2013;34:3363-3369.
124. Nichols AC, Dhaliwal SS, Palma DA, et al. Does HPV type affect outcome in oropharyngeal cancer? *J Otolaryngol Head Neck Surg*. 2013;42:9.
125. Psychogios G, Mantsopoulos K, Agaimy A, et al. Prognostic factors in limited (T1-2, N0-1) oropharyngeal carcinoma treated with surgery ± adjuvant therapy. *Head Neck*. 2013;35:1752-1758.
126. Melkane AE, Auperin A, Saulnier P, et al. Human papillomavirus prevalence and prognostic implication in oropharyngeal squamous cell carcinomas. *Head Neck*. 2014;36:257-265.
127. Deng Z, Hasegawa M, Aoki K, et al. A comprehensive evaluation of human papillomavirus positive status and p16INK4a overexpression as a prognostic biomarker in head and neck squamous cell carcinoma. *Int J Oncol*. 2014;45:67-76.
128. Meyer MF, Seuthe IM, Drebber U, et al. Valosin-containing protein (VCP/p97)-expression correlates with prognosis of HPV- negative oropharyngeal squamous cell carcinoma (OSCC). *PLoS One*. 2014;9:e114170.
129. Egloff AM, Lee JW, Langer CJ, et al. Phase II study of cetuximab in combination with cisplatin and radiation in unresectable, locally advanced head and neck squamous cell carcinoma: Eastern cooperative oncology group trial E3303. *Clin Cancer Res*. 2014;20:5041-5051.
130. Hasegawa M, Maeda H, Deng Z, et al. Prediction of concurrent chemoradiotherapy outcome in advanced oropharyngeal cancer. *Int J Oncol*. 2014;45:1017-1026.
131. Nomura F, Sugimoto T, Kitagaki K, et al. Clinical characteristics of Japanese oropharyngeal squamous cell carcinoma positive for human papillomavirus infection. *Acta Otolaryngol*. 2014;134:1265-1274.
132. Cai C, Chernock RD, Pittman ME, El-Mofty SK, Thorstad WL, Lewis JS. Keratinizing-type squamous cell carcinoma of the oropharynx: p16 overexpression is associated with positive high-risk HPV status and improved survival. *Am J Surg Pathol*. 2014;38:809-815.

133. Vermorken JB, Psyrri A, Mesía R, et al. Impact of tumor HPV status on outcome in patients with recurrent and/or metastatic squamous cell carcinoma of the head and neck receiving chemotherapy with or without cetuximab: retrospective analysis of the phase III EXTREME trial. *Ann Oncol*. 2014;25:801-807.
134. Lorch JH, Hanna GJ, Posner MR, et al. Human papillomavirus and induction chemotherapy versus concurrent chemoradiotherapy in locally advanced oropharyngeal cancer: The Dana Farber Experience. *Head Neck*. 2015.
135. Goodman MT, Saraiya M, Thompson TD, et al. Human papillomavirus genotype and oropharynx cancer survival in the United States of America. *Eur J Cancer*. 2015;51:2759-2767.
136. Lam EW, Chan JY, Chan AB, et al. Prevalence, clinicopathological characteristics, and outcome of human papillomavirus-associated oropharyngeal cancer in Southern Chinese patients. *Cancer Epidemiol Biomarkers Prev*. 2015.
137. Gillison ML. Current topics in the epidemiology of oral cavity and oropharyngeal cancers. *Head Neck*. 2007;29:779-792.
138. Smeets SJ, Hesselink AT, Speel EJ, et al. A novel algorithm for reliable detection of human papillomavirus in paraffin embedded head and neck cancer specimen. *Int J Cancer*. 2007;121:2465-2472.
139. Gillison ML, Shah KV. Human papillomavirus-associated head and neck squamous cell carcinoma: mounting evidence for an etiologic role for human papillomavirus in a subset of head and neck cancers. *Curr Opin Oncol*. 2001;13:183-188.
140. Chaturvedi AK, Engels EA, Anderson WF, Gillison ML. Incidence trends for human papillomavirus-related and -unrelated oral squamous cell carcinomas in the United States. *J Clin Oncol*. 2008;26:612-619.
141. Frisch M, Hjalgrim H, Jaeger AB, Biggar RJ. Changing patterns of tonsillar squamous cell carcinoma in the United States. *Cancer Causes Control*. 2000;11:489-495.
142. Shiboski CH, Schmidt BL, Jordan RC. Tongue and tonsil carcinoma: increasing trends in the U.S. population ages 20-44 years. *Cancer*. 2005;103:1843-1849.
143. Näsman A, Attner P, Hammarstedt L, et al. Incidence of human papillomavirus (HPV) positive tonsillar carcinoma in Stockholm, Sweden: an epidemic of viral-induced carcinoma? *Int J Cancer*. 2009;125:362-366.
144. Zelnik M, Kantner JF. Sexual activity, contraceptive use and pregnancy among metropolitan-area teenagers: 1971-1979. *Fam Plann Perspect*. 1980;12:230-231, 233-237.
145. Warren CW, Santelli JS, Everett SA, et al. Sexual behavior among U.S. high school students, 1990-1995. *Fam Plann Perspect*. 1998;30:170-172, 200.
146. Jit M, Choi YH, Edmunds WJ. Economic evaluation of human papillomavirus vaccination in the United Kingdom. *BMJ*. 2008;337:a769.
147. Kim JJ, Goldie SJ. Cost effectiveness analysis of including boys in a human papillomavirus vaccination programme in the United States. *BMJ*. 2009;339:b3884.
148. Seto K, Marra F, Raymakers A, Marra CA. The cost effectiveness of human papillomavirus vaccines: a systematic review. *Drugs*. 2012;72:715-743.
149. Lawton MD, Nathan M, Asboe D. HPV vaccination to prevent anal cancer in men who have sex with men. *Sex Transm Infect*. 2013;89:342-343.
150. Georgousakis M, Jayasinghe S, Brotherton J, Gilroy N, Chiu C, Macartney K. Population-wide vaccination against human papillomavirus in adolescent boys: Australia as a case study. *Lancet Infect Dis*. 2012;12:627-634.

151. UK CR. Cancer Research UK Oral cancer incidence statistics 2010-2012: available via <http://www.cancerresearchuk.org/health-professional/cancer-statistics/statistics-by-cancer-type/oral-cancer/incidence#ref-4>.
152. Conway DI, Stockton DL, Warnakulasuriya KA, Ogden G, Macpherson LM. Incidence of oral and oropharyngeal cancer in United Kingdom (1990-1999) -- recent trends and regional variation. *Oral Oncol.* 2006;42:586-592.
153. Louie KS, Mehanna H, Sasieni P. Trends in head and neck cancers in England from 1995 to 2011 and projections up to 2025. *Oral Oncol.* 2015;51:341-348.
154. Mehanna H, Jones TM, Gregoire V, Ang KK. Oropharyngeal carcinoma related to human papillomavirus. *BMJ.* 2010;340:c1439.
155. Szkaradkiewicz A, Kruk-Zagajewska A, Wal M, Jopek A, Wierzbicka M, Kuch A. Epstein-Barr virus and human papillomavirus infections and oropharyngeal squamous cell carcinomas. *Clin Exp Med.* 2002;2:137-141.
156. Koskinen WJ, Chen RW, Leivo I, et al. Prevalence and physical status of human papillomavirus in squamous cell carcinomas of the head and neck. *Int J Cancer.* 2003;107:401-406.
157. Wells LA, Junor EJ, Conn B, Pattle S, Cuschieri K. Population-based p16 and HPV positivity rates in oropharyngeal cancer in Southeast Scotland. *J Clin Pathol.* 2015;68:849-852.
158. Auluck A, Hislop G, Bajdik C, Poh C, Zhang L, Rosin M. Trends in oropharyngeal and oral cavity cancer incidence of human papillomavirus (HPV)-related and HPV-unrelated sites in a multicultural population: the British Columbia experience. *Cancer.* 2010;116:2635-2644.
159. Schwartz SR, Yueh B, McDougall JK, Daling JR, Schwartz SM. Human papillomavirus infection and survival in oral squamous cell cancer: a population-based study. *Otolaryngol Head Neck Surg.* 2001;125:1-9.
160. Haraf DJ, Nodzinski E, Brachman D, et al. Human papilloma virus and p53 in head and neck cancer: clinical correlates and survival. *Clin Cancer Res.* 1996;2:755-762.
161. Sisk EA, Bradford CR, Jacob A, et al. Human papillomavirus infection in "young" versus "old" patients with squamous cell carcinoma of the head and neck. *Head Neck.* 2000;22:649-657.
162. Hong A, Dobbins T, Lee CS, et al. Relationships between epidermal growth factor receptor expression and human papillomavirus status as markers of prognosis in oropharyngeal cancer. *Eur J Cancer.* 2010;46:2088-2096.
163. Settle K, Posner MR, Schumaker LM, et al. Racial survival disparity in head and neck cancer results from low prevalence of human papillomavirus infection in black oropharyngeal cancer patients. *Cancer Prev Res (Phila).* 2009;2:776-781.
164. Weinberger PM, Merkley MA, Khichi SS, et al. Human papillomavirus-active head and neck cancer and ethnic health disparities. *Laryngoscope.* 2010;120:1531-1537.
165. Molina MA, Cheung MC, Perez EA, et al. African American and poor patients have a dramatically worse prognosis for head and neck cancer: an examination of 20,915 patients. *Cancer.* 2008;113:2797-2806.
166. Gourin CG, Podolsky RH. Racial disparities in patients with head and neck squamous cell carcinoma. *Laryngoscope.* 2006;116:1093-1106.
167. Heffernan CB, O'Neill JP, Timon C. Oncogenic impact of human papilloma virus in head and neck cancer. *J Laryngol Otol.* 2010;124:941-944.
168. Califano J, van der Riet P, Westra W, et al. Genetic progression model for head and neck cancer: implications for field cancerization. *Cancer Res.* 1996;56:2488-2492.
169. Braakhuis BJ, Snijders PJ, Keune WJ, et al. Genetic patterns in head and neck cancers that contain or lack transcriptionally active human papillomavirus. *J Natl Cancer Inst.* 2004;96:998-1006.

170. Wu CL, Sloan P, Read AP, Harris R, Thakker N. Deletion mapping on the short arm of chromosome 3 in squamous cell carcinoma of the oral cavity. *Cancer Res.* 1994;54:6484-6488.
171. Califano J, Westra WH, Meininger G, Corio R, Koch WM, Sidransky D. Genetic progression and clonal relationship of recurrent premalignant head and neck lesions. *Clin Cancer Res.* 2000;6:347-352.
172. Subramanya D, Grivas PD. HPV and cervical cancer: updates on an established relationship. *Postgrad Med.* 2008;120:7-13.
173. Yugawa T, Kiyono T. Molecular mechanisms of cervical carcinogenesis by high-risk human papillomaviruses: novel functions of E6 and E7 oncoproteins. *Rev Med Virol.* 2009;19:97-113.
174. Wentzensen N, Vinokurova S, von Knebel Doeberitz M. Systematic review of genomic integration sites of human papillomavirus genomes in epithelial dysplasia and invasive cancer of the female lower genital tract. *Cancer Res.* 2004;64:3878-3884.
175. Thorland EC, Myers SL, Gostout BS, Smith DI. Common fragile sites are preferential targets for HPV16 integrations in cervical tumors. *Oncogene.* 2003;22:1225-1237.
176. Kraus I, Driesch C, Vinokurova S, et al. The majority of viral-cellular fusion transcripts in cervical carcinomas cotranscribe cellular sequences of known or predicted genes. *Cancer Res.* 2008;68:2514-2522.
177. Peter M, Stransky N, Couturier J, et al. Frequent genomic structural alterations at HPV insertion sites in cervical carcinoma. *J Pathol.* 2010;221:320-330.
178. Peter M, Rosty C, Couturier J, Radvanyi F, Teshima H, Sastre-Garau X. MYC activation associated with the integration of HPV DNA at the MYC locus in genital tumors. *Oncogene.* 2006;25:5985-5993.
179. Steenbergen RD, Hermsen MA, Walboomers JM, et al. Integrated human papillomavirus type 16 and loss of heterozygosity at 11q22 and 18q21 in an oral carcinoma and its derivative cell line. *Cancer Res.* 1995;55:5465-5471.
180. Ragin CC, Reshmi SC, Gollin SM. Mapping and analysis of HPV16 integration sites in a head and neck cancer cell line. *Int J Cancer.* 2004;110:701-709.
181. Gewin L, Galloway DA. E box-dependent activation of telomerase by human papillomavirus type 16 E6 does not require induction of c-myc. *J Virol.* 2001;75:7198-7201.
182. Van Doorslaer K, Burk RD. Association between hTERT activation by HPV E6 proteins and oncogenic risk. *Virology.* 2012;433:216-219.
183. Kiyono T, Foster SA, Koop JI, McDougall JK, Galloway DA, Klingelutz AJ. Both Rb/p16INK4a inactivation and telomerase activity are required to immortalize human epithelial cells. *Nature.* 1998;396:84-88.
184. Vega-Peña A, Illades-Aguiar B, Flores-Alfaro E, et al. Risk of progression of early cervical lesions is associated with integration and persistence of HPV-16 and expression of E6, Ki-67, and telomerase. *J Cytol.* 2013;30:226-232.
185. Kim NW, Piatyszek MA, Prowse KR, et al. Specific association of human telomerase activity with immortal cells and cancer. *Science.* 1994;266:2011-2015.
186. Mirghani H, Amen F, Tao Y, Deutsch E, Levy A. Increased radiosensitivity of HPV-positive head and neck cancers: Molecular basis and therapeutic perspectives. *Cancer Treat Rev.* 2015;41:844-852.
187. Kimple RJ, Smith MA, Blitzer GC, et al. Enhanced radiation sensitivity in HPV-positive head and neck cancer. *Cancer Res.* 2013;73:4791-4800.
188. Gubanov E, Brown B, Ivanov SV, et al. Downregulation of SMG-1 in HPV-positive head and neck squamous cell carcinoma due to promoter hypermethylation correlates with improved survival. *Clin Cancer Res.* 2012;18:1257-1267.

189. Brumbaugh KM, Otterness DM, Geisen C, et al. The mRNA surveillance protein hSMG-1 functions in genotoxic stress response pathways in mammalian cells. *Mol Cell*. 2004;14:585-598.
190. Gupta AK, Lee JH, Wilke WW, et al. Radiation response in two HPV-infected head-and-neck cancer cell lines in comparison to a non-HPV-infected cell line and relationship to signaling through AKT. *Int J Radiat Oncol Biol Phys*. 2009;74:928-933.
191. Vu HL, Sikora AG, Fu S, Kao J. HPV-induced oropharyngeal cancer, immune response and response to therapy. *Cancer Lett*. 2010;288:149-155.
192. Klozar J, Tachezy R, Rotnáglóvá E, Koslabová E, Saláková M, Hamsíková E. Human papillomavirus in head and neck tumors: epidemiological, molecular and clinical aspects. *Wien Med Wochenschr*. 2010;160:305-309.
193. Singhi AD, Westra WH. Comparison of human papillomavirus in situ hybridization and p16 immunohistochemistry in the detection of human papillomavirus-associated head and neck cancer based on a prospective clinical experience. *Cancer*. 2010;116:2166-2173.
194. Gillison ML. Human papillomavirus and prognosis of oropharyngeal squamous cell carcinoma: implications for clinical research in head and neck cancers. *J Clin Oncol*. 2006;24:5623-5625.
195. Allen CT, Lewis JS, El-Mofty SK, Haughey BH, Nussenbaum B. Human papillomavirus and oropharynx cancer: biology, detection and clinical implications. *Laryngoscope*. 2010;120:1756-1772.
196. Schache AG, Liloglou T, Risk JM, et al. Validation of a novel diagnostic standard in HPV-positive oropharyngeal squamous cell carcinoma. *Br J Cancer*. 2013;108:1332-1339.
197. Cooper K, Herrington CS, Stickland JE, Evans MF, McGee JO. Episomal and integrated human papillomavirus in cervical neoplasia shown by non-isotopic in situ hybridisation. *J Clin Pathol*. 1991;44:990-996.
198. Hafkamp HC, Speel EJ, Haesevoets A, et al. A subset of head and neck squamous cell carcinomas exhibits integration of HPV 16/18 DNA and overexpression of p16INK4A and p53 in the absence of mutations in p53 exons 5-8. *Int J Cancer*. 2003;107:394-400.
199. Weinberger PM, Yu Z, Kountourakis P, et al. Defining molecular phenotypes of human papillomavirus-associated oropharyngeal squamous cell carcinoma: validation of three-class hypothesis. *Otolaryngol Head Neck Surg*. 2009;141:382-389.
200. Wiest T, Schwarz E, Enders C, Flechtenmacher C, Bosch FX. Involvement of intact HPV16 E6/E7 gene expression in head and neck cancers with unaltered p53 status and perturbed pRb cell cycle control. *Oncogene*. 2002;21:1510-1517.
201. Grønhøj Larsen C, Gyldenløve M, Jensen DH, et al. Correlation between human papillomavirus and p16 overexpression in oropharyngeal tumours: a systematic review. *Br J Cancer*. 2014;110:1587-1594.
202. Jordan RC, Lingen MW, Perez-Ordóñez B, et al. Validation of methods for oropharyngeal cancer HPV status determination in US cooperative group trials. *Am J Surg Pathol*. 2012;36:945-954.
203. El-Naggar AK, Westra WH. p16 expression as a surrogate marker for HPV-related oropharyngeal carcinoma: a guide for interpretative relevance and consistency. *Head Neck*. 2012;34:459-461.
204. Lewis JS. p16 Immunohistochemistry as a standalone test for risk stratification in oropharyngeal squamous cell carcinoma. *Head Neck Pathol*. 2012;6 Suppl 1:S75-82.
205. Merlano MC, Denaro N, Vivenza D, et al. p16 cutoff in head and neck squamous cell carcinoma: correlation between tumor and patient characteristics and outcome. *Int J Biol Markers*. 2015:0.

206. Junor E, Kerr G, Oniscu A, et al. Benefit of chemotherapy as part of treatment for HPV DNA-positive but p16-negative squamous cell carcinoma of the oropharynx. *Br J Cancer*. 2012;106:358-365.
207. Ukpo OC, Flanagan JJ, Ma XJ, Luo Y, Thorstad WL, Lewis JS. High-risk human papillomavirus E6/E7 mRNA detection by a novel in situ hybridization assay strongly correlates with p16 expression and patient outcomes in oropharyngeal squamous cell carcinoma. *Am J Surg Pathol*. 2011;35:1343-1350.
208. Martró E, Valencia MJ, Tarrats A, et al. Comparison between two human papillomavirus genotyping assays targeting the L1 or E6/E7 region in cervical cancer biopsies. *Enferm Infecc Microbiol Clin*. 2012;30:225-229.
209. Burger RA, Monk BJ, Kurosaki T, et al. Human papillomavirus type 18: association with poor prognosis in early stage cervical cancer. *J Natl Cancer Inst*. 1996;88:1361-1368.
210. Im SS, Wilczynski SP, Burger RA, Monk BJ. Early stage cervical cancers containing human papillomavirus type 18 DNA have more nodal metastasis and deeper stromal invasion. *Clin Cancer Res*. 2003;9:4145-4150.
211. Kónya J, Veress G, Hernádi Z, Soós G, Czeglédy J, Gergely L. Correlation of human papillomavirus 16 and 18 with prognostic factors in invasive cervical neoplasias. *J Med Virol*. 1995;46:1-6.
212. Thibaudeau E, Fortin B, Coutlée F, et al. HPV Prevalence and Prognostic Value in a Prospective Cohort of 255 Patients with Locally Advanced HNSCC: A Single-Centre Experience. *Int J Otolaryngol*. 2013;2013:437815.
213. Cognetti DM, Weber RS, Lai SY. Head and neck cancer: an evolving treatment paradigm. *Cancer*. 2008;113:1911-1932.
214. Calais G, Alfonsi M, Bardet E, et al. Randomized trial of radiation therapy versus concomitant chemotherapy and radiation therapy for advanced-stage oropharynx carcinoma. *J Natl Cancer Inst*. 1999;91:2081-2086.
215. Masterson L, Moualed D, Masood A, et al. De-escalation treatment protocols for human papillomavirus-associated oropharyngeal squamous cell carcinoma. *Cochrane Database Syst Rev*. 2014;2:CD010271.
216. Lindel K, Beer KT, Laissue J, Greiner RH, Aebbersold DM. Human papillomavirus positive squamous cell carcinoma of the oropharynx: a radiosensitive subgroup of head and neck carcinoma. *Cancer*. 2001;92:805-813.
217. Evans M, Powell NG. The changing aetiology of head and neck cancer: the role of human papillomavirus. *Clin Oncol (R Coll Radiol)*. 2010;22:538-546.
218. Mehannah H. Determination of Epidermal growth factor receptor inhibitor (cetuximab) versus Standard Chemotherapy (cisplatin) early And Late Toxicity Events in Human Papillomavirus positive oropharyngeal squamous cell carcinoma.
219. Trotti A, Gillison M. Phase III Trial of Radiotherapy Plus Cetuximab Versus Chemoradiotherapy in HPV-Associated Oropharynx Cancer.
220. Schrag D. The price tag on progress--chemotherapy for colorectal cancer. *N Engl J Med*. 2004;351:317-319.
221. Griffin S, Walker S, Sculpher M, et al. Cetuximab plus radiotherapy for the treatment of locally advanced squamous cell carcinoma of the head and neck. *Health Technol Assess*. 2009;13 Suppl 1:49-54.
222. Greenhalgh J, Bagust A, Boland A, et al. Cetuximab for the treatment of recurrent and/or metastatic squamous cell carcinoma of the head and neck. *Health Technol Assess*. 2009;13 Suppl 3:49-54.

223. O'Sullivan B, Huang SH, Siu LL, et al. Deintensification candidate subgroups in human papillomavirus-related oropharyngeal cancer according to minimal risk of distant metastasis. *J Clin Oncol*. 2013;31:543-550.
224. Blanchard P, Baujat B, Holostenco V, et al. Meta-analysis of chemotherapy in head and neck cancer (MACH-NC): a comprehensive analysis by tumour site. *Radiother Oncol*. 2011;100:33-40.
225. Pignon JP, Bourhis J, Domenge C, Designé L. Chemotherapy added to locoregional treatment for head and neck squamous-cell carcinoma: three meta-analyses of updated individual data. MACH-NC Collaborative Group. Meta-Analysis of Chemotherapy on Head and Neck Cancer. *Lancet*. 2000;355:949-955.
226. Pignon JP, le Maître A, Maillard E, Bourhis J, Group M-NC. Meta-analysis of chemotherapy in head and neck cancer (MACH-NC): an update on 93 randomised trials and 17,346 patients. *Radiother Oncol*. 2009;92:4-14.
227. Brotherston DC, Poon I, Le T, et al. Patient preferences for oropharyngeal cancer treatment de-escalation. *Head Neck*. 2013;35:151-159.
228. Hinni ML, Nagel T, Howard B. Oropharyngeal cancer treatment: the role of transoral surgery. *Curr Opin Otolaryngol Head Neck Surg*. 2015;23:132-138.
229. Nichols AC, Yoo J, Hammond JA, et al. Early-stage squamous cell carcinoma of the oropharynx: radiotherapy vs. trans-oral robotic surgery (ORATOR)--study protocol for a randomized phase II trial. *BMC Cancer*. 2013;13:133.
230. van Loon JW, Smeele LE, Hilgers FJ, van den Brekel MW. Outcome of transoral robotic surgery for stage I-II oropharyngeal cancer. *Eur Arch Otorhinolaryngol*. 2015;272:175-183.
231. Buckley L, Gupta R, Ashford B, Jabbour J, Clark JR. Oropharyngeal cancer and human papilloma virus: evolving diagnostic and management paradigms. *ANZ J Surg*. 2015.
232. Ford SE, Brandwein-Gensler M, Carroll WR, Rosenthal EL, Magnuson JS. Transoral robotic versus open surgical approaches to oropharyngeal squamous cell carcinoma by human papillomavirus status. *Otolaryngol Head Neck Surg*. 2014;151:606-611.
233. Gupta T, Kannan S, Ghosh-Laskar S, Agarwal JP. Systematic Review and Meta-analysis of Conventionally Fractionated Concurrent Chemoradiotherapy versus Altered Fractionation Radiotherapy Alone in the Definitive Management of Locoregionally Advanced Head and Neck Squamous Cell Carcinoma. *Clin Oncol (R Coll Radiol)*. 2016;28:50-61.
234. Zhang L, Jiang N, Shi Y, Li S, Wang P, Zhao Y. Induction chemotherapy with concurrent chemoradiotherapy versus concurrent chemoradiotherapy for locally advanced squamous cell carcinoma of head and neck: a meta-analysis. *Sci Rep*. 2015;5:10798.
235. Petrelli F, Coinu A, Riboldi V, et al. Concomitant platinum-based chemotherapy or cetuximab with radiotherapy for locally advanced head and neck cancer: a systematic review and meta-analysis of published studies. *Oral Oncol*. 2014;50:1041-1048.
236. Marta GN, Silva V, de Andrade Carvalho H, et al. Intensity-modulated radiation therapy for head and neck cancer: systematic review and meta-analysis. *Radiother Oncol*. 2014;110:9-15.
237. Thurlow JK, Peña Murillo CL, Hunter KD, et al. Spectral clustering of microarray data elucidates the roles of microenvironment remodeling and immune responses in survival of head and neck squamous cell carcinoma. *J Clin Oncol*. 2010;28:2881-2888.
238. Roepman P, de Koning E, van Leenen D, et al. Dissection of a metastatic gene expression signature into distinct components. *Genome Biol*. 2006;7:R117.
239. Salem AF, Al-Zoubi MS, Whitaker-Menezes D, et al. Cigarette smoke metabolically promotes cancer, via autophagy and premature aging in the host stromal microenvironment. *Cell Cycle*. 2013;12:818-825.

240. Hassona Y, Cirillo N, Lim KP, et al. Progression of genotype-specific oral cancer leads to senescence of cancer-associated fibroblasts and is mediated by oxidative stress and TGF- β . *Carcinogenesis*. 2013;34:1286-1295.
241. Erez N, Truitt M, Olson P, Arron ST, Hanahan D. Cancer-Associated Fibroblasts Are Activated in Incipient Neoplasia to Orchestrate Tumor-Promoting Inflammation in an NF-kappaB-Dependent Manner. *Cancer Cell*. 2010;17:135-147.
242. Marsh D, Suchak K, Moutasim KA, et al. Stromal features are predictive of disease mortality in oral cancer patients. *J Pathol*. 2011;223:470-481.
243. Pitiyage GN, Slijepcevic P, Gabrani A, et al. Senescent mesenchymal cells accumulate in human fibrosis by a telomere-independent mechanism and ameliorate fibrosis through matrix metalloproteinases. *J Pathol*. 2011;223:604-617.
244. Coppe JP, Boysen M, Sun CH, et al. A role for fibroblasts in mediating the effects of tobacco-induced epithelial cell growth and invasion. *Mol Cancer Res*. 2008;6:1085-1098.
245. Parkinson EK. Senescence as a modulator of oral squamous cell carcinoma development. *Oral Oncol*. 2010;46:840-853.
246. Coppé JP, Patil CK, Rodier F, et al. Senescence-associated secretory phenotypes reveal cell-nonautonomous functions of oncogenic RAS and the p53 tumor suppressor. *PLoS Biol*. 2008;6:2853-2868.
247. Parrinello S, Coppe JP, Krtolica A, Campisi J. Stromal-epithelial interactions in aging and cancer: senescent fibroblasts alter epithelial cell differentiation. *J Cell Sci*. 2005;118:485-496.
248. Pyeon D, Newton MA, Lambert PF, et al. Fundamental differences in cell cycle deregulation in human papillomavirus-positive and human papillomavirus-negative head/neck and cervical cancers. *Cancer Res*. 2007;67:4605-4619.
249. Tsai KK, Stuart J, Chuang YY, Little JB, Yuan ZM. Low-dose radiation-induced senescent stromal fibroblasts render nearby breast cancer cells radioresistant. *Radiat Res*. 2009;172:306-313.
250. Ferris RL, Martinez I, Sirianni N, et al. Human papillomavirus-16 associated squamous cell carcinoma of the head and neck (SCCHN): a natural disease model provides insights into viral carcinogenesis. *Eur J Cancer*. 2005;41:807-815.
251. de Roda Husman AM, Walboomers JM, van den Brule AJ, Meijer CJ, Snijders PJ. The use of general primers GP5 and GP6 elongated at their 3' ends with adjacent highly conserved sequences improves human papillomavirus detection by PCR. *J Gen Virol*. 1995;76 (Pt 4):1057-1062.
252. Kennedy IM, Haddow JK, Clements JB. A negative regulatory element in the human papillomavirus type 16 genome acts at the level of late mRNA stability. *J Virol*. 1991;65:2093-2097.
253. Seedorf K, Krämer G, Dürst M, Suhai S, Röwekamp WG. Human papillomavirus type 16 DNA sequence. *Virology*. 1985;145:181-185.
254. Wald AI, Hoskins EE, Wells SI, Ferris RL, Khan SA. Alteration of microRNA profiles in squamous cell carcinoma of the head and neck cell lines by human papillomavirus. *Head Neck*. 2011;33:504-512.
255. Hanahan D, Weinberg RA. Hallmarks of cancer: the next generation. *Cell*. 2011;144:646-674.
256. Liang CC, Park AY, Guan JL. In vitro scratch assay: a convenient and inexpensive method for analysis of cell migration in vitro. *Nat Protoc*. 2007;2:329-333.
257. Zhang D, Chen ZG, Liu SH, et al. Galectin-3 gene silencing inhibits migration and invasion of human tongue cancer cells in vitro via downregulating β -catenin. *Acta Pharmacol Sin*. 2013;34:176-184.

258. Morley SM, D'Alessandro M, Sexton C, et al. Generation and characterization of epidermolysis bullosa simplex cell lines: scratch assays show faster migration with disruptive keratin mutations. *Br J Dermatol.* 2003;149:46-58.
259. Inoue H, Miyazaki Y, Kikuchi K, et al. Podoplanin promotes cell migration via the EGF-Src-Cas pathway in oral squamous cell carcinoma cell lines. *J Oral Sci.* 2012;54:241-250.
260. Draper BK, Komurasaki T, Davidson MK, Nanney LB. Epiregulin is more potent than EGF or TGF α in promoting in vitro wound closure due to enhanced ERK/MAPK activation. *J Cell Biochem.* 2003;89:1126-1137.
261. Chen P, Gupta K, Wells A. Cell movement elicited by epidermal growth factor receptor requires kinase and autophosphorylation but is separable from mitogenesis. *J Cell Biol.* 1994;124:547-555.
262. Silva D, Cáceres M, Arancibia R, Martínez C, Martínez J, Smith PC. Effects of cigarette smoke and nicotine on cell viability, migration and myofibroblastic differentiation. *J Periodontal Res.* 2012;47:599-607.
263. Brusevold IJ, Aasrum M, Bryne M, Christoffersen T. Migration induced by epidermal and hepatocyte growth factors in oral squamous carcinoma cells in vitro: role of MEK/ERK, p38 and PI-3 kinase/Akt. *J Oral Pathol Med.* 2012;41:547-558.
264. Rose MT. Effect of growth factors on the migration of equine oral and limb fibroblasts using an in vitro scratch assay. *Vet J.* 2012;193:539-544.
265. Kramer N, Walzl A, Unger C, et al. In vitro cell migration and invasion assays. *Mutat Res.* 2013;752:10-24.
266. Balló H, Koldovsky P, Hoffmann T, et al. Establishment and characterization of four cell lines derived from human head and neck squamous cell carcinomas for an autologous tumor-fibroblast in vitro model. *Anticancer Res.* 1999;19:3827-3836.
267. White JS, Weissfeld JL, Ragin CC, et al. The influence of clinical and demographic risk factors on the establishment of head and neck squamous cell carcinoma cell lines. *Oral Oncol.* 2007;43:701-712.
268. Virgilio L, Shuster M, Gollin SM, et al. FHIT gene alterations in head and neck squamous cell carcinomas. *Proc Natl Acad Sci U S A.* 1996;93:9770-9775.
269. Lin CJ, Grandis JR, Carey TE, et al. Head and neck squamous cell carcinoma cell lines: established models and rationale for selection. *Head Neck.* 2007;29:163-188.
270. Zhao M, Rosenbaum E, Carvalho AL, et al. Feasibility of quantitative PCR-based saliva rinse screening of HPV for head and neck cancer. *Int J Cancer.* 2005;117:605-610.
271. Sambrook J, Russell DW. *Molecular cloning : a laboratory manual.* 3rd ed. Cold Spring Harbor, N.Y.: Cold Spring Harbor Laboratory Press; 2001.
272. Storesund T, Hayashi K, Kolltveit KM, Bryne M, Schenck K. Salivary trefoil factor 3 enhances migration of oral keratinocytes. *Eur J Oral Sci.* 2008;116:135-140.
273. Davy C, Doorbar J. *Human papillomaviruses : methods and protocols.* Totowa, N.J.: Humana Press; 2005.
274. Masuda H, Zhang D, Bartholomeusz C, Doihara H, Hortobagyi GN, Ueno NT. Role of epidermal growth factor receptor in breast cancer. *Breast Cancer Res Treat.* 2012;136:331-345.
275. Blanco-Prieto S, Vázquez-Iglesias L, Rodríguez-Girondo M, et al. Serum calprotectin, CD26 and EGF to establish a panel for the diagnosis of lung cancer. *PLoS One.* 2015;10:e0127318.
276. Kwon MJ, Kim DH, Park HR, et al. Frequent hepatocyte growth factor overexpression and low frequency of c-Met gene amplification in human papillomavirus-negative tonsillar squamous cell carcinoma and their prognostic significances. *Hum Pathol.* 2014;45:1327-1338.

277. Sun Y, Nelson PS. Molecular pathways: involving microenvironment damage responses in cancer therapy resistance. *Clin Cancer Res.* 2012;18:4019-4025.
278. Kalluri R, Weinberg RA. The basics of epithelial-mesenchymal transition. *J Clin Invest.* 2009;119:1420-1428.
279. Zoni E, van der Pluijm G, Gray PC, Kruithof-de Julio M. Epithelial Plasticity in Cancer: Unmasking a MicroRNA Network for TGF- β -, Notch-, and Wnt-Mediated EMT. *J Oncol.* 2015;2015:198967.
280. Fuxe J, Karlsson MC. TGF- β -induced epithelial-mesenchymal transition: a link between cancer and inflammation. *Semin Cancer Biol.* 2012;22:455-461.
281. Moustakas A, Heldin CH. Induction of epithelial-mesenchymal transition by transforming growth factor β . *Semin Cancer Biol.* 2012;22:446-454.
282. Levovitz C, Chen D, Ivansson E, et al. TGF β receptor 1: an immune susceptibility gene in HPV-associated cancer. *Cancer Res.* 2014;74:6833-6844.
283. Guan X, Sturgis EM, Lei D, et al. Association of TGF-beta1 genetic variants with HPV16-positive oropharyngeal cancer. *Clin Cancer Res.* 2010;16:1416-1422.
284. Peralta-Zaragoza O, Bermúdez-Morales V, Gutiérrez-Xicotencatl L, Alcocer-González J, Recillas-Targa F, Madrid-Marina V. E6 and E7 oncoproteins from human papillomavirus type 16 induce activation of human transforming growth factor beta1 promoter throughout Sp1 recognition sequence. *Viral Immunol.* 2006;19:468-480.
285. Hatakeyama H, Mizumachi T, Sakashita T, Kano S, Homma A, Fukuda S. Epithelial-mesenchymal transition in human papillomavirus-positive and -negative oropharyngeal squamous cell carcinoma. *Oncol Rep.* 2014;32:2673-2679.
286. Dumont P, Burton M, Chen QM, et al. Induction of replicative senescence biomarkers by sublethal oxidative stresses in normal human fibroblast. *Free Radic Biol Med.* 2000;28:361-373.
287. Morgan E, Varro R, Sepulveda H, et al. Cytometric bead array: a multiplexed assay platform with applications in various areas of biology. *Clin Immunol.* 2004;110:252-266.
288. .
289. Acosta JC, O'Loughlen A, Banito A, et al. Chemokine signaling via the CXCR2 receptor reinforces senescence. *Cell.* 2008;133:1006-1018.
290. Rudisch A, Dewhurst MR, Horga LG, et al. High EMT Signature Score of Invasive Non-Small Cell Lung Cancer (NSCLC) Cells Correlates with NF κ B Driven Colony-Stimulating Factor 2 (CSF2/GM-CSF) Secretion by Neighboring Stromal Fibroblasts. *PLoS One.* 2015;10:e0124283.
291. McMahon GA, Dignam JD, Gentry LE. Structural characterization of the latent complex between transforming growth factor beta 1 and beta 1-latency-associated peptide. *Biochem J.* 1996;313 (Pt 1):343-351.
292. Zheng X, Jiang F, Katakowski M, Zhang ZG, Lu QE, Chopp M. ADAM17 promotes breast cancer cell malignant phenotype through EGFR-PI3K-AKT activation. *Cancer Biol Ther.* 2009;8:1045-1054.
293. Rios-Doria J, Sabol D, Chesebrough J, et al. A Monoclonal Antibody to ADAM17 Inhibits Tumor Growth by Inhibiting EGFR and Non-EGFR-Mediated Pathways. *Mol Cancer Ther.* 2015;14:1637-1649.
294. Harding J, Burtneß B. Cetuximab: an epidermal growth factor receptor chimeric human-murine monoclonal antibody. *Drugs Today (Barc).* 2005;41:107-127.
295. Bonner JA, Harari PM, Giralt J, et al. Radiotherapy plus cetuximab for squamous-cell carcinoma of the head and neck. *N Engl J Med.* 2006;354:567-578.
296. Vermorken JB, Mesia R, Rivera F, et al. Platinum-based chemotherapy plus cetuximab in head and neck cancer. *N Engl J Med.* 2008;359:1116-1127.

297. Uchino E, Tsuzuki T, Inoue K. The effects of age and sex on seven elements of Sprague - Dawley rat organs. *Lab Anim.* 1990;24:253-264.
298. Mirghani H, Amen F, Moreau F, Guigay J, Hartl DM, Lacau St Guily J. Oropharyngeal cancers: relationship between epidermal growth factor receptor alterations and human papillomavirus status. *Eur J Cancer.* 2014;50:1100-1111.
299. Crusius K, Auvinen E, Steuer B, Gaissert H, Alonso A. The human papillomavirus type 16 E5-protein modulates ligand-dependent activation of the EGF receptor family in the human epithelial cell line HaCaT. *Exp Cell Res.* 1998;241:76-83.
300. Kim SH, Juhnn YS, Kang S, et al. Human papillomavirus 16 E5 up-regulates the expression of vascular endothelial growth factor through the activation of epidermal growth factor receptor, MEK/ ERK1,2 and PI3K/Akt. *Cell Mol Life Sci.* 2006;63:930-938.
301. Bertotti A, Sassi F. Molecular Pathways: Sensitivity and Resistance to Anti-EGFR Antibodies. *Clin Cancer Res.* 2015;21:3377-3383.
302. Weickhardt AJ, Price TJ, Chong G, et al. Dual targeting of the epidermal growth factor receptor using the combination of cetuximab and erlotinib: preclinical evaluation and results of the phase II DUX study in chemotherapy-refractory, advanced colorectal cancer. *J Clin Oncol.* 2012;30:1505-1512.
303. Matar P, Rojo F, Cassia R, et al. Combined epidermal growth factor receptor targeting with the tyrosine kinase inhibitor gefitinib (ZD1839) and the monoclonal antibody cetuximab (IMC-C225): superiority over single-agent receptor targeting. *Clin Cancer Res.* 2004;10:6487-6501.
304. de Bock CE, Wang Y. Clinical significance of urokinase-type plasminogen activator receptor (uPAR) expression in cancer. *Med Res Rev.* 2004;24:13-39.
305. Hildenbrand R, Schaaf A, Dorn-Beineke A, et al. Tumor stroma is the predominant uPA-, uPAR-, PAI-1-expressing tissue in human breast cancer: prognostic impact. *Histol Histopathol.* 2009;24:869-877.
306. Thunø M, Macho B, Eugen-Olsen J. suPAR: the molecular crystal ball. *Dis Markers.* 2009;27:157-172.
307. Stephens RW, Nielsen HJ, Christensen IJ, et al. Plasma urokinase receptor levels in patients with colorectal cancer: relationship to prognosis. *J Natl Cancer Inst.* 1999;91:869-874.
308. Eugen-Olsen J, Gustafson P, Sidenius N, et al. The serum level of soluble urokinase receptor is elevated in tuberculosis patients and predicts mortality during treatment: a community study from Guinea-Bissau. *Int J Tuberc Lung Dis.* 2002;6:686-692.
309. Schneider UV, Nielsen RL, Pedersen C, Eugen-Olsen J. The prognostic value of the suPARnostic ELISA in HIV-1 infected individuals is not affected by uPAR promoter polymorphisms. *BMC Infect Dis.* 2007;7:134.
310. Begum FD, Høgdall CK, Kjaer SK, et al. The prognostic value of plasma soluble urokinase plasminogen activator receptor (suPAR) levels in stage III ovarian cancer patients. *Anticancer Res.* 2004;24:1981-1985.
311. Bao YN, Cao X, Luo DH, et al. Urokinase-type plasminogen activator receptor signaling is critical in nasopharyngeal carcinoma cell growth and metastasis. *Cell Cycle.* 2014;13:1958-1969.
312. Magnussen S, Rikardsen OG, Hadler-Olsen E, Uhlin-Hansen L, Steigen SE, Svineng G. Urokinase plasminogen activator receptor (uPAR) and plasminogen activator inhibitor-1 (PAI-1) are potential predictive biomarkers in early stage oral squamous cell carcinomas (OSCC). *PLoS One.* 2014;9:e101895.
313. Soria G, Ben-Baruch A. The inflammatory chemokines CCL2 and CCL5 in breast cancer. *Cancer Lett.* 2008;267:271-285.

314. Soria G, Yaal-Hahoshen N, Azenshtein E, et al. Concomitant expression of the chemokines RANTES and MCP-1 in human breast cancer: a basis for tumor-promoting interactions. *Cytokine*. 2008;44:191-200.
315. Zang J, Li C, Zhao LN, et al. Prognostic value of vascular endothelial growth factor in patients with head and neck cancer: A meta-analysis. *Head Neck*. 2013;35:1507-1514.
316. Kyzas PA, Cunha IW, Ioannidis JP. Prognostic significance of vascular endothelial growth factor immunohistochemical expression in head and neck squamous cell carcinoma: a meta-analysis. *Clin Cancer Res*. 2005;11:1434-1440.
317. Wilkie MD, Emmett MS, Santosh S, et al. Relative expression of vascular endothelial growth factor isoforms in squamous cell carcinoma of the head and neck. *Head Neck*. 2014.
318. Fei J, Hong A, Dobbins TA, et al. Prognostic significance of vascular endothelial growth factor in squamous cell carcinomas of the tonsil in relation to human papillomavirus status and epidermal growth factor receptor. *Ann Surg Oncol*. 2009;16:2908-2917.
319. Baruah P, Lee M, Wilson PO, et al. Impact of p16 status on pro- and anti-angiogenesis factors in head and neck cancers. *Br J Cancer*. 2015;113:653-659.
320. Li G, He L, Zhang E, et al. Overexpression of human papillomavirus (HPV) type 16 oncoproteins promotes angiogenesis via enhancing HIF-1 α and VEGF expression in non-small cell lung cancer cells. *Cancer Lett*. 2011;311:160-170.
321. Van Damme J, Proost P, Lenaerts JP, Opdenakker G. Structural and functional identification of two human, tumor-derived monocyte chemotactic proteins (MCP-2 and MCP-3) belonging to the chemokine family. *J Exp Med*. 1992;176:59-65.
322. Hwang TL, Lee LY, Wang CC, Liang Y, Huang SF, Wu CM. CCL7 and CCL21 overexpression in gastric cancer is associated with lymph node metastasis and poor prognosis. *World J Gastroenterol*. 2012;18:1249-1256.
323. Jung DW, Che ZM, Kim J, Kim K, Kim KY, Williams D. Tumor-stromal crosstalk in invasion of oral squamous cell carcinoma: a pivotal role of CCL7. *Int J Cancer*. 2010;127:332-344.
324. Levine SJ. Molecular mechanisms of soluble cytokine receptor generation. *J Biol Chem*. 2008;283:14177-14181.
325. Wang J, Sharma A, Ghamande SA, et al. Serum protein profile at remission can accurately assess therapeutic outcomes and survival for serous ovarian cancer. *PLoS One*. 2013;8:e78393.
326. Gadducci A, Ferdeghini M, Castellani C, et al. Serum levels of tumor necrosis factor (TNF), soluble receptors for TNF (55- and 75-kDa sTNFr), and soluble CD14 (sCD14) in epithelial ovarian cancer. *Gynecol Oncol*. 1995;58:184-188.
327. Gadducci A, Ferdeghini M, Fanucchi A, et al. Serum levels of soluble receptors for tumor necrosis factor (p55 and p75 sTNFr) in endometrial cancer. *Anticancer Res*. 1996;16:3125-3128.
328. Wu B, Wang W, Zhan Y, et al. CXCL13, CCL4, and sTNFR as circulating inflammatory cytokine markers in primary and SLE-related autoimmune hemolytic anemia. *J Transl Med*. 2015;13:112.
329. Sikora JP, Kuzański W, Andrzejewska E. Soluble cytokine receptors sTNFR I and sTNFR II, receptor antagonist IL-1ra, and anti-inflammatory cytokines IL-10 and IL-13 in the pathogenesis of systemic inflammatory response syndrome in the course of burns in children. *Med Sci Monit*. 2009;15:CR26-31.
330. Jacobson SH, Lu Y, Brauner A. Tumour necrosis factor soluble receptors I and II and interleukin-1 receptor antagonist in acute pyelonephritis in relation to bacterial virulence-associated traits and renal function. *Nephrol Dial Transplant*. 1996;11:2209-2214.

331. Dong W, Xu J, Qiao Z, Wang N, Yu R. [Expression and significance of serum soluble tumor necrosis factor receptor-I in patients with head and neck neoplasm]. *Zhonghua Er Bi Yan Hou Ke Za Zhi*. 2001;36:468-470.
332. Chen W, Gao Q, Han S, Pan F, Fan W. The CCL2/CCR2 axis enhances IL-6-induced epithelial-mesenchymal transition by cooperatively activating STAT3-Twist signaling. *Tumour Biol*. 2015;36:973-981.
333. Yadav A, Kumar B, Datta J, Teknos TN, Kumar P. IL-6 promotes head and neck tumor metastasis by inducing epithelial-mesenchymal transition via the JAK-STAT3-SNAIL signaling pathway. *Mol Cancer Res*. 2011;9:1658-1667.
334. Chuang JY, Huang YL, Yen WL, Chiang IP, Tsai MH, Tang CH. Syk/JNK/AP-1 signaling pathway mediates interleukin-6-promoted cell migration in oral squamous cell carcinoma. *Int J Mol Sci*. 2014;15:545-559.
335. Rokavec M, Öner MG, Li H, et al. IL-6R/STAT3/miR-34a feedback loop promotes EMT-mediated colorectal cancer invasion and metastasis. *J Clin Invest*. 2014;124:1853-1867.
336. Acosta JC, O'Loughlen A, Banito A, Raguz S, Gil J. Control of senescence by CXCR2 and its ligands. *Cell Cycle*. 2008;7:2956-2959.
337. Wauman J, De Ceuninck L, Vanderroost N, Lievens S, Tavernier J. RNF41 (Nrdp1) controls type 1 cytokine receptor degradation and ectodomain shedding. *J Cell Sci*. 2011;124:921-932.
338. Ogura H, Murakami M, Okuyama Y, et al. Interleukin-17 promotes autoimmunity by triggering a positive-feedback loop via interleukin-6 induction. *Immunity*. 2008;29:628-636.
339. Ahuja SK, Murphy PM. The CXC chemokines growth-regulated oncogene (GRO) alpha, GRObeta, GROgamma, neutrophil-activating peptide-2, and epithelial cell-derived neutrophil-activating peptide-78 are potent agonists for the type B, but not the type A, human interleukin-8 receptor. *J Biol Chem*. 1996;271:20545-20550.
340. Popper KR. *The Logic of scientific discovery*: [S.l.] : Hutchinson, 1972 (1977).
341. Guo H, Liu Z, Xu B, et al. Chemokine receptor CXCR2 is transactivated by p53 and induces p38-mediated cellular senescence in response to DNA damage. *Aging Cell*. 2013;12:1110-1121.
342. Kay AB, Lee TH. Neutrophil chemotactic factor of anaphylaxis. *J Allergy Clin Immunol*. 1982;70:317-320.
343. Lee TH, Nagy L, Nagakura T, Walport MJ, Kay AB. Identification and partial characterization of an exercise-induced neutrophil chemotactic factor in bronchial asthma. *J Clin Invest*. 1982;69:889-899.
344. Atkins PC, Norman M, Zweiman B, Rosenblum F. Further characterization and biologic activity of ragweed antigen--induced neutrophil chemotactic activity in man. *J Allergy Clin Immunol*. 1979;64:251-258.
345. Zarogoulidis P, Katsikogianni F, Tsiouda T, Sakkas A, Katsikogiannis N, Zarogoulidis K. Interleukin-8 and interleukin-17 for cancer. *Cancer Invest*. 2014;32:197-205.
346. Kundu JK, Surh YJ. Inflammation: gearing the journey to cancer. *Mutat Res*. 2008;659:15-30.
347. Hierholzer C, Kalff JC, Omert L, et al. Interleukin-6 production in hemorrhagic shock is accompanied by neutrophil recruitment and lung injury. *Am J Physiol*. 1998;275:L611-621.
348. Pietras K, Ostman A. Hallmarks of cancer: interactions with the tumor stroma. *Exp Cell Res*. 2010;316:1324-1331.
349. Rose-John S. IL-6 trans-signaling via the soluble IL-6 receptor: importance for the pro-inflammatory activities of IL-6. *Int J Biol Sci*. 2012;8:1237-1247.
350. Hanahan D, Weinberg RA. The hallmarks of cancer. *Cell*. 2000;100:57-70.

351. Aikawa T, Gunn J, Spong SM, Klaus SJ, Korc M. Connective tissue growth factor-specific antibody attenuates tumor growth, metastasis, and angiogenesis in an orthotopic mouse model of pancreatic cancer. *Mol Cancer Ther.* 2006;5:1108-1116.
352. Ijichi H, Chytil A, Gorska AE, et al. Inhibiting Cxcr2 disrupts tumor-stromal interactions and improves survival in a mouse model of pancreatic ductal adenocarcinoma. *J Clin Invest.* 2011;121:4106-4117.
353. Kim SA, Lee EK, Kuh HJ. Co-culture of 3D tumor spheroids with fibroblasts as a model for epithelial-mesenchymal transition in vitro. *Exp Cell Res.* 2015;335:187-196.
354. Yang Z, Sun Z, Liu H, et al. Connective tissue growth factor stimulates the proliferation, migration and differentiation of lung fibroblasts during paraquat-induced pulmonary fibrosis. *Mol Med Rep.* 2015;12:1091-1097.
355. Itoh Y, Joh T, Tanida S, et al. IL-8 promotes cell proliferation and migration through metalloproteinase-cleavage proHB-EGF in human colon carcinoma cells. *Cytokine.* 2005;29:275-282.
356. Luppi F, Longo AM, de Boer WI, Rabe KF, Hiemstra PS. Interleukin-8 stimulates cell proliferation in non-small cell lung cancer through epidermal growth factor receptor transactivation. *Lung Cancer.* 2007;56:25-33.
357. Kyriakakis E, Cavallari M, Pfaff D, et al. IL-8-mediated angiogenic responses of endothelial cells to lipid antigen activation of iNKT cells depend on EGFR transactivation. *J Leukoc Biol.* 2011;90:929-939.
358. Moser B, Clark-Lewis I, Zwahlen R, Baggiolini M. Neutrophil-activating properties of the melanoma growth-stimulatory activity. *J Exp Med.* 1990;171:1797-1802.
359. Bechara C, Chai H, Lin PH, Yao Q, Chen C. Growth related oncogene-alpha (GRO-alpha): roles in atherosclerosis, angiogenesis and other inflammatory conditions. *Med Sci Monit.* 2007;13:RA87-90.
360. Verbeke H, Struyf S, Laureys G, Van Damme J. The expression and role of CXC chemokines in colorectal cancer. *Cytokine Growth Factor Rev.* 2011;22:345-358.
361. Wang D, Wang H, Brown J, et al. CXCL1 induced by prostaglandin E2 promotes angiogenesis in colorectal cancer. *J Exp Med.* 2006;203:941-951.
362. Chiu ST, Hsieh FJ, Chen SW, Chen CL, Shu HF, Li H. Clinicopathologic correlation of up-regulated genes identified using cDNA microarray and real-time reverse transcription-PCR in human colorectal cancer. *Cancer Epidemiol Biomarkers Prev.* 2005;14:437-443.
363. Bièche I, Chavey C, Andrieu C, et al. CXC chemokines located in the 4q21 region are up-regulated in breast cancer. *Endocr Relat Cancer.* 2007;14:1039-1052.
364. Allen C, Duffy S, Teknos T, et al. Nuclear factor-kappaB-related serum factors as longitudinal biomarkers of response and survival in advanced oropharyngeal carcinoma. *Clin Cancer Res.* 2007;13:3182-3190.
365. Khurram SA, Bingle L, McCabe BM, Farthing PM, Whawell SA. The chemokine receptors CXCR1 and CXCR2 regulate oral cancer cell behaviour. *J Oral Pathol Med.* 2014;43:667-674.
366. Qian Y, Wang Y, Li DS, et al. The chemokine receptor-CXCR2 plays a critical role in the invasion and metastases of oral squamous cell carcinoma in vitro and in vivo. *J Oral Pathol Med.* 2014;43:658-666.
367. De Filippo K, Dudeck A, Hasenberg M, et al. Mast cell and macrophage chemokines CXCL1/CXCL2 control the early stage of neutrophil recruitment during tissue inflammation. *Blood.* 2013;121:4930-4937.
368. Zhao H, Zhu H, Jin Q, et al. Association of high expression of Groβ with clinical and pathological characteristics of unfavorable prognosis in gastrointestinal stromal tumors. *Dis Markers.* 2015;2015:171035.

369. Doll D, Keller L, Maak M, et al. Differential expression of the chemokines GRO-2, GRO-3, and interleukin-8 in colon cancer and their impact on metastatic disease and survival. *Int J Colorectal Dis.* 2010;25:573-581.
370. Wang B, Khachigian LM, Esau L, et al. A key role for early growth response-1 and nuclear factor-kappaB in mediating and maintaining GRO/CXCR2 proliferative signaling in esophageal cancer. *Mol Cancer Res.* 2009;7:755-764.
371. Wang B, Hendricks DT, Wamunyokoli F, Parker MI. A growth-related oncogene/CXC chemokine receptor 2 autocrine loop contributes to cellular proliferation in esophageal cancer. *Cancer Res.* 2006;66:3071-3077.
372. Cross AK, Richardson V, Ali SA, Palmer I, Taub DD, Rees RC. Migration responses of human monocytic cell lines to alpha- and beta-chemokines. *Cytokine.* 1997;9:521-528.
373. Smith DF, Galkina E, Ley K, Huo Y. GRO family chemokines are specialized for monocyte arrest from flow. *Am J Physiol Heart Circ Physiol.* 2005;289:H1976-1984.
374. Al-Alwan LA, Chang Y, Mogas A, et al. Differential roles of CXCL2 and CXCL3 and their receptors in regulating normal and asthmatic airway smooth muscle cell migration. *J Immunol.* 2013;191:2731-2741.
375. Farioli-Vecchioli S, Cinà I, Ceccarelli M, et al. Tis21 knock-out enhances the frequency of medulloblastoma in Patched1 heterozygous mice by inhibiting the Cxcl3-dependent migration of cerebellar neurons. *J Neurosci.* 2012;32:15547-15564.
376. Zhang H, Ning H, Banie L, et al. Adipose tissue-derived stem cells secrete CXCL5 cytokine with chemoattractant and angiogenic properties. *Biochem Biophys Res Commun.* 2010;402:560-564.
377. Wuyts A, Proost P, Lenaerts JP, Ben-Baruch A, Van Damme J, Wang JM. Differential usage of the CXC chemokine receptors 1 and 2 by interleukin-8, granulocyte chemotactic protein-2 and epithelial-cell-derived neutrophil attractant-78. *Eur J Biochem.* 1998;255:67-73.
378. Van Damme J, Wuyts A, Froyen G, et al. Granulocyte chemotactic protein-2 and related CXC chemokines: from gene regulation to receptor usage. *J Leukoc Biol.* 1997;62:563-569.
379. Tian H, Huang P, Zhao Z, Tang W, Xia J. HIF-1 α plays a role in the chemotactic migration of hepatocarcinoma cells through the modulation of CXCL6 expression. *Cell Physiol Biochem.* 2014;34:1536-1546.
380. Tokumaru S, Sayama K, Yamasaki K, et al. SOCS3/CIS3 negative regulation of STAT3 in HGF-induced keratinocyte migration. *Biochem Biophys Res Commun.* 2005;327:100-105.
381. Boccaccio C, Andò M, Tamagnone L, et al. Induction of epithelial tubules by growth factor HGF depends on the STAT pathway. *Nature.* 1998;391:285-288.
382. Daly AJ, McIlreavey L, Irwin CR. Regulation of HGF and SDF-1 expression by oral fibroblasts--implications for invasion of oral cancer. *Oral Oncol.* 2008;44:646-651.
383. Sun R, Zhang Q, Guo L, et al. HGF stimulates proliferation through the HGF/c-Met pathway in nasopharyngeal carcinoma cells. *Oncol Lett.* 2012;3:1124-1128.
384. Xu P, Li Y, Yang S, Yang H, Tang J, Li M. Micro-ribonucleic acid 143 (MiR-143) inhibits oral squamous cell carcinoma (OSCC) cell migration and invasion by downregulation of phospho-c-Met through targeting CD44 v3. *Oral Surg Oral Med Oral Pathol Oral Radiol.* 2015;120:43-51.
385. Tao X, Hill KS, Gaziova I, et al. Silencing Met receptor tyrosine kinase signaling decreased oral tumor growth and increased survival of nude mice. *Oral Oncol.* 2014;50:104-112.
386. Schoppet M, Preissner KT, Hofbauer LC. RANK ligand and osteoprotegerin: paracrine regulators of bone metabolism and vascular function. *Arterioscler Thromb Vasc Biol.* 2002;22:549-553.

387. Wittrant Y, Théoleyre S, Chipoy C, et al. RANKL/RANK/OPG: new therapeutic targets in bone tumours and associated osteolysis. *Biochim Biophys Acta*. 2004;1704:49-57.
388. Goranov SE, Goranova-Marinova VS. Bone lesions in multiple myeloma--the OPG/RANK-ligand system. *Folia Med (Plovdiv)*. 2004;46:5-11.
389. Bruce AG, Linsley PS, Rose TM. Oncostatin M. *Prog Growth Factor Res*. 1992;4:157-170.
390. Chen SH, Benveniste EN. Oncostatin M: a pleiotropic cytokine in the central nervous system. *Cytokine Growth Factor Rev*. 2004;15:379-391.
391. Mosley B, De Imus C, Friend D, et al. Dual oncostatin M (OSM) receptors. Cloning and characterization of an alternative signaling subunit conferring OSM-specific receptor activation. *J Biol Chem*. 1996;271:32635-32643.
392. Gómez-Lechón MJ. Oncostatin M: signal transduction and biological activity. *Life Sci*. 1999;65:2019-2030.
393. Gearing DP, Comeau MR, Friend DJ, et al. The IL-6 signal transducer, gp130: an oncostatin M receptor and affinity converter for the LIF receptor. *Science*. 1992;255:1434-1437.
394. Grant SL, Begley CG. The oncostatin M signalling pathway: reversing the neoplastic phenotype? *Mol Med Today*. 1999;5:406-412.
395. Ko HS, Choi SK, Kang HK, et al. Oncostatin M stimulates cell migration and proliferation by down-regulating E-cadherin in HTR8/SVneo cell line through STAT3 activation. *Reprod Biol Endocrinol*. 2013;11:93.
396. Fossey SL, Bear MD, Kiseberth WC, Pennell M, London CA. Oncostatin M promotes STAT3 activation, VEGF production, and invasion in osteosarcoma cell lines. *BMC Cancer*. 2011;11:125.
397. Zhu M, Che Q, Liao Y, et al. Oncostatin M activates STAT3 to promote endometrial cancer invasion and angiogenesis. *Oncol Rep*. 2015;34:129-138.
398. Li N, Fu H, Tie Y, et al. miR-34a inhibits migration and invasion by down-regulation of c-Met expression in human hepatocellular carcinoma cells. *Cancer Lett*. 2009;275:44-53.
399. Ke AW, Shi GM, Zhou J, et al. Role of overexpression of CD151 and/or c-Met in predicting prognosis of hepatocellular carcinoma. *Hepatology*. 2009;49:491-503.
400. West NR, Murray JI, Watson PH. Oncostatin-M promotes phenotypic changes associated with mesenchymal and stem cell-like differentiation in breast cancer. *Oncogene*. 2014;33:1485-1494.
401. West NR, Murphy LC, Watson PH. Oncostatin M suppresses oestrogen receptor- α expression and is associated with poor outcome in human breast cancer. *Endocr Relat Cancer*. 2012;19:181-195.
402. Hibi K, Goto T, Sakuraba K, et al. Methylation of OSMR gene is frequently observed in non-invasive colorectal cancer. *Anticancer Res*. 2011;31:1293-1295.
403. Lacreusette A, Lartigue A, Nguyen JM, et al. Relationship between responsiveness of cancer cells to Oncostatin M and/or IL-6 and survival of stage III melanoma patients treated with tumour-infiltrating lymphocytes. *J Pathol*. 2008;216:451-459.
404. Richards CD. The enigmatic cytokine oncostatin m and roles in disease. *ISRN Inflamm*. 2013;2013:512103.
405. Zarling JM, Shoyab M, Marquardt H, Hanson MB, Lioubin MN, Todaro GJ. Oncostatin M: a growth regulator produced by differentiated histiocytic lymphoma cells. *Proc Natl Acad Sci U S A*. 1986;83:9739-9743.
406. Rose-John S, Scheller J, Elson G, Jones SA. Interleukin-6 biology is coordinated by membrane-bound and soluble receptors: role in inflammation and cancer. *J Leukoc Biol*. 2006;80:227-236.

407. Müllberg J, Schooltink H, Stoyan T, et al. The soluble interleukin-6 receptor is generated by shedding. *Eur J Immunol.* 1993;23:473-480.
408. Matthews V, Schuster B, Schütze S, et al. Cellular cholesterol depletion triggers shedding of the human interleukin-6 receptor by ADAM10 and ADAM17 (TACE). *J Biol Chem.* 2003;278:38829-38839.
409. Saftig P, Reiss K. The "A Disintegrin And Metalloproteases" ADAM10 and ADAM17: novel drug targets with therapeutic potential? *Eur J Cell Biol.* 2011;90:527-535.
410. Lust JA, Donovan KA, Kline MP, Greipp PR, Kyle RA, Maihle NJ. Isolation of an mRNA encoding a soluble form of the human interleukin-6 receptor. *Cytokine.* 1992;4:96-100.
411. Coxon A, Rex K, Meyer S, et al. Soluble c-Met receptors inhibit phosphorylation of c-Met and growth of hepatocyte growth factor: c-Met-dependent tumors in animal models. *Mol Cancer Ther.* 2009;8:1119-1125.
412. Athauda G, Giubellino A, Coleman JA, et al. c-Met ectodomain shedding rate correlates with malignant potential. *Clin Cancer Res.* 2006;12:4154-4162.
413. Wajih N, Walter J, Sane DC. Vascular origin of a soluble truncated form of the hepatocyte growth factor receptor (c-met). *Circ Res.* 2002;90:46-52.
414. Scheller J, Chalaris A, Garbers C, Rose-John S. ADAM17: a molecular switch to control inflammation and tissue regeneration. *Trends Immunol.* 2011;32:380-387.
415. Buraschi S, Pal N, Tyler-Rubinstein N, Owens RT, Neill T, Iozzo RV. Decorin antagonizes Met receptor activity and down-regulates {beta}-catenin and Myc levels. *J Biol Chem.* 2010;285:42075-42085.
416. Choe JY, Yun JY, Nam SJ, Kim JE. Expression of c-Met Is Different along the Location and Associated with Lymph Node Metastasis of Head and Neck Carcinoma. *Korean J Pathol.* 2012;46:515-522.
417. Lewis MP, Lygoe KA, Nystrom ML, et al. Tumour-derived TGF-beta1 modulates myofibroblast differentiation and promotes HGF/SF-dependent invasion of squamous carcinoma cells. *Br J Cancer.* 2004;90:822-832.
418. Knowles LM, Stabile LP, Egloff AM, et al. HGF and c-Met participate in paracrine tumorigenic pathways in head and neck squamous cell cancer. *Clin Cancer Res.* 2009;15:3740-3750.
419. Bennett JH, Morgan MJ, Whawell SA, et al. Metalloproteinase expression in normal and malignant oral keratinocytes: stimulation of MMP-2 and -9 by scatter factor. *Eur J Oral Sci.* 2000;108:281-291.
420. Dimou A, Non L, Chae YK, Tester WJ, Syrigos KN. MET gene copy number predicts worse overall survival in patients with non-small cell lung cancer (NSCLC); a systematic review and meta-analysis. *PLoS One.* 2014;9:e107677.
421. Aune G, Lian AM, Tingulstad S, et al. Increased circulating hepatocyte growth factor (HGF): a marker of epithelial ovarian cancer and an indicator of poor prognosis. *Gynecol Oncol.* 2011;121:402-406.
422. Peng Z, Zhu Y, Wang Q, et al. Prognostic significance of MET amplification and expression in gastric cancer: a systematic review with meta-analysis. *PLoS One.* 2014;9:e84502.
423. Yu S, Yu Y, Zhao N, Cui J, Li W, Liu T. C-Met as a prognostic marker in gastric cancer: a systematic review and meta-analysis. *PLoS One.* 2013;8:e79137.
424. Liu Y, Yu XF, Zou J, Luo ZH. Prognostic value of c-Met in colorectal cancer: a meta-analysis. *World J Gastroenterol.* 2015;21:3706-3710.
425. Gao H, Guan M, Sun Z, Bai C. High c-Met expression is a negative prognostic marker for colorectal cancer: a meta-analysis. *Tumour Biol.* 2015;36:515-520.

426. Aebersold DM, Kollar A, Beer KT, Laissue J, Greiner RH, Djonov V. Involvement of the hepatocyte growth factor/scatter factor receptor c-met and of Bcl-xL in the resistance of oropharyngeal cancer to ionizing radiation. *Int J Cancer*. 2001;96:41-54.
427. Montag M, Dyckhoff G, Lohr J, et al. Angiogenic growth factors in tissue homogenates of HNSCC: expression pattern, prognostic relevance, and interrelationships. *Cancer Sci*. 2009;100:1210-1218.
428. Baschnagel AM, Williams L, Hanna A, et al. c-Met expression is a marker of poor prognosis in patients with locally advanced head and neck squamous cell carcinoma treated with chemoradiation. *Int J Radiat Oncol Biol Phys*. 2014;88:701-707.
429. Qian CN, Guo X, Cao B, et al. Met protein expression level correlates with survival in patients with late-stage nasopharyngeal carcinoma. *Cancer Res*. 2002;62:589-596.
430. Liu X, Wang Q, Yang G, et al. A novel kinase inhibitor, INCB28060, blocks c-MET-dependent signaling, neoplastic activities, and cross-talk with EGFR and HER-3. *Clin Cancer Res*. 2011;17:7127-7138.
431. Shah MA, Wainberg ZA, Catenacci DV, et al. Phase II study evaluating 2 dosing schedules of oral foretinib (GSK1363089), cMET/VEGFR2 inhibitor, in patients with metastatic gastric cancer. *PLoS One*. 2013;8:e54014.
432. Choueiri TK, Vaishampayan U, Rosenberg JE, et al. Phase II and biomarker study of the dual MET/VEGFR2 inhibitor foretinib in patients with papillary renal cell carcinoma. *J Clin Oncol*. 2013;31:181-186.
433. Seiwert T, Sarantopoulos J, Kallender H, McCallum S, Keer HN, Blumenschein G. Phase II trial of single-agent foretinib (GSK1363089) in patients with recurrent or metastatic squamous cell carcinoma of the head and neck. *Invest New Drugs*. 2013;31:417-424.
434. Cecchi F, Rabe DC, Bottaro DP. Targeting the HGF/Met signaling pathway in cancer therapy. *Expert Opin Ther Targets*. 2012;16:553-572.
435. Qian F, Engst S, Yamaguchi K, et al. Inhibition of tumor cell growth, invasion, and metastasis by EXEL-2880 (XL880, GSK1363089), a novel inhibitor of HGF and VEGF receptor tyrosine kinases. *Cancer Res*. 2009;69:8009-8016.
436. Eder JP, Vande Woude GF, Boerner SA, LoRusso PM. Novel therapeutic inhibitors of the c-Met signaling pathway in cancer. *Clin Cancer Res*. 2009;15:2207-2214.
437. Bonfils C, Beaulieu N, Fournel M, Ste-Croix H, Besterman J, Maroun C. The combination of MGCD265, a Met/VEGFR inhibitor in clinical development, and erlotinib potently inhibits tumor growth by altering multiple pathways including glycolysis 2012.
438. Liu L, Siegmund A, Xi N, et al. Discovery of a potent, selective, and orally bioavailable c-Met inhibitor: 1-(2-hydroxy-2-methylpropyl)-N-(5-(7-methoxyquinolin-4-yloxy)pyridin-2-yl)-5-methyl-3-oxo-2-phenyl-2,3-dihydro-1H-pyrazole-4-carboxamide (AMG 458). *J Med Chem*. 2008;51:3688-3691.
439. You WK, Sennino B, Williamson CW, et al. VEGF and c-Met blockade amplify angiogenesis inhibition in pancreatic islet cancer. *Cancer Res*. 2011;71:4758-4768.
440. Pan BS, Chan GK, Chenard M, et al. MK-2461, a novel multitargeted kinase inhibitor, preferentially inhibits the activated c-Met receptor. *Cancer Res*. 2010;70:1524-1533.
441. Schroeder GM, An Y, Cai ZW, et al. Discovery of N-(4-(2-amino-3-chloropyridin-4-yloxy)-3-fluorophenyl)-4-ethoxy-1-(4-fluorophenyl)-2-oxo-1,2-dihydropyridine-3-carboxamide (BMS-777607), a selective and orally efficacious inhibitor of the Met kinase superfamily. *J Med Chem*. 2009;52:1251-1254.
442. Buchanan SG, Hendle J, Lee PS, et al. SGX523 is an exquisitely selective, ATP-competitive inhibitor of the MET receptor tyrosine kinase with antitumor activity in vivo. *Mol Cancer Ther*. 2009;8:3181-3190.

443. Timofeevski SL, McTigue MA, Ryan K, et al. Enzymatic characterization of c-Met receptor tyrosine kinase oncogenic mutants and kinetic studies with aminopyridine and triazolopyrazine inhibitors. *Biochemistry*. 2009;48:5339-5349.
444. Carboni JM, Wittman M, Yang Z, et al. BMS-754807, a small molecule inhibitor of insulin-like growth factor-1R/IR. *Mol Cancer Ther*. 2009;8:3341-3349.
445. Albrecht BK, Harmange JC, Bauer D, et al. Discovery and optimization of triazolopyridazines as potent and selective inhibitors of the c-Met kinase. *J Med Chem*. 2008;51:2879-2882.
446. Smolen GA, Sordella R, Muir B, et al. Amplification of MET may identify a subset of cancers with extreme sensitivity to the selective tyrosine kinase inhibitor PHA-665752. *Proc Natl Acad Sci U S A*. 2006;103:2316-2321.
447. Christensen JG, Schreck R, Burrows J, et al. A selective small molecule inhibitor of c-Met kinase inhibits c-Met-dependent phenotypes in vitro and exhibits cytoreductive antitumor activity in vivo. *Cancer Res*. 2003;63:7345-7355.
448. Zou HY, Li Q, Lee JH, et al. An orally available small-molecule inhibitor of c-Met, PF-2341066, exhibits cytoreductive antitumor efficacy through antiproliferative and antiangiogenic mechanisms. *Cancer Res*. 2007;67:4408-4417.
449. Nakagawa T, Tohyama O, Yamaguchi A, et al. E7050: a dual c-Met and VEGFR-2 tyrosine kinase inhibitor promotes tumor regression and prolongs survival in mouse xenograft models. *Cancer Sci*. 2010;101:210-215.
450. Wang X, Le P, Liang C, et al. Potent and selective inhibitors of the Met [hepatocyte growth factor/scatter factor (HGF/SF) receptor] tyrosine kinase block HGF/SF-induced tumor cell growth and invasion. *Mol Cancer Ther*. 2003;2:1085-1092.
451. Munshi N, Jeay S, Li Y, et al. ARQ 197, a novel and selective inhibitor of the human c-Met receptor tyrosine kinase with antitumor activity. *Mol Cancer Ther*. 2010;9:1544-1553.
452. Eathiraj S, Palma R, Volckova E, et al. Discovery of a novel mode of protein kinase inhibition characterized by the mechanism of inhibition of human mesenchymal-epithelial transition factor (c-Met) protein autophosphorylation by ARQ 197. *J Biol Chem*. 2011;286:20666-20676.
453. Taverna P, Huang L, Choy G, Azab M. Amuvatinib (MP-470), a multi-targeted tyrosine kinase inhibitor and DNA repair suppressor, synergizes with Etoposide (VP-16) in Small Cell Lung Cancer (SCLC) cell lines and xenografts: EORTC Conference; 2010.
454. Welsh JW, Mahadevan D, Ellsworth R, Cooke L, Bearss D, Stea B. The c-Met receptor tyrosine kinase inhibitor MP470 radiosensitizes glioblastoma cells. *Radiat Oncol*. 2009;4:69.
455. Morotti A, Mila S, Accornero P, Tagliabue E, Ponzetto C. K252a inhibits the oncogenic properties of Met, the HGF receptor. *Oncogene*. 2002;21:4885-4893.
456. Schiering N, Knapp S, Marconi M, et al. Crystal structure of the tyrosine kinase domain of the hepatocyte growth factor receptor c-Met and its complex with the microbial alkaloid K-252a. *Proc Natl Acad Sci U S A*. 2003;100:12654-12659.
457. Bellon SF, Kaplan-Lefko P, Yang Y, et al. c-Met inhibitors with novel binding mode show activity against several hereditary papillary renal cell carcinoma-related mutations. *J Biol Chem*. 2008;283:2675-2683.
458. Porter J. Small molecule c-Met kinase inhibitors: a review of recent patents. *Expert Opin Ther Pat*. 2010;20:159-177.
459. Logan TF. Foretinib (XL880): c-MET inhibitor with activity in papillary renal cell cancer. *Curr Oncol Rep*. 2013;15:83-90.

460. T Y, C-J Y, P-J C, Y C, R L. A Phase I/II Study Of Foretinib, An Oral Multikinase Inhibitor Targeting MET, RON, AXL, TIE-2 AND VEGFR In Advanced Hepatocellular Carcinoma (HCC). *J Hepatol* 54: S268, abstr 6652011.
461. Vargas GA, Hoeflich A, Jehle PM. Hepatocyte growth factor in renal failure: promise and reality. *Kidney Int.* 2000;57:1426-1436.
462. Brandes F, Schmidt K, Wagner C, et al. Targeting cMET with INC280 impairs tumour growth and improves efficacy of gemcitabine in a pancreatic cancer model. *BMC Cancer.* 2015;15:71.
463. Boccaccio C, Comoglio PM. Invasive growth: a MET-driven genetic programme for cancer and stem cells. *Nat Rev Cancer.* 2006;6:637-645.
464. Graziani A, Gramaglia D, Cantley LC, Comoglio PM. The tyrosine-phosphorylated hepatocyte growth factor/scatter factor receptor associates with phosphatidylinositol 3-kinase. *J Biol Chem.* 1991;266:22087-22090.
465. O'Brien LE, Tang K, Kats ES, Schutz-Geschwender A, Lipschutz JH, Mostov KE. ERK and MMPs sequentially regulate distinct stages of epithelial tubule development. *Dev Cell.* 2004;7:21-32.
466. Graziani A, Gramaglia D, dalla Zonca P, Comoglio PM. Hepatocyte growth factor/scatter factor stimulates the Ras-guanine nucleotide exchanger. *J Biol Chem.* 1993;268:9165-9168.
467. Monga SP, Mars WM, Padiaditakis P, et al. Hepatocyte growth factor induces Wnt-independent nuclear translocation of beta-catenin after Met-beta-catenin dissociation in hepatocytes. *Cancer Res.* 2002;62:2064-2071.
468. Papkoff J, Aikawa M. WNT-1 and HGF regulate GSK3beta activity and beta-catenin signaling in mammary epithelial cells. *Biochem Biophys Res Commun.* 1998;247:851-858.
469. Liu Y, Wang T, Yan J, et al. HGF/c-Met signalling promotes Notch3 activation and human vascular smooth muscle cell osteogenic differentiation in vitro. *Atherosclerosis.* 2011;219:440-447.
470. Ohnishi T, Daikuhara Y. Hepatocyte growth factor/scatter factor in development, inflammation and carcinogenesis: its expression and role in oral tissues. *Arch Oral Biol.* 2003;48:797-804.
471. Zhang YW, Vande Woude GF. HGF/SF-met signaling in the control of branching morphogenesis and invasion. *J Cell Biochem.* 2003;88:408-417.
472. Syed ZA, Yin W, Hughes K, Gill JN, Shi R, Clifford JL. HGF/c-met/Stat3 signaling during skin tumor cell invasion: indications for a positive feedback loop. *BMC Cancer.* 2011;11:180.
473. Yao X, Liu H, Zhang X, et al. Cell Surface GRP78 Accelerated Breast Cancer Cell Proliferation and Migration by Activating STAT3. *PLoS One.* 2015;10:e0125634.
474. Dunkel Y, Ong A, Notani D, et al. STAT3 protein up-regulates Gα-interacting vesicle-associated protein (GIV)/Girdin expression, and GIV enhances STAT3 activation in a positive feedback loop during wound healing and tumor invasion/metastasis. *J Biol Chem.* 2012;287:41667-41683.
475. Devarajan E, Huang S. STAT3 as a central regulator of tumor metastases. *Curr Mol Med.* 2009;9:626-633.
476. de Jong KP, van Gameren MM, Bijzet J, et al. Recombinant human interleukin-6 induces hepatocyte growth factor production in cancer patients. *Scand J Gastroenterol.* 2001;36:636-640.
477. [http://www.selleckchem.com/products/XL880\(GSK1363089](http://www.selleckchem.com/products/XL880(GSK1363089) E-h.
478. Kataoka Y, Mukohara T, Tomioka H, et al. Foretinib (GSK1363089), a multi-kinase inhibitor of MET and VEGFRs, inhibits growth of gastric cancer cell lines by blocking inter-receptor tyrosine kinase networks. *Invest New Drugs.* 2012;30:1352-1360.

479. Goel HL, Mercurio AM. VEGF targets the tumour cell. *Nat Rev Cancer*. 2013;13:871-882.
480. Uribe P, Gonzalez S. Epidermal growth factor receptor (EGFR) and squamous cell carcinoma of the skin: molecular bases for EGFR-targeted therapy. *Pathol Res Pract*. 2011;207:337-342.
481. Zuo JH, Zhu W, Li MY, et al. Activation of EGFR promotes squamous carcinoma SCC10A cell migration and invasion via inducing EMT-like phenotype change and MMP-9-mediated degradation of E-cadherin. *J Cell Biochem*. 2011;112:2508-2517.
482. Tumor Z, Katebzadeh S, Guerra C, Bhushan L, Alkam T, Henson BS. RhoC mediates epidermal growth factor-stimulated migration and invasion in head and neck squamous cell carcinoma. *Neoplasia*. 2015;17:141-151.
483. Pickhard AC, Margraf J, Knopf A, et al. Inhibition of radiation induced migration of human head and neck squamous cell carcinoma cells by blocking of EGF receptor pathways. *BMC Cancer*. 2011;11:388.
484. Ooft ML, Braunius WW, Heus P, et al. Prognostic significance of the EGFR pathway in nasopharyngeal carcinoma: a systematic review and meta-analysis. *Biomark Med*. 2015;9:997-1010.
485. Keller J, Nimnual AS, Shroyer KR, et al. Ron tyrosine kinase receptor synergises with EGFR to confer adverse features in head and neck squamous cell carcinoma. *Br J Cancer*. 2013;109:482-492.
486. Ang KK, Andratschke NH, Milas L. Epidermal growth factor receptor and response of head-and-neck carcinoma to therapy. *Int J Radiat Oncol Biol Phys*. 2004;58:959-965.
487. Kalyankrishna S, Grandis JR. Epidermal growth factor receptor biology in head and neck cancer. *J Clin Oncol*. 2006;24:2666-2672.
488. Kyzas PA, Stefanou D, Batistatou A, Agnantis NJ. Prognostic significance of VEGF immunohistochemical expression and tumor angiogenesis in head and neck squamous cell carcinoma. *J Cancer Res Clin Oncol*. 2005;131:624-630.
489. Salven P, Heikkilä P, Anttonen A, Kajanti M, Joensuu H. Vascular endothelial growth factor in squamous cell head and neck carcinoma: expression and prognostic significance. *Mod Pathol*. 1997;10:1128-1133.
490. Sauter ER, Nesbit M, Watson JC, Klein-Szanto A, Litwin S, Herlyn M. Vascular endothelial growth factor is a marker of tumor invasion and metastasis in squamous cell carcinomas of the head and neck. *Clin Cancer Res*. 1999;5:775-782.
491. Tsuchiya S, Yamabe M, Yamaguchi Y, Kobayashi Y, Konno T, Tada K. Establishment and characterization of a human acute monocytic leukemia cell line (THP-1). *Int J Cancer*. 1980;26:171-176.
492. Sanceau J, Wijdenes J, Revel M, Wietzerbin J. IL-6 and IL-6 receptor modulation by IFN-gamma and tumor necrosis factor-alpha in human monocytic cell line (THP-1). Priming effect of IFN-gamma. *J Immunol*. 1991;147:2630-2637.
493. Ishibe S, Karihaloo A, Ma H, et al. Met and the epidermal growth factor receptor act cooperatively to regulate final nephron number and maintain collecting duct morphology. *Development*. 2009;136:337-345.
494. Hov H, Tian E, Holien T, et al. c-Met signaling promotes IL-6-induced myeloma cell proliferation. *Eur J Haematol*. 2009;82:277-287.
495. Nechemia-Arbely Y, Shriki A, Denz U, et al. Early hepatocyte DNA synthetic response posthepatectomy is modulated by IL-6 trans-signaling and PI3K/AKT activation. *J Hepatol*. 2011;54:922-929.
496. Heinrich PC, Behrmann I, Haan S, Hermanns HM, Müller-Newen G, Schaper F. Principles of interleukin (IL)-6-type cytokine signalling and its regulation. *Biochem J*. 2003;374:1-20.

497. Vermeulen L, De Sousa E Melo F, van der Heijden M, et al. Wnt activity defines colon cancer stem cells and is regulated by the microenvironment. *Nat Cell Biol.* 2010;12:468-476.
498. Peplow PV, Chatterjee MP. A review of the influence of growth factors and cytokines in in vitro human keratinocyte migration. *Cytokine.* 2013;62:1-21.
499. Sun R, Jaruga B, Kulkarni S, Sun H, Gao B. IL-6 modulates hepatocyte proliferation via induction of HGF/p21cip1: regulation by SOCS3. *Biochem Biophys Res Commun.* 2005;338:1943-1949.
500. Zarnegar R, Michalopoulos GK. The many faces of hepatocyte growth factor: from hepatopoiesis to hematopoiesis. *J Cell Biol.* 1995;129:1177-1180.
501. Yamasaki K, Hanakawa Y, Tokumaru S, et al. Suppressor of cytokine signaling 1/JAB and suppressor of cytokine signaling 3/cytokine-inducible SH2 containing protein 3 negatively regulate the signal transducers and activators of transcription signaling pathway in normal human epidermal keratinocytes. *J Invest Dermatol.* 2003;120:571-580.
502. Druzgal CH, Chen Z, Yeh NT, et al. A pilot study of longitudinal serum cytokine and angiogenesis factor levels as markers of therapeutic response and survival in patients with head and neck squamous cell carcinoma. *Head Neck.* 2005;27:771-784.
503. Jones SA, Horiuchi S, Topley N, Yamamoto N, Fuller GM. The soluble interleukin 6 receptor: mechanisms of production and implications in disease. *FASEB J.* 2001;15:43-58.
504. Knüpfner H, Preiss R. sIL-6R: more than an agonist? *Immunol Cell Biol.* 2008;86:87-91.
505. Drucker C, Gewiese J, Malchow S, Scheller J, Rose-John S. Impact of interleukin-6 classic- and trans-signaling on liver damage and regeneration. *J Autoimmun.* 2010;34:29-37.
506. Gewiese-Rabsch J, Drucker C, Malchow S, Scheller J, Rose-John S. Role of IL-6 trans-signaling in CCl₄ induced liver damage. *Biochim Biophys Acta.* 2010;1802:1054-1061.
507. Peters M, Blinn G, Jostock T, et al. Combined interleukin 6 and soluble interleukin 6 receptor accelerates murine liver regeneration. *Gastroenterology.* 2000;119:1663-1671.
508. Dominitzki S, Fantini MC, Neufert C, et al. Cutting edge: trans-signaling via the soluble IL-6R abrogates the induction of FoxP3 in naive CD4+CD25 T cells. *J Immunol.* 2007;179:2041-2045.
509. Zhang L, Zhao Y. The regulation of Foxp3 expression in regulatory CD4(+)CD25(+)T cells: multiple pathways on the road. *J Cell Physiol.* 2007;211:590-597.
510. Bettelli E, Carrier Y, Gao W, et al. Reciprocal developmental pathways for the generation of pathogenic effector TH17 and regulatory T cells. *Nature.* 2006;441:235-238.
511. Molling JW, de Gruijl TD, Glim J, et al. CD4(+)CD25hi regulatory T-cell frequency correlates with persistence of human papillomavirus type 16 and T helper cell responses in patients with cervical intraepithelial neoplasia. *Int J Cancer.* 2007;121:1749-1755.
512. Ivashkiv LB, Hu X. Signaling by STATs. *Arthritis Res Ther.* 2004;6:159-168.
513. Larsen L, Röpke C. Suppressors of cytokine signalling: SOCS. *APMIS.* 2002;110:833-844.
514. Ghosh A, Pechota A, Coleman D, Upchurch GR, Eliason JL. Cigarette smoke-induced MMP2 and MMP9 secretion from aortic vascular smooth cells is mediated via the Jak/Stat pathway. *Hum Pathol.* 2015;46:284-294.
515. NICE technology appraisal guidance [TA145] – 2008 r.
516. Takeuchi S, Wang W, Li Q, et al. Dual inhibition of Met kinase and angiogenesis to overcome HGF-induced EGFR-TKI resistance in EGFR mutant lung cancer. *Am J Pathol.* 2012;181:1034-1043.
517. Yano S, Wang W, Li Q, et al. Hepatocyte growth factor induces gefitinib resistance of lung adenocarcinoma with epidermal growth factor receptor-activating mutations. *Cancer Res.* 2008;68:9479-9487.

518. Yamada T, Takeuchi S, Kita K, et al. Hepatocyte growth factor induces resistance to anti-epidermal growth factor receptor antibody in lung cancer. *J Thorac Oncol*. 2012;7:272-280.
519. Mueller KL, Madden JM, Zoratti GL, Kuperwasser C, List K, Boerner JL. Fibroblast-secreted hepatocyte growth factor mediates epidermal growth factor receptor tyrosine kinase inhibitor resistance in triple-negative breast cancers through paracrine activation of Met. *Breast Cancer Res*. 2012;14:R104.
520. Wang W, Li Q, Yamada T, et al. Crosstalk to stromal fibroblasts induces resistance of lung cancer to epidermal growth factor receptor tyrosine kinase inhibitors. *Clin Cancer Res*. 2009;15:6630-6638.
521. Turke AB, Zejnullahu K, Wu YL, et al. Preexistence and clonal selection of MET amplification in EGFR mutant NSCLC. *Cancer Cell*. 2010;17:77-88.
522. Song N, Liu S, Zhang J, et al. Cetuximab-induced MET activation acts as a novel resistance mechanism in colon cancer cells. *Int J Mol Sci*. 2014;15:5838-5851.
523. Kim SM, Kwon OJ, Hong YK, et al. Activation of IL-6R/JAK1/STAT3 signaling induces de novo resistance to irreversible EGFR inhibitors in non-small cell lung cancer with T790M resistance mutation. *Mol Cancer Ther*. 2012;11:2254-2264.
524. Liu L, Shi H, Liu Y, et al. Synergistic effects of foretinib with HER-targeted agents in MET and HER1- or HER2-coactivated tumor cells. *Mol Cancer Ther*. 2011;10:518-530.
525. Group NCT. MET/VEGFR2 Inhibitor GSK1363089 and Erlotinib Hydrochloride or Erlotinib Hydrochloride Alone in Treating Patients With Locally Advanced or Metastatic Non-Small Cell Lung Cancer That Has Not Responded to Previous Chemotherapy. Clinicaltrials.gov ID: NCT01068587.
526. Group NCT. Study of Foretinib in Combination With Lapatinib in Patients With Metastatic Breast Cancer. Clinicaltrials.gov ID: NCT01138384.
527. Paulsson J, Micke P. Prognostic relevance of cancer-associated fibroblasts in human cancer. *Semin Cancer Biol*. 2014;25:61-68.
528. Bhowmick NA, Neilson EG, Moses HL. Stromal fibroblasts in cancer initiation and progression. *Nature*. 2004;432:332-337.
529. Cirri P, Chiarugi P. Cancer-associated-fibroblasts and tumour cells: a diabolic liaison driving cancer progression. *Cancer Metastasis Rev*. 2012;31:195-208.
530. De Wever O, Demetter P, Mareel M, Bracke M. Stromal myofibroblasts are drivers of invasive cancer growth. *Int J Cancer*. 2008;123:2229-2238.
531. Orimo A, Tomioka Y, Shimizu Y, et al. Cancer-associated myofibroblasts possess various factors to promote endometrial tumor progression. *Clin Cancer Res*. 2001;7:3097-3105.
532. Räsänen K, Vaheri A. Activation of fibroblasts in cancer stroma. *Exp Cell Res*. 2010;316:2713-2722.
533. Gaggioli C, Hooper S, Hidalgo-Carcedo C, et al. Fibroblast-led collective invasion of carcinoma cells with differing roles for RhoGTPases in leading and following cells. *Nat Cell Biol*. 2007;9:1392-1400.
534. Goruppi S, Dotto GP. Mesenchymal stroma: primary determinant and therapeutic target for epithelial cancer. *Trends Cell Biol*. 2013;23:593-602.
535. Capparelli C, Guido C, Whitaker-Menezes D, et al. Autophagy and senescence in cancer-associated fibroblasts metabolically supports tumor growth and metastasis via glycolysis and ketone production. *Cell Cycle*. 2012;11:2285-2302.
536. Elkhattouti A, Hassan M, Gomez CR. Stromal Fibroblast in Age-Related Cancer: Role in Tumorigenesis and Potential as Novel Therapeutic Target. *Front Oncol*. 2015;5:158.

537. Yang G, Rosen DG, Zhang Z, et al. The chemokine growth-regulated oncogene 1 (Gro-1) links RAS signaling to the senescence of stromal fibroblasts and ovarian tumorigenesis. *Proc Natl Acad Sci U S A*. 2006;103:16472-16477.
538. Laberge RM, Awad P, Campisi J, Desprez PY. Epithelial-mesenchymal transition induced by senescent fibroblasts. *Cancer Microenviron*. 2012;5:39-44.
539. Bachman KE, Park BH. Dual nature of TGF-beta signaling: tumor suppressor vs. tumor promoter. *Curr Opin Oncol*. 2005;17:49-54.
540. Pardali K, Moustakas A. Actions of TGF-beta as tumor suppressor and pro-metastatic factor in human cancer. *Biochim Biophys Acta*. 2007;1775:21-62.
541. Al-toub M, Almusa A, Almajed M, et al. Pleiotropic effects of cancer cells' secreted factors on human stromal (mesenchymal) stem cells. *Stem Cell Res Ther*. 2013;4:114.
542. Bhowmick NA, Chytil A, Plieth D, et al. TGF-beta signaling in fibroblasts modulates the oncogenic potential of adjacent epithelia. *Science*. 2004;303:848-851.
543. Oyanagi J, Kojima N, Sato H, et al. Inhibition of transforming growth factor- β signaling potentiates tumor cell invasion into collagen matrix induced by fibroblast-derived hepatocyte growth factor. *Exp Cell Res*. 2014;326:267-279.
544. Schauer IG, Sood AK, Mok S, Liu J. Cancer-associated fibroblasts and their putative role in potentiating the initiation and development of epithelial ovarian cancer. *Neoplasia*. 2011;13:393-405.
545. Schauer IG, Zhang J, Xing Z, et al. Interleukin-1 β promotes ovarian tumorigenesis through a p53/NF- κ B-mediated inflammatory response in stromal fibroblasts. *Neoplasia*. 2013;15:409-420.
546. Coppé JP, Desprez PY, Krtolica A, Campisi J. The senescence-associated secretory phenotype: the dark side of tumor suppression. *Annu Rev Pathol*. 2010;5:99-118.
547. Nyström ML, Thomas GJ, Stone M, Mackenzie IC, Hart IR, Marshall JF. Development of a quantitative method to analyse tumour cell invasion in organotypic culture. *J Pathol*. 2005;205:468-475.
548. Ota H, Miki N. Microtechnology-based three-dimensional spheroid formation. *Front Biosci (Elite Ed)*. 2013;5:37-48.
549. Raghavan S, Ward MR, Rowley KR, et al. Formation of stable small cell number three-dimensional ovarian cancer spheroids using hanging drop arrays for preclinical drug sensitivity assays. *Gynecol Oncol*. 2015;138:181-189.
550. Colley HE, Hearnden V, Jones AV, et al. Development of tissue-engineered models of oral dysplasia and early invasive oral squamous cell carcinoma. *Br J Cancer*. 2011;105:1582-1592.
551. Dongari-Bagtzoglou A, Kashleva H. Development of a highly reproducible three-dimensional organotypic model of the oral mucosa. *Nat Protoc*. 2006;1:2012-2018.
552. Pinnock A, Murdoch C, Moharamzadeh K, Whawell S, Douglas CW. Characterisation and optimisation of organotypic oral mucosal models to study Porphyromonas gingivalis invasion. *Microbes Infect*. 2014;16:310-319.
553. Jenei V, Nyström ML, Thomas GJ. Measuring invasion in an organotypic model. *Methods Mol Biol*. 2011;769:223-232.
554. T S, S S, H K, P B, S M, J S. A Phase II study of the efficacy and safety of foretinib, a novel receptor tyrosine kinase inhibitor, given on an intermittent five days on nine days off (5/9) schedule in patients with recurrent or metastatic squamous cell cancer of the head and neck. Vol 8 (12 suppl), B6. *Mol Cancer Ther* 2009.
555. Shapiro GI, McCallum S, Adams LM, et al. A Phase 1 dose-escalation study of the safety and pharmacokinetics of once-daily oral foretinib, a multi-kinase inhibitor, in patients with solid tumors. *Invest New Drugs*. 2013;31:742-750.

556. Chang YC, Nieh S, Chen SF, Jao SW, Lin YL, Fu E. Invasive pattern grading score designed as an independent prognostic indicator in oral squamous cell carcinoma. *Histopathology*. 2010;57:295-303.
557. Hartmann S, Neckel N, Seher A, et al. Erlotinib and gefitinib responsiveness in head and neck cancer cell lines—a comparing analysis with cetuximab. *Clin Oral Investig*. 2015.
558. Lynch TJ, Bell DW, Sordella R, et al. Activating mutations in the epidermal growth factor receptor underlying responsiveness of non-small-cell lung cancer to gefitinib. *N Engl J Med*. 2004;350:2129-2139.
559. Ontario HQ. Epidermal Growth Factor Receptor Mutation (EGFR) Testing for Prediction of Response to EGFR-Targeting Tyrosine Kinase Inhibitor (TKI) Drugs in Patients with Advanced Non-Small-Cell Lung Cancer: An Evidence-Based Analysis. *Ont Health Technol Assess Ser*. 2010;10:1-48.
560. Lococo F, Paci M, Rapicetta C, et al. Preliminary Evidence on the Diagnostic and Molecular Role of Circulating Soluble EGFR in Non-Small Cell Lung Cancer. *Int J Mol Sci*. 2015;16:19612-19630.
561. Hennigan S, Kavanaugh A. Interleukin-6 inhibitors in the treatment of rheumatoid arthritis. *Ther Clin Risk Manag*. 2008;4:767-775.
562. Vij N, Sharma A, Thakkar M, Sinha S, Mohan RR. PDGF-driven proliferation, migration, and IL8 chemokine secretion in human corneal fibroblasts involve JAK2-STAT3 signaling pathway. *Mol Vis*. 2008;14:1020-1027.
563. Nakamura T, Matsumoto K, Kiritoshi A, Tano Y. Induction of hepatocyte growth factor in fibroblasts by tumor-derived factors affects invasive growth of tumor cells: in vitro analysis of tumor-stromal interactions. *Cancer Res*. 1997;57:3305-3313.
564. Gharavi NM, Alva JA, Mouillesseaux KP, et al. Role of the Jak/STAT pathway in the regulation of interleukin-8 transcription by oxidized phospholipids in vitro and in atherosclerosis in vivo. *J Biol Chem*. 2007;282:31460-31468.
565. de la Iglesia N, Konopka G, Lim KL, et al. Deregulation of a STAT3-interleukin 8 signaling pathway promotes human glioblastoma cell proliferation and invasiveness. *J Neurosci*. 2008;28:5870-5878.
566. Gu FM, Li QL, Gao Q, et al. IL-17 induces AKT-dependent IL-6/JAK2/STAT3 activation and tumor progression in hepatocellular carcinoma. *Mol Cancer*. 2011;10:150.
567. Mesa RA. Ruxolitinib, a selective JAK1 and JAK2 inhibitor for the treatment of myeloproliferative neoplasms and psoriasis. *IDrugs*. 2010;13:394-403.
568. Pandey A, Fernandez MM, Steen H, et al. Identification of a novel immunoreceptor tyrosine-based activation motif-containing molecule, STAM2, by mass spectrometry and its involvement in growth factor and cytokine receptor signaling pathways. *J Biol Chem*. 2000;275:38633-38639.
569. Leonard WJ, O'Shea JJ. Jaks and STATs: biological implications. *Annu Rev Immunol*. 1998;16:293-322.
570. Fujitani Y, Hibi M, Fukada T, et al. An alternative pathway for STAT activation that is mediated by the direct interaction between JAK and STAT. *Oncogene*. 1997;14:751-761.
571. Scuto A, Kujawski M, Kowolik C, et al. STAT3 inhibition is a therapeutic strategy for ABC-like diffuse large B-cell lymphoma. *Cancer Res*. 2011;71:3182-3188.
572. Arribas J, Coodly L, Vollmer P, Kishimoto TK, Rose-John S, Massagué J. Diverse cell surface protein ectodomains are shed by a system sensitive to metalloprotease inhibitors. *J Biol Chem*. 1996;271:11376-11382.

- 573.** Perez-Torres M, Valle BL, Maihle NJ, Negron-Vega L, Nieves-Alicea R, Cora EM. Shedding of epidermal growth factor receptor is a regulated process that occurs with overexpression in malignant cells. *Exp Cell Res.* 2008;314:2907-2918.
- 574.** Cripps C, Winqvist E, Devries MC, Stys-Norman D, Gilbert R, Group HaNCDS. Epidermal growth factor receptor targeted therapy in stages III and IV head and neck cancer. *Curr Oncol.* 2010;17:37-48.
- 575.** Lawless C, Wang C, Jurk D, Merz A, Zglinicki T, Passos JF. Quantitative assessment of markers for cell senescence. *Exp Gerontol.* 2010;45:772-778.
- 576.** Zillhardt M, Park SM, Romero IL, et al. Foretinib (GSK1363089), an orally available multikinase inhibitor of c-Met and VEGFR-2, blocks proliferation, induces anoikis, and impairs ovarian cancer metastasis. *Clin Cancer Res.* 2011;17:4042-4051.

Appendix I: STR Profiling of Cell Lines

22/10/2013

Cell line STR profile report

CR-UK Centre Genomics Facility
Leeds Institute of Molecular Medicine

Reference data for UPCLSCC152

Reference profile from :

D3	TH01	D21	D18	Peak 2	D2	D13	D7	D16	CEBP10	Peak D	Amel	YWA	D8	TP0X	FGA
S1328	(2n+11)	S11	S21	(2n+13)	S178	S217	S228	S238	(2n2)	(2n21)	(2n+2)	(2n+2)	S1179	(2n2)	(2n+1)

Sample data

Sample UPCLSCC152_KH_Sep13

D3	TH01	D21	D18	Peak 2	D2	D13	D7	D16	CEBP10	Peak D	Amel	YWA	D8	TP0X	FGA
S1328	(2n+11)	S11	S21	(2n+13)	S178	S217	S228	S238	(2n2)	(2n21)	(2n+2)	(2n+2)	S1179	(2n2)	(2n+1)
G105924	7.9.3	28.31	18	11.12	11.12	11	9.10	12.13	11.12	11	XV	17	12	8	20
G105928	7.9.3	28.31	18	11.12	11.12	11	9.10	12.13	11.12	11	XV	17	12	8	20

Statistics are tabulated using the format:
 cell line _ marker _ value of 1st band _ date of receipt or other unique identifier

Analysis

Sample match to reference

No reference profile available.

DSMZAB Very close match to UPCL-SCC-090 (DSMZ ACC 670).

DSMZ STR profile database :
 <http://www.rockefeller.edu/genetics/strdb/>
 <http://www.genenetwork.org/strdb/>
 Statistics Z177 cell lines from ATCC, DSMZ, JCRB & NINDS.

CLMABD No record retrieved.

Cell line integrated molecular authentication (CLIMA) database
 <http://biomedinformatics.sagepub.com/>

CGP Cell line not included in CGP dataset.

Centre Genome Project STR data :
 <http://www.genenetwork.org/strdb/>
 (registration required). <http://www.genenetwork.org/strdb/>
 Details of CGP data available only to registered users.

CLABD Very similar to UPCL-SCC-090 (see accompanying information).

Database of STR profiles generated by the CR-UK Genomics Facility

Comment
UPCL-SCC-090 and UPCL-SCC-152 are derived from the same patient (White et al., 2007 Oral Oncol. 43 701). The two cell lines have extremely similar STR profiles (see accompanying information): the percentage match between the two profiles is 93.6%, and the two cell lines cannot be categorically distinguished by STR profiling.

22/10/2013

Cell line STR profile report

CR-UK Centre Genomics Facility
Leeds Institute of Molecular Medicine

Reference data for UPCLSCC090

Reference profile	DSMZ	ACC 070	CO (kb)	TH01 (kb)	D21 S11 (kb)	D18 S21 (kb)	Power E (kb)	D5 S818 (kb)	D13 S317 (kb)	D7 S828 (kb)	D16 S538 (kb)	CGF190 (kb)	Power D (kb)	Amel (kb)	VWA (kb)	D8 S1178 (kb)	TPOX (kb)	FGA (kb)
from :																		
			11.358	7				11.12	11	8.10	12.13	11.12	X,Y	17		8		

Sample data

Sample	UPCLSCC090_KH_Sep13	CO (kb)	TH01 (kb)	D21 S11 (kb)	D18 S21 (kb)	Power E (kb)	D5 S818 (kb)	D13 S317 (kb)	D7 S828 (kb)	D16 S538 (kb)	CGF190 (kb)	Power D (kb)	Amel (kb)	VWA (kb)	D8 S1178 (kb)	TPOX (kb)	FGA (kb)
		14	7	20.21	14.18	11.12	11.12	11	8.10	12.13	11.12	11	X,Y	17	12	8	20

Samples are labelled using the format: `cell_line_sample_date_of_receipt_or_other_unique_identifier`

Analysis Sample match to reference Matches DSMZ reference profile at 979 markers.

DSMZ00 Matches UPCL-SCC-090 (DSMZ ACC 070).

CLMAD0 Not done.

CGP0 Cell line not included in CGP dataset.

Comment

UPCL-SCC-090 and UPCL-SCC-152 are derived from the same patient [White et al., 2007; Oral Oncol. 43 701]. The two cell lines have extremely similar STR profiles (see accompanying information); the percentage match between the two profiles is 99.8%, and the two cell lines cannot be categorically distinguished by STR profiling.

DSMZ STR profile database:
<http://www.dsmz.de/str/str-service.html>
(registration required)
Database 2278 and data from ATCC, DSMZ, JCRB & WIKEN

Cell line independent molecular authentication (CLINA) database
<http://bioinformatics.sagepub.com>

Cancer Genome Project STR data
<http://www.sanger.ac.uk/research/projects/cancer-genome-project/>
(registration required)
Details of CGP data available only to registered users

Experimental data generated using Promega PowerPlex 16 system.

We recommend that a minimum of two profiles are generated for each sample, to control for PCR artefacts such as allele dropout. This is of particular importance when generating reference profiles of new cell lines for publication or for validation of reference to published profiles.

22/10/2013

Cell line STR profile report

CR-UK Centre Genomics Facility
Leeds Institute of Molecular Medicine

Reference data for UPCISCC089

Reference profile from :

DI	TH01	D21	D18	Peak E	D5	D13	D7	D16	CSF1PO	Peak D	Amt1	VWA	D8	TPOX	FGA
(bp1)	(bp11)	(bp1)	(bp1)	(bp15)	(bp11)	(bp17)	(bp12)	(bp12)	(bp1)	(bp21)	(bp12)	(bp12)	(bp17)	(bp12)	(bp1)
15	8	28,312	14,20	10,13	12	12,14	8,12	12	11,14	12,14	X	17,18	10,16,17	8	28

Samples are labelled using the format: cell line name, _index of lab head, _date of receipt or other unique identifier

Sample data

Sample **UPCISCC089_KH_Sep13**

DI	TH01	D21	D18	Peak E	D5	D13	D7	D16	CSF1PO	Peak D	Amt1	VWA	D8	TPOX	FGA
(bp1)	(bp11)	(bp1)	(bp1)	(bp15)	(bp11)	(bp17)	(bp12)	(bp12)	(bp1)	(bp21)	(bp12)	(bp12)	(bp17)	(bp12)	(bp1)
15	8	28,312	14,20	10,13	12	12,14	8,12	12	11,14	12,14	X	17,18	10,16,17	8	28

Analysis Sample match to No reference profile available.
reference

DSMZdb

No close match.

DSMZ STR profile database:
<http://www.genet.byu.edu/strdb/strdb.html>
(registration required)
Searches Z178 and from ATCC, DSMZ, JCRB & NIKEN.

CLIMAPdb

No record retrieved.

Cell line integrated molecular authentication (CLIMAP) database
<http://bioinformatics.sage.ac.uk/>

CCP

Cell line not included in CCP dataset.

Cancer Genomes Project STR data:
<http://www.sanger.ac.uk/Research/Projects/cancer-genomes/>
(registration required)
Details of CCP data available only to registered users.

CLAVAdb

No match (database contains experimental data from 213 different cell lines on 20.09.2013).

Database of STR profiles generated by the CR-UK Genomics Facility

Comment

22/10/2013

Cell line STR profile report

CR-UK Centre Genomics Facility
Leeds Institute of Molecular Medicine

Reference data for UPICISCC072

Reference profile	DSMZ	ACC 607	Q1	THS1 (chr11)	Q21 SFI	Q18 SFI	PlusE (chr15)	Q1 SFI	Q13 SFI	Q7 SFI	Q16 SFI	CER10 (chr4)	PlusD (chr21)	Amel (chr12)	YMA SFI	Q8 SFI	THOX (chr2)	PSA (chr1)
			14	6			7	14	11	11,12	11,12	11		X	15		8	

Sample data

Sample	UPICISCC072_KH_Sep13	Q1 SFI	THS1 (chr11)	Q21 SFI	Q18 SFI	PlusE (chr15)	Q1 SFI	Q13 SFI	Q7 SFI	Q16 SFI	CER10 (chr4)	PlusD (chr21)	Amel (chr12)	YMA SFI	Q8 SFI	THOX (chr2)	PSA (chr1)
		17	6	no result	12,16	7	14	11	11,12	11,12	11	13	X	15	13,15	8	23
		17	6	no result	12,16	7	14	11	11,12	11,12	11	13	X	15	13,15	8	23

Stratify are labelled using the format:
 cell line name, _ marker of the band, _ date of receipt or other unique identifier

Analysis

Sample match to **Matches DSMZ reference profile at 9/9 markers.**
reference

DSMZ06 Matches UPICISCC-072 (DSMZ ACC 607).

CLMMA0D Not done.

CQP Cell line not included in CQP dataset.

Comment

DSMZ STR profile database :
<http://www.dsmz.de/ftp/strdb.html>
(registration required)
Searches 2275 cell lines from ATCC, DSMZ, JCRB & KRCRI.

Cell line integrated molecular authentication (CLMMA) address
<http://biobanbank.sagepub.com>

Experimental data generated using Promega PowerPlex 16 system.

We warrant that a minimum of two profiles are generated for each sample, to enable for PCR analysis such as allele dropout. This is of particular importance when generating reference profiles of new cell lines for publication or for validation of differences to published profiles.

21/10/2013

Cell line STR profile report

CR-UK Centre Genomics Facility
Leeds Institute of Molecular Medicine

Reference data for UDSCC2

Reference profile available.
from :

D3	THS1	D21	D18	Peak E	D5	D13	D7	D16	CE190	Peak D	Amel	YWA	D8	TPXK	TGA
S1328	(2n+1)	S11	S51	(2n+1)	S818	S317	S529	S539	(2n)	(2n+1)	(2n+1)	(2n+2)	S1179	(2n+2)	(2n+1)

Sample data

Sample UDSCC2_KH_Sep13

GV95926A	D3	THS1	D21	D18	Peak E	D5	D13	D7	D16	CE190	Peak D	Amel	YWA	D8	TPXK	TGA
	S1328	(2n+1)	S11	S51	(2n+1)	S818	S317	S529	S539	(2n)	(2n+1)	(2n+1)	(2n+2)	S1179	(2n+2)	(2n+1)
GV95926B	14,16	8,9	20	12,17	10	10,11	8	8,9	11,13	11,12	13	XY	15,18	13,15	8,10	20,27

Stratify are labelled using the format: cell line name _ position of the band _ date of receipt or other unique identifier

Analysis

Sample match to reference

No reference profile available.

DSMZ26

No close match.

DSMZ STR profile database:
http://www.azylab.org/STRdb.html
(registration required)
Shawnee Z179 cell lines from ATCC, DSMZ, JCRB & NIKEN.

CLMAD6

No record retrieved.

Cell line integrated molecular authentication (CLMAD) database
http://stemcellbank.sagepub.com

CCP

Cell line not included in CCP dataset.

Genex Genome Project STR data:
http://www.sanger.ac.uk/Research/Projects/Genex/genexstrdb/
(registration required)
Details of CCP data available only to registered users.

CLAD6

No match (database contains experimental data from 213 different cell lines on 26.09.2013).

Database of STR profiles generated by the CR-UK Genomics Facility

Comment

Experimental data generated using Promega PowerPlex 16 system.

We recommend that a minimum of two profiles are generated for each sample, to control for PCR artefacts such as allele dropout. This is of particular importance when generating reference profiles of new cell lines for publication or for validation of differences to published profiles.

21/10/2013

Cell line STR profile report

CR-UK Centre Genomics Facility
Leeds Institute of Molecular Medicine

Reference data for HTEE6E7

Reference profile from : No profile available.

Reference	Profile																										
01	10.17	TH01	6.8	021	20.21	018	12.18	02	10.13	013	8.11	07	8.2	018	9.11	CEP10	11	8.14	X	WGA	17.18	08	10.13	TH0X	11	PCNA	20.22
01	10.17	TH01	6.8	021	20.21	018	12.18	02	10.13	013	8.11	07	8.2	018	9.11	CEP10	11	8.14	X	WGA	17.18	08	10.13	TH0X	11	PCNA	20.22
01	10.17	TH01	6.8	021	20.21	018	12.18	02	10.13	013	8.11	07	8.2	018	9.11	CEP10	11	8.14	X	WGA	17.18	08	10.13	TH0X	11	PCNA	20.22
01	10.17	TH01	6.8	021	20.21	018	12.18	02	10.13	013	8.11	07	8.2	018	9.11	CEP10	11	8.14	X	WGA	17.18	08	10.13	TH0X	11	PCNA	20.22
01	10.17	TH01	6.8	021	20.21	018	12.18	02	10.13	013	8.11	07	8.2	018	9.11	CEP10	11	8.14	X	WGA	17.18	08	10.13	TH0X	11	PCNA	20.22

Samples are labelled using the format: cell_line_name _ position_of_the_lane _ date_of_receipt_or_other_unique_identifier

Analysis

Sample match to reference: No reference profile available.

OSMAZB: No close match.

CLMAAD: No record retrieved.

COP: Cell line not included in COP dataset.

CLAD: Matches a cell line received for analysis under the name 10EGE7HTE. Given the similarity between the names of the two cell lines, it seems possible that they derive from the same source.

Comment: It may be worth attempting to confirm that HTEE6E7 and 10EGE7HTE are, in fact, the same cell line.

Experimental data generated using Promega PowerPlex 16 system.

We recommend that a minimum of two profiles are generated for each sample. It is vital for PCR amplification when generating reference profiles of new cell lines for publication or for validation of reference profiles.

21/10/2013

Cell line STR profile report

CR-UK Centre Genomics Facility
Leeds Institute of Molecular Medicine

Reference data for 93WU147T

Reference profile from :	No profile available.														
D3	TH01	D21	D18	Peak 6	D5	D13	D7	D16	CEBP10	Peak D	Amel	YWA	D8	TP53	TGA
S1326	(26/11)	S11	S31	(26/15)	S618	S317	S529	S539	(26/2)	(26/21)	(26/12)	(26/12)	S1179	(26/2)	(26/1)

Sample data

Sample 93WU147T_KH_Sep13

CS	TH01	D21	D18	Peak 6	D5	D13	D7	D16	CEBP10 <th>Peak D</th> <th>Amel</th> <th>YWA</th> <th>D8</th> <th>TP53</th> <th>TGA</th>	Peak D	Amel	YWA	D8	TP53	TGA	
S1326	(26/11)	S11	S31	(26/15)	S618	S317	S529	S539	(26/2)	(26/21)	(26/12)	(26/12)	S1179	(26/2)	(26/1)	
CHROM24	15.17	7.8	20.21	18	11.12	11.12	12	10.11	9.11	11.12	12.14	X	18	13.19	9.11	22
CHROM28	15.17	7.8	20.21	18	11.12	11.12	12	10.11	9.11	11.12	12.14	X	18	13.19	9.11	22

Samples are labelled using the format: cell line name, index of lab head, date of receipt or other unique identifier

Analysis

Sample match to reference

No reference profile available.

DGMZAB

No close match.

CLMABD

No record retrieved.

CGP

Cell line not included in CGP database.

CLAB

No match (database contains experimental data from 213 different cell lines on 26.09.2013).

Comment

Experimental data generated using Promega PowerPlex 16 system.
We recommend that a selection of two profiles are generated for each sample, to assist for PCR products such as when shipped. This is of particular importance when generating reference profiles of new cell lines for publication or for inclusion of differences to published profiles.